DISPERSANT EFFECTIVENESS UNDER HIGH SALINITY CONDITIONS FOLLOWING A SUBSURFACE JET RELEASE OF OIL

Brian Robinson, Thomas King, Scott Ryan
Department of Fisheries and Oceans Canada
Bedford Institute of Oceanography, Dartmouth, Nova Scotia, Canada

Robyn Conmy
U.S. Environmental Protection Agency
Office of Research and Development, Cincinnati, Ohio, USA

Michel Boufadel, Lin Zhao, Feng Gao
Department of Civil and Environmental Engineering
New Jersey Institute of Technology, Newark, New Jersey, USA

INTRODUCTION

Potential oil exploration and production activities in close proximity to hypersaline water bodies, such as brine channels in the Arctic or brine pools in the Gulf of Mexico (GoM), necessitates characterization of Dispersant Effectiveness (DE) at high salinities. The 2010 GoM Deepwater Horizon (DWH) oil spill was the largest and deepest oil release ever to be treated with chemical dispersants as the primary mitigation tool, demonstrating that dispersants could be injected directly into a high pressure oil blowout at a depth of 1500 m. Yet, if such a release were to occur into hypersaline waters, it is currently unknown whether dispersants would be an effective response tool, particularly during extreme mixing of brine with overlying seawater. To investigate the effect of hypersaline conditions on DE, a series of experiments were conducted using an underwater jet release of oil in a flume tank.

DESCRIPTION OF FLUME TANK FACILITY

Subsurface injection experiments were conducted in a flume tank located at the Bedford Institute of Oceanography in Dartmouth, Nova Scotia, Canada. The tank has inner dimensions of 30 m x 2 m x 0.6 m (LxWxH) with an operational water volume of 30,000 L. All experiments were conducted using a natural supply of seawater that had been pumped through 5 µm and 25 µm bag filters.

The tank is equipped with a high flow seawater pumping system connected to a series of influent and effluent manifolds that are capable of generating horizontal water currents of up to 5 cm s^{-1} in the tank.

The subsurface oil injector consists of a stainless steel pressure vessel that can hold up to 2 L of oil. Inside the pressure vessel was a coil of copper tubing that was connected to a circulating water bath which allowed for maintaining the oil temperature at 20°C. The pressure vessel was pressurized to 50 psi (ANS) or 90 psi (IFO) by connecting it to a tank of compressed nitrogen. A series of valves were used to connect the pressure vessel to an injector nozzle inside the tank. The nozzle had an orifice diameter of 2.4 mm and was oriented 20 cm off the bottom of the tank and pointed in a horizontal down current direction. Injection times ranged between 5-7 seconds resulting in a 350 g oil release.

The BIO wave tank and flume tank facility.

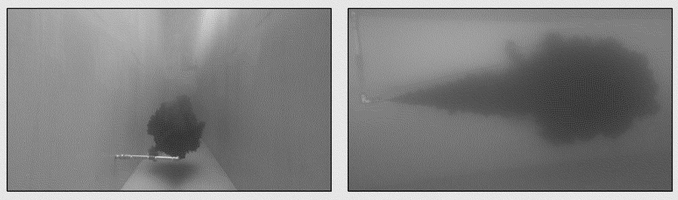

Underwater images of a subsurface oil injection experiment.

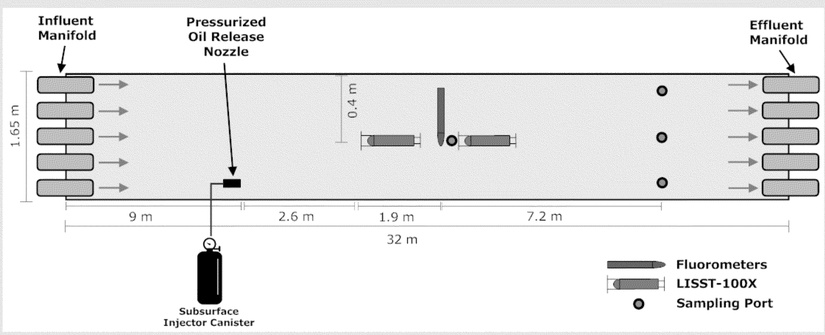

Figure 1: Cross section of the flume tank used in this study showing the high flow seawater manifold system (left) and the subsurface injection system and insitu instrument package (right).

EXPERIMENTAL METHODS

A series of 10 subsurface injection flume tank experiments were conducted to evaluate the horizontal transport of subsurface oil droplets under four test salinities. Two different oil types were used – Alaska North Slope (ANS) crude and Intermediate Fuel Oil 120 (IFO). Each oil type was tested without dispersant treatment as well as with the dispersant Corexit 9500A at a dispersant-to-oil ratio (DOR) of 1:25. The experiments were conducted in the fall of 2016 and average water temperatures were 14.1°C for experiments with ANS and 9.5°C for experiments for experiments with IFO-120. A complete list of the experimental treatment conditions can be found in the table below.

To monitor the transport of dispersed oil in the tank, a series of insitu instruments were deployed at various locations in the tank. Oil droplet sizes between 2.5-500 µm were measured using two LISST-100X particle size analyzers (Sequoia Scientific) which were located 2.6 m and 4.5 m downstream of the subsurface oil release. Also deployed in the tank were a series of four commercially available hydrocarbon fluorometers (Turner Cyclops C7 Refined and Crude Optics, Chelsea UV Aquatracka Refined Optics, Wetlabs ECO) so that their response to dispersed oil resulting from a subsurface release could be evaluated. Discrete water samples were collected during each experiment for chemical analysis of BTEX (benzene, toluene, ethylebenzene and xylene) and TPH (Total Petroleum Hydrocarbons).

		Water Temp (°C)	Air Temp (°C)	Salinity (ppt)
Experiment ID	**Oil Type**	**(Avg)**	**(Avg)**	
SubHS-1, 2, 3, 4	ANS Crude	14.1±1.1	11.6±4.1	28, 50, 75, 100
SubHS-7, 8, 9, 10	ANS Crude	9.5±0.6	7.7±1.6	28, 50, 75, 100

	Viscosity @ Selected Temperatures cPoise		Density @ 40°C g ml^{-1}
	15°C	40°C	
ANS	18.9	8.3	0.8600
IFO-120	2481.5	240.3	0.9411

REFERENCES

Conmy et al. 2013. Submersible Optical Sensors Exposed to Chemically Dispersed Crude Oil: Wave Tank Simulations for Improved Oil Spill Monitoring. Environmental Science and Technology, 48:1803-1810.

Li et al. 2016. Reynolds Number Scaling to Predict Droplet Size Distribution in Dispersed and Undispersed Subsurface Oil Releases. Marine Pollution Bulletin, 113:332-342.

Zhao et al. 2016. Underwater oil jet: Hydrodynamics and droplet size distribution. The Chemical Engineering Journal, 299:292-303

DROPLET SIZE RESULTS

Data obtained from the LISST was used to generate the oil droplet size distribution (DSD) plots shown in Figure 2 below. The use of dispersants had the greatest impact on oil droplet sizes for both oil types. For the ANS crude oil experiments, without the use of dispersant the resulting oil droplet size had a D50 of 75 µm, while with Corexit 9500A at a DOR of 1:25 the D50 was reduced to 12 µm. For the IFO-120 experiments, the more viscous product resulted in overall larger droplets with dispersant having less of an effect compared to ANS. A D50 of 104 µm was obtained in IFO-120 experiments without the use of dispersant, while a D50 of 88 µm was obtained with the use of Corexit. Salinity appeared to have very little effect on the DSD for both oil types, with or without dispersant application.

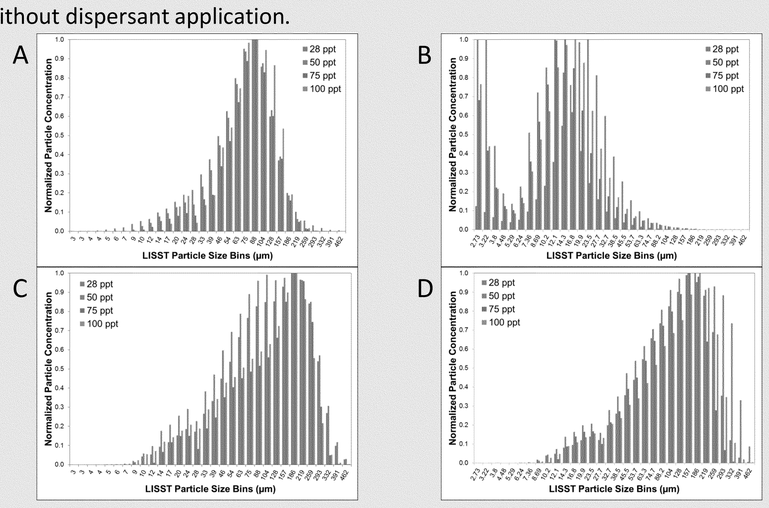

Figure 2: Droplet size distribution at four different test salinities for (A) ANS, (B) ANS+Corexit, (C) IFO, and (D) IFO+Corexit.

The impact of increased salinity on oil droplet buoyancy was calculated using Stokes Law. Based on the oil droplet rise velocities shown in Figure 3, droplets less 500 µm would remain submerged during the entire length of the experiment. The impact of salinity on oil droplet rise velocities would be more noticeable for larger droplets (i.e. 2mm or greater in diameter).

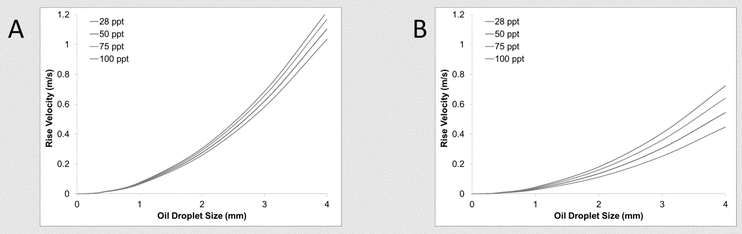

Figure 3: Droplet size rise velocities for (A) ANS Crude and (B) IFO-120 at four test salinities.

WATER COLUMN HYDROCARBON RESULTS

The use of in-situ fluorometers during oil spill response is becoming increasingly common due to their relative ease of deployment and sensitivity to a range of petroleum hydrocarbons. However, there are numerous in-situ fluorometers available commercially, each using different optical properties and thus having varying responses to different crude oil types. An example of the realtime response from the four different hydrocarbon fluorometers deployed during these experiments is shown in Figure 4. All four instruments gave a higher signal response to ANS crude oil compared to IFO-120. In addition, experiments using ANS that had been dispersed with Corexit 9500 had on average twice the signal response compared to ANS oil alone. There was little difference in the intensity of the fluorometer response for IFO-120 with and without dispersant treatment. Measurement of water column hydrocarbon concentrations found that there were significant differences between the two oils (Table 1). For the volatile hydrocarbon (BTEX) results, the ANS crude generated concentrations that were approximately an order of magnitude greater than IFO-120. The use of dispersant also resulted in BTEX concentrations that were approximately double compared to experiments that did not use dispersant. Total oil concentrations (TPH) in the water column were also higher for both ANS and IFO-120 when treated with dispersant, while IFO-120 had slightly higher TPH concentrations for experiments both with and without dispersant compared to ANS.

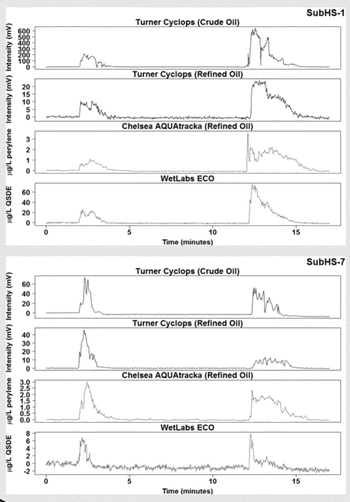

Figure 4 (Left) shows the insitu fluorometer response for ANS Crude (top) and IFO-120 (bottom). The first peak on each plot is for an oil injection without dispersant treatment, while the second peak is for oil and dispersant.

Table 1 (right) summarizes the average water column hydrocarbon chemistry results for BTEX and TPH analyses.

BTEX (ppb)		
	ANS	IFO-120
No Dispersant	195.0	37.3
With Dispersant	513.7	51.1

TPH (ppm)		
	ANS	IFO-120
No Dispersant	20.1	34.8
With Dispersant	33.3	37.9

SUMMARY

A series of subsurface oil injection experiments were conducted to evaluate the effect of hypersaline conditions on dispersant effectiveness. Under the conditions used in this study, salinities of up to 100 ppt did not have a significant effect on crude oil dispersion. Higher salinities would have an impact on oil droplet rise velocities, although these effects were not observed in our shallow water test tank. In situ fluorometer response varied across the different instruments that were deployed. A stronger signal on all instruments for the ANS crude oil may have been a result of its chemical composition as well as the oil droplet size distribution generated by this oil.

ED_001324_00000685-00001

To: McClellan, Kim[Mcclellan.Kim@epa.gov]
Cc: Yeardley, Roger[Yeardley.Roger@epa.gov]; Conmy, Robyn[Conmy.Robyn@epa.gov]
From: Dapper, Marilyn
Sent: Fri 1/6/2017 4:52:03 PM
Subject: Appendices for Robyn's paper "Dispersant Effectiveness..."
Dispersant Effectiveness combined Appendices A to H plus supplemental table A.pdf

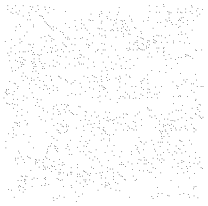

Hi, Kim,

I've attached the appendices for Robyn Conmy's paper, "Dispersant Effectiveness…," (EPA/600/F-16/250). Because of its size, it will need to be published separately from the paper. So, we will need a separate EPA number for it. Can you help/advise us on how to get this number?

Thank you,

Marilyn Dapper

Executive Assistant (SEE)

Environmental Protection Agency

Land Remediation & Pollution Control Division

26 W. Martin Luther King Dr.

Cincinnati, OH 45268

513.569.7925

IAA No. E12PG00037

Final Report Appendices

Dispersant Effectiveness, In-Situ Droplet Size Distribution and Numerical Modeling to Assess Subsurface Dispersant Injection as a Deepwater Blowout Oil Spill Response Option

and

Evaluation of Oil Fluorescence Characteristics to Improve Forensic Response Tools

Submitted to:

Bureau of Safety and Environmental Enforcement

Submitted by:

Robyn N. Conmy, Ph.D.
U.S. Environmental Protection Agency, Office of Research and Development
26 W. Martin Luther King Drive, Cincinnati, OH 45268
*Tel: 513-569-7090, Fax: 513-569-7620, Email: conmy.robyn@epa.gov

Thomas King, M.Sc.; Brian Robinson, M.Sc; Scott Ryan, M.Sc; Youyu Lu, Ph.D.;
Department of Fisheries and Oceans Canada, Bedford Institute of Oceanography
1 Challenger Drive, Dartmouth, Nova Scotia, Canada B2Y 4A2
Tel: 902-426-4172, Tom.King@mar.dfo-mpo.gc.ca

Mary Abercrombie, M.Sc.
University of South Florida, College of Marine Science
140 7th Ave South, St. Petersburg, FL 33701
*Tel: 727-553-1140, Email: mabercrombie@marine.usf.edu

Michel Boufadel, Ph.D.
New Jersey Institute of Technology, Civil and Environmental Engineering
University Heights, Newark, NJ 07102
Tel: 973-596-5657, Email: michel.boufadel@njit.edu

Haibo Niu, Ph.D.
Dalhousie University, Department of Engineering
PO Box 550, Truro, N.S. Canada
Tel: 902-893-6714, Email: haibo.niu@dal.ca

September 30, 2016

ED_001324_00000687-00001

LIST OF APPENDICES

APPENDIX A – Experiment Logs
APPENDIX B – Analytical Chemistry Results
APPENDIX C – Jet Release LISST Oil Droplet Size Distribution Histograms
APPENDIX D – Jet Release LISST Oil Droplet Size Distribution Time Series Contours
APPENDIX E – Submersible Fluorescence Time Series
APPENDIX F – Excitation Emission Matrix Contours
APPENDIX G – VDROP-J and JETLAG Numerical Plume Modeling Report
APPENDIX H – Weber Number Scaling Numerical Plume Modeling Report

ED_001324_00000687-00002

ED_001324_00000687-00003

APPENDIX A – Experiment Logs for subsurface injection experiments with Alaskan North Slope crude, IFO-120, South Louisiana crude and Gas Condensate.

Table A1. Log sheet for subsurface injection experiments with ANS and Corexit 9500 for cold water temperatures.

Experiment ID	Date	Oil Type	Oil Amount (g)	Dispersant-to-Oil Ratio DOR	Oil Temp. °C	Seawater Temp. °C	Air Temp. °C	Salinity ppt	Oil Injection Time seconds	Injection Pressure psi	Weather Conditions
SubANS-1	22-May-14	ANS	208.0	0	80	11.4	11.0	28.1	4	40	Calm
SubANS-2R	02-Dec-14	ANS	290.5	1:200	80	6.4	0.0	27.7	5	40	clear/windy
SubANS-3	23-May-14	ANS	284.5	1:100	80	11.2	14.0	28.0	5	40	Clear, calm
SubANS-4R	03-Dec-14	ANS	287.2	1:20	80	6.8	0.5	28.6	5	40	breezy
SubANS-5	26-May-14	ANS	279.3	0	80	8.4	9.0	28.6	5	40	Overcast
SubANS-6R	02-Dec-14	ANS	335.0	1:200	80	6.1	-2.0	27.7	5	40	light wind
SubANS-7	30-May-14	ANS	276.3	1:100	80	8.5	17.0	29.1	5	40	Clear, calm
SubANS-8R	03-Dec-14	ANS	297.2	1:20	80	7.0	4.5	28.8	5	40	rainy/breezy
SubANS-9	02-Jun-14	ANS	281.4	0	80	9.7	17	29.1	5	40	Clear, calm
SubANS-10R	17-Dec-14	ANS	344.5	1:200	80	5.4	2.0	26.5	5	40	calm
SubANS-11	06-Jun-14	ANS	276.8	1:100	80	10.7	14.0	29.0	5	40	Overcast
SubANS-12R	03-Dec-14	ANS	295.7	1:20	80	7.3	6.5	28.8	5	40	rain
Averages			288.0			8.2	7.8	28.3			

ED_001324_00000687-00004

Table A2. Log sheet for subsurface injection experiments with IFO-120 and Corexit 9500 for cold water temperatures.

Experiment ID	Date	Oil Type	Oil Amount (g)	Dispersant-to-Oil Ratio DOR	Oil Temp. °C	Seawater Temp. °C	Air Temp. °C	Salinity ppt	Oil Injection Time seconds	Injection Pressure psi	Weather Conditions
SubIFO-1R	17-Dec-14	IFO-120	253.6	0	80	4.9	1.0	25.9	10	60	calm
SubIFO-2R	04-Dec-14	IFO-120	208.2	1:200	80	6.7	6.0	28.1	7	60	windy
SubIFO-3	20-Jun-14	IFO-120	213.9	1:100	80	13.2	12.4	27.9	7	62	Partly cloudy, windy
SubIFO-4R	05-Dec-14	IFO-120	219.6	1:20	80	5.6	-3.5	29.3	10	30	sunny calm
SubIFO-5	17-Jun-14	IFO-120	275.1	0	80	12.0	20.0	28.7	7	62	Clear, calm
SubIFO-6R	04-Dec-14	IFO-120	215.6	1:200	80	6.6	5	27.4	8	60	windy
SubIFO-7R	10-Dec-14	IFO-120	239.3	1:100	80	7.5	9.0	28.4	8	60	heavy rain/wind
SubIFO-8R	05-Dec-14	IFO-120	243.3	1:20	80	5.4	-3.5	28.4	10	60	sunny breezy
SubIFO-9	17-Jun-14	IFO-120	359.6	0	80	12.7	20.3	29.0	7	62	Clear, sunny
SubIFO-10R	04-Dec-14	IFO-120	221.7	1:200	80	6.6	4.5	27.2	8	60	windy
SubIFO-11R	17-Dec-14	IFO-120	N/A	1:100	80	4.9	0.5	25.8	10	60	calm
SubIFO-12R	10-Dec-14	IFO-120	204.8	1:20	80	6.8	7.0	29.5	9	60	rain/wind
Averages			241.3			7.7	6.6	28.0			

ED_001324_00000687-00005

Table A3. Log sheet for subsurface injection experiments with ANS and Corexit 9500 for warm water temperatures.

Experiment ID	Date	Oil Type	Oil Amount (g)	Dispersant-to-Oil Ratio DOR	Oil Temp. °C	Seawater Temp. °C	Air Temp. °C	Salinity ppt	Oil Injection Time seconds	Injection Pressure psi	Weather Conditions
SubANS-13	05-Sep-14	ANS	303.7	0	80	17.7	19.0	29.4	5	40	sunny
SubANS-14	08-Sep-14	ANS	295.2	1:200	80	16.0	18.0	29.8	5	40	sunny
SubANS-15R	10-Sep-14	ANS	304.3	1:100	80	13.8	16.5	30.0	5	40	cloudy, calm
SubANS-16	10-Sep-14	ANS	291.9	1:20	80	14.7	19.0	30.0	5	40	partly sunny
SubANS-17	05-Sep-14	ANS	299.6	0	80	18.1	23.5	29.5	5	40	sunny, calm
SubANS-18	08-Sep-14	ANS	297.7	1:200	80	16.2	19.0	29.7	5	40	sunny
SubANS-19	09-Sep-14	ANS	283.4	1:100	80	15.3	18.5	29.9	5	40	sunny, calm
SubANS-20	11-Sep-14	ANS	289.6	1:20	80	14.1	16.0	30.0	5	40	overcast, calm
SubANS-21	08-Sep-14	ANS	297.1	0	80	15.1	14.5	29.8	5	40	sunny
SubANS-22	09-Sep-14	ANS	281.8	1:200	80	14.2	14.0	30.0	5	40	cloudy, calm
SubANS-23	10-Sep-14	ANS	284.4	1:100	80	13.4	16.0	30.1	5	40	partly cloudy
SubANS-24	11-Sep-14	ANS	285.8	1:20	80	13.6	17.5	30.0	5	40	sunny, calm
Average			292.9			15.2	17.6	29.9			

ED_001324_00000687-00006

Table A4. Log sheet for subsurface injection experiments with IFO-120 and Corexit 9500 for warm water temperatures.

Experiment ID	Date	Oil Type	Oil Amount (g)	Dispersant-to-Oil Ratio DOR	Oil Temp. °C	Seawater Temp. °C	Air Temp. °C	Salinity ppt	Oil Injection Time seconds	Injection Pressure psi	Weather Conditions
SubIFO-13	12-Sep-14	IFO-120	256.8	0	80	14.9	18.5	29.9	7	60	Sunny, breezy
SubIFO-14	15-Sep-14	IFO-120	279.0	1:200	80	13.5	14.0	30.0	8	60	Sunny, breezy
SubIFO-15	16-Sep-14	IFO-120	336.2	1:100	80	14.0	12.0	30.0	8	60	sunny, calm
SubIFO-16	17-Sep-14	IFO-120	315.9	1:20	80	14.7	14.0	29.9	7	60	Clear, calm
SubIFO-17	12-Sep-14	IFO-120	293.3	0	80	14.7	20.0	30.0	8	60	sunny, windy
SubIFO-18	15-Sep-14	IFO-120	331.8	1:200	80	13.8	16.5	30.0	8	60	cloudy, breezy
SubIFO-19	16-Sep-14	IFO-120	353.8	1:100	80	14.7	14.0	30.0	7	60	overcast, calm
SubIFO-20	17-Sep-14	IFO-120	345.6	1:20	80	15.2	18.0	29.9	7	60	Sunny, breezy
SubIFO-21	12-Sep-14	IFO-120	303.6	0	80	15.2	20.0	30.0	8	60	sunny, windy
SubIFO-22	15-Sep-14	IFO-120	363.3	1:200	80	14.0	16.5	30.0	8	60	cloudy
SubIFO-23	16-Sep-14	IFO-120	352.6	1:100	80	14.7	16.5	30.0	7	60	overcast, calm
SubIFO-24	17-Sep-14	IFO-120	380.0	1:20	80	16.0	20.0	30.0	7	60	sunny, calm
Average			326.0			14.6	16.7	30.0			

ED_001324_00000687-00007

Table A5. Log sheet for subsurface injection experiments with Gas Condensate and Corexit 9500 for warm water temperatures.

Experiment ID	Date	Oil Type	Oil Amount (g)	Dispersant-to-Oil Ratio DOR	Oil Temp. °C	Seawater Temp. °C	Air Temp. °C	Salinity ppt	Oil Injection Time seconds	Injection Pressure psi	Weather Conditions
SubCND-01	15-Jun-15	Condensate	169.3	None	ambient	10.0	20.5	27.4	4	40psi	Clear, calm
SubCND-02R	17-Jun-15	Condensate	299.8	None	ambient	11.1	17.2	27.8	6	40psi	Windy, partly sunny
SubCND-03	16-Jun-15	Condensate	328.6	None	ambient	10.0	14.5	28.5	6	40psi	Overcast
SubCND-04	16-Jun-15	Condensate	308.9	1:20	ambient	10.8	17.0	28.4	6	40psi	Overcast, breezy
SubCND-05	17-Jun-15	Condensate	308.7	1:20	ambient	11.9	16.5	26.7	6	40psi	Windy
SubCND-06	17-Jun-15	Condensate	301.8	1:20	ambient	11.6	17.0	27.2	6	40psi	Windy, partly sunny
SubCND-07	15-Jun-15	None	-	None	-	10.0	20.5	27.4	5	40psi	Clear, calm
Average			288.4			11.5	18.4	27.5			

ED_001324_00000687-00008

Table A6. Log sheet for subsurface injection experiments with ANS and Finasol OSR 52 for warm water temperatures.

Experiment ID	Date	Oil Type	Oil Amount (g)	Dispersant-to-Oil Ratio DOR	Oil Temp. °C	Seawater Temp. °C	Air Temp. °C	Salinity ppt	Oil Injection Time seconds	Injection Pressure psi	Weather Conditions
SubFIN-01	09-Jul-15	ANS	275.6	1:20	80	16.6	17.5	26.9	5	40psi	Sunny
SubFIN-02	09-Jul-15	ANS	279.7	1:20	80	17.4	23.5	27.2	5	40psi	Sunny
SubFIN-03	17-Jul-15	ANS	268.4	1:20	80	16.8	24.0	28.3	5	40psi	Sunny, breezy
SubFIN-04	13-Jul-15	ANS	251.4	1:100	80	17.0	24.0	27.8	5	40psi	Sunny, calm
SubFIN-05	13-Jul-15	ANS	261.7	1:100	80	18.6	27.5	27.6	5	40psi	Sunny, calm
SubFIN-06	13-Jul-15	ANS	258.0	1:100	80	20.8	30.0	27.5	5	40psi	Sunny, calm
SubFIN-07	15-Jul-15	ANS	283.0	1:200	80	14.2	19.0	28.7	5	40psi	Foggy
SubFIN-08	15-Jul-15	ANS	264.8	1:200	80	17.5	23.5	28.0	5	40psi	Sunny
SubFIN-09	17-Jul-15	ANS	267.9	1:200	80	17.0	22.0	28.0	5	40psi	Sunny
Average			267.8			17.3	23.4	27.8			

ED_001324_00000687-00009

Table A7. Log sheet for subsurface injection experiments with IFO-120 and Finasol OSR 52 for warm water temperatures.

Experiment ID	Date	Oil Type	Oil Amount (g)	Dispersant-to-Oil Ratio DOR	Oil Temp. °C	Seawater Temp. °C	Air Temp. °C	Salinity ppt	Oil Injection Time seconds	Injection Pressure psi	Weather Conditions
SubFIN-10	30-Jul-15	IFO-120	131.6	1:200	80	17.5	15.0	28.0	6	60psi	Light fog
SubFIN-11	30-Jul-15	IFO-120	264.9	1:100	80	18.7		26.2	6	60psi	Sunny, calm
SubFIN-12	30-Jul-15	IFO-120	297.5	1:20	80	20.3	27.5	25.9	6	60psi	Sunny
Average			231.3			18.8	21.3	26.7			

ED_001324_00000687-00010

Table A8. Log sheet for subsurface injection experiments with SLC and Corexit 9500 for warm water temperatures.

Experiment ID	Date	Oil Type	Oil Amount (g)	Dispersant-to-Oil Ratio DOR	Oil Temp. °C	Seawater Temp. °C	Air Temp. °C	Salinity ppt	Oil Injection Time seconds	Injection Pressure psi	Weather Conditions
SubSLC-01	23-Jul-15	MC252	317.3	0	80	16.6	18.0	27.7	6	40psi	Calm, overcast
SubSLC-02	24-Jul-15	MC252	315.2	1:200	80	17.0	19.5	28.1	6	40psi	Sunny, calm
SubSLC-03	27-Jul-15	MC252	317.5	1:100	80	16.9	17.5	28.5	6	40psi	Light rain
SubSLC-04	28-Jul-15	MC252	317.1	1:20	80	17.4	18.5	27.6	6	40psi	Rain
SubSLC-05	23-Jul-15	MC252	322.0	0	80	17.0	24.5	27.8	6	40psi	Sunny, calm
SubSLC-06	24-Jul-15	MC252	319.5	1:200	80	17.1	23.0	28.1	6	40psi	Sunny
SubSLC-07	27-Jul-15	MC252	322.9	1:100	80	17.0	18.5	28.5	6	40psi	Rain
SubSLC-08	28-Jul-15	MC252	318.0	1:20	80	17.8	18.5	27.2	6	40psi	Drizzle, breezy
SubSLC-09	23-Jul-15	MC252	329.4	0	80	17.2	24.5	27.9	6	40psi	Sunny
SubSLC-10	24-Jul-15	MC252	325.2	1:200	80	17.1	23.5	28.4	6	40psi	Overcast
SubSLC-11	27-Jul-15	MC252	330.6	1:100	80	17.0	18.5	28.0	6	40psi	Rain
SubSLC-12	28-Jul-15	MC252	321.1	1:20	80	18.1	21.0	27.3	6	40psi	Windy, drizzle
Average			321.3			17.2	20.5	27.9			

ED_001324_00000687-00011

APPENDIX B – Analytical TPH and BTEX analytical chemistry values for each experiment time point.

Table B1. Total Petroleum Hydrocarbon (TPH) and Benzene-Toluene-Ethylbenzene-Xylene (BTEX) values for subsurface injection experiments of ANS with Corexit 9500 for warm water experiments. TPH method detection limit is < 1 ppm, represented by 0 in top table. Effluent samples are represented with # E in time column.

Time (min)	TPH (ppm) DOR = 0			TPH (ppm) DOR = 1:200			TPH (ppm) DOR = 1:100			TPH (ppm) DOR = 1:20		
	SUBANS13	SUBANS17	SUBANS21	SUBANS14	SUBANS18	SUBANS22	SUBANS15R	SUBANS19	SUBANS23	SUBANS16	SUBANS20	SUBANS24
0	0	0	0	0	1	0	Data missing	0	0	0	0	1
2	37	0	127	72	84	67		32	46	34	8	41
2.5	174	253	359	237	132	128		159	65	72	60	113
3	57	149	60	98	177	97		103	159	82	77	44
3.5	24	35	60	11	17	40		25	31	27	62	49
4	2	8	146	4	2	15		1	5	7	5	13
4.5	0	1	14	1	2	3		0	2	20	1	3
5	0	0	34	0	0	1		0	0	4	0	1
5.5	0	0	36	0	0	0		0	0	1	0	0
6	0	0	7	0	0	0		0	0	0	1	2
6.5	0	0	3	0	0	1		1	0	0	1	0
7	0	0	4	0	0	0		1	0	1	1	0
8	0	0	3	0	0	0		0	0	0	0	0
10	0	0	1	0	0	0		0	0	0	1	0
12	0	0	1	0	0	0		0	0	1	0	0
14	0	0	1	0	0	0		0	0	0	0	0
2 E	0	0	0	0	0	0		0	0	0	0	0
4 E	0	0	0	0	0	0		0	0	0	0	0
6 E	0	0	2	0	0	0		0	0	0	0	0
8 E	7	37	12	19	6	10		15	16	32	18	17
10 E	12	13	5	11	23	13		21	25	19	18	29
12 E	8	5	4	8	18	10		5	10	6	7	5
14 E	3	3	3	4	11	4		2	3	3	3	2

Time (min)	BTEX (ppb) DOR = 0			BTEX (ppb) DOR = 1:200			BTEX (ppb) DOR = 1:100			BTEX (ppb) DOR = 1:20		
	SUBANS13	SUBANS17	SUBANS21	SUBANS14	SUBANS18	SUBANS22	SUBANS15R	SUBANS19	SUBANS23	SUBANS16	SUBANS20	SUBANS24
0	0	0	0	2	3	1	Data missing	0	0	2	0	2
2	0	0	744	106	16	312		16	124	88	0	13
3	161	1333	920	1218	2063	1447		791	1161	1529	1445	636
4	14	248	1883	94	65	346		45	127	140	262	209
5	2	15	514	10	15	21		7	14	72	9	22
6	6	6	317	8	7	5		6	4	15	19	23
7	2	2	102	6	6	4		8	3	7	12	3
8	4	1	92	5	6	3		3	2	4	9	3
10	1	1	59	4	5	2		3	2	4	11	2
12	3	4	39	3	5	2		3	2	4	4	2
14	3	1	31	3	4	2		3	1	4	3	2
6 E	0	0	71	1	1	3		2	0	5	0	1
8 E	37	107	195	255	145	178		331	312	517	408	393
10 E	37	50	122	193	278	349		379	322	232	267	298
12 E	27	77	88	152	232	168		74	163	107	108	76
14 E	75	10	59	87	109	62		32	44	48	49	27

ED_001324_00000687-00012

Table B2. Total Petroleum Hydrocarbon (TPH) and Benzene-Toluene- Ethylbenzene -Xylene (BTEX) values for subsurface injection experiments of ANS with Corexit 9500 for cold water experiments. TPH method detection limit is < 1 ppm, represented by 0 in top table. Effluent samples are represented with # E in time column.

Time (min)	TPH (ppm) DOR = 0			TPH (ppm) DOR = 1:200			TPH (ppm) DOR = 1:100			TPH (ppm) DOR = 1:20		
	SUBANS1	SUBANS5	SUBANS9	SUBANS2R	SUBANS6R	SUBANS10R	SUBANS3	SUBANS7	SUBANS11	SUBANS4R	SUBANS8R	SUBANS12R
0	0	0	0	1	0	0	0	1	0	0	0	1
2	214	17	132	70	109	201	5	189	106	2	25	301
2.5	66	0	48	150	192	110	269	87	88	79	160	114
3	7	0	60	131	83	3	18	18	37	71	46	42
3.5	1	0	4	35	27	5	34	2	7	44	5	29
4	1	0	1	3	10	4	1	1	2	11	6	34
4.5	1	0	0	2	13	2	1	0	0	15	3	10
5	1	0	0	2	4	1	0	0	0	4	3	4
5.5	0	0	0	1	2	1	0	0	0	1	2	1
6	0	0	1	1	1	0	0	0	0	0	5	1
6.5	0	0	0	0	0	1	0	0	0	0	3	1
7	0	0	0	0	0	1	0	0	0	0	1	0
8	0	0	0	0	0	1	0	0	0	0	1	0
10	0	0	0	0	0	1	0	0	0	0	0	0
12	0	0	0	0	0	0	0	0	0	0	0	0
14	0	0	0	0	0	1	0	0	0	0	0	0
2 E	0	0	0	0	0	1	0	0	0	0	0	0
4 E	0	0	0	0	0	1	0	0	0	0	0	0
6 E	0	0	0	0	0	20	0	0	1	0	0	1
8 E	7	8	4	16	19	32	13	4	12	4	4	12
10 E	6	0	4	5	34	8	5	9	11	23	13	23
12 E	6	1	5	7	17	5	10	6	4	12	10	12
14 E	2	1	2	13	4	5	5	1	2	5	14	6

Time (min)	BTEX (ppb) DOR = 0			BTEX (ppb) DOR = 1:200			BTEX (ppb) DOR = 1:100			BTEX (ppb) DOR = 1:20		
	SUBANS1	SUBANS5	SUBANS9	SUBANS2R	SUBANS6R	SUBANS10R	SUBANS3	SUBANS7	SUBANS11	SUBANS4R	SUBANS8R	SUBANS12R
0	1	1	3	0	1	0	1	1	1	0	1	5
2	940	1303	2604	0	638	774	1	2488	1937	19	18	52
3	123	341	1437	1599	1143	274	350	566	1034	1046	470	570
4	5	11	36	109	133	200	52	21	69	163	63	469
5	3	5	13	52	71	18	11	7	13	145	66	72
6	3	4	8	6	16	7	7	6	7	11	100	21
7	2	3	7	3	6	14	4	5	6	8	16	12
8	2	3	7	3	4	8	4	4	5	5	8	7
10	1	3	5	3	3	3	3	3	4	4	3	5
12	1	3	5	2	2	2	4	3	3	2	3	5
14	1	2	5	2	2	3	2	3	3	2	2	4
6 E	no sample	no sample	no sample	0	0	898	no sample	no sample	no sample	5	17	73
8 E	no sample	no sample	no sample	295	348	418	no sample	no sample	no sample	150	121	232
10 E	no sample	no sample	no sample	338	417	185	no sample	no sample	no sample	360	216	336
12 E	no sample	no sample	no sample	170	215	128	no sample	no sample	no sample	205	186	163
14 E	no sample	no sample	no sample	95	no sample	78	no sample	no sample	no sample	78	197	58

ED_001324_00000687-00013

Table B3. Total Petroleum Hydrocarbon (TPH) and Benzene-Toluene- Ethylbenzene -Xylene (BTEX) values for subsurface injection experiments of ANS with Finasol OSR 52 for warm water experiments. TPH method detection limit is < 1 ppm, represented by 0 in top table. Effluent samples are represented with # E in time column.

Time (min)	TPH (ppm) DOR = 1:200			TPH (ppm) DOR = 1:100			TPH (ppm) DOR = 1:20		
	SUBFIN-07	SUBFIN-08	SUBFIN-09	SUBFIN-04	SUBFIN-05	SUBFIN-06	SUBFIN-01	SUBFIN-02	SUBFIN-03
0	0	1	16	7	1	0	0	1	0
2	68	42	13	84	9	24	84	38	17
2.5	147	164	111	214	123	66	113	150	206
3	78	28	106	116	109	67	97	122	197
3.5	35	24	59	113	99	48	22	113	109
4	22	2	5	6	16	26	8	17	6
4.5	4	2	13	15	17	9	9	18	31
5	2	0	4	7	13	6	3	10	18
5.5	0	0	4	4	8	4	1	4	12
6	2	0	1	2	3	3	1	4	4
6.5	0	0	1	2	2	2	1	3	2
7	0	0	0	1	2	0	1	2	1
8	1	0	0	1	2	2	1	2	1
10	0	0	0	2	2	0	1	1	0
12	0	0	0	0	1	1	1	1	1
14	0	0	0	0	1	0	0	1	0
2 E	0	0	0	0	1	0	1	2	0
4 E	0	0	0	1	0	0	1	1	0
6 E	0	0	0	2	1	1	1	1	1
8 E	18	25	15	22	17	24	20	12	21
10 E	23	9	11	20	23	18	21	19	16
12 E	6	5	6	6	10	6	7	13	11
14 E	2	2	4	3	3	4	3	5	5

Time (min)	BTEX (ppb) DOR = 1:200			BTEX (ppb) DOR = 1:100			BTEX (ppb) DOR = 1:20		
	SUBFIN-07	SUBFIN-08	SUBFIN-09	SUBFIN-04	SUBFIN-05	SUBFIN-06	SUBFIN-01	SUBFIN-02	SUBFIN-03
0	0	1	0	0	2	1	1	6	2
2	81	187	0	28	1	1	0	28	1
3	894	908	1056	1063	766	535	585	1203	1937
4	467	238	304	527	337	305	439	530	589
5	201	45	36	144	224	78	95	143	184
6	11	13	21	37	50	22	24	47	59
7	16	10	15	16	17	10	9	16	19
8	9	8	8	8	9	6	4	8	12
10	6	6	5	1	6	4	3	5	8
12	3	5	4	3	5	3	2	4	5
14	4	5	2	5	3	2	2	3	5
6 E	0	3	0	0	0	0	0	0	1
8 E	390	444	287	464	312	413	380	229	287
10 E	385	192	253	331	373	308	365	327	261
12 E	119	123	132	105	148	129	115	183	188
14 E	58	66	68	51	51	65	52	68	87

ED_001324_00000687-00014

Table B4. Total Petroleum Hydrocarbon (TPH) and Benzene-Toluene- Ethylbenzene -Xylene (BTEX) values for subsurface injection experiments of IFO 120 with Corexit 9500 for warm water experiments. TPH method detection limit is < 1 ppm, represented by 0 in top table. Effluent samples are represented with # E in time column.

Time (min)	TPH (ppm) DOR = 0			TPH (ppm) DOR = 1:200			TPH (ppm) DOR = 1:100			TPH (ppm) DOR = 1:20		
	SUBIFO13	SUBIFO17	SUBIFO21	SUBIFO14	SUBIFO18	SUBIFO22	SUBIFO15	SUBIFO19	SUBIFO23	SUBIFO16	SUBIFO20	SUBIFO24
0	6	4	0	0	0	0	3	2	1	0	0	1
2	16	69	151	87	20	108	187	162	202	27	159	103
2.5	56	155	117	87	55	113	81	414	344	129	171	127
3	35	43	32	14	16	411	58	30	101	110	4	107
3.5	31	9	16	10	11	8	6	1	4	45	1	4
4	4	8	2	4	18	5	2	0	1	15	1	2
4.5	3	3	0	2	10	5	8	1	0	4	0	0
5	8	4	1	2	5	0	1	1	0	2	1	1
5.5	4	7	0	4	5	0	1	0	0	0	0	0
6	5	2	0	2	2	0	1	0	1	1	1	1
6.5	0	1	1	2	1	0	1	1	0	0	0	0
7	0	2	1	2	0	0	1	1	0	1	0	0
8	0	2	1	1	0	0	0	0	1	0	0	0
10	0	1	0	1	0	0	1	0	0	0	0	0
12	0	1	1	1	0	0	0	0	0	0	1	0
14	0	0	1	0	0	0	0	0	1	0	0	1
2 E	0	0	0	1	0	0	0	0	0	0	0	0
4 E	0	0	0	0	lost	0	0	0	0	0	0	0
6 E	0	0	0	0	0	0	0	1	0	0	0	0
8 E	3	15	9	4	2	13	3	17	15	2	40	51
10 E	5	39	21	5	13	22	10	15	46	13	25	31
12 E	2	15	4	6	8	7	7	5	14	30	7	7
14 E	1	4	2	1	3	2	2	3	3	1	3	4

Time (min)	BTEX (ppb) DOR = 0			BTEX (ppb) DOR = 1:200			BTEX (ppb) DOR = 1:100			BTEX (ppb) DOR = 1:20		
	SUBIFO13	SUBIFO17	SUBIFO21	SUBIFO14	SUBIFO18	SUBIFO22	SUBIFO15	SUBIFO19	SUBIFO23	SUBIFO16	SUBIFO20	SUBIFO24
0	0	0	3	0	0	2	0	1	1	0	2	2
2	11	9	68	98	0	138	166	6	89	4	123	15
3	40	111	42	40	32	75	144	102	277	64	22	163
4	5	37	1	3	26	5	3	2	4	5	1	5
5	1	1	1	8	9	1	0	2	2	0	1	2
6	1	1	1	3	1	1	0	2	2	0	1	2
7	0	0	1	3	1	1	0	1	2	0	1	2
8	0	0	1	0	1	1	0	1	2	0	1	2
10	0	0	1	0	1	1	0	2	2	0	1	2
12	1	0	1	0	1	1	0	1	2	0	1	2
14	0	0	1	0	1	1	0	1	2	0	1	2
6 E	0	0	1	0	1	1	0	17	1	0	1	2
8 E	8	5	20	8	7	31	11	28	40	20	62	69
10 E	7	18	27	10	27	32	19	16	33	51	25	36
12 E	2	6	8	4	11	11	10	11	19	11	8	15
14 E	0	1	1	1	6	4	2	4	6	3	5	7

ED_001324_00000687-00015

Table B5. Total Petroleum Hydrocarbon (TPH) and Benzene-Toluene- Ethylbenzene -Xylene (BTEX) values for subsurface injection experiments of IFO 120 with Corexit 9500 for cold water experiments. TPH method detection limit is < 1 ppm, represented by 0 in top table. Effluent samples are represented with # E in time column.

Time (min)	TPH (ppm) DOR = 0			TPH (ppm) DOR = 1:200			TPH (ppm) DOR = 1:100			TPH (ppm) DOR = 1:20		
	SUBIFO1R	SUBIFO5	SUBIFO9	SUBIFO2R	SUBIFO6R	SUBIFO10R	SUBIFO3	SUBIFO7R	SUBIFO11R	SUBIFO4R	SUBIFO8R	SUBIFO12R
0	0	0	2	1	2	1	5	0	1	1	0	1
2	111	118	210	30	12	1	110	1	36	7	2	28
2.5	50	165	55	15	14	30	135	28	29	11	107	69
3	3	32	7	4	1	35	10	19	2	2	81	39
3.5	3	2	1	1	2	11	3	5	1	6	36	10
4	1	1	1	1	1	2	1	5	1	4	2	2
4.5	1	1	1	1	0	1	1	10	1	2	2	2
5	1	1	1	0	1	1	1	7	1	1	2	1
5.5	1	0	1	0	0	1	1	4	0	1	1	1
6	0	0	1	0	0	0	1	3	1	1	1	1
6.5	1	0	1	1	0	0	1	3	0	2	1	0
7	1	0	2	1	0	1	1	4	1	1	1	1
8	1	0	1	0	0	0	1	1	1	1	1	0
10	1	0	1	1	0	1	1	1	1	0	1	1
12	0	1	1	0	1	0	1	1	1	1	1	1
14	1	1	1	1	0	0	1	1	0	1	1	0
2 E	0	0	0	0	0	1	0	0	1	0	0	0
4 E	0	0	0	0	1	1	1	1	1	0	1	1
6 E	2	0	0	1	1	1	1	1	0	0	1	0
8 E	4	4	13	0	2	0	2	0	2	5	2	1
10 E	1	6	15	1	3	3	5	2	1	2	10	9
12 E	1	5	5	1	1	1	2	2	1	2	7	4
14 E	0	2	3	0	1	1	1	2	1	1	1	2

	BTEX (ppb) DOR = 0			BTEX (ppb) DOR = 1:200			BTEX (ppb) DOR = 1:100			BTEX (ppb) DOR = 1:20		
Time (min)	SUBIFO1R	SUBIFO5	SUBIFO9	SUBIFO2R	SUBIFO6R	SUBIFO10R	SUBIFO3	SUBIFO7R	SUBIFO11R	SUBIFO4R	SUBIFO8R	SUBIFO12R
0	1	0	0	0	0	1	0	0	0	0	2	0
2	3	73	277	20	30	1	22	1	7	0	225	7
3	6	53	10	1	1	32	20	25	4	4	164	94
4	1	1	1	0	0	2	1	4	0	5	14	3
5	1	0	1	0	0	2	0	15	0	0	4	1
6	1	1	1	0	0	2	0	2	0	0	2	0
7	1	1	0	0	0	2	0	8	0	0	2	0
8	1	1	0	0	0	2	0	1	0	0	2	0
10	1	0	0	0	0	2	0	1	0	0	2	0
12	1	0	0	0	0	2	0	0	0	0	2	0
14	1	0	0	0	0	2	0	0	0	0	2	0
6 E	14	no sample	no sample	0	0	1	no sample	0	0	0	2	0
8 E	5	no sample	no sample	1	4	1	no sample	1	5	5	8	1
10 E	1	no sample	no sample	2	1	5	no sample	3	1	2	27	16
12 E	1	no sample	no sample	1	0	2	no sample	6	0	1	11	6
14 E	1	no sample	no sample	0	0	2	no sample	4	0	1	3	0

ED_001324_00000687-00016

Table B6. Total Petroleum Hydrocarbon (TPH) and Benzene-Toluene- Ethylbenzene -Xylene (BTEX) values for subsurface injection experiments of IFO 120 with Finasol OSR 52 for warm water experiments. TPH method detection limit is < 1 ppm, represented by 0 in top table. Effluent samples are represented with # E in time column.

Time (min)	TPH (ppm) DOR = 1:200 SUBFIN-10	TPH (ppm) DOR = 1:100 SUBFIN-11	TPH (ppm) DOR = 1:20 SUBFIN-12
0	1	2	0
2	45	55	3
2.5	14	170	181
3	10	14	117
3.5	3	19	46
4	2	4	9
4.5	2	3	2
5	1	3	3
5.5	0	2	2
6	2	1	2
6.5	1	2	2
7	1	1	0
8	1	2	1
10	1	2	0
12	1	0	0
14	1	0	1
2 E	1	2	2
4 E	1	1	1
6 E	0	0	0
8 E	1	8	11
10 E	0	5	28
12 E	0	3	9
14 E	0	2	4

Time (min)	BTEX (ppb) DOR = 1:200 SUBFIN-10	BTEX (ppb) DOR = 1:100 SUBFIN-11	BTEX (ppb) DOR = 1:20 SUBFIN-12
0	0	1	0
2	17	22	10
3	24	59	180
4	1	11	6
5	1	2	1
6	0	1	1
7	0	1	1
8	0	1	0
10	0	1	0
12	0	1	0
14	0	1	0
6 E	0	1	0
8 E	3	20	46
10 E	4	9	53
12 E	1	4	16
14 E	0	2	8

ED_001324_00000687-00017

Table B7. Total Petroleum Hydrocarbon (TPH) and Benzene-Toluene- Ethylbenzene -Xylene (BTEX) values for subsurface injection experiments of SLC with Corexit 9500 for warm water experiments. TPH method detection limit is < 1 ppm, represented by 0 in top table. Effluent samples are represented with # E in time column.

Time (min)	TPH (ppm) DOR = 0			TPH (ppm) DOR = 1:200			TPH (ppm) DOR = 1:100			TPH (ppm) DOR = 1:20		
	SUBSLC-01	SUBSLC-05	SUBSLC-09	SUBSLC-02	SUBSLC-06	SUBSLC-10	SUBSLC-03	SUBSLC-07	SUBSLC-11	SUBSLC-04	SUBSLC-08	SUBSLC-12
0	1	3	2	3	0	1	0	0	2	2	3	1
2	48	13	100	6	3	4	8	26	11	2	4	1
2.5	156	140	130	130	110	195	262	119	171	22	56	32
3	105	120	106	75	29	111	164	100	60	120	130	131
3.5	52	109	104	87	20	38	122	45	22	85	93	115
4	48	111	40	45	28	8	30	16	8	69	55	42
4.5	9	29	39	56	10	4	13	7	6	57	23	18
5	2	10	22	17	9	3	3	4	13	28	12	9
5.5	4	3	10	14	4	2	3	2	6	10	6	4
6	3	3	3	7	3	2	1	3	7	6	3	2
6.5	2	3	4	3	0	1	1	2	4	3	2	2
7	1	0	4	3	2	2	2	2	2	2	2	2
8	1	1	2	3	0	1	2	2	1	3	2	1
10	1	1	2	3	0	1	1	1	2	2	1	1
12	1	0	1	1	0	1	1	0	1	2	1	1
14	0	0	2	3	2	1	1	1	1	2	1	1
2 E	2	1	1	1	0	1	0	0	1	2	1	1
4 E	2	2	1	2	0	1	1	0	1	2	1	1
6 E	1	1	1	1	0	1	1	0	1	2	1	2
8 E	13	12	11	16	12	14	4	5	7	8	11	17
10 E	11	9	5	10	7	12	13	17	17	12	13	17
12 E	10	12	8	11	10	7	9	9	12	15	11	13
14 E	8	5	6	9	4	2	7	4	6	9	7	6

	BTEX (ppb) DOR = 0			BTEX (ppb) DOR = 1:200			BTEX (ppb) DOR = 1:100			BTEX (ppb) DOR = 1:20		
Time (min)	SUBSLC-01	SUBSLC-05	SUBSLC-09	SUBSLC-02	SUBSLC-06	SUBSLC-10	SUBSLC-03	SUBSLC-07	SUBSLC-11	SUBSLC-04	SUBSLC-08	SUBSLC-12
0	2	6	3	1	2	2	1	1	4	0	1	8
2	141	1	523	0	2	12	54	359	6	0	1	3
3	1082	1268	1161	1046	578	1794	2058	1518	590	2455	1038	708
4	316	1507	721	664	457	464	923	668	77	1128	494	890
5	58	74	548	380	317	87	124	91	152	118	110	65
6	17	59	44	199	129	23	60	40	136	34	42	35
7	17	24	31	49	32	14	25	14	55	17	20	16
8	10	19	21	28	15	8	21	9	15	7	9	10
10	8	13	15	9	7	7	7	6	19	6	8	8
12	6	12	13	6	6	6	6	4	0	4	5	7
14	6	12	11	5	6	5	4	4	5	3	5	6
6 E	0	0	0	0	1	0	6	0	1	0	5	1
8 E	337	335	212	252	396	344	140	249	224	371	337	220
10 E	263	371	174	240	199	323	265	444	394	6	392	197
12 E	207	296	276	211	335	190	210	225	264	371	258	343
14 E	136	130	185	184	113	64	162	110	147	136	146	222

ED_001324_00000687-00018

Table B8. Total Petroleum Hydrocarbon (TPH) and Benzene-Toluene- Ethylbenzene -Xylene (BTEX) values for subsurface injection experiments of Gas Condensate with Corexit 9500 for warm water experiments. TPH method detection limit is < 1 ppm, represented by 0 in top table. Effluent samples are represented with # E in time column.

Time (min)	TPH (ppm) DOR = 0			TPH (ppm) DOR = 1:20		
	SUBCND-01	SUBCND-02R	SUBCND-03	SUBCND-04	SUBCND-05	SUBCND-06
0	0	0	0	0	0	0
2	4	41	29	76	50	25
2.5	4	12	12	32	102	42
3	2	1	3	17	35	5
3.5	0	2	0	9	2	26
4	0	2	0	2	3	2
4.5	0	1	0	4	5	0
5	0	1	0	0	4	0
5.5	0	1	0	1	9	0
6	0	0	0	0	7	0
6.5	0	1	0	0	2	0
7	0	0	0	0	0	0
8	0	0	0	0	3	0
10	0	0	0	0	2	1
12	0	1	0	0	2	0
14	0	0	0	0	1	0
2 E	0	0	0	0	0	0
4 E	0	0	0	0	1	0
6 E	0	0	0	0	0	0
8 E	1	1	2	5	3	4
10 E	0	1	1	9	3	5
12 E	0	1	0	8	4	7
14 E	0	1	0	3	5	3

Time (min)	BTEX (ppb) DOR = 0			BTEX (ppb) DOR = 1:20		
	SUBCND-01	SUBCND-02R	SUBCND-03	SUBCND-04	SUBCND-05	SUBCND-06
0	1	4	4	5	1	13
2	998	2326	4041	6345	4418	1298
3	706	186	772	3665	2618	1261
4	41	741	72	323	1104	532
5	19	28	36	46	1195	252
6	18	99	25	28	962	35
7	15	27	22	18	355	40
8	11	29	17	15	863	26
10	11	29	12	11	186	27
12	6	18	15	9	269	24
14	6	12	7	7	371	17
6 E	1	3	324	336	61	8
8 E	322	228	579	834	462	683
10 E	282	174	205	1393	553	853
12 E	90	135	86	1012	633	848
14 E	43	84	34	459	636	520

ED_001324_00000687-00019

APPENDIX C – Jet Release LISST Oil Droplet Size Distribution Histograms*

**Note that LISST histogram plots have constrained Y-axes, thus lines which extend slightly above the top of the plot area represent values which were truncated.*

ED_001324_00000687-00020

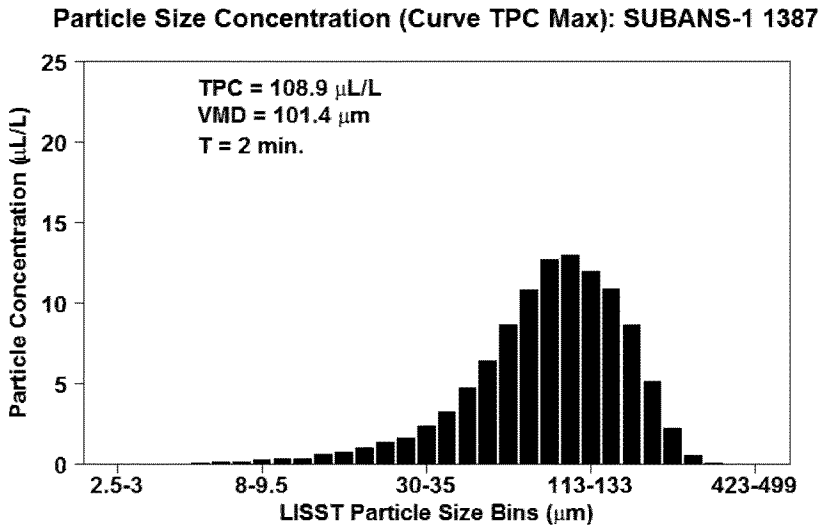

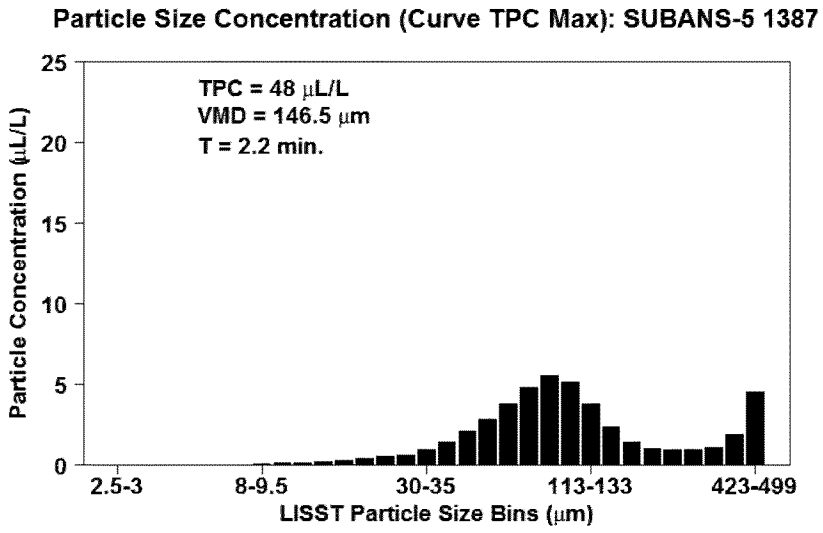

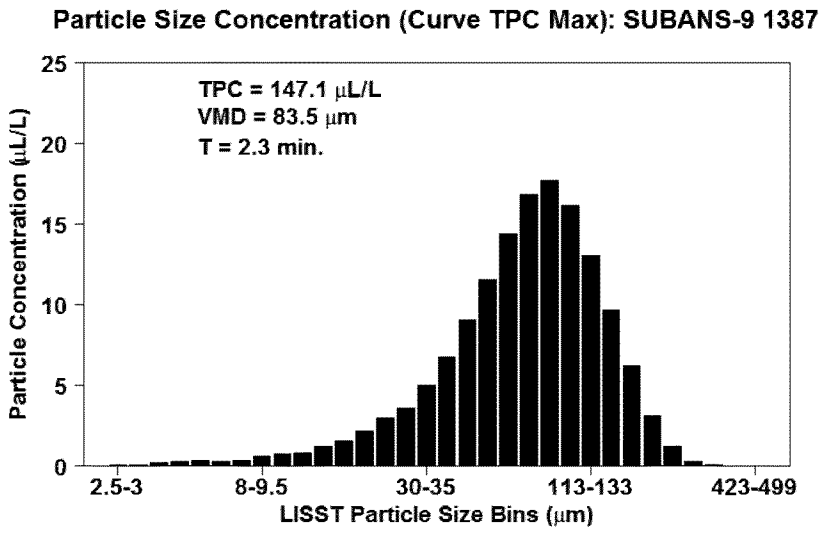

Appendix C - Figure C1. LISST DSD plot for ANS, no dispersant, cold water experiments.

ED_001324_00000687-00021

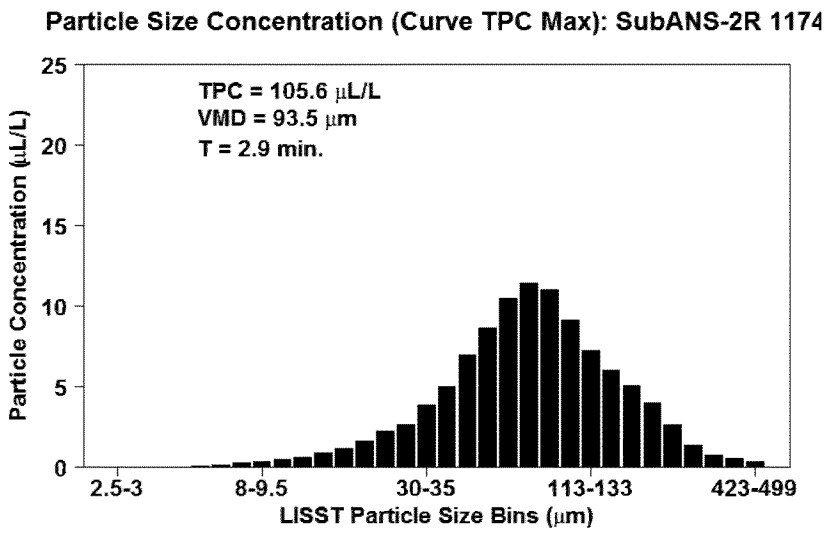

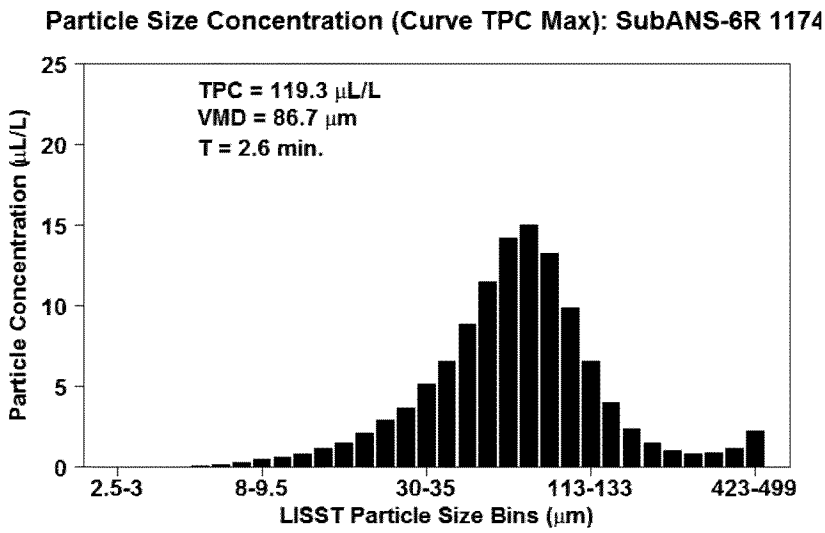

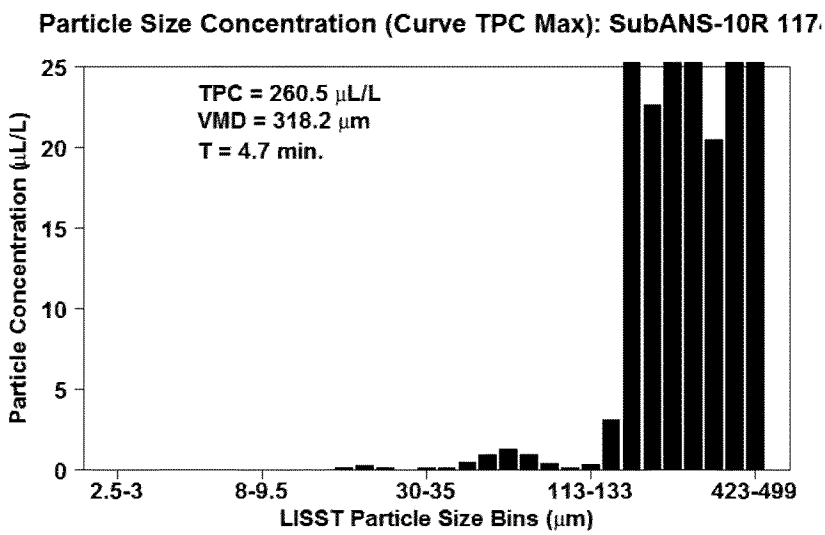

Appendix C - Figure C2. LISST DSD plot for ANS, DOR 1:200 (Corexit 9500), cold water experiments.

ED_001324_00000687-00022

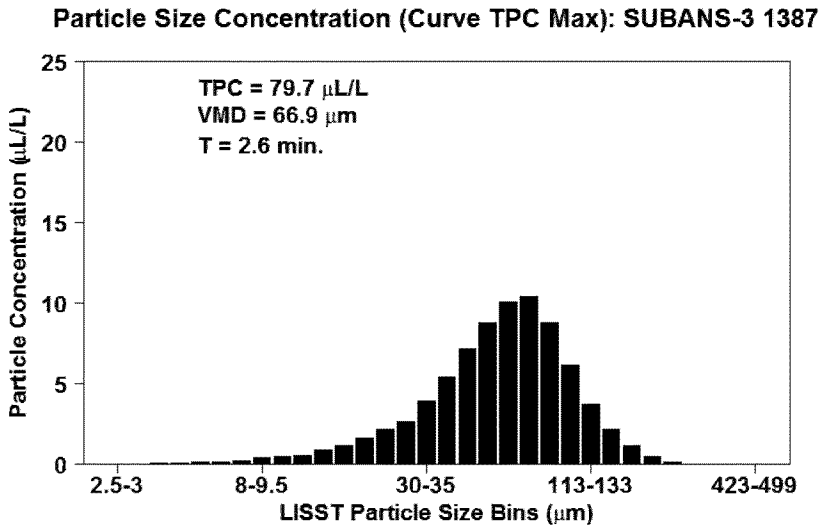

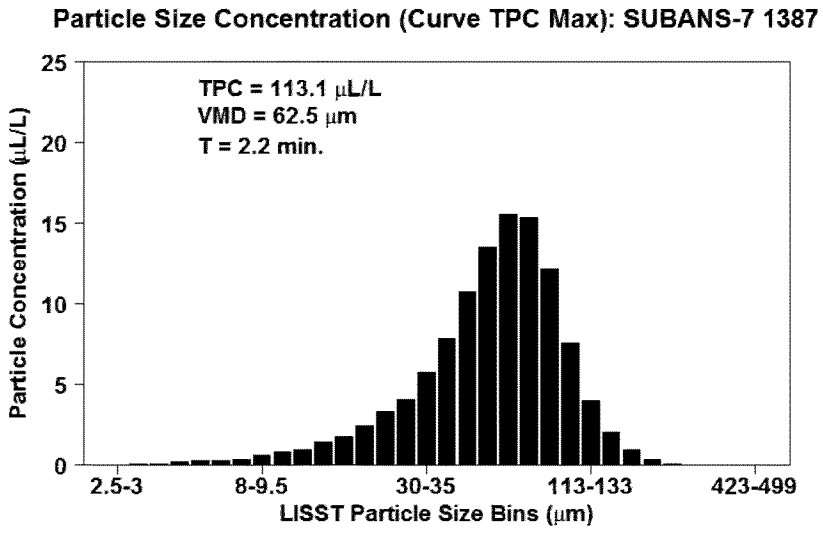

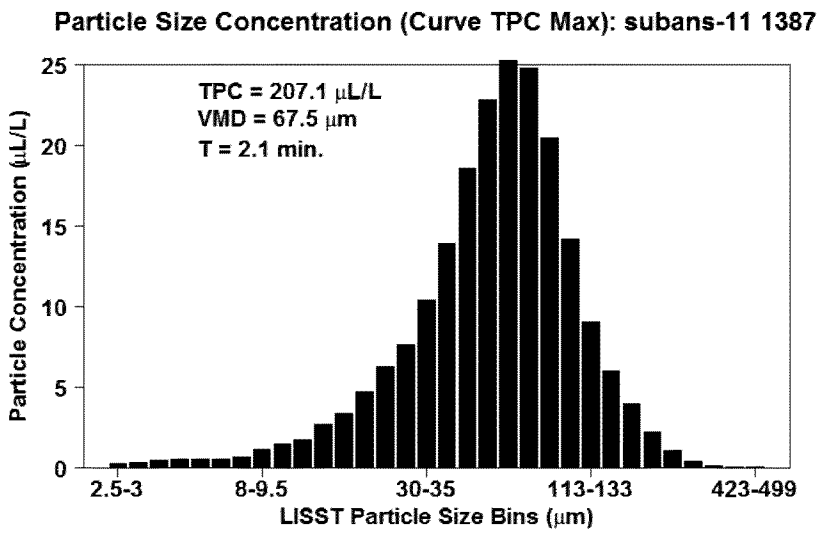

Appendix C - FigureC3. LISST DSD plot for ANS, DOR 1:100 (Corexit 9500), cold water experiments.

ED_001324_00000687-00023

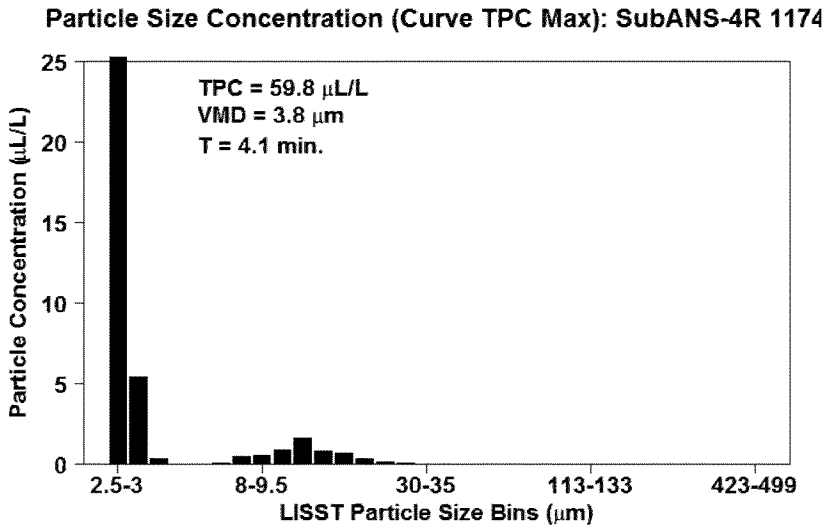

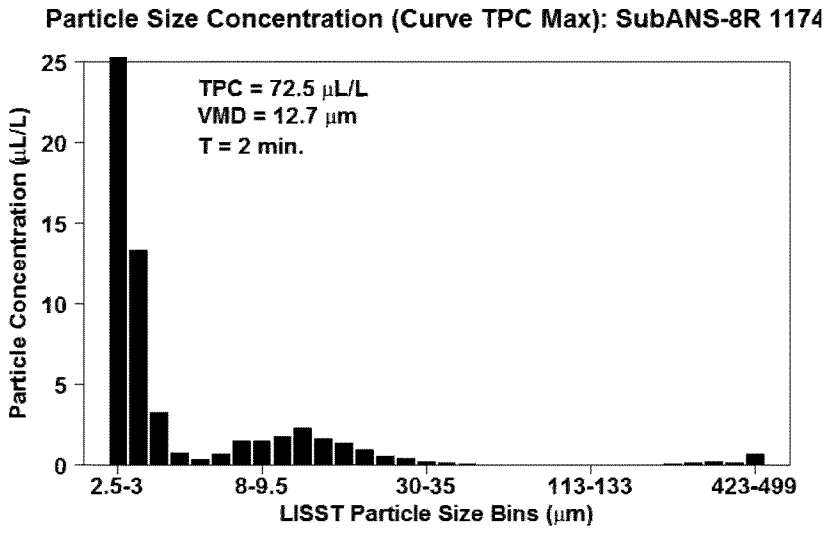

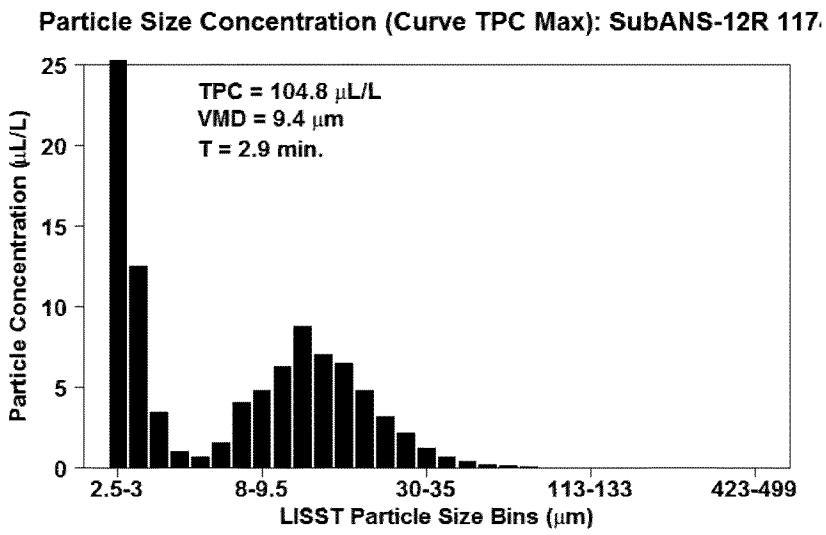

Appendix C - Figure C4. LISST DSD plot for ANS, DOR 1:20 (Corexit 9500), cold water experiments.

ED_001324_00000687-00024

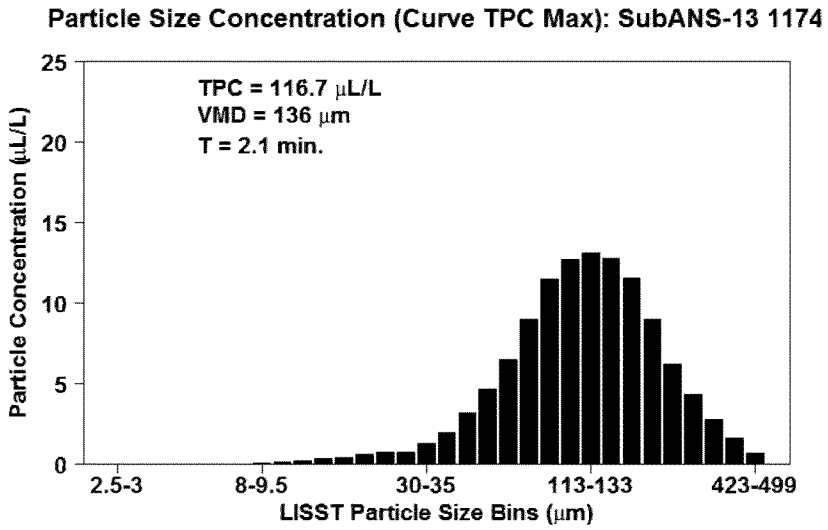

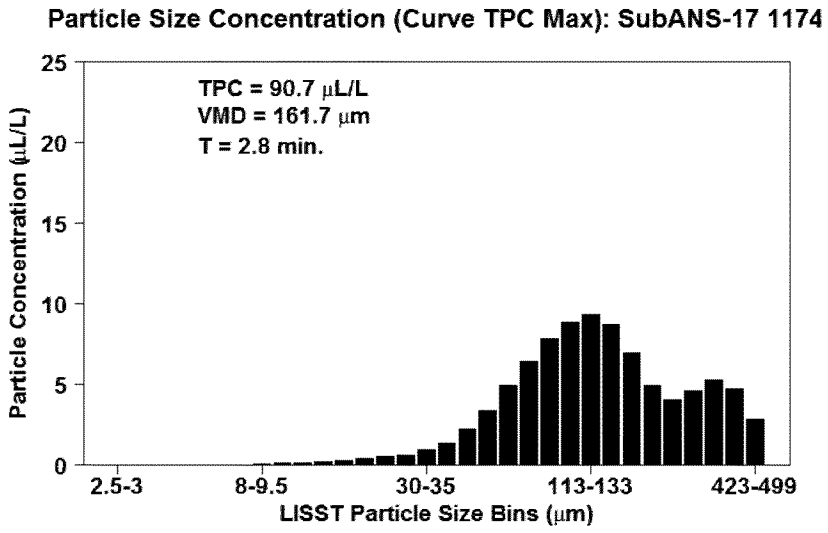

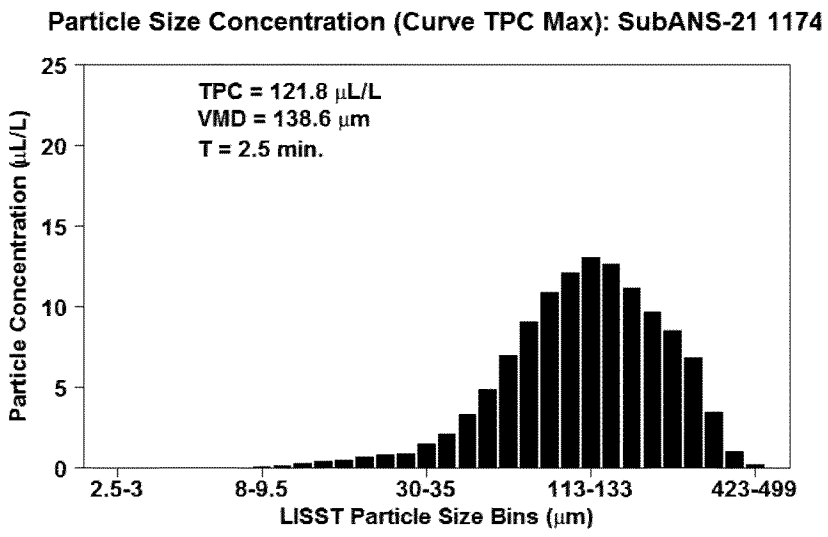

Appendix C - Figure C5. LISST DSD plot for ANS, DOR 0 (Corexit 9500), warm water experiments.

ED_001324_00000687-00025

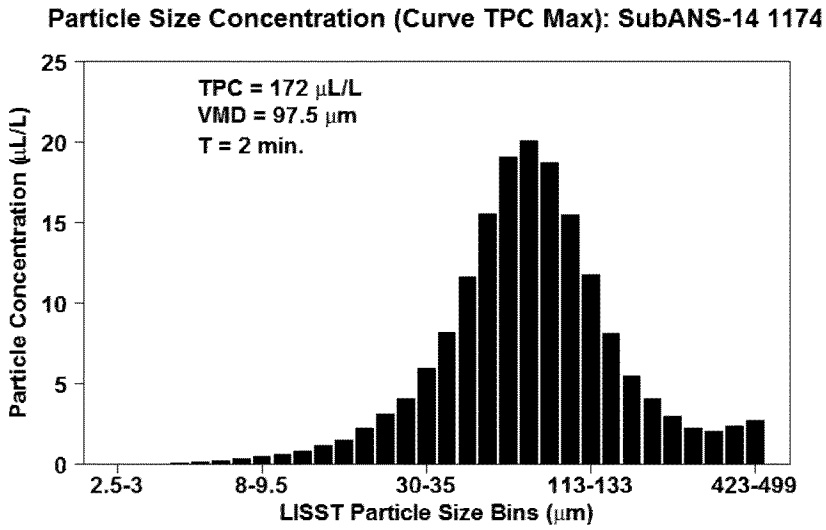

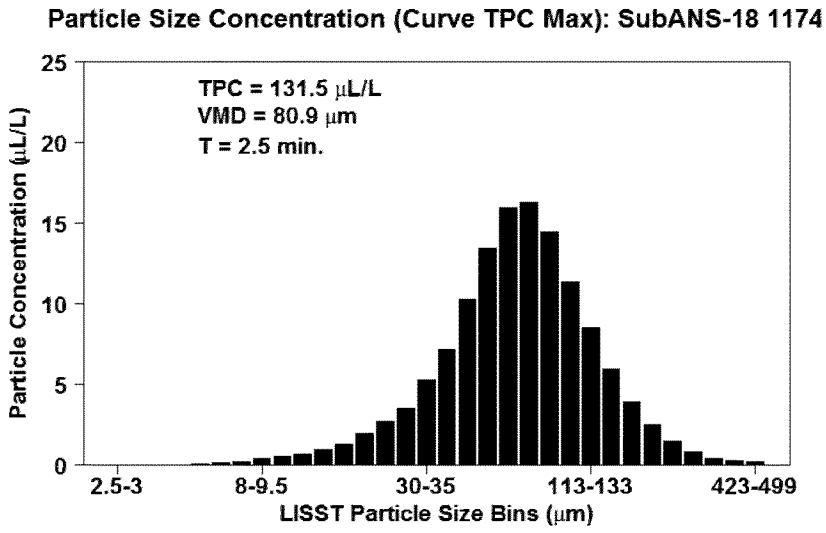

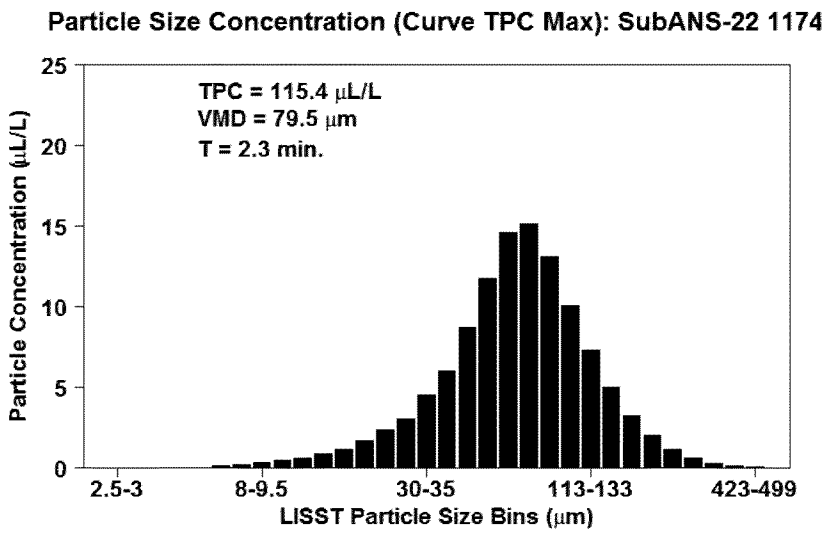

Appendix C - Figure C6. LISST DSD plot for ANS, DOR 1:200 (Corexit 9500), warm water experiments.

ED_001324_00000687-00026

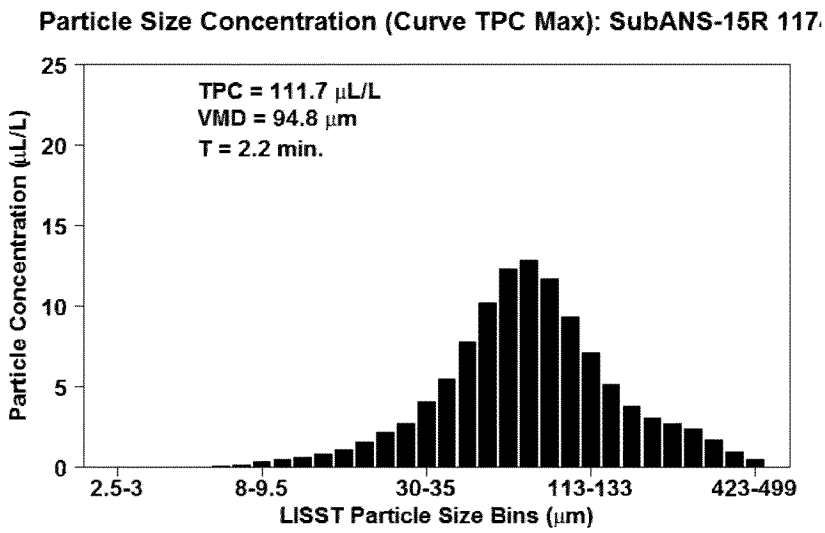

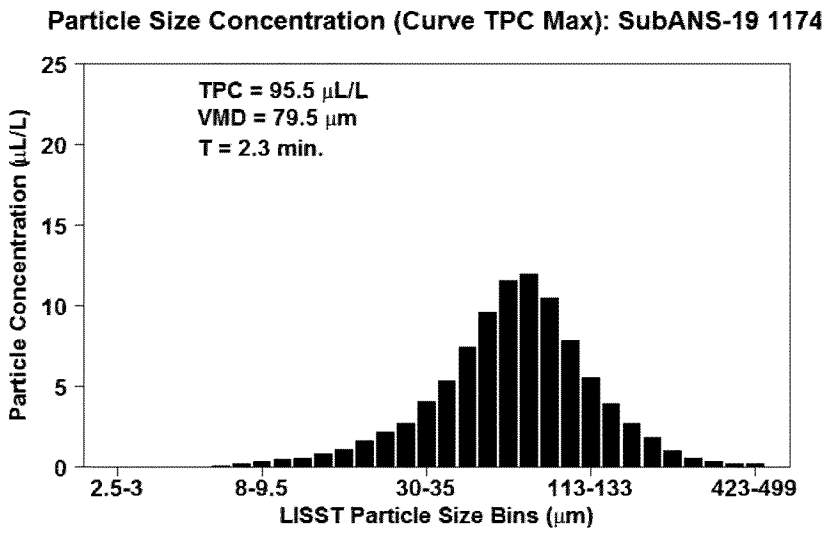

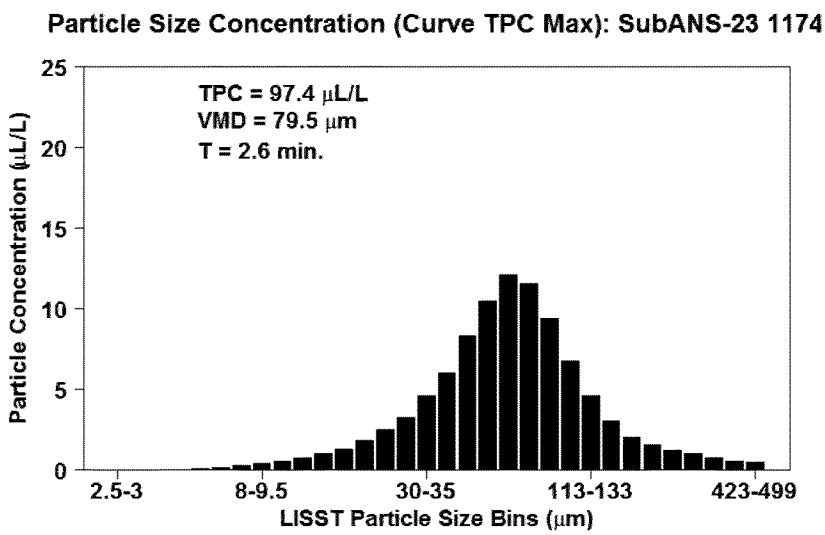

Appendix C - Figure C7. LISST DSD plot for ANS, DOR 1:100 (Corexit 9500), warm water experiments.

ED_001324_00000687-00027

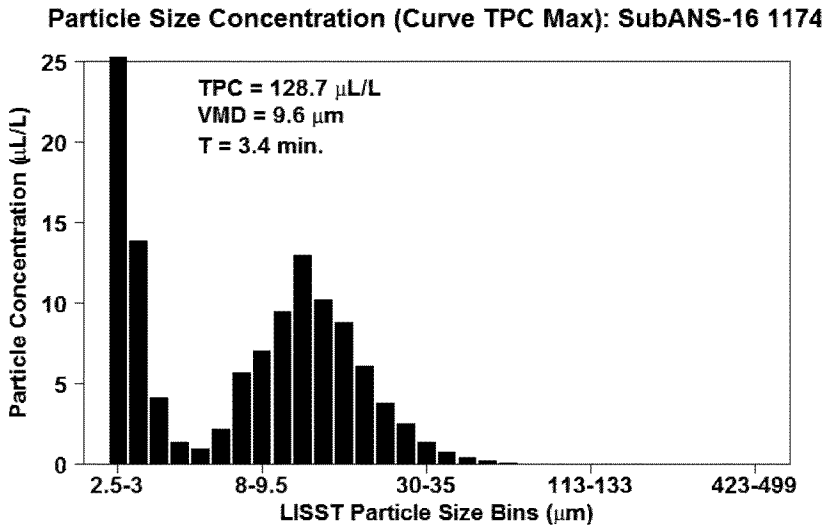

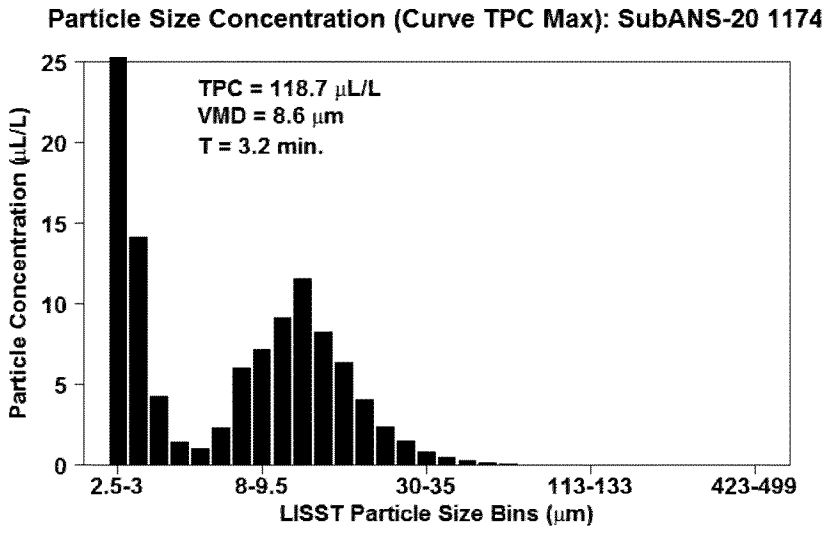

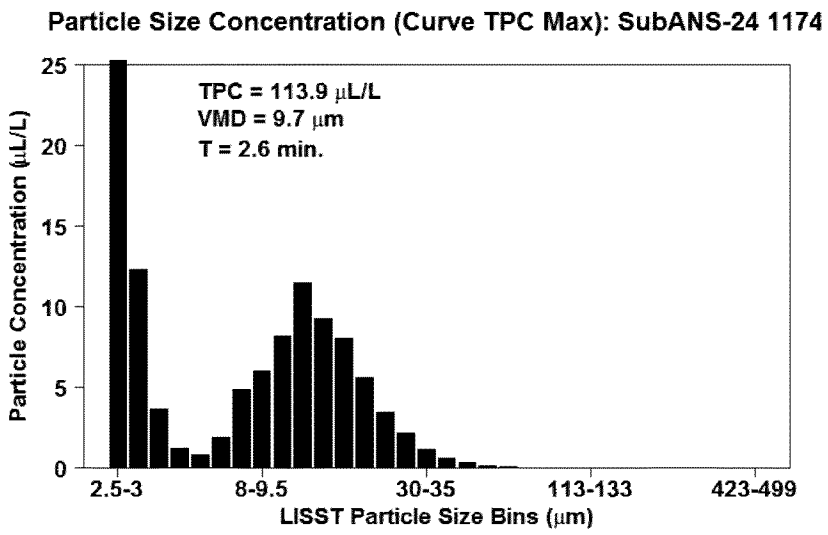

Appendix C - Figure C8. LISST DSD plot for ANS, DOR 1:20 (Corexit 9500), warm water experiments.

ED_001324_00000687-00028

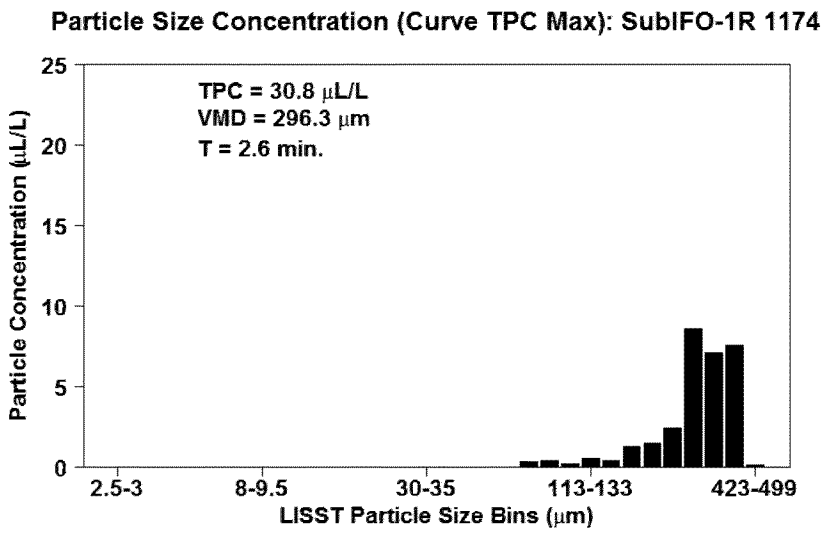

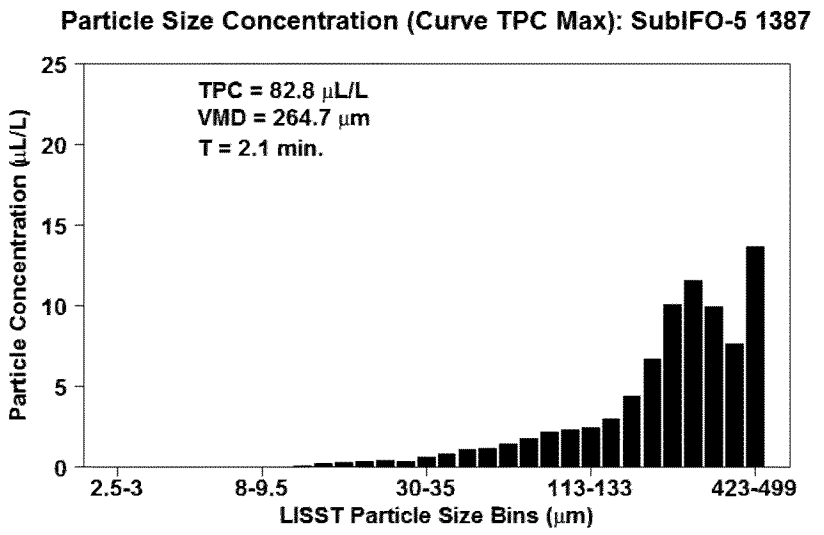

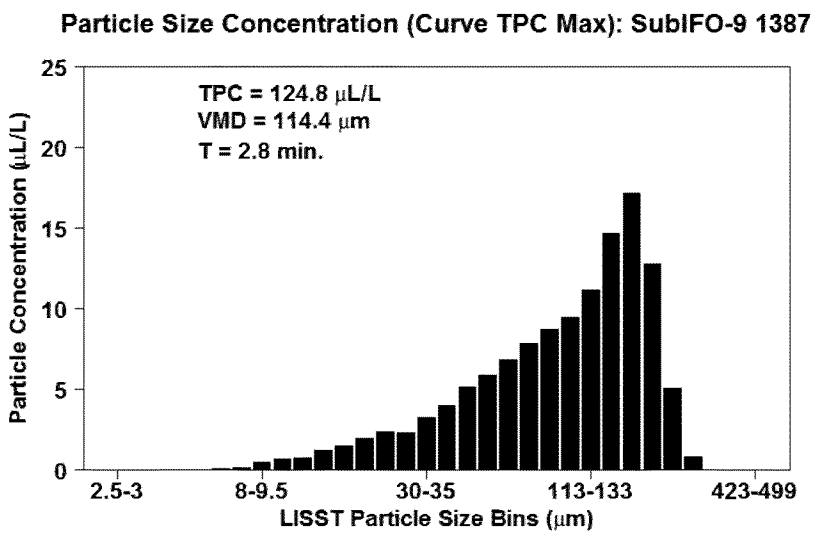

Appendix C - Figure C9. LISST DSD plot for IFO-120, no dispersant, cold water experiments.

ED_001324_00000687-00029

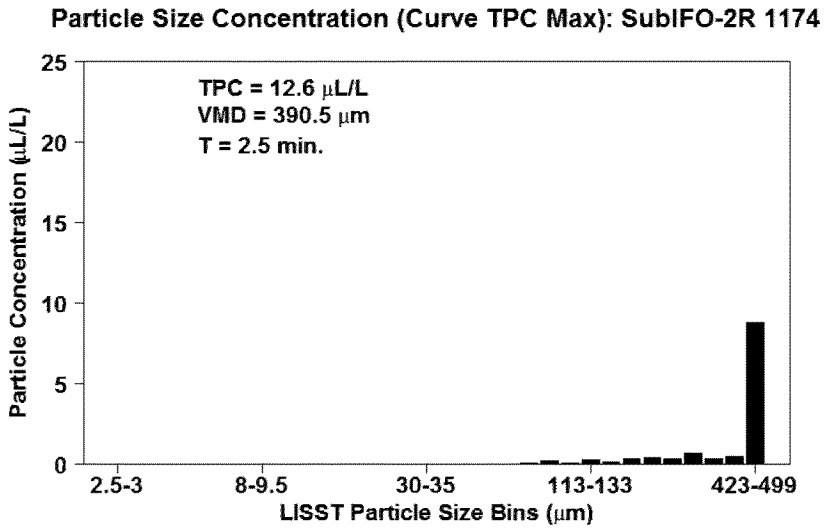

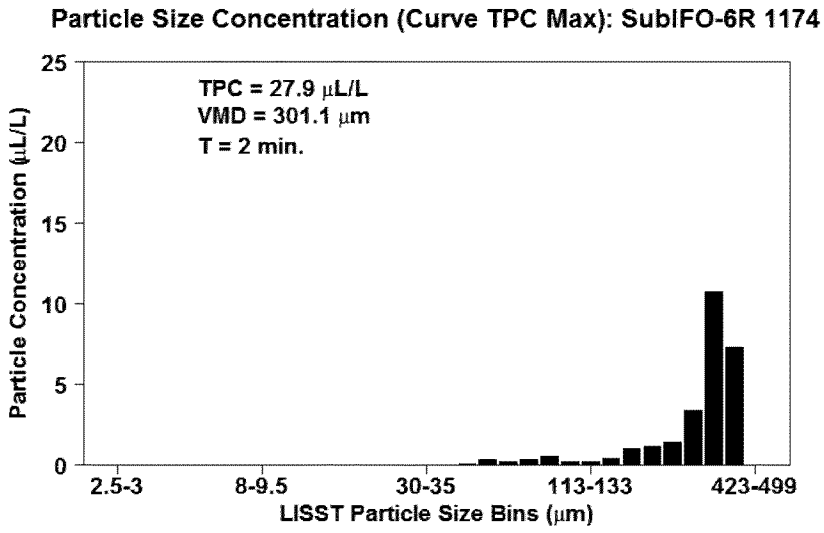

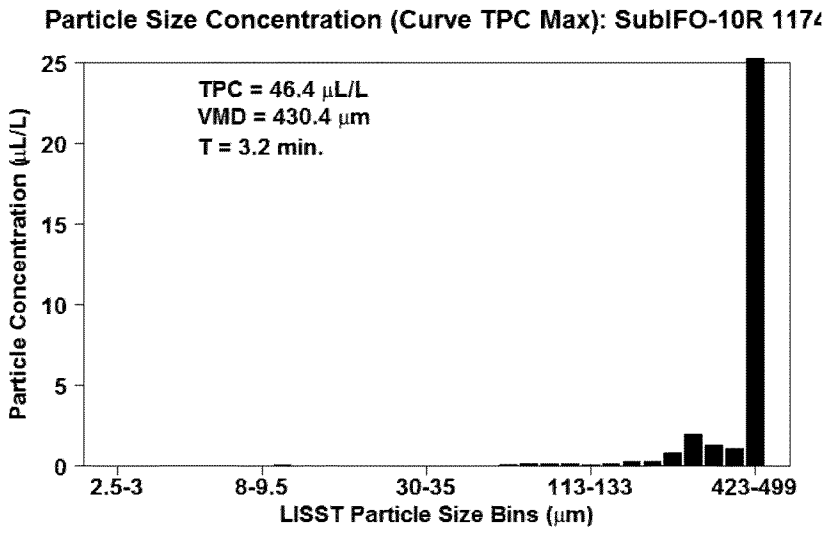

Appendix C - Figure C10. LISST DSD plot for IFO-120, DOR 1:200 (Corexit 9500), cold experiments.

ED_001324_00000687-00030

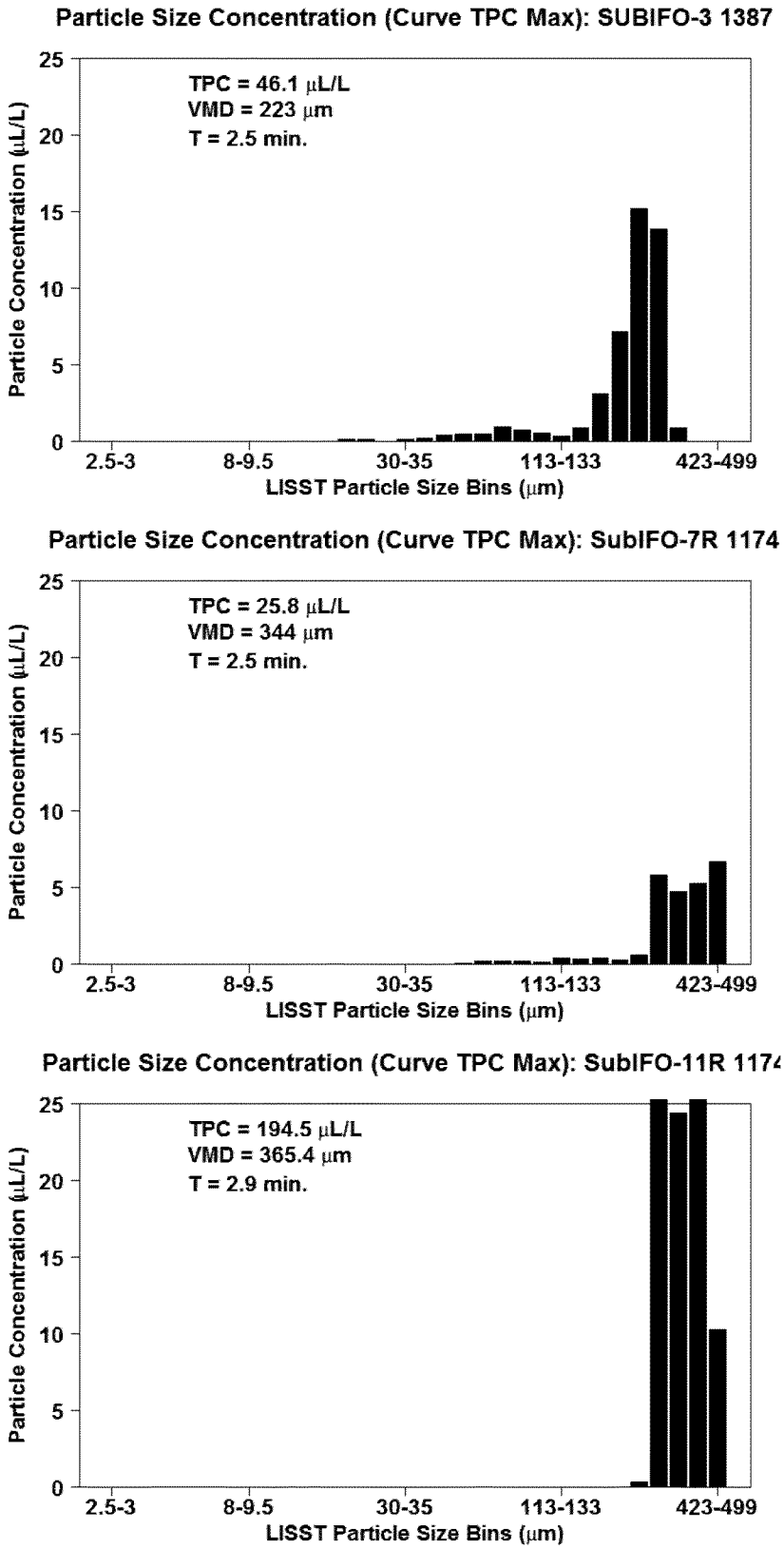

Appendix C - Figure C11. LISST DSD plot for IFO-120, DOR 1:100 (Corexit 9500), cold experiments.

ED_001324_00000687-00031

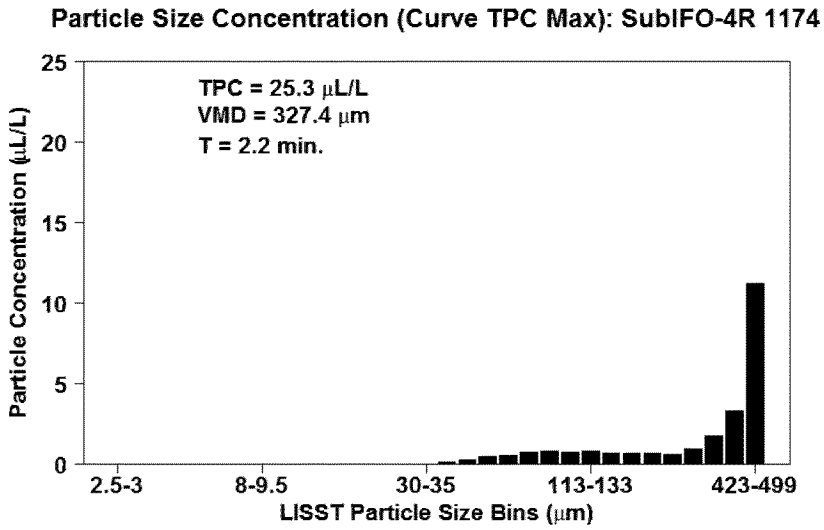

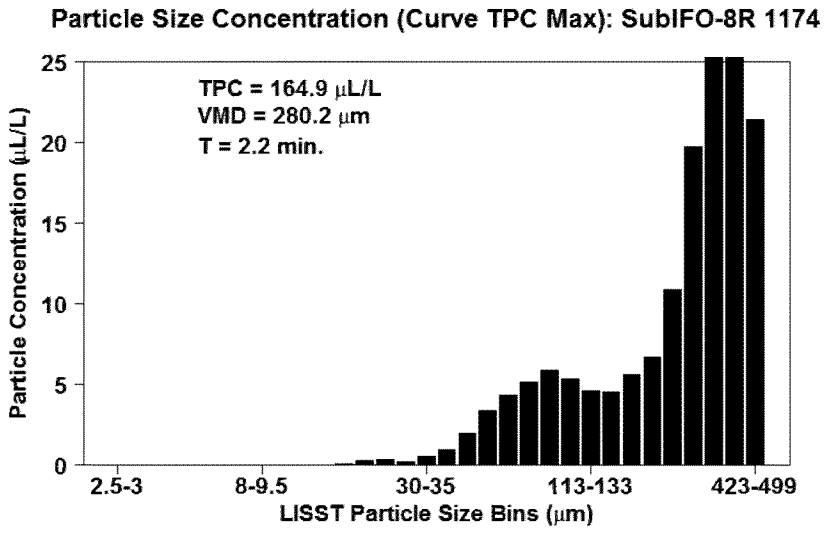

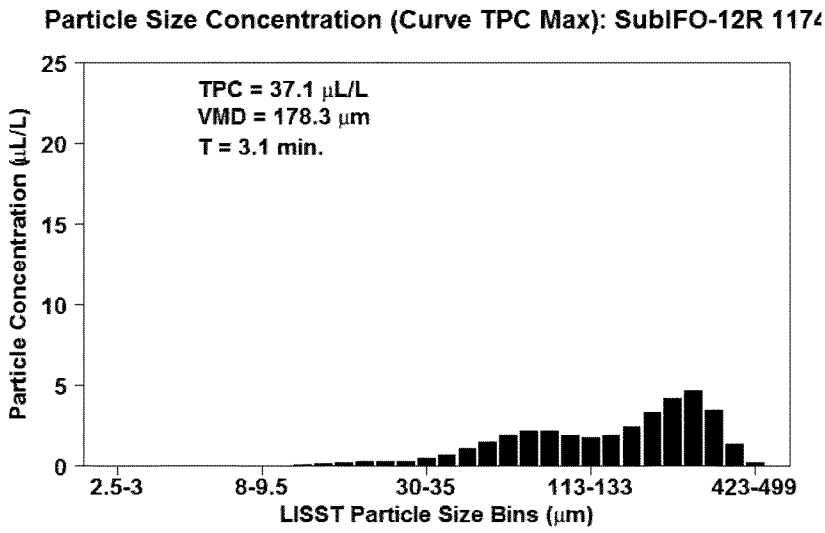

Appendix C - Figure C12. LISST DSD plot for IFO-120, DOR 1:20 (Corexit 9500), cold water experiments.

ED_001324_00000687-00032

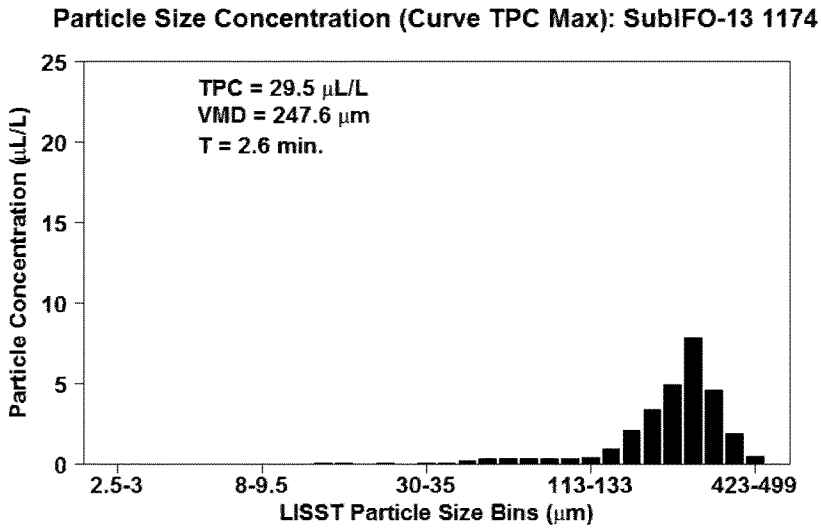

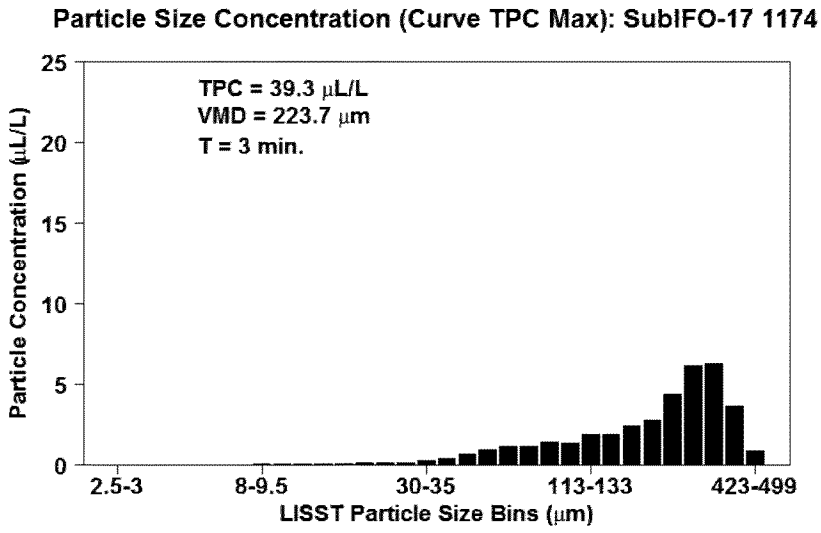

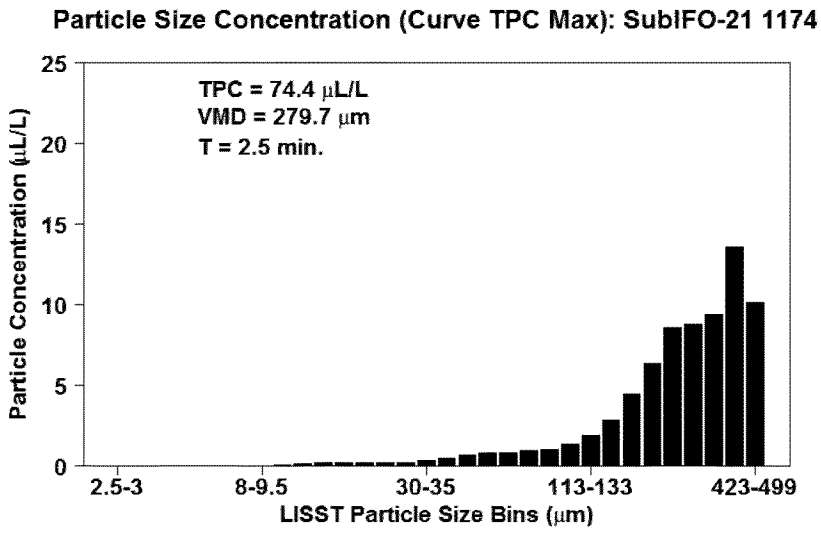

Appendix C - Figure C13. LISST DSD plot for IFO-120, no dispersant, warm water experiments.

ED_001324_00000687-00033

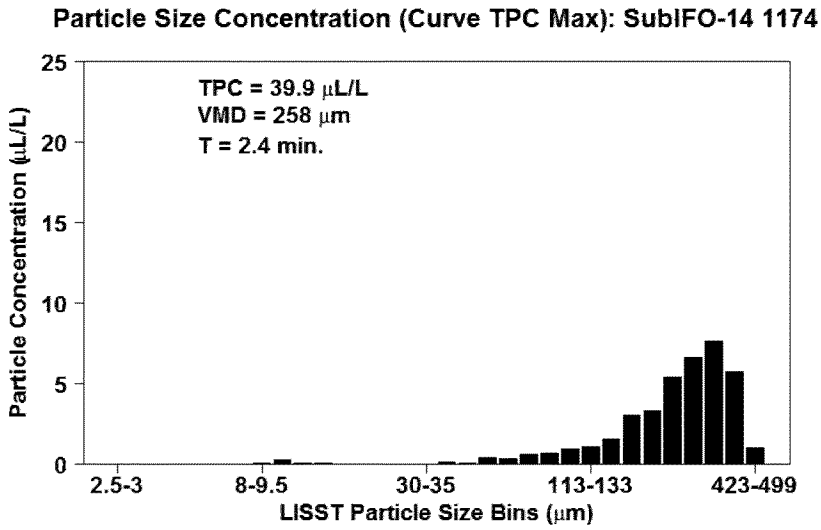

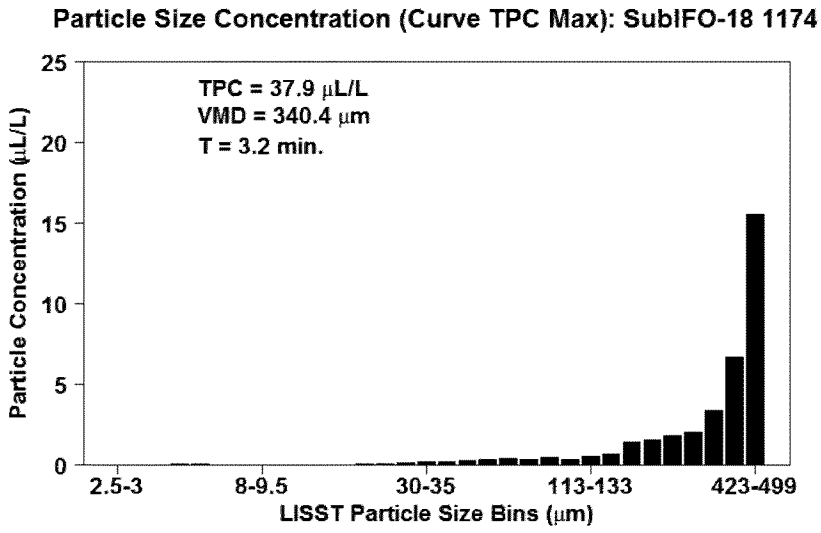

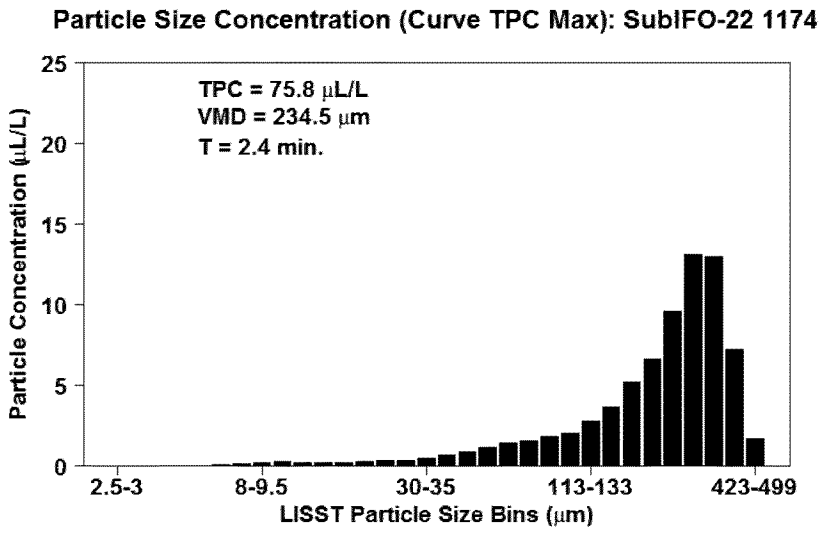

Appendix C - Figure C14. LISST DSD plot for IFO-120, DOR 1:200 (Corexit 9500), warm experiments.

ED_001324_00000687-00034

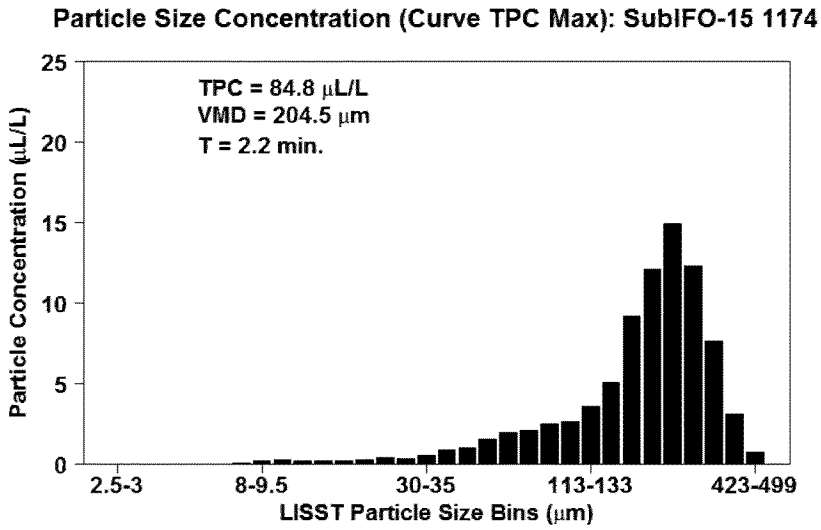

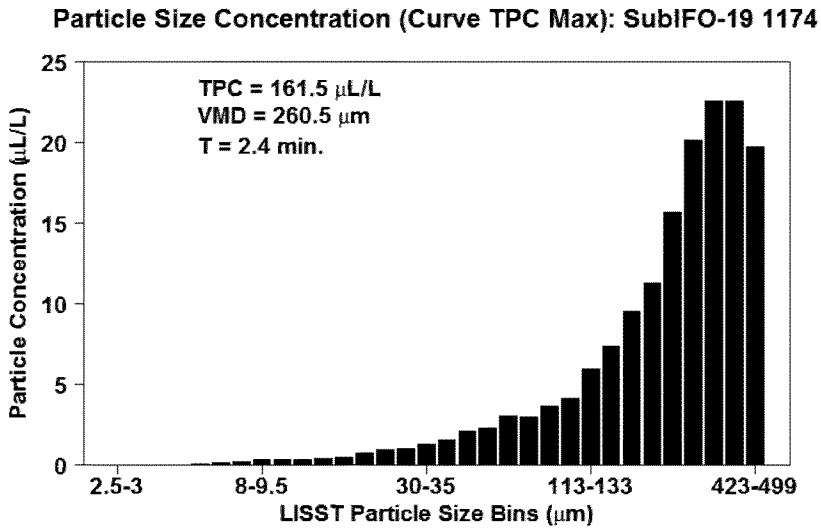

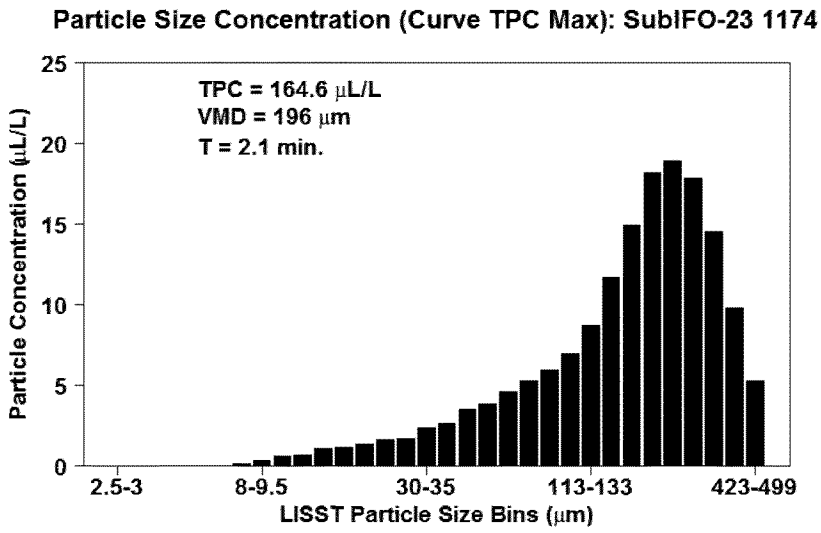

Appendix C - Figure C15. LISST DSD plot for IFO-120, DOR 1:100 (Corexit 9500), warm experiments.

ED_001324_00000687-00035

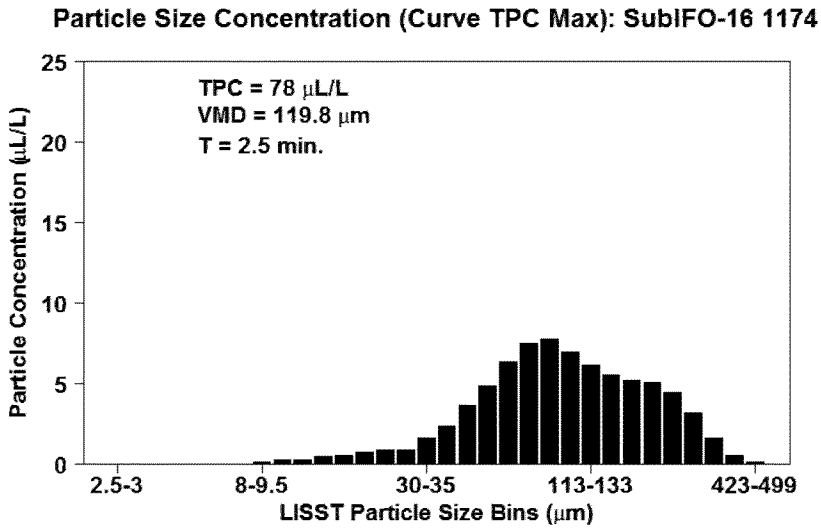

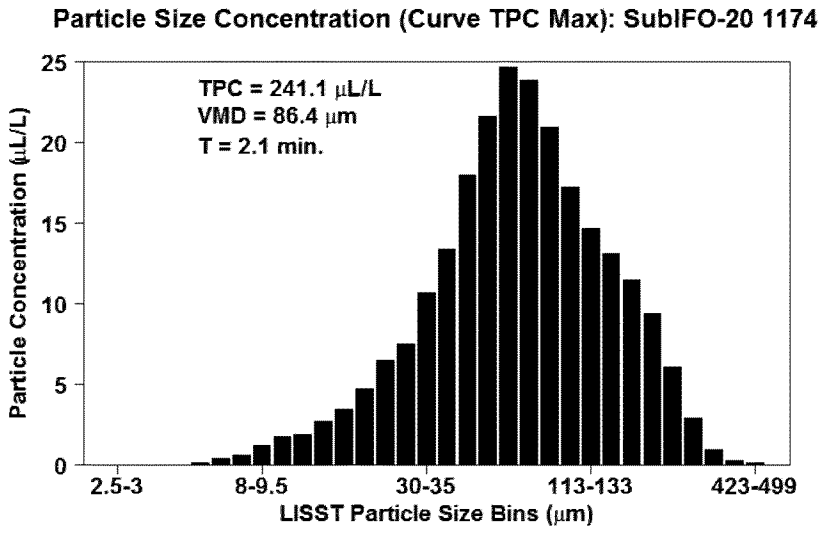

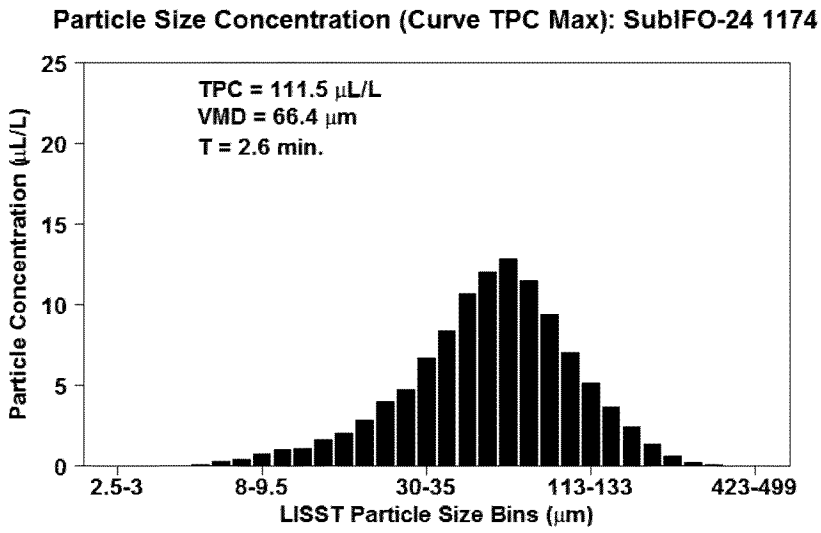

Appendix C - Figure C16. LISST DSD plot for IFO-120, DOR 1:20 (Corexit 9500), warm experiments.

ED_001324_00000687-00036

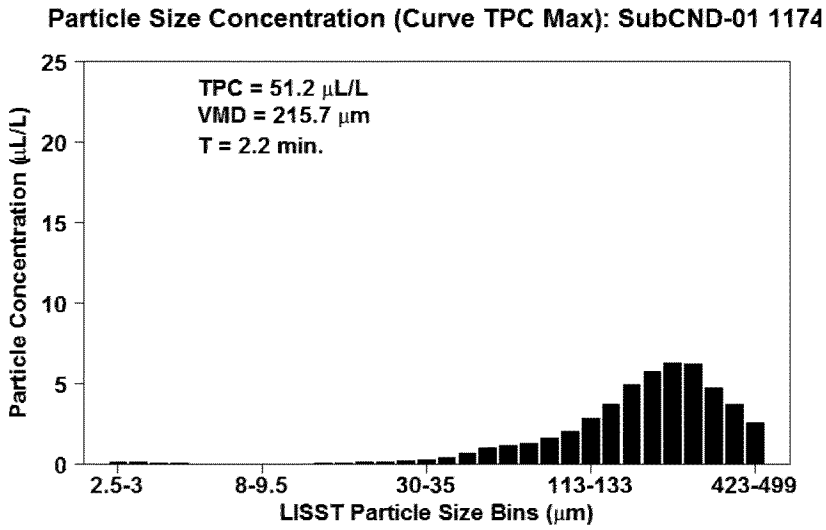

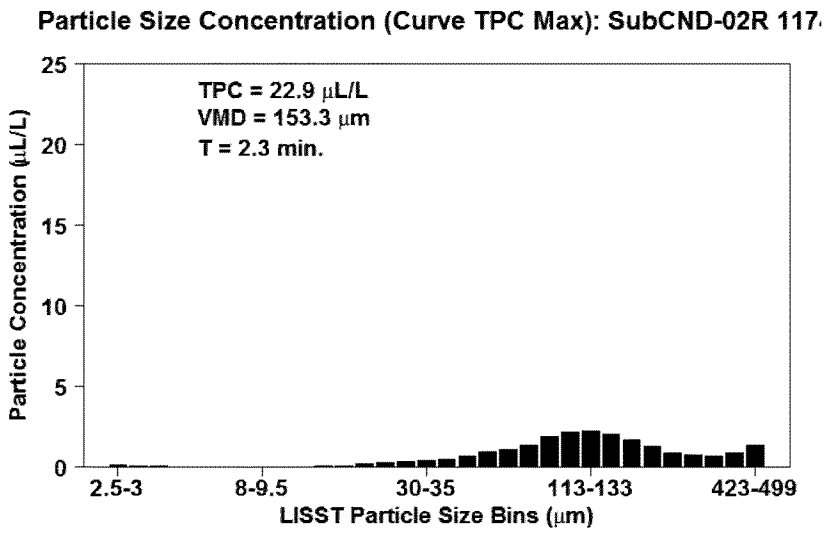

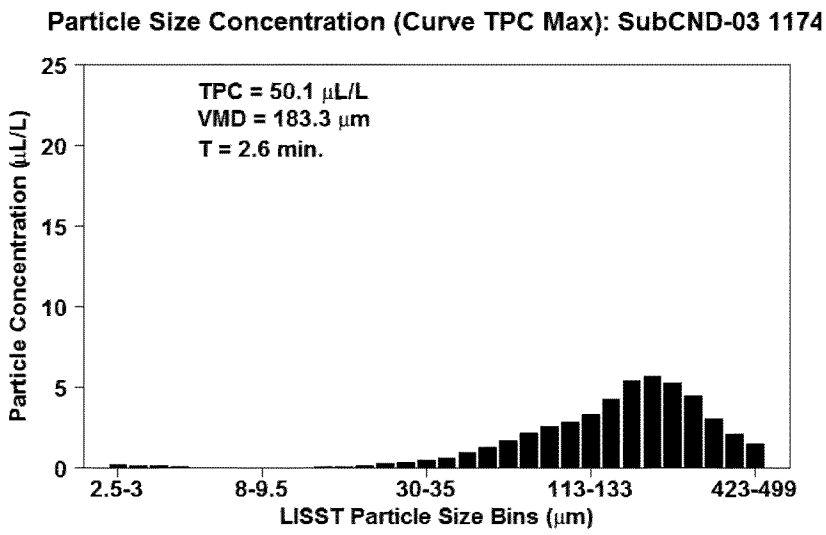

Appendix C - Figure C17. LISST DSD plot for Gas Condensate, no dispersant.

ED_001324_00000687-00037

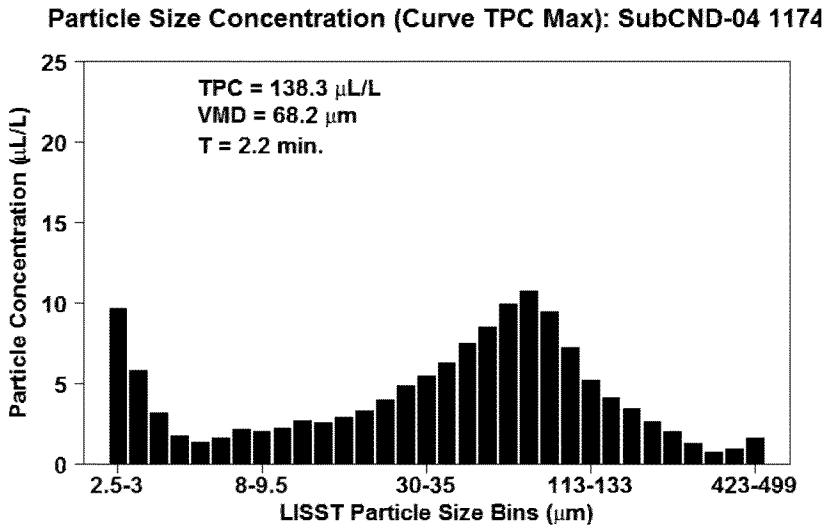

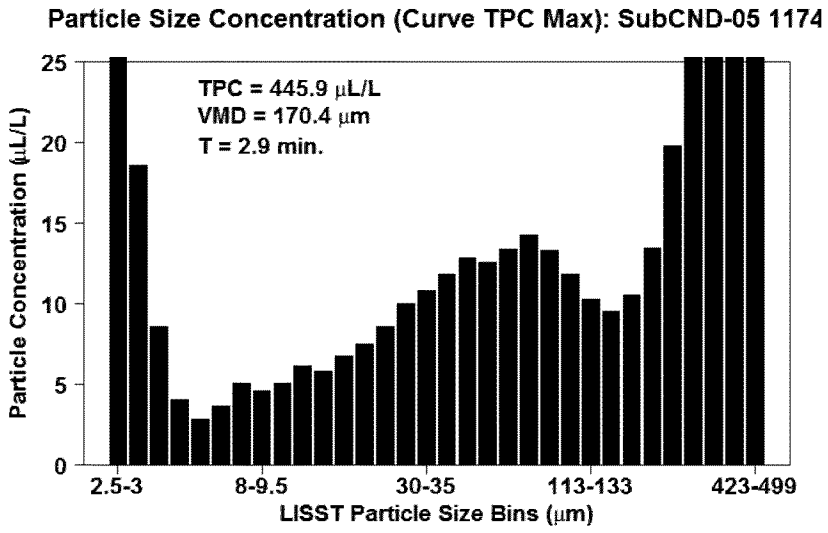

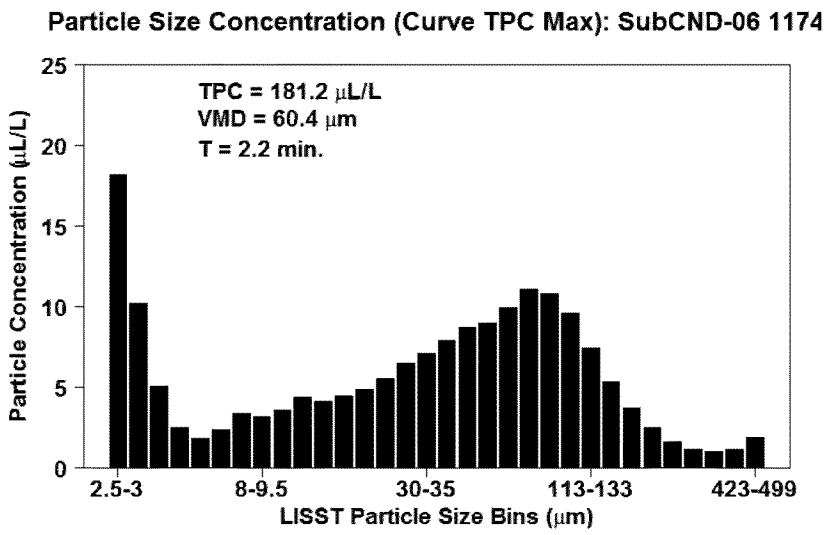

Appendix C - Figure C18. LISST DSD plot for Gas Condensate, DOR 1:20 (Corexit 9500).

ED_001324_00000687-00038

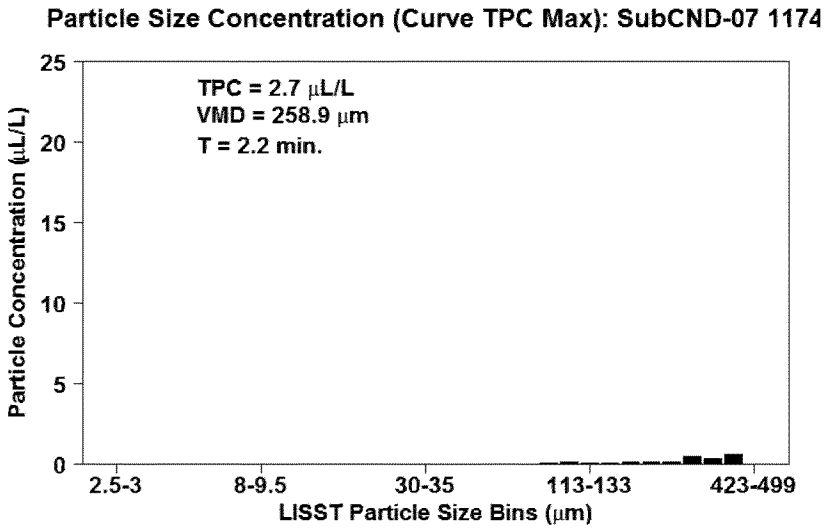

Appendix C - Figure C19. LISST DSD plot for air injection, no dispersant.

ED_001324_00000687-00039

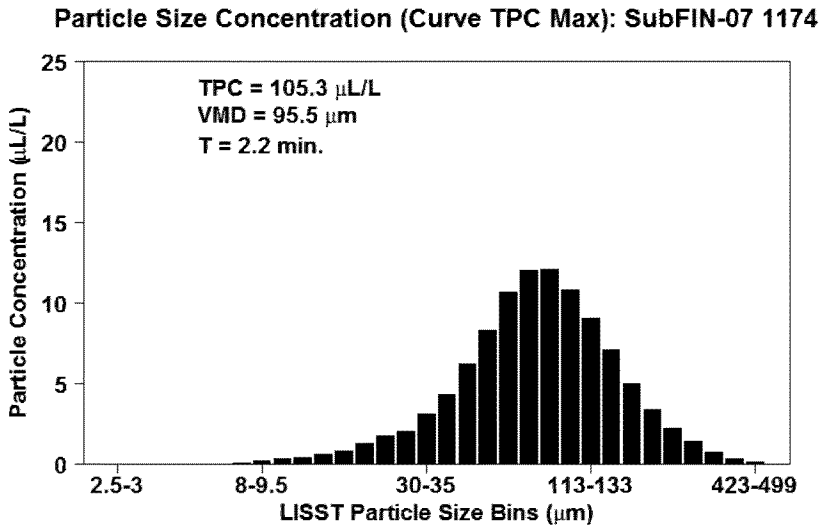

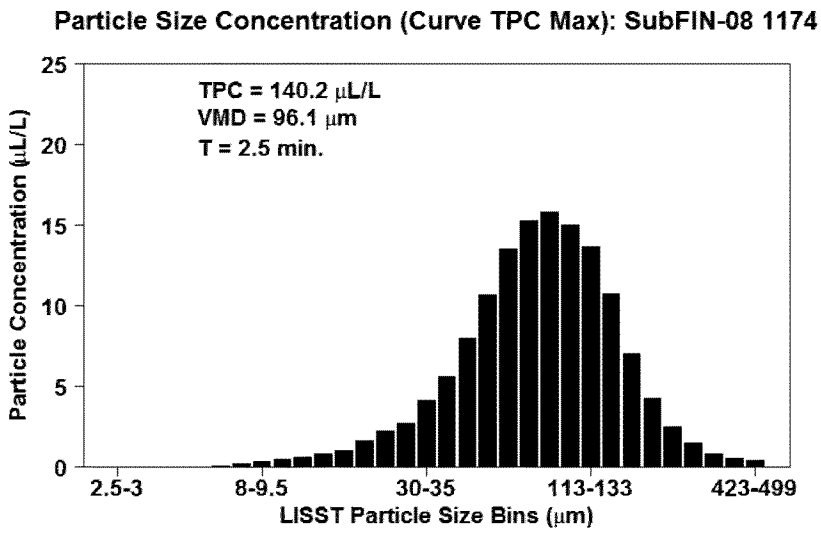

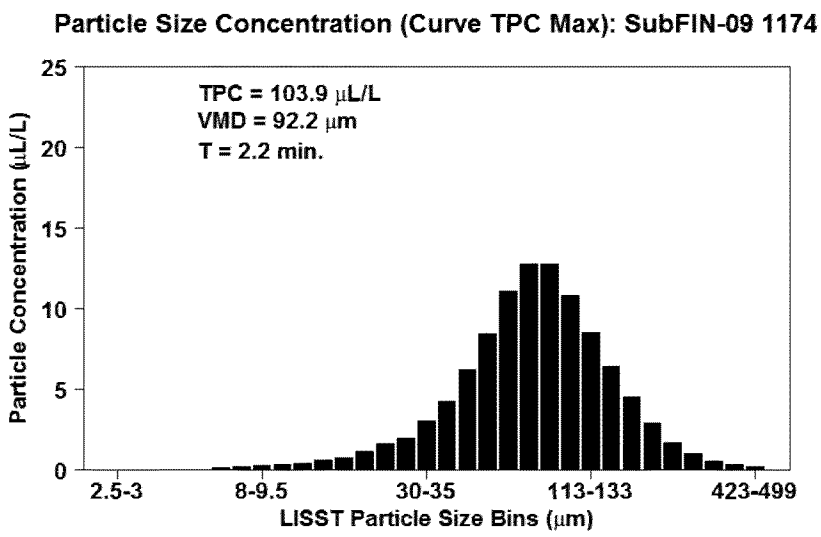

Appendix C - Figure C20. LISST DSD plot for ANS, DOR 1:200 (Finasol OSR 52), warm experiments.

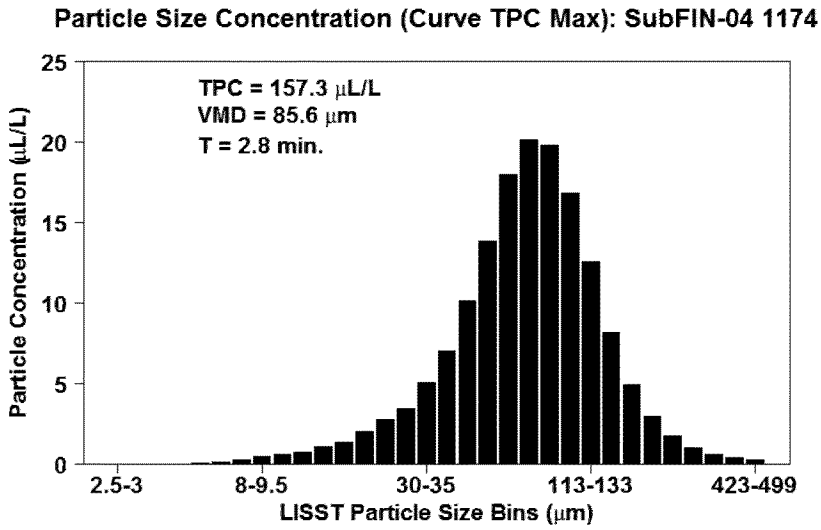

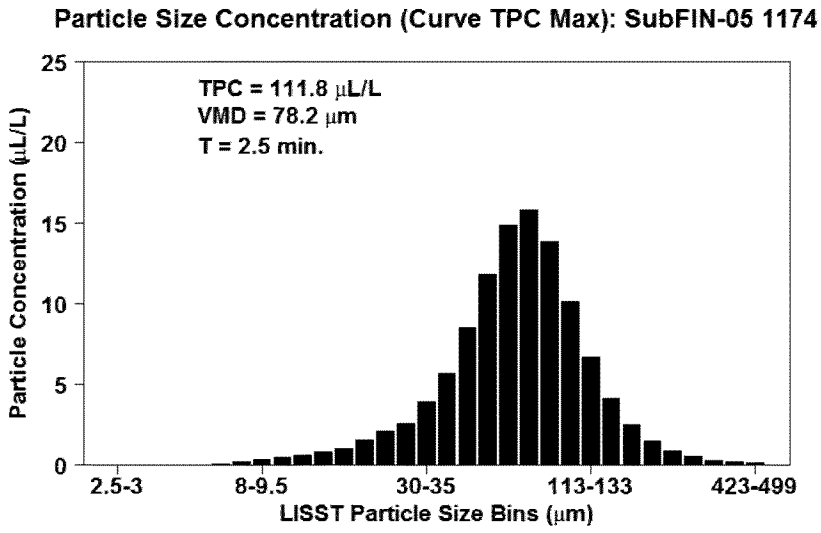

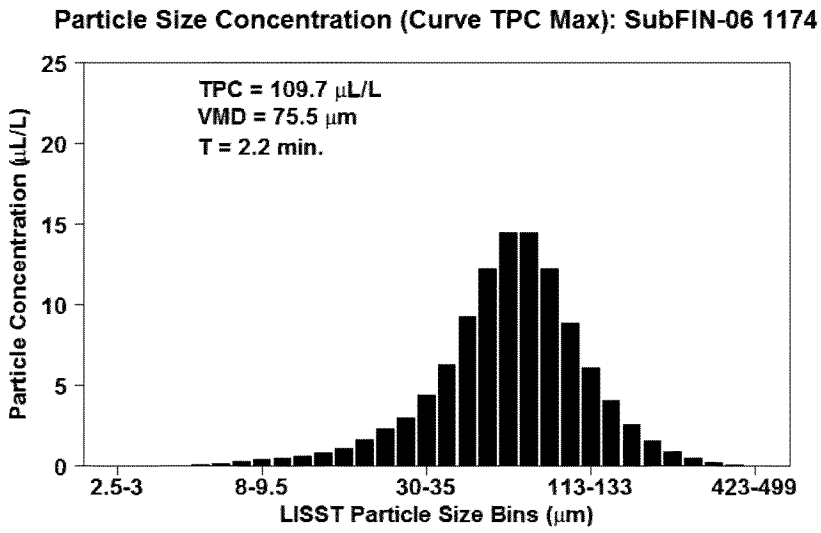

Appendix C - Figure C21. LISST DSD plot for ANS, DOR 1:100 (Finasol OSR 52), warm experiments.

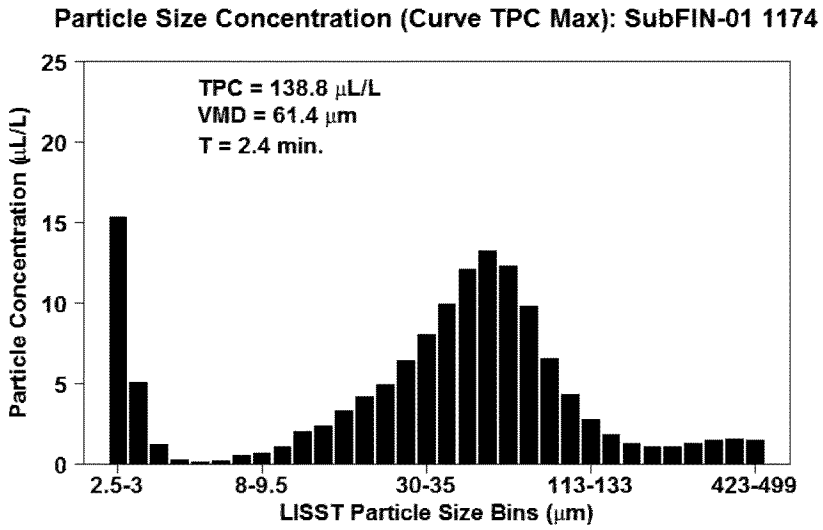

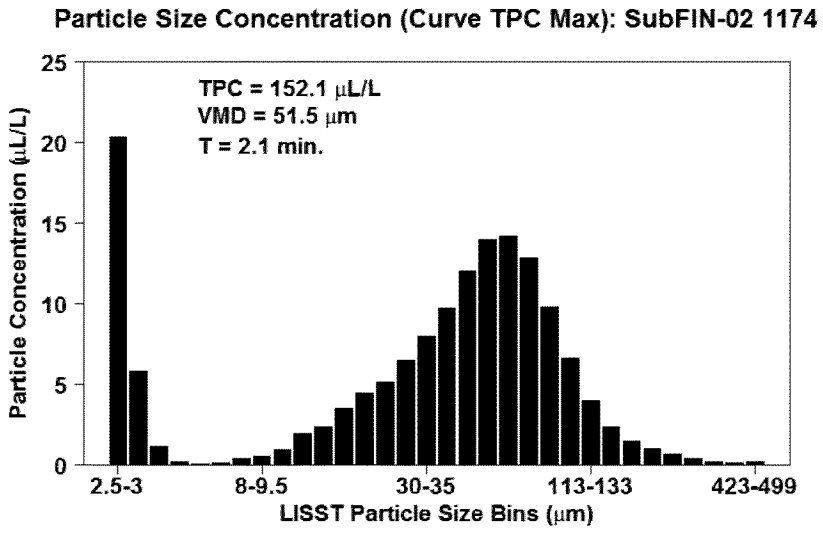

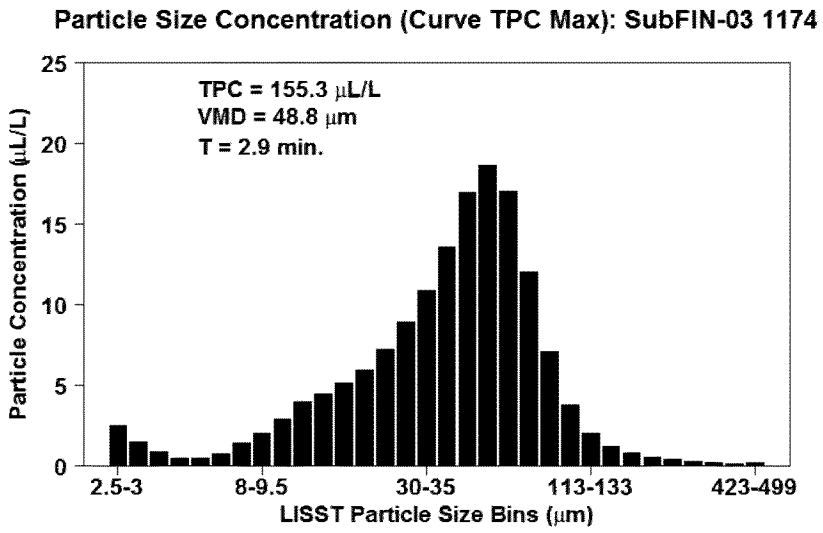

Appendix C - Figure C22. LISST DSD plot for ANS, DOR 1:20 (Finasol OSR 52), warm water experiments.

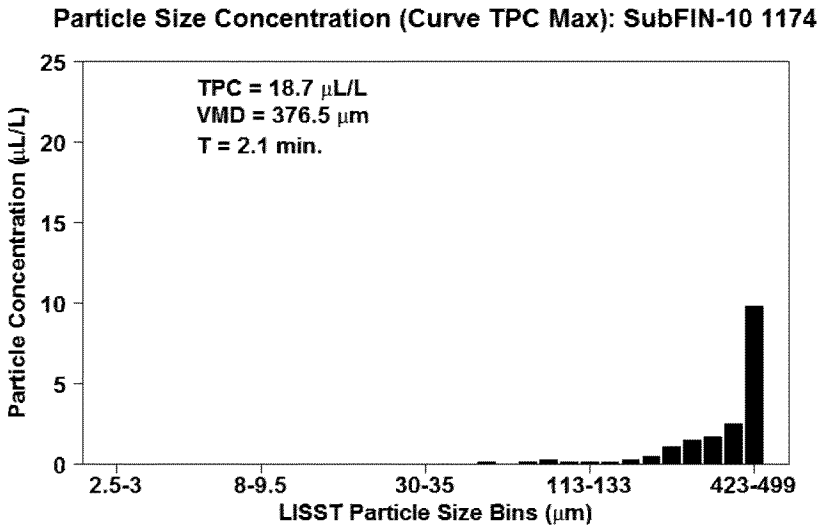

Appendix C - Figure C23. LISST DSD plot for IFO-120, DOR 1:200 (Finasol OSR 52), warm water experiments.

ED_001324_00000687-00043

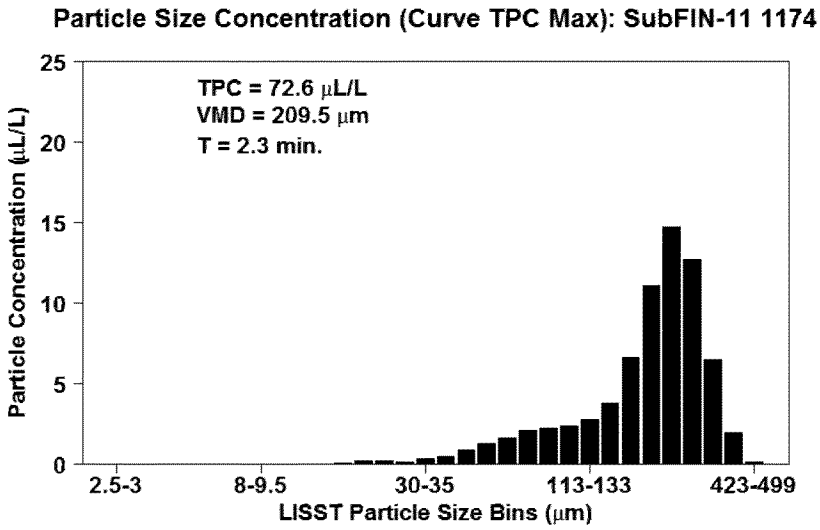

Appendix C - Figure C24. LISST DSD plot for IFO-120, DOR 1:100 (Finasol OSR 52), warm experiments.

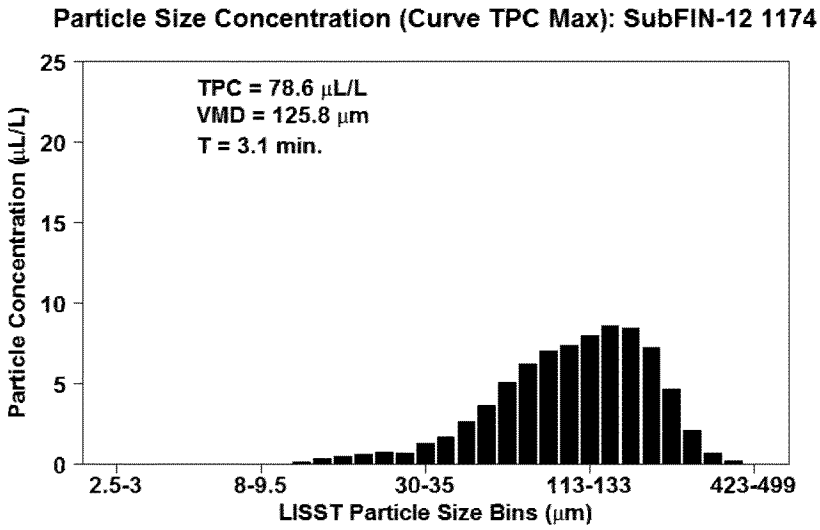

Appendix C - Figure C25. LISST DSD plot for IFO-120, DOR 1:20 (Finasol OSR 52), warm experiments.

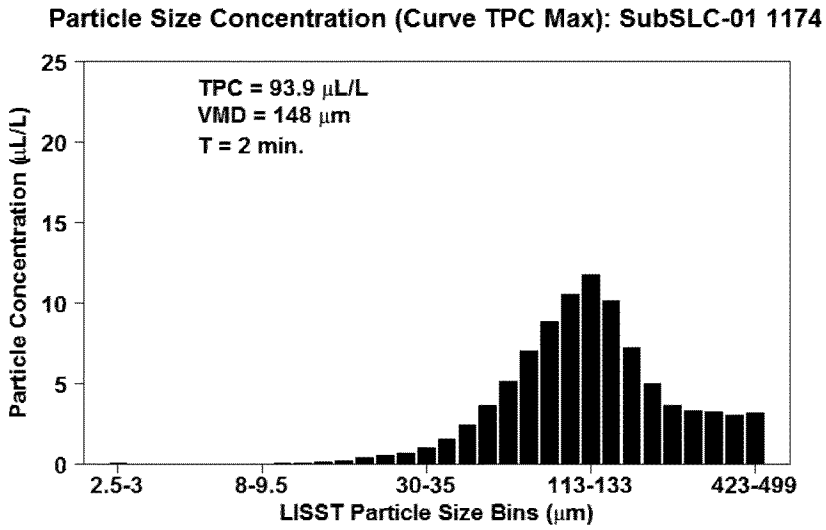

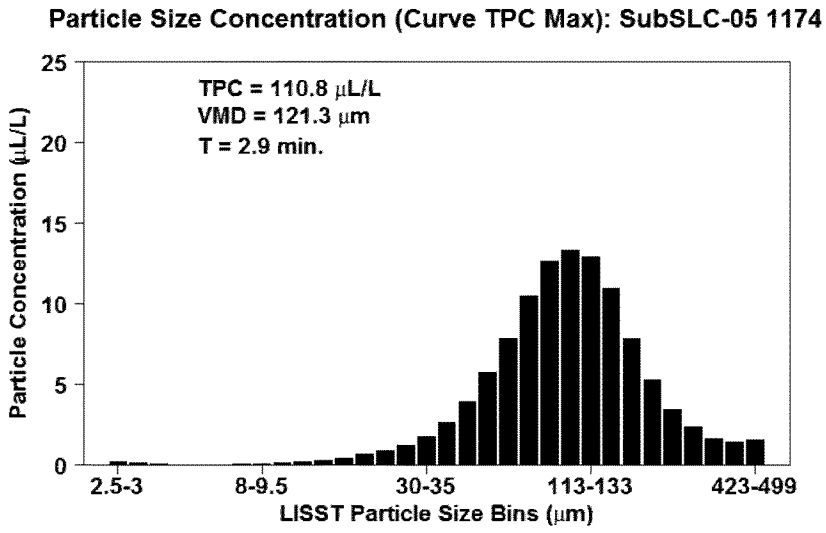

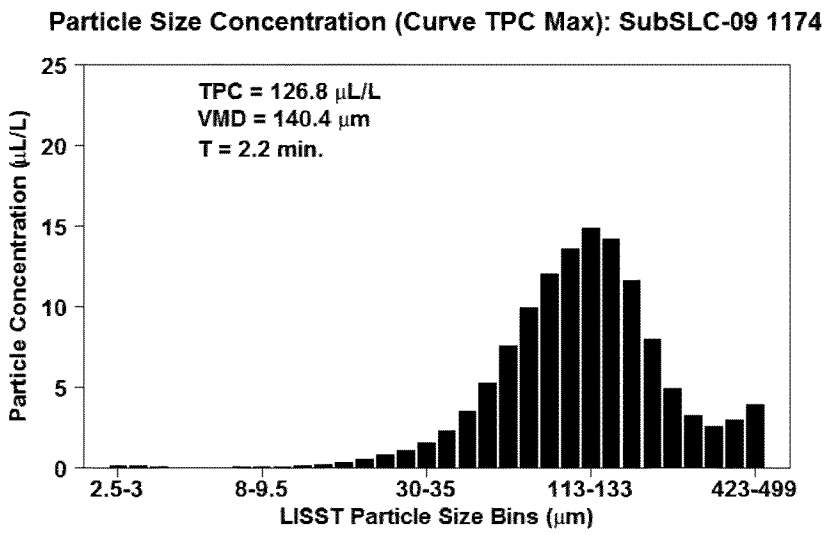

Appendix C - Figure C26. LISST DSD plot for SLC, no dispersant, warm water experiments.

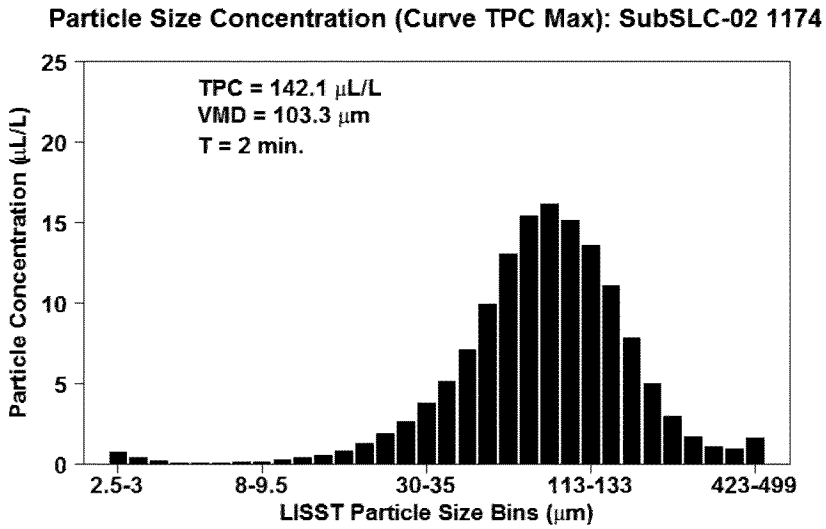

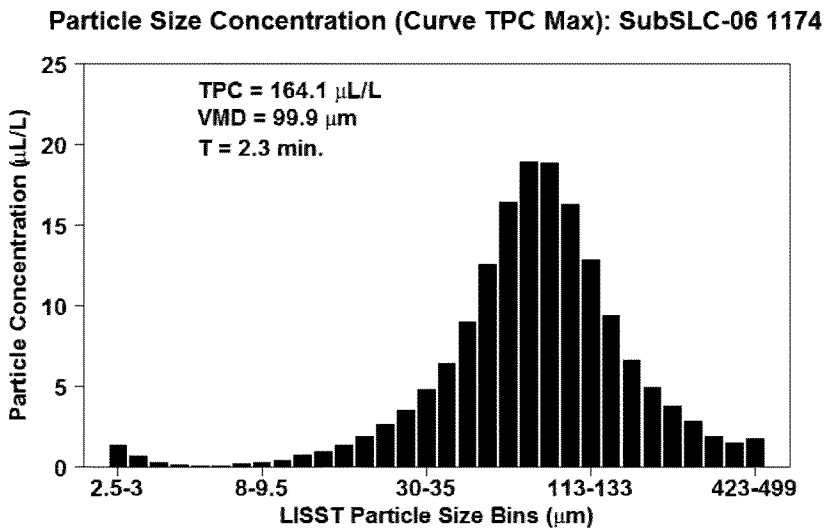

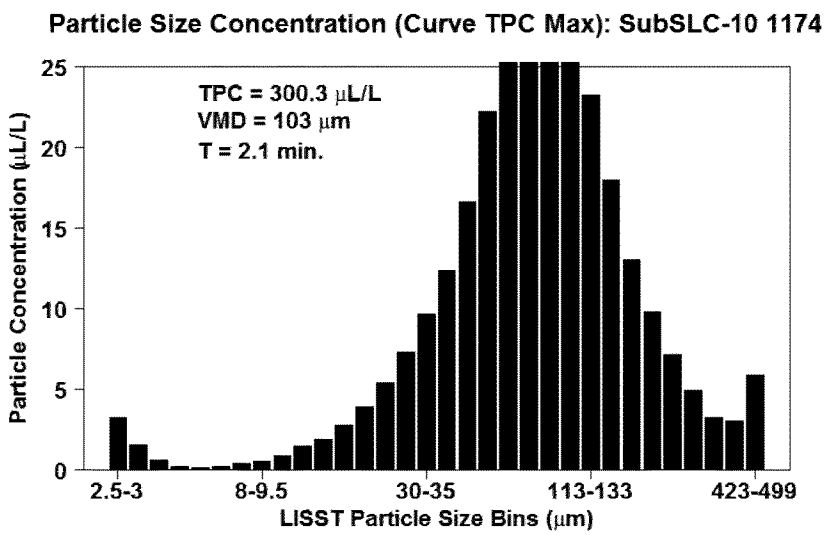

Appendix C - Figure C27. LISST DSD plot for SLC, DOR 1:200 (Corexit 9500), warm water experiments.

ED_001324_00000687-00047

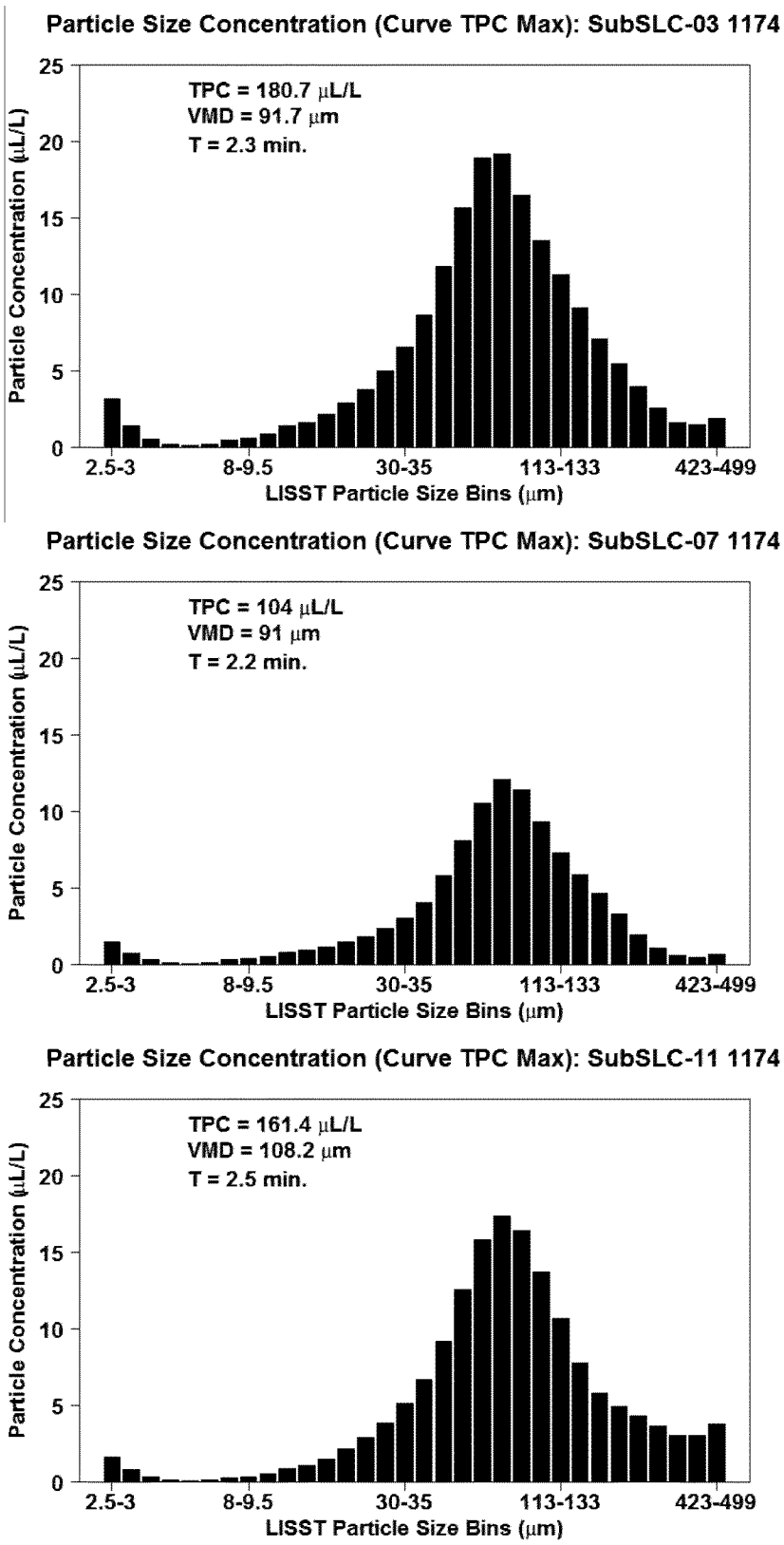

Appendix C - Figure C28. LISST DSD plot for SLC, DOR 1:100 (Corexit 9500), warm water experiments.

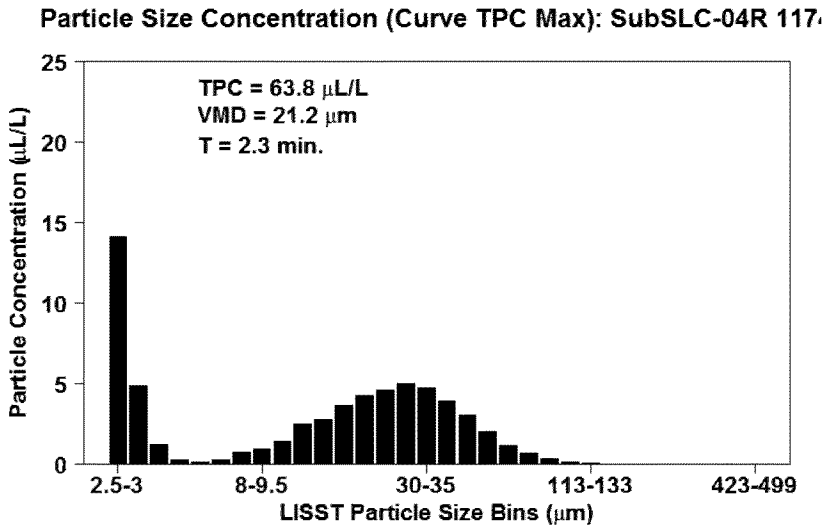

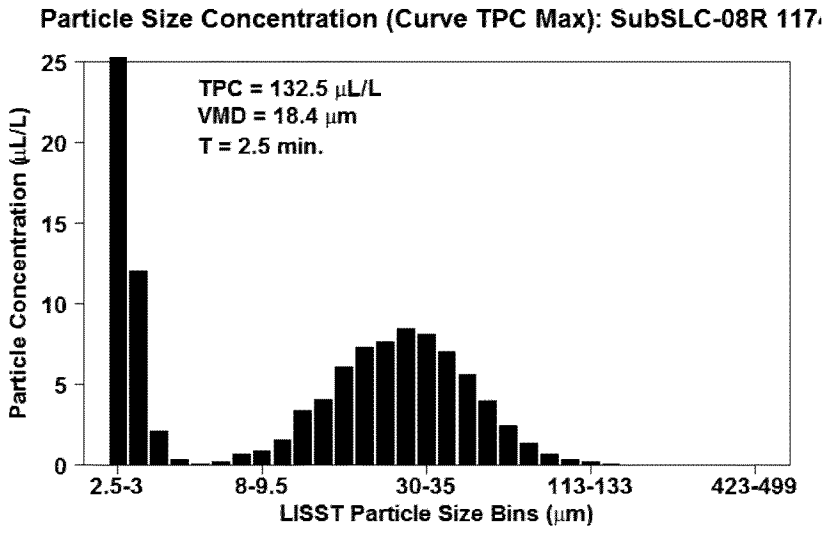

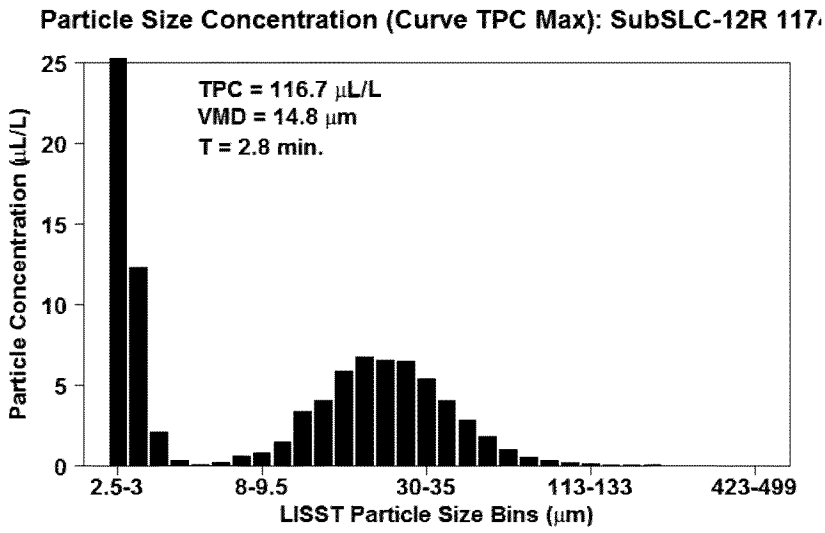

Appendix C - Figure C29. LISST DSD plot for SLC, DOR 1:20 (Corexit 9500), warm water experiments.

APPENDIX D – Jet Release LISST Oil Droplet Size Distribution Time Series Contours

ED_001324_00000687-00050

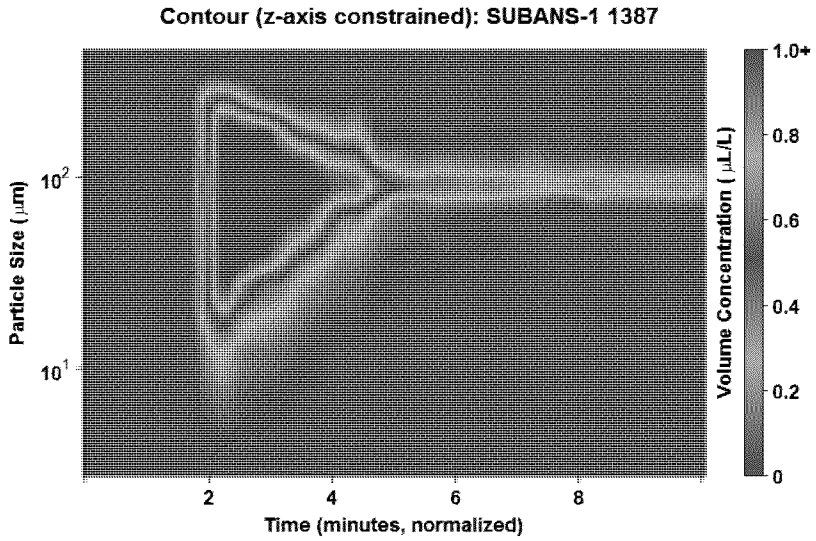
Contour (z-axis constrained): SUBANS-1 1387
Particle Size (μm)
10^2
10^1
2
4
6
8
Time (minutes, normalized)
Volume Concentration (μL/L)
1.0+
0.8
0.6
0.4
0.2
0

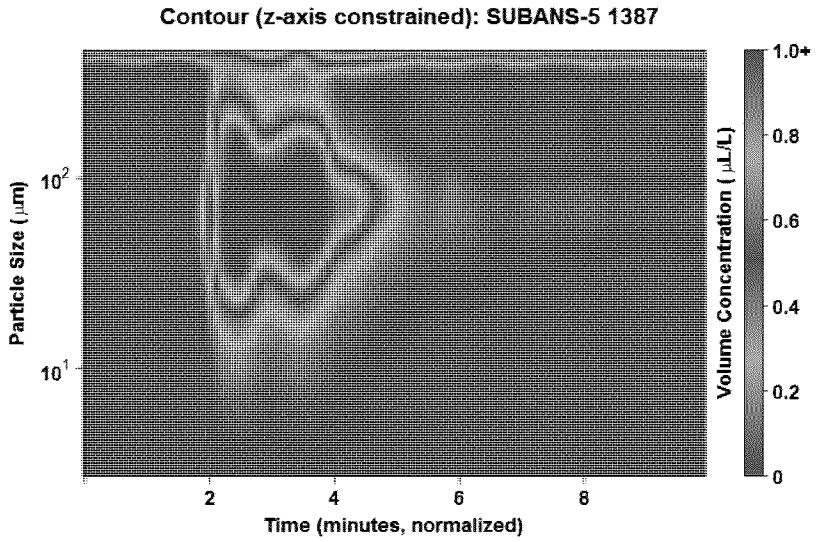
Contour (z-axis constrained): SUBANS-5 1387
Particle Size (μm)
10^2
10^1
2
4
6
8
Time (minutes, normalized)
Volume Concentration (μL/L)
1.0+
0.8
0.6
0.4
0.2
0

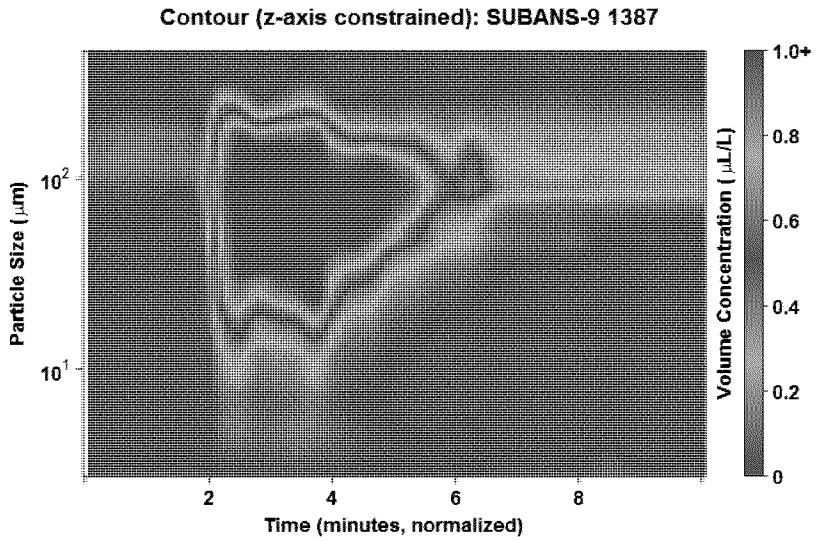
Contour (z-axis constrained): SUBANS-9 1387
Particle Size (μm)
10^2
10^1
2
4
6
8
Time (minutes, normalized)
Volume Concentration (μL/L)
1.0+
0.8
0.6
0.4
0.2
0

Appendix D - Figure D1. LISST contour plot for ANS, no dispersant, cold water experiments.

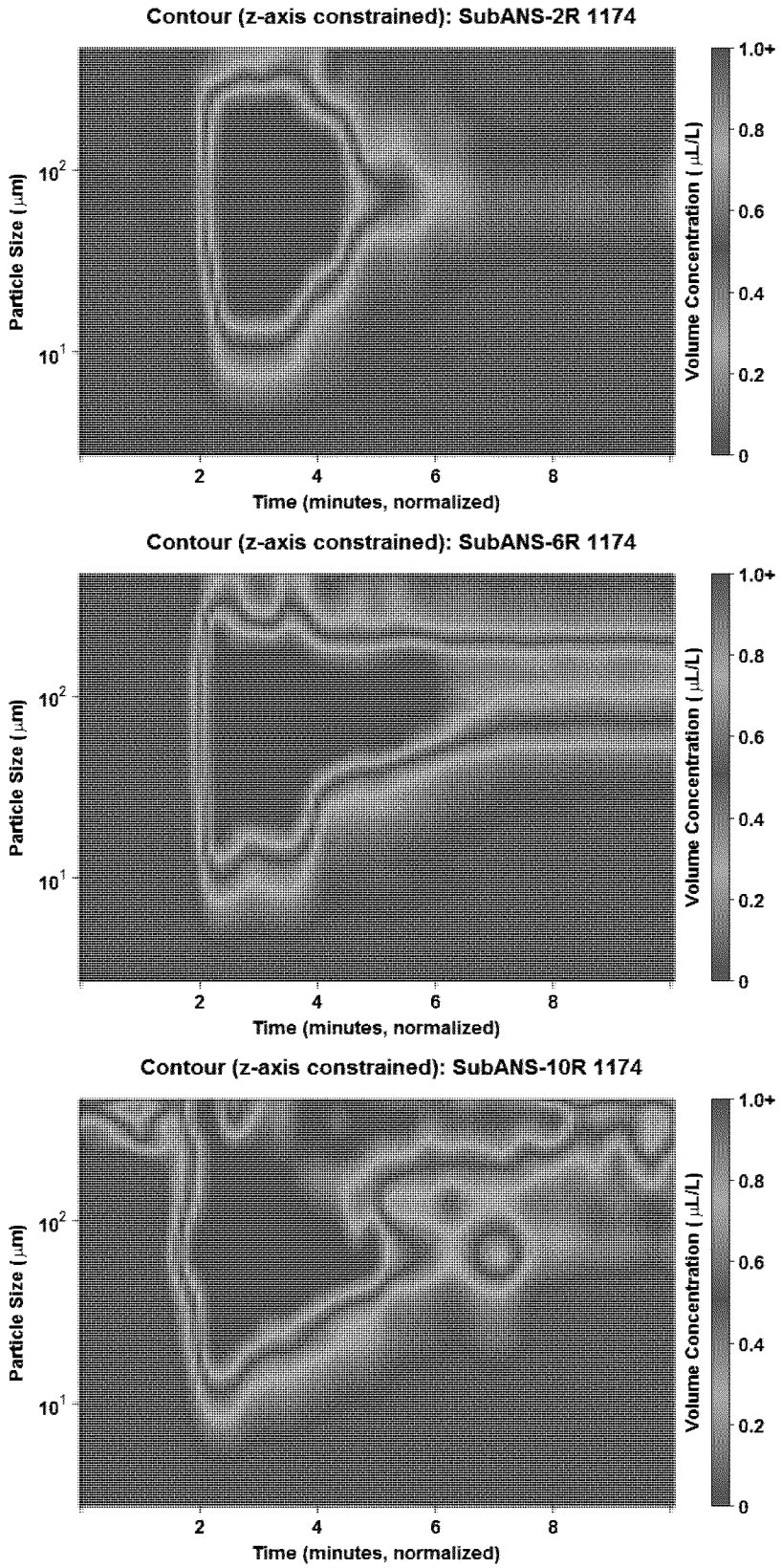

Appendix D - FigureD2. LISST contour plot for ANS, DOR 1:200 (Corexit 9500), cold water experiment.

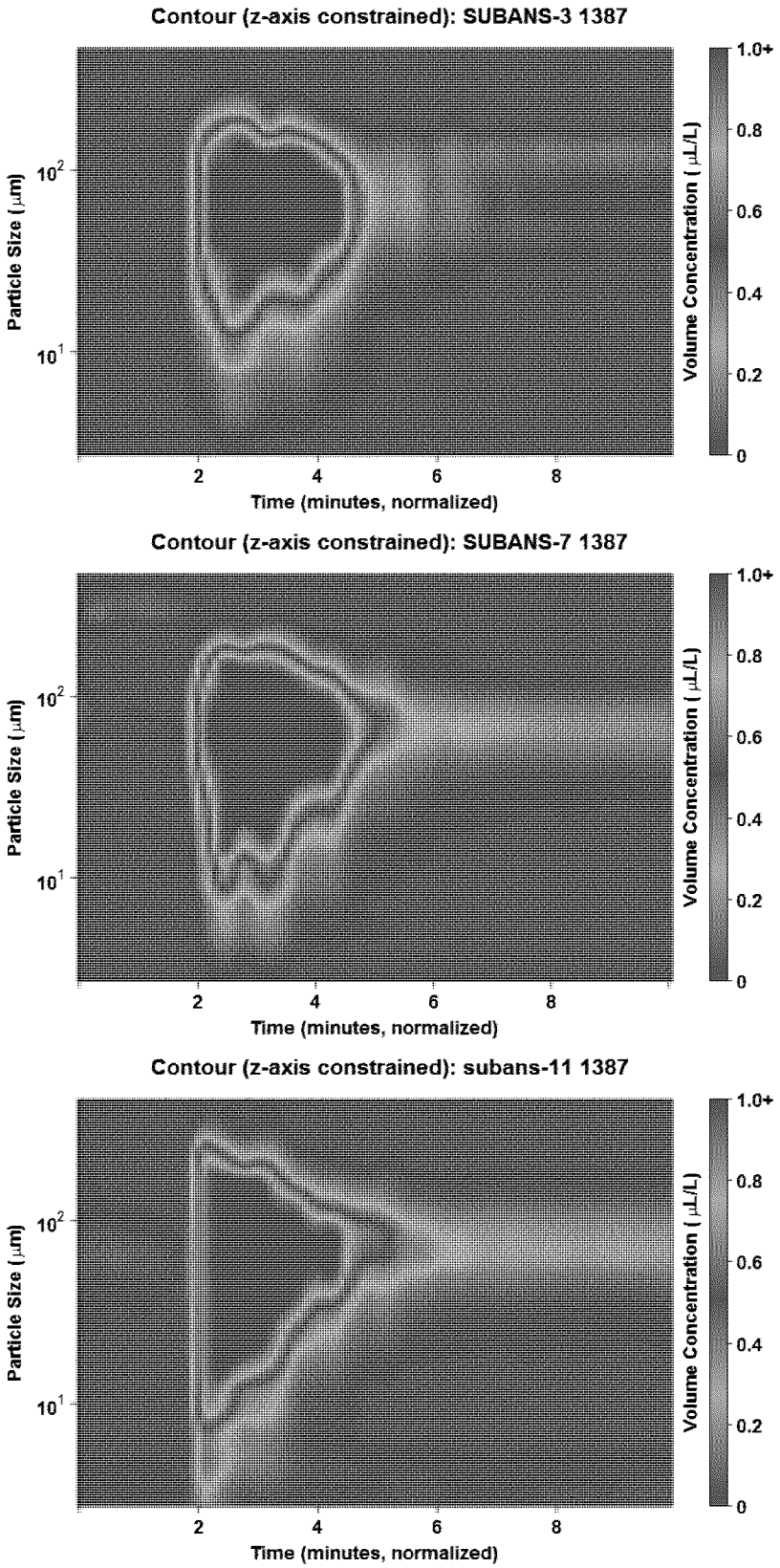

Appendix D - Figure D3. LISST contour plot for ANS, DOR 1:100 (Corexit 9500), cold water experiment.

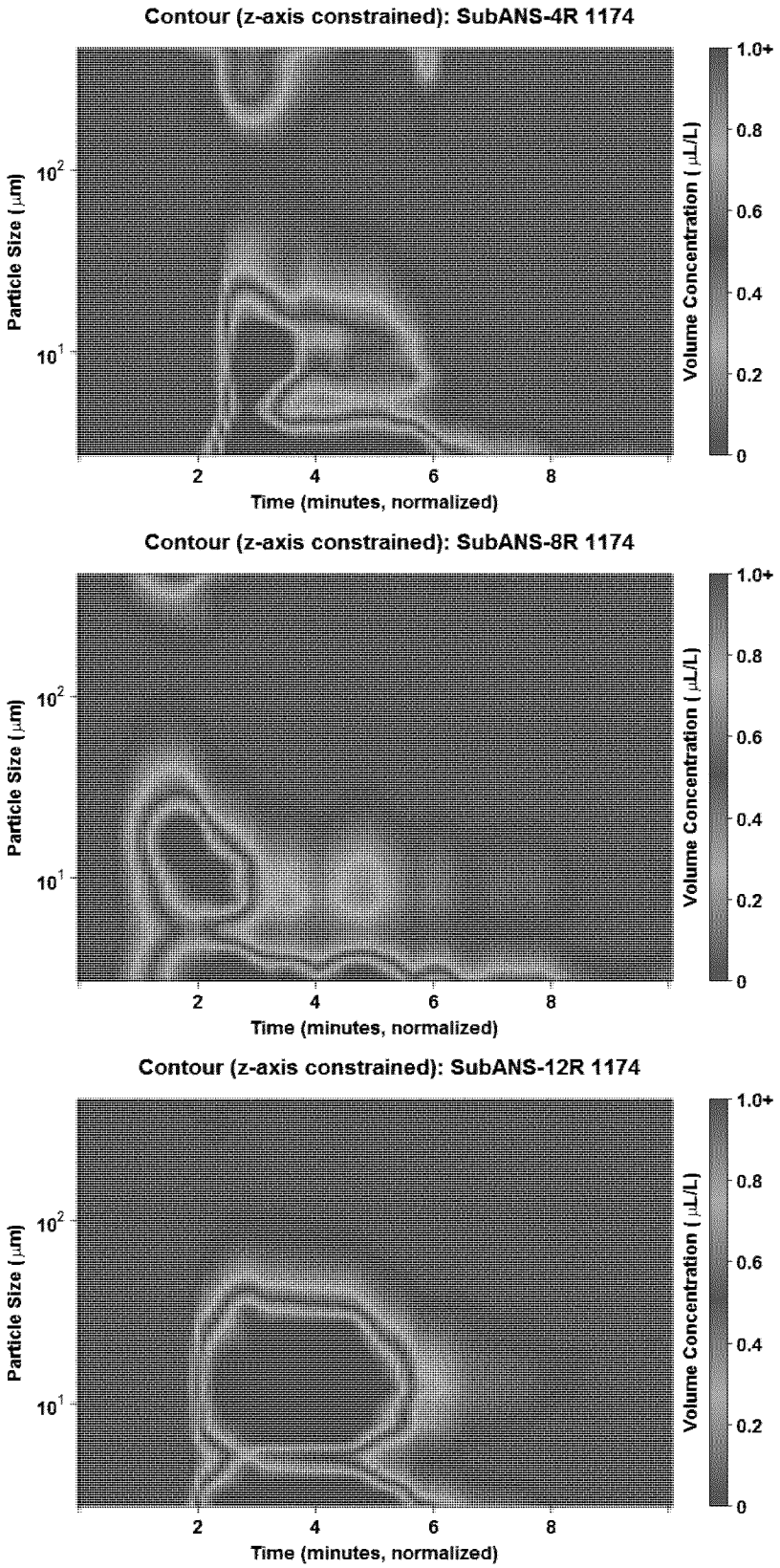

ED_001324_00000687-00054

Appendix D - Figure D4. LISST contour plot for ANS, DOR 1:20 (Corexit 9500), cold water experiment.

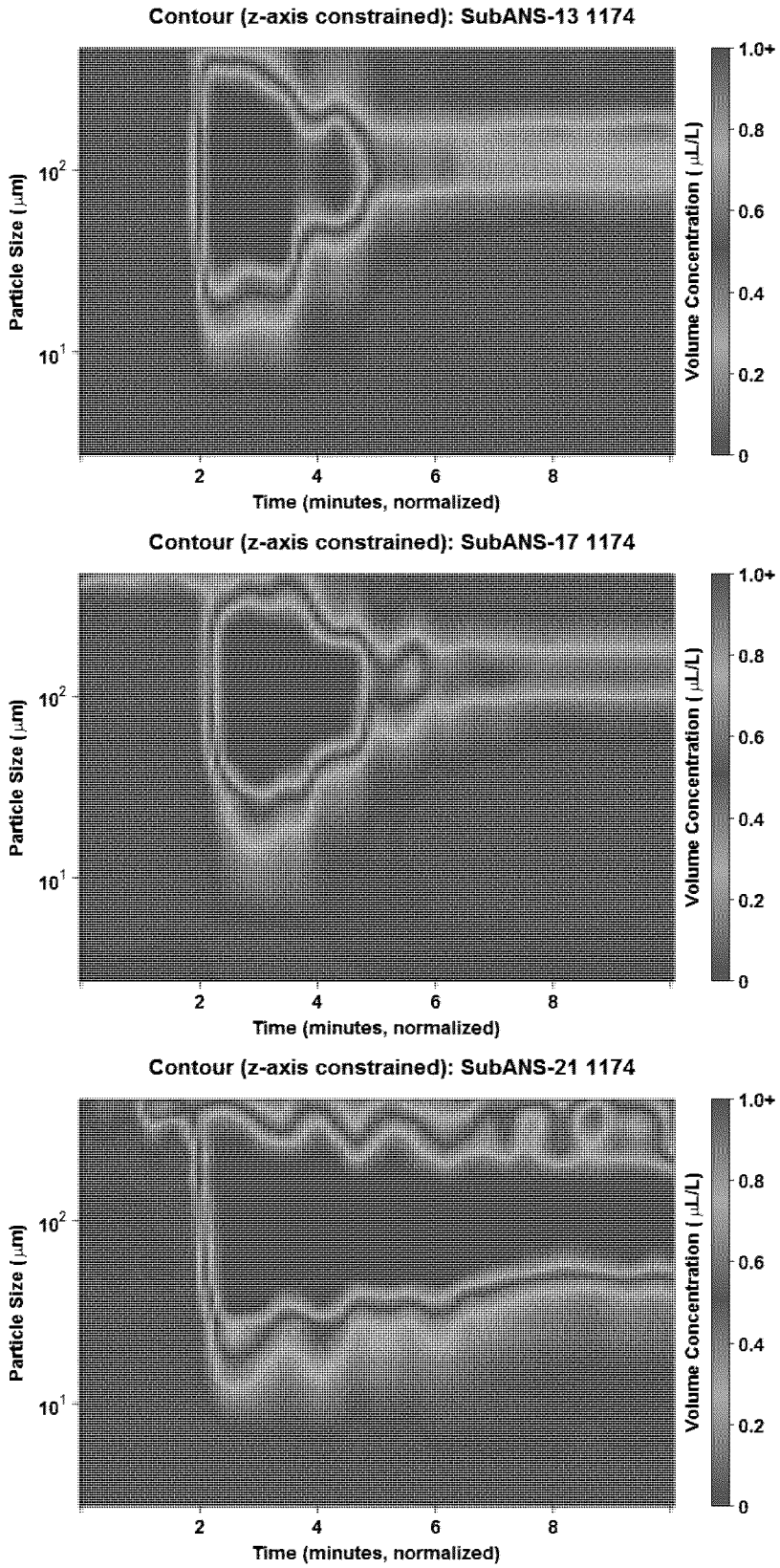

ED_001324_00000687-00055

Appendix D - Figure D5. LISST contour plot for ANS, no dispersant (Corexit 9500), warm experiment.

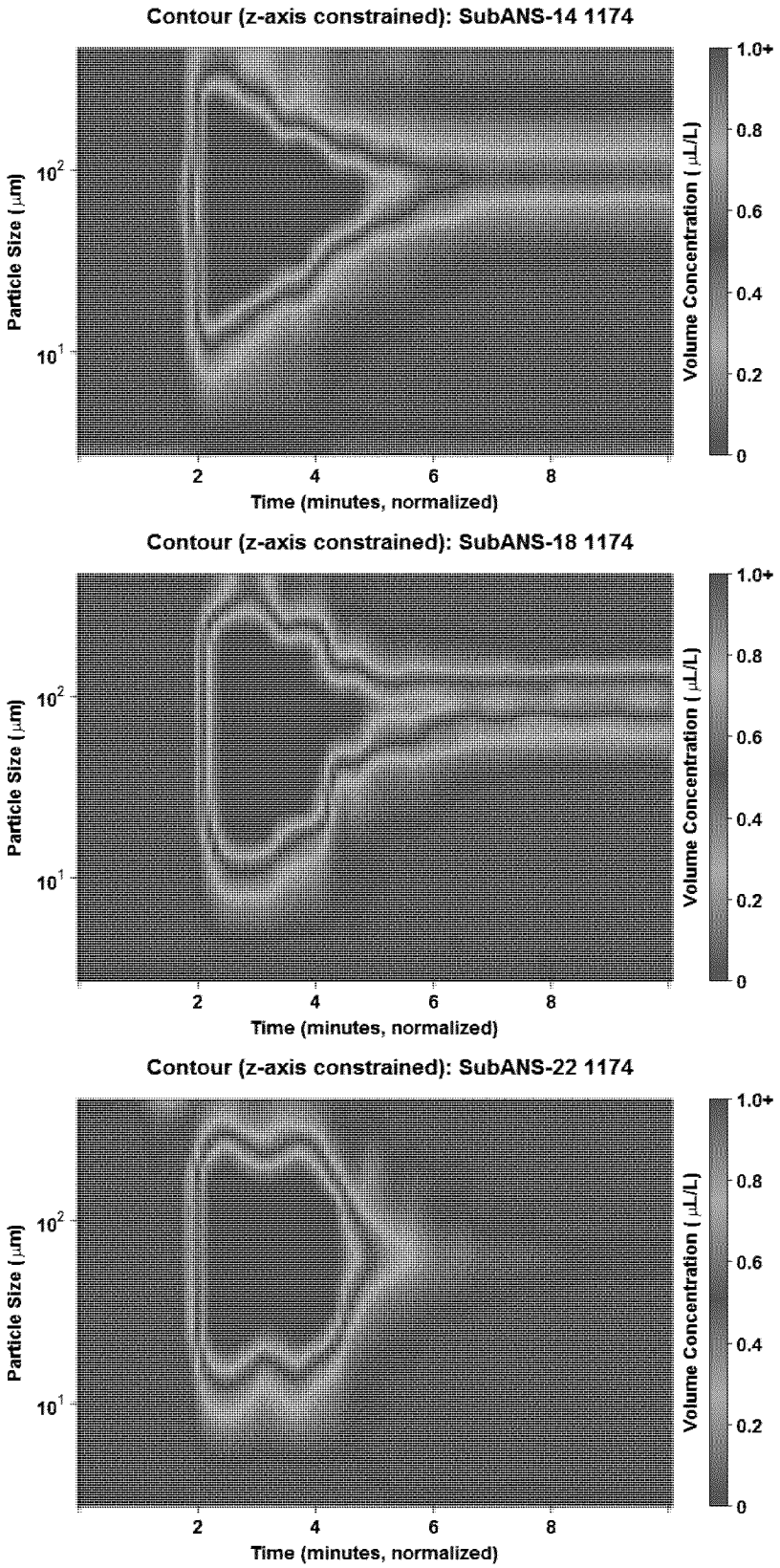

ED_001324_00000687-00056

Appendix D - Figure D6. LISST contour plot for ANS, DOR 1:200 (Corexit 9500), warm experiment.

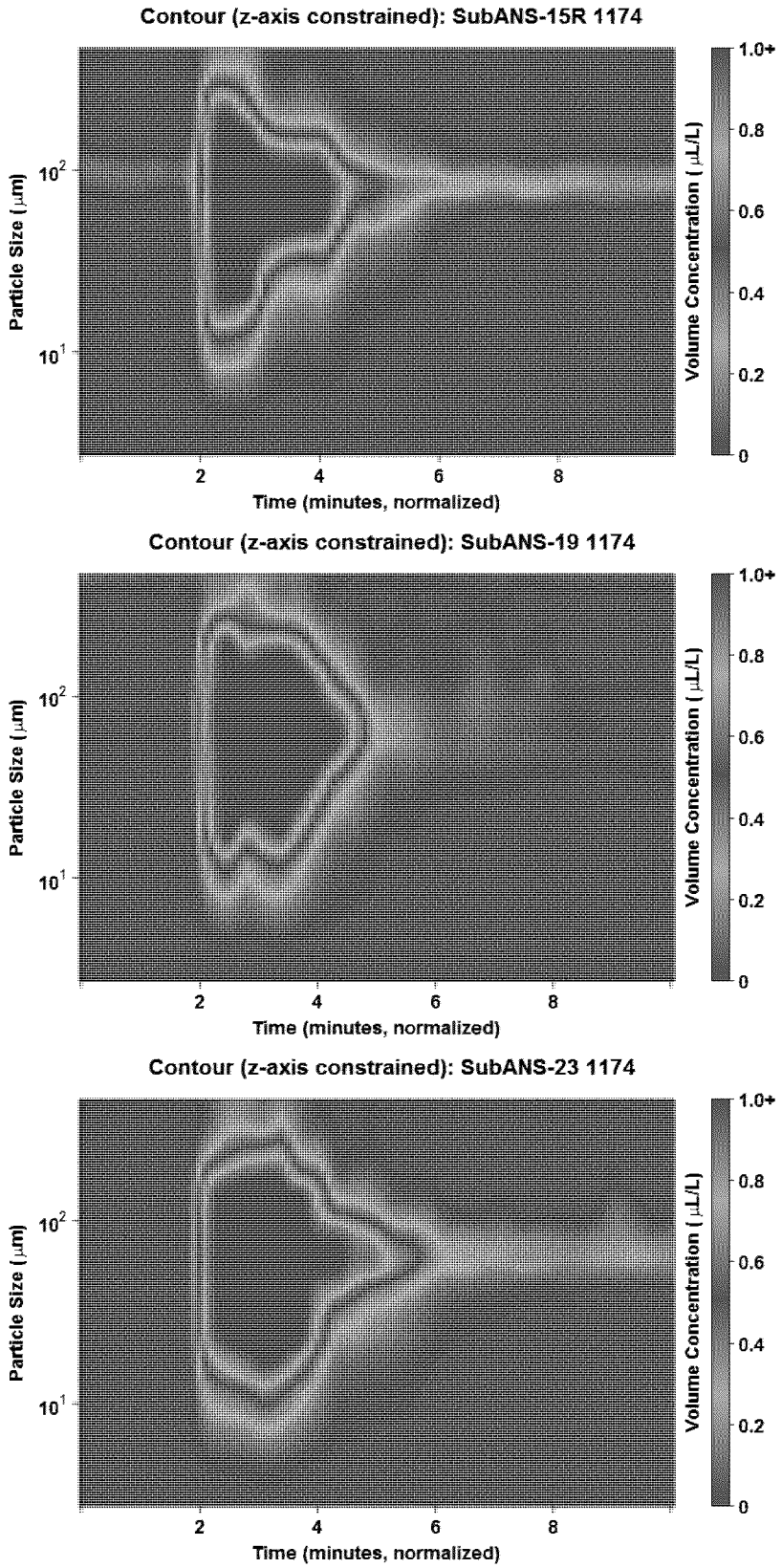

Appendix D - Figure D7. LISST contour plot for ANS, DOR 1:100 (Corexit 9500), warm experiment.

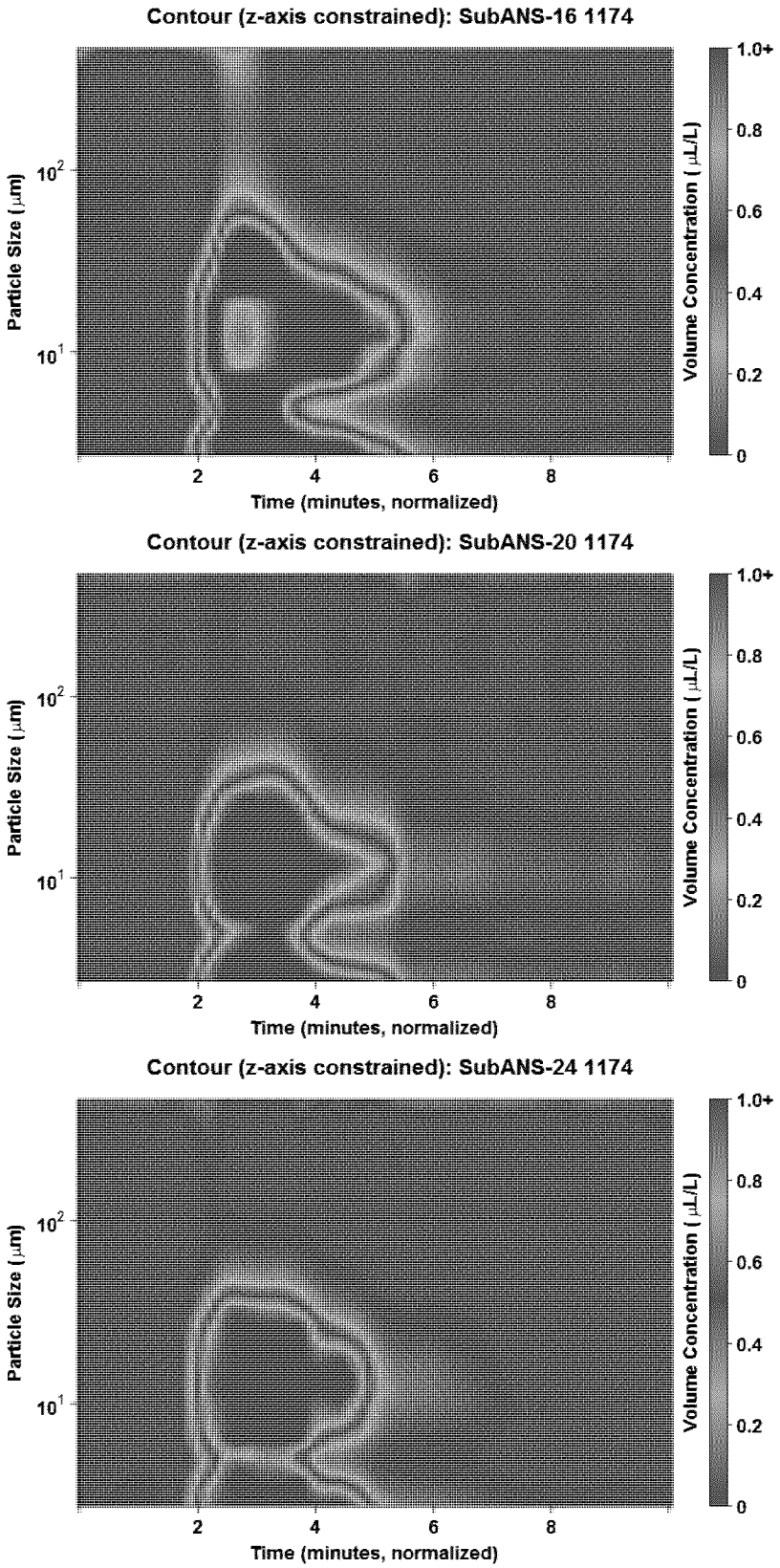

Appendix D - Figure D8. LISST contour plot for ANS, DOR 1:20 (Corexit 9500), warm experiment.

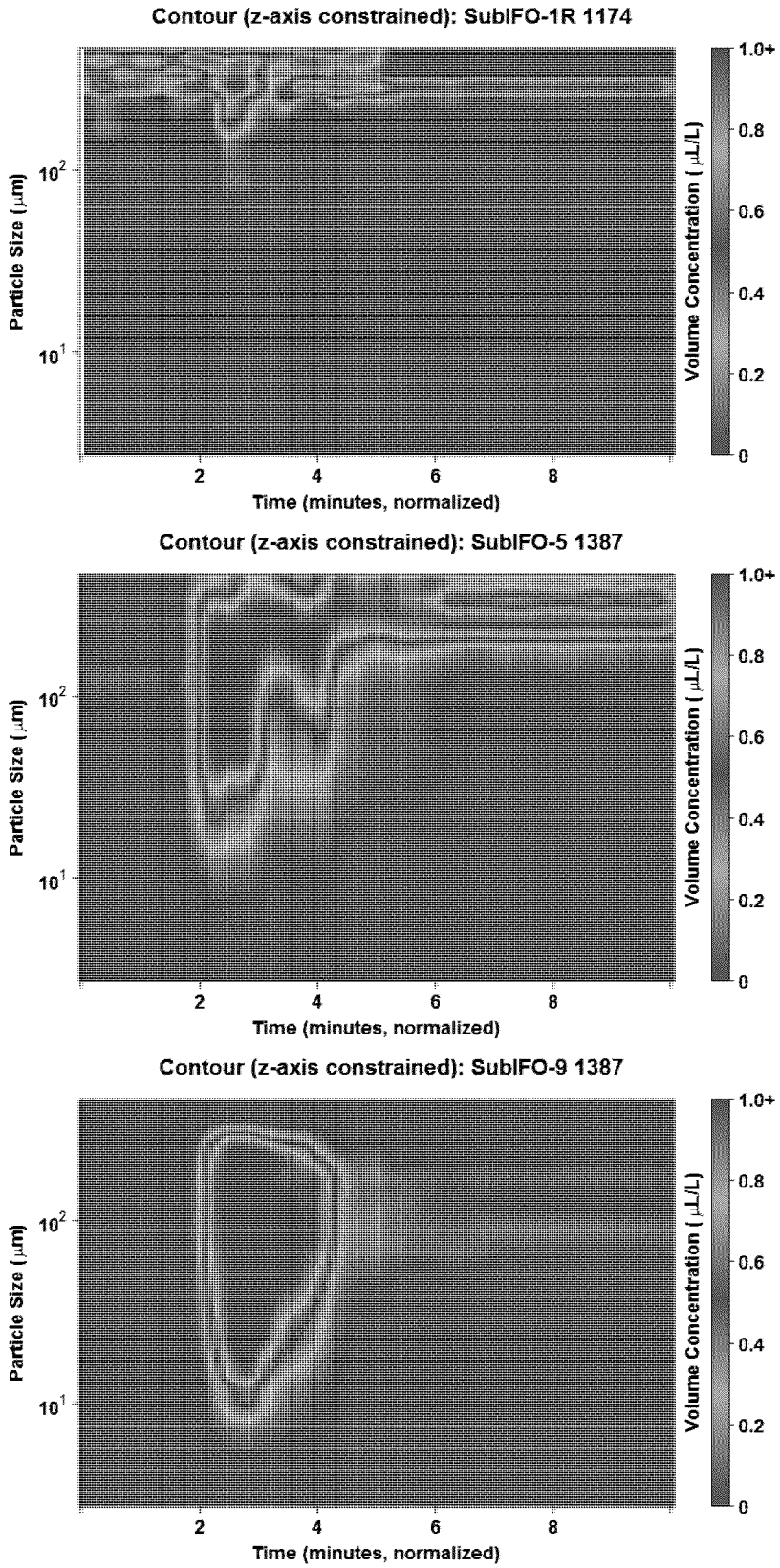

Appendix D - Figure D9. LISST contour plot for IFO-120, no dispersant, cold water experiment.

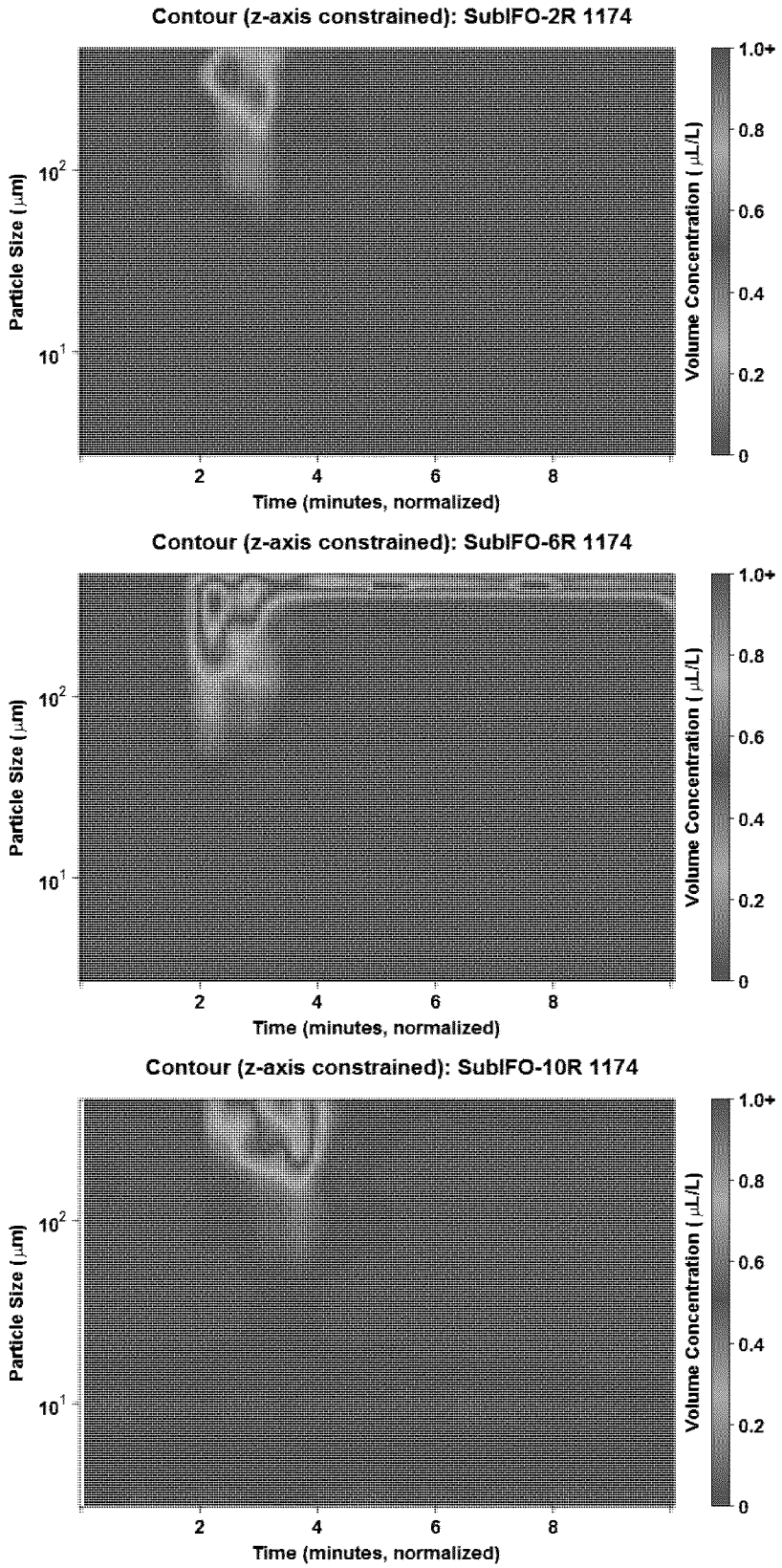

Appendix D - Figure D10. LISST contour plot for IFO-120, DOR 1:200 (Corexit 9500), cold experiment.

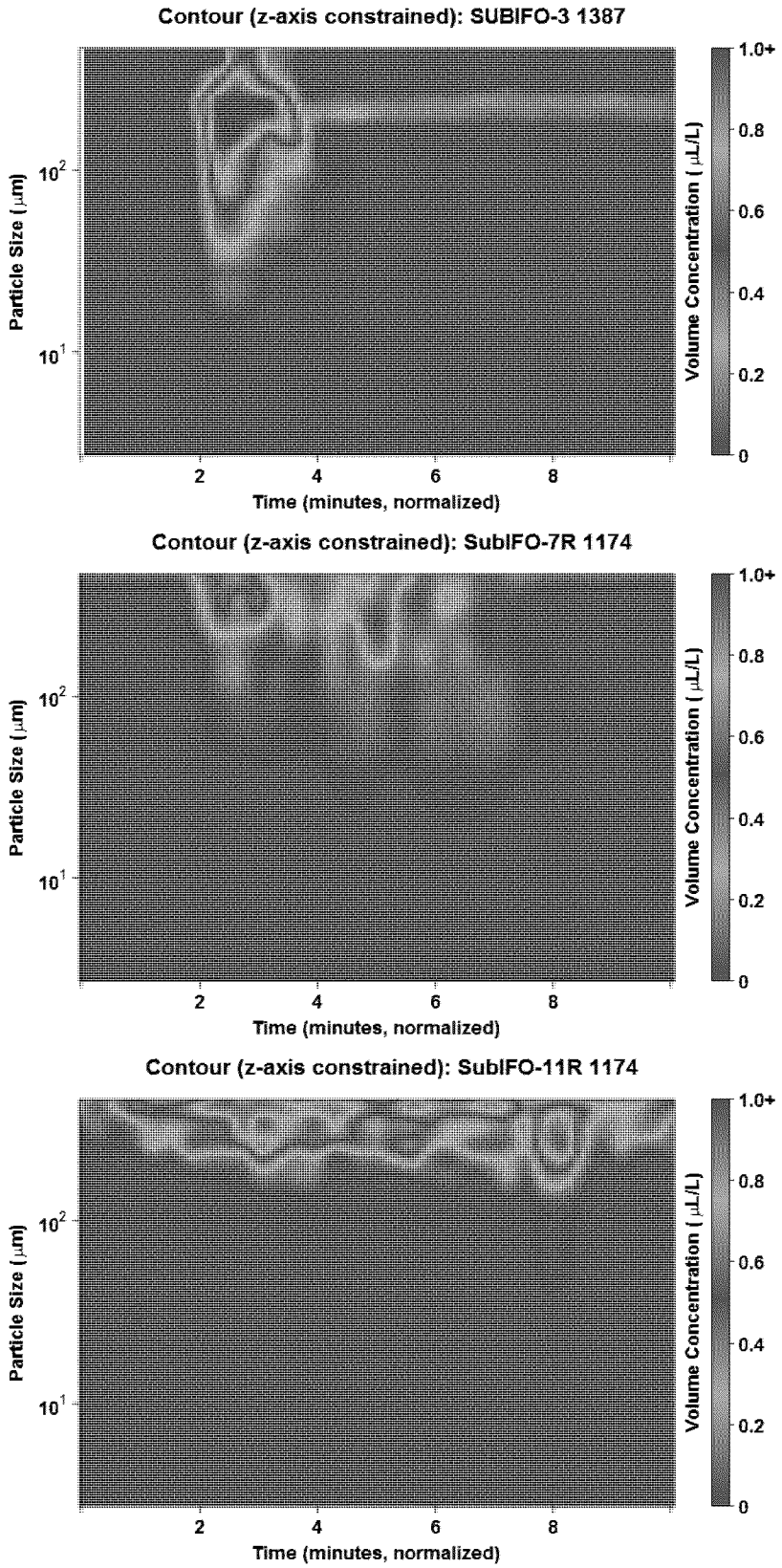

Appendix D - Figure D11. LISST contour plot for IFO-120, DOR 1:100 (Corexit 9500), cold experiment.

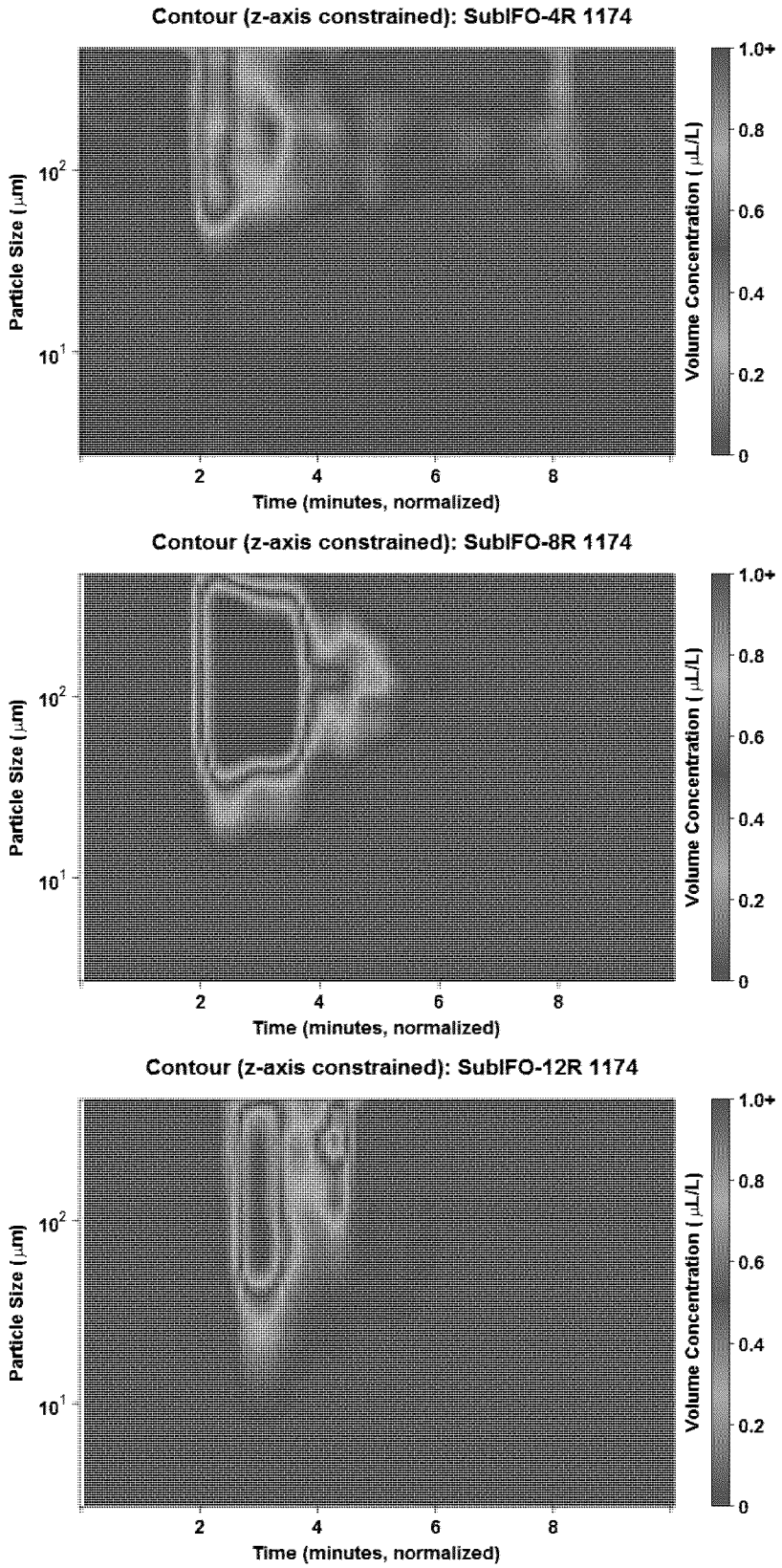

Appendix D - Figure D12. LISST contour plot for IFO-120, DOR 1:20 (Corexit 9500), cold experiment.

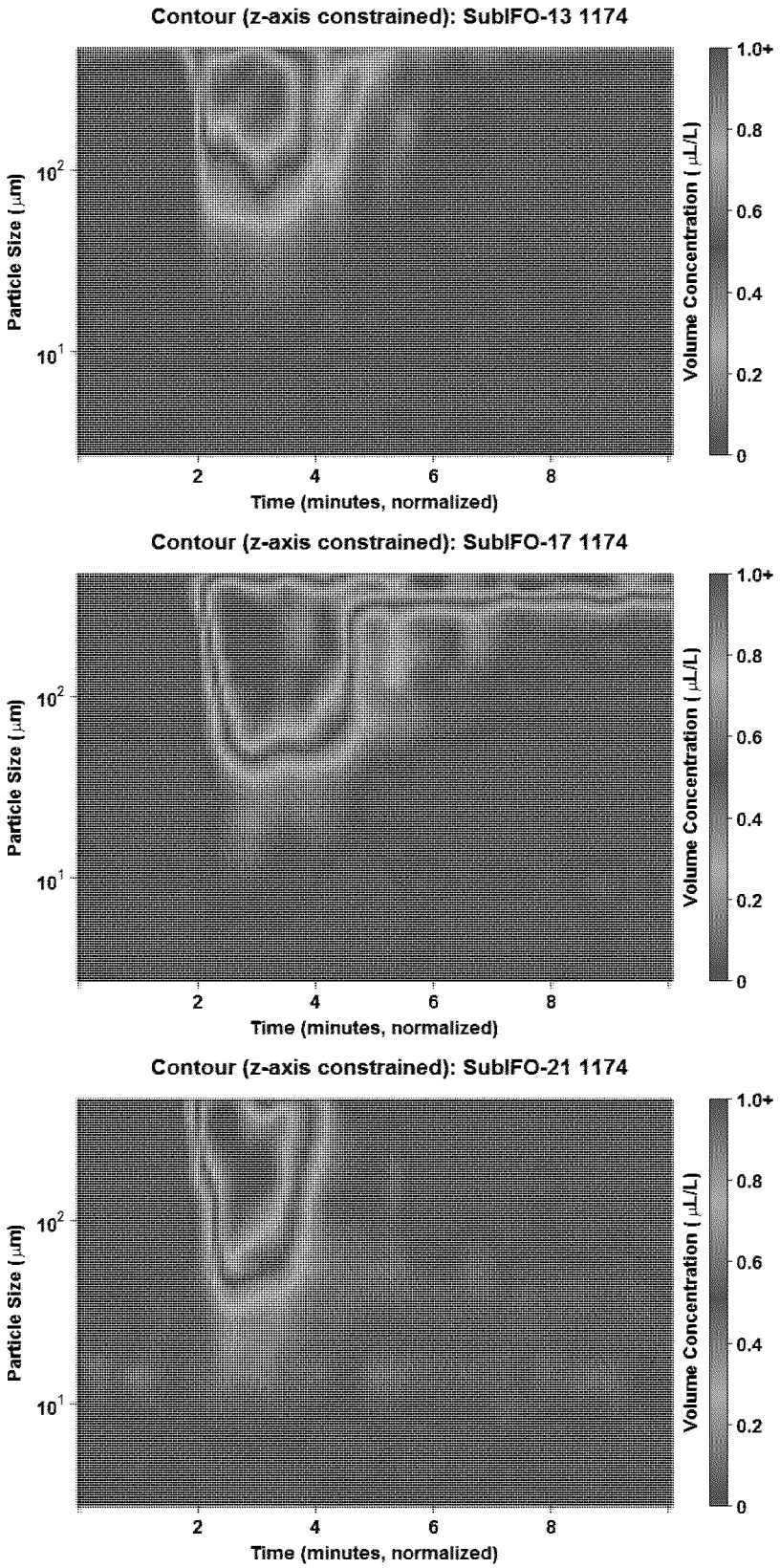

ED_001324_00000687-00063

Appendix D - Figure D13. LISST contour plot for IFO-120, no dispersant, warm water experiment.

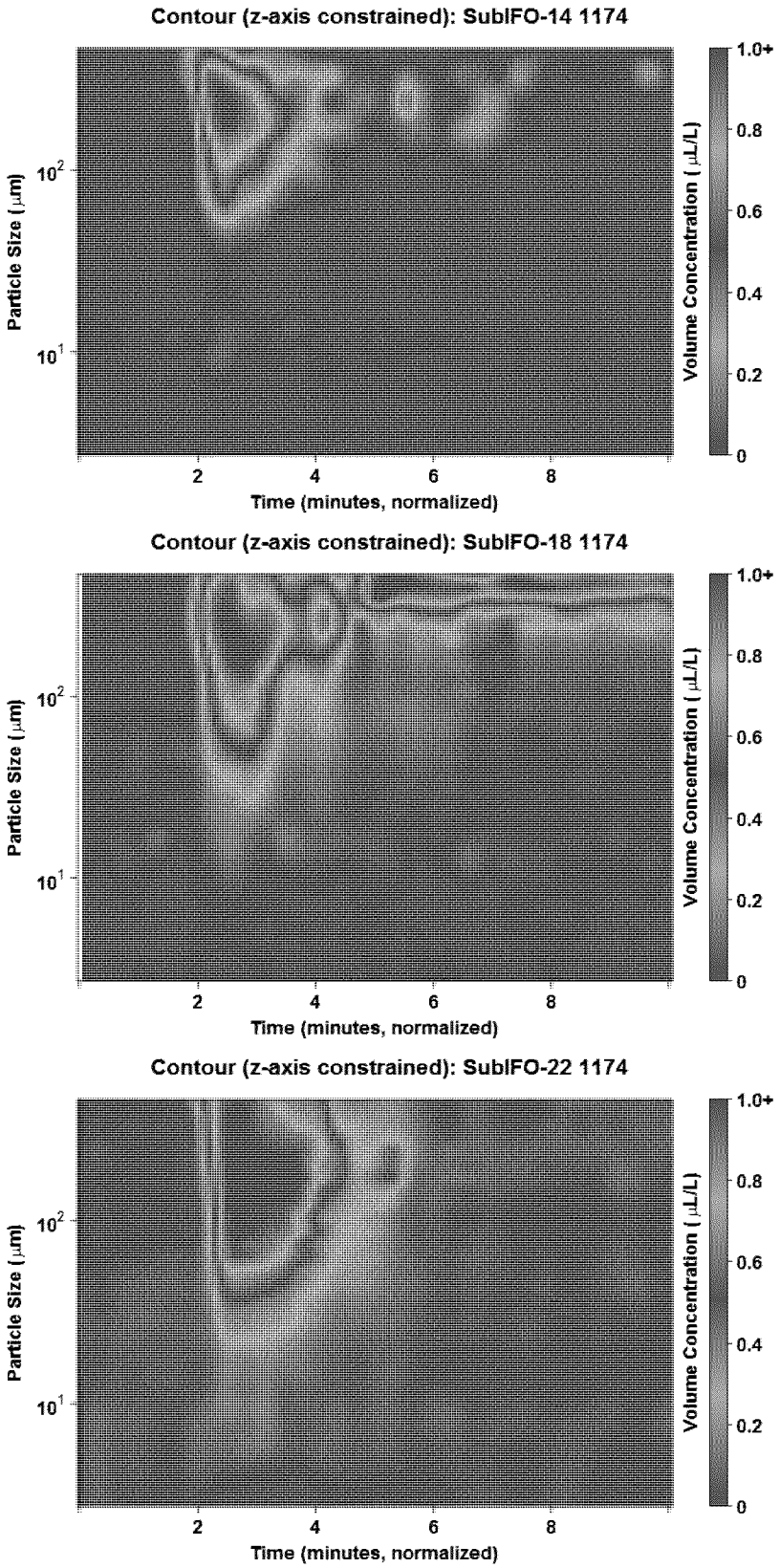

Appendix D - Figure D14. LISST contour plot for IFO-120, DOR 1:200 (Corexit 9500), warm experiment.

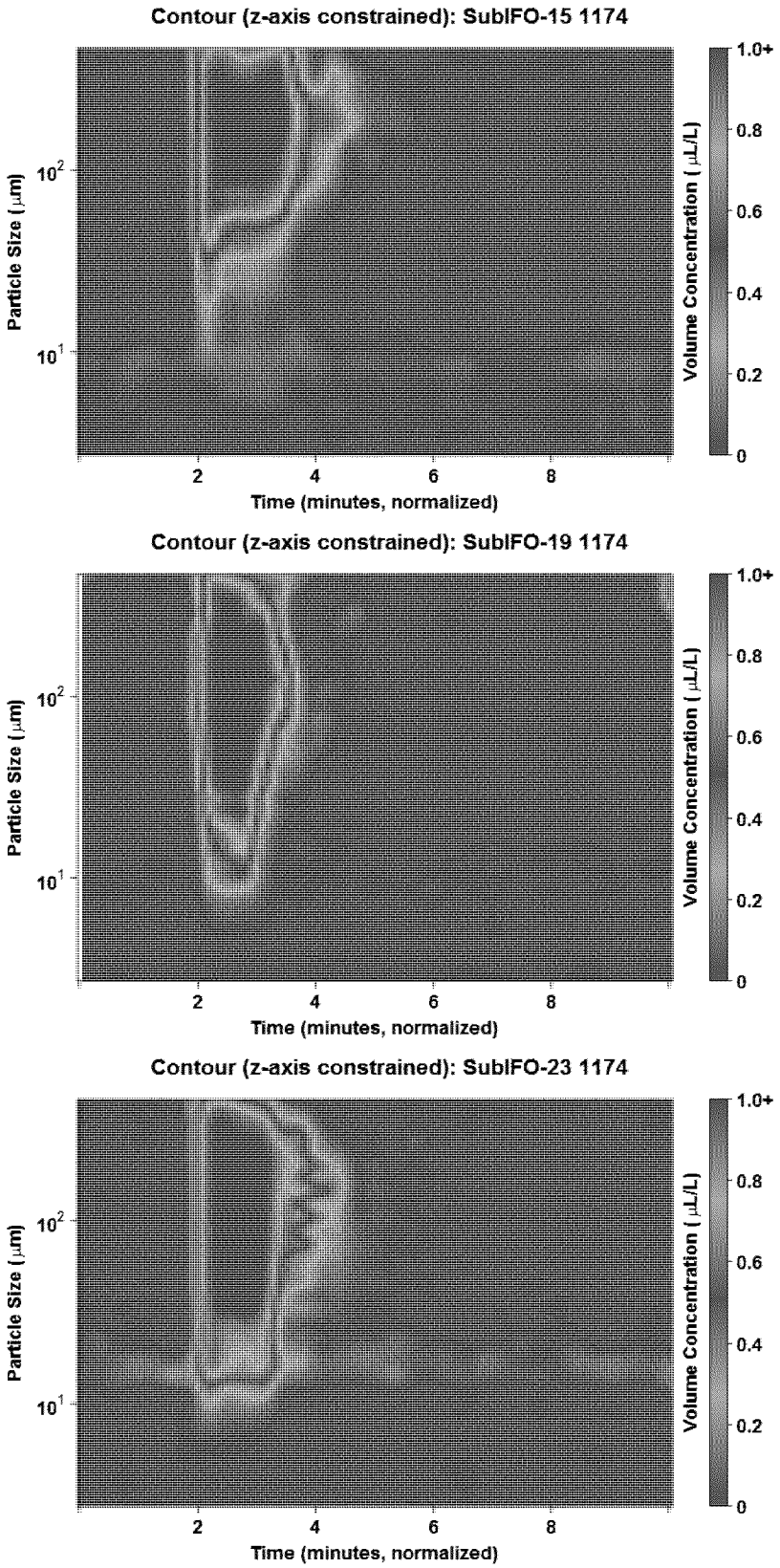

Appendix D - Figure D15. LISST contour plot for IFO-120, DOR 1:100 (Corexit 9500), warm experiment.

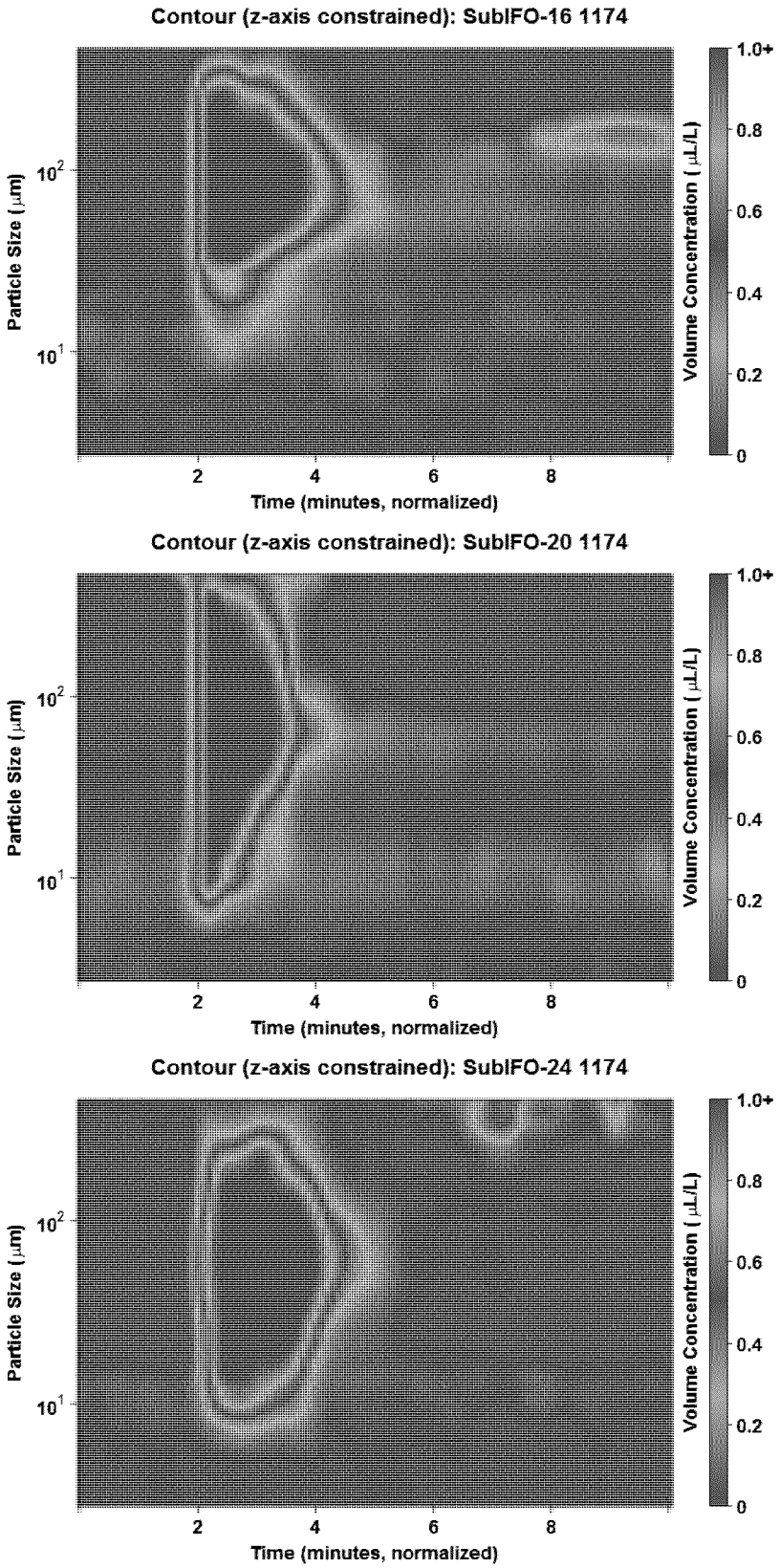

Appendix D - Figure D16. LISST contour plot for IFO-120, DOR 1:20 (Corexit 9500), warm experiment.

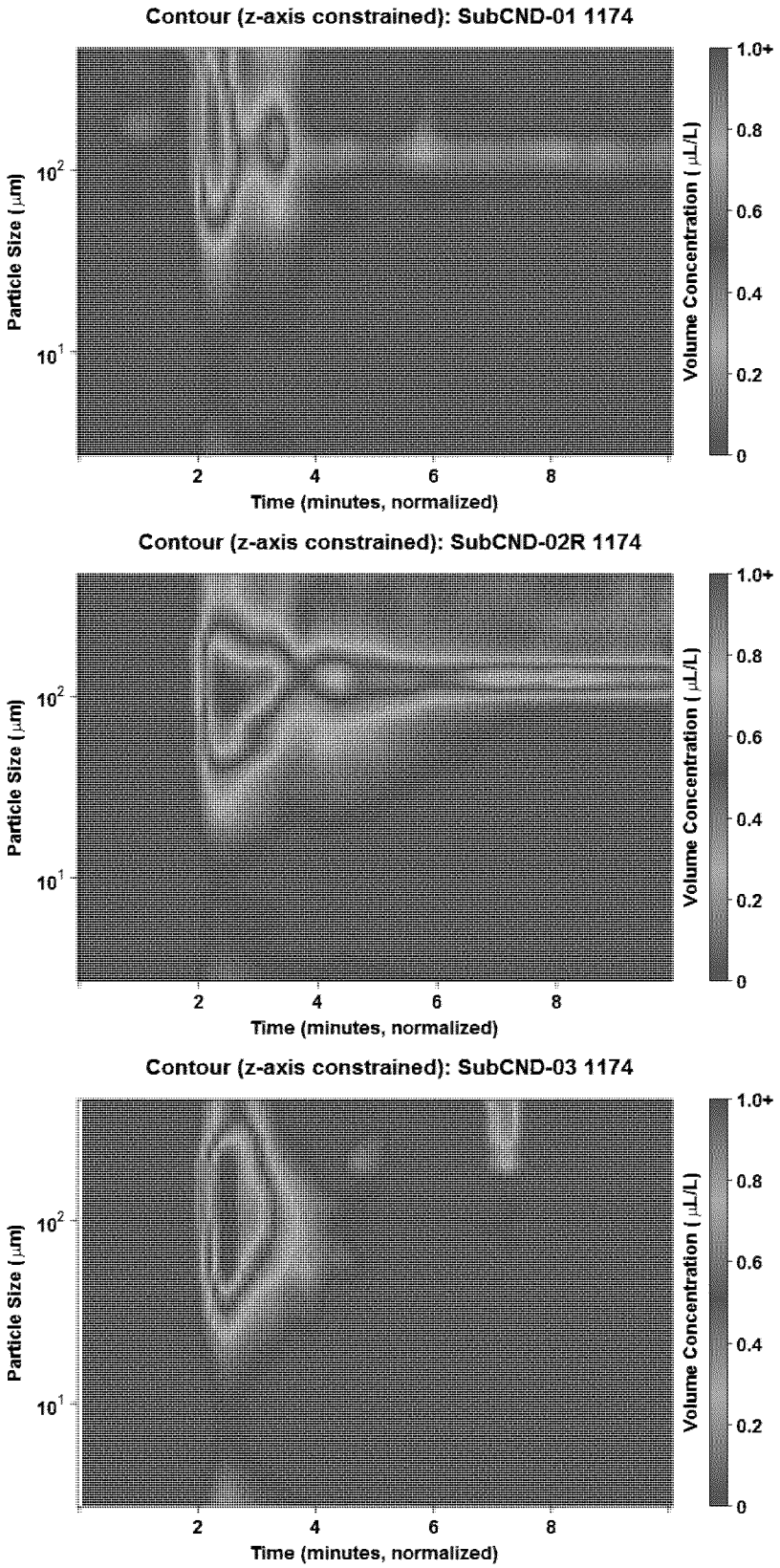

Appendix D - Figure D17. LISST contour plot for Gas Condensate, no dispersant.

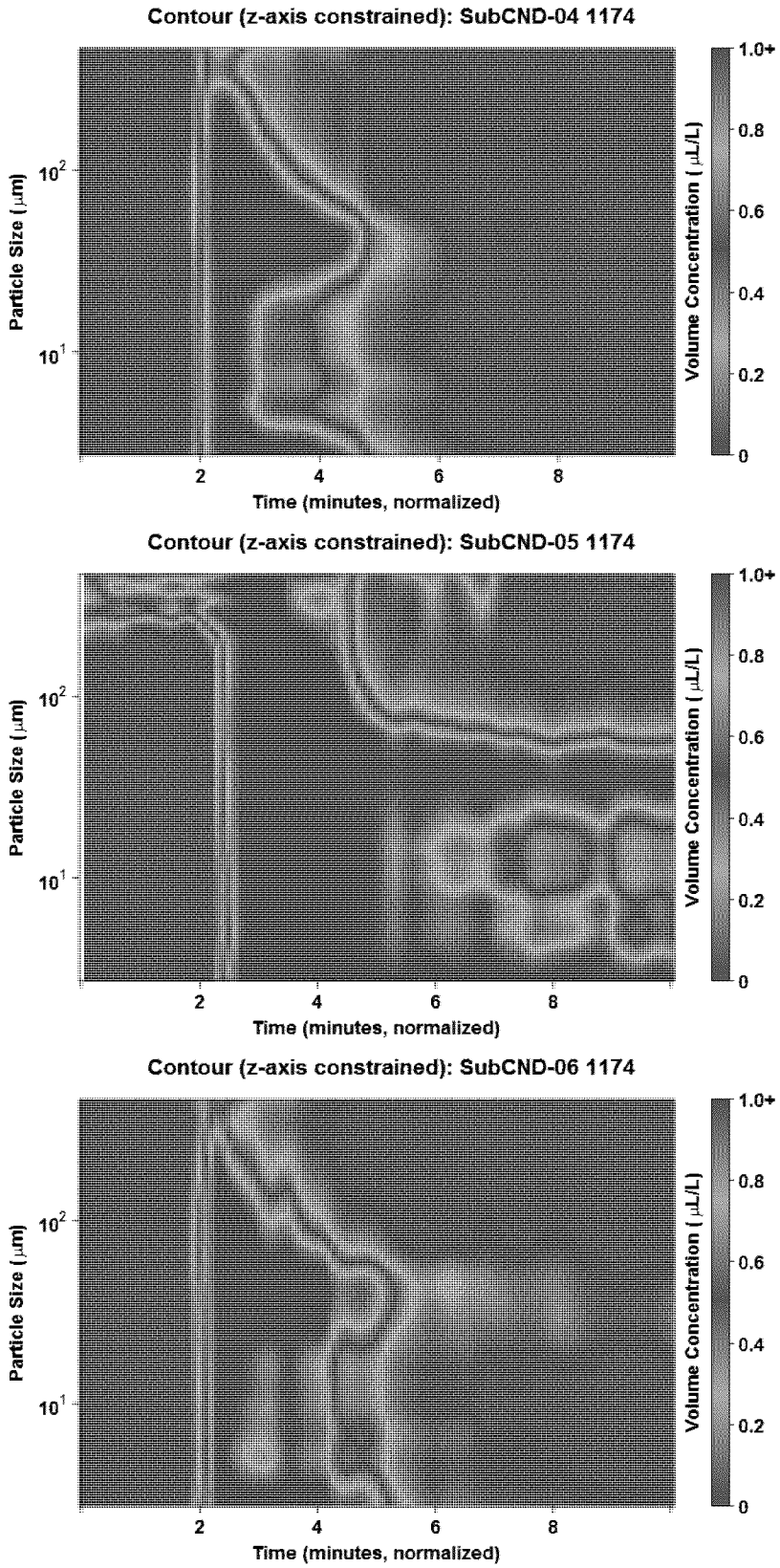

ED_001324_00000687-00068

Appendix D - Figure D18. LISST contour plot for Gas Condensate, DOR 1:20 (Corexit 9500).

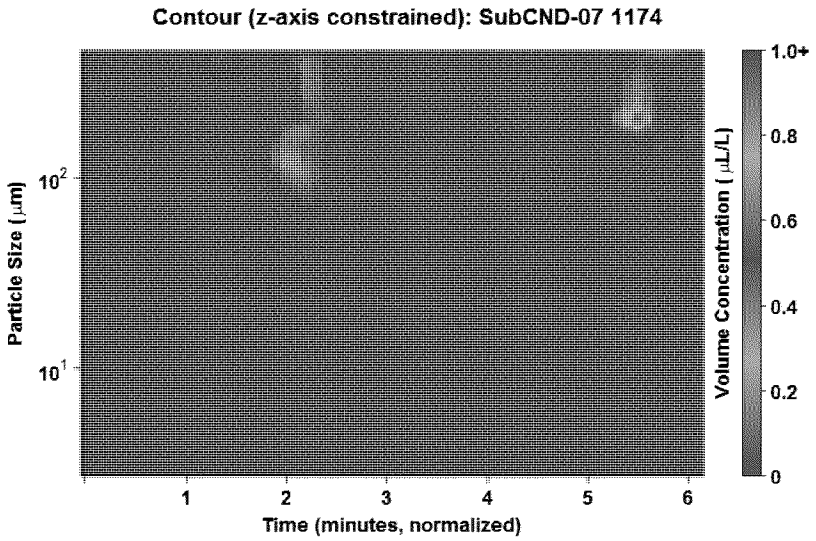

Appendix D - Figure D19. LISST contour plot for air injection, no dispersant.

ED_001324_00000687-00069

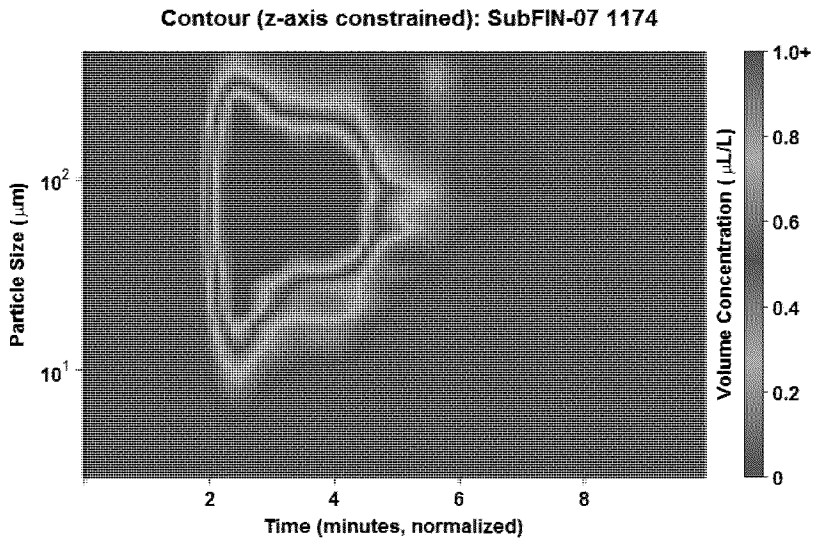

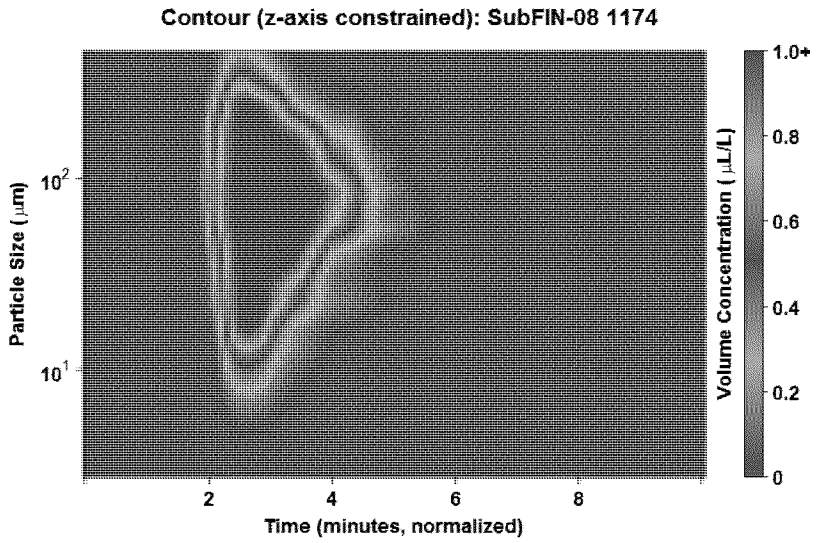

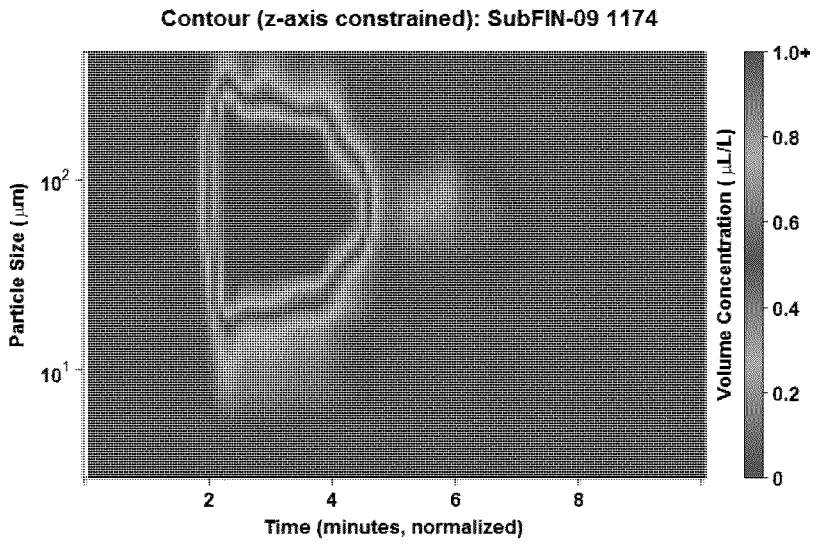

Appendix D - Figure D20. LISST contour plot for ANS, DOR 1:200 (Finasol OSR 52), warm experiment.

ED_001324_00000687-00070

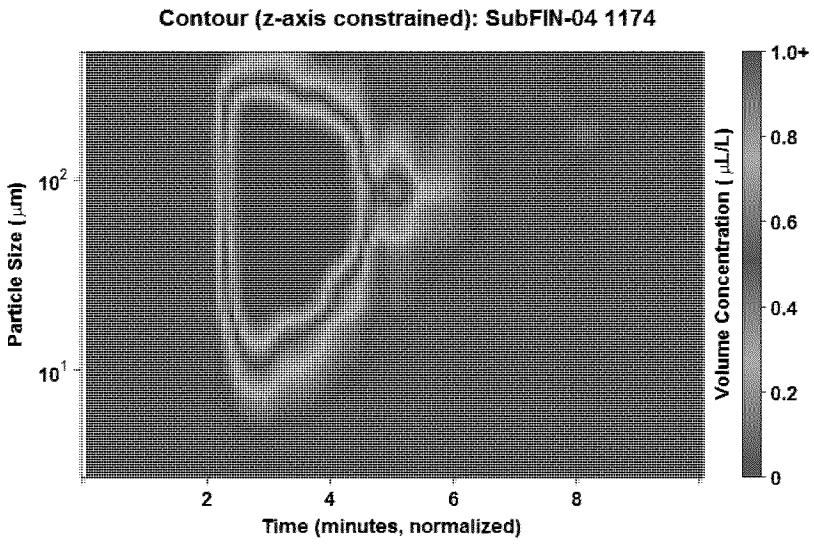

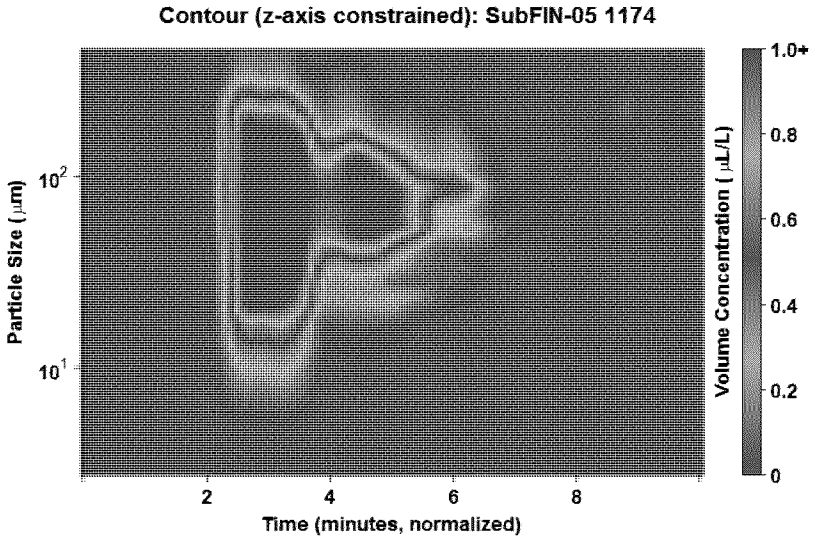

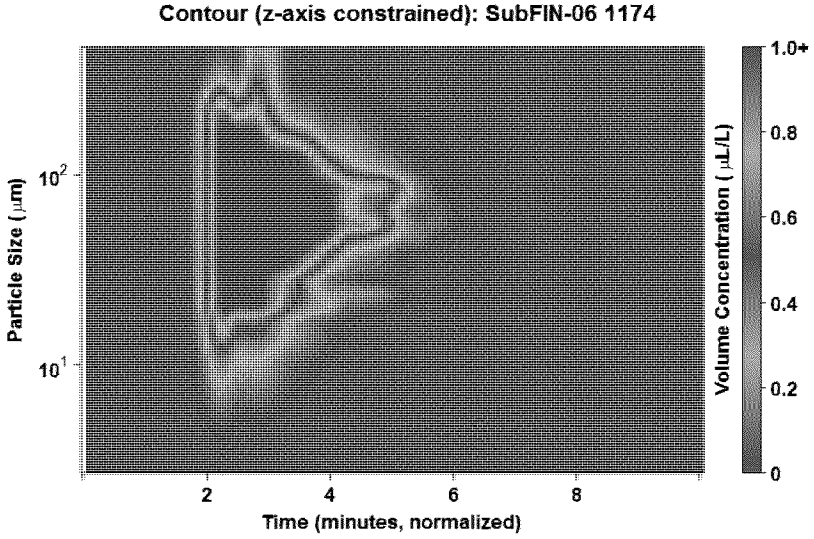

Appendix D - Figure D21. LISST contour plot for ANS, DOR 1:100 (Finasol OSR 52), warm experiment.

ED_001324_00000687-00071

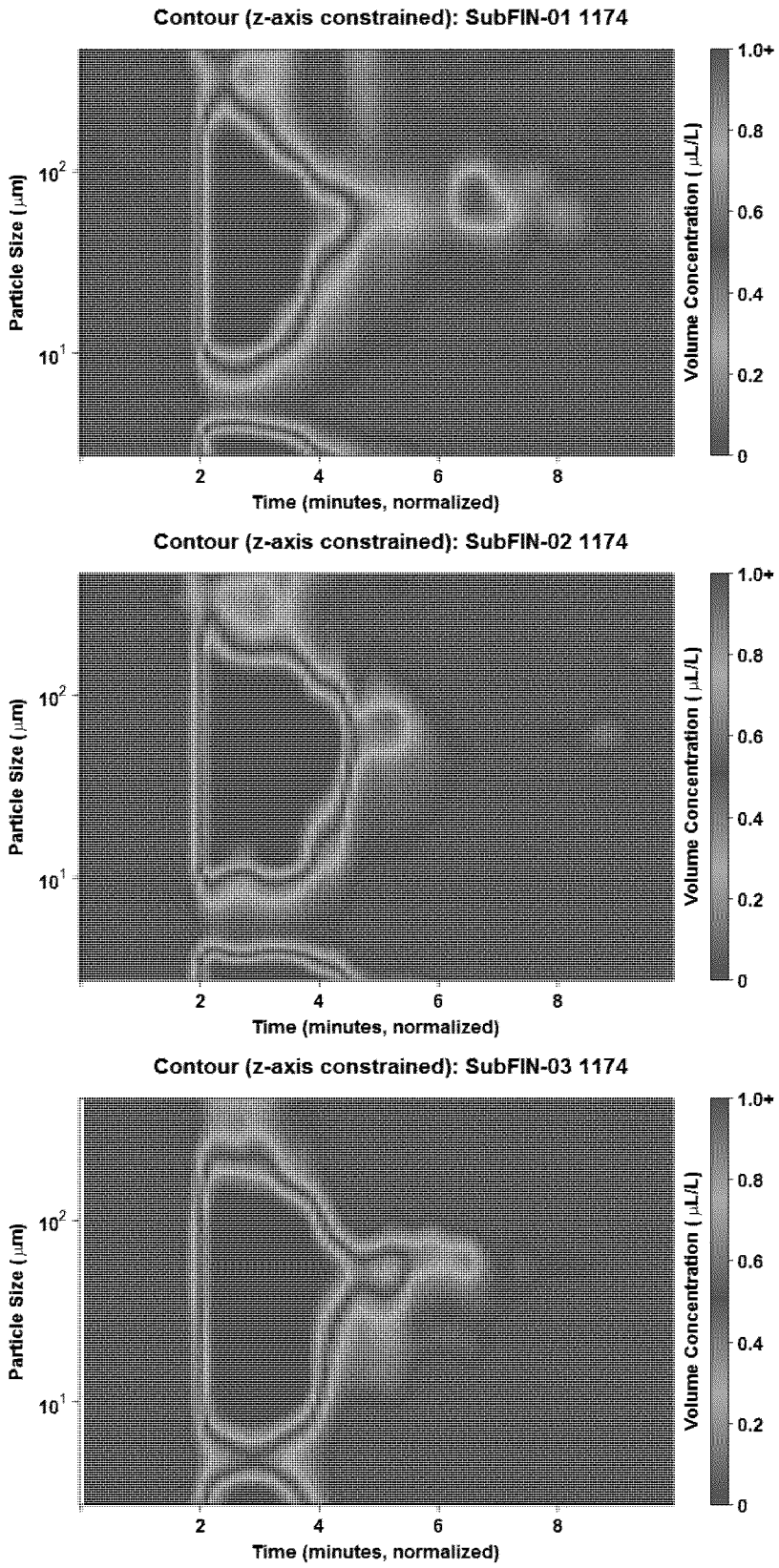

Appendix D - Figure D22. LISST contour plot for ANS, DOR 1:20 (Finasol OSR 52), warm experiment.

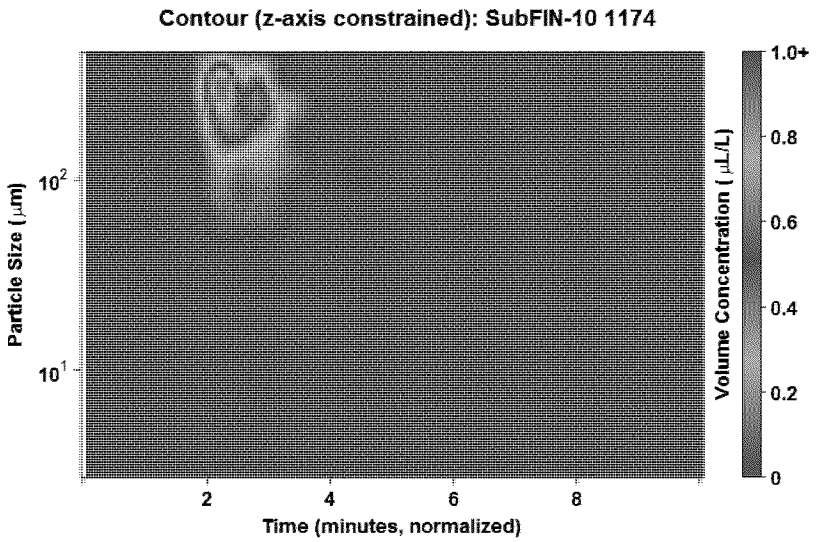

Appendix D - Figure D23. LISST contour plot for IFO-120, DOR 1:200 (Finasol OSR 52), warm experiment.

ED_001324_00000687-00073

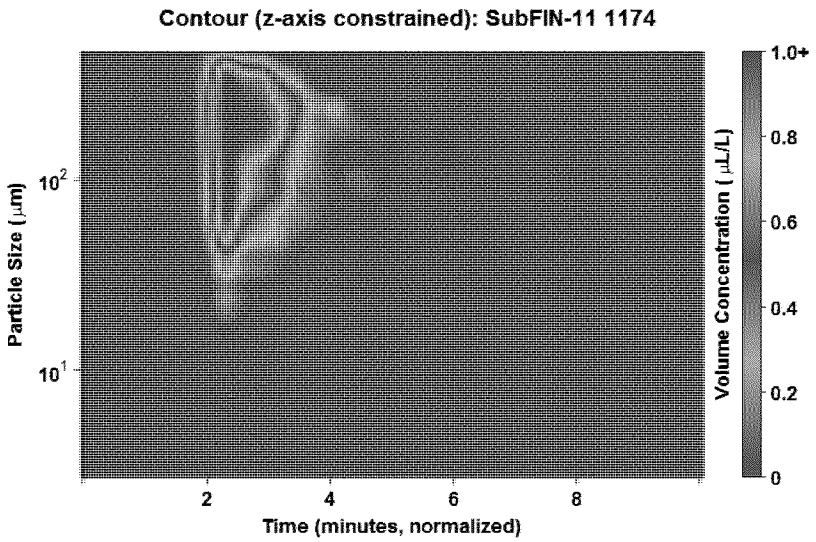

Appendix D - Figure D24. LISST contour plot for IFO-120, DOR 1:100 (Finasol OSR 52), warm experiment.

ED_001324_00000687-00074

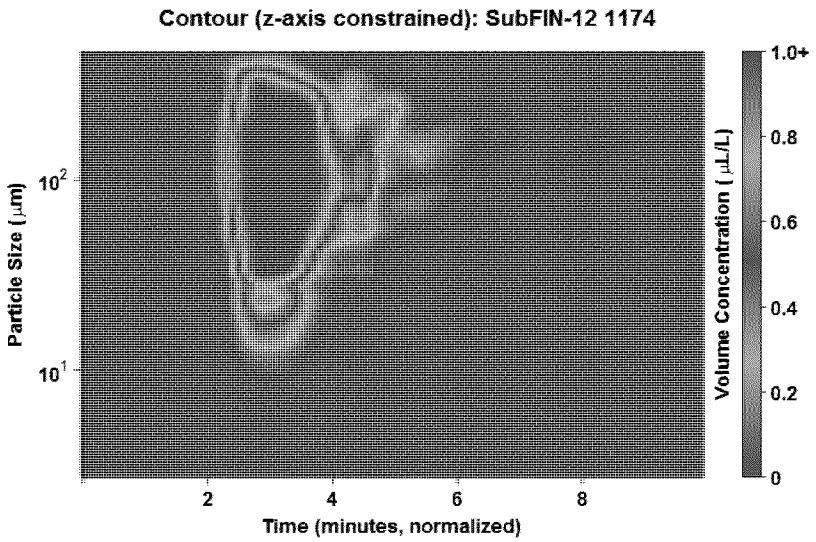

Appendix D - Figure D25. LISST contour plot for IFO-120, DOR 1:20 (Finasol OSR 52), warm experiment.

ED_001324_00000687-00075

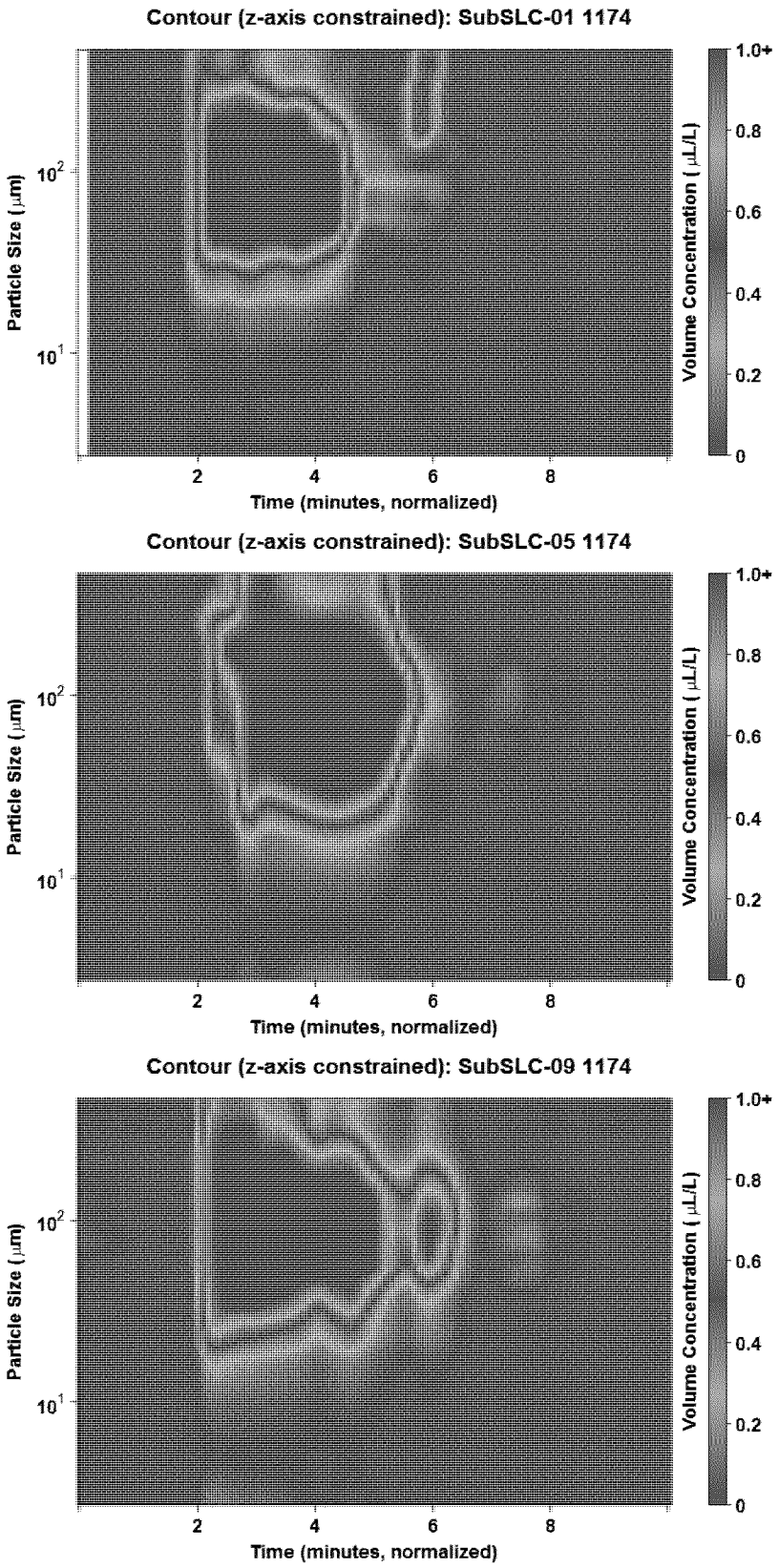

Appendix D - Figure D26. LISST contour plot for SLC, no dispersant, warm water experiment.

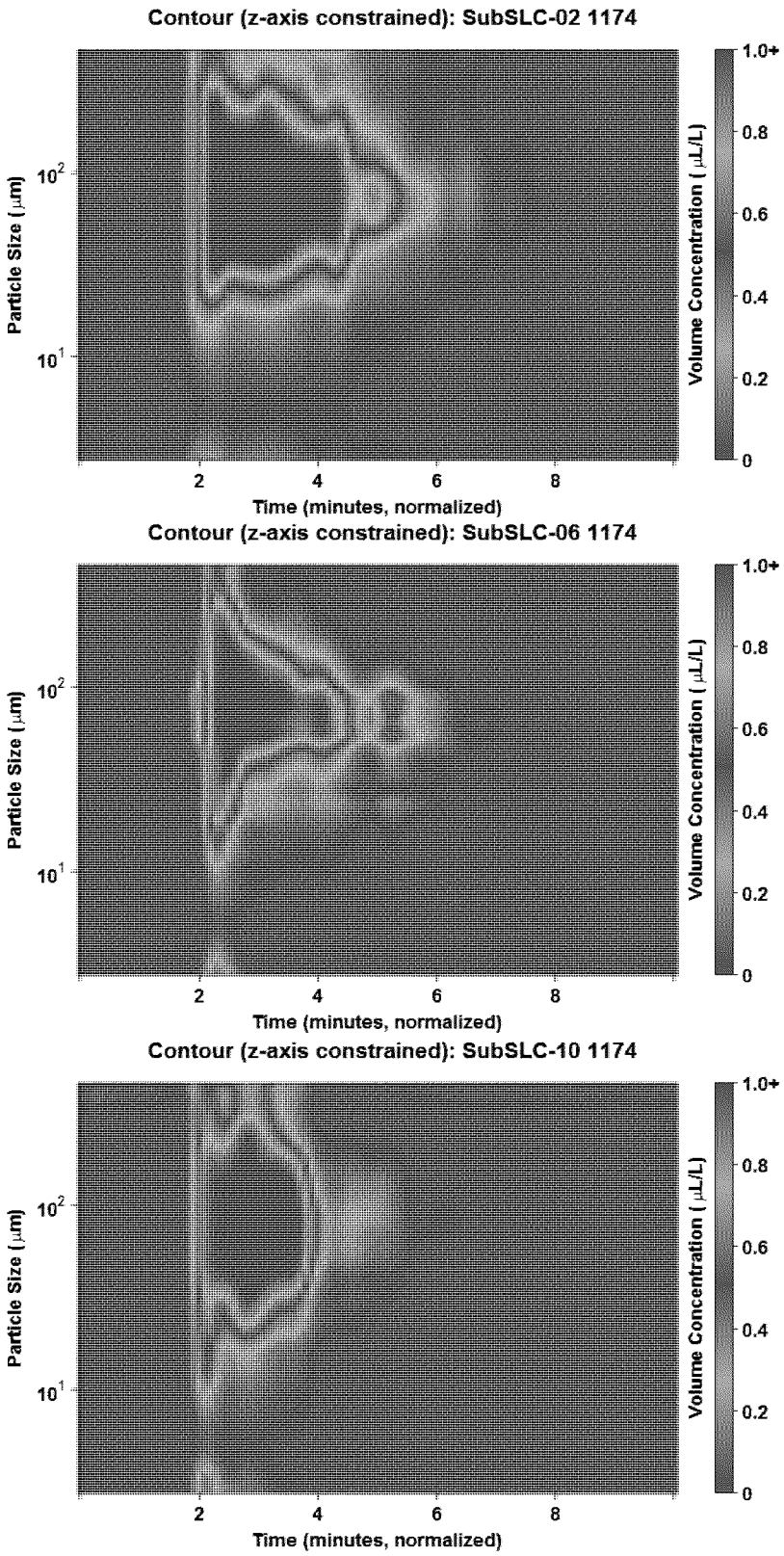

Appendix D - Figure D27. LISST contour plot for SLC, DOR 1:200 (Corexit 9500), warm water experiment.

ED_001324_00000687-00077

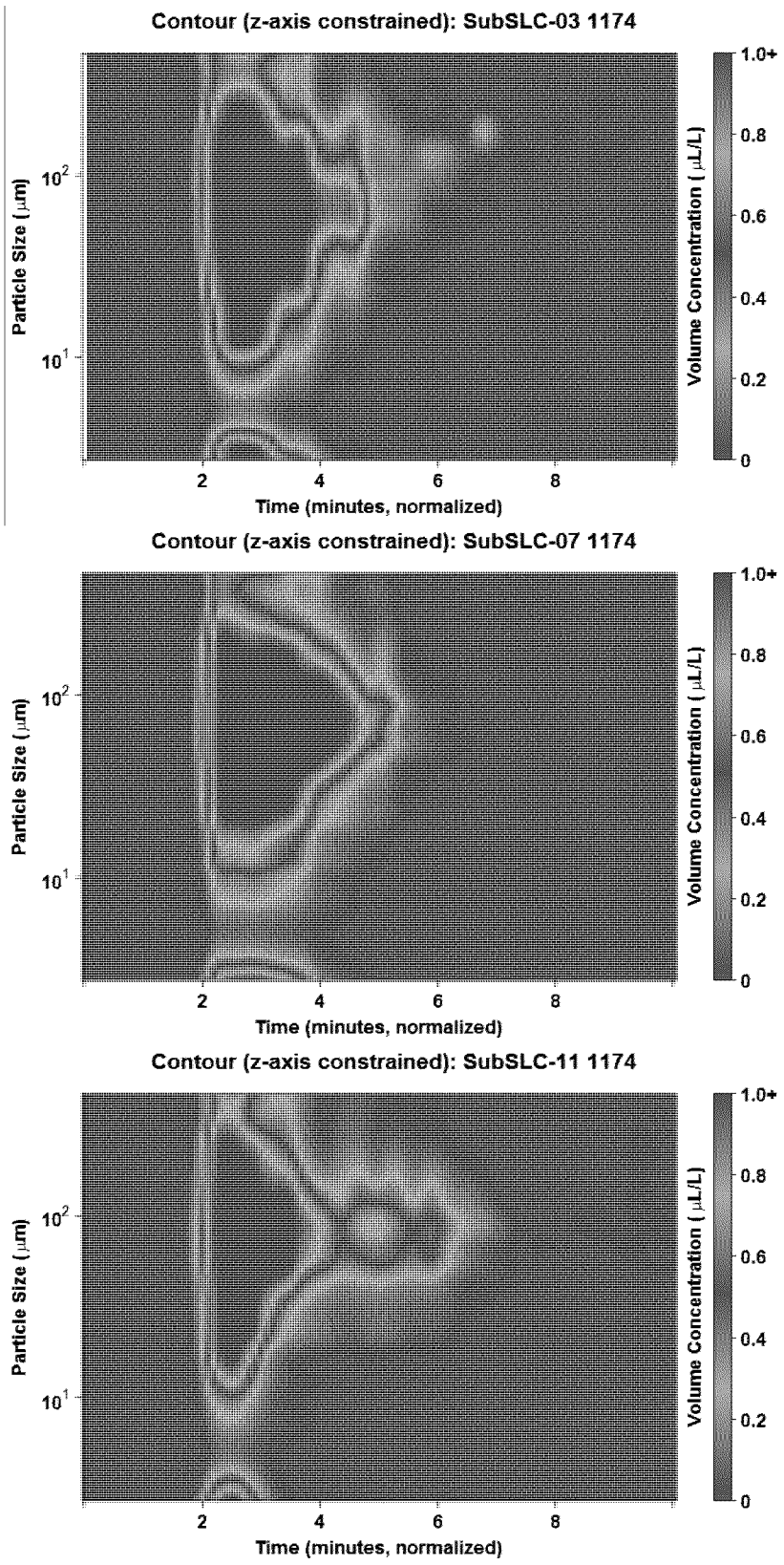

Appendix D - Figure D28. LISST contour plot for SLC, DOR 1:100 (Corexit 9500), warm experiment.

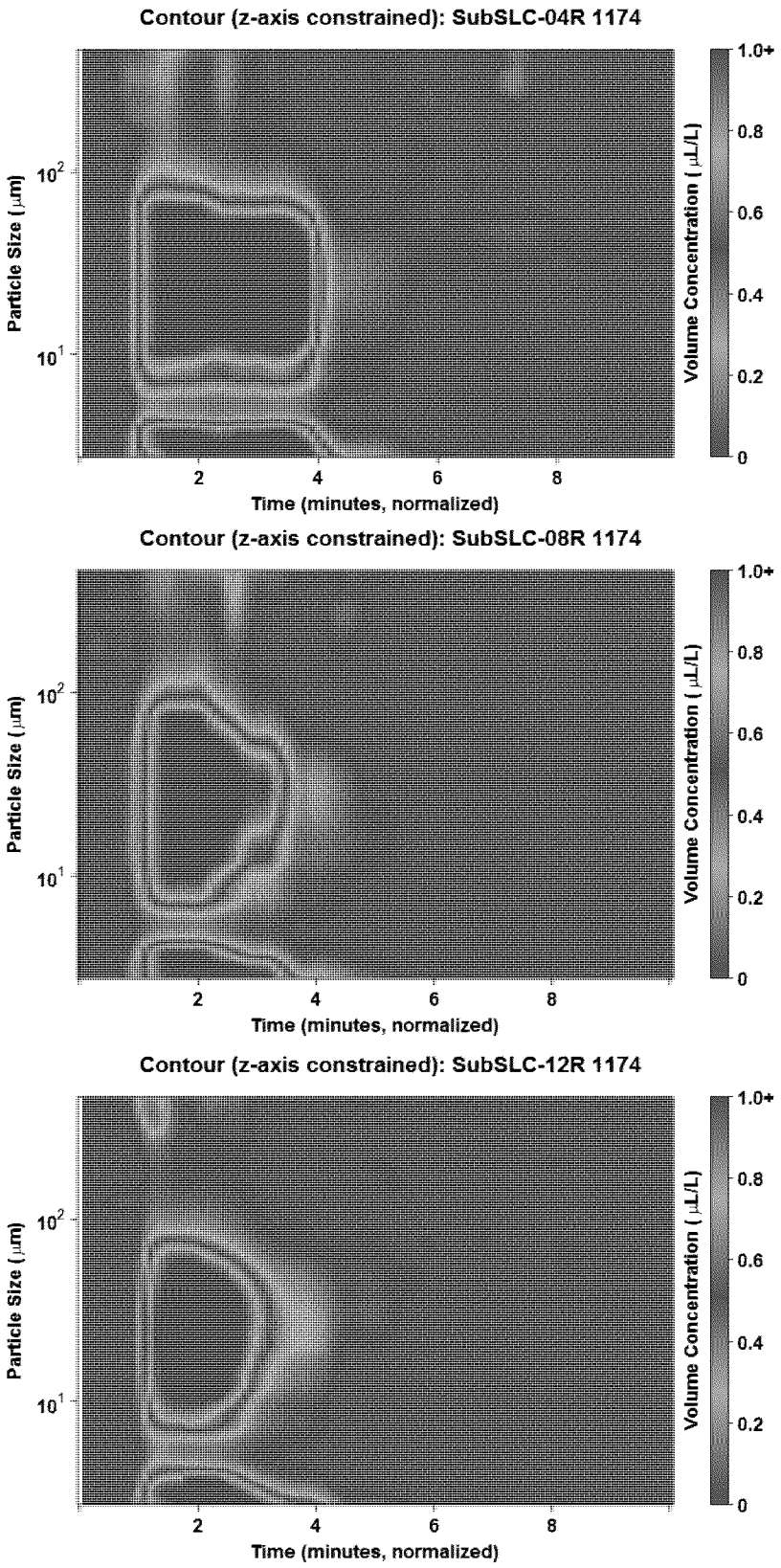

Appendix D - Figure D29. LISST contour plot for SLC, DOR 1:20 (Corexit 9500), warm water experiment.

APPENDIX E – Submersible Fluorescence Time Series

ED_001324_00000687-00080

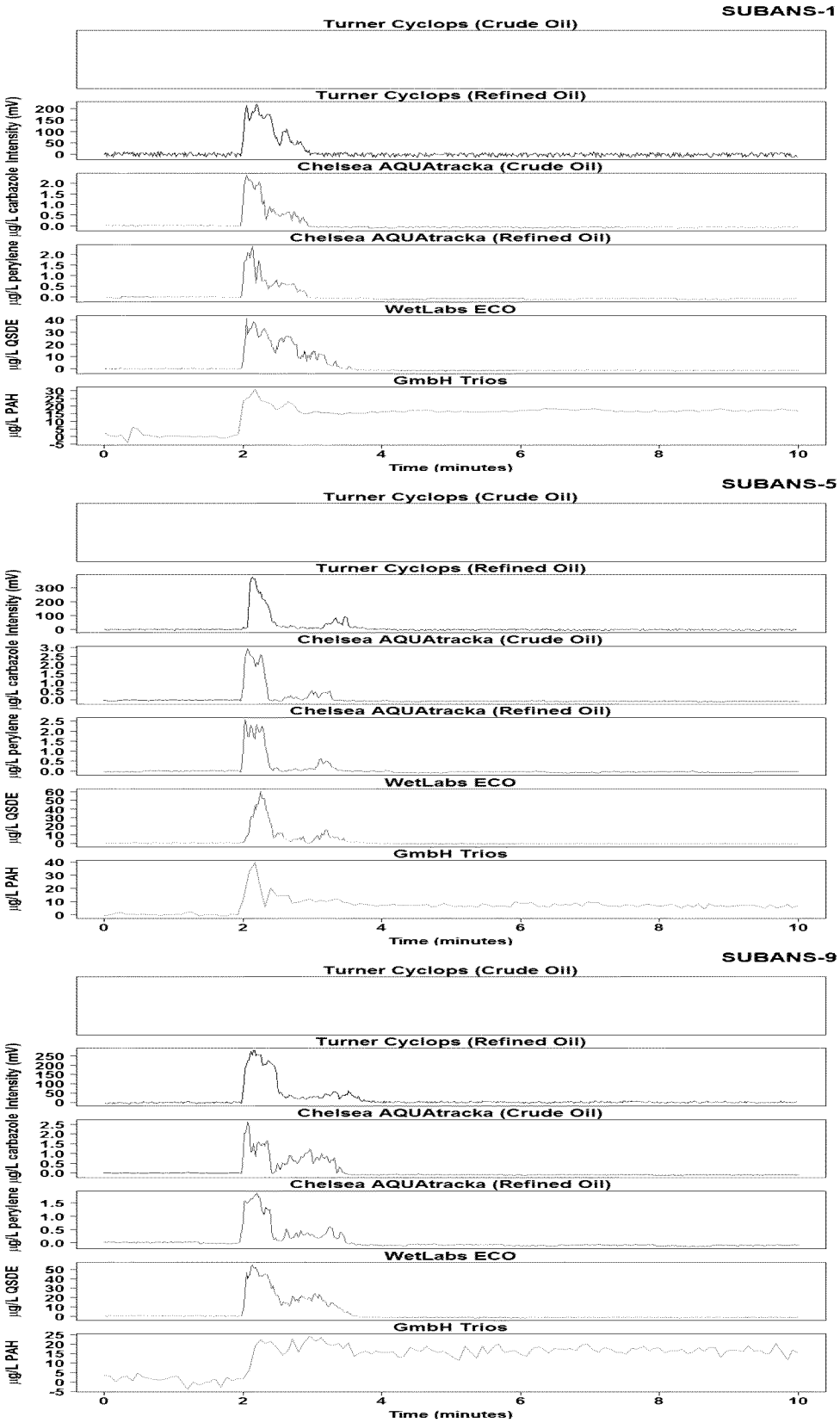

Appendix E - Figure E1. Raw in-situ fluorometer signal for ANS, no dispersant, cold experiment.

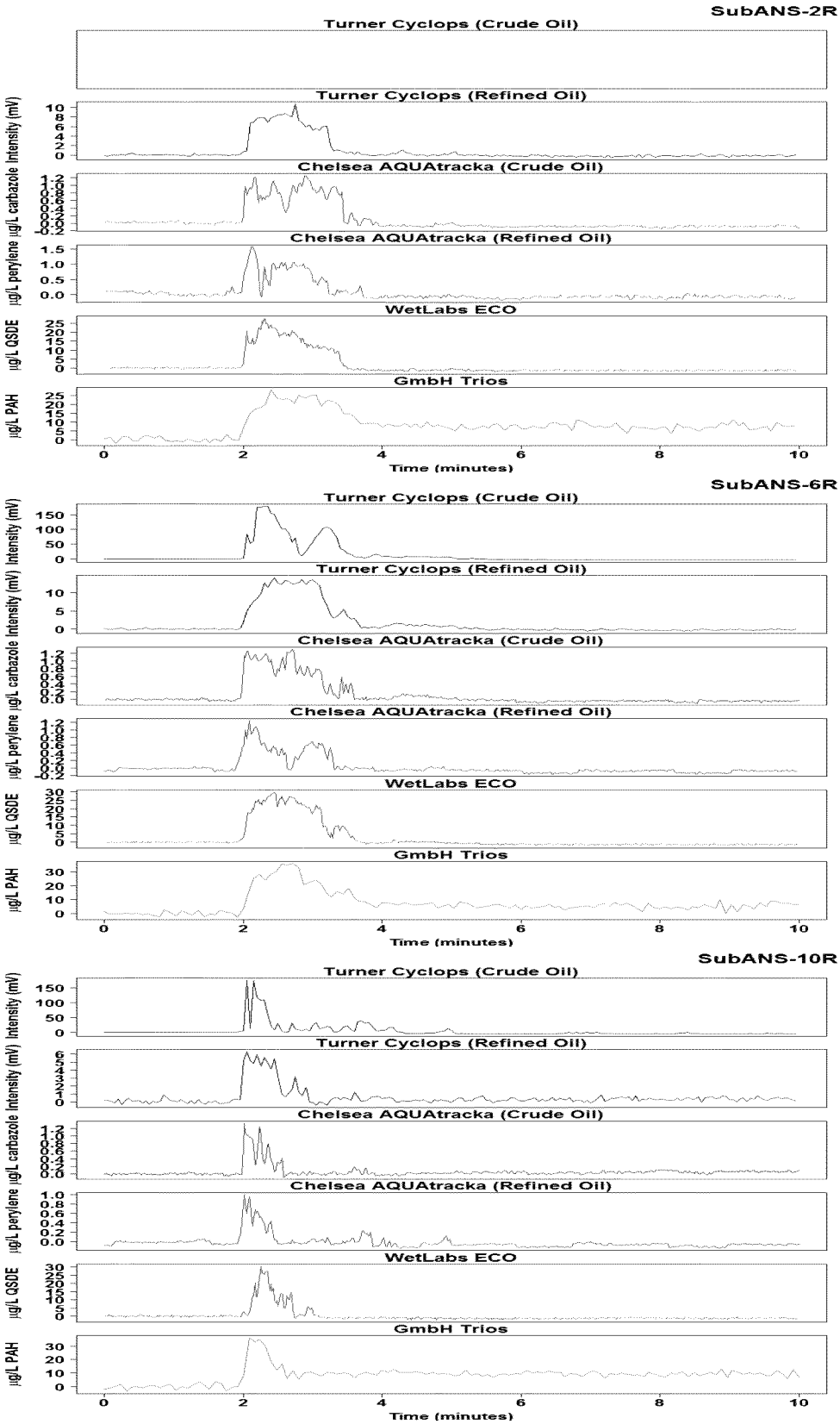

Appendix E - Figure E2. Raw in-situ fluorometer signal for ANS, DOR 1:200 (Corexit 9500), cold expt.

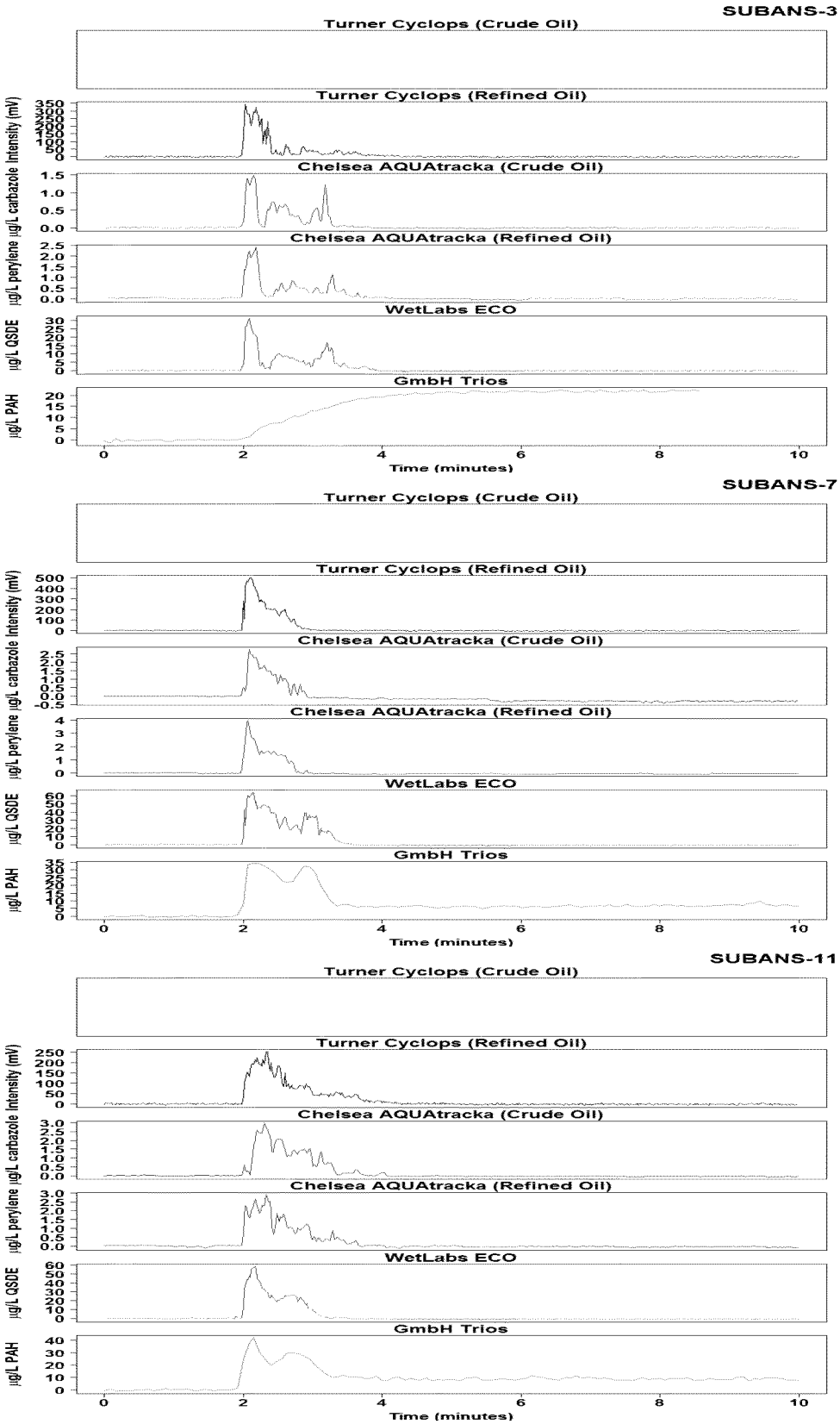

Appendix E - Figure E3. Raw in-situ fluorometer signal for ANS, DOR 1:100 (Corexit 9500), cold expt.

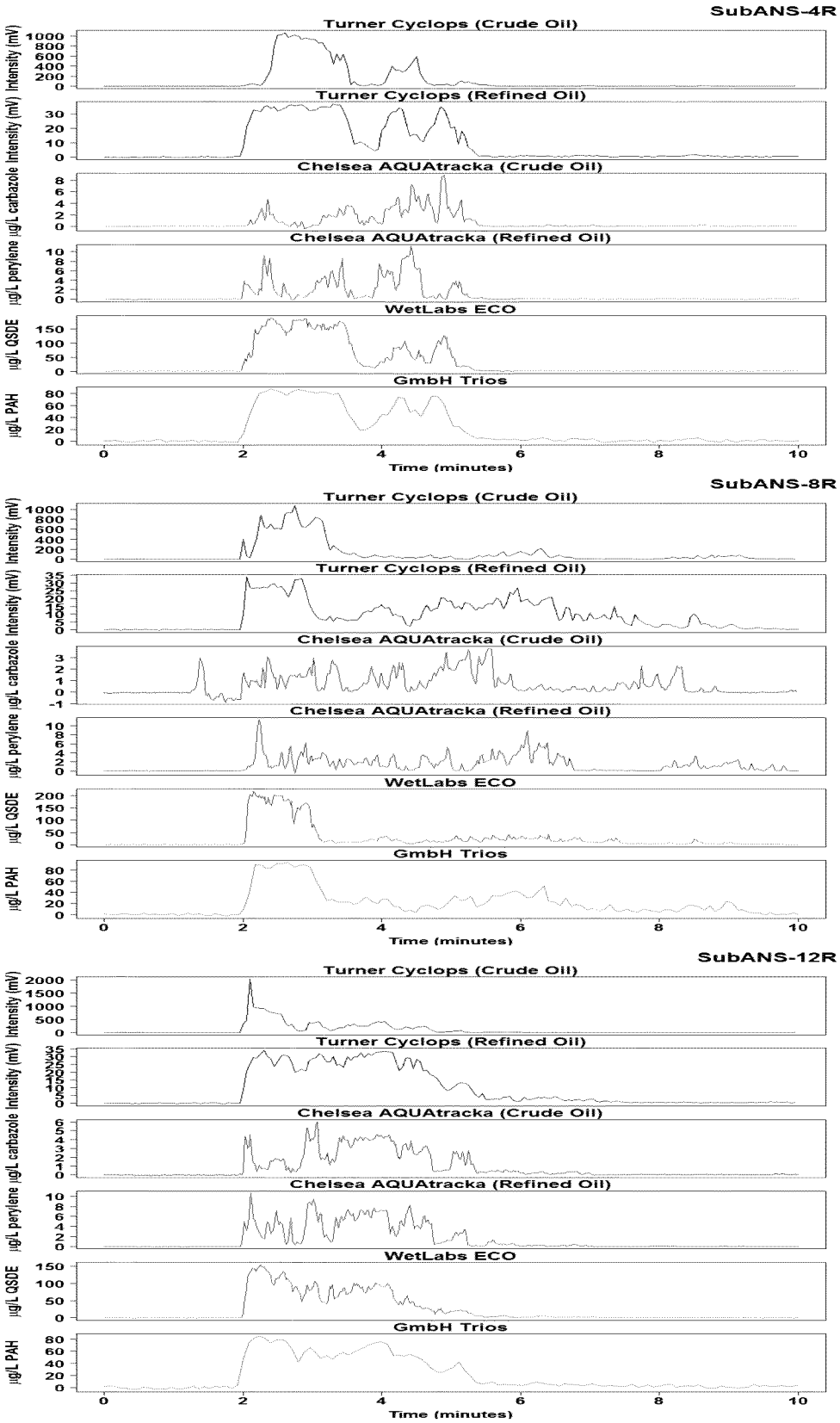

Appendix E - Figure E4. Raw in-situ fluorometer signal for ANS, DOR 1:20 (Corexit 9500), cold expt.

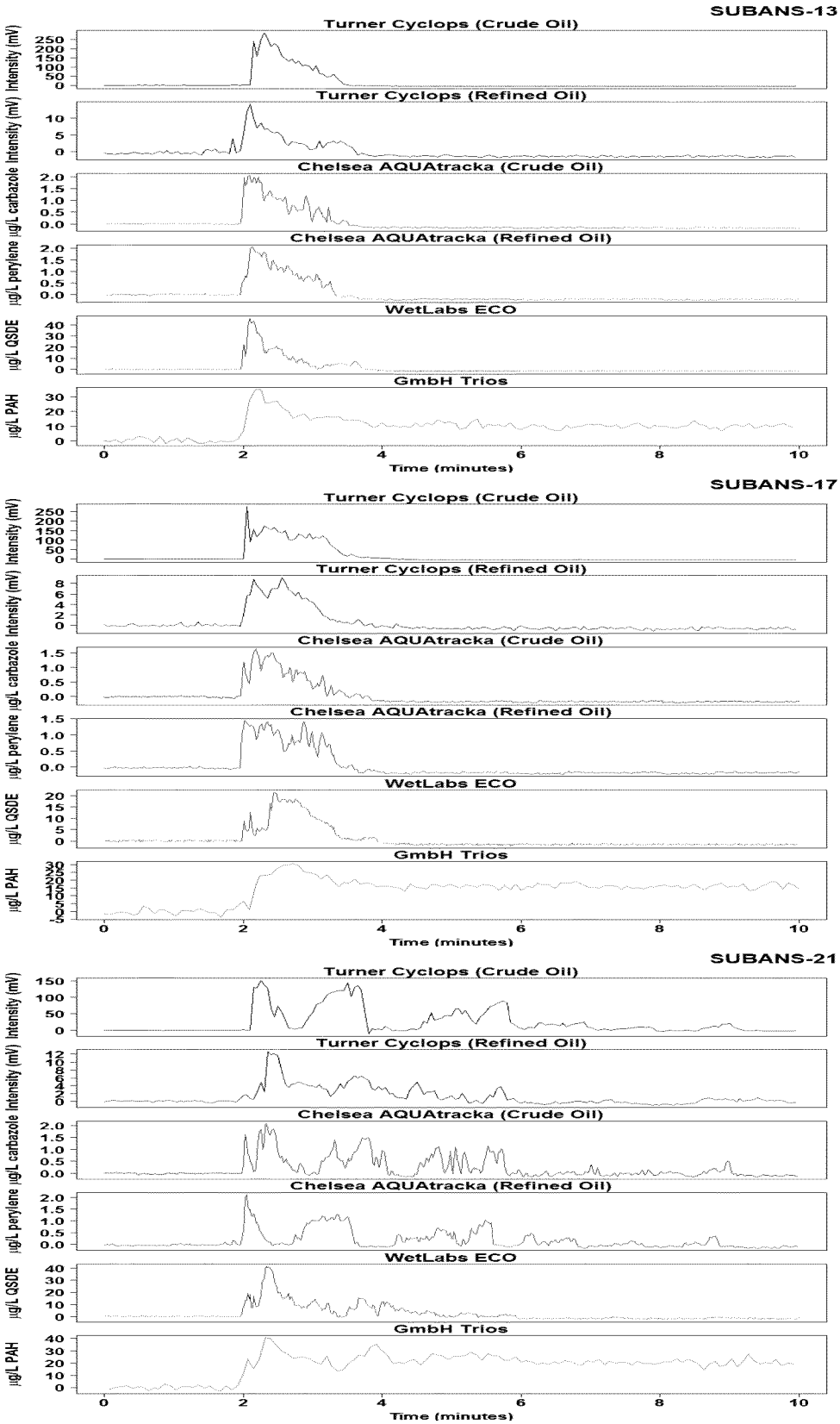

Appendix E - Figure E5. Raw in-situ fluorometer signal for ANS, DOR 0 (Corexit 9500), warm expt.

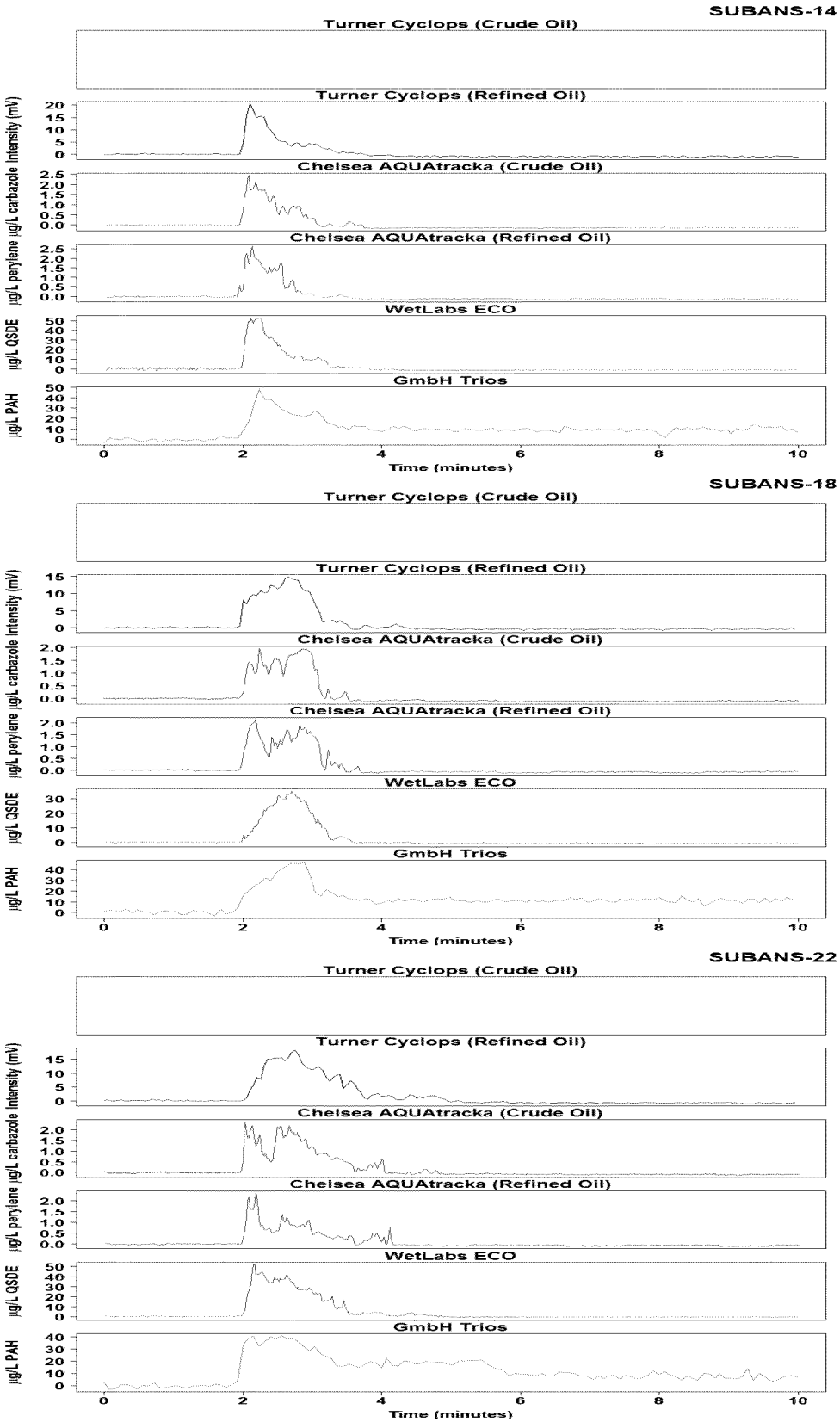

Appendix E - Figure E6. Raw in-situ fluorometer signal for ANS, DOR 1:200 (Corexit 9500), warm expt.

ED_001324_00000687-00086

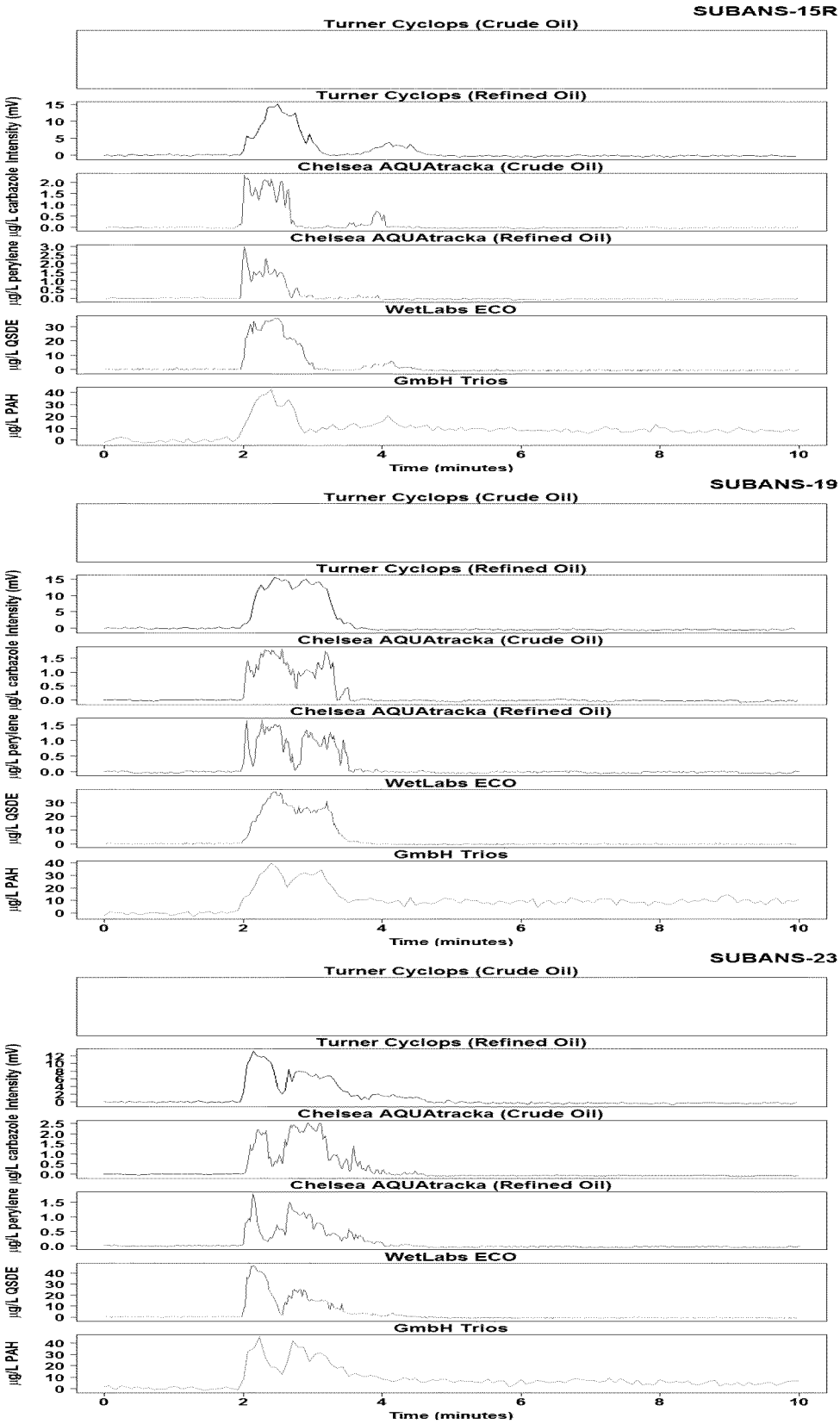

Appendix E - Figure E7. Raw in-situ fluorometer signal for ANS, DOR 1:100 (Corexit 9500), warm expt.

ED_001324_00000687-00087

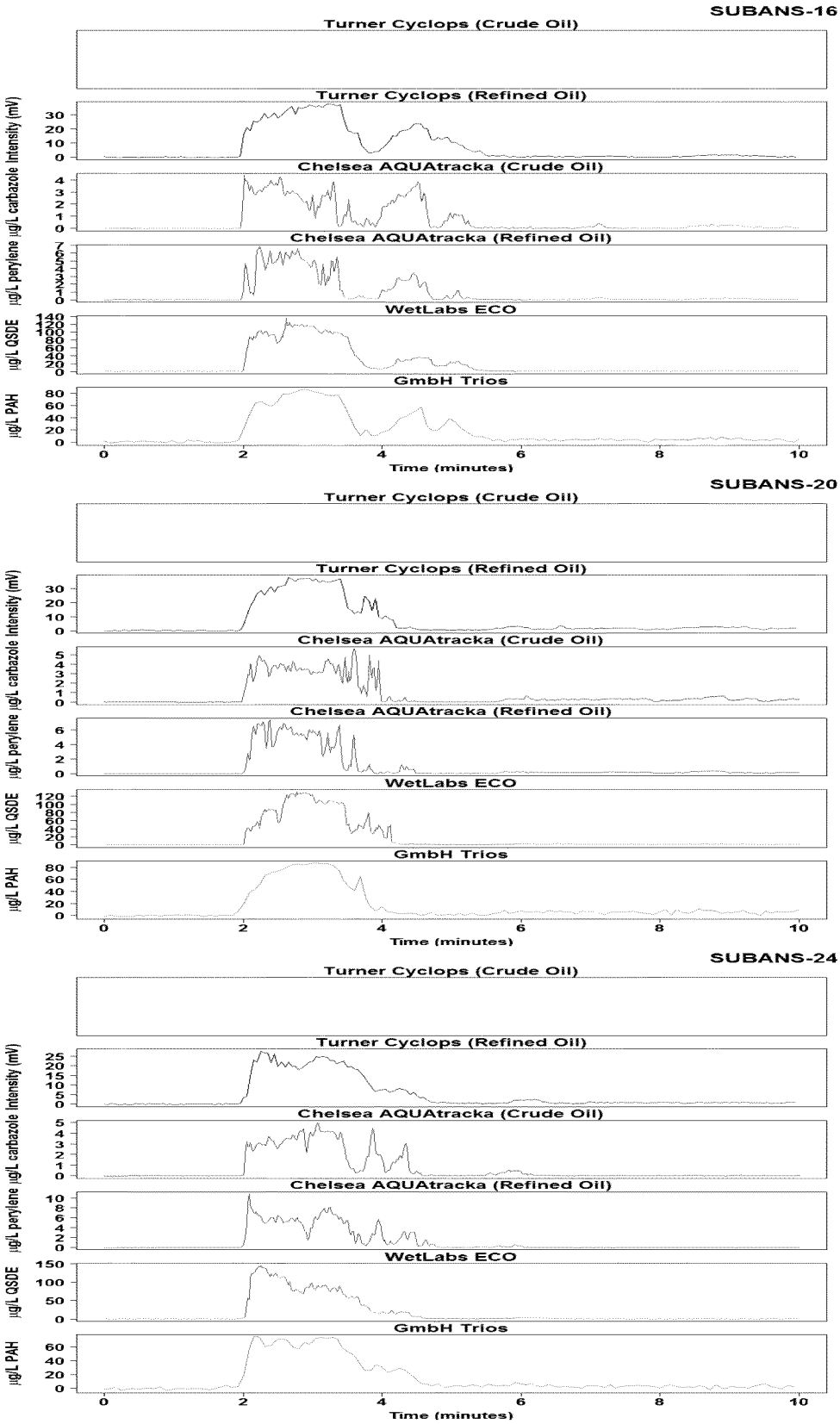

Appendix E - Figure E8. Raw in-situ fluorometer signal for ANS, DOR 1:20 (Corexit 9500), warm expt.

ED_001324_00000687-00088

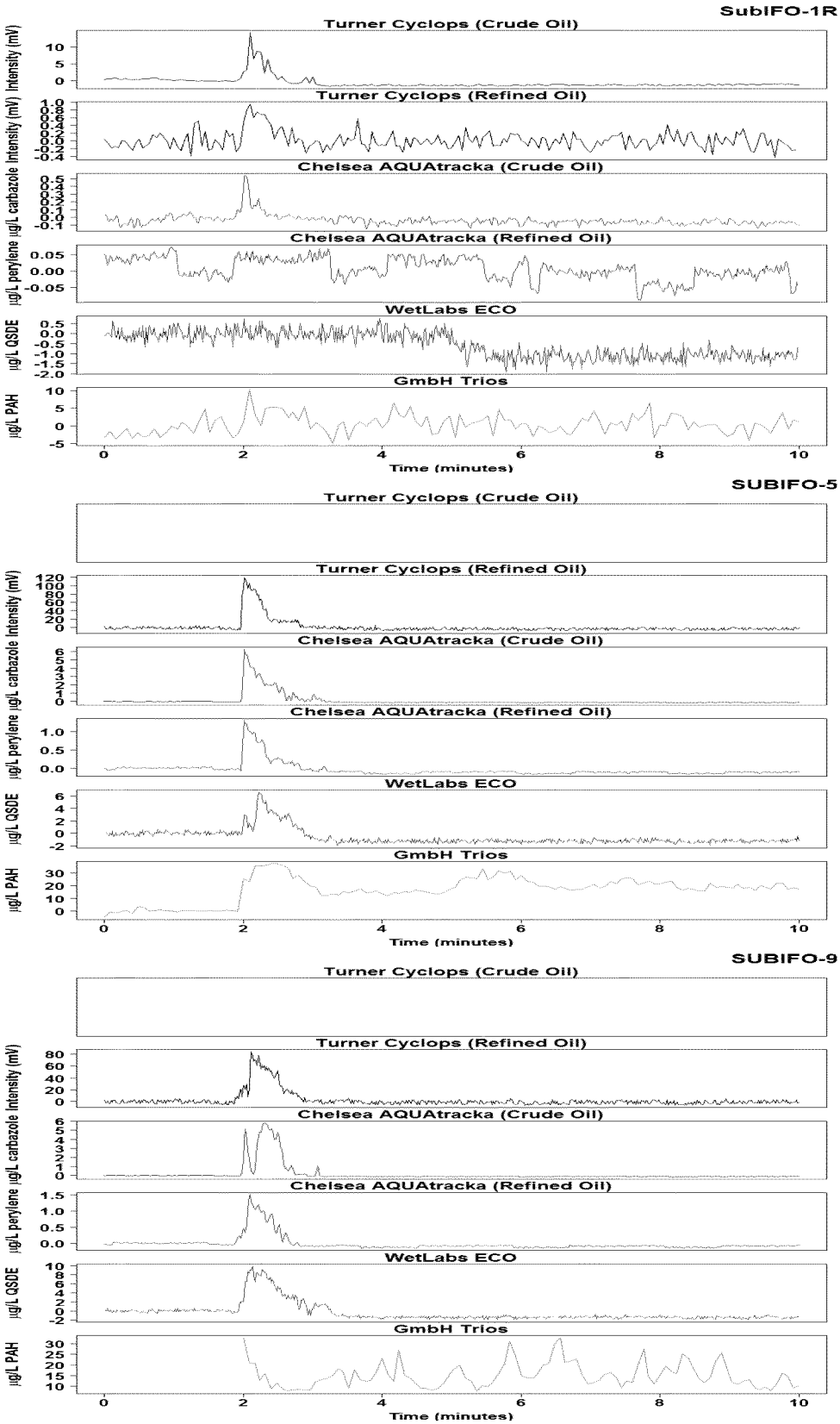

Appendix E - Figure E9. Raw in-situ fluorometer signal, IFO-120, no dispersant, cold water expt.

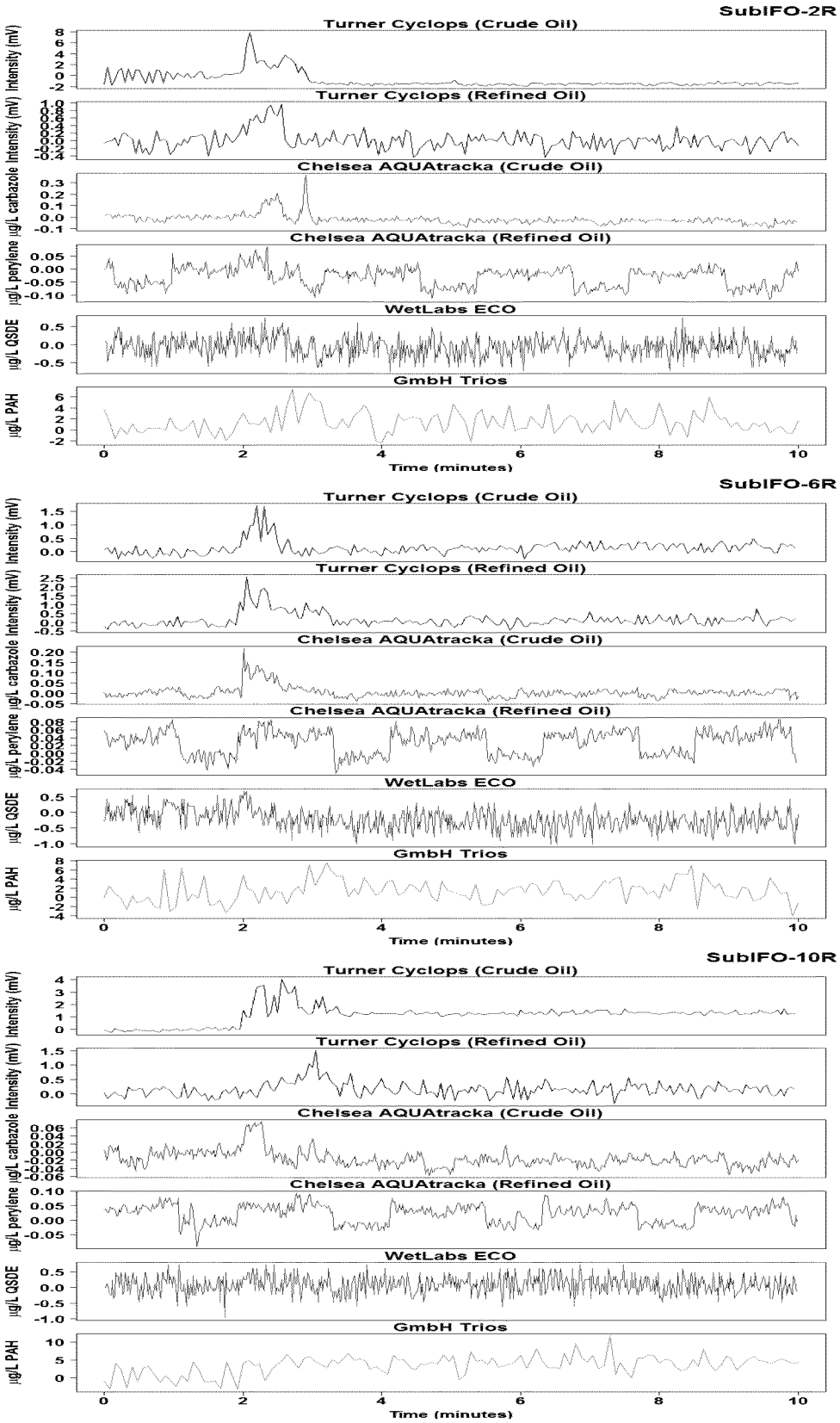

Appendix E - Figure E10. Raw in-situ fluorometer signal, IFO-120, DOR 1:200 (Corexit 9500), cold expt.

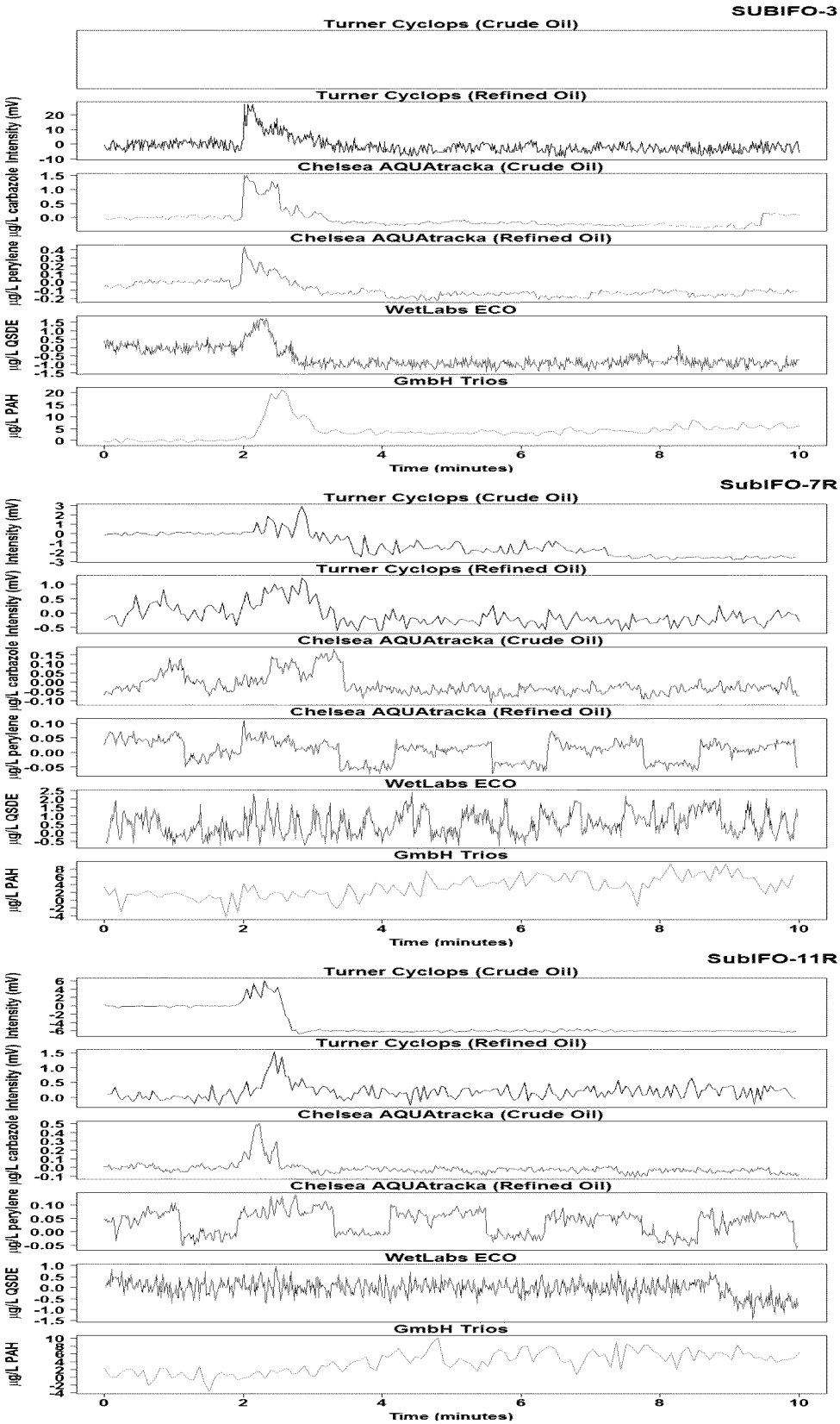

Appendix E - Figure E11. Raw in-situ fluorometer signal, IFO-120, DOR 1:100 (Corexit 9500), cold expt.

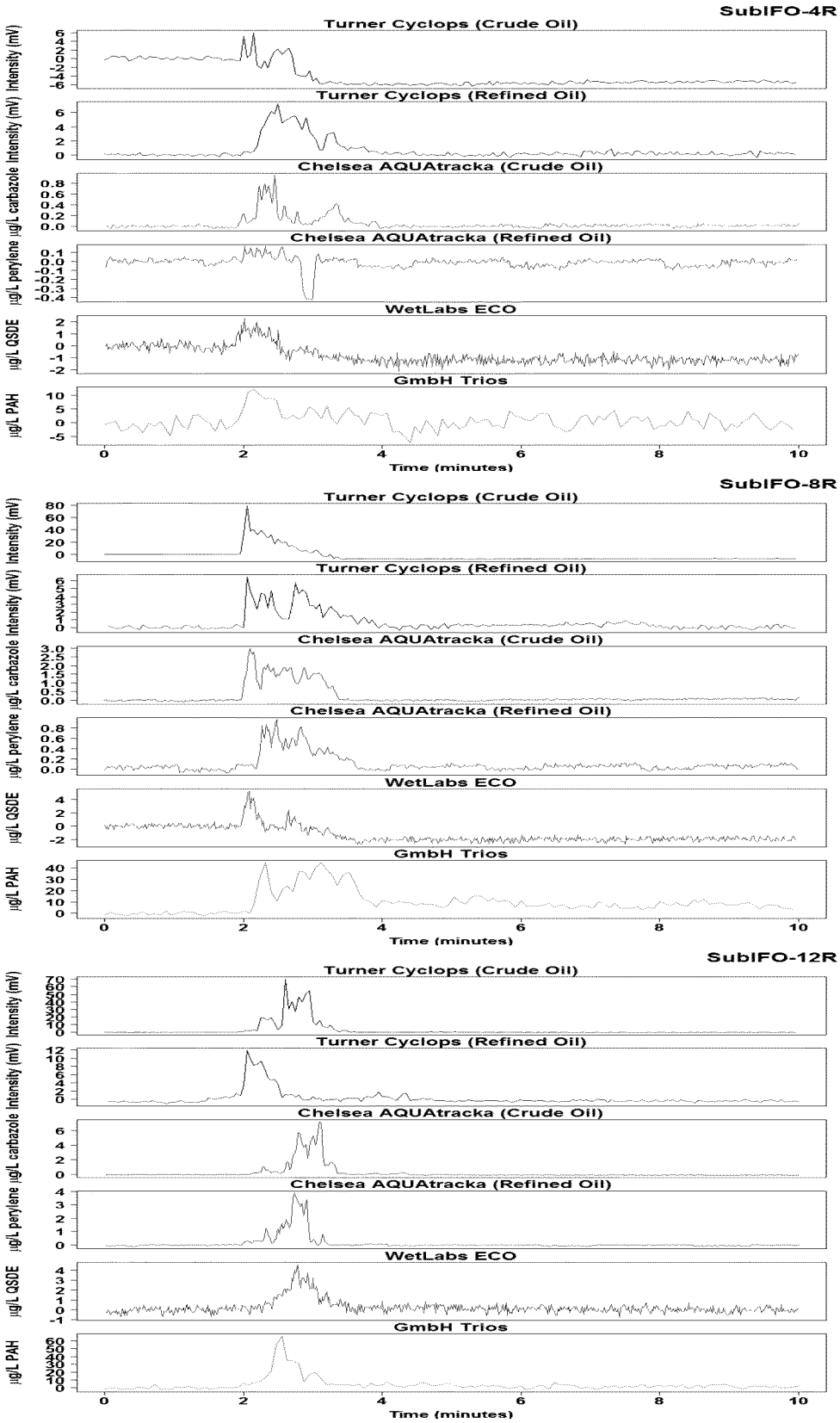

Appendix E - Figure E12. Raw in-situ fluorometer signal, IFO-120, DOR 1:20 (Corexit 9500), cold expt.

ED_001324_00000687-00092

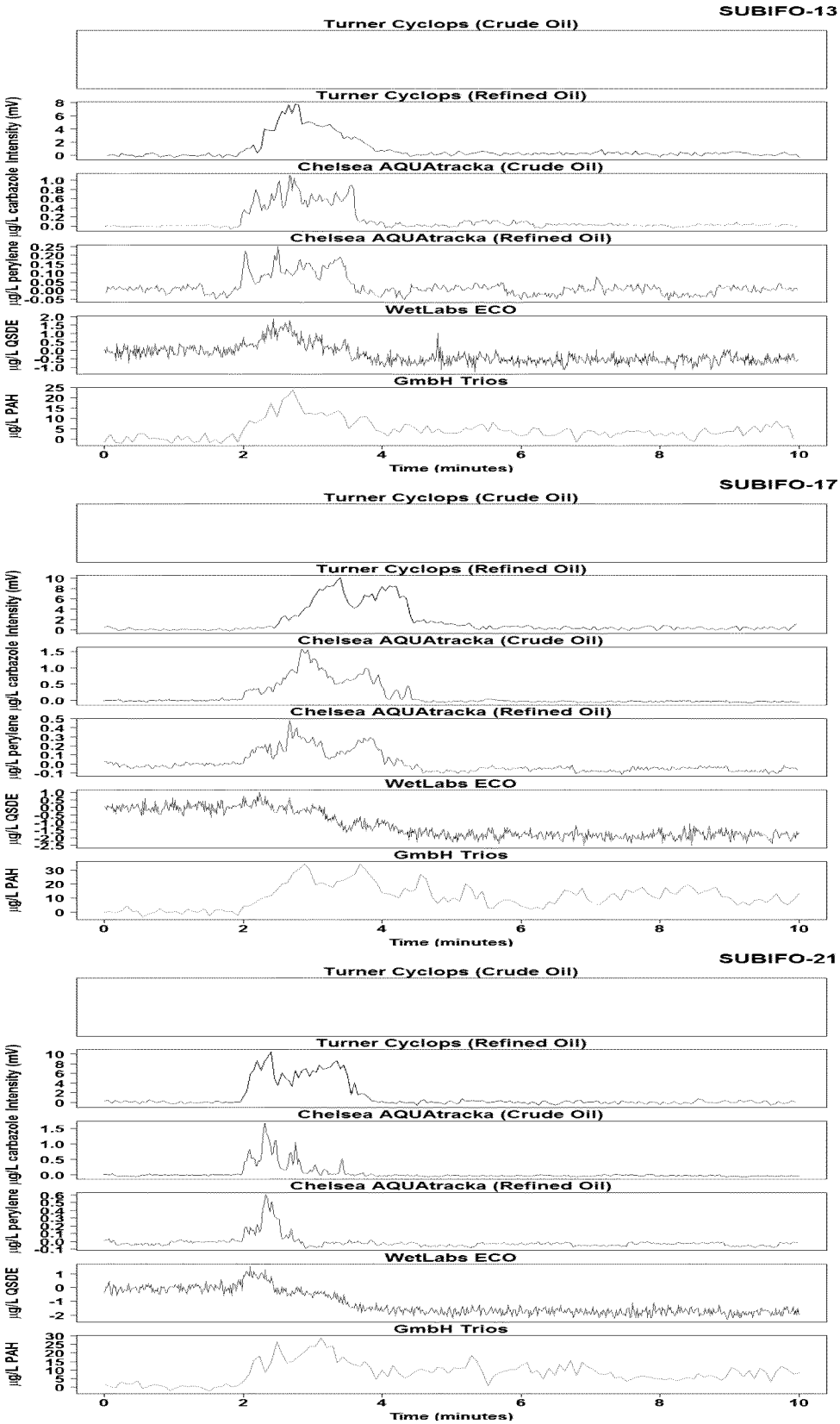

Appendix E - Figure E13. Raw in-situ fluorometer signal for IFO-120, no dispersant, warm water expt.

ED_001324_00000687-00093

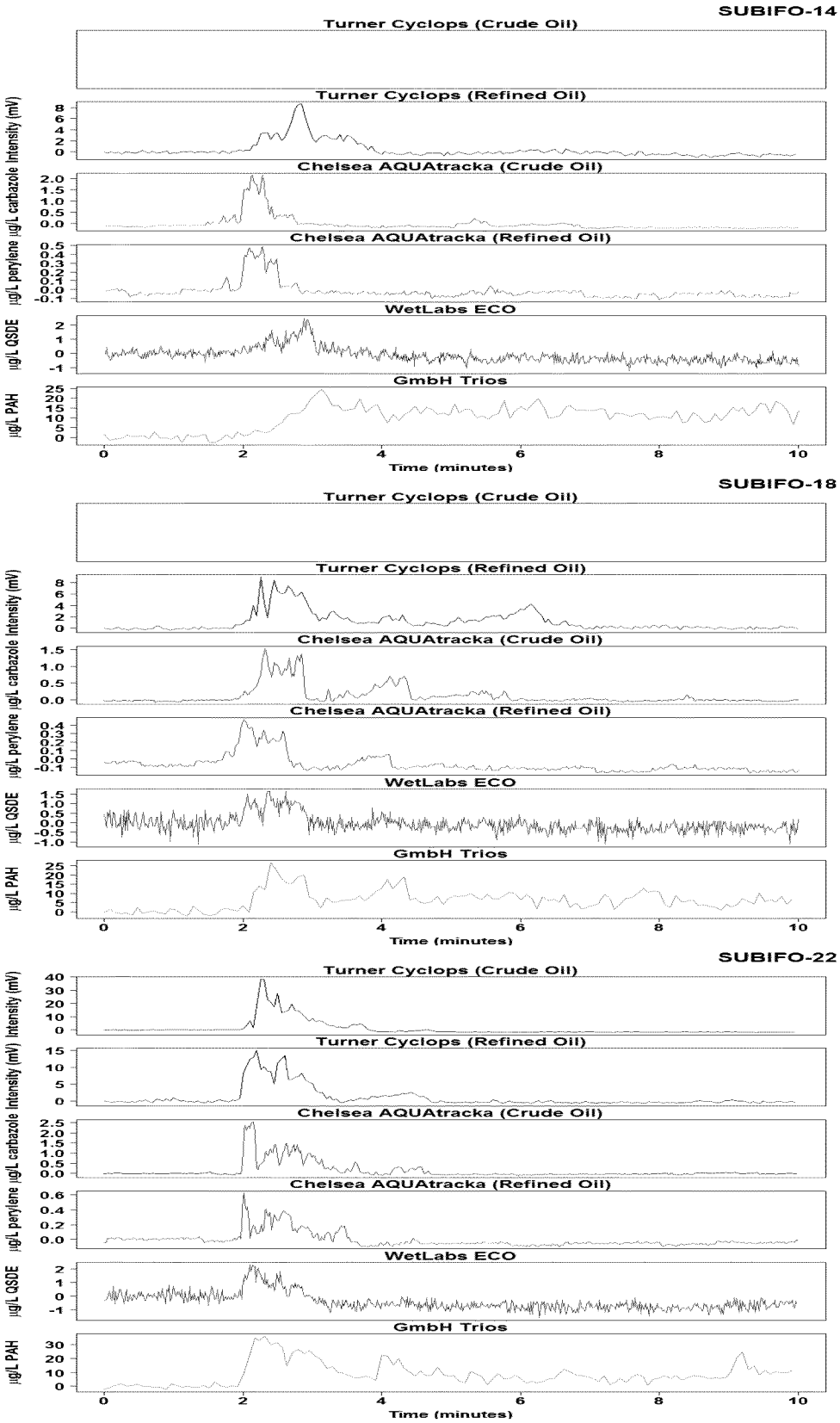

Appendix E - Figure E14. Raw in-situ fluorometer signal, IFO-120, DOR 1:200 (Corexit 9500) warm expt.

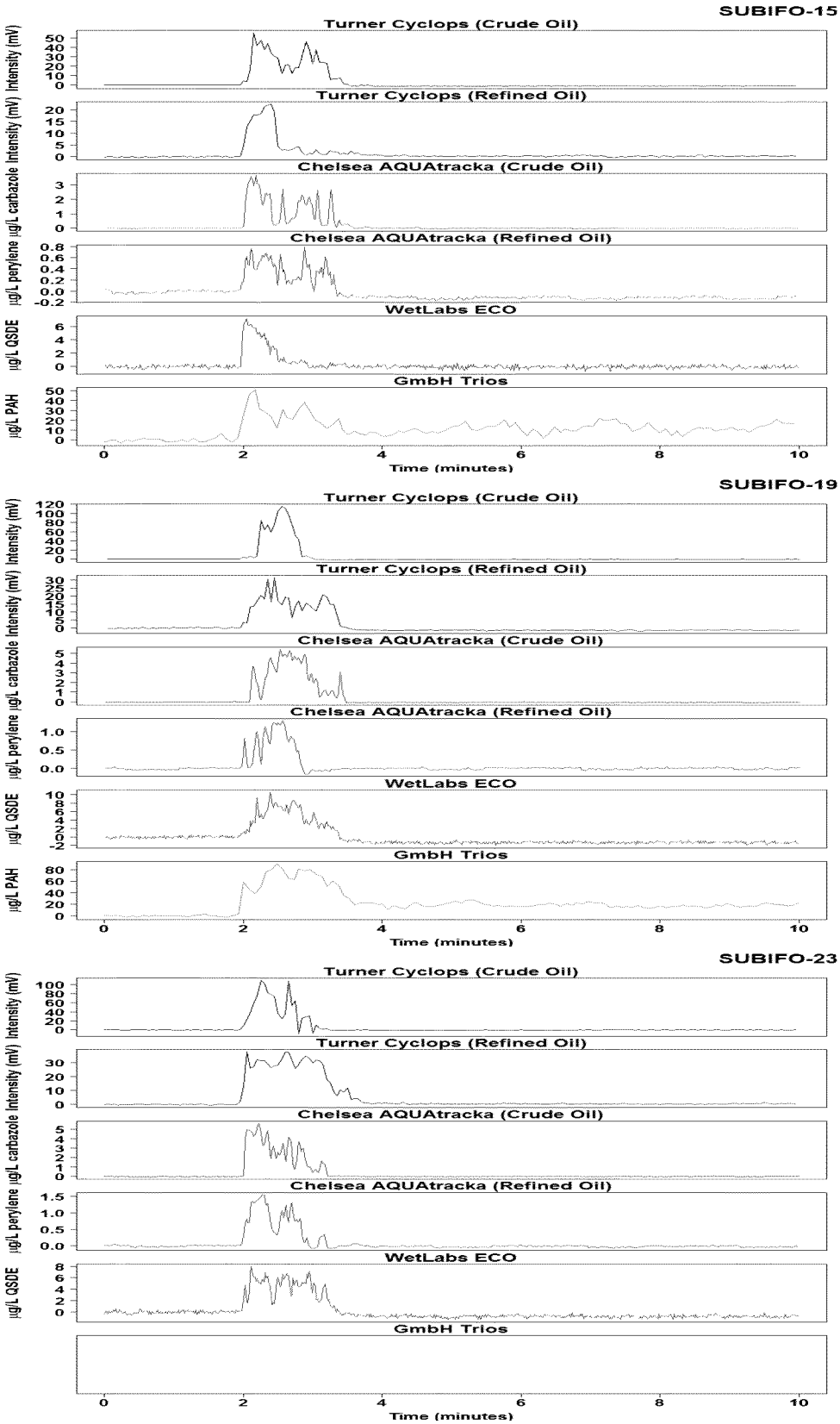

Appendix E - Figure E15. Raw in-situ fluorometer signal, IFO-120, DOR 1:100 (Corexit 9500) warm expt.

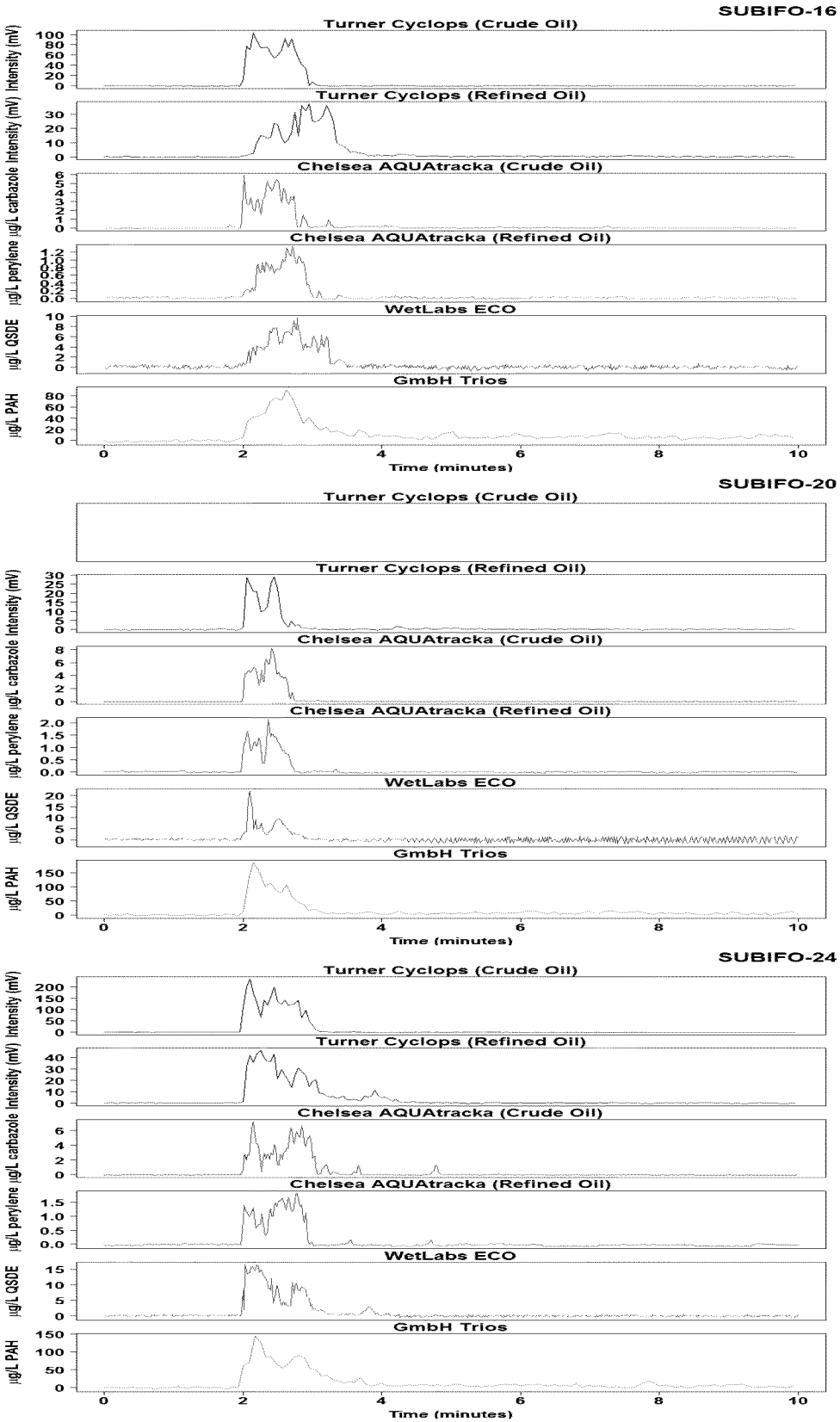

Appendix E - Figure E16. Raw in-situ fluorometer signal, IFO-120, DOR 1:20 (Corexit 9500), warm expt.

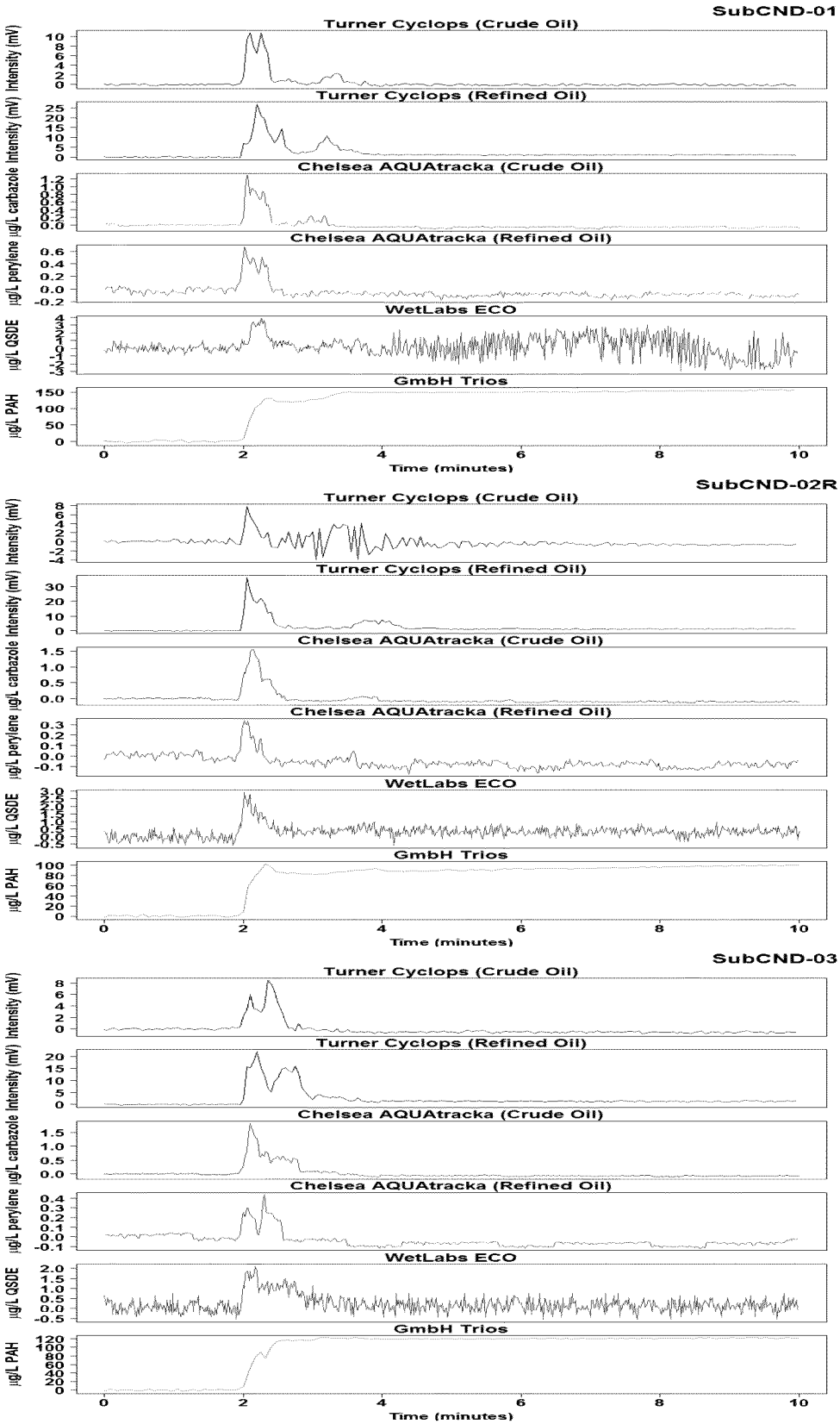

Appendix E - Figure E17. Raw in-situ fluorometer signal for Gas Condensate, no dispersant.

ED_001324_00000687-00097

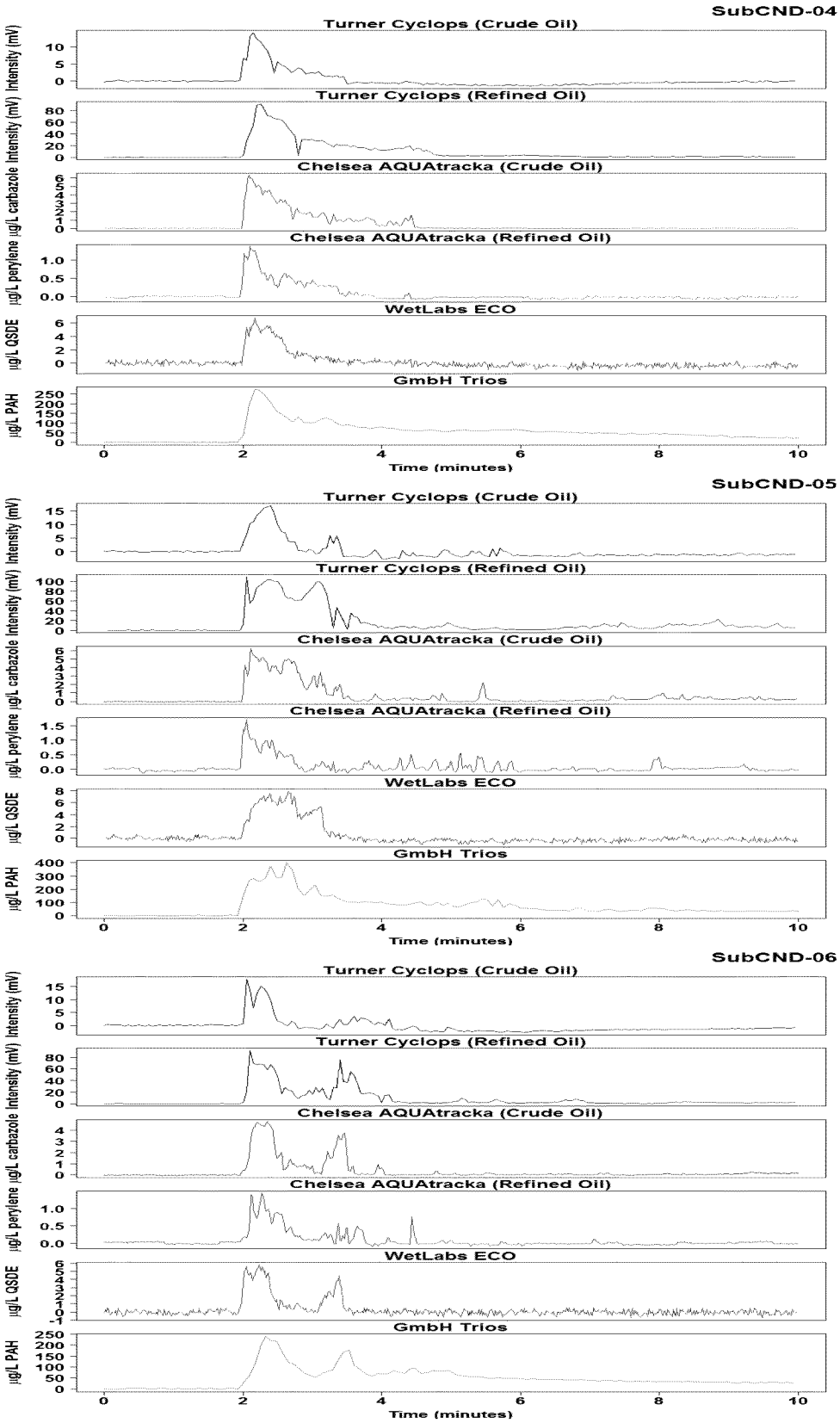

Appendix E - Figure E18. Raw in-situ fluorometer signal for Gas Condensate, DOR 1:20 (Corexit 9500).

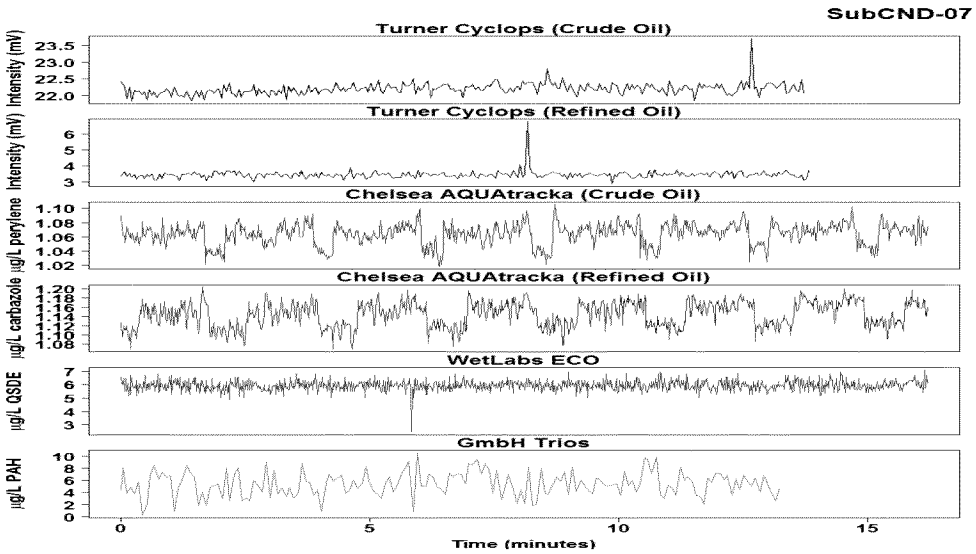

Appendix E - Figure E19. Raw in-situ fluorometer signal for air injection, no dispersant.

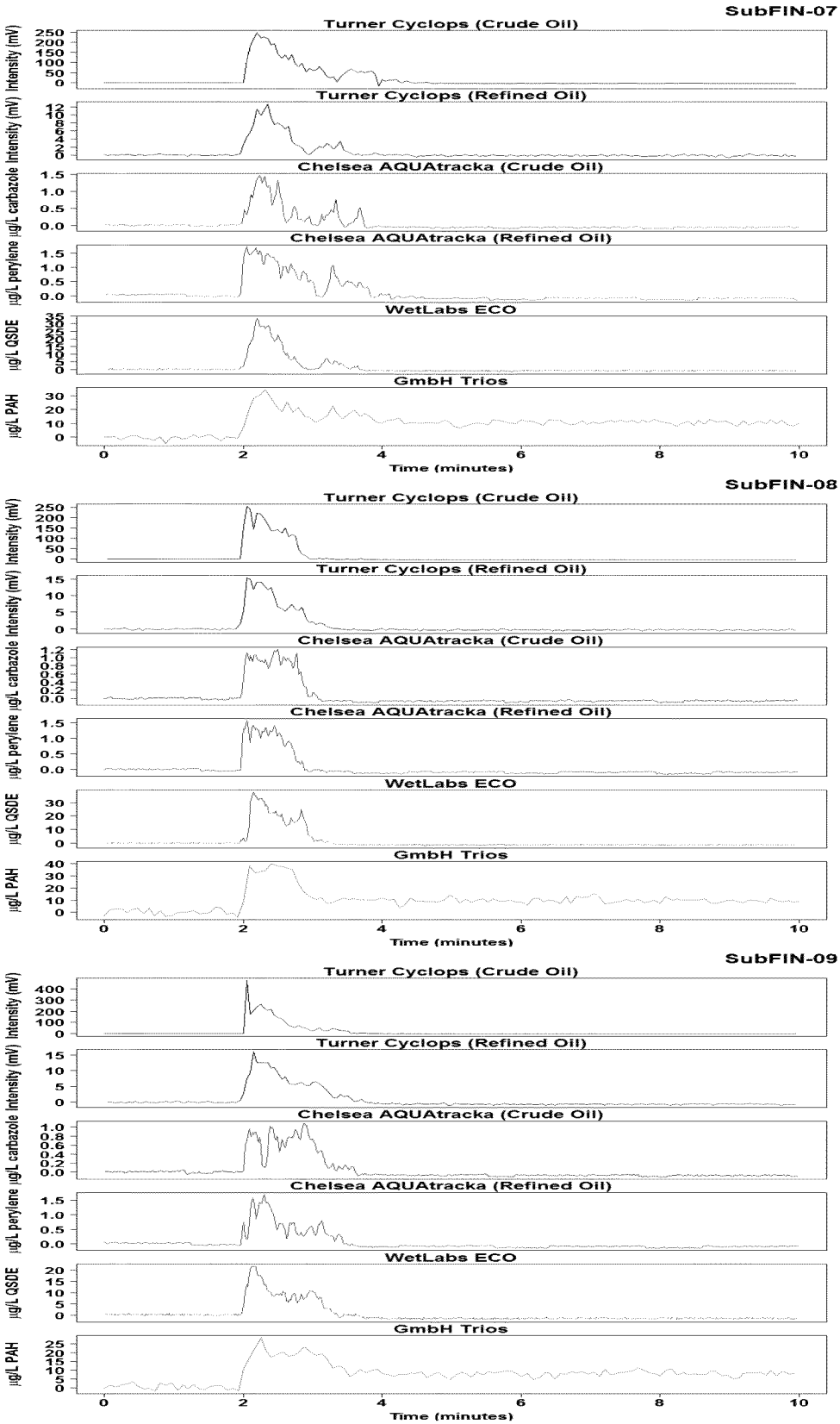

Appendix E - Figure E20. Raw in-situ fluorometer signal, ANS, DOR 1:200 (Finasol OSR 52), warm expt.

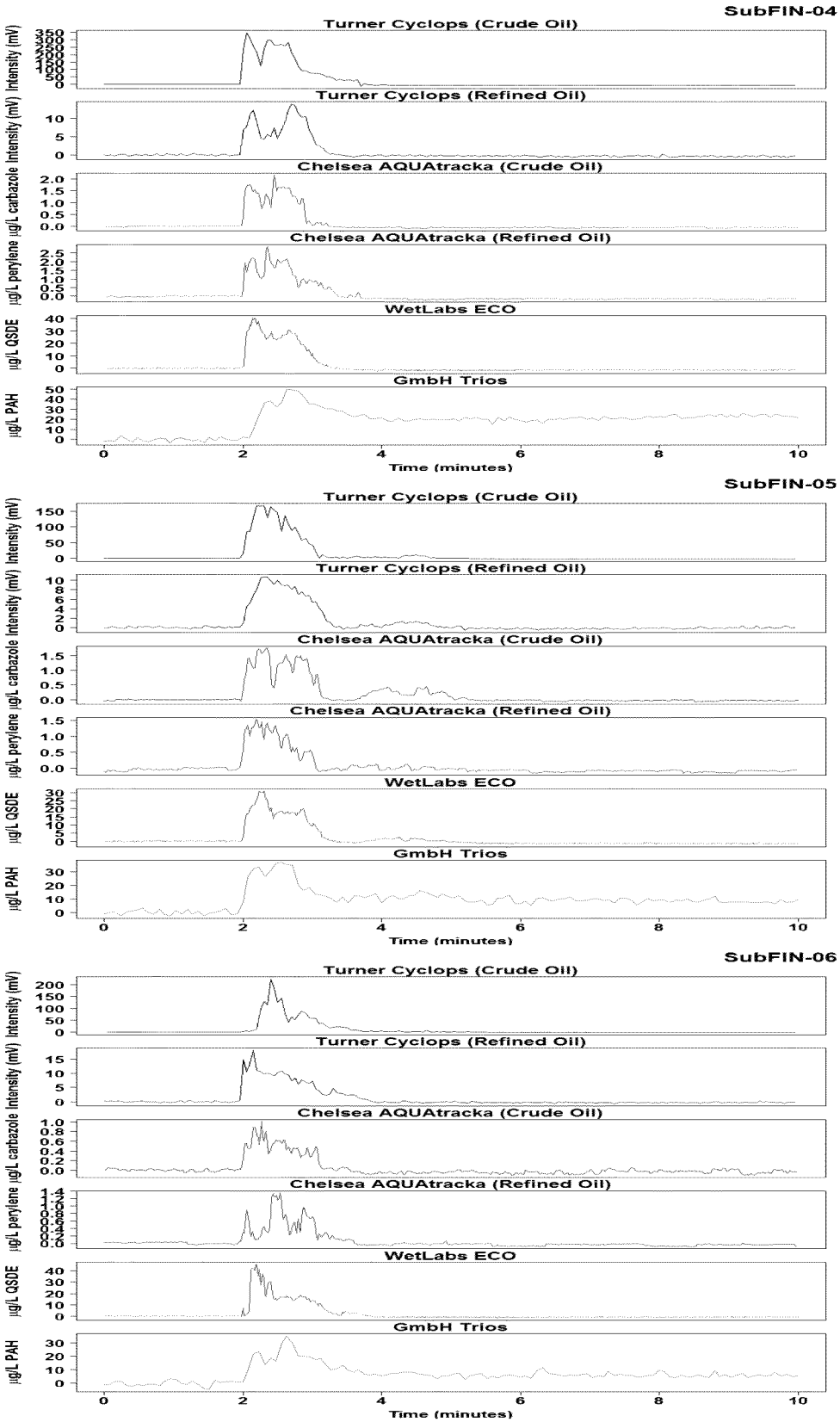

Appendix E - Figure E21. Raw in-situ fluorometer signal ANS, DOR 1:100 (Finasol OSR 52) warm expt.

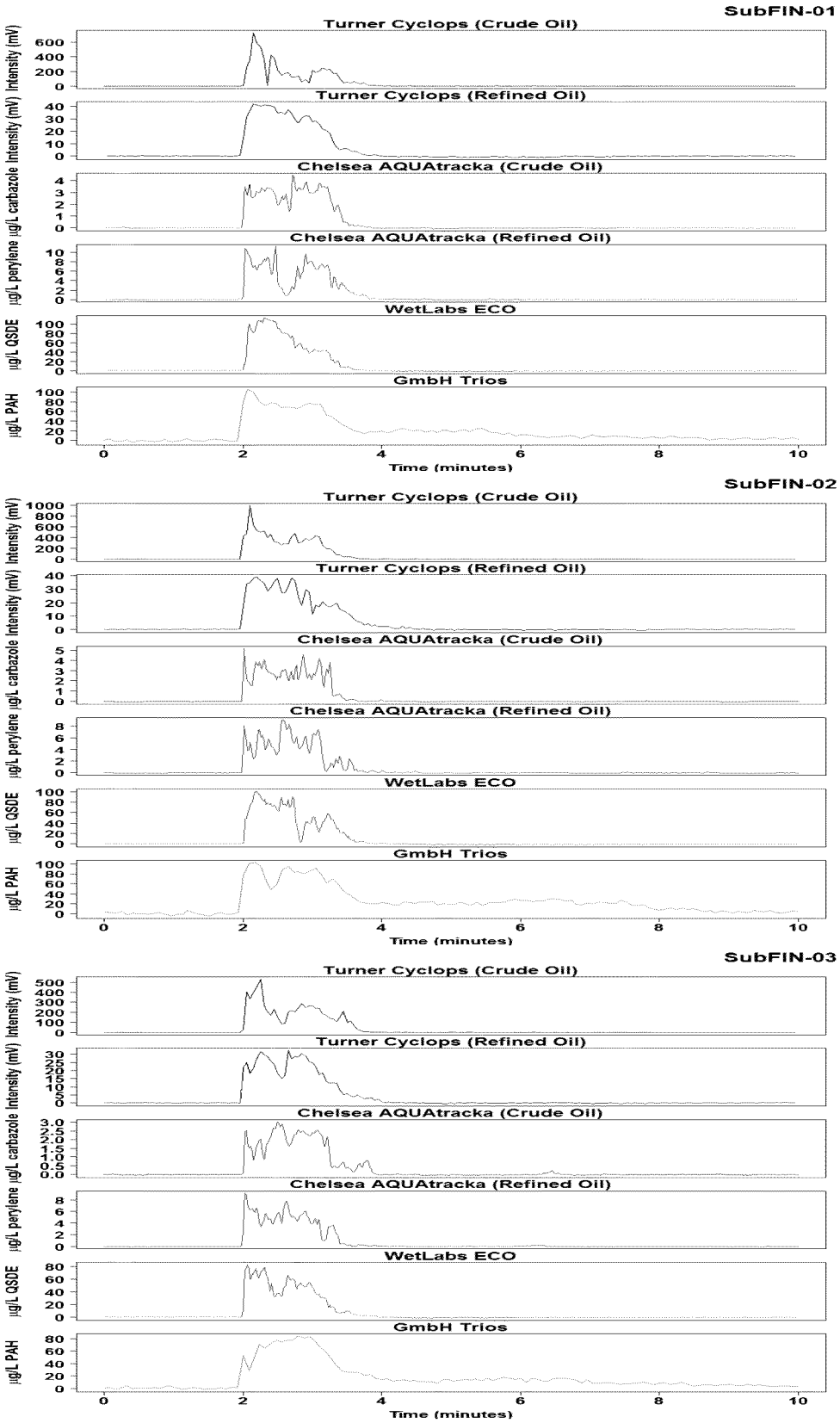

Appendix E - Figure E22. Raw in-situ fluorometer signal for ANS, DOR 1:20 (Finasol OSR 52) warm expt.

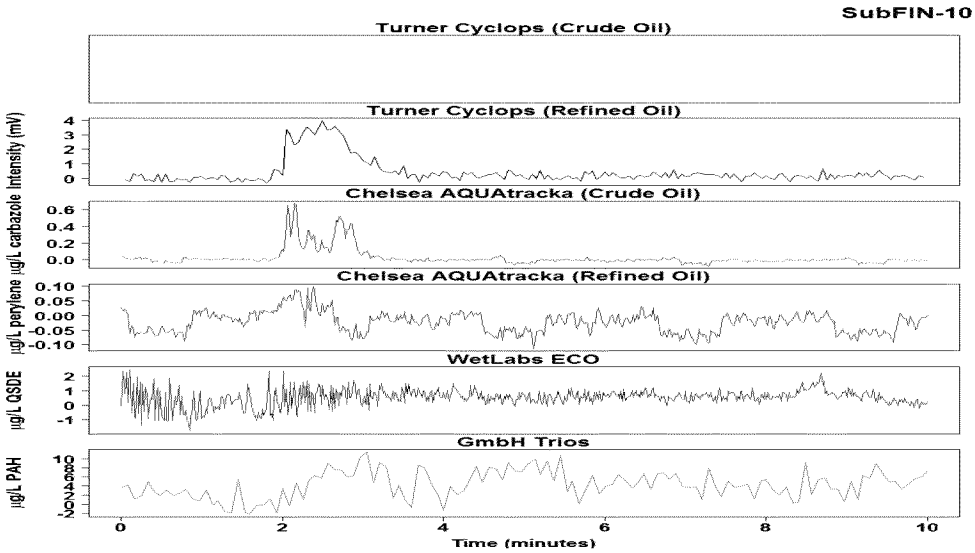

Appendix E - Figure E23. Raw in-situ fluorometer signal for IFO-120, DOR 1:200 (Finasol OSR 52), warm water experiment.

ED_001324_00000687-00103

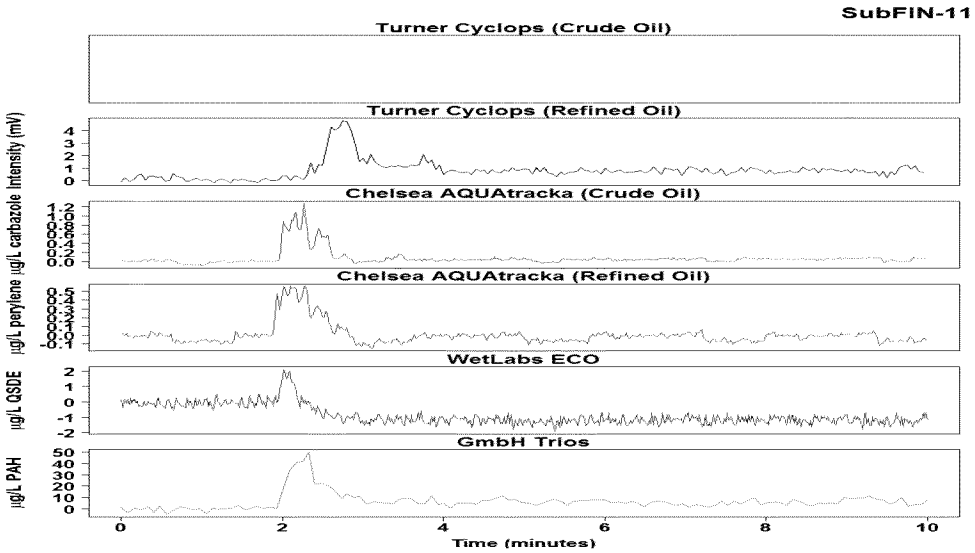

Appendix E - Figure E24. Raw in-situ fluorometer signal for IFO-120, DOR 1:100 (Finasol OSR 52), warm water experiment.

ED_001324_00000687-00104

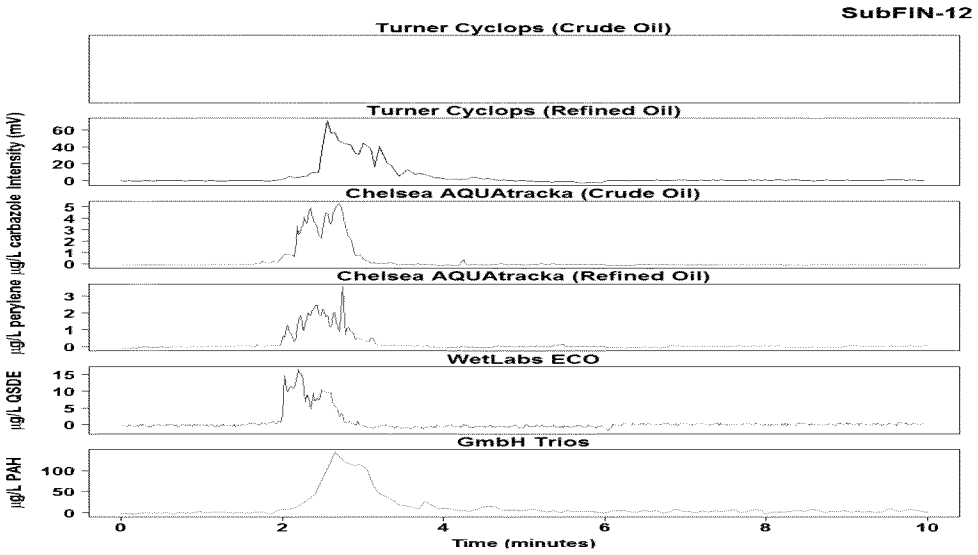

Appendix E - Figure E25. Raw in-situ fluorometer signal IFO-120, DOR 1:20 (Finasol OSR 52) warm expt.

ED_001324_00000687-00105

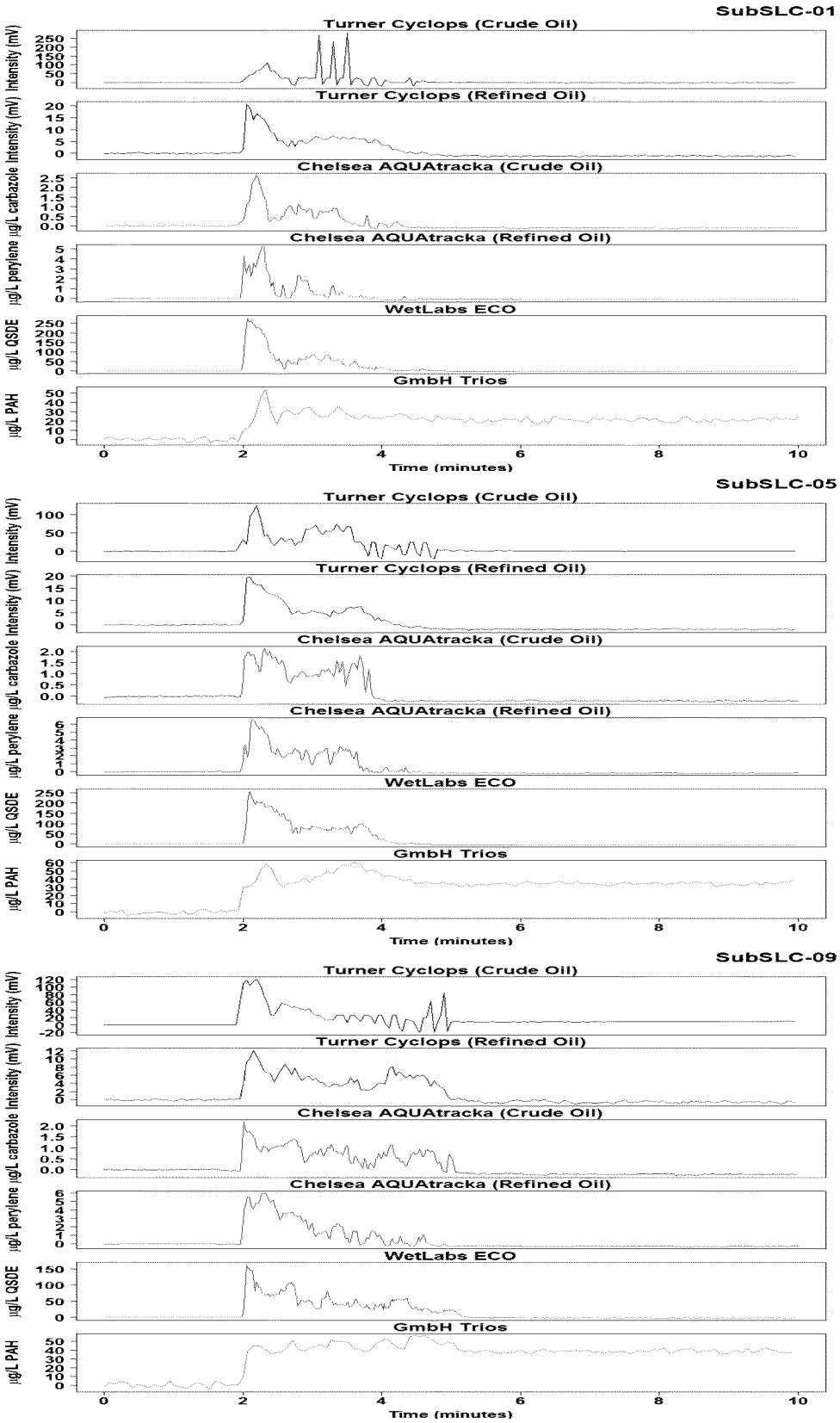

Appendix E - Figure E26. Raw in-situ fluorometer signal for SLC, no dispersant, warm water expt.

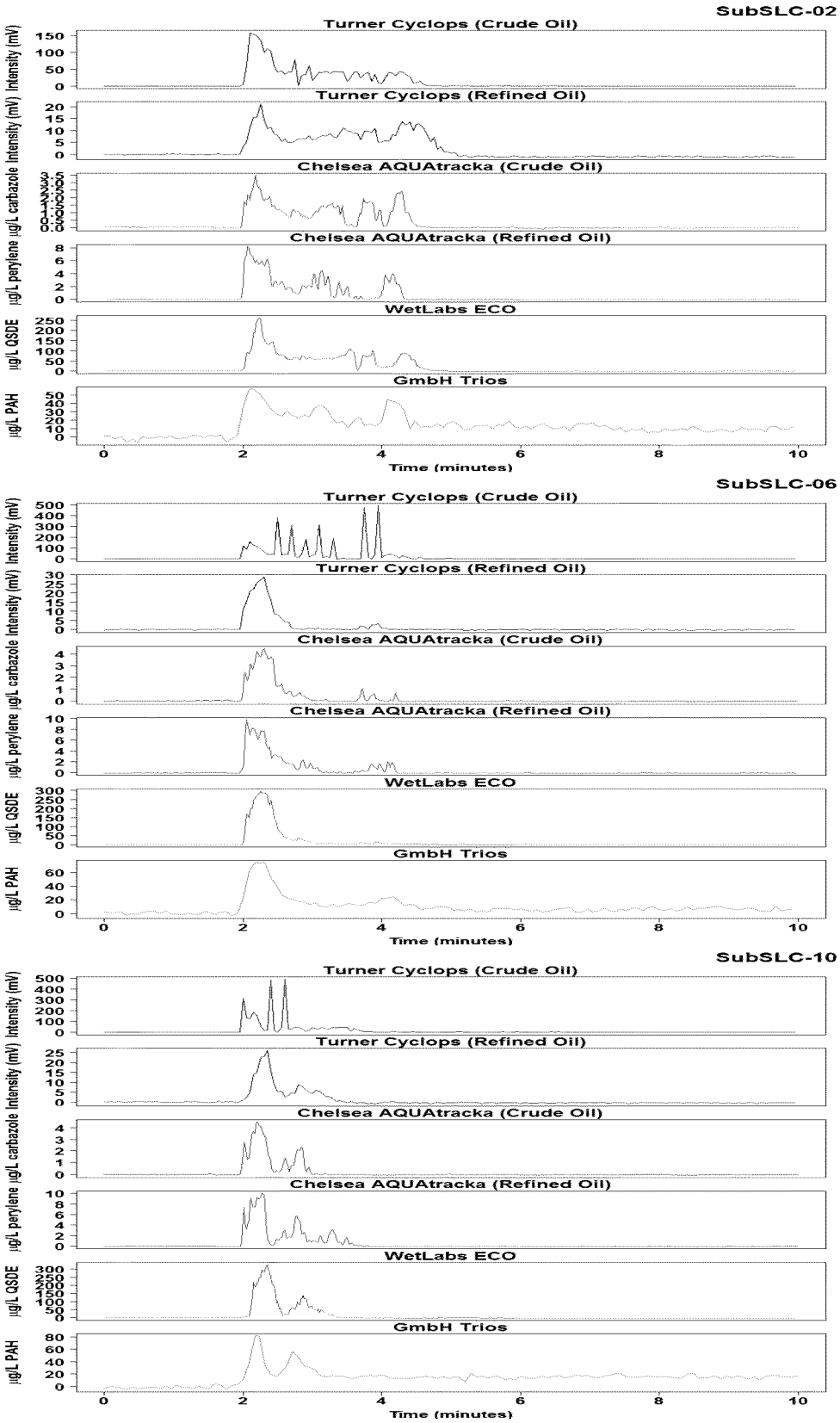

Appendix E - Figure E27. Raw in-situ fluorometer signal for SLC, DOR 1:200 (Corexit 9500), warm expt.

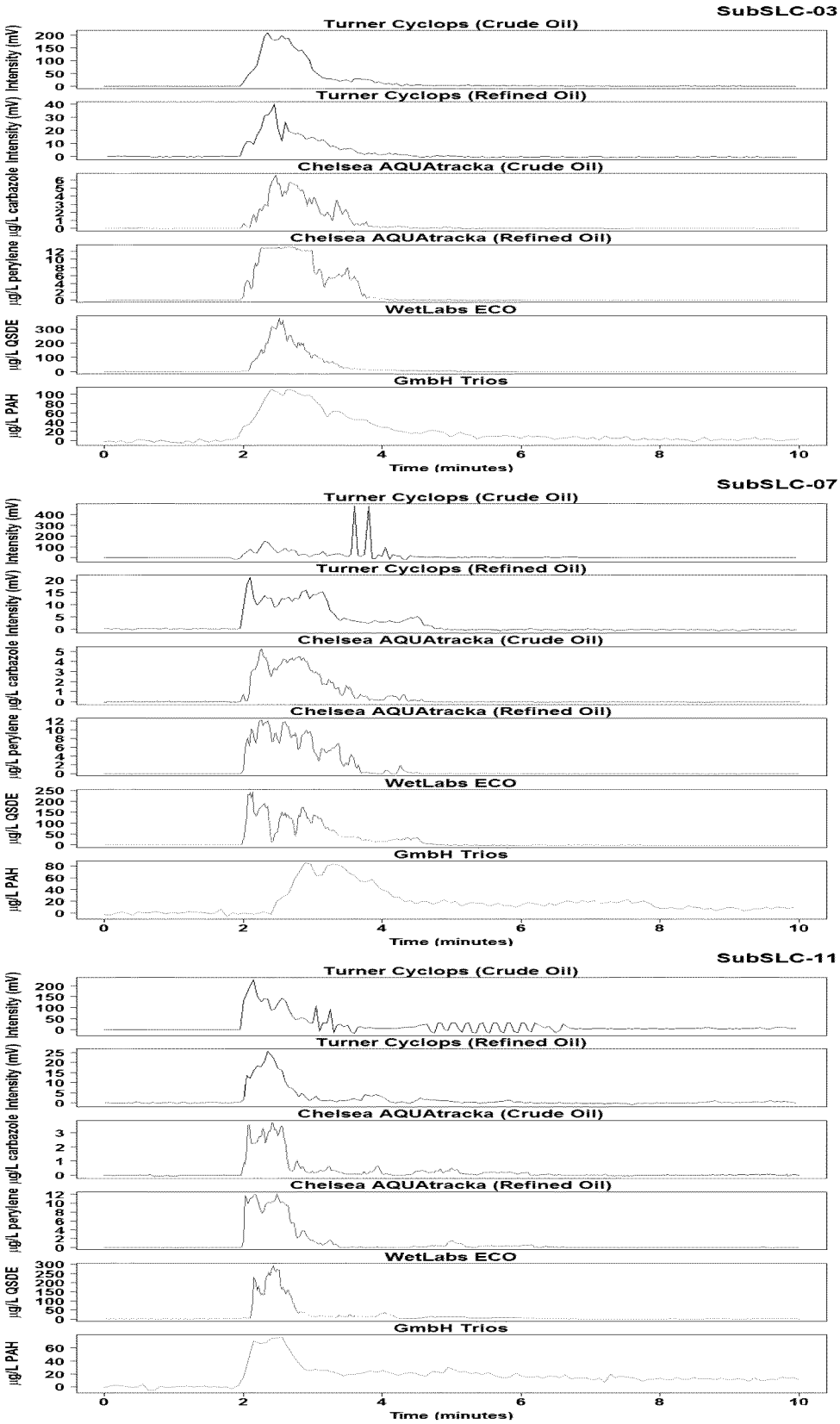

Appendix E - Figure E28. Raw in-situ fluorometer signal for SLC, DOR 1:100 (Corexit 9500), warm expt.

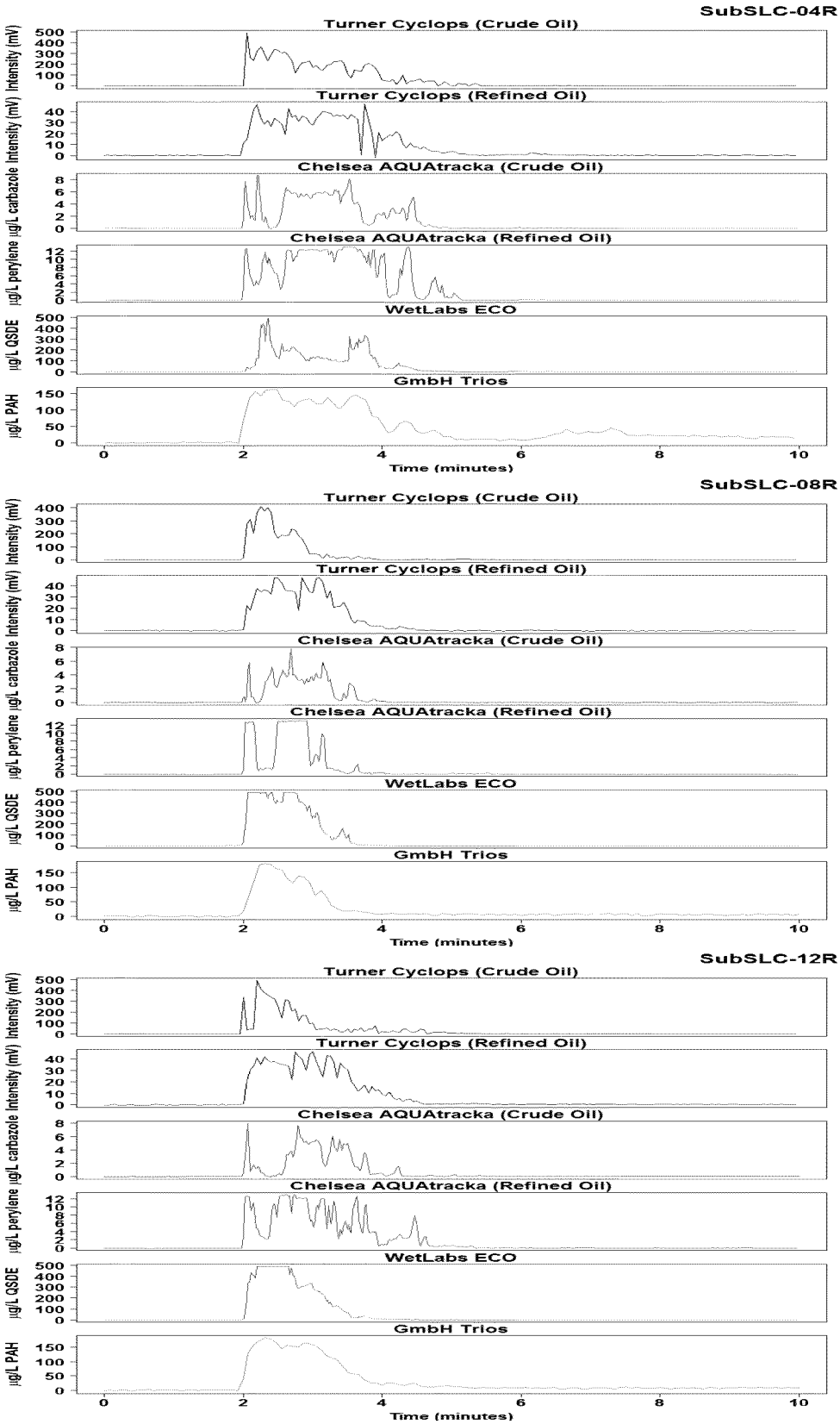

Appendix E - Figure E29. Raw in-situ fluorometer signal for SLC, DOR 1:20 (Corexit 9500), warm expt.

ED_001324_00000687-00110

IAA No. E12PG00037

Final Report Appendix F Excitation Emission Matrix Contours

Dispersant Effectiveness, In-Situ Droplet Size Distribution and Numerical Modeling to Assess Subsurface Dispersant Injection as a Deepwater Blowout Oil Spill Response Option

and

Evaluation of Oil Fluorescence Characteristics to Improve Forensic Response Tools

Submitted to:

Bureau of Safety and Environmental Enforcement

Submitted by:

Robyn N. Conmy, Ph.D.
U.S. Environmental Protection Agency, Office of Research and Development
26 W. Martin Luther King Drive, Cincinnati, OH 45268
*Tel: 513-569-7090, Fax: 513-569-7620, Email: conmy.robyn@epa.gov

Thomas King, M.Sc.; Brian Robinson, M.Sc; Scott Ryan, M.Sc; Youyu Lu, Ph.D.;
Department of Fisheries and Oceans Canada, Bedford Institute of Oceanography
1 Challenger Drive, Dartmouth, Nova Scotia, Canada B2Y 4A2
Tel: 902-426-4172, Tom.King@mar.dfo-mpo.gc.ca

Mary Abercrombie, M.Sc.
University of South Florida, College of Marine Science
140 7th Ave South, St. Petersburg, FL 33701
*Tel: 727-553-1140, Email: mabercrombie@marine.usf.edu

Michel Boufadel, Ph.D.
New Jersey Institute of Technology, Civil and Environmental Engineering
University Heights, Newark, NJ 07102
Tel: 973-596-5657, Email: michel.boufadel@njit.edu

Haibo Niu, Ph.D.
Dalhousie University, Department of Engineering
PO Box 550, Truro, N.S. Canada
Tel: 902-893-6714, Email: haibo.niu@dal.ca

September 30, 2016

ED_001324_00000687-00111

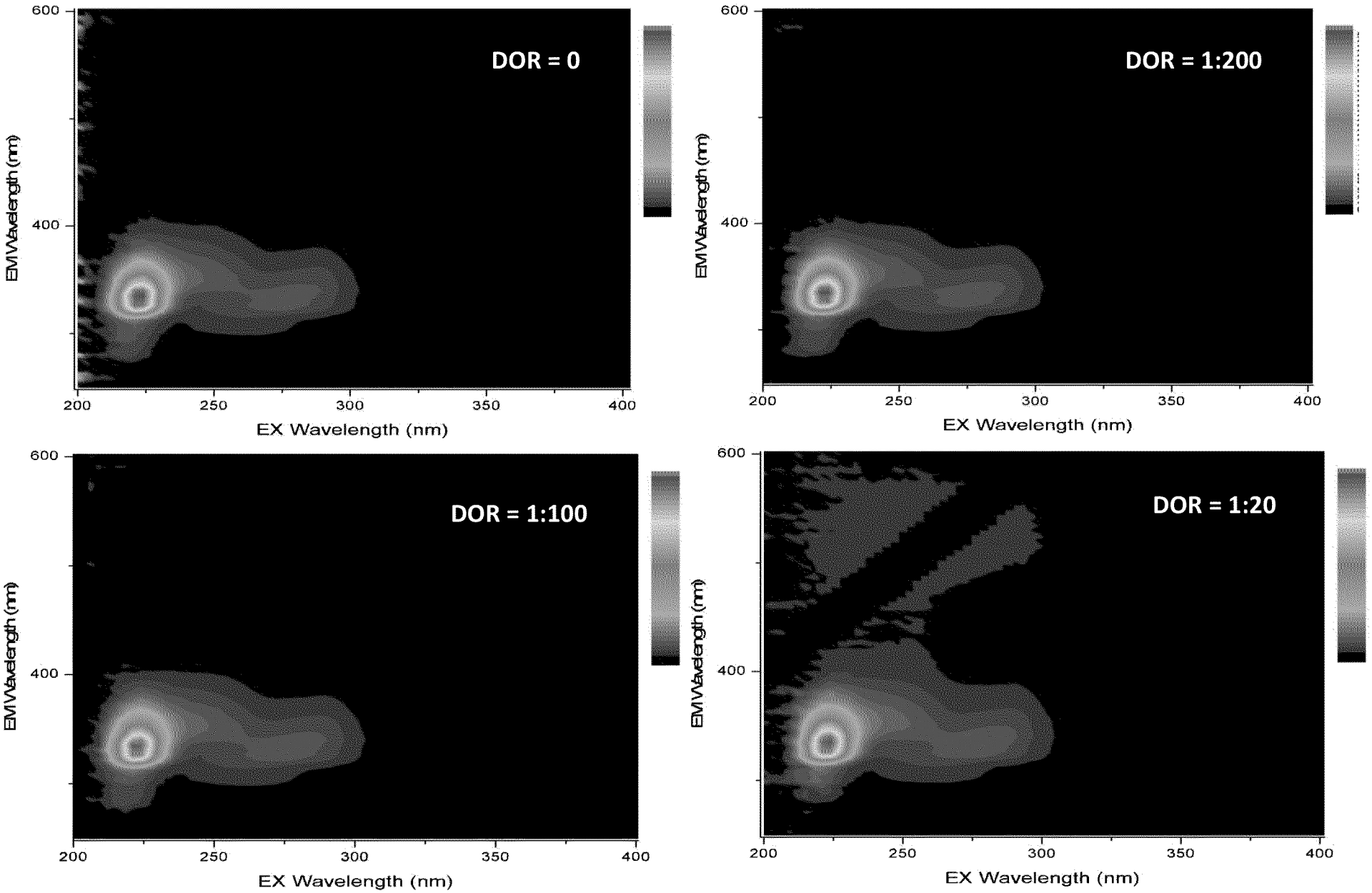

Appendix F - Figure F1. Light Oil Category – IFO-40 oil with dispersant EEMs. Colored contours represent intensity, scaled to maximum fluorescence peak (red).

ED_001324_00000687-00112

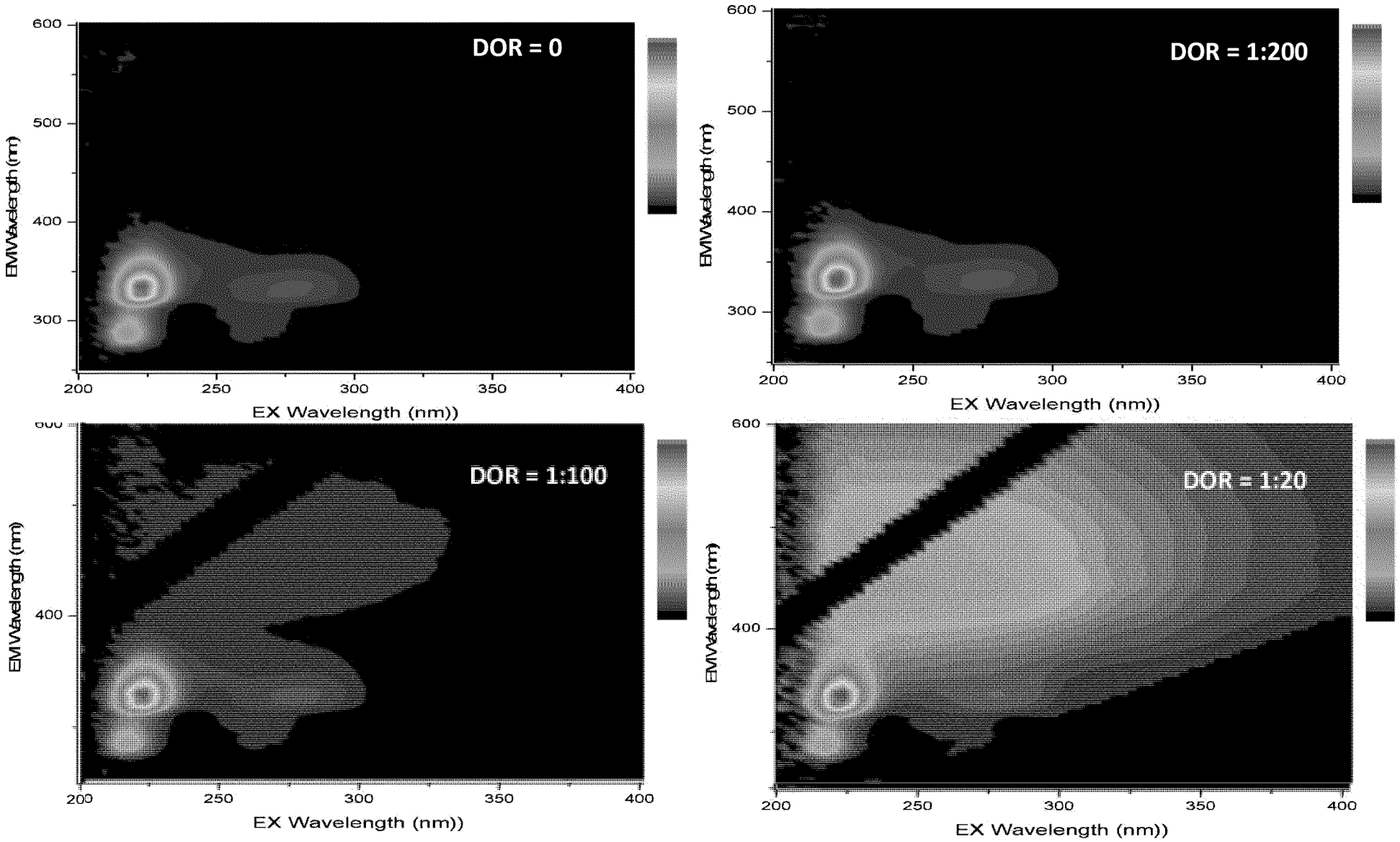

Appendix F - Figure F2. Light Oil Category – Arabian Light crude oil with dispersant EEMs. Colored contours represent intensity, scaled to maximum fluorescence peak (red).

ED_001324_00000687-00113

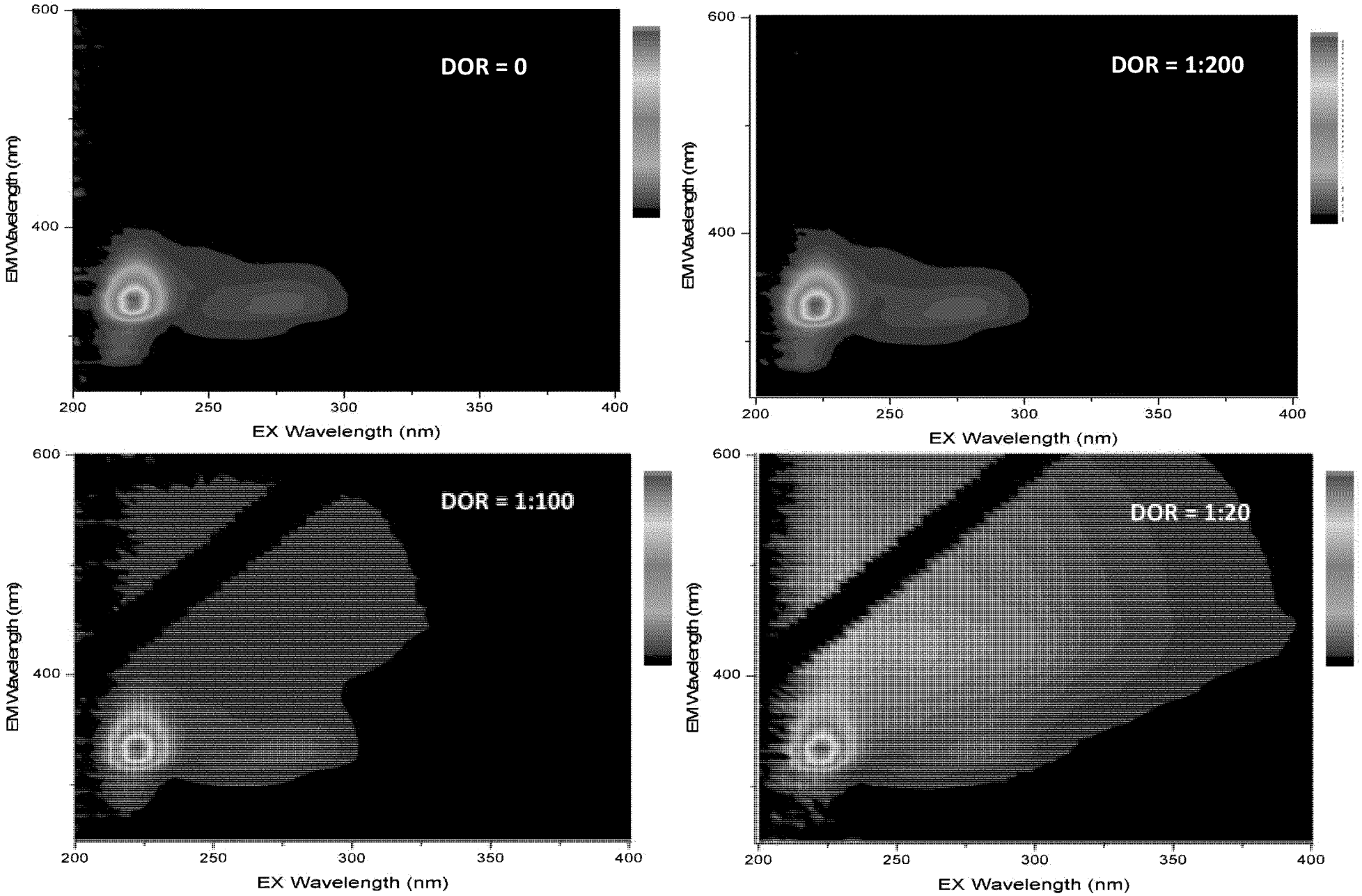

Appendix F - Figure F3. Light Oil Category – Brent crude oil with dispersant EEMs. Colored contours represent intensity, scaled to maximum fluorescence peak (red).

ED_001324_00000687-00114

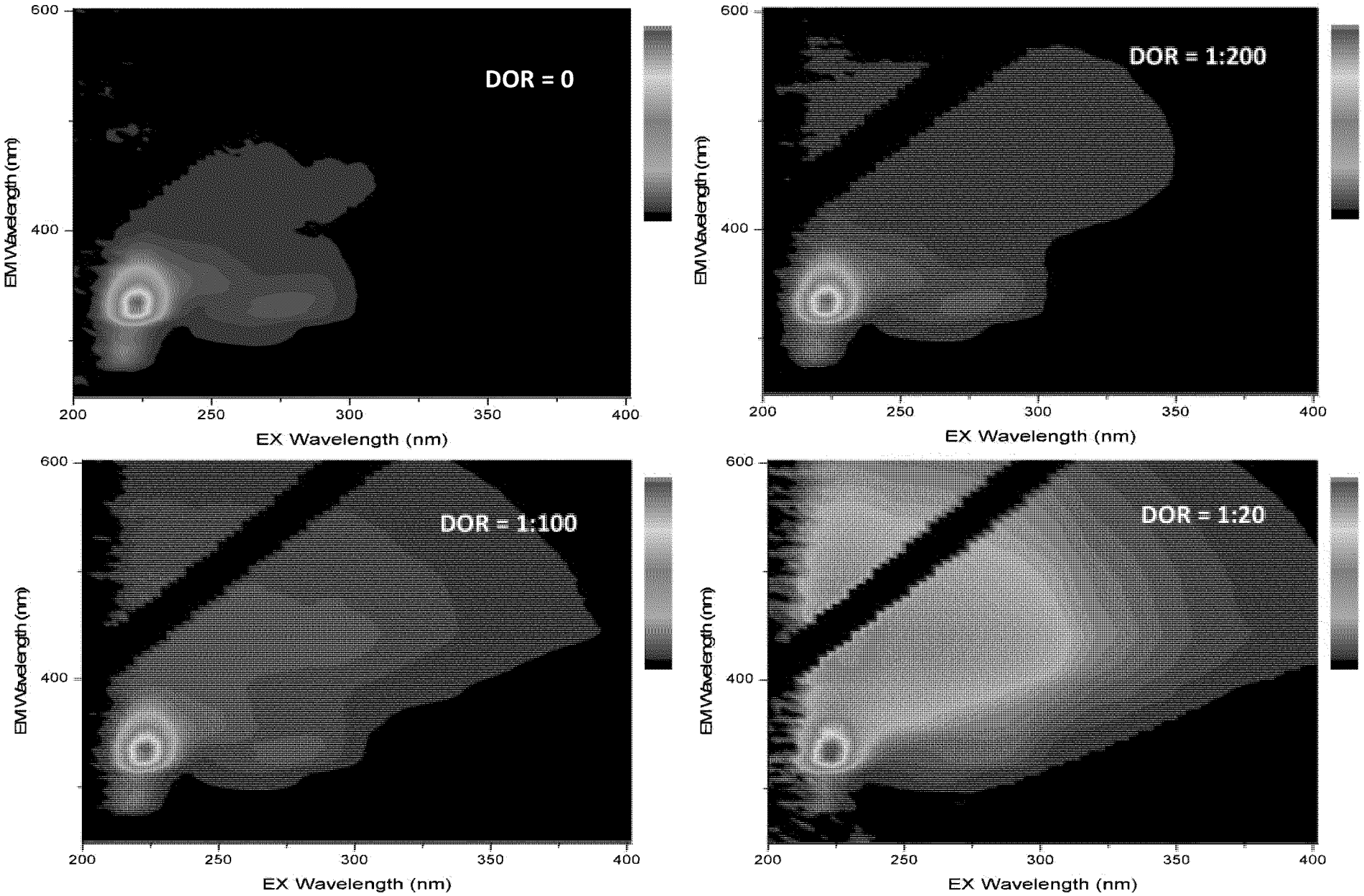

Appendix F - Figure F4. Light Oil Category – Federated crude oil with dispersant EEMs. Colored contours represent intensity, scaled to maximum fluorescence peak (red).

ED_001324_00000687-00115

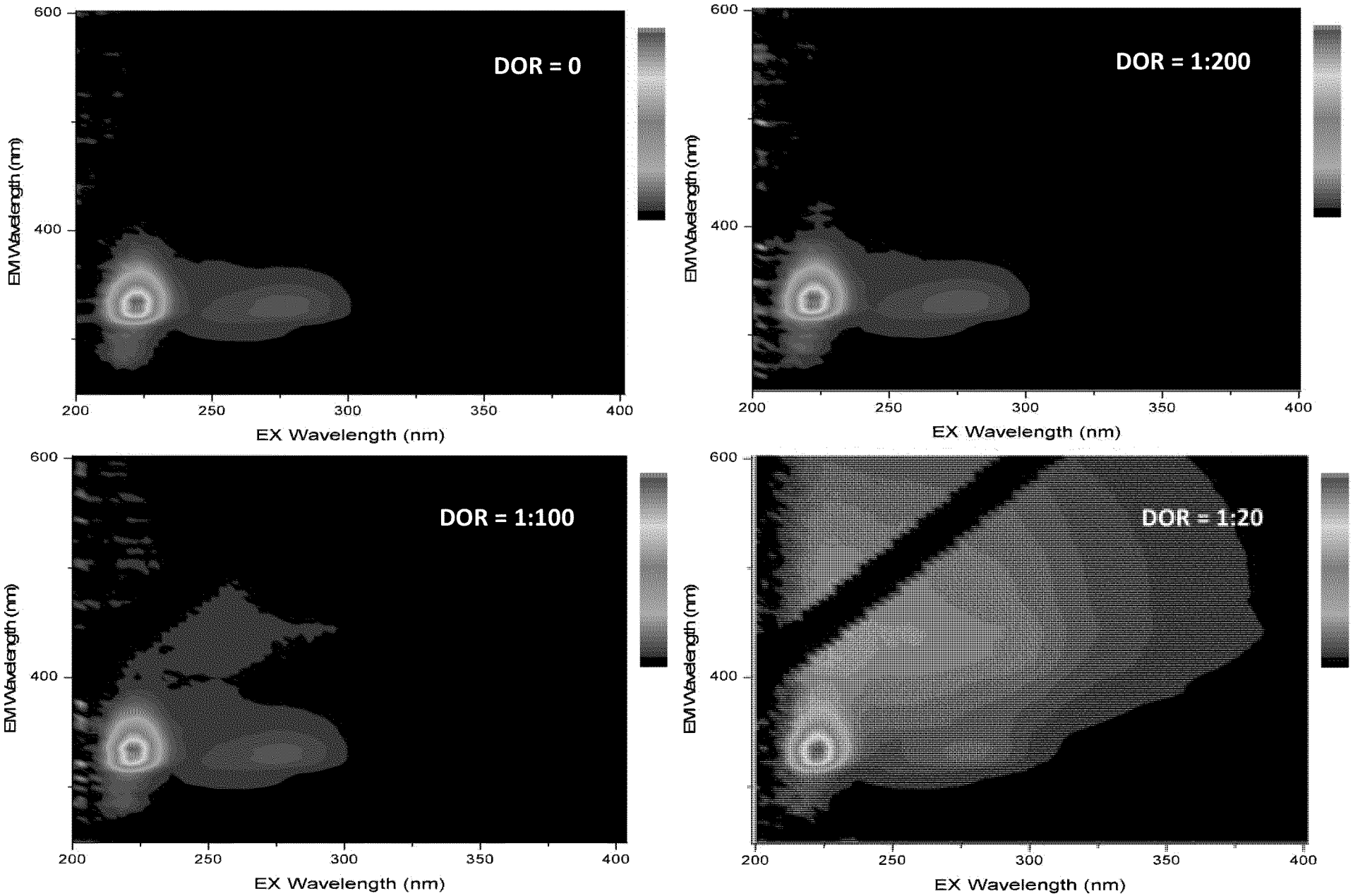

Appendix F - Figure F5. Light Oil Category – Gullfaks crude oil with dispersant EEMs. Colored contours represent intensity, scaled to maximum fluorescence peak (red).

ED_001324_00000687-00116

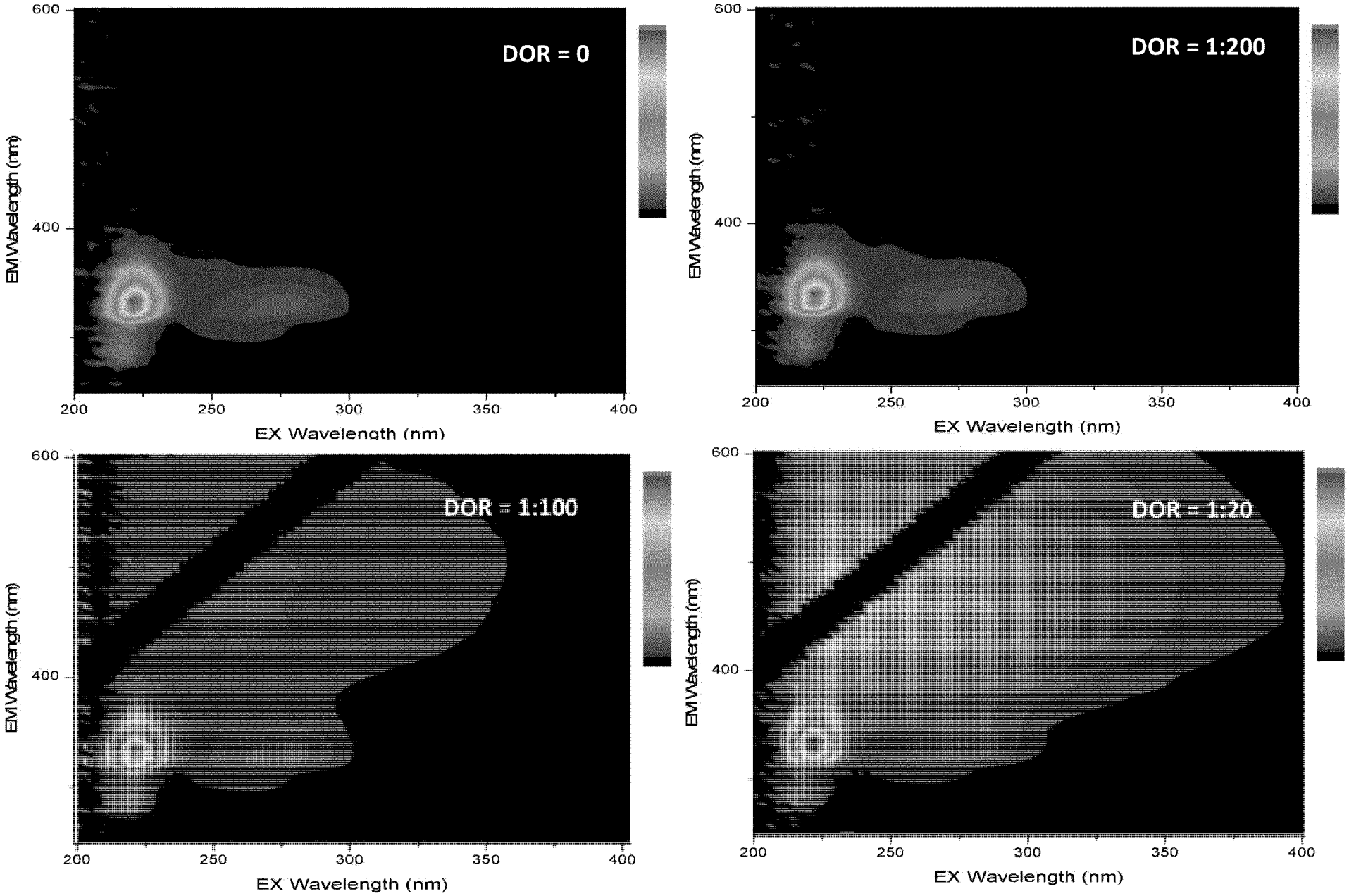

Appendix F - Figure F6. Light Oil Category – Hibernia crude oil with dispersant EEMs. Colored contours represent intensity, scaled to maximum fluorescence peak (red).

ED_001324_00000687-00117

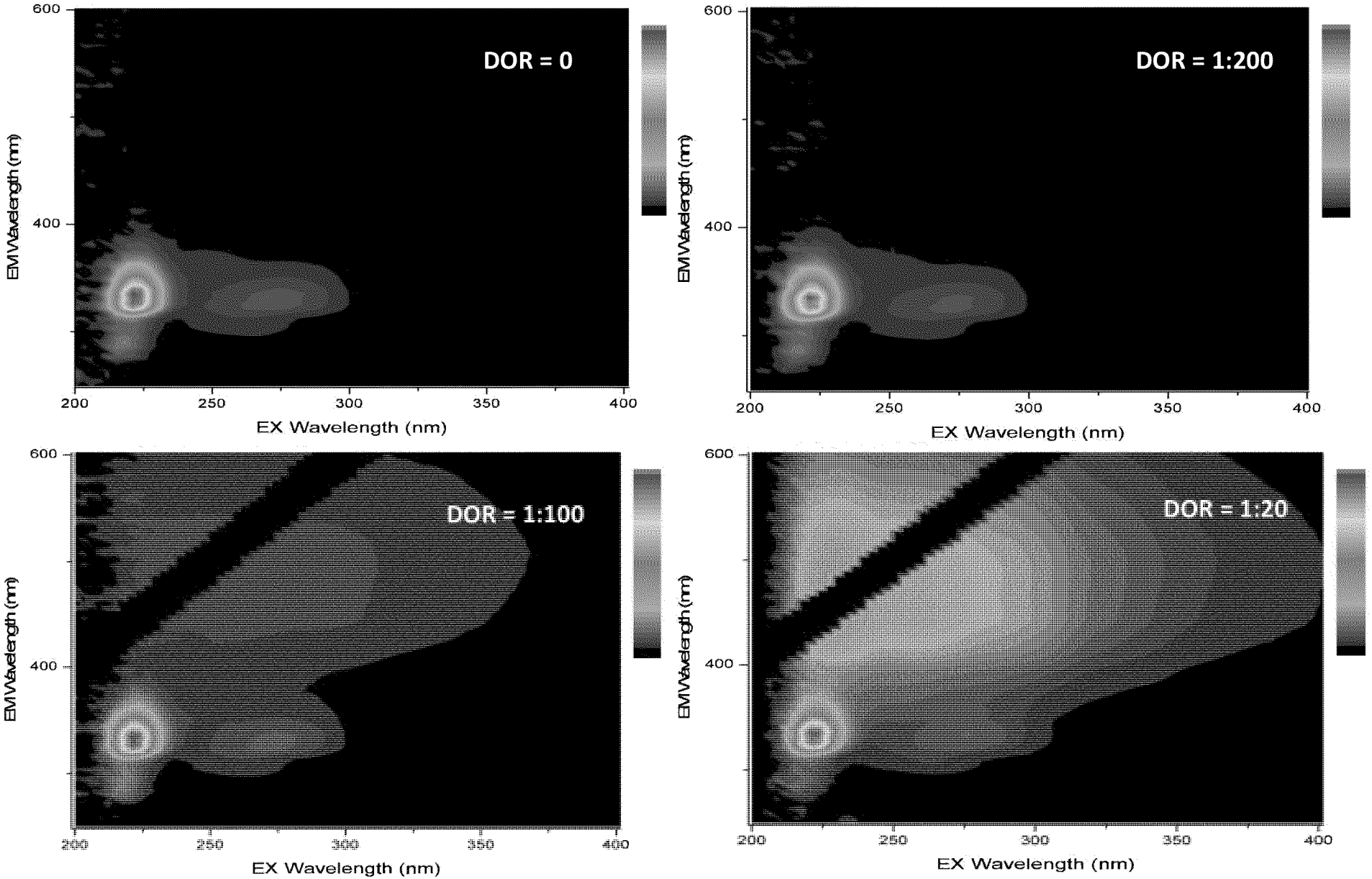

Appendix F - Figure F7. Light Oil Category – MC252 (Discoverer Enterprise) crude oil with dispersant EEMs. Colored contours represent intensity, scaled to maximum fluorescence peak (red).

ED_001324_00000687-00118

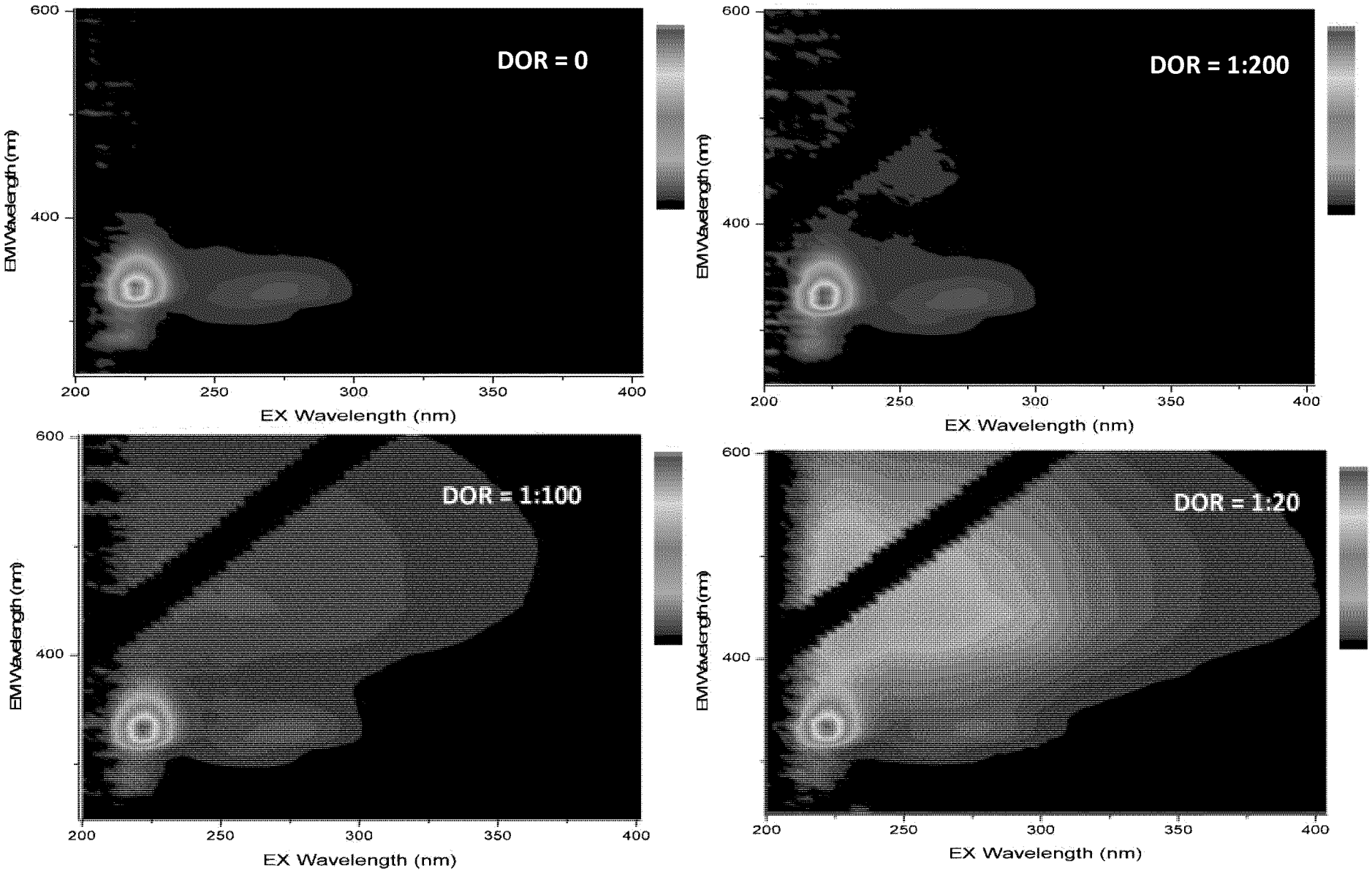

Appendix F - Figure F8. Light Oil Category– MC252 (Generic) crude oil with dispersant EEMs. Colored contours represent intensity, scaled to maximum fluorescence peak (red).

ED_001324_00000687-00119

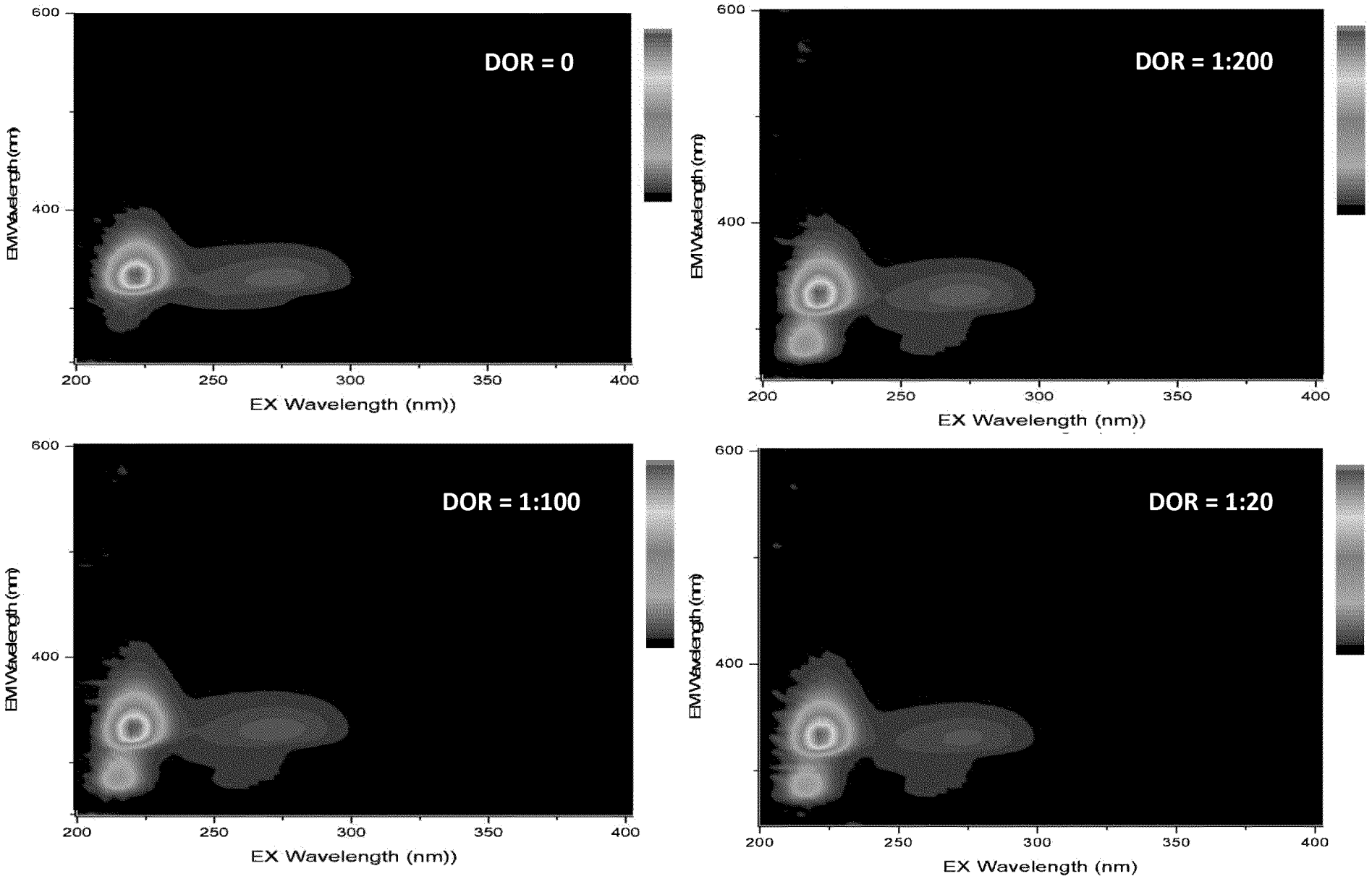

Appendix F - Figure F9. Light Oil Category – Scotian Shelf Condensate crude oil with dispersant EEMs. Colored contours represent intensity, scaled to maximum fluorescence peak (red).

ED_001324_00000687-00120

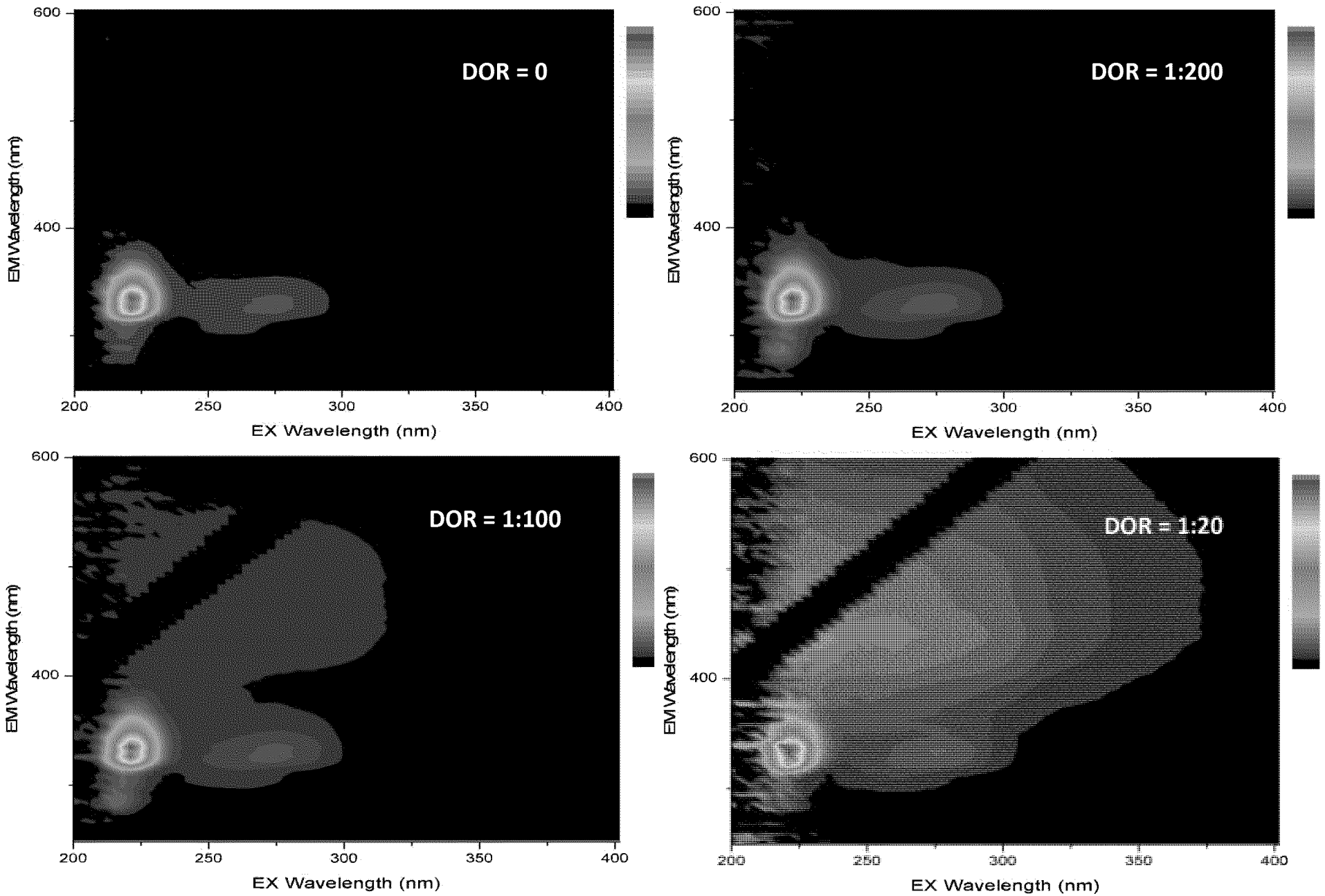

Appendix F - Figure F10. Light Oil Category– Sea Rose crude oil with dispersant EEMs. Colored contours represent intensity, scaled to maximum fluorescence peak (red).

ED_001324_00000687-00121

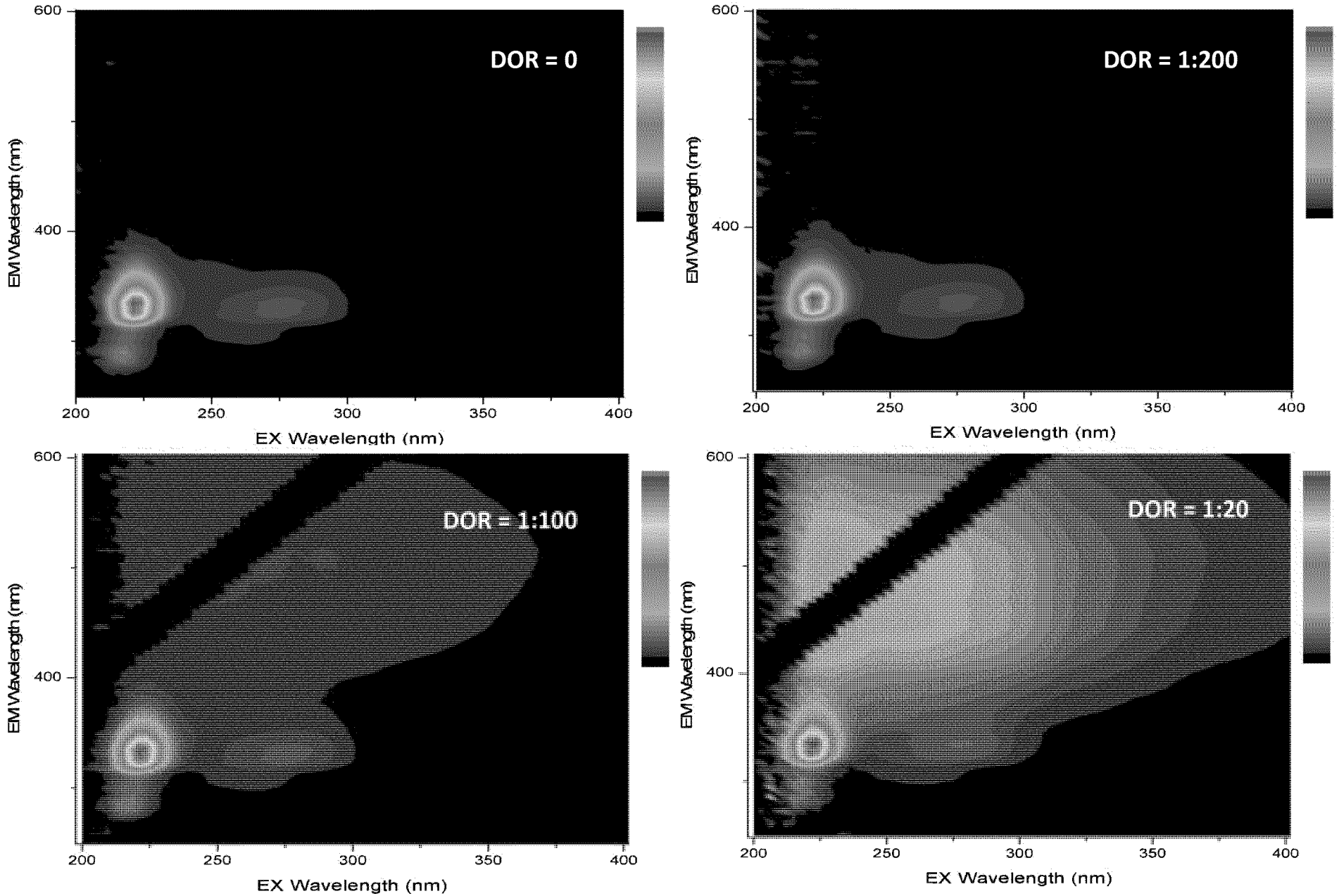

Appendix F - Figure F11. Light Oil Category – Terra Nova crude oil with dispersant EEMs. Colored contours represent intensity, scaled to maximum fluorescence peak (red).

ED_001324_00000687-00122

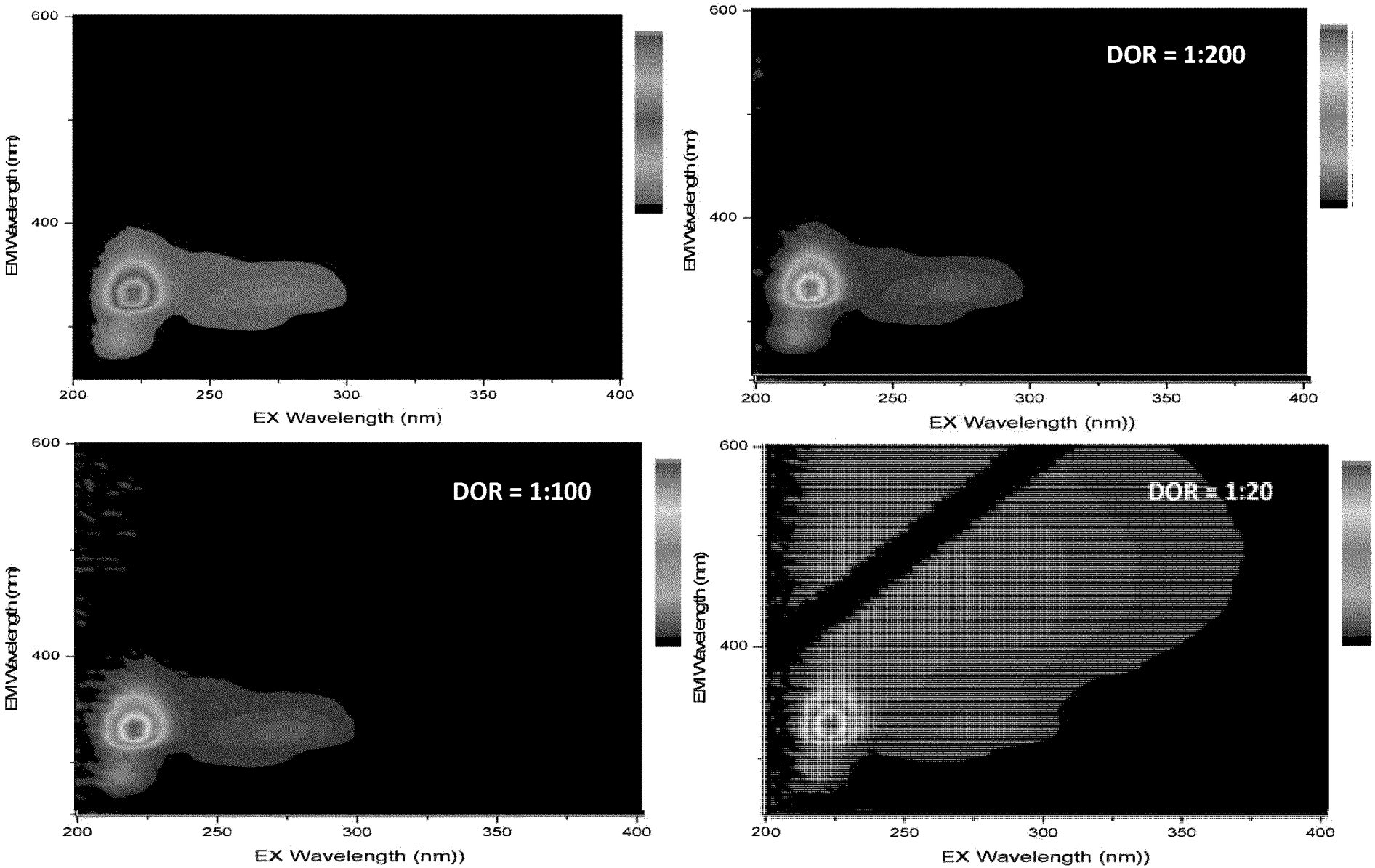

Appendix F - Figure F12. Medium Oil Category - ANS (Alaskan North Slope) crude oil with dispersant EEMs. Colored contours represent intensity, scaled to maximum fluorescence peak (red).

ED_001324_00000687-00123

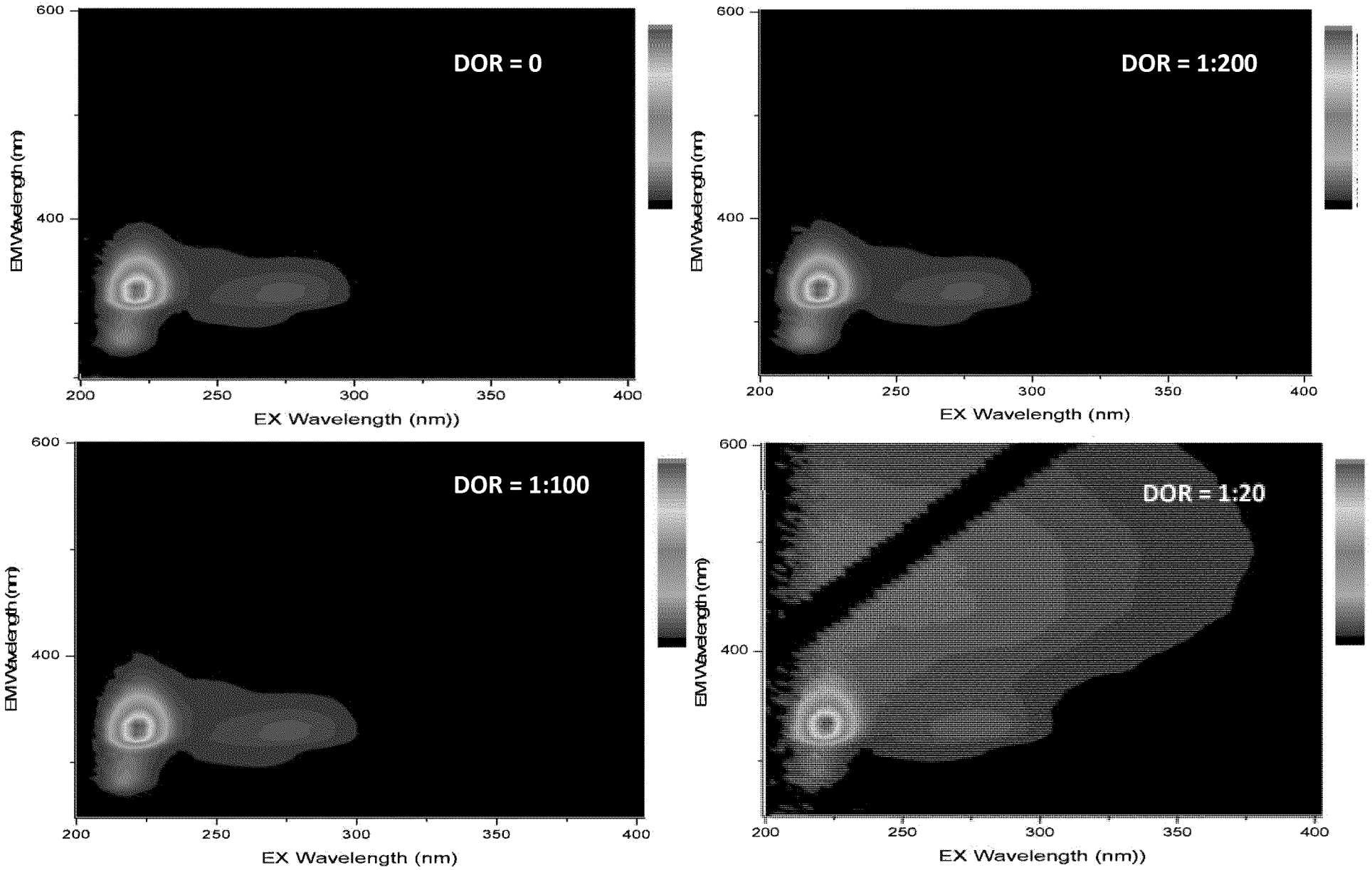

Appendix F - Figure F13. Medium Oil Category - 10% Weathered ANS (Alaskan North Slope) crude oil with dispersant EEMs. Colored contours represent intensity, scaled to maximum fluorescence peak (red).

ED_001324_00000687-00124

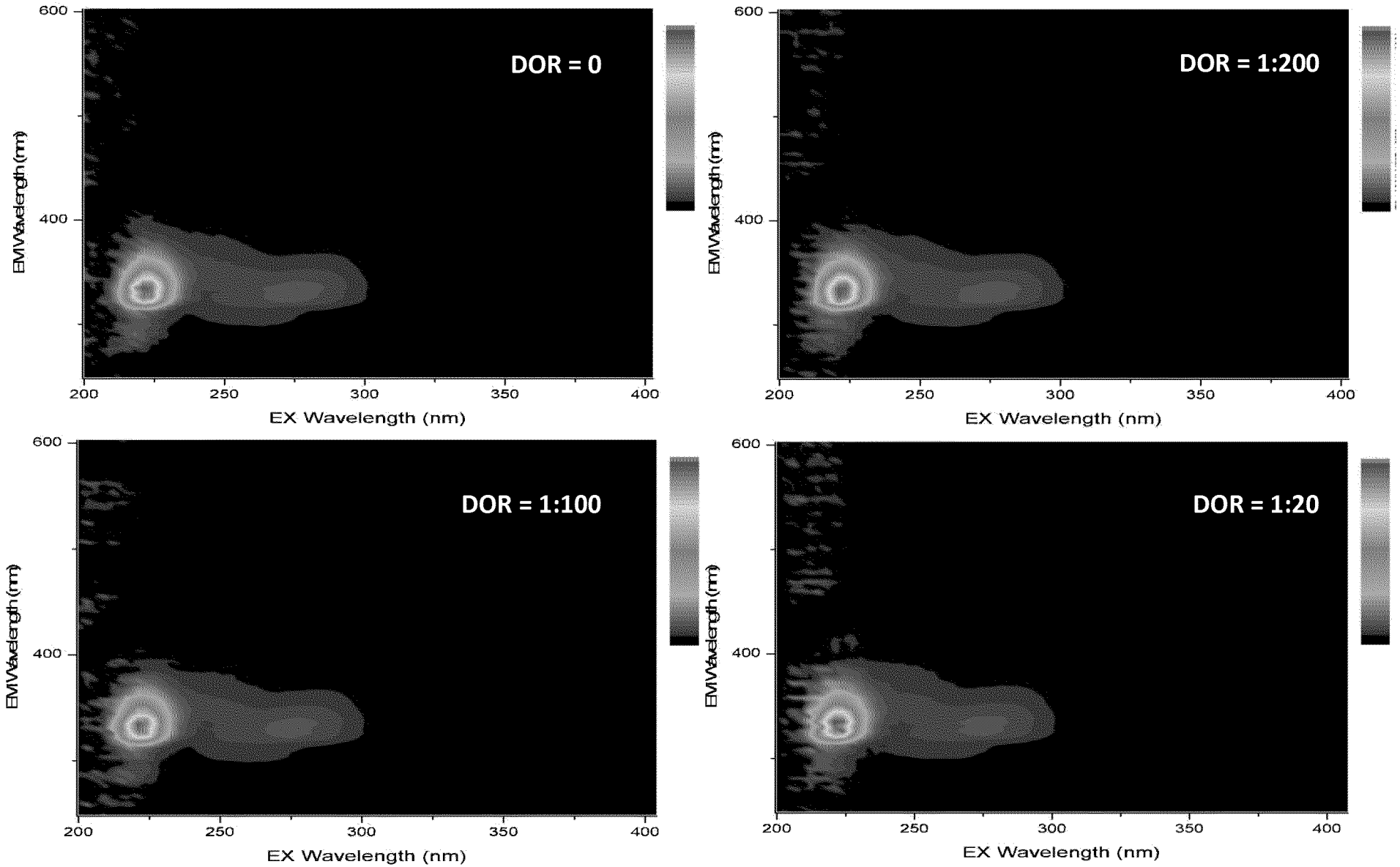

Appendix F - Figure F14. Medium Oil Category – Heavy IFO-120 oil with dispersant EEMs. Colored contours represent intensity, scaled to maximum fluorescence peak (red).

ED_001324_00000687-00125

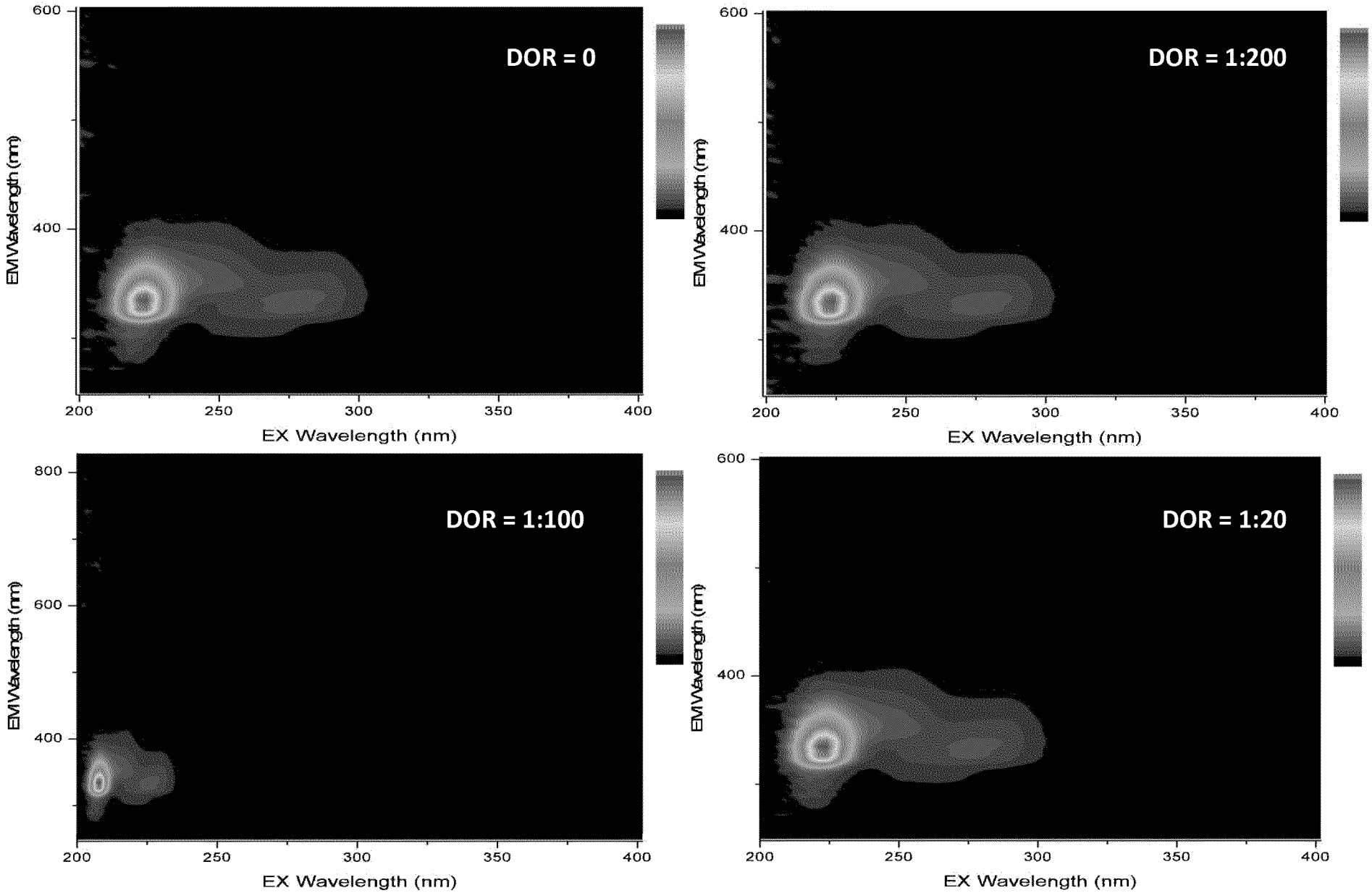

Appendix F - Figure F15. Medium Oil Category - Heavy IFO-180 oil with dispersant EEMs. Colored contours represent intensity, scaled to maximum fluorescence peak (red).

ED_001324_00000687-00126

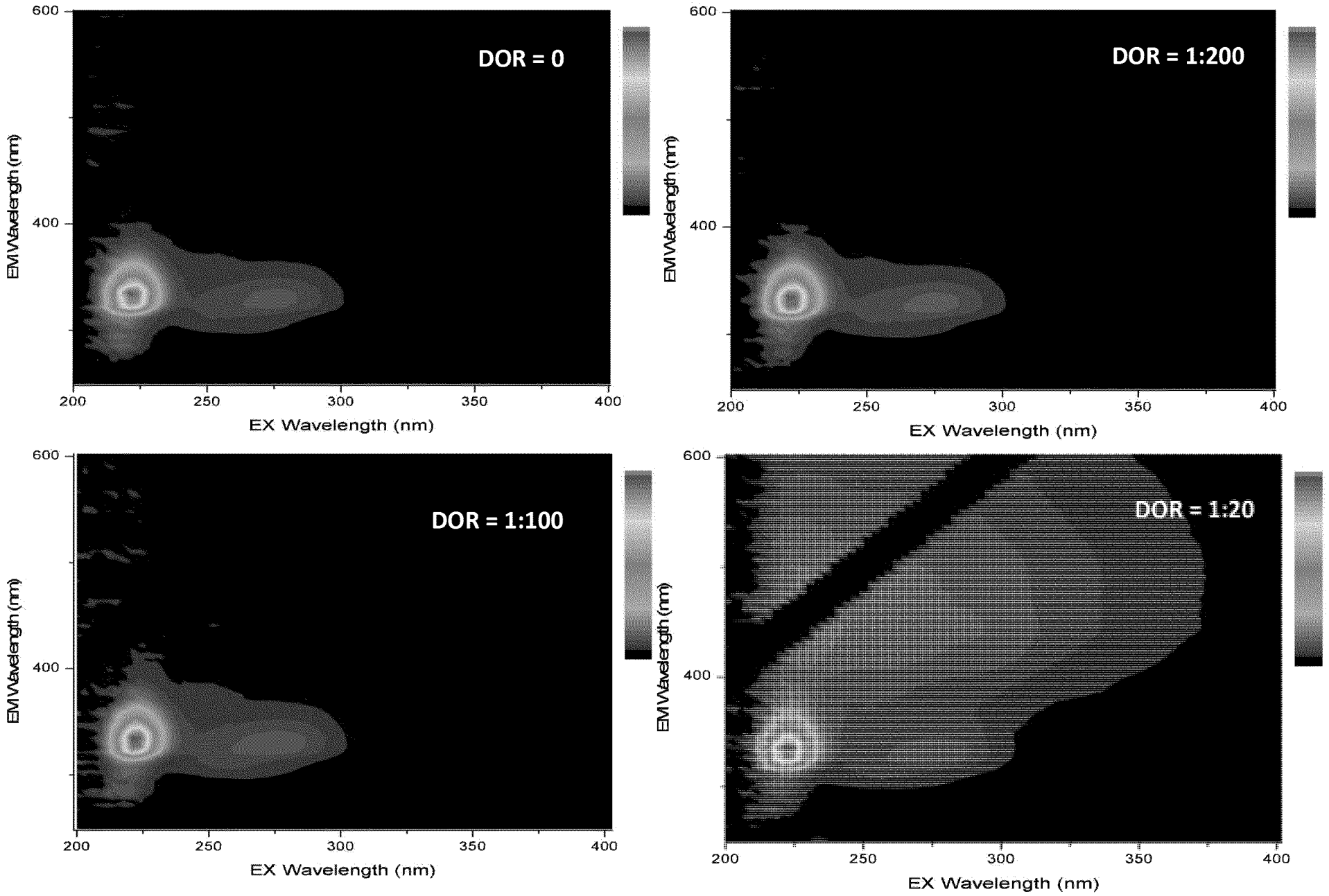

Appendix F - Figure F16. Medium Oil Category - Heidrun crude oil with dispersant EEMs. Colored contours represent intensity, scaled to maximum fluorescence peak (red).

ED_001324_00000687-00127

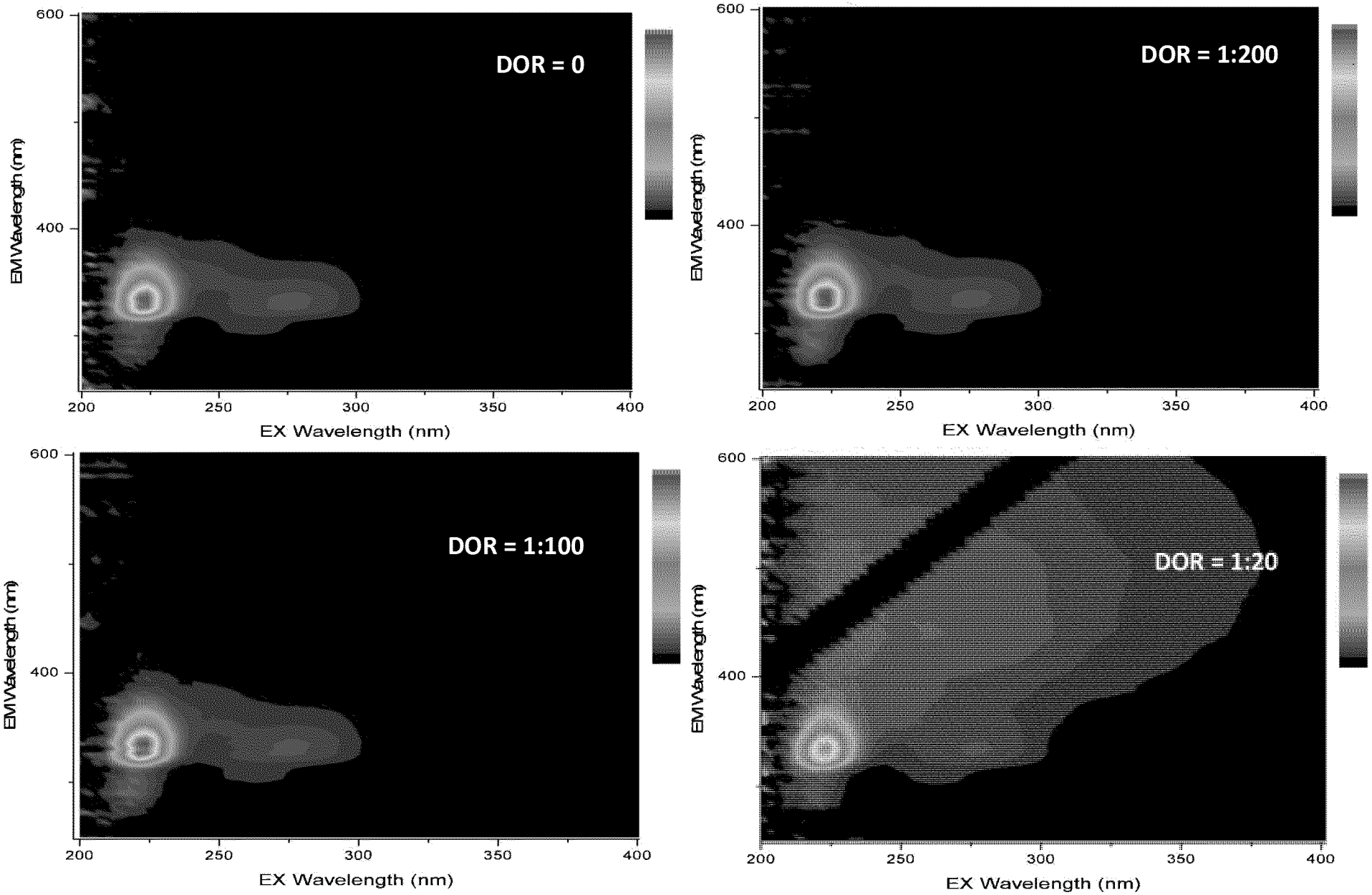

Appendix F - Figure F17. Medium Oil Category - Lago crude oil with dispersant EEMs. Colored contours represent intensity, scaled to maximum fluorescence peak (red).

ED_001324_00000687-00128

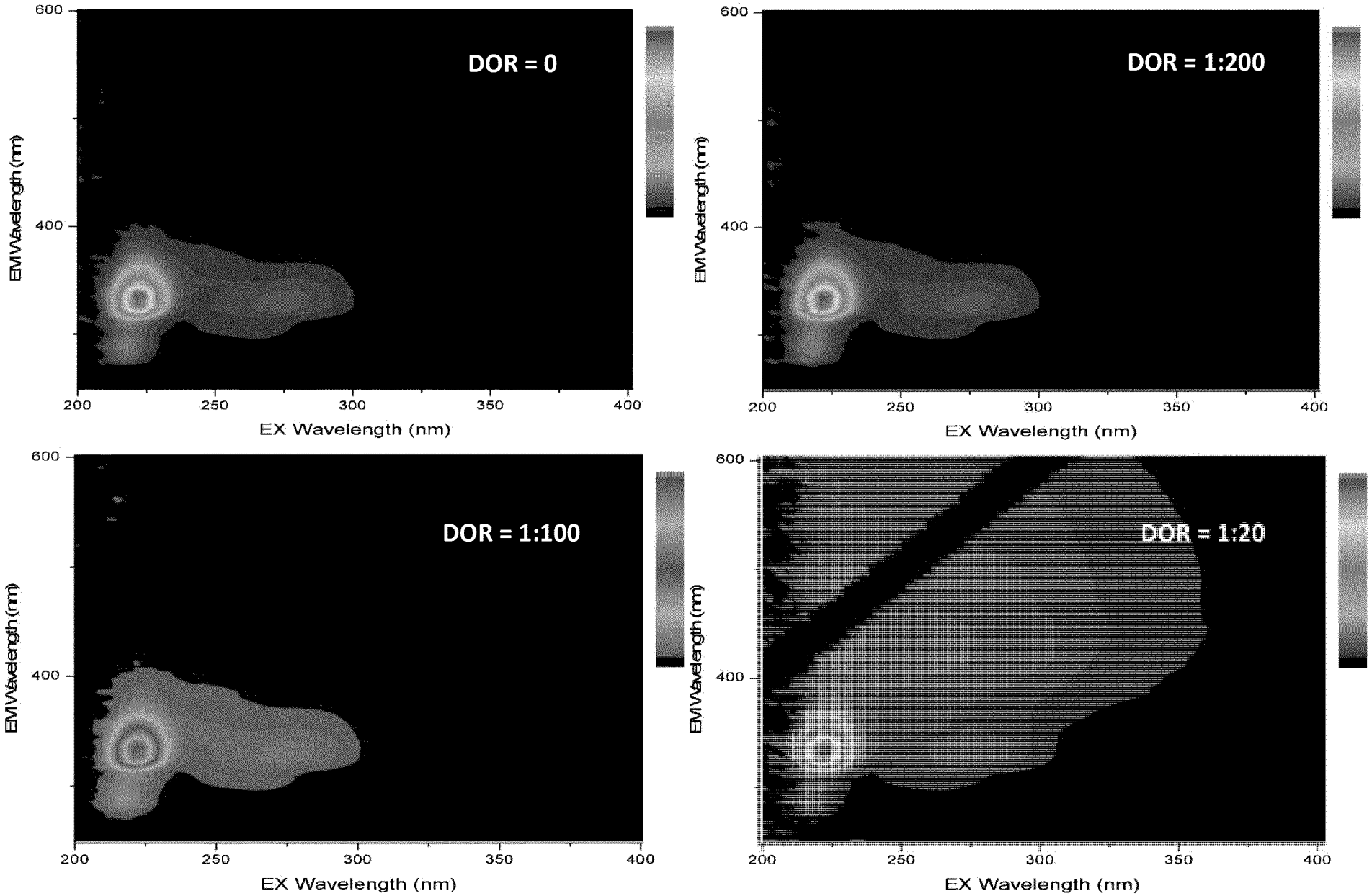

Appendix F - Figure F18. Medium Oil Category- Mesa crude oil with dispersant EEMs. Colored contours represent intensity, scaled to maximum fluorescence peak (red).

ED_001324_00000687-00129

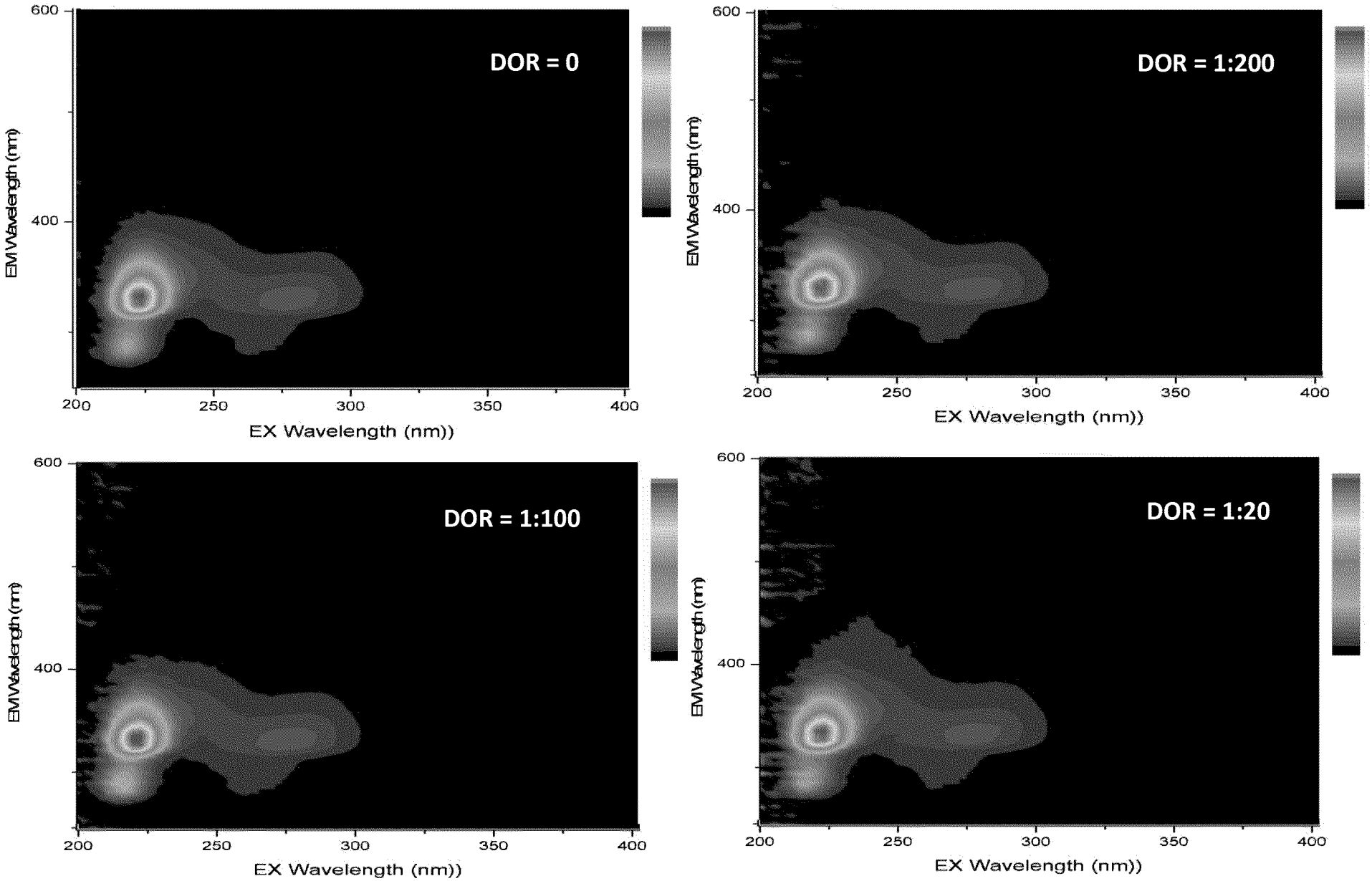

Appendix F - Figure F19. Medium Oil Category – Santa Clara crude oil with dispersant EEMs. Colored contours represent intensity, scaled to maximum fluorescence peak (red).

ED_001324_00000687-00130

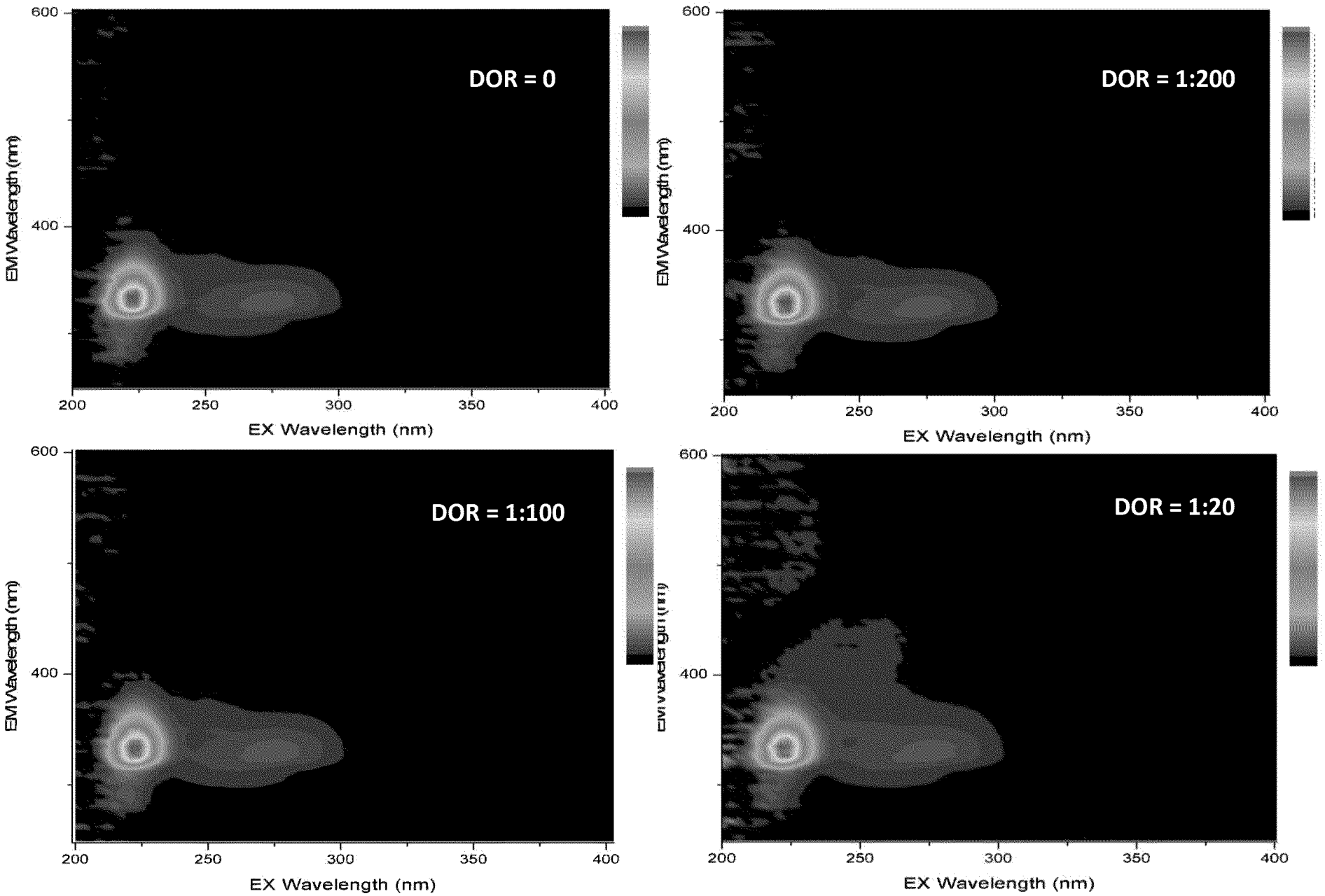

Appendix F - Figure F20. Medium Oil Category - Vasconia crude oil with dispersant EEMs. Colored contours represent intensity, scaled to maximum fluorescence peak (red).

ED_001324_00000687-00131

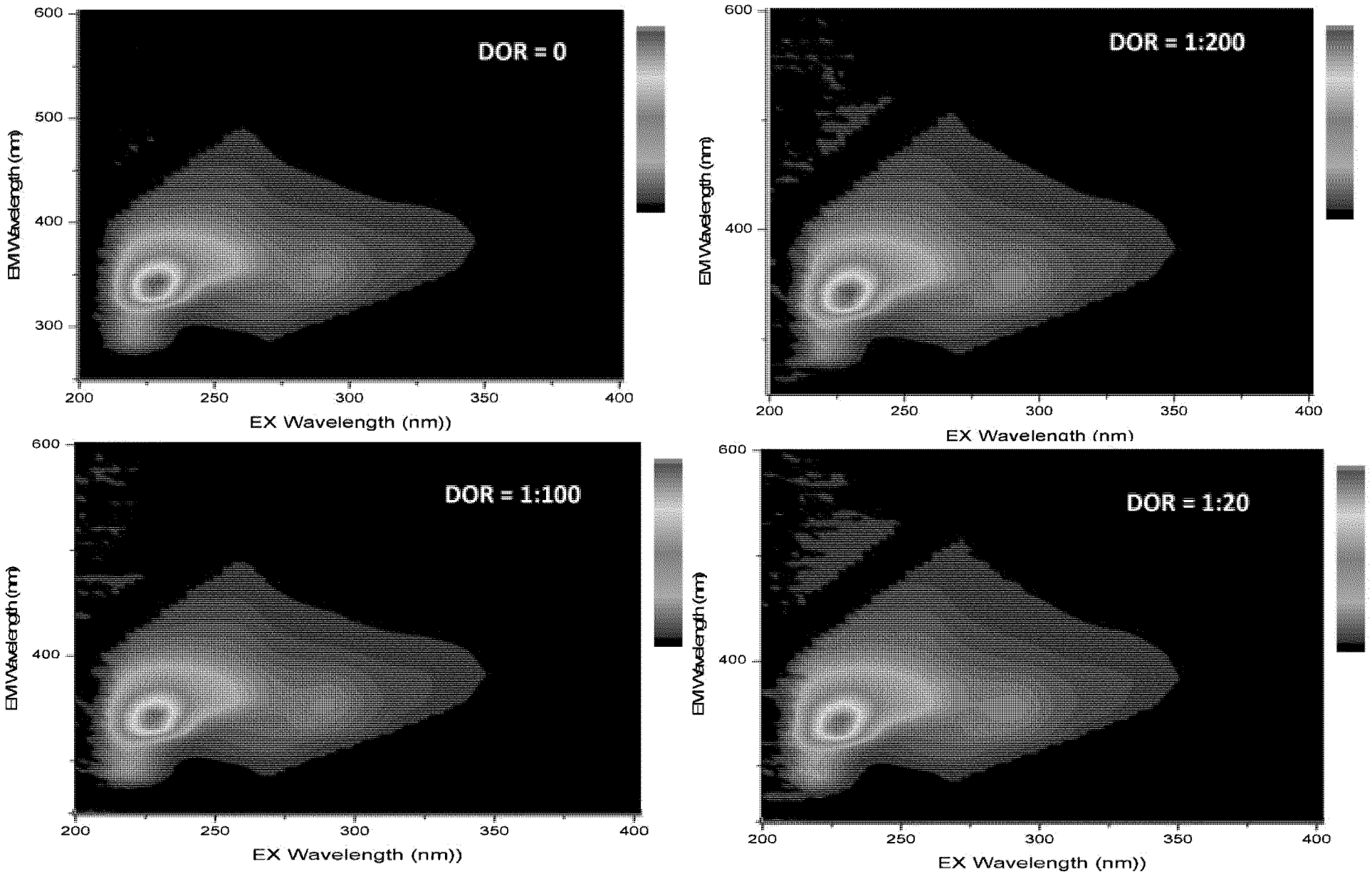

Appendix F - Figure F21. Heavy Oil Category - Belridge crude oil with dispersant EEMs. Colored contours represent intensity, scaled to maximum fluorescence peak (red).

ED_001324_00000687-00132

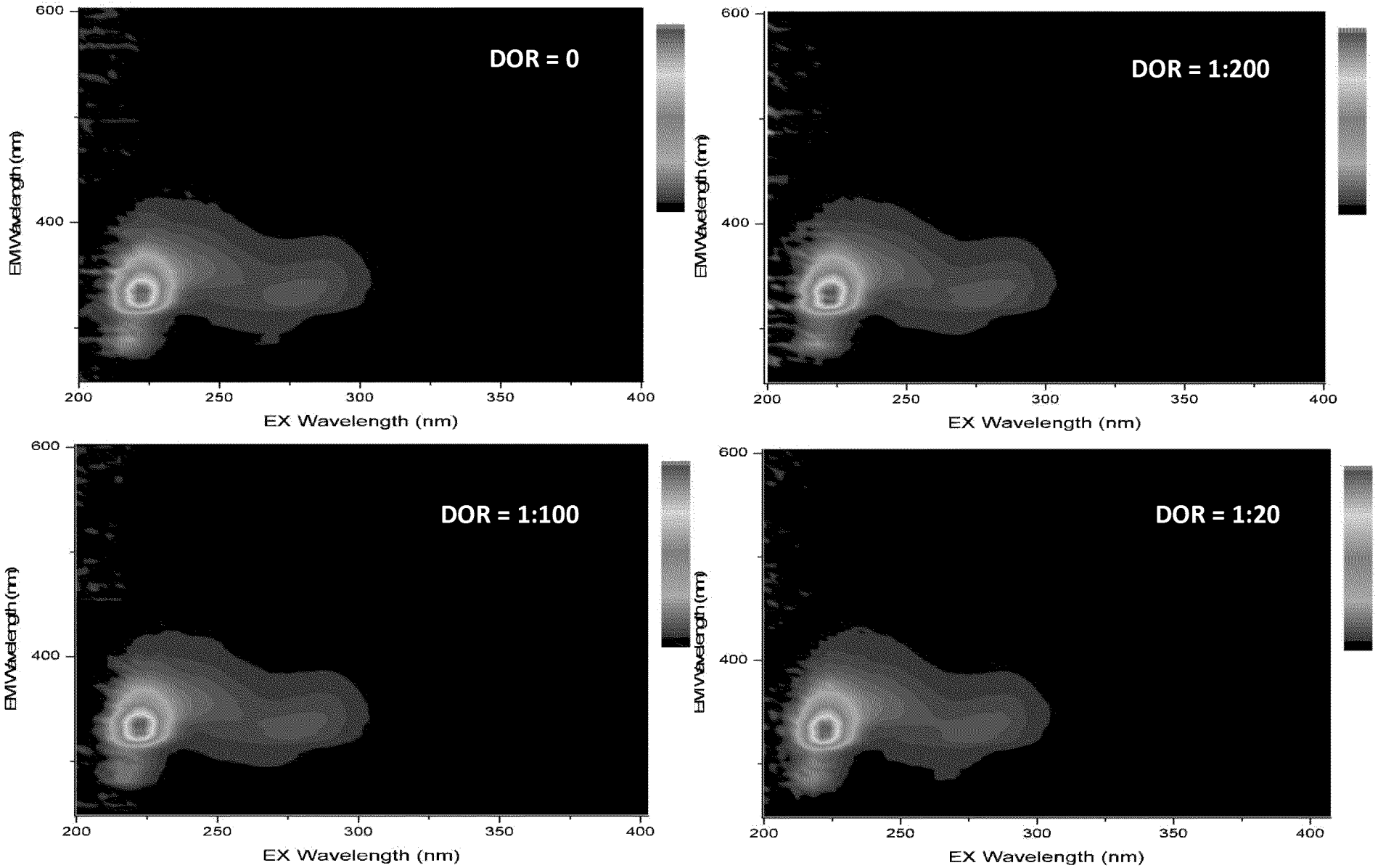

Appendix F - Figure F22. Heavy Oil Category - Hondo crude oil with dispersant EEMs. Colored contours represent intensity, scaled to maximum fluorescence peak (red).

ED_001324_00000687-00133

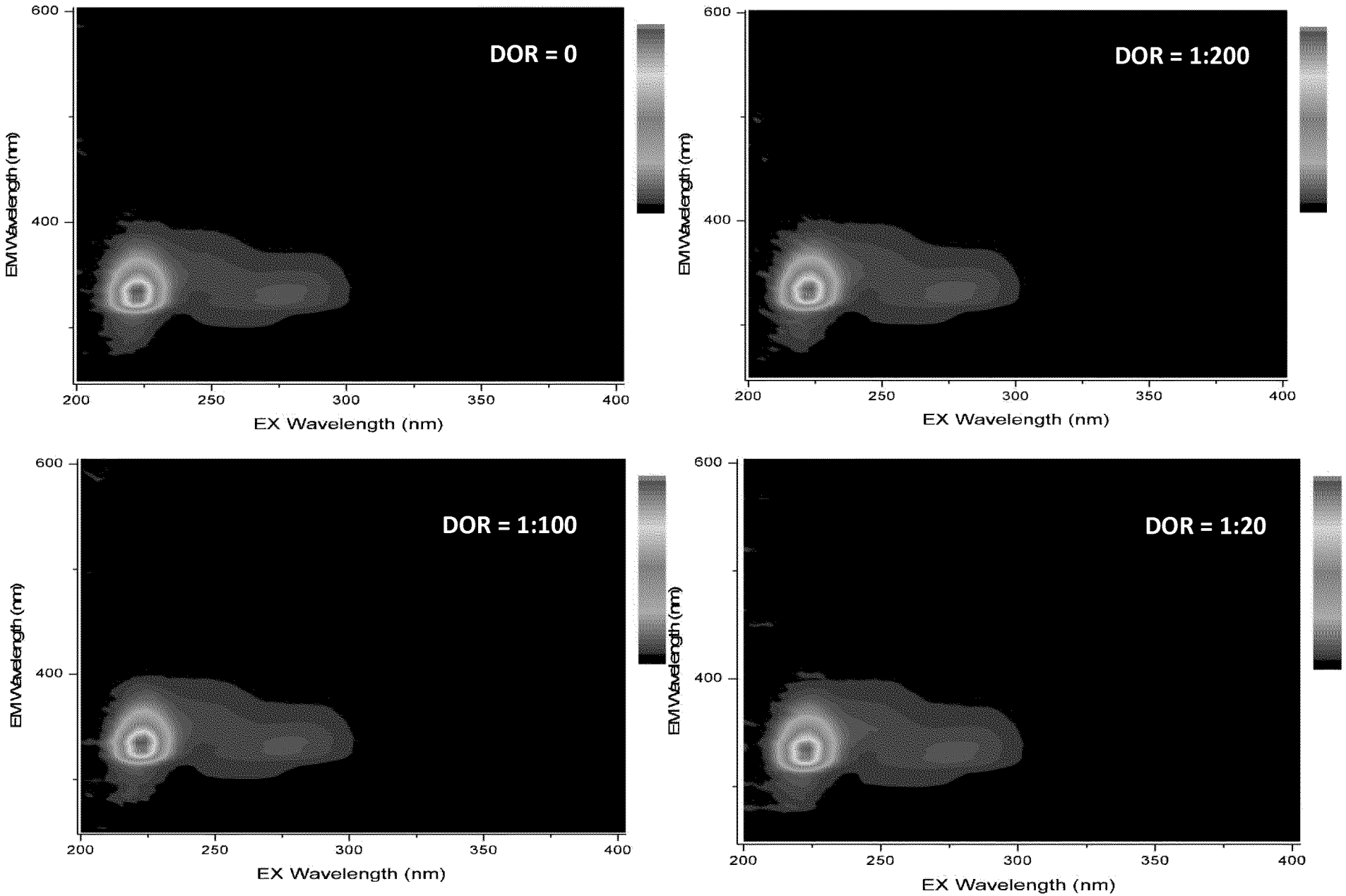

Appendix F - Figure F23. Heavy Oil Category – IFO-300 crude oil with dispersant EEMs. Colored contours represent intensity, scaled to maximum fluorescence peak (red).

ED_001324_00000687-00134

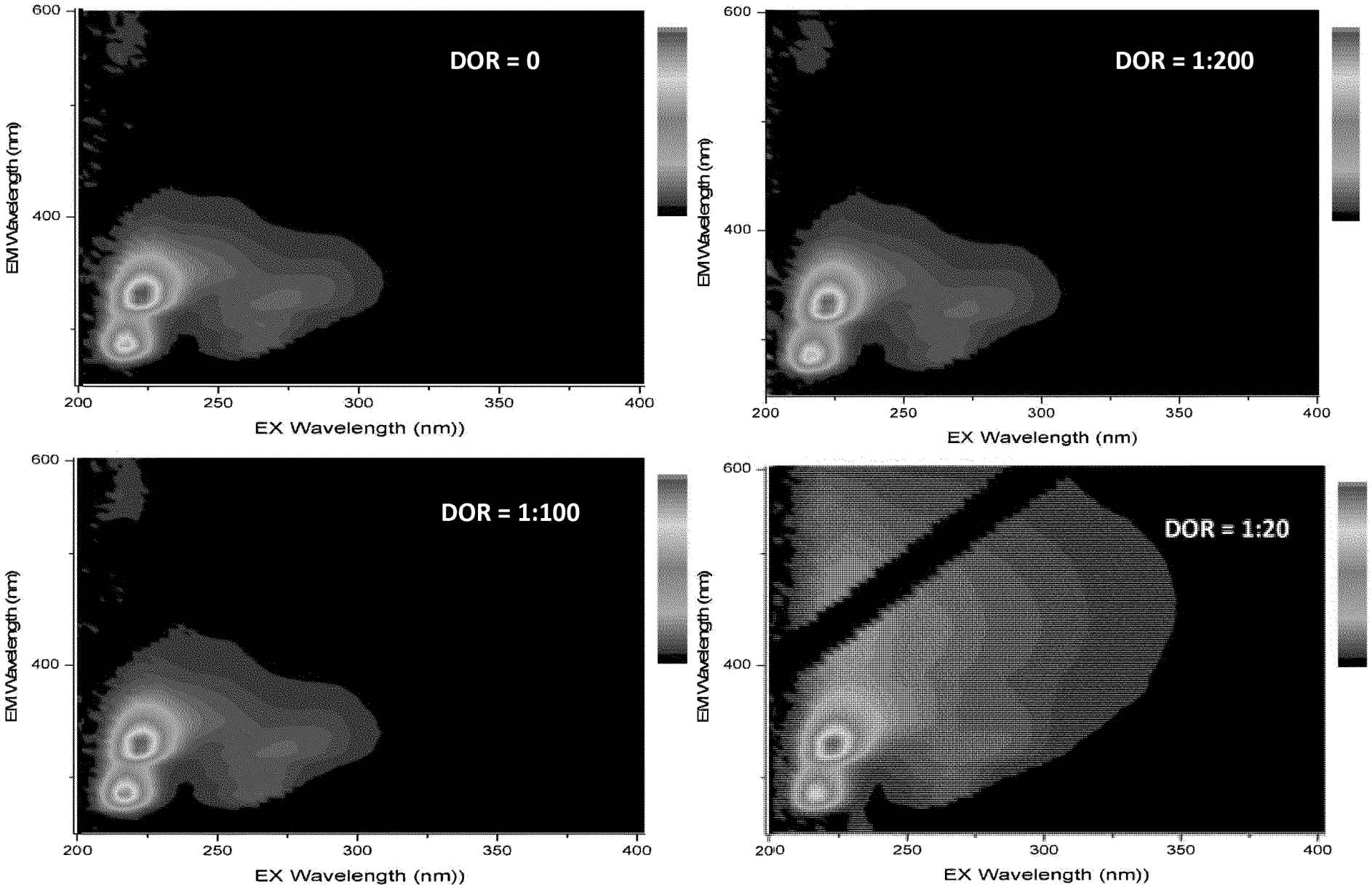

Appendix F - Figure F24. Dilbit Oil Category – Access Western Blend oil with dispersant EEMs. Colored contours represent intensity, scaled to maximum fluorescence peak (red).

ED_001324_00000687-00135

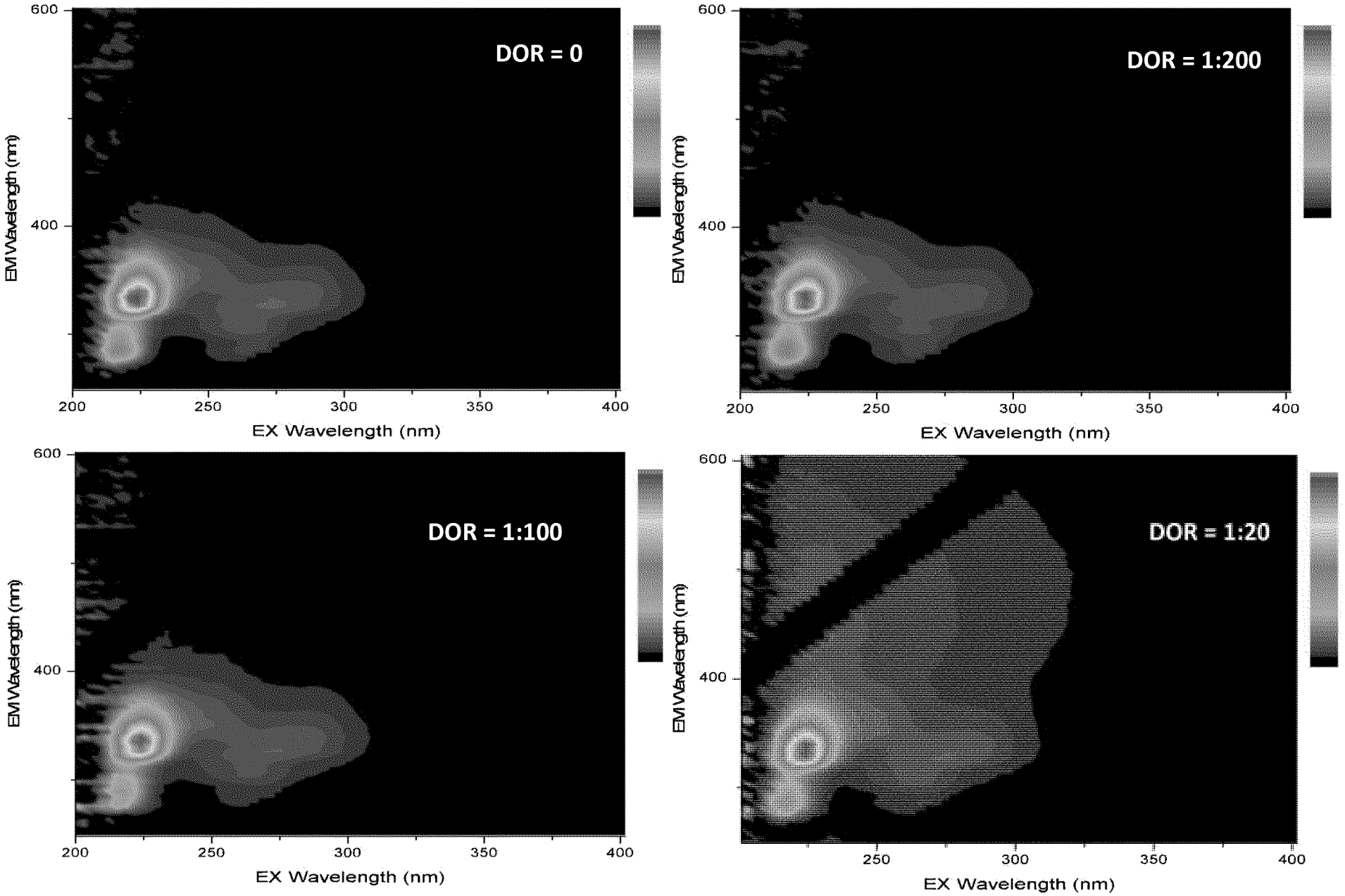

Appendix F - Figure F25. Dilbit Oil Category – Cold Lake oil with dispersant EEMs. Colored contours represent intensity, scaled to maximum fluorescence peak (red).

ED_001324_00000687-00136

ED_001324_00000687-00137

IAA No. E12PG00037

Final Report

Dispersant Effectiveness, In-Situ Droplet Size Distribution and Numerical Modeling to Assess Subsurface Dispersant Injection as a Deepwater Blowout Oil Spill Response Option

and

Evaluation of Oil Fluorescence Characteristics to Improve Forensic Response Tools

APPENDIX G VDROP-J and JETLAG Numerical Plume Modeling

Report on Simulated Oil Plume Advanced Numerical Modeling using VDROP-J and JETLAG

Prepared by:

Michel C. Boufadel, PhD, PE and Feng Gao

New Jersey Institute of Technology
Civil and Environmental Engineering
University Heights, Newark, NJ 07102
973-596-5657
Michel.boufadel@njit.edu

ED_001324_00000687-00138

Introduction

The goal was to develop the needed tools to simulate the horizontal release of oil from a horizontal orifice. The models were to be calibrated (i.e., trained) by simulating the release of oil from a 2.4 mm orifice in the BIO tank (32 m long, 0.6 m wide, and 2.0 m tall, but contains water at a depth of 1.5 m). The BIO tank contains also currents at a n approximate speed of 5.0 cm/s along the duration of the jet.

The orifice had an elevation of 0.25 m from the inside bottom of the tank, and thus the distance between it and the water surface is 1.25 m. The diameter of the orifice was 2.4 mm. The oil was Alaskan North Slope (ANS) whose density ρ = 866 kg/m3, dynamic viscosity μ=11.5 cp, and interfacial tension with water □ =0.02 N/m. The oil mass flow rate was 58g (approximately 0.06 liter per second, 3.6 liter per minute, around 1.0 gpm). The oil temperature in the canister was 80 ℃ while the water temperature in the tank was 15 ℃. Due to the short duration of the experiments and the relatively small volume of released oil, it is unlikely that the oil temperature raised the water temperature by a measurable amount.

Based on the volumetric oil flow rate and the diameter of the orifice, the average oil exit velocity is 13.3 m/s. In the absence of dispersant, the Reynolds and Weber numbers are:

$$\mathrm{Re} \square \frac{\square . V . D}{\square} \square \frac{(866)(13.3)(0.0024)}{0.0113} \square 2{,}500 \quad (1)$$

$$\mathrm{We} \square \frac{\square . V^2 . D}{\square} \square \frac{(866)(13.3)^2(0.0024)}{0.02} \square 18{,}000 \quad (2)$$

Another important number is the Ohnsorge number given as:

$$Oh \square \frac{We^{0.5}}{\mathrm{Re}} \square \frac{\square}{(\square\square D)^{0.5}} \square \frac{(0.0115)}{(866 \square 0.02 \square 0.0024)^{0.5}} \square 0.055 \quad (3)$$

Based on Figure 1 ofJohansen et al. (2013), the resulting jet is in the atomization regime (the blue dot in the graph).

ED_001324_00000687-00139

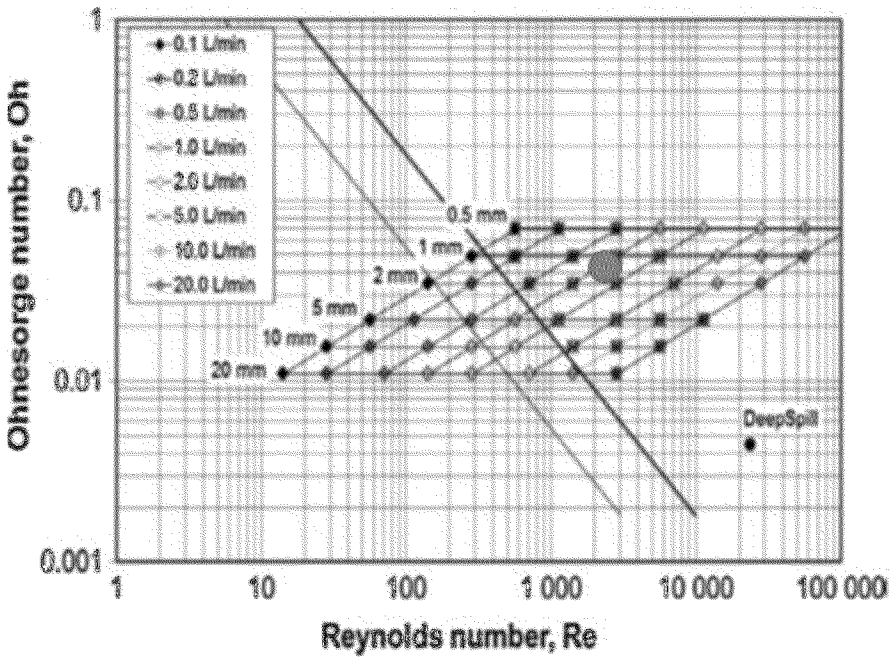

Figure 1: Experimental conditions plotted in the diagram of the Ohnesorge vs. Reynolds number as obtained by Johansen et al. (2013).The injection rate varied from 0.1 to 20 L/min, with nozzle diameters varied from 0.5 to 20 mm. The oil viscosity is presumed to be 5 cP. The thick line in the diagram shows the boundary between transitional and atomization breakup. The blue disk represents the experimental conditions of the BIO tank (this study).

Technical Approach

There are two major challenges with modeling oil jets. The first is the hydrodynamics of the jet and the other is the formation of droplets. However, we approach this problem first from an engineering point of view where we attempt to understand the engineering properties of the jet, and then by zooming in on the hydrodynamics of the jet and the movement of oil droplets. For this purpose, we use first the models VDROP -J and JETLAG, which provide the average hydrodynamics properties along the centerline of the jet. The model VDROP -J provides also the centerline droplet size distribution. In the second step, we use the models Fluent a Computational Fluid Dynamics (CFD) model and the model NEMO3D for tracking the individual oil droplets.

The layout of the document is as follows: The next Secti on addresses the modeling using the engineering approach. The following section addresses the detailed hydrodynamics of the plume and the movement of individual oil droplets as they interact with their surroundings. In that Section, we address the droplet size distribution within the plume, which would help to design future experiments.

ED_001324_00000687-00140

Engineering Properties of Jet Hydrodynamics

For jet hydrodynamics, we use herein the models VDROP and JETLAG to capture the behavior of the plume. While the model VDROP p rovides the centerline velocity based on correlations from the literature, the model JETLAG provides the average velocity within the plume. To allow comparison, we used the Gaussian approximation for the velocity profile across the jet, and we computed the peak (centerline) velocity from JETLAG. The resulting velocity along the centerline of the plume is reported in Figure2 for VDROP and for JETLAG in the presence of a current Ua=3.0 cm/s and in the absence of current (Ua=0 cm/s). The agreement is very go od between the two cases lending further credence that VDROP-J is compatible with numerical models of plumes such as JETLAG.

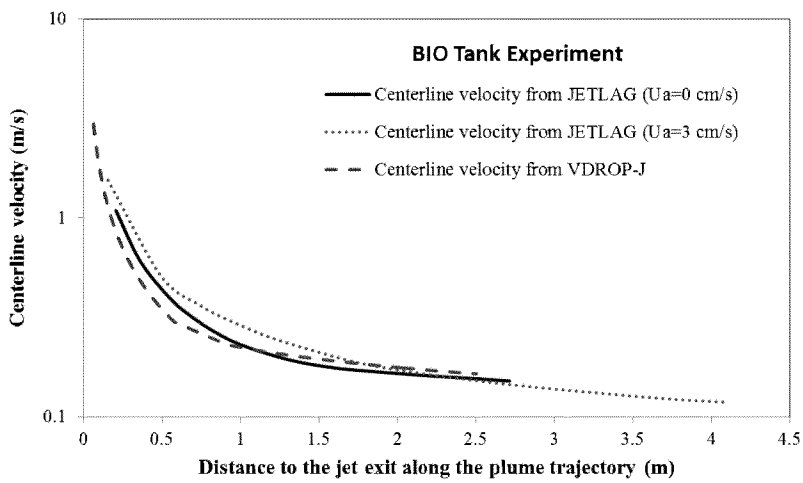

Figure 2: The velocity along the centerline of the jet/plume using VDROP -J and JETLAG. The velocity along the centerline of the jet/plume using VDROP -J and JETLAG. Note that the agreement was particularly good considering that no fitting was conducted, rather each model was run with the parameters stated in the Problem Statement Section.

The holdup is defined as the ratio of the volume of oil at a particular location in the plume to the total volume (oil+water) at that location. The value of the holdup affects the droplet size distribution, and reflects the intensity of water entrainment into the jet/p lume; a large holdup value results in a high rate of coalescence between droplets. Figure 3 reports the holdup along the centerline using VDROP -J and JETLAG, and one clearly notes that the agreement is good further reflecting the compatibility of VDROP -J with JETLAG for evaluating the mass of oil in the jet/plume. The holdup decreased sharply from around 10% at few centimeters from the pipe exit to almost 0.5% after 2.5 m. Thus at 2.5 m, 99.50% of the fluid in the plume is made up of water.

ED_001324_00000687-00141

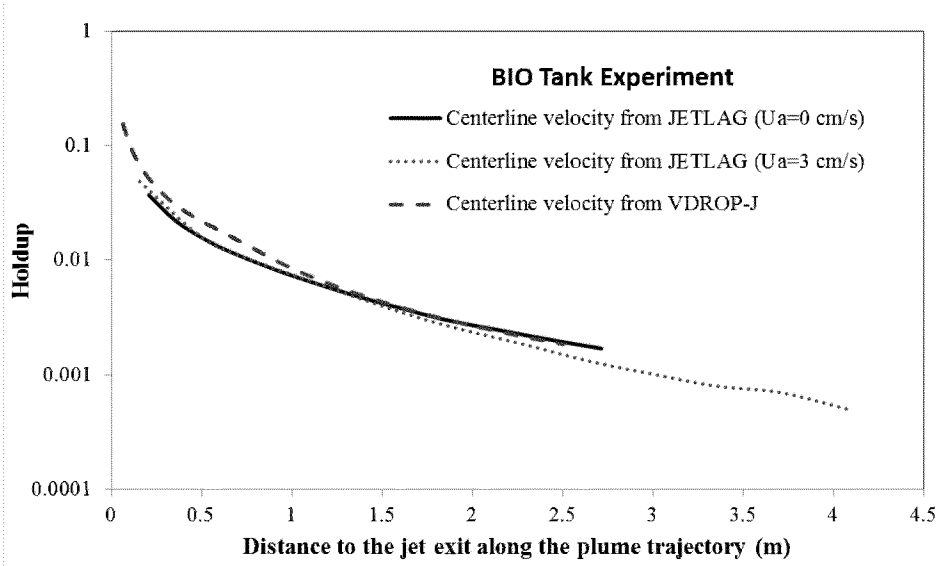

Figure 3: Holdup (ratio of oil volume to total volume of fluid) as function of distance from the pipe exit. Note the rapid decrease, which required a logarithmic scale for the holdup.

Figure 4 shows the simulation results from JETLAG for the shape of the plume. It shows the centerline along with the lower and upper bound of the plume along the vertical plan (note that the plume is circular, and thus three dimensional). The location of the LISST used in the experiments is also reported, and its results will be discussed later in this document.

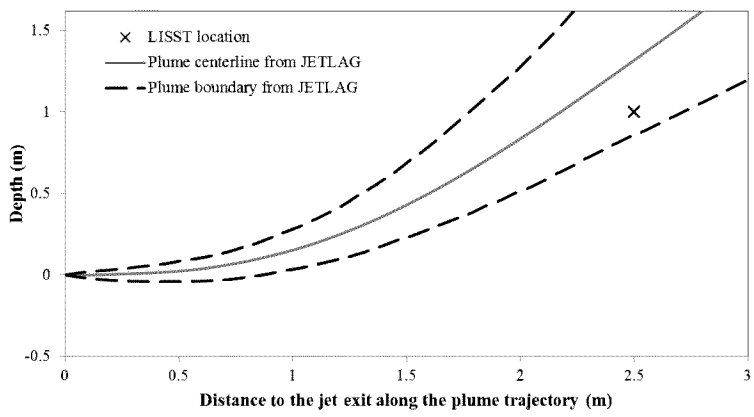

Figure 4: Plume centerline and boundaries based on the model JETLAG. The LISST was located within the plume near the lower edge of the plume.

ED_001324_00000687-00142

Droplet Size Distribution

Using only the parameters from the Problem Statement, we obtained the breakage constant Kb=0.1 from the correlation in Zhao et al. (2014). We then used VDROP-J to predict the droplet size distribution at the location of the LISST (given in Figure 5), and we compared it to the observed data from the LISST in Figure 4, which shows an exceptional agreement. The only adjustable parameter was the initial droplet size, selected at 500 microns herein. The initial size of the droplets results from the so-called primary breakup, and it depends on shear flow near the orifice and thus cannot be predicted by VDROP-J, which relies on turbulence away from boundaries.

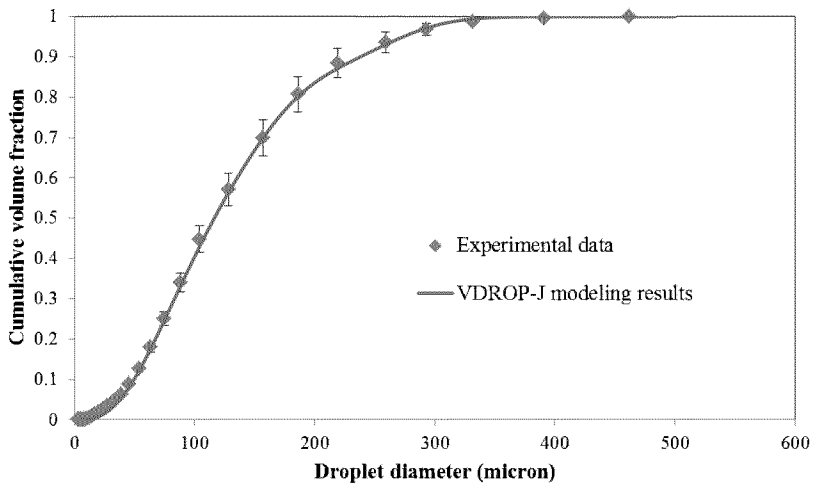

Figure 5: Droplet size distribution obtainedfrom VDROP-J and from the LISST (location reported in Figure 3) in the absence of dispersant.

Based on the good agreement between the model VDROP-J and experimental data, one can predict the DSD at various locations in the plume, as illustrated in Figure5; it is clear that the DSD changes drastically in the first meter of its trajectory, and the DSD does not change much afterward. This is reasonable as the mixing energy decreases rapidly with distance from the orifice (to the power "-4").

ED_001324_00000687-00143

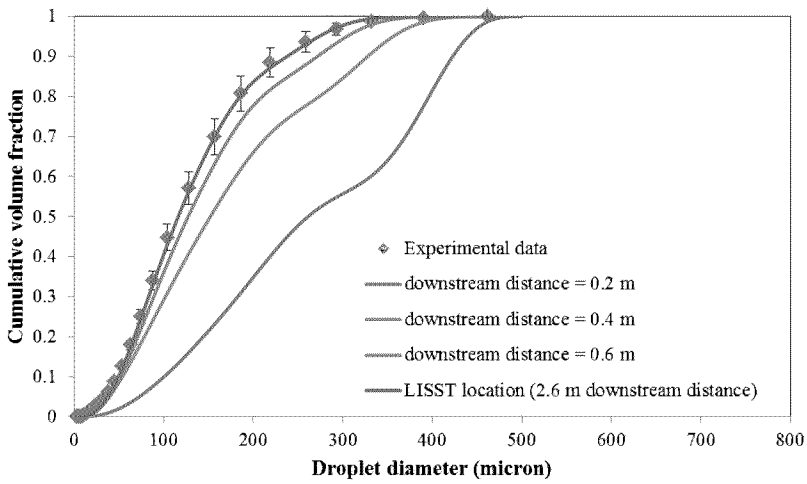

Figure 6: The droplet size distribution at various locations from the orifice along the centerline. The DSD essentially reached the steady state distribution within less than a meter.

The impact of dispersant was evaluated by premixing the oil with dispersant at the DOR of 1:20, and releasing oil at the same rate as before (see Problem Statement). The experimental and modeling results are reported in Figure 7. In the VDROP -J model, th e same parameters used earlier were used again with the exception of the interfacial tension, which was calibrated to be 0.0013 N/m, a reduction of 15 folds. The results in Figure 6 show a reasonable fit of the model to the data. The fit is good for larg er sizes, but it is relatively poor at the smaller sizes. To better illustrate this discrepancy, we used a different scale in the lower panel of Figure 7. The discrepancy is due to the fact that the oil and dispersants were premixed resulting in the so-called tip-streaming, whereby the oil peels off from the droplet without the action of mixing. It is a pure chemical process that VDROP-J is not designed to handle.

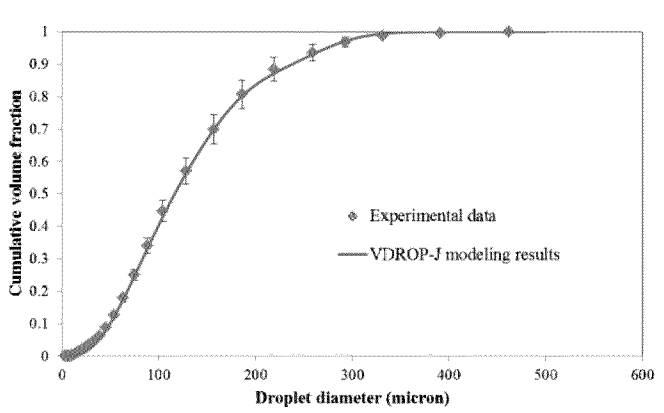

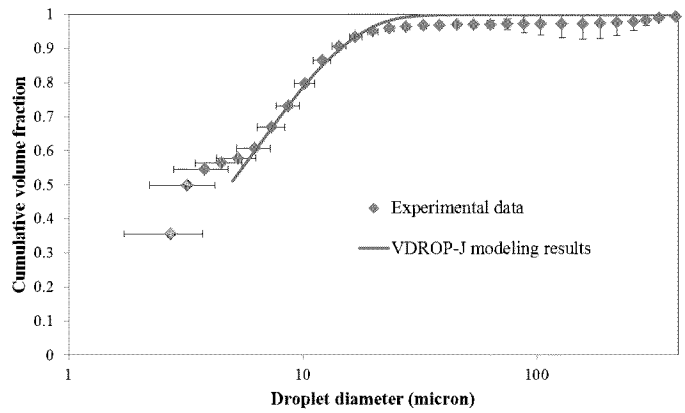

Figure 7: Droplet size distribution in the presence of d ispersant obtained at the location of the LISST in Figure 4. The difference between the two graphs is that the lower one has a logarithmic scale for the size axis.

Computational Fluid Dynamics

Evaluating the hydrodynamic properties of an oil jet (e.g., a blowout) is very difficult for a variety of reasons including: 1) The oil jet velocity is very large at the orifice (e.g., around 15 m/s for our experiment), and drops sharply with distance, and 2) there are multiple phases present, namely oil, water, and oil droplets in water, and 3) the turbulent energy and the presence of eddies prevents accurate evaluation of average speeds. For example, when using an acoustic Doppler velocimeter (ADV), one obtains different readings depending on the phase passing in front of the ADV. Hence, one needs a robust method to study the oil jet underwater numerically to complement experimental measurement.

We used computational fluid dynamics (CFD) to simulate the experiment of oil jet carried out at Bedford Institute of Ocean ography in Canada. In the CFD simulation, the computational domain consisted of 2,777,029 nodes. The turbulence model k □□ was selected, as it is most appropriate for such problems because of its usefulness of application in free -shear layer flows, calculation stability, and relative easiness of convergence (Aronson et al., 2000; Pope, 2000; Wilcox, 1998). The model relies on solving two equations to model the turbulent kinetic energy and the turbulence dissipation rate. The k □□ model belongs to th e family of RANS (Reynolds Average Navier Stokes) models, which aim to solve for the average flow field of turbulent flow (Eaton and Johnston, 1981).

In the present simulation, the achievement of steady state was observed based on monitoring the conservation of mass (e.g. the inflow rate of the oil equates the rate of the outflow of oil with a maximum of 1% difference. A m esh independent study was performed to ensure that the simulation results does not change with the further refinement of mesh . This was done by

ED_001324_00000687-00145

monitoring the average pressure at the outlet to see whether it changes with mesh refinement. After approximately 1 0,000 iterations, the simu lation reache d steady state with first order of accuracy as the mass conservation information was monitored. All simulations were run in parallel on 20 processors located on the NRDP Computational Laboratory.

Figure 8 shows results of CFD where the profile of the plume that was modelled based on an oil flow rate of 1.0 L/second. The purple lines represent the contours of the holdup, which is equal to the volume of oil divided by the volume of fluids in a given control volume. The holdup at the exit is 1.0, and one notes that it decreases to a few percent and even lower with 0.5 m. The contours of the velocity magnitude show velocities larger than 0.2 to 0.3 m/s within the plume but a sharp decrease at the edge of the plume. One also shows the velocity vect ors outside of the plume reflecting the entrainment of fluids (i.e., water) to the plume, especially near the exit to the tank.

Figure 9 shows the edge of the plume (delineated using 10% of the velocity) along with three locations for obtaining cross secti ons. Figures 10, 11, and 12 show cross sections of the holdup (lines) and velocity magnitude.

Figure 10 shows that the cross section is more or less circular as the exit point to the tank was circular. The lack of perfect circularity is due mesh discret ization. It appears that the bottom of the tank, which was at 25 cm below the exit, has an effect on the general flow circulation, as the flow vectors below the jet are different from those above it. But it is not sure if the bottom has any measurable effects on the hydrodynamics within the plume.

ED_001324_00000687-00146

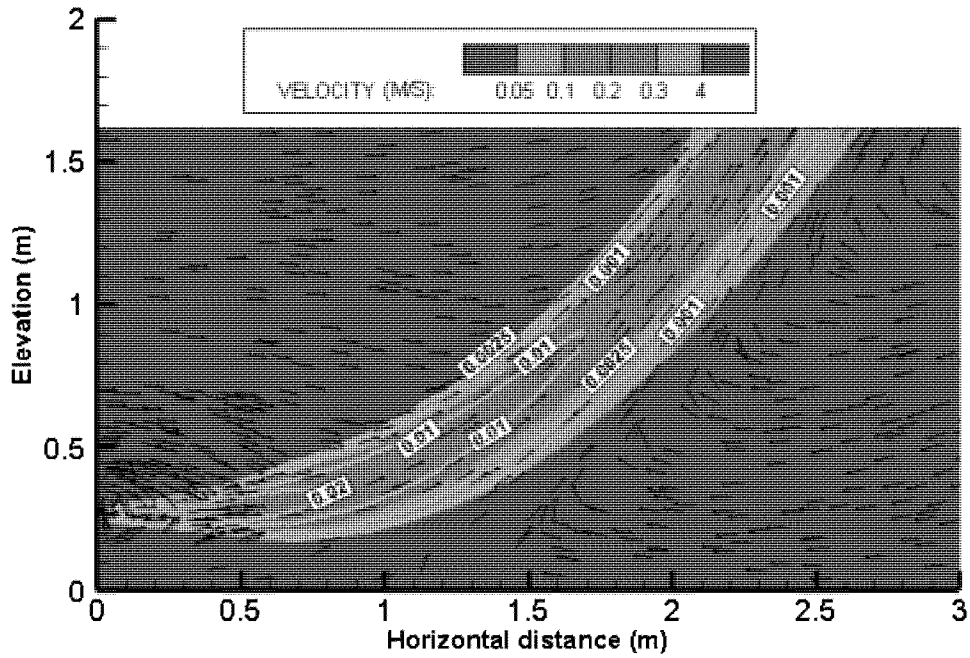

Figure 8: The profile of the plume through a vertical plane passing through the center axis. The figure shows the contour of the velocity magnitude (flooded colors) and the holdup (volume of oil to total liquid volume), using purple lines. The arrows indicate the velocity component in the plan of the figure. The length of the velocity vector does not represent the magnitude but only represents the direction.

ED_001324_00000687-00147

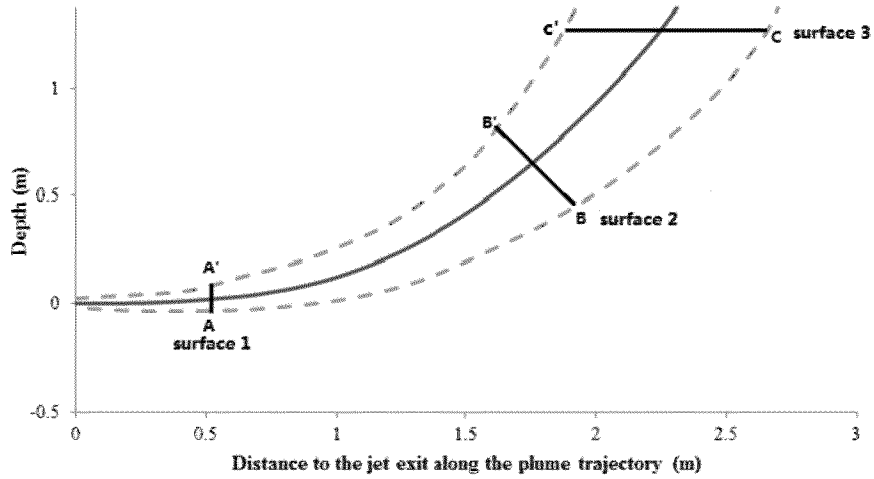

Figure 9: The locations of cut cross sections along the plume trajectory. The cross sections are numbered as surface-1, surface-2 and surface-3 as they are distant away from the orifice. "Surface1" is 0.5 m away from the orifice and perpendicula r to the horizontal direction. "Surface -2" is centered at 0.81 m above the jet orifice and 45°to the tank bottom. "Surface-3" is parallel to the horizontal, and 10 cm below the water surface. The green curve denotes the center line of the jet plume and the dotted orange lines denote the edge of the plume (which is defined by 10 % of the centerline velocity magnitude). The cross sections are cut while being at downstream locations (i.e., one sees the jet coming toward them).

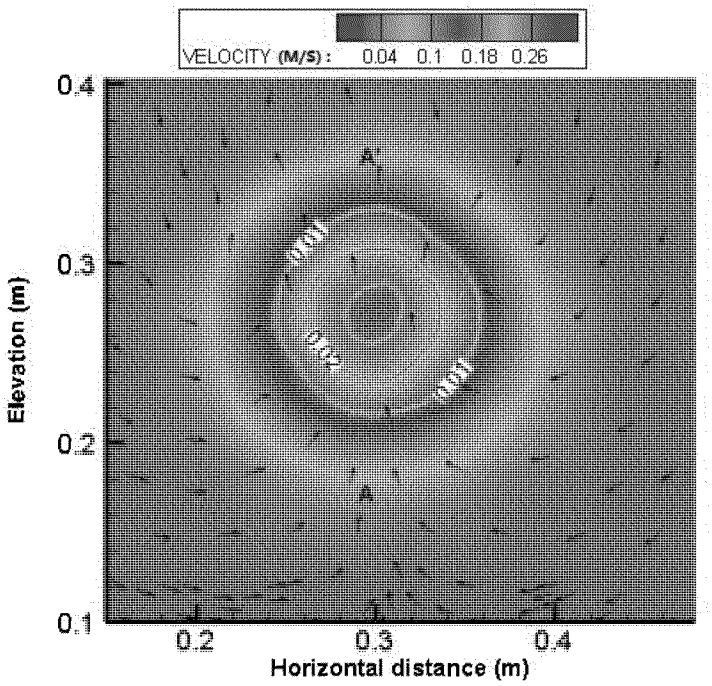

Figure 10: Surface-1 (Purple lines indicate the contour of the holdup, continuous flood contour indicates the velocity magnitude. The arrow vectors indicate the velocity vectors that parallel to the present surface)

Figure 11 shows the c ross section B-B' (see Figure 9). One notes that the plume is no longer circular in comparison to Figure 10. Also, the center of the plume is closer to the top portion of the plume than it is to the bottom of the plume. First, note that the velocity in this cross section is going in the direction of B-B', which means it is upward. We believe the non -circular shape of the plume in Figure 11 is due to two complementary processes: 1) The close distance to the top portion of the plume is most likely due to buoyancy which has more effects on the center of the plume than on the edge of the plume because the center of the plume has more oil in it. Therefore, the buoyancy of the center of the plume is larger than that of the top, causing the center to be closer to the top of the plume. The converse occurs for the bottom of the plume. 2) As buoyancy pulls the plume upward, we believe that the lower edge of the plume is carried further out due to inertia.

ED_001324_00000687-00149

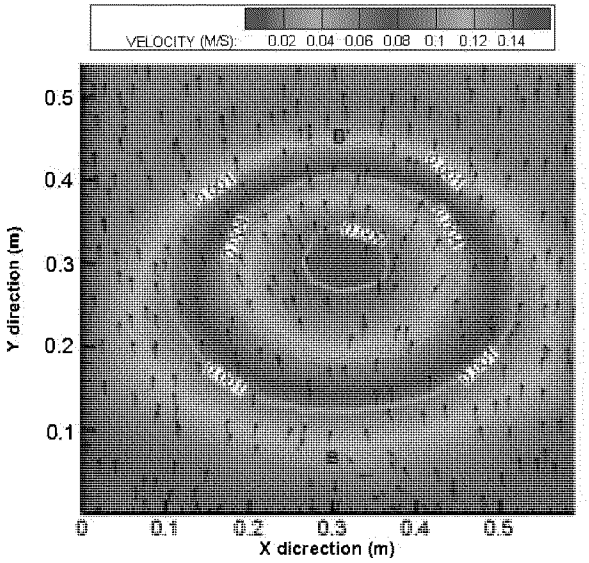

Figure 11: Surface-2 (Purple lines indicate the contour of the holdup, continuous flood contour indicates the velocity magnitude. The arrow vectors indicate the velocity vectors that parallel to the present surface)

Figure 12 shows the cross section C -C' where the velocity vectors are outward (i.e., away from the plume). Notice that the width of the plume is determined by the width of the tank (i.e., 0.60 m). Notice also that the velocity magnitude did not drop a lot from Figure 11, which is probably due to the fact that the plume reached the water surface and is thus confined to move horizontally. In this figure, the effect of inertia discussed for Figure 11 is more prevalent, as one notes that the distance between the center of the plume and the downstream edge of the plume (i.e., toward B) is much larger than in the opposite direction. Note that the downstream edge of the plume here is the lower edge of the plume of Figure 11.

ED_001324_00000687-00150

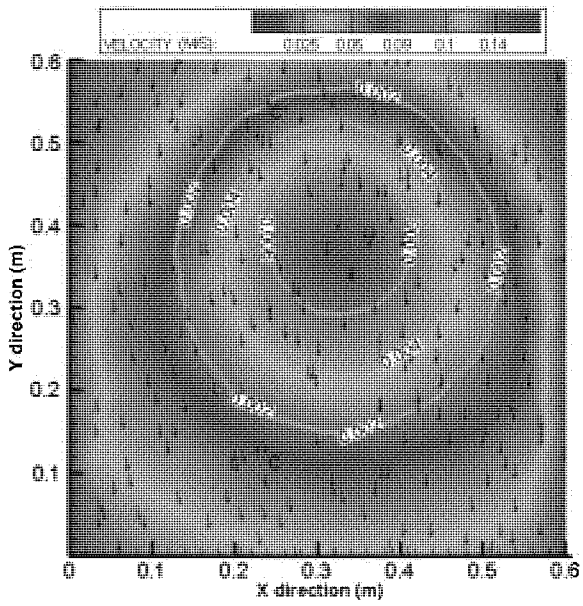

Figure 12: Surface -3 (Purple curve indicates the contour of the holdup, continuous flood contour indicates the velocity magnitude. The arrow vectors indicate the velocity vectors that parallel to the present surface)

The eddy diffusivity is defined as:

$$D \square 0.9 \frac{k^2}{\square} \qquad (4)$$

where k is the kinetic energy due to turbulence per unit mass and□ is energy dissipation rate per unit mass (watt/kg), and it reflects the intensity of turbulent mixing. The unit of D is m^2/s.

Figure 13 shows the eddy diffusivity profile in a vertical plane passing through the center axis of the plume. The eddy diffusivity is important for the mixing of oil and water within the plume, and it was used later to predict the movement of indivi dual oil droplets. One notes that the plume has a core of high mixing surrounded by a layer of relatively small mixing. This is probably due to the fact that the edge of the plume is "constrained" by the entrainment of water into it, a process that tends to reduce mixing. However, the entrainment does not seem to affect the core of the plume.

ED_001324_00000687-00151

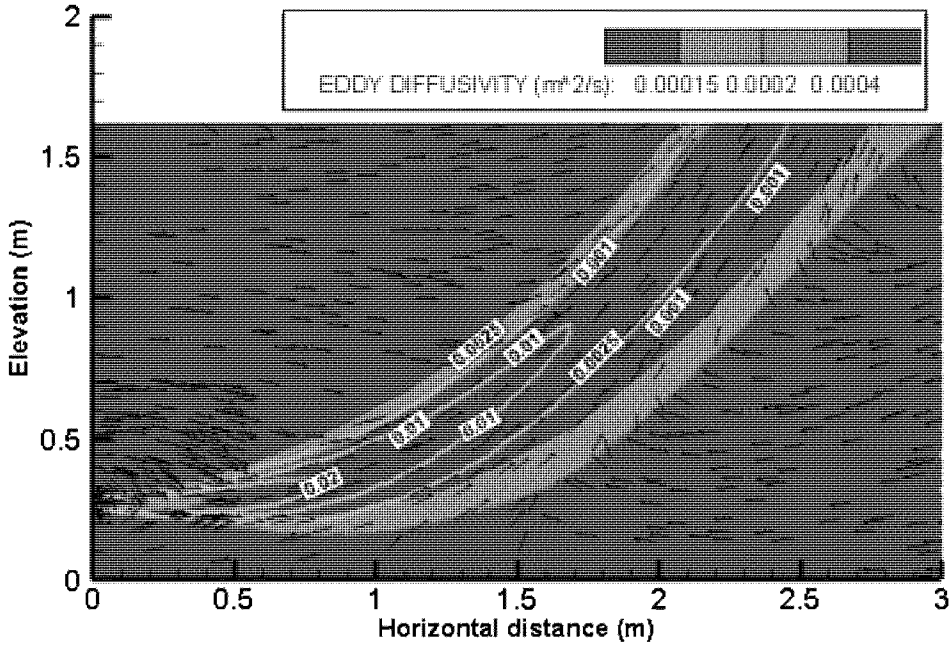

Figure 13: The profile of eddy diffusivity of the plume (Purple lines indicates the contour of the holdup, flood contour indicates eddy diffusivity. The arrow vectors indicate the velocity vectors that parallel to the present surface. The length of the velocity vector does not represent the magnitude but only represent the direction.

Figures 14, 15, and 16 report the eddy diffusivity at the cross sections used earlier (see Figure 9). One notes that the eddy diffusivity magnitude in Figure 14 (cross section 1) and Figure 15 (cross section 2) is comparable. However, one notes a large decrease for Figure 16 (cross section 3). This is probably because the eddy diffusivity is due to the k turbulence model, and turbulence was unhindered between cross section 1 and cross section 2. However, cross section 3 was only 0.10 m below the water surface where turbulent eddies were quashed by the water surface, which acted as a boundary.

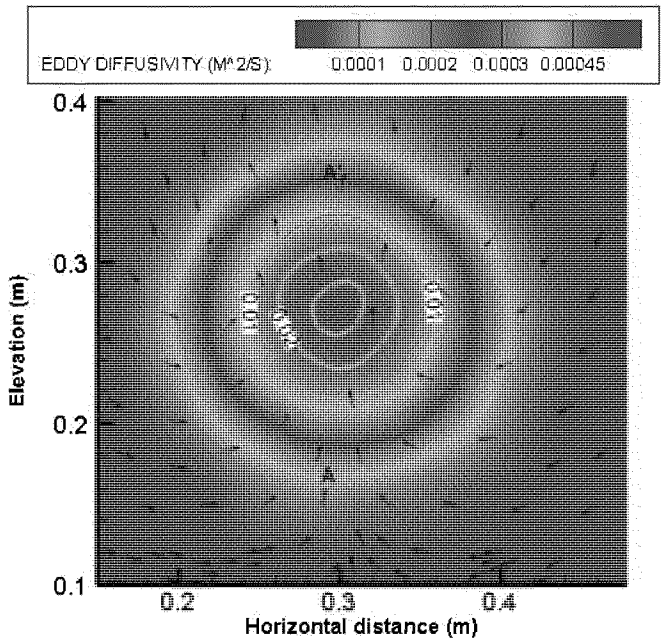

Figure 14: Surface-1, purple lines indicate the contour of the holdup, continuous flood contour indicates eddy diffusivity. The arrow vectors indicate the velocity vectors that parallel to the present surface

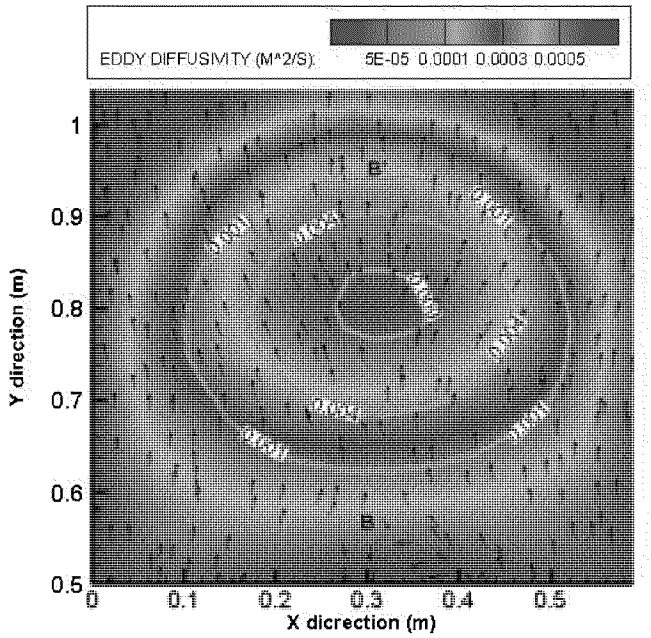

Figure 15: Surface-2 (Purple lines indicate the contour of the holdup, continuous flood contour indicates eddy diffusivity and the arrow vectors indicate the velocity vectors that are parallel to the present surface)

ED_001324_00000687-00153

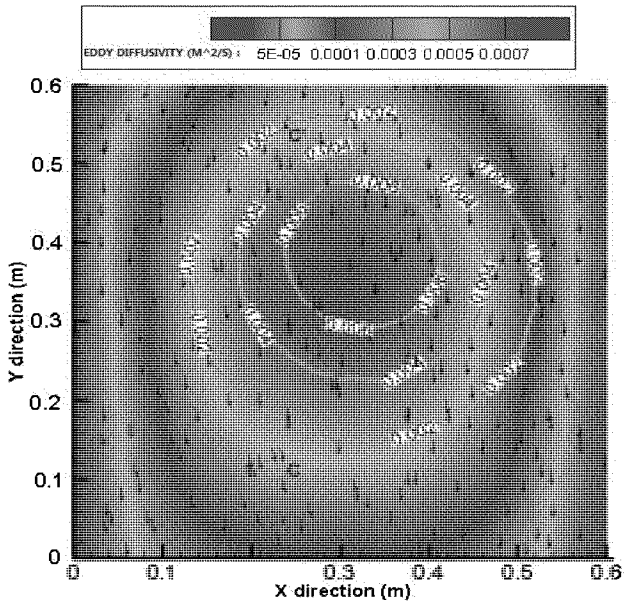

Figure 16: Surface-3 (Purple lines indicates the contour of the holdup, flood contour indicates eddy diffusivity and the arrow vectors indicate the velocity vectors that parallel to the present surface)

The value of the energy dissipation rate □ (watt/kg) is commonly needed to determine the breakup of oil droplets and their coalescence. Although, we have not conducted the breakup of oil droplets within the current framework, we provide herein the values of □ for future (imminent) application. Figure 17 shows the profile contour of □, where the values drop sharply with the centerline distance (note the logarithmic scale of the contours).

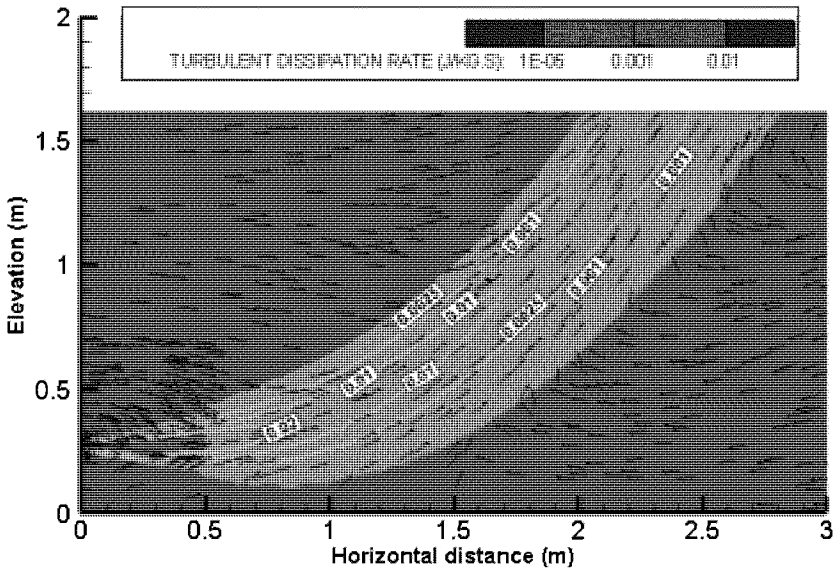

Figure 17: The profile of turbulent dissipation rate in the plume. Purple lines indicates the contour of the holdup, continuous flood contour indicates turbulent dissipation rate. The arrows indicate velocity vectors components that are parallel to the page surface. The length of the veloci ty vector does not represent the magnitude but only represent the direction.

Figure 18, 19, and 20 show the contours of □ in cross sections 1, 2, and 3, respectively (see Figure 9 for reference). While the maximum value is at or nea r the center, one notes a sharp decrease of□ between cross sections. The decrease is much sharper than that of the eddy diffusivity, which is probably because the turbulent kinetic energy k behaved more or less similar to□, and thus the ratio in Eq. 4 remained more or less uniform with distance from the source.

ED_001324_00000687-00155

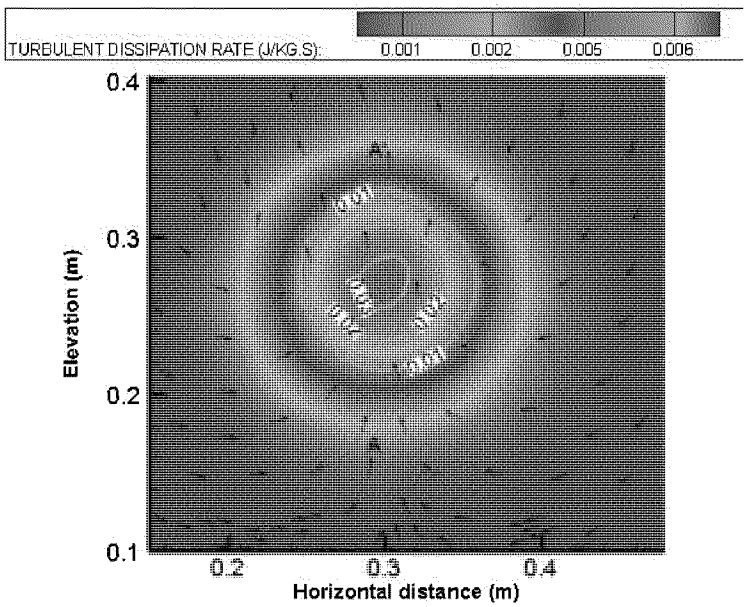

Figure 18: Surface-1 (Purple lines indicates the contour of the holdup, continuous flood contour indicates eddy diffusivity. The arrow vectors indicate the velocity vectors that parallel to the present surface)

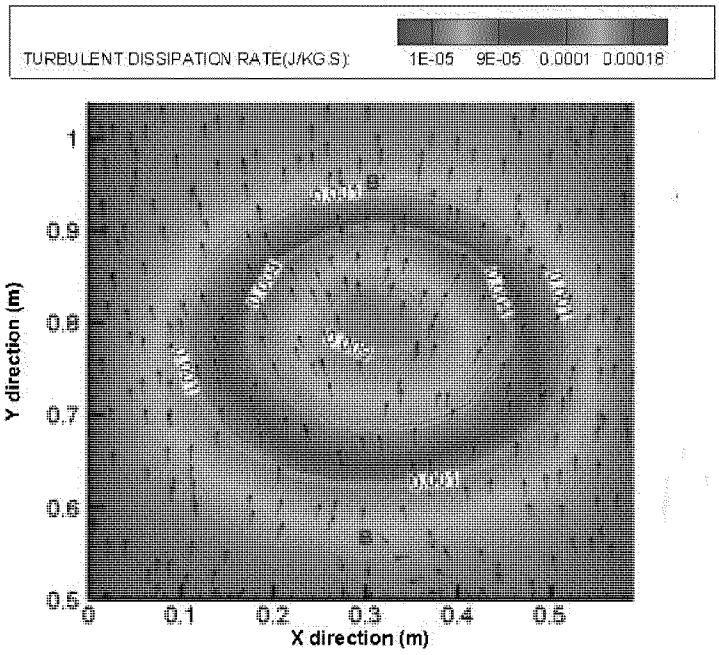

Figure 19: Surface-2 (Purple lines indicates the contour of the holdup, continuous flood contour indicates turbulent dissipation r ate. The arrow vectors indicate the velocity vectors that parallel to the present surface)

ED_001324_00000687-00156

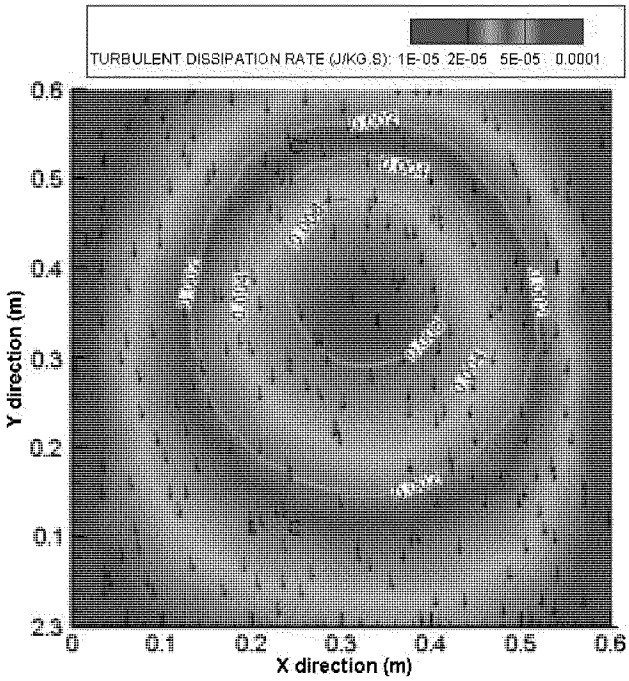

Figure 20: Surface-3 (Purple lines indicate the contour of the holdup, continuous flood contour indicates turbulent dissipation rate. The arrow vectors indicate the velocity vectors that parallel to the present surface)

Figure 21 reports the variation of □ along the centerline of the plume, where one notes a sharp decrease with distance (note the logarithmic scale on the vertical). Theoretical arguments in water jets revealed that □ decreases proportional to x^{-4}, where x is the centerline distance from the source.

ED_001324_00000687-00157

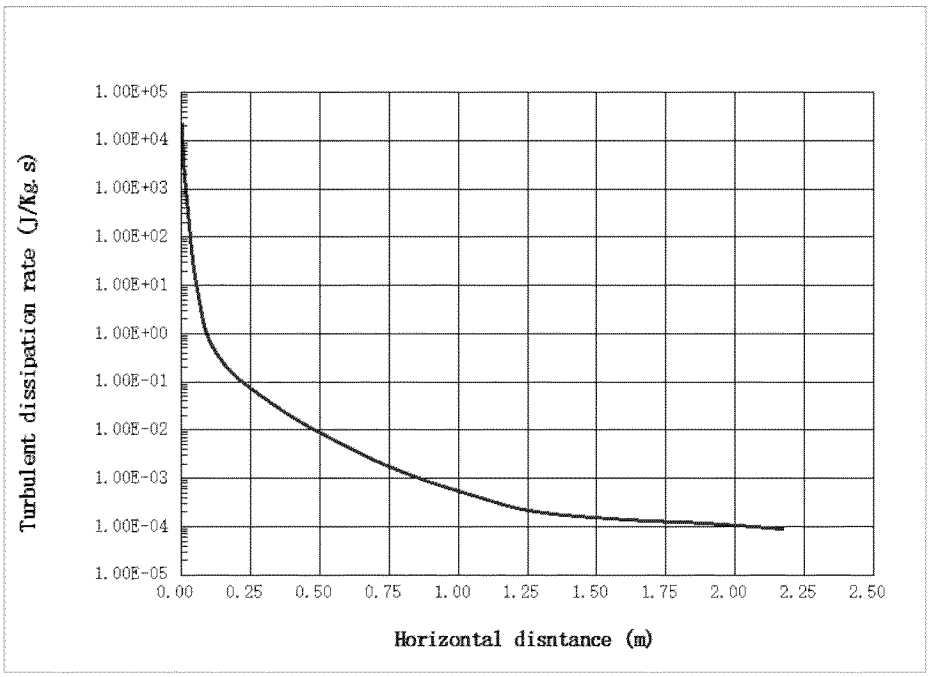

Figure 21: Turbulent dissipation rate along the centerline of the plume (The turbulent dissipation rate decreases sharply when exiting the orifice.)

<u>Particle tracking using Lagrangian method coupled with CFD</u>

In the experiment of oil jet underwater, we observed that some oil droplets exit the plume and rise up individually. This interesting phenomenon gives rise to how the oil droplets behave when exiting the jet orifice. In the present model, we aim to understand how oil droplets behave after exiting the orifice (e.g., how the large oil droplets exit the plume and oil droplets of which diameters remain within the plume. However, CFD (Computational Fluid Dynamics) does not consider the behavior of single droplet s. For example, RANS (Reynold Averaged Navier Stokes Equations) in CFD considers the oil and water fully mixed, which is different from the real situation, where they are in different phases: oil droplets in water.

We modelled herein the trajectories of oil droplets using a Lagrangian method coupled with CFD data. The flow field was obtained from the CFD simulations (Section I), and used as input to our particle tracking model NEMO3D.

The velocity of water is:

$$\vec{U} = u.\vec{x} + v.\vec{y} + w.\vec{z} \qquad (5)$$

The velocity of the particle is:

ED_001324_00000687-00158

$$\overrightarrow{U_p} \square u_p.\vec{x} \square \mathrm{v_p}.\vec{y} \square w_p.\vec{z}$$

(6)

For particle tracking:

$$\frac{d\vec{S}_p}{dt} \square \vec{U}_p \square \overrightarrow{R\sqrt{2D\square t}}$$

(7)

Where

$$\overrightarrow{S_p} \square X_p.\vec{x} \square Y_p.\vec{y} \square Z_p.\vec{z}$$

(8)

Equation (3) is thus written in each of the coordinate directions:

$$\frac{dX_p}{dt} \square u_p \square R\sqrt{2D_x \square t}$$

(9a)

$$\backslash \frac{dY_p}{dt} \square \mathrm{v}_p \square R\sqrt{2D_y \square t}$$

(9b)

$$\frac{dZ_p}{dt} \square w_p \square R\sqrt{2D_z \square t}$$

(9c)

Where Dx, Dy, and Dz are the eddy diffusivities computed in Section I (Eq. 4). The velocities $\mathrm{u_p}, \mathrm{v_p}$ and $\mathrm{w_p}$ are given based on the momentum equation. In the x direction:

$$\frac{du_p}{dt} \square (\frac{f_1}{\square_d})*(\mathrm{U}\cos \square \square U_p \cos\square) \square (\frac{f_1}{\square_d})*(\mathrm{u} \square u_p)$$

(10)

Momentum equation in the y direction:

$$\frac{d\mathrm{v}_p}{dt} \square (\frac{f_1}{\square_d})*(\mathrm{U}\sin \square \square U_p \sin\square) \square (\frac{f_1}{\square_d})*(\mathrm{v} \square \mathrm{v}_p)$$

(11)

ED_001324_00000687-00159

Momentum equation in the z direction:

$$\frac{dw_p}{dt} = \left(\frac{f_1}{\tau_d}\right)*(w - w_p) - \frac{\rho_w - \rho_o}{\rho_w} * g$$

(12)

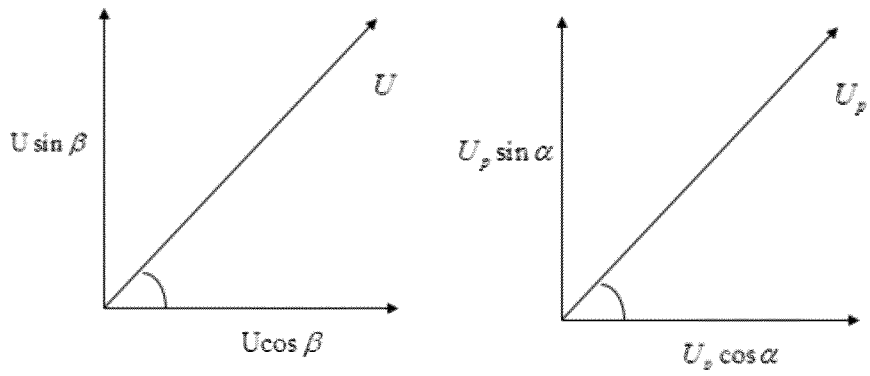

Figure 22: The angles of the velocities in cylindrical coordinates for the water velocity U (left panel) and for the oil droplet velocity U_p (right panel).

The parameter τ_d is the Stokes drag coefficient given as:

$$\tau_d = \frac{\rho_o * D^2}{18 * \mu_w}$$

(13)

The parameter f_1 is a correction for the Stokes coefficient to account for situations where the flow is not laminar, but when the droplet Reynolds number $\mathrm{Re} = \frac{\rho_w * u_s * D}{\mu_w}$ is less than 100. It is calculated based on the following equations (Miller et al., 1998):

$$f_1 = 1 - 0.0545\mathrm{Re} - 0.1*\mathrm{Re}^{\frac{1}{2}}(1 - 0.03*\mathrm{Re})$$

(14)

The slip velocity for the calculation of the Reynolds number is given by the Euclidean norm:

$$u_s = \|\vec{U} - \vec{U}_p\| = \left(\left(u - u_p\right)^2 + \left(v - v_p\right)^2 + \left(w - w_p\right)^2\right)^{1/2}$$

(15)

By putting equation (5) -(14) into the NEMO 3D code, one can obtain the trajectories of the oil droplets with different diameters.

The oil droplets with different diameters rise up not only because of the flow filed velocity, but also due to the individual velocities of its own. As shown in Figure 23, oil droplets with larger diameters rise ahead of the centerline of the plume, and oil droplets with a 1000 microns exist the plume at around 0.5 m from the orifice in the horizontal direction. The present method can predict at which point the oil droplets will exit the plume. In addition, when combined with LISST data, one can also estimate how much percentage of oil droplets with large diameters will exit the plume after released.

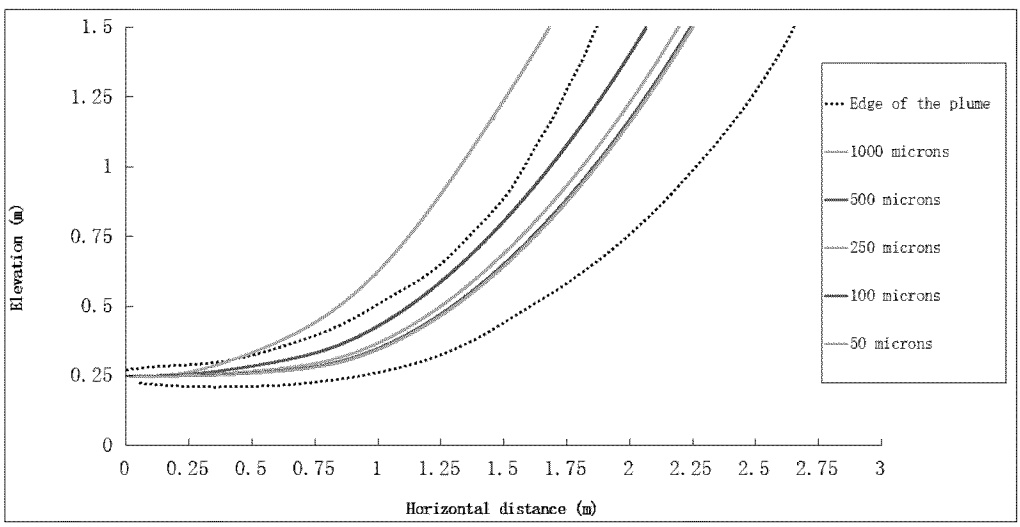

Figure 23: The trajectories of oil droplets with different diameters. The edge of the plume is defined by 10 % of the centerline velocity.

When the inertia terms are not estimated for oil droplets, the buoyancy effect is estimated by terminal velocity directly (e.g., the right hand side of Equation (9a), (9b), (9c) is zero) while the present method uses equation (5)-(14) to consider the effect of inertia and buoyancy.

Figure 24 shows the evaluation of the combined effect of inertia and buoyancy effect on oil droplets when rising; the oil droplet trajectories rise faster when the inertial effects are not accounted for. This is because the jet is horizontal and tends to propel the droplets horizontally. Thus, not accounting for the inertia of droplets overestimate their rise rate. The difference becomes more pronounced for the large oil droplets, such as 500 and 1000 microns, which is because the large droplets have a higher buoyancy (due to their large volume) and have larger inertia due to their large mass. The results in Figure 24 demonstrate that one needs to account

ED_001324_00000687-00161

for both the effects of inertia and buoyancy when considering the movement of oil droplets in jets.

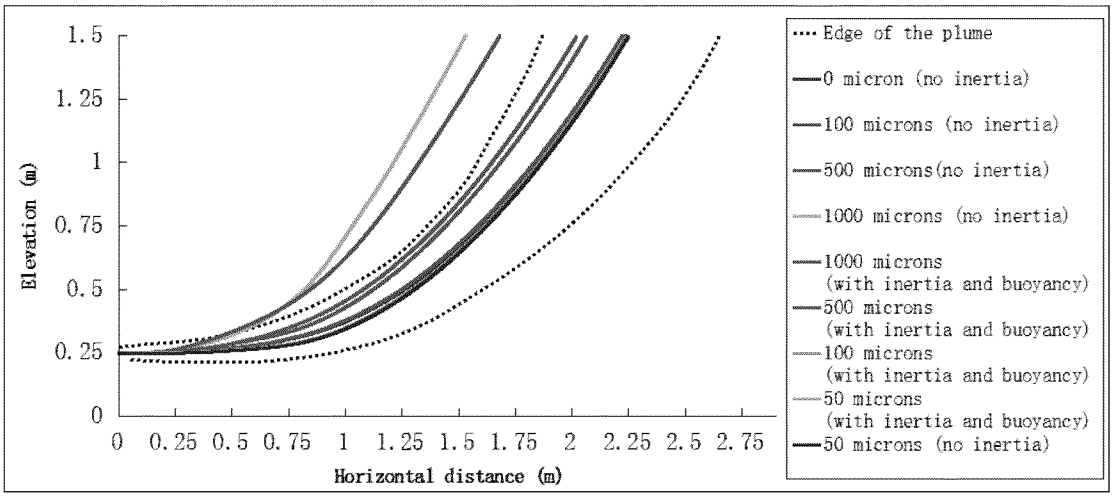

Figure 24: Evaluation of the effects of inertia and buoyancy on oil droplets trajectories. In the absence of inertia, oil droplets rise faster.

Figures 25 through 28 show the trajectories of oil droplets of various sizes. Figures 25 and 26 show identical results, which suggests that the mixing due to eddy diffusivity was large enough to minimize the effect of buoyancy between 50 and 100 microns. However, the effect of buoyancy seems to become important for droplets of size 500microns (Figure 27) and 1,000 microns (Figure 28). For the latter, the droplet trajectories were outside of the 10% boundary of the plume.

ED_001324_00000687-00162

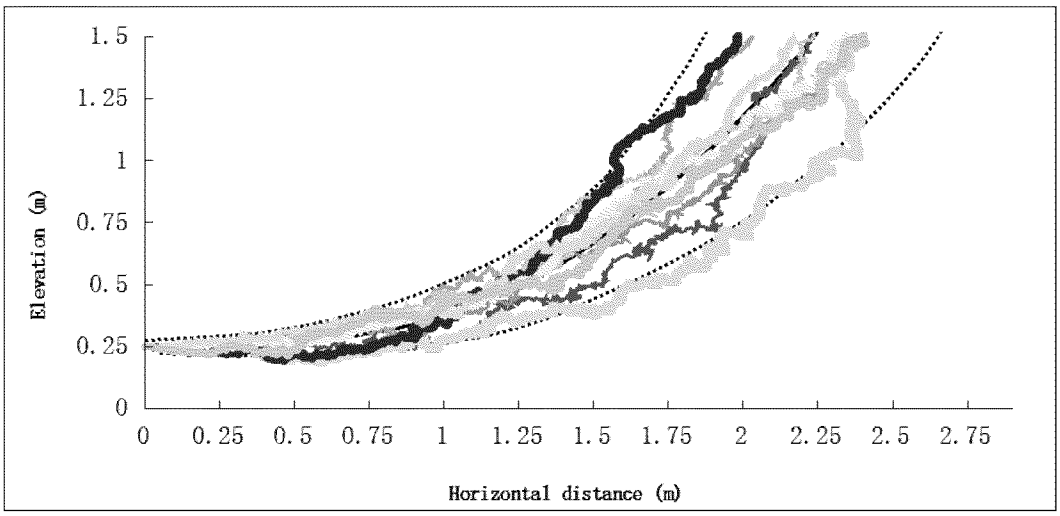

Figure 25: The trajectories of oil droplets when the diameter is 50 microns (with inertia and turbulent diffusion)

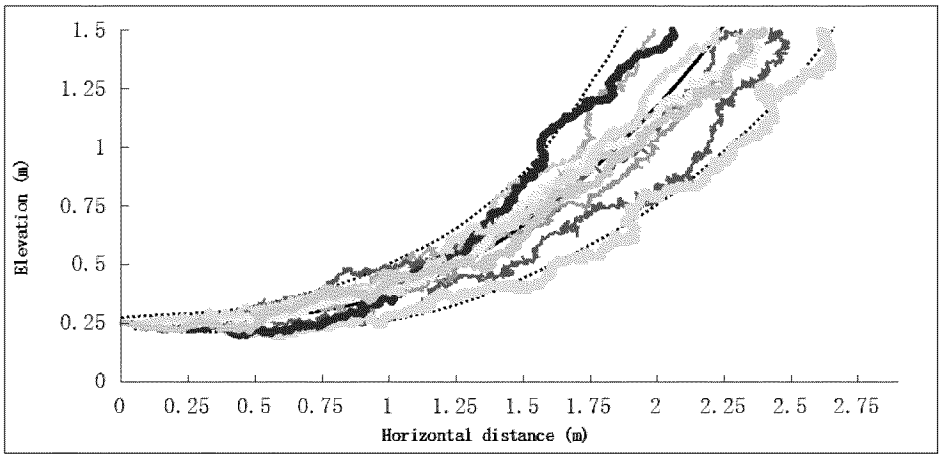

Figure 26: The trajectories of oil droplets when the diameter is 100 microns (with inertia and turbulent diffusion)

ED_001324_00000687-00163

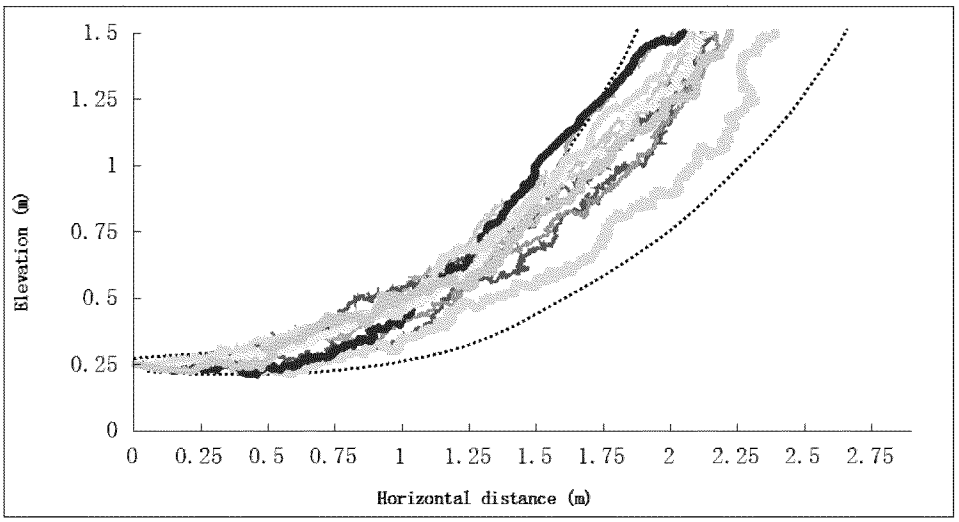

Figure 27: The trajectories of oil droplets when the oil droplet diameter is 500 microns with inertia and turbulent diffusion.

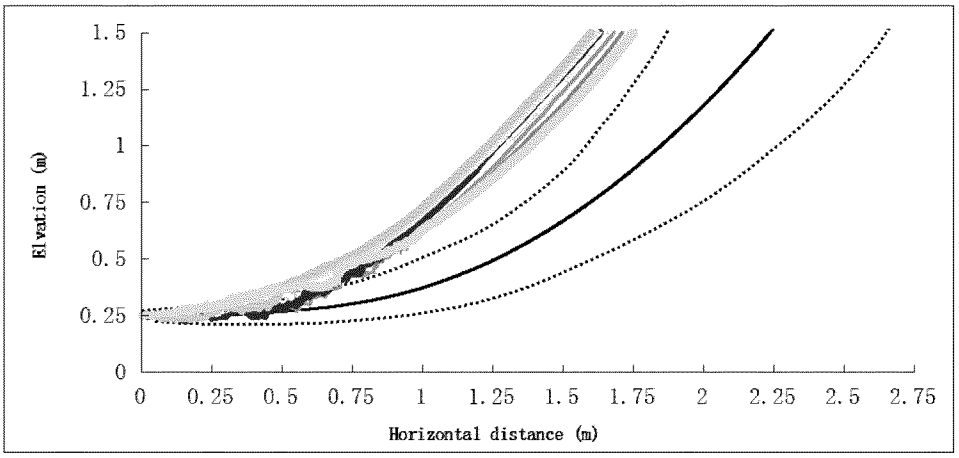

Figure 28: The trajectories of oil droplets when the diameter is 1000 microns, with inertia and turbulent diffusion.

ED_001324_00000687-00164

References

Aronson, D., Chroneer, Z., Elofsson, P., Fellbom, H., 2000. Comparison between CFD and PIV measurements in a passenger compartment. SAE Technical Paper.

Eaton, J., Johnston, J., 1981. A review of research on subsonic turbulent flow reattachment. AIAA journal 19, 1093-1100.

Johansen, Ø., Brandvik, P.J., Farooq, U., 2013. Droplet breakup in subsea oil releases – Part 2: Predictions of droplet size distributions with and without injection of chemical dispersants. Mar Pollut Bull 73, 327-335.

Miller, R., Harstad, K., Bellan, J., 1998. Evaluation of equilibrium and non-equilibrium evaporation models for many-droplet gas-liquid flow simulations. International Journal of Multiphase Flow 24, 1025-1055.

Pope, S.B., 2000. Turbulent flows. Cambridge university press.

Wilcox, D.C., 1998. Turbulence modeling for CFD. DCW industries La Canada, CA.

Zhao, L., Boufadel, M.C., Socolofsky, S.A., Adams, E., King, T., Lee, K., 2014. Evolution of droplets in subsea oil and gas blowouts: Development and validation of the numerical model VDROP-J. Marine pollution bulletin 83, 58-69.

ED_001324_00000687-00165

IAA No. E12PG00037

Final Report

Dispersant Effectiveness, In-Situ Droplet Size Distribution and Numerical Modeling to Assess Subsurface Dispersant Injection as a Deepwater Blowout Oil Spill Response Option

and

Evaluation of Oil Fluorescence Characteristics to Improve Forensic Response Tools

APPENDIX H
Weber Number Scaling Numerical Modeling Prediction of Droplet Size Distribution from Subsurface Oil Releases with and without Chemical Dispersants

By

Haibo Niu and Linlu Weng

Water Studies Laboratory

Department of Engineering

Dalhousie University (Truro Campus)

Truro, NS, Canada

DALHOUSIE UNIVERSITY

ED_001324_00000687-00166

1 Introduction

The increased in offshore oil and gas exploration in deep waters increases the risk of deepwater oil spills. One recent example is the Deepwater Horizon (DWH) incident in the Gulf of Mexico. Oil released from subsurface blowouts breaks up into droplets and the sizes of these droplets have strong impacts on the subsequent fate of oil in the marine environment (Chen and Yapa, 2007; Bradvik et al., 2013; Johansen et al., 2013). With a density smaller than that of the ambient seawater, larger oil droplets will rise to the sea surface more rapidly than smaller droplets and will reach surface closer to the spill location than the smaller droplets. Better knowledge on droplet size distributions resulting from subsurface oil releases will help us predict whether the oil will surface and if so, when and where and what the oil slick thickness be (Chen and Yapa, 2003).

Currently, both our knowledge on the droplet size distributions and our capability to predict the distributions are limited. Before the DWH incident, only very few experimental work have been conducted to measure droplet size distribution from subsurface releases and only few studied the effects of chemical dispersant on droplet sizes. Topham (1975) was probably the earliest work studying droplets from subsurface releases and he has reported droplet size ranging from 0.5 mm (detection limit) to 3 mm for Norman Wells crude and a peak diameter of 15 μm for Swan Hills crude. The field experimental data from the Canadian Arctic gathered by Dome Petroleum gave a range from 50 μm to 2.1 mm (Buist et al., 1981). Masutani and Adams (2001) conducted jet experiments on an oil-water system using four types of crude oil and studied the different modes of jet breakup. Johansen et al. (2003) was the only full-scale deep water experiment, they observed that droplet sizes resulting from the release of diesel at 844 m depth were from 1 to 10 mm.

While DWH is the first oil spill occurring at significant depth (~1500m), it is also the first time where chemical dispersants were directly injected into the subsurface oil release to enhance the dispersion of oil over a large water column (Louis et al., 2011). A total of 18,379 barrels of dispersant were used at the DWH incident (The Federal Interagency Solutions Group, 2010). When a chemical dispersant is added at the depth of the wellhead, the surfactant is expected to break the oil into small droplets. The only available data on the effects of dispersant on droplet sizes is Brandvik et al. (2013). Brandvik et al (2013) have studied the effects of dispersant by using seven different dispersant-oil-ratios (DORs) and the peak droplet sizes were found strongly affected by DORs.

Very few publications are available on predicting the droplet sizes. Chen and Yapa (2007) developed a method based on the maximum entropy formalism using the "deepspill" experimental data. Currently, this method is mainly applied to subsurface releases without chemical dispersant. However, the feasibility of this method is yet to be validated in the case of subsurface release with chemical dispersant. More recently, Johansen et al. (2013) have incorporated new experimental data for the subsurface release cases with chemical dispersant application developed a modified Weber number approach to predict the droplet sizes. Zhao et al. (2014) used the same data set with a droplet breakup rate approach. However, all of these available approaches were based on one single set of experimental data on subsurface oil-dispersant interaction (Brandvik et al., 2013) by using one type of oil (Oseberg Blend). There is an urgent need to validate these models with extensive experimental data on more oil types.

ED_001324_00000687-00167

Furthermore, although it appears likely that subsurface *in-situ* use of chemical dispersants may be very effective for countering deepwater oil spills, many uncertainties still exist. For example, assumptions of the optimum DOR are based on empirical data mostly obtained from bench-scale experimental protocols that have been designed for testing at standard temperatures and pressures (STP), whereas conditions at a wellhead on the ocean floor or anywhere along a riser beneath the ocean surface could be significantly different. Dispersant effectiveness as a function of dispersant type, oil type, and DOR must be better understood for application in deepwater environments. Furthermore, the interaction of dispersant and crude oil at depth under different turbulence regimes may also have significant implication in optimizing operational performance of subsurface dispersant injection. Improved understanding of these issues should provide better support in decision-making for subsurface dispersant application.

To fill the existing knowledge gaps, extensive experimental studies have been conducted in a flow-through wave tank located at the Bedford Institute of Oceanography (BIO) with an underwater high flow rate oil release system. Accordingly, the objective of this project is to: 1) analyze these newly gained experimental data from BIO; 2) develop a method that can effectively predict the droplet size distributions of oil released from subsurface, with and without application of chemical dispersant; and 3) incorporate the newly developed method with an oil spill model to study its effects on fate and transport of oil from subsurface releases.

2 Methodology

2.1 Maximum Entropy Formalism (MEF) Approach

Probability density function (PDF) such as Rosin-Rammler or Nukiyama-Tanasawa distribution, are established correlations for the droplet size distribution. However, more theoretical foundations were needed for these correlation. Maximum entropy formalism (MEF) approach was used by Chen and Yapa (2007) to develop model for estimating oil droplet size distribution.

To estimate a droplet spectrum, the probability density function (PDF) needs to be connected to a characteristic size (e.g. δ_{max}, δ_{30}, or δ_{32}) (Chen and Yapa, 2007). δ_{max} is the maximum droplet size, δ_{30} is the mass mean volume equivalent diameter, and δ_{32} is the Sauter mean (volume surface) diameter. δ_{max} is determined by diameter of the nozzle D and the Weber number (We) as follows:

$$\delta_{max} = kDWe^{-3/5} \tag{1}$$

By knowing δ_{max}, δ_{30} and δ_{32} can be estimated as follows:

$$\delta_{30} = \left[\int_0^{\delta_{max}} f\,\delta^3 d\delta\right]^{1/3} \tag{2}$$

$$\delta_{32} = \left[\int_0^{\delta_{max}} f\,\delta^2 d\delta\right]^{-1} \delta_{30}^3 \tag{3}$$

where f is PDF defined as:

ED_001324_00000687-00168

$$f \square 3 \square_1^2 \exp \square \square_0 \square \square_1 \square_1 3 \square \square_2 \square_1^3 u_1 \square \square_3 (\square_1^3 u_1^2 \square \square_1^2 B) \square \tag{4}$$

Where δ_1 is nondimensional droplet diameter. u_1 is nondimensional droplet velocity. After solving the Lagrangian multiplier λ_i ($\lambda_0, \lambda_1, \lambda_2, \lambda_3$), which are evaluated by several nonlinear constraint equations, mentioned in the Chen and Yapa (2007) the droplet size number based distribution can be obtained in Equation $f_N \square \frac{dN}{d(\square/\square_{30})} \square A \exp \square \square \frac{\square_{30}}{\square} \square B \square \frac{\square}{\square_{30}} \square^C \square$ (5 (Chen and Yapa, 2007). It indicates that the droplet distributions are controlled by two tuning coefficients B and C:

$$f_N \square \frac{dN}{d(\square/\square_{30})} \square A \exp \square \square \frac{\square_{30}}{\square} \square B \square \frac{\square}{\square_{30}} \square^C \square \tag{5}$$

Where f_N is a number based probability density function, N is the droplet number, δ_{30} is the volume mean diameter, A is a term that accounts for normalization conditions. Their result seems to be less biased. Due to the limited data, the effects of oil properties were neglected. The applicability of the formulation for chemically dispersed oil will be tested in future study.

2.2 Droplet Breakup Approach

Maximum Entropy Formalism (MEF) Approach was widely used in flow atomization and spray; there is less of consideration of oil property. Zhao et al. (2014) has developed a VDROP -J model which considers the effects of both oil viscosity and oil-water interfacial tension (ITF). In a liquid-liquid dispersion system, a population balance equation is proposed as follows:

$$\frac{\square n(d_i,t)}{\square t} \square \underbrace{\square_{j=i+1}^{n} \square d_i, d_j \square g \square d_j \square n \square d_j, t \square}_{\text{droplet breakup}}$$
$$\square \underbrace{\square_{j=1}^{n} \square_{k=1}^{n} \square d_j, d_k \square n \square d_j, t \square n \square d_k, t \square \square n \square d_i, t \square \square_{j=i+1}^{n} \square d_i, d_j \square n \square d_j, t \square}_{\text{droplet coalescence}} \tag{6}$$

Where n is number concentration of droplets of diameter d_i at a given time t. The term $\beta(d_i, d_j)$ is the breakage probability density function (dimensionless)for the creation of droplet of diameter d_i due to breakage of droplets of (a larger) diameter d_j, and $g(d_j)$ is the breakage frequency of droplets of diameter d_j. The first term represents the birth of droplets d_i resulting from the breakup of droplets d_j, while the second term represents the death of droplets d_i due to breakup into smaller droplets. For droplets coalescence, the term $\Gamma(d_k, d_j)$ is the coalescence rate (m^3/s). The first term of droplet coalescence represents the birth of droplets d_i as a results of coalescence events occurring between droplets d_k and d_j to form drops with the

ED_001324_00000687-00169

size of d_i, while the second term represents deaths of droplets d_i due to the coalescence of drops d_i with all other drops (including drops of size d_i themselves) to form larger drops.

The breakage rate $g(d_i)$ is given by:

$$g(d_i) = K_b \int_{n_e} S_{ed}(u_e^2 - u_d^2)^{1/2} BE \, dn_e \tag{7}$$

where S_{ed} represents the collisional cross section of eddy and droplet (m^2), u_e is the turbulent velocity of an eddy (m/s), u_d is droplet velocity (m/s), n_e is number concentration of eddies (number of eddies/m^3), BE is the breakup efficiency which is related with the IFT, dn_e is the number of eddies of size between μ_e and μ_d are the velocities of eddies and droplet and K_b is a system-dependent parameter for droplet breakup, and would need to be obtained by calibration to experimental data. Based on exper imental data, the K_b was found can be approximated by (Zhao et al., 2014):

$$K_b = 3.57 \times \rho U^2 D^{-0.63} \tag{8}$$

where ρ is density (kg/m^3), U is velocity (m/s), and D is droplet diameter (m) In Figure 1, an example is given for the comparison of VDROPJ with the experimental data (Brandvik et al., 2013). For a given release condition (e.g., same oil type, discharge nozzle size, and exit velocity), same K_b (0.11 in this case) will be obtained. Therefore, Equation 8 does not consider the effects of chemical dispersant on droplet sizes or shape of the curves. To fit the droplet size distributions with model, other parameters such as ITF or known dispersion efficiency must be used to adjust the shape ofthe curve. Both Zhao et al. (2014) and Johansen et al. (2013) indicated IFTs (15.5, 0.05 and 0.09) from three experiments based on DOR of 0, 1:50, and 1:25, respectively. The measured IFT (0.09) for DOR=1:25 is actually higher than the IFT (0.05) for DOR=1:50.This is against to the IFT fitting produced by Zhao et al. (2014) which indicated that the higher IFT would lead to a closer curve to the untreated condition (DOR = 0). The author may use estimated efficiencies of 10% and 80% for the case of DOR=1:50 and 1:25 during the fitting, respectively.

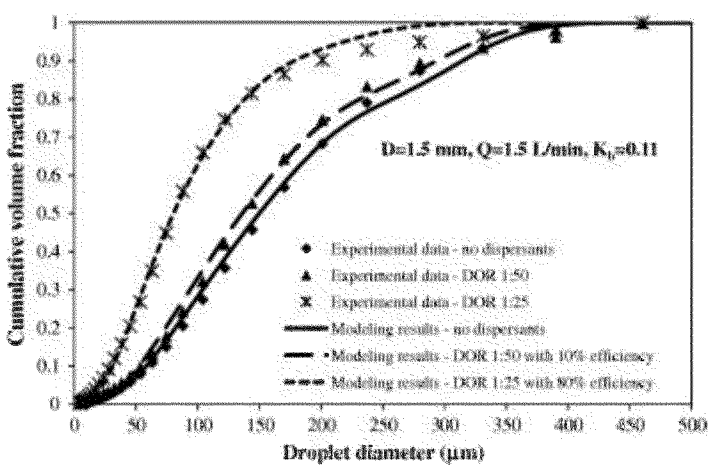

Figure 1: Comparison of oil droplet size distribution between VDROP-J and experimental data.

(*Source: Zhao et al. 2014*)

ED_001324_00000687-00170

2.3 Modified Weber Number Approach

There is no validation conducted for theMEF and droplet breakup approaches for droplet size prediction with chemical dispersant application. However, chemical dispersion is one of the important technologies in offshore oil spill response, and promising in responding to deepwater release. Thus, an approach in predicting droplet size with chemical dispersant is desired.

Johansen et al. (2013) has proposed a modified Weber number approach for such purpose based on the conventional Weber number approach by Wang and Calabreses (1986). In Johansen et al. (2013), Weber number scaling law was used to fit their experimental data, expressed as:

$$d'/D \propto \mathrm{Awe}^{-3/5} \tag{9}$$

where d' is characteristic droplet diameter (m) D is the nozzle diameter (m), A is a factor of proportionality and $We = \rho U^2 D/\sigma$ is the Weber number, ρ is density of the liquid in the jet (oil) (kg/m^3) U is the exit velocity (m/s), and σ is the interfacial tension between oil and water (N/m or kg/s^2). However, this simple Weber scaling law only fit well on DOR=0, for other DOR experiments, this scaling law do not fit it. Based on these available data, a new prediction model (modified weber number) is used for oil droplet size distribution with and without chemical dispersant.

The modified Weber number, *We**, is defined as follows:

$$We^* = \frac{We}{1 + B\,Vi\,(d_{50}/D)^{1/3}} \tag{10}$$

where *We* is the Weber number, $Vi = We/Re$ is the viscosity number, d_{50} is the median droplet diameter (m), *D* is the nozzle size(m), *B* is an empirical coefficient determined by experimental analysis. The relative droplet size *d50/D* can be expressed as:

$$(d_{50}/D) = A\,(We^*)^{-3/5} \tag{11}$$

where *A* is an empirical constant. Based on the data from Brandvik (2013) and Johansen et al. (2013) the value of *A* and *B* can be determined as A = 15.0 and B = 0.8.

Once d_{50} is determined, the droplet size distribution can be estimated using either lognormal or Rosin-Rammler distribution. Johansen et al. (2013) has concluded that Rosin-Rammler (Equation 12) distribution gives better fit of experimental data overall.

$$V(d) = 1 - \exp\left[-0.693\,(d/d_{50})^{\alpha}\right] \tag{12}$$

where *V(d)* is the cumulative distribution, and α is the spreading-parameter.

Although the mathematical formulations of three methods described above are of different level of complexity, all three methods require two or three tuning coefficients determined from regression. It seems that the efficiency and accuracy of droplet size prediction from these three methods are more or less the

ED_001324_00000687-00171

same. Comparatively, the complexity of the modified Weber number approach is lower than the other two, leading to advantage in real-world application. Therefore, the modified Weber number approach is selected in this study to fit the new experimental data with performance validation.

3 Prediction of Droplet Size Distribution

3.1 Experimental settings

A series of experiments of droplet size measurement for two types of oils (IFO-120 and ANS) have been conducted by the COOGER in BIO. The current flow rate for the experiments is set to 1 cm/s and the oil temperature is set to 80°C. The detailed settings of the other parameters (i.e., oil amount, water temperature, injection time, and flow in the tank) are listed in Tables 1 and 2. 24 experiments were conducted for each types of oil by consideration of seasonal conditions (spring and summer). As shown in Tables 1 and 2, the experiment No.1 to 12 were set based on spring condition with slightly lower water temperature (mostly lower than 10°C). In contrast, the experiments of No. 13 to 24 were set based on summer condition with warm water temperature (mostly higher than 10 °C). The "R" marked in the experiment No. denoted a repeated experiment with slightly adjusted conditions (e.g., different DOR). In addition, some of the repeated experiments (i.e., 6R, 7R, 10R and 11R), which were scheduled in spring but not conducted due to abnormal weather conditions with rising water temperature, were actually conducted late fall.

There were four dispersant-oil ratios (0, 1:250, 1:100, and 1:25) for the spring condition. Comparatively, the settings of dispersant-oil ratios are slightly different from which in the spring condition, which are 1:200 and 1:20.

Table 1: Experimental settings for droplet size analysis for IFO-120

No.	Factors		Measurements					
	Oil	DOR	Date	Oil Amount (g)	Water Temperature (°C)	Injection Time (sec)	Flow in the Tank (gpm)	Injection Pressure (psi)
1	IFO-120	0	9-Jun-14	145.2	13.0	5	600	40
2	IFO-120	1:250	20-Jun-14	199.6	12.2	7	600	62
2R	IFO-120	1:200	04-Dec-14	208.2	6.7	7	600	60
3	IFO-120	1:100	20-Jun-14	213.9	13.2	7	600	62
4	IFO-120	1:25	11-Jun-14	179.1	12.8	9	600	40

ED_001324_00000687-00172

4R	IFO-120	1:20	05-Dec-14	219.6	5.6	10	600	30
5	IFO-120	0	17-Jun-14	275.1	12.0	7	600	62
6R	IFO-120	1:200	04-Dec-14	215.6	6.6	8	600	60
7R	IFO-120	1:100	10-Dec-14	239.3	7.5	8	600	60
8	IFO-120	1:25	11-Jun-14	255.8	13.2	9	600	40
8R	IFO-120	1:20	05-Dec-14	243.3	5.4	10	600	60
9	IFO-120	0	17-Jun-14	359.6	12.7	7	600	62
10R	IFO-120	1:200	04-Dec-14	221.7	6.6	8	600	60
11R	IFO-120	1:100	17-Dec-14	N/A	4.9	10	600	60
12	IFO-120	1:25	16-Jun-14	354.8	12.5	9	600	62
12R	IFO-120	1:20	10-Dec-14	204.8	6.8	9	600	60
13	IFO-120	0	12-Sep-14	256.8	14.9	7	600	60
14	IFO-120	1:200	15-Sep-14	279	13.5	8	600	60
15	IFO-120	1:100	16-Sep-14	336.2	14.0	8	600	60
16	IFO-120	1:20	17-Sep-14	315.9	14.7	7	600	60
17	IFO-120	0	12-Sep-14	293.3	14.7	8	600	60
18	IFO-120	1:200	15-Sep-14	331.8	13.8	8	600	60
19	IFO-120	1:100	16-Sep-14	353.8	14.7	7	600	60
20	IFO-120	1:20	17-Sep-14	345.6	15.2	7	600	60
21	IFO-120	0	12-Sep-14	303.6	15.2	8	600	60
22	IFO-120	1:200	15-Sep-14	363.3	14.0	8	600	60
23	IFO-120	1:100	16-Sep-14	352.6	14.7	7	600	60
24	IFO-120	1:20	17-Sep-14	380	16.0	7	600	60

Note: R indicates repeated experiment.

ED_001324_00000687-00173

Table 2: Experimental settings for droplet size analysis for ANS

No.	Factors		Measurements					
	Oil	DOR	Date	Oil Amount (g)	Water T (°C)	Injection Time (sec)	Flow in the Tank (gpm)	Injection pressure (psi)
1	ANS	0	22-May-14	208.0	11.4	4	600	40
2	ANS	1:250	23-May-14	280.0	10.6	5	600	40
2R*	ANS	1:200	02-Dec-14	290.5	6.4	5	600	40
3	ANS	1:100	23-May-14	284.5	11.2	5	600	40
4	ANS	1:25	26-May-14	283.0	8.4	5	600	40
4R	ANS	1:20	03-Dec-14	287.2	6.8	5	600	40
5	ANS	0	26-May-14	279.3	8.4	5	600	40
6	ANS	1:250	30-May-14	279.7	7.7	5	600	40
6R	ANS	1:200	02-Dec-14	335.0	6.1	5	600	40
7	ANS	1:100	30-May-14	276.3	8.5	5	600	40
8	ANS	1:25	02-Jun-14	277.4	9.4	5	600	40
8R	ANS	1:20	03-Dec-14	297.2	7.0	5	600	40
9	ANS	0	02-Jun-14	281.4	9.7	5	600	40
10	ANS	1:250	06-Jun-14	281.0	10.3	5	600	40
10R	ANS	1:200	17-Dec-14	344.5	5.4	5	600	40
11	ANS	1:100	06-Dec-14	276.8	10.7	5	600	40
12	ANS	1:25	09-Jun-14	280.6	12.5	5	600	40
12R	ANS	1:20	10-Dec-14	295.7	7.3	5	600	40
13	ANS	0	05-Sep-14	303.7	17.7	5	600	40

ED_001324_00000687-00174

14	ANS	1:200	08-Sep-14	295.2	16.0	5	600	40
15R	ANS	1:100	10-Sep-14	304.3	13.8	5	600	40
16	ANS	1:20	10-Sep-14	291.9	14.7	5	600	40
17	ANS	0	05-Sep-14	299.6	18.1	5	600	40
18	ANS	1:200	08-Sep-14	297.7	16.2	5	600	40
19	ANS	1:100	09-Sep-14	283.4	15.3	5	600	40
20	ANS	1:20	11-Sep-14	289.6	14.1	5	600	40
21	ANS	0	08-Sep-14	297.1	15.1	5	600	40
22	ANS	1:200	09-Sep-14	281.8	14.2	5	600	40
23	ANS	1:100	10-Sep-14	284.4	13.4	5	600	40
24	ANS	1:20	11-Sep-14	285.8	13.6	5	600	40
25	ANS	1:50	11-Sep-14	316.2	17.6	6	600	40

Note: R indicates repeated experiment.

3.2 Measured Droplet Size Distributions

The droplet size distributions of IFO-120 based on different DOR and seasonal conditions are shown in Figures 2 to10. In addition, the droplet size distributions of ANS are listed in Figures 11 to 21. The ranges of DOR for the ANS experiment (Figures 11 to 20) were the same as which for the IFO -120. A series of experiments with DOR =1:50 are currently conducting by COOGER (one set of result is listed in Figure 21), further analysis will be conducted for this case.

As shown in Figure 2, the distribution and corresponding median of the droplet size distribution from experiment No. 1, 5, and 9 based on same type of oil (IFO -120), DOR = 0, seasonal condition (spring, similar water temperature) but different oil amount, injection time, and injection pressure. In addition, t he first two experiments (No. 1 and 5) have the same peak diameter (d_p = 259 μm), but slightly different d_{50} (258 μm in No. 1 and 176 in No. 5) . The third experiment showed smaller d_{50} (186 μm) and d_p (100 μm). This may be caused by relatively large plume or more smaller droplets caught by LISST.

In summer condition, the experiment 13 and 21 has same d_p (391 μm) and very similar d_{50} (263 μm in No. 13 and 264 in No. 21) , while the experiment 17 has a slightly smaller d_{50} (192 μm) and d_p (293 μm) with similar settings from which in spring condition . However, the droplet size distributions form No. 13 and 21 are not completed due to the limited measuring window of the LISST. Thus, the data from these two experiments will not be included in the further analysis. Comparing results from summer and spring, the d_p

ED_001324_00000687-00175

and d_{50} from summer is relatively higher than which from spring. Since the only significant different setting from summer to spring is the water temperature, which may be another factor that affecting the oil droplet size.

The droplet size distributions with similar conditions but different DOR in spring are listed in Figures 4, 5, 7, and 9. By comparing the d_p and d_{50} in the experiments with different DOR, it indicates that the change of droplet size is relatively insignificant with DOR from 0 to 1:100 (Figures 2, 5, and 7). However, a significant decrease droplet size is observed with DOR increasing from 1:100 to 1:20. Therefore, there are may be a threshold of DOR dosage that significantly changes the effects of dispersant on droplet size.

The droplet size distributions with similar conditions but different DOR in summer are listed in Figures 6, 8, and 10. For the warm cases (14, 18, and 22), experiment No.18 showed strong effects of truncation due to the maximum diameter can be measured by LISST instrument was 500μm. Both experiments 14 and 22 have similar but slightly smaller d_{50} compared with untreated cases (No.13 and 21), but the d_p from warm water are much smaller. This indicates that dispersant started to play a role in this case but the effects are not very strong.

For the case of DOR=1:100 with spring condition, the shape of the distribution and calculated d_{50} and d_p in experiment No.3 are very similar to the untreated case and DOR=1:250 cases of experiment No.5 and No.2, and the dispersant did not show a strong effects on the droplet distribution (Figure 7) . Similar as experiment No. 18, experiment No.7R also showed strong effects of truncation. For the summer condition cases (Figure 8), although d_{50} and d_p for experiment No.15 does not change significantly compared with DOR=1:200 cases (e.g. No.14), d50 from experiment No. 19 and 23 are much smaller and the overall oil concentration are much higher. This indicates high dispersant effectiveness.

For the case of DOR=1:25 (or 20) with spring condition (Experiment No. 4, 8, and 12), while the first experiment showed very low oil concentration compared with the other two experiments. The second and the third experiments repeated very well with much higher oil concentration and smaller d_p (128 μm for No. 8 and 104 μm for No. 12) and d_{50} (99 μm for No. 8 and 93 μm for No. 12) (Figure 9). Similar trends can be observed for the summer condition cases (Figure 10).

Compared the droplet size distributions from spring to summer conditions with same DOR, the droplet sizes from the results in summer experiment are significantly smaller than which in winter condition. The only known parameter that is different from the spring and summer condition with same DOR is the water temperature. Therefore, temperature may help facilitate the effect of dispersant on reduction the droplet size. In general, the results from the cases with spring and summer conditions indicate very high effectiveness of chemical dispersants.

Compared with the droplet sizes of IFO -120, the droplet sizes of ANS are significantly smaller. The droplet size distributions from three experiments (No. 1, 5 and 9) with untreated ANS in spring conditions are shown in Figure 11. The d_p (75 - 88 μm) and d_{50} (68 - 81 μm) are different but not significant in these three experiments. However, there is an abnormal peak observed in No. 5, which may due to unknown effects (further experiments and analyses shall be needed). The droplet sizes from the experiments with summer condition (No. 13, 17 and 21) (Figure 12) are similar (d_p = 104 - 128 μm d_{50} = 89 - 101 μm) and higher than which from experiments with spring condition.

ED_001324_00000687-00176

For the case of DOR=1:250 with spring condition, three experiments (No. 2, 6 and 10) have been conducted (Figure 13). In addition, three repeated experiments (No. 2R, 6R and 10R) with DOR=1:200 have also been conducted (Figure 14). Experiment No. 2 shows two d_p in one distribution which may due to influences from environment, and thus is difficult to be analyzed. Nevertheless, the droplet size distributions from No. 6 and 10 are highly similar with same d_p (75 μm) and similar d_{50} (63 μm for No. 6 and 66 μm for No. 10). The repeated experiments with DOR=1:200 show similar situation, the shape of the distribution and calculated d_{50} and d_p are very similar between No. 2R and 6R; while the situation of No. 10R is similar to which of No. 2. Compared with the untreated case (d_p = 75 - 88 μm), the smaller d_p (< 75 μm) in DOR=1:200 (or 250) show the effect of dispersant on oil droplet distribution. The droplet size distributions from the experiments (14, 18, and 22) based on summer condition are highly similar with identical d_p (75 μm) and very close d_{50} (64 - 65 μm). Experiments with DOR=1:200 (or 250) have slightly smaller d_{50} (64 - 65 μm) compared with untreated cases (13, 17 and 21)(d_{50} = 68 - 81 μm), as well as the d_p (75 μm for DOR = 200 or 250 and 75 - 88 μm for DOR = 0). This indicates that the effect of dispersant on ANS is more significantly than which on IFO-120 with very insignificant change of droplet size from DOR = 0 to 1:200.

Three experiments have been conducted for DOR=1:100 with spring condition (Figure 16). The d_{50} (55 - 58 μm) in experiment No.3, 7 and 11 are smaller than the DOR=1:200 (or 250) cases (d_{50} = 64 - 65 μm) while d_p (75 μm) are same. For the summer condition cases (Figure 17), d_{50} and d_p for experiment No.15R does not change significantly compared with DOR=1:200 cases (e.g. No.14), while the ones from experiment 19 and 23 are relatively smaller.

For the case of DOR=1: 25 with spring condition, the d_p (12 μm) and d_{50} (3 - 10 μm) from corresponding experiments (No. 8 and 12) are significantly lower than which from the experiments with DOR=1: 200 and 1: 100; while data from experiment No.4 appears abnormal distribution and could not be analyzed (Figure 18). The situations from the repeated experiments (No. 4R, 8R, and 12R) with DOR = 1:20 (Figure 19) are very similar to the original one (DOR = 1:25). Furthermore, similar trends can be observed for the summer condition cases (Figure 20). Figure 21 is a trial experiment of DOR=1:50 which is done in the summer of 2015, which indicate the droplet size of ANS is steadily decrease with increase DOR. It should also be noted that the droplet size distributions are significantly different from the experiments with DOR = 1:20 or 25 to the others. This may be cause by over dose of chemical dispersant. The other peaks in the distributions (Figures 18, 19 and 20) may be caused by the over-dosed dispersant or the unknown background components that were affected by the dispersant.

In general, the chemical dispersant plays an importance role in reduce the droplet size of ANS no matter in spring or summer conditions. The effectiveness of dispersant in reducing droplet size is higher on ANS than which on IFO-120. There may be thresholds for the dose of chemical dispersant to some oils (e.g., IFO-120) but will need further experiments to analyze. There may also be over dose of dispersant to some oils (e.g., ANS) when the DOR is high, eventually affecting the droplet size distribution. Future experiment will also need for this particular issue.

ED_001324_00000687-00177

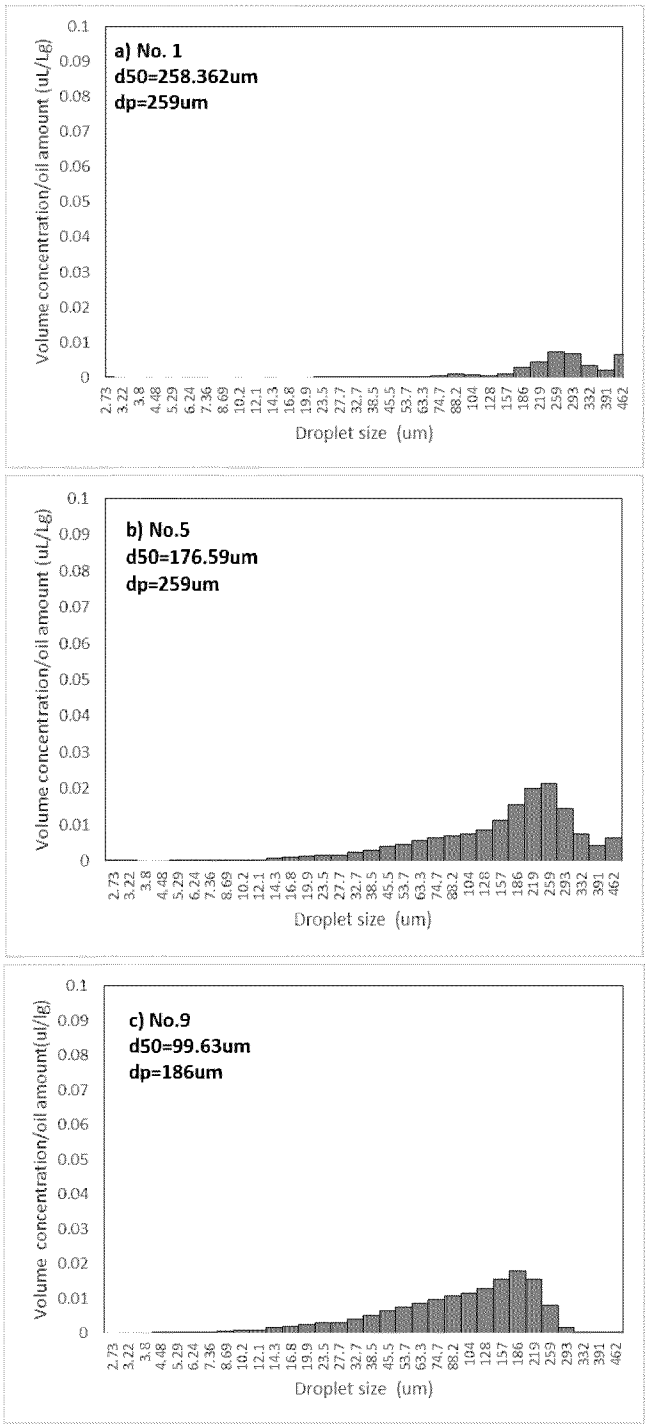

Figure 2: Experimental droplet size distribution of IFO-120 based on experiment a) No. 1, b) No. 5, and c) No.9 with DOR = 0 in spring condition

ED_001324_00000687-00178

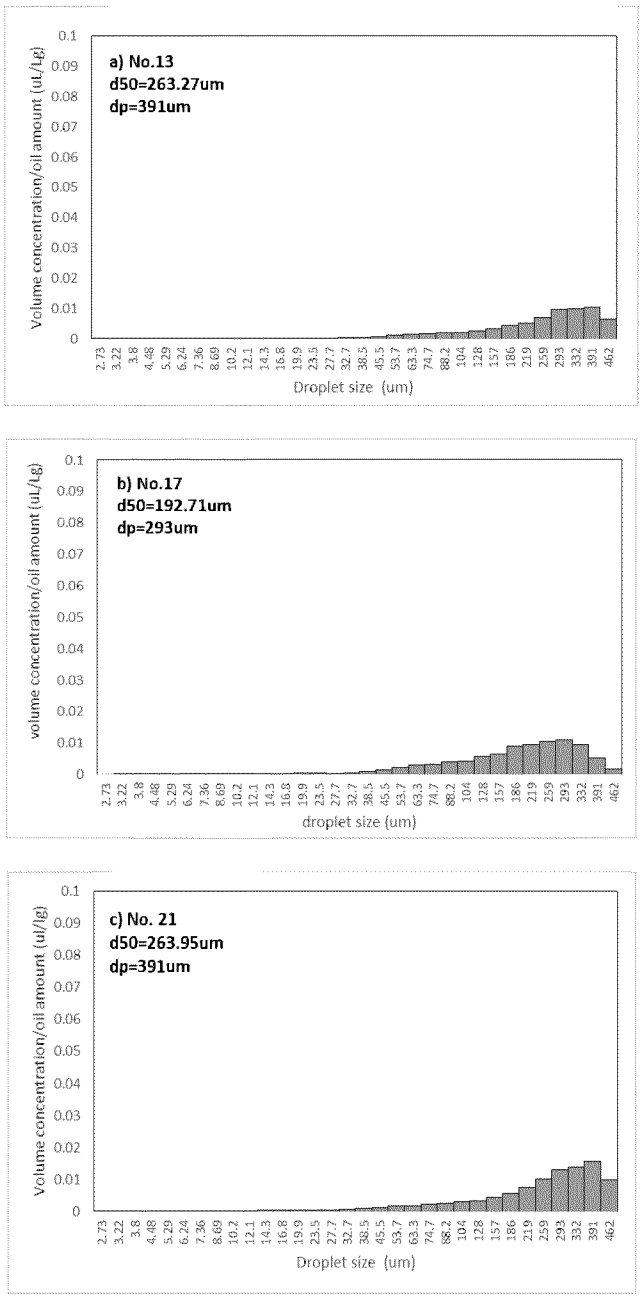

Figure 3: Experimental droplet size distribution of IFO-120 based on experiment a) No. 13, b) No. 17, and c) No. 21 with DOR = 0 in summer condition

ED_001324_00000687-00179

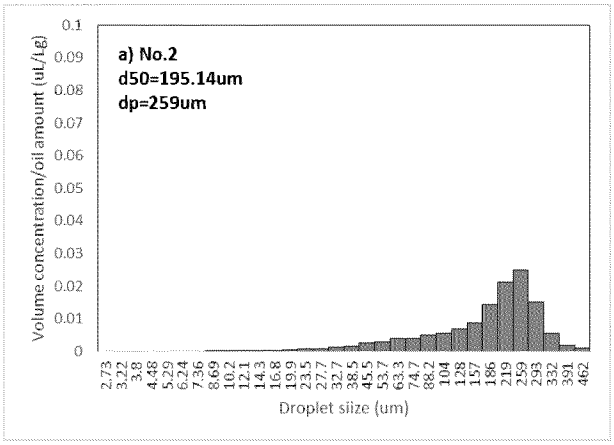

Figure 4: Experimental droplet size distribution of IFO-120 based on experiment a) No. 2 with DOR = 1: 250 in spring condition

ED_001324_00000687-00180

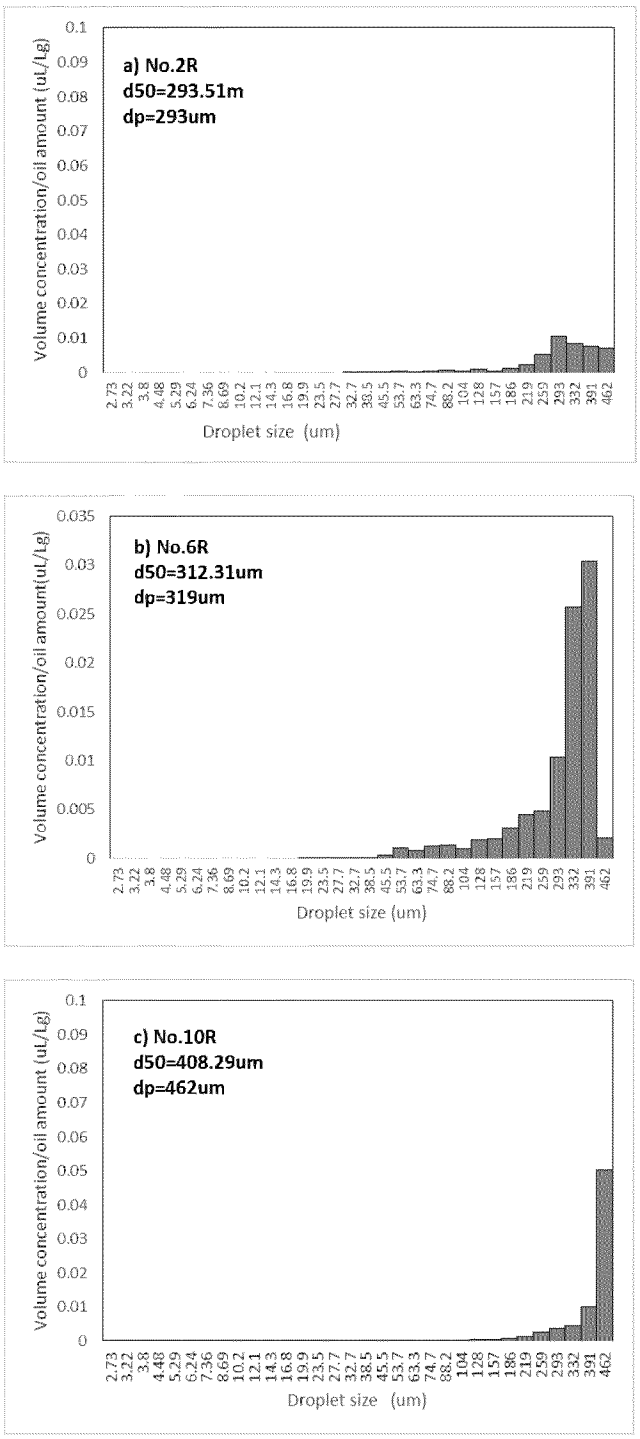

Figure 5: Experimental droplet size distribution of IFO-120 based on experiment a) No. 2R, b) No. 6R, and c) No.10R with DOR = 1: 200 in spring condition

ED_001324_00000687-00181

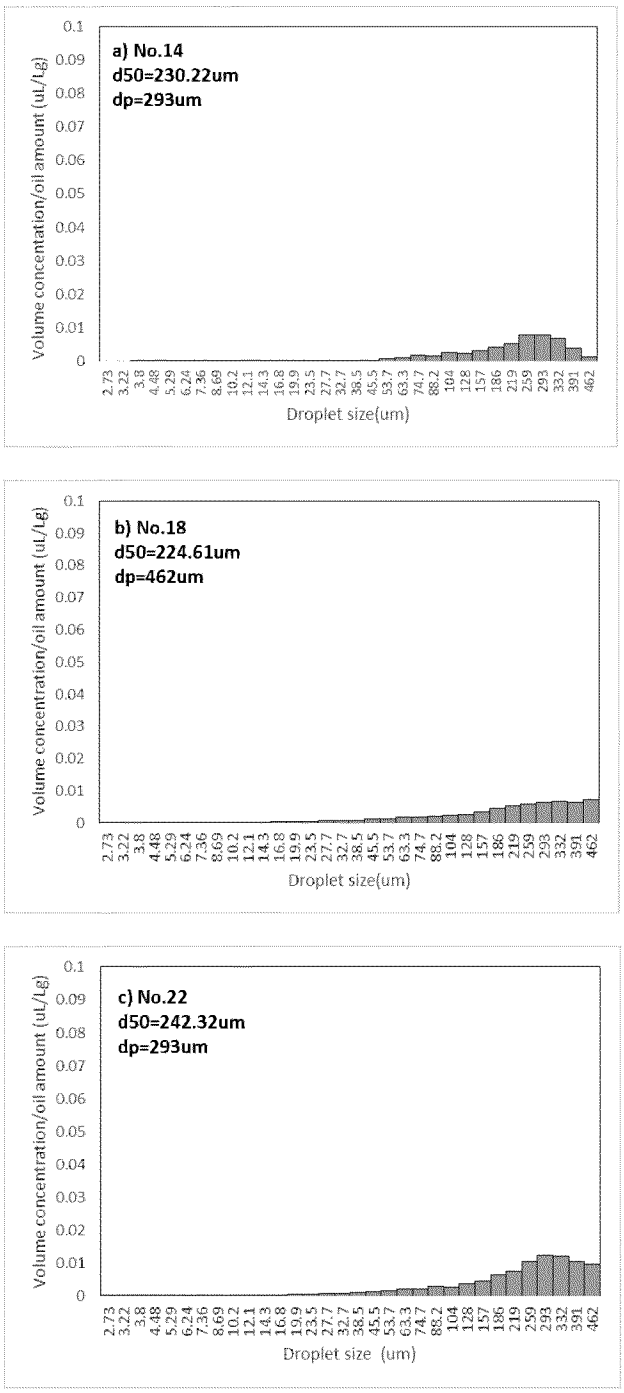

Figure 6: Experimental droplet size distribution of IFO-120 based on experiment a) No. 14, b) No. 18, and c) No. 22 with DOR = 1:200 in summer condition

ED_001324_00000687-00182

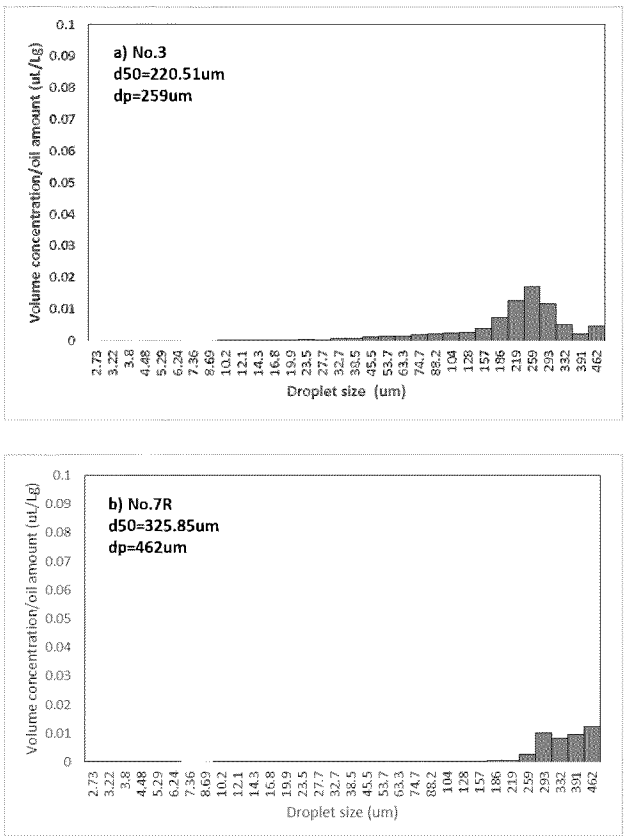

Figure 7: Experimental droplet size distribution of IFO-120 based on experiment a) No. 3, and b) No. 7, with DOR = 1:100 in spring condition

ED_001324_00000687-00183

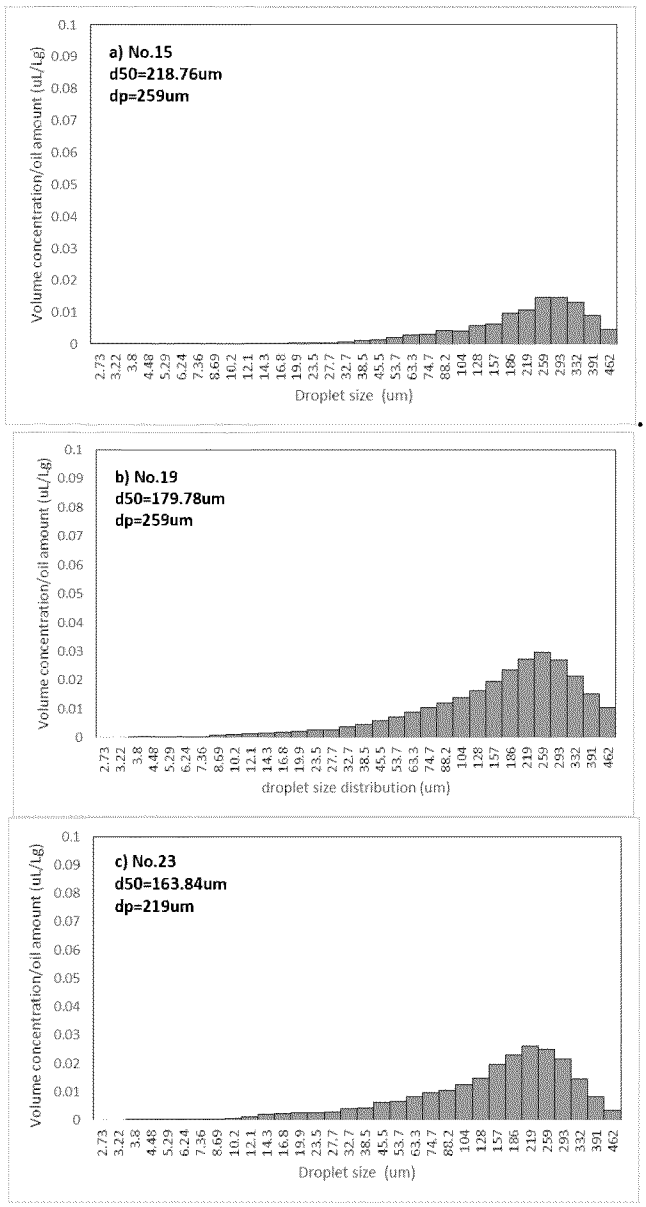

Figure 8: Experimental droplet size distribution of IFO-120 based on experiment a) No. 15, b) No. 19, and c) No.23 with DOR = 1:100 in summer condition

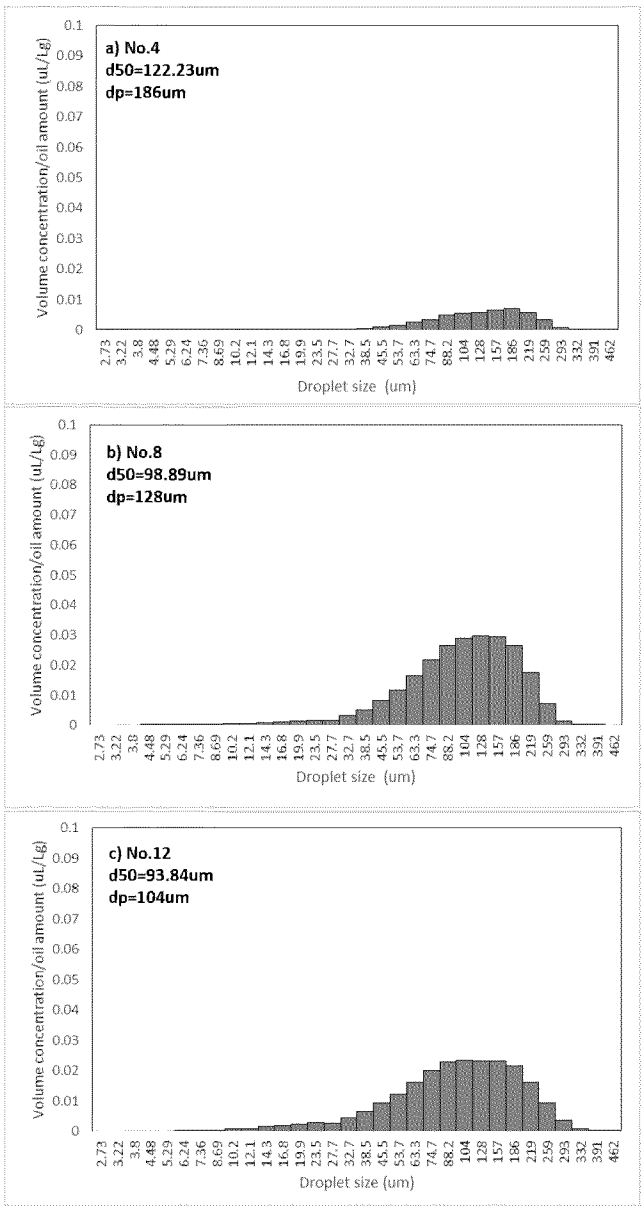

Figure 9: Experimental droplet size distribution of IFO-120 based on experiment a) No. 4, b) No. 8, and c) No.12 with DOR = 1:25 in spring condition

ED_001324_00000687-00185

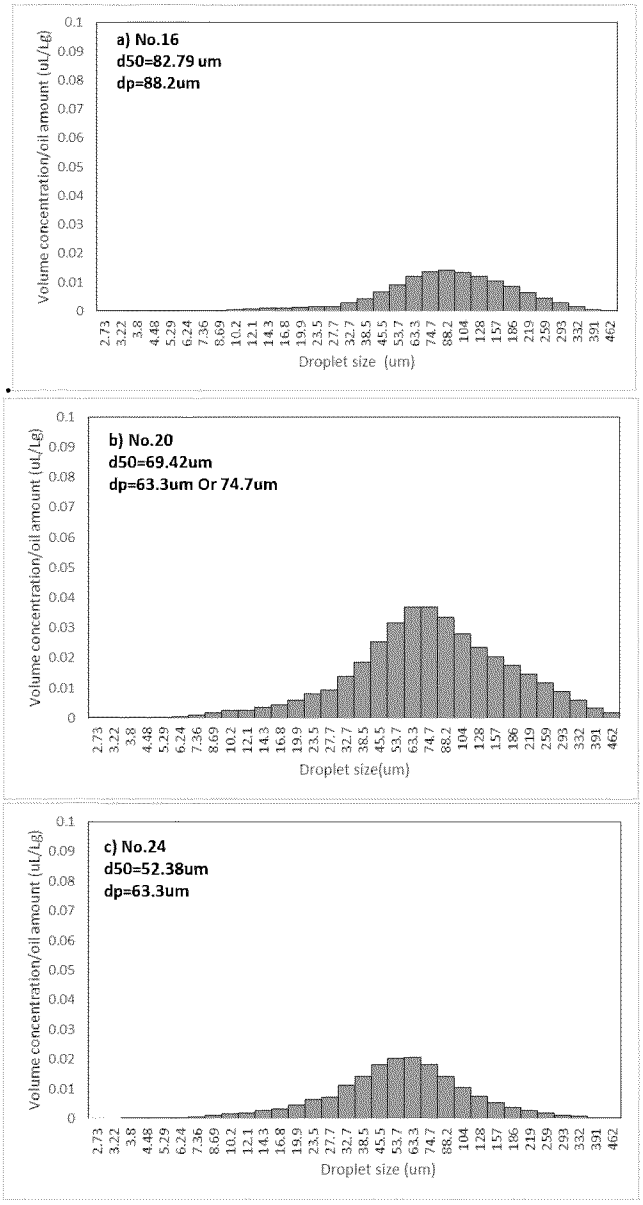

Figure 10: Experimental droplet size distribution of IFO-120 based on experiment a) No. 16, b) No. 20, and c) No.24 with DOR = 1:20 in summer condition

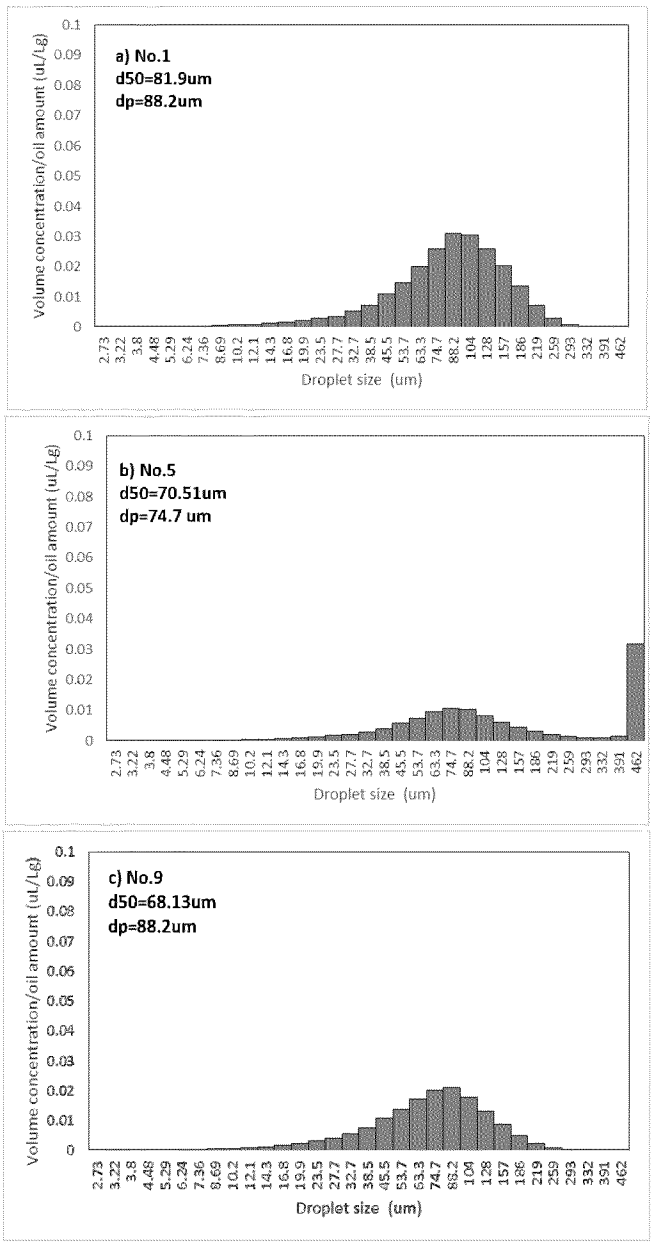

Figure 11: Experimental droplet size distribution of ANS based on experiment a) No. 1, b) No. 5, and c) No. 9 with DOR = 0 in spring condition

ED_001324_00000687-00187

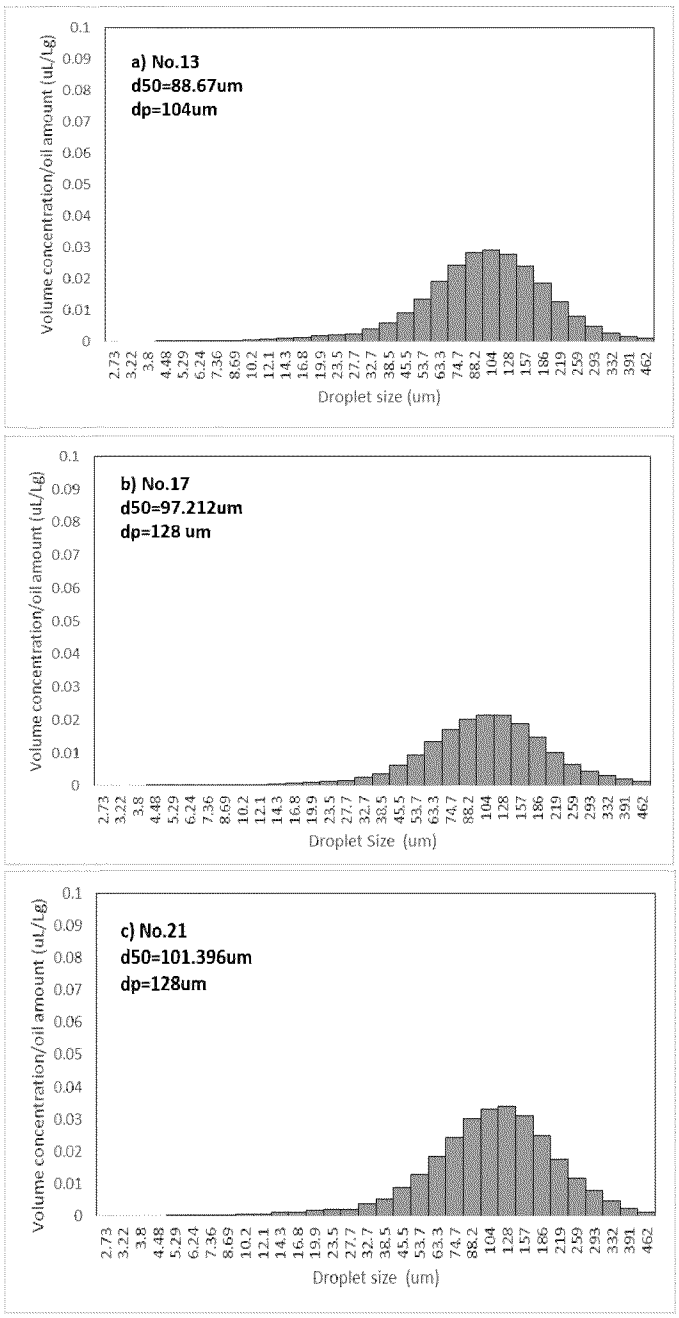

Figure 12: Experimental droplet size distribution of ANS based on experiment a) No. 13, b) No. 17, and c) No. 21 with DOR = 0 in summer condition

ED_001324_00000687-00188

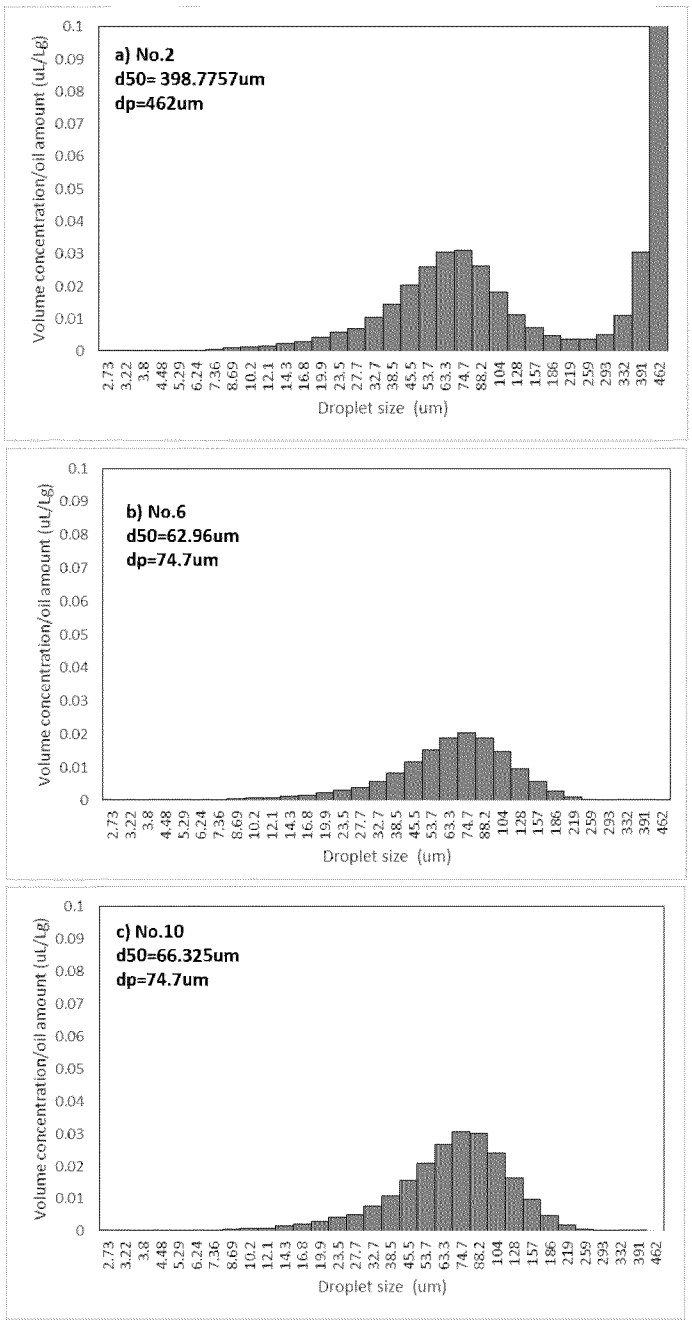

Figure 13: Experimental droplet size distribution of ANS based on experiment a) No. 2, b) No. 6, and c) No. 10 with DOR = 1:250 in spring condition

ED_001324_00000687-00189

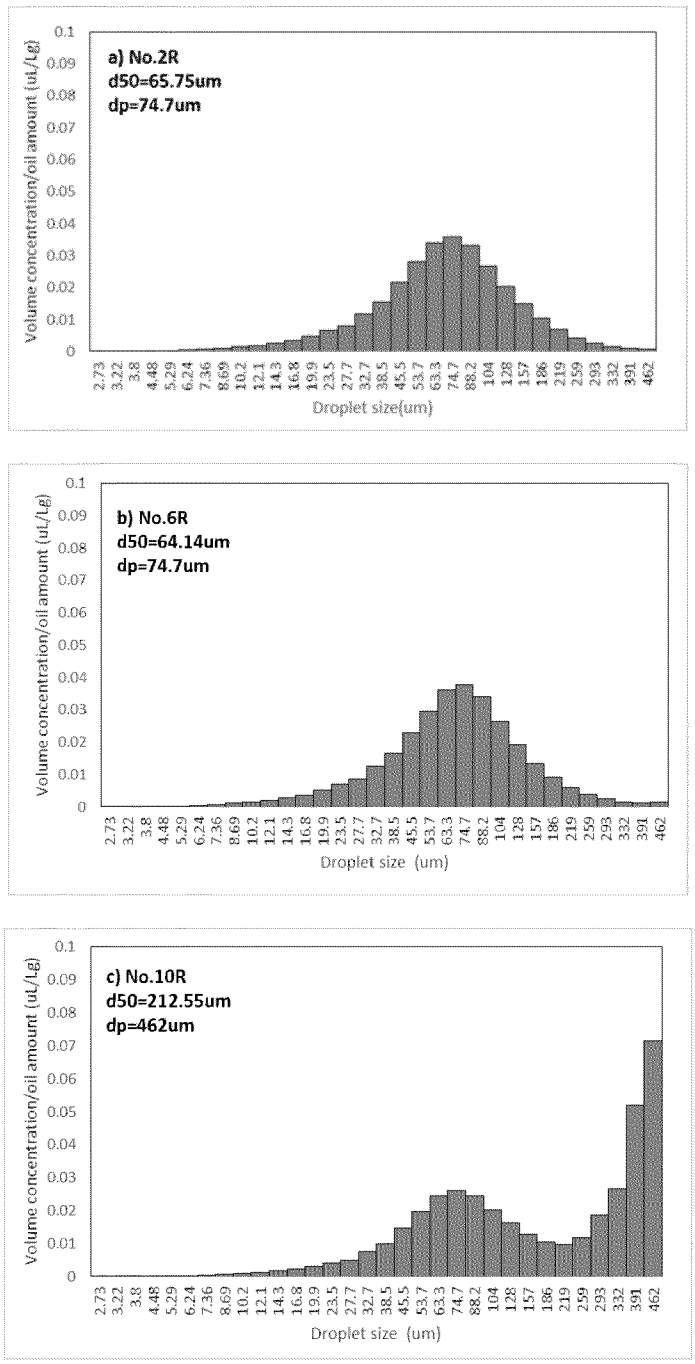

Figure 14: Experimental droplet size distribution of ANS based on experiment a) No. 2R, b) No. 6R, and c) No. 10R with DOR = 1:200 in spring condition

ED_001324_00000687-00190

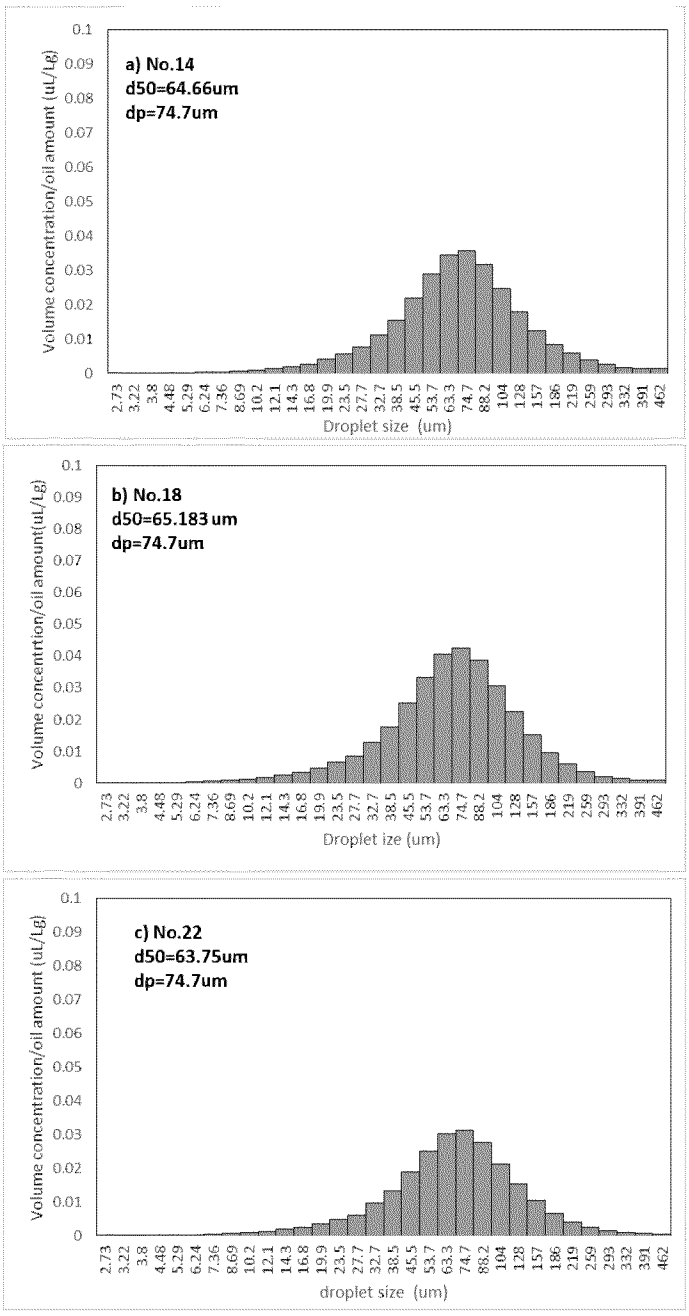

Figure 15: Experimental droplet size distribution of ANS based on experiment a) No. 14, b) No. 18, and c) No. 22 with DOR = 1:200 in summer condition

ED_001324_00000687-00191

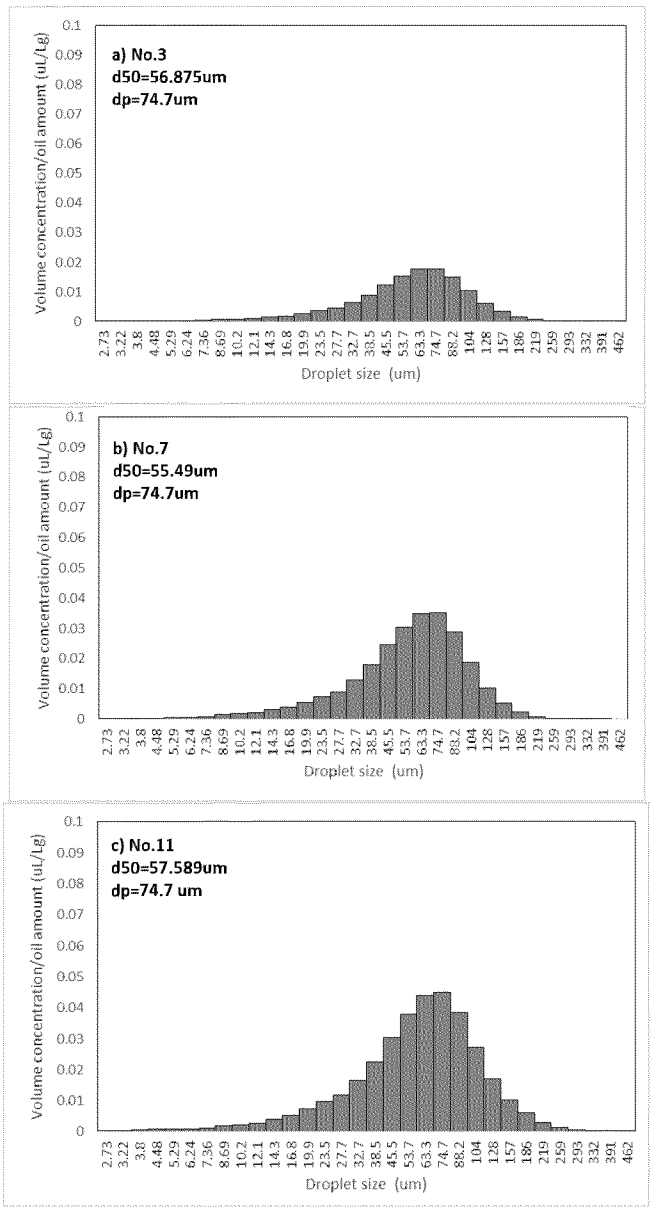

Figure 16: Experimental droplet size distribution of ANS based on experiment a) No. 3, b) No. 7, and c) No. 11 with DOR = 1:100 in spring condition

ED_001324_00000687-00192

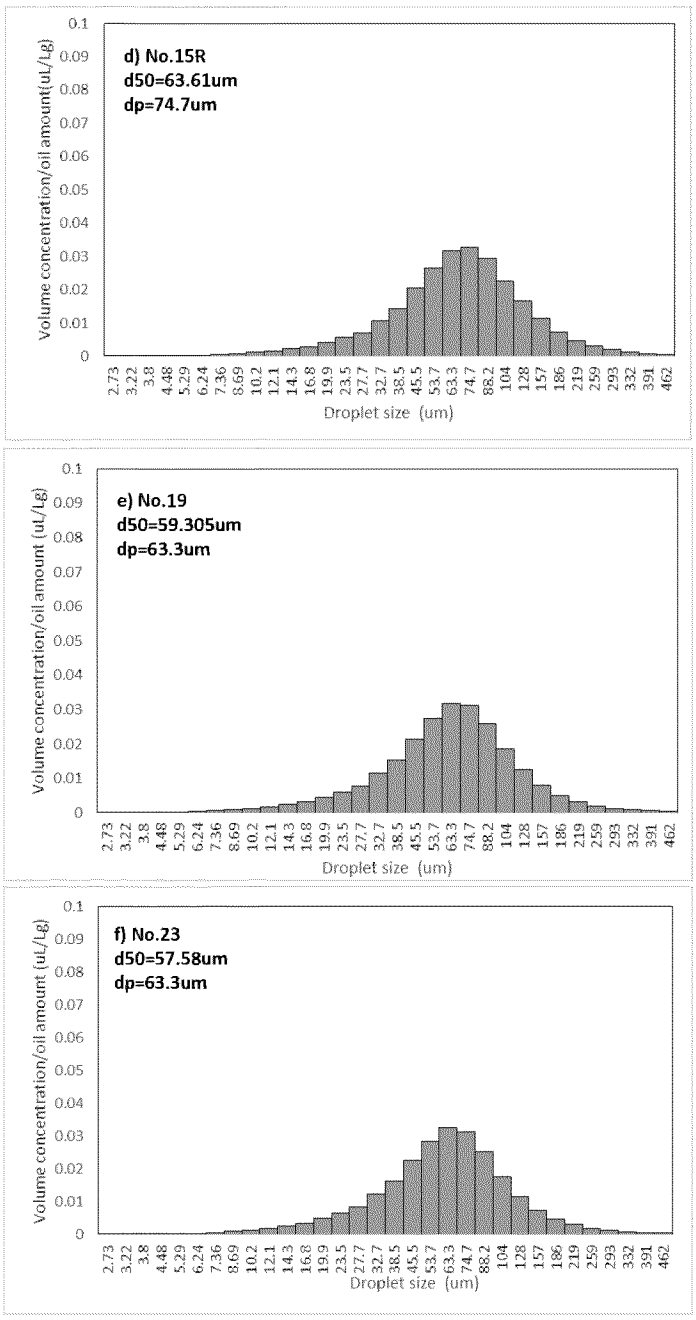

Figure 17: Experimental droplet size distribution of ANS based on experiment a) No. 15R, b) No. 19, and c) No. 23 with DOR = 1:100 in spring condition

ED_001324_00000687-00193

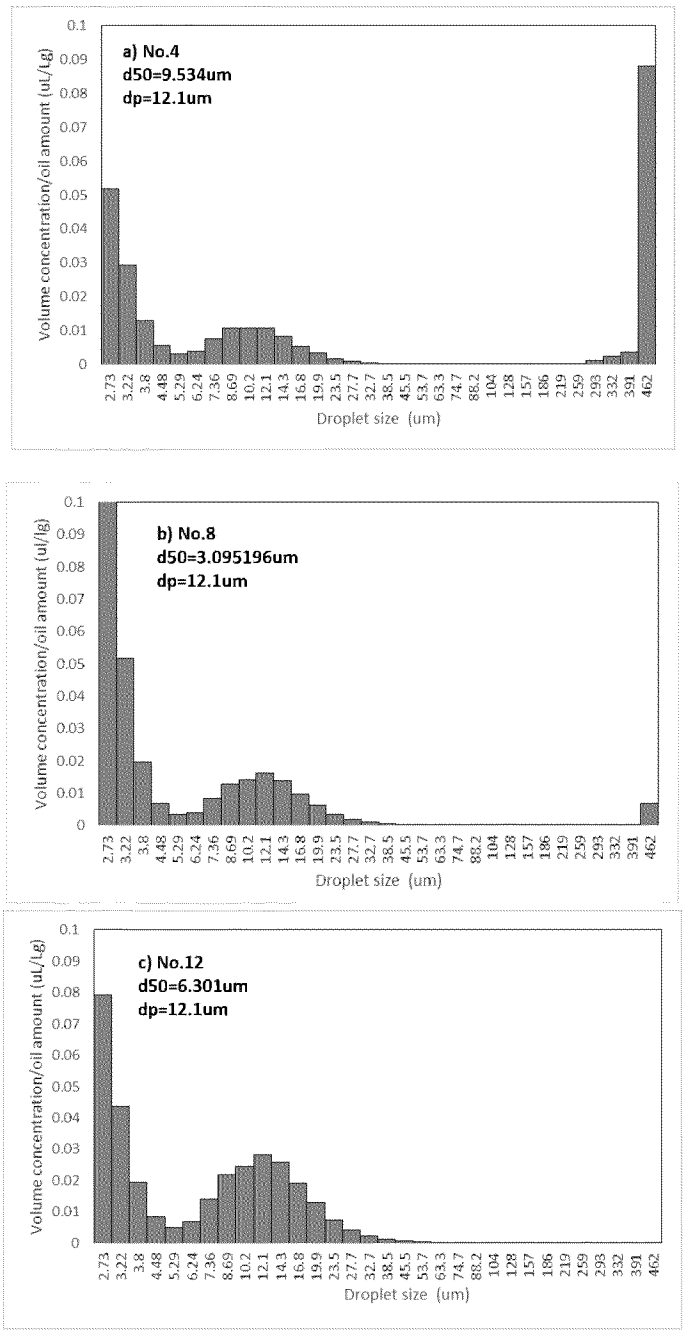

Figure 18: Experimental droplet size distribution of ANS based on experiment a) No. 4, b) No. 8, and c) No. 12 with DOR = 1:25 in spring condition

ED_001324_00000687-00194

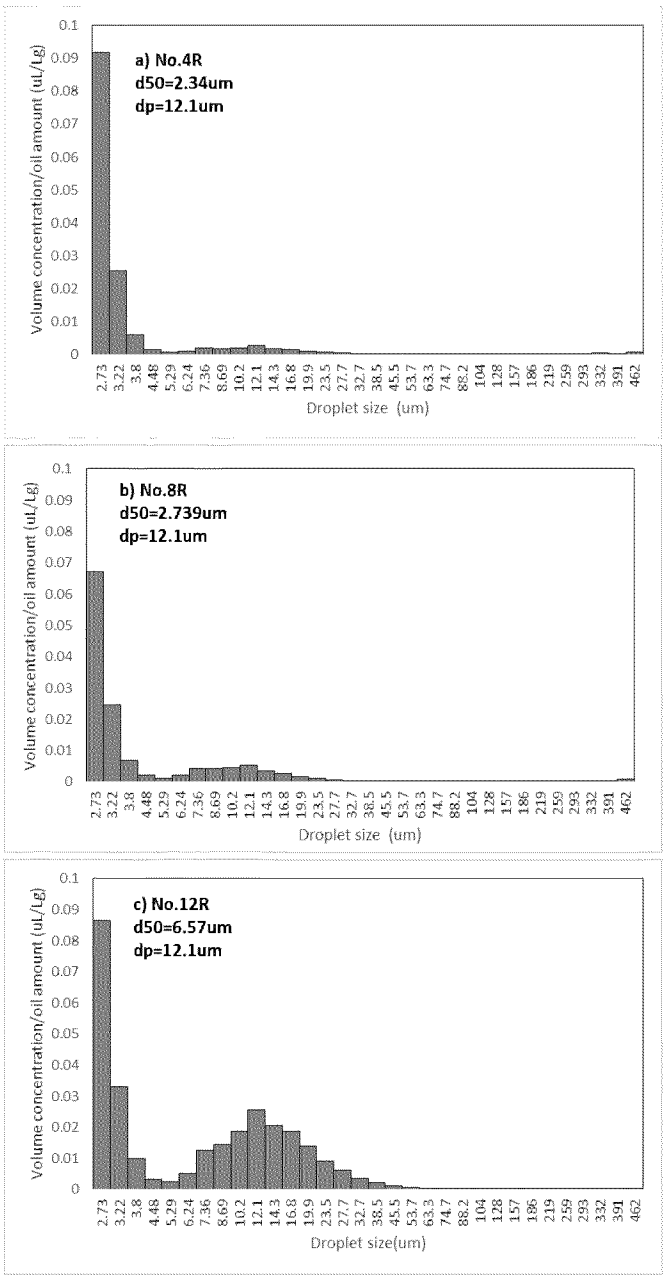

Figure 19: Experimental droplet size distribution of ANS based on experiment a) No. 4R, b) No. 8R, and c) No. 12R with DOR = 1:20 in spring condition

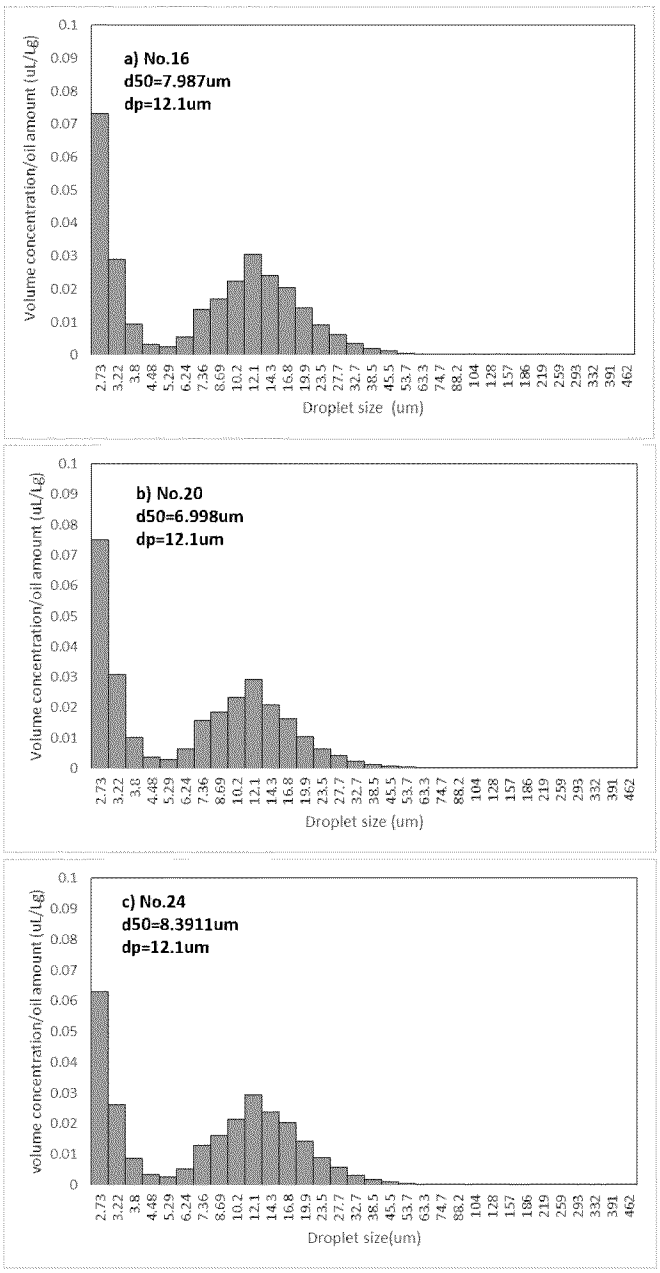

Figure 20: Experimental droplet size distribution of ANS based on experiment a) No. 16, b) No. 20, and c) No. 24 with DOR = 1:20 in Summer condition

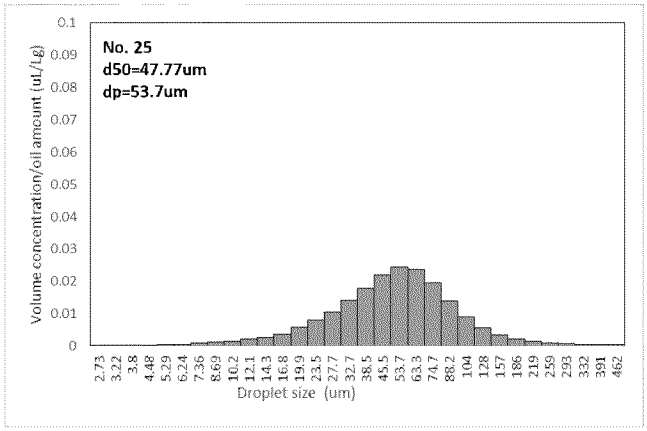

Figure 21: Experimental droplet size distribution of ANS based on experiment with DOR = 1:50 in summer condition

3.3 Data Fitting with Modified Weber Number Approach

Based on experimental settings (Table 1 and 2) and measured droplet size distributions (Figures 2 to 21), as well as the additional measurements on oilviscosity and IFT, the Weber number (*We*), Viscosity number (*Vi*) and Reynold number (*Re*) were calculated. The values of calculated and additional measured parameters for IFO-120 and ANS are listed in Tables 3 and 4. By normalize the d_{50} with the preset nozzle size in the experiments (D = 2.387 mm), the relationship between relative volume median droplet sizes (d_{50}/D) and modified Weber number (We* in Equation 11) for corresponding oils can be determined as in Figures 22 and 23. In comparison purpose, the corresponding data for Oseberg Blend based on the SINTEF tower tank experiments are also included in these figures.

As shown in Figure 22, for the treated IFO-120 crude oil with DOR ≤ 1:100, the modified Weber number approach fits the measured data IFO -120 well. The empirical constant A has been determined based on Equation 11 with regression approach. The empirical constant A for IFO-120 with DOR ≤ 1:100 is $A = 5$ which is significantly lower than the one for Oseberg Blend ($A = 15$, Johnsen et al., 2013). In the case of DOR > 1:100, the value of regressed constant is $A = 2.54$ for IFO-120 and $A = 8.7$ for Oseberg Blend. It indicates an about 45% of A values for both oils from DOR ≤ 1:100 to DOR > 1:100.

The regressions of constant A for ANS with different DOR conditions are listed in Figure 23. A reduction of 45% of A values is observed for ANS from DOR ≤ 1:100 to DOR > 1:100. It can be seen that the fitting situation for the regression of IFO-120 is better than which of ANS. Nevertheless, the trends of A with the change of DOR are consistent for IFO-120, ANS, and Oseberg Blend. Furthermore, the change of A values may be caused by the significant reduction of IFT. For the Oseberg Blend, when the DOR changed from 0 to 1:100 to 1:25, the corresponding IFTs were redu ced from 15.5 to 0.5 to 0.09 mN/m (Johansen et al., 2013). However, the change of IFTs measured in the COOGER's experiments are from 46.78 (mN/m) to 56.97 (DOR=1:100), and 49.09 (1:20), which are much less significant than which from Johansen et al., 2013 If similar magnitude of reduction as Johansen et al. (2013) is applied to IFO-120, the two fitted line could get much closer. Therefore, besides the oil properties, measured IFT played a significant role in determining the values of empirical constant A and it must be examined further.

ED_001324_00000687-00197

ED_001324_00000687-00198

Table 3: Data analyses for droplet size distribution of IFO-120

No.	Factors		Parameters								
	Oil	DOR	Q (L/min)	Viscosity (mPa·s)	d_{50} (μm)	dp (μm)	U (m/s)	IFT (mN/m)	We	Vi	Re
1	IFO-120	0	1.8063	44	230	259	5.6	46.78	1.55×10^3	5.27	293.5
1R	IFO-120	0									
2	IFO-120	1:250	1.7729	45	197.3	259	6.6	57.84	1.74×10^3	5.14	338.0
2R	IFO-120	1:200	1.849	45	293.510	293	6.887	57.84	1.89×10^3	5.36	352.556
3	IFO-120	1:100	1.8999	42	223.1	259	7.1	56.97	2.02×10^3	5.22	388.1
*4**	IFO-120	*1:25*	*1.2373*	*40*	*122.2*	*186*	*4.6*	*49.09*	*9.96×10^2*	*3.75*	*265.4*
4R	IFO-120	1:20	1.365	40	195.310	462	5.058	49.09	1.21×10^3	4.14	292.84
5	IFO-120	0	2.4435	44	176.6	259	9.1	46.78	4.08×10^3	8.56	476.4
6R	IFO-120	1:200	1.676	45	312.310	319	6.241	57.84	1.55×10^3	4.86	319.451
7R	IFO-120	1:100	1.86	42	341.750	462	6.927	56.97	1.94×10^3	5.11	379.893
8	IFO-120	1:25	1.7672	40	98.9	128	6.6	49.09	2.02×10^3	5.36	379
8R	IFO-120	1:20	1.513	40	177.920	293	5.634	49.09	1.49×10^3	4.59	324.444
9	IFO-120	0	3.1941	44	100.4	186	11.9	46.78	6.97×10^3	11.19	622.7

ED_001324_00000687-00199

10R	IFO-120	1:200	1.723	45	408.290	462	6.417	57.84	1.64×10^3	4.99	328.489
11R	IFO-120	1:100	N/A	42	370.340	462	N/A	56.97	N/A	N/A	N/A
12	IFO-120	1:25	2.4511	40	93.8	128	9.1	49.09	3.91×10^3	7.44	525.7
12R	IFO-120	1:20	1.415	40	211.340	293	5.27	49.09	1.3×10^3	4.29	303.449
13*	IFO-120	0	2.281	44	263.3	391	8.5	46.78	3.13×10^3	7.89	444.7
14	IFO-120	1:200	2.1684	45	230.2	259	8.1	57.84	2.29×10^3	6.28	413.4
15	IFO-120	1:100	2.613	42	215.2	259	9.7	56.97	3.37×10^3	7.17	533.7
16	IFO-120	1:20	2.8059	40	82.8	88.2	10.5	49.09	4.51×10^3	8.52	601.8
17	IFO-120	0	2.2795	44	192.7	293	8.5	46.78	3.13×10^3	7.99	444.5
18*	IFO-120	1:200	2.5788	45	224	462	9.6	57.84	3.24×10^3	7.47	491.6
19	IFO-120	1:100	3.1426	42	179.8	259	11.7	56.97	4.88×10^3	8.63	641.9
20	IFO-120	1:20	3.0697	40	69.38	74.7	11.4	49.09	5.40×10^3	9.32	658.4
21*	IFO-120	0	2.3596	44	254.6	391	8.8	46.78	3.35×10^3	8.27	460.1
22*	IFO-120	1:200	2.8236	45	245.9	293	10.5	57.84	3.88×10^3	8.18	538.3
23	IFO-120	1:100	3.1319	42	167.8	219	11.7	56.97	4.85×10^3	8.60	639.7
24	IFO-120	1:20	3.3753	40	52.6	63.3	12.6	49.09	6.53×10^3	10.24	723.9

Table 4: Data analyses for droplet size distribution of ANS

ED_001324_00000687-00200

No.	Factors		Parameters								
	Oil	DOR	Q (L/min)	Viscosity (mPa·s)	d_{50} (μm)	dp (μm)	U (m/s)	IFT (mN/m)	We	Vi	Re
1	ANS	0	3.617	7.2	81.9	88.2	13.471	63.97	5.84×10^3	1.52	3852.38
2*	ANS	1:250	3.895	8.2	398.780	462	14.507	60.52	7.16×10^3	1.97	3642.77
2R	ANS	1:200	4.041	8.2	65.750	74.7	15.051	60.52	7.71×10^3	2.04	3779.38
3	ANS	1:100	3.958	8.3	56.875	74.7	14.740	55.94	8.00×10^3	2.19	3656.72
*4**	ANS	*1:25*	*3.937*	*7.6*	*9.534*	*10.2*	*14.663*	*42.07*	1.08×10^3	*2.64*	*3972.47*
4R	ANS	*1:20*	*3.995*	*7.6*	*2.340*	*12.1*	*14.880*	*42.07*	1.08×10^4	*2.69*	*4031.43*
5	ANS	0	3.885	7.2	70.512	74.7	14.471	63.97	6.74×10^3	1.63	4138.34
6*	ANS	1:250	3.891	8.2	62.961	74.7	14.492	60.52	7.14×10^3	1.96	3638.87
6R	ANS	1:200	4.66	8.2	64.140	74.7	17.357	60.52	1.02×10^4	2.35	4358.32
7	ANS	1:100	3.844	8.3	55.487	74.7	14.316	55.94	7.54×10^3	2.12	3551.38
8*	ANS	1:25	3.859	7.6	3.095	12.1	14.373	42.07	1.01×10^4	2.6	3893.87
8R	ANS	1:20	4.134	7.6	2.739	12.1	15.398	42.07	1.16×10^4	2.78	4171.8
9	ANS	0	3.915	7.2	68.131	88.2	14.580	63.97	6.84×10^3	1.64	4169.46
10*	ANS	1:250	3.909	8.2	66.325	74.7	14.559	60.52	7.21×10^3	1.97	3655.78
10R*	ANS	1:200	4.792	8.2	212.55	462	17.849	60.52	1.08×10^4	2.42	4481.91

ED_001324_00000687-00201

11	ANS	1:100	3.851	8.3	57.589	74.7	14.341	55.94	7.57×10^3	2.13	355.76
12*	ANS	1:25	3.904	7.6	6.301	12.1	14.538	42.07	1.03×10^4	2.63	3938.78
12R	ANS	1:20	4.144	7.6	6.570	12.1	15.321	42.07	1.15×10^4	2.77	4150.74
13	ANS	0	4.225	7.2	88.870	104	15.735	63.97	7.97×10^3	1.77	4499.9
14	ANS	1:200	4.107	8.2	64.661	74.7	15.295	60.52	7.96×10^3	2.07	3840.5
15R	ANS	1:100	4.233	8.3	63.604	74.7	15.766	55.94	9.15×10^3	2.34	3911.2
16	ANS	1:20	4.061	7.6	7.987	12.1	15.124	42.07	1.12×10^4	2.73	4097.4
17	ANS	0	4.168	7.2	97.212	128	15.523	63.97	$7{,}76\times10^3$	1.75	4439.1
18	ANS	1:200	4.141	8.2	65.183	74.7	15.424	60.52	8.09×10^3	2.09	3873
19	ANS	1:100	3.942	8.3	59.305	63.3	14.683	55.94	7.94×10^3	2.18	3642.6
20	ANS	1:20	4.029	7.6	6.999	12.1	15.005	42.07	1.1×10^4	2.71	4065.1
21	ANS	0	4.133	7.2	101.396	128	15.393	63.97	7.63×10^3	1.73	4402.1
22	ANS	1:200	3.920	8.2	63.747	74.7	14.600	60.52	7.25×10^3	1.98	3666.2
23	ANS	1:100	3.956	8.3	57.583	63.3	14.735	55.94	7.99×10^3	2.19	3655.4
24	ANS	1:20	3.976	7.6	8.391	12.1	14.808	42.07	1.07×10^4	2.68	4011.8

*Note: * mark means these data were not considered in the prediction of droplet size distribution due to incomplete measured distribution.*

ED_001324_00000687-00202

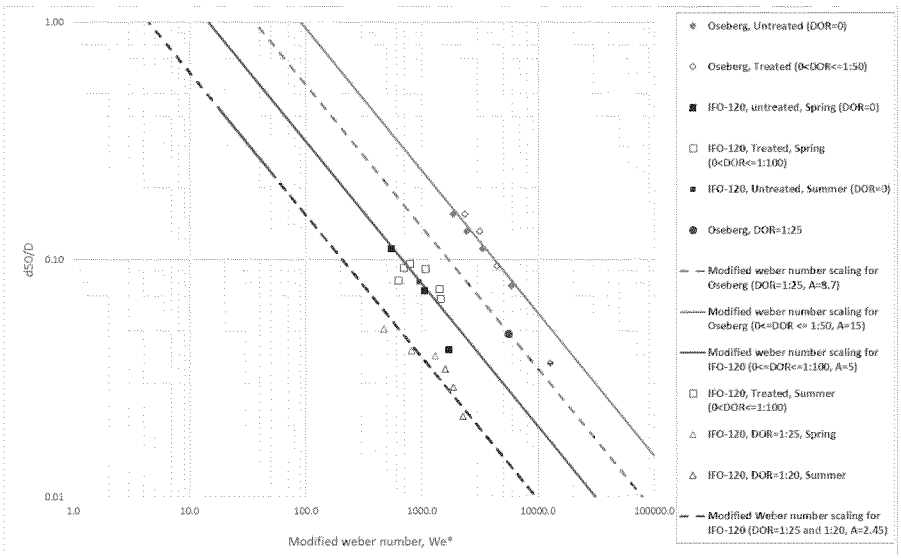

Figure 22: Data regression for constant *A* from modified Weber number and d_{50}/D for IFO-120

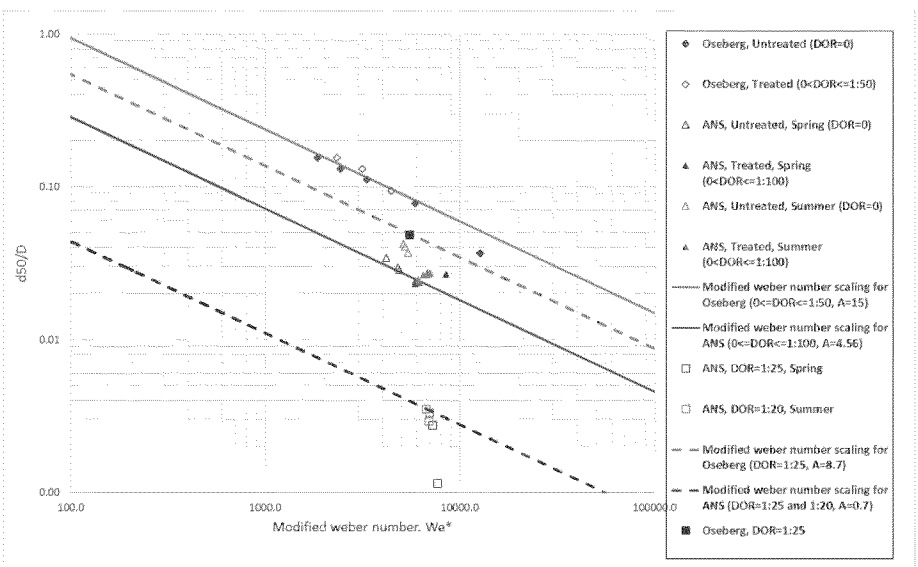

Figure 23: Data regression for constant *A* from modified Weber number and d_{50}/D for ANS

3.4 IFT and Reynolds Number Scaling

Due fact that the effects of oil/dispersant in water concentration affects IFT and in situ sampling may be impractical, as suggested by Johansen et al. (2013), some method for prediction of IFT related to a given DOR will be useful. IFT measurements with a variety of oils premixed with different dosages of dispersants might help to establish such relationships in more general terms. As demonstrated by MacKay and Hossain (1982), with same amount of oil and dispersant, the water volume affects the IFT significantly. In the direct sampling methods, the amount of oil/dispersant in 1L of sample from different experiments could vary significantly and therefore affects the IFT measurements. For example for Murban oil with DOR=1:1333, the IFT was 3.7 and 7.9 (mN/m) for 100 and 800 mL of water, respectively. Brandvik et al. (2013) provide a more advantage method for more consistent IFT measurement compared with the direct sampling methods. In this method, oil/water samples were collected at 1.5 m height above the nozzle in 1 L long necked measuring flask. Oil appeared as droplets in the water withsize distribution depending on the DOR and method of dispersant application. The surface oil layer in the narrow neck of the bottle and was collected for IFT measurements after 24 h. using spinning drop method as described by Khelifa and So (2009), the Dataphysics Spinning Drop Tensiometer SVT-20N with control and calculation software SVTS 20 IFT was used. The IFT in this study were measured using a different method by premix 10 mg oil - dispersant in 100 mL seawater.

Before such a relationship is establish, we believe that the use of IFT should be avoided and the use of Modified Weber number approach should be re -considered. Wang and Calabrese (1986) have found that droplet breakup was governed by the Weber number scaling for small viscosity numbers ($Vi \rightarrow 0$), but that a Reynolds number scaling would apply for large viscosity number ($Vi >> 1$):

$$d_{50} / D = C \cdot Re^{-3/4} \tag{13}$$

where $C = A^{5/4}B^{3/4}$, and the Re is the Reynolds number given by

$$Re = \frac{\rho U D}{\mu} \tag{14}$$

where ρ is the density of oil, U is the exit velocity, D is the nozzle diameter, and μ is the dynamic viscosity. Using of Reynolds scaling instead of modified Weber number scaling have the apparent advantage of avoiding the inconsistency IFT measurements and can make comparison of data from different sources easier.

The application of this concept for existing experimental data has been shown in Figure 24 . The calculated and observed d_{50}/D correlates very well. In addition, the volume median diameters for IFO-120 are plotted against Reynolds number in Figure 25 together with data for Oseberg Blend by Brandvik et al. (2013). It can be seen from the plot that Reynolds scaling fits the data well. Values of empirical constants A were obtained for all IFO -120 combined (exclude DOR=1:25 (or 20)) and Oseberg Blend through regression analysis. A was 6.1 for combined data while the A for Oseberg Blend is 16.8. The data has shown that with the d50/D is slightly bigger (higher A) for summer condition cases than winter condition cases

ED_001324_00000687-00204

with same Reynolds number (Figure 25). The cases for ANS show quite dif ference compared with IFO-120 cases. The DOR=0 and ≤1:100 experimental data points are more closed to Oseberg Blend data, the A for combined data of ANS (excluded DOR=1:25 (or 20)) is 10.5 (Figure 26). It is unclear if this is associated with uncertainties due to limited experimental data points or it is actually due to the effects of different water temperature. With more experimental data available, this observation will be revisited. Without considering the effects of temperature, the difference in *A* between IFO-120 and Oseberg Blend are considered to be the effects of oil type.

Furthermore, *A* has been reduced from 16.8 to 8.7 (49% reduction) for Oseberg, from 6.1 to 3.21 (47% reduction) for IFO-120 and 10.5 to 1.75 (83% reduction) for ANS (Figures 24 and 25). This is reduction can be used to model the effects of chemical dispersant on droplet size. Based on the experimental data on the three oils, it is proposed that a constant value *A* could be selected for Reynolds number scaling depending on oil types for cases of DOR ≤ 1:100. For DOR of 1:25, a 50% reduction of *A* may be used and a linear interpolation may be used to estimate *A* values for other DOR greater than 1:100 but less than 1:25 for Oseberg Blend and IFO-120. However, the change *A* values for ANS does not follow the linear relation. Data points of DOR = 1:50 for ANS is close to the one of DOR = 1:100 but relatively far from which of DOR=1:25 (or 20). This may be caused by the effects of oil type and further interpolations for the relation of DOR and A value for ANS will be needed in future study.

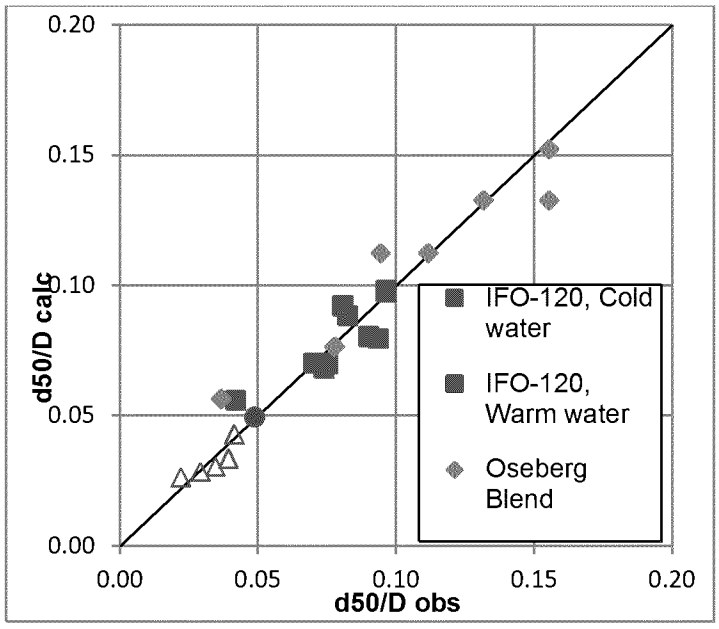

Figure 24: Measured (obs) and computed (calc) relative droplet sizes d50/D from experiments with IFO-120 and Oseberg Blend

ED_001324_00000687-00205

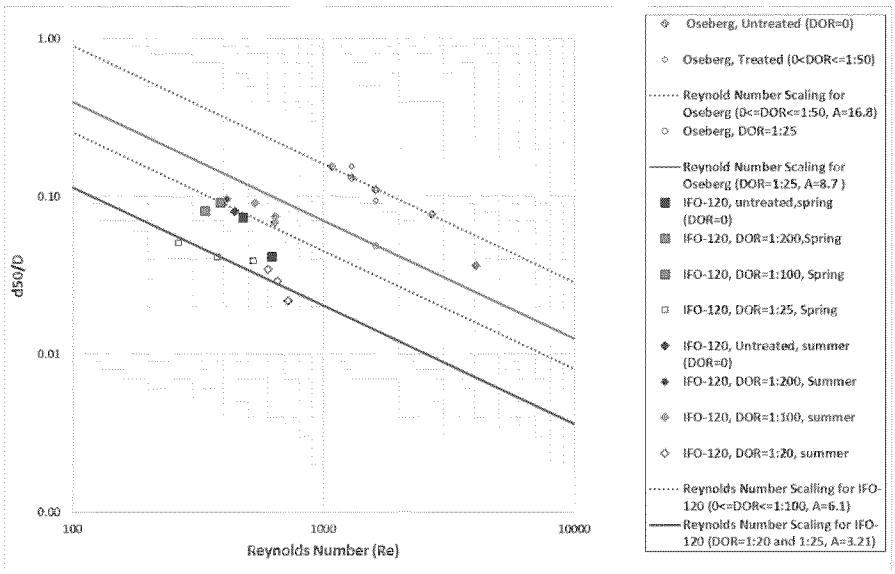

Figure 25: Data regression for constant *A* from Reynolds number and d_{50}/D for IFO-120

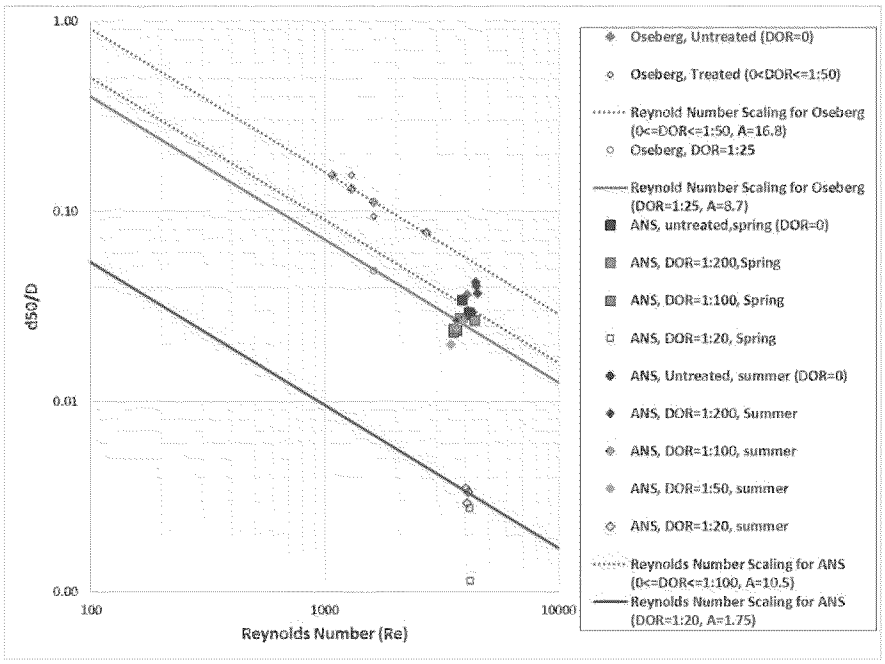

Figure 26: Data regression for constant *A* from Reynolds number and d_{50}/D for ANS

3.5 Determination of Distribution Shape using Two-Step Rosin-Rammler Method

The sections above described how to predict the characteristic diameter, d_{50}, for different types of oils (i.e., IFO-120 and ANS). Correspondingly, further prediction of the statistical distribution for the droplet sizes around the characteristic diameter will be conducted in this section. According to Lefebvre (1989),

two most commonly used distribution are lognormal and Rosin-Rammler distributions. Johansen et al. (2013) has also concluded that there is currently no theoretical basis for choosing the right distribution function and the choice of function must be based on empirical data.

Johansen et al. (2013) have found that Rosin-Rammler could provide better overall fit of the experiment data and they have derived a spreading coefficient $\alpha = 1.8$ for the corresponding distribution. In this study, Rosin-Rammler distribution was also selected and corresponding regression analysis has been conducted to calculate the best spreading coefficients (Tables 5 and 6).

The initial data analysis has indicated that the distributions of the data with $d/d_{50} <= 1$ and $d/d_{50} > 1$ are significantly varied. Thus, it would be difficult and/or inaccurate to predict the measured IFO-120 and ANS data by only a single distribution.

In order to address this challenge, a two-step Rosin-Rammler approach was introduced by advancing from the Rosin-Rammler approach proved by Johansen et al. (2013). The proposed approach uses two separate spreading coefficients: α_1 for $d/d_{50} <= 1$ and α_2 for $d/d_{50} > 1$, providing better fit of the data in all cases. The data distribution and the corresponding regression results are shown in Figures 27 to 42. Regressed based on the single Rosin-Rammler distribution, the overall spreading coefficient (α) for IFO-120 is 2.33 which is larger than that for Oseberg Blend (1.8). For ANS, $\alpha = 1.77$, is smaller than which for Oseberg Blend ($\alpha = 1.8$). According to the two-step Rosin-Rammler approach, the average α_1 for IFO-120 is 2.01 and α_2 is 2.74. In addition, the average α_1 for ANS is 1.78 and α_2 is 1.63. Furthermore, the regression coefficients (R^2) for the regressions based on single and two-step Rosin-Rammler distributions were also calculated for both IFO-120 and ANS under different DOR and seasonal conditions (Figures 27 to 42). The R^2 for two-step Rosin-Rammler are higher than which for the single one in most of the case, indicating the advantage of the proposed two-step Rosin-Rammler approach.

Table 5: Spreading coefficient for Rosin-Rammler distribution of IFO-120

			All Data			Average		
			Single	2-step		Single	2-step	
			α	α_1	α_2	α	α_1	α_2
Summer	Untreated	No.13*	/	/	/			
		No.17	1.86	1.53	2.20			
		No.21*	/	/	/	1.86	1.53	2.20
	1:20	No.16	1.75	2.13	1.44			
		No.20	1.55	1.95	1.18			
		No.24	1.85	2..05	1.50	1.72	2.04	1.37
	1:100	No.15	1.96	1.50	2.54			
		No.19	1.57	1.30	2.00			
		No.23	1.59	1.31	1.975	1.71	1.37	2.17

ED_001324_00000687-00207

			All Data			Average		
	1:200	No.14	2.39	1.85	3.10			
		No.18*	/	/	/			
		No.22*	/	/	/	2.39	1.85	3.10
Spring	Untreated	No.1*	/	/	/			
		No.5	1.66	1.32	2.14			
		No.9	1.54	1.49	1.632	1.60	1.41	1.89
	1:25	No.4	2.13	2.24	2.10			
		No.8	2.05	2.31	1.83			
		No.12	1.77	1.99	1.62	1.98	2.18	1.85
	1:100	No.3	2.61	1.98	3.31			
		No.7R*	/	/	/			
		No.11R*	/	/	/	2.61	1.98	3.31
	1:250	No.2	2.39	1.72	3.20			
		No.6R*	/	/	/			
		No.10R*	/	/	/	2.39	1.72	3.20
Average						2.33	2.01	2.74

Note: "/" indicates that the data is unavailable due to incomplete droplet size distribution from measurement

Table 6: Spreading coefficient for Rosin-Rammler distribution of ANS

			All Data			Average		
			Single α	2-Step:		Single	2-step	
			α	α_1	α_2	α	α_1	α_2
summer	Untreated	No. 13	1.93	2.32	1.57			
		No. 17	1.87	2.29	1.51			
		No. 21	1.9	2.3	1.58	1.90	2.30	1.55
	1:20	No. 16	1.12	0.62	1.39			
		No. 20	1.12	0.61	1.34	1.14	0.64	1.41
		No. 24	1.17	0.68	1.49			
	1:100	No. 15R	1.99	2.24	1.65			

ED_001324_00000687-00208

			All Data			Average		
		No. 19	2.05	2.24	1.67	2.02	2.23	1.66
		No. 23	2.03	2.20	1.66			
	1:200	No. 14	1.96	2.26	1.49	2.02	2.27	1.57
		No. 18	2.03	2.29	1.61			
		No. 22	2.06	2.25	1.622			
Spring	Untreated	No. 1	2.08	2.00	1.90	2.04	2.01	1.93
		No. 5*	/	/	/			
		No. 9	1.99	2.02	1.95			
	1:20	No. 4R*	/	/	/	0.98	0.49	1.10
		No. 8R*	/	/	/			
		No. 12R	0.98	0.49	1.10			
	1:100	No. 3	2.14	2.17	2.11	2.10	2.11	2.09
		No. 7	2.15	2.13	2.18			
		No. 11	2.00	2.03	1.97			
	1:200 (and 250)	No. 2R	1.87	2.11	1.50	2.01	2.19	1.73
		No. 6R	1.92	2.16	1.54			
		No. 10	2.23	2.30	2.15			
Average						1.77	1.78	1.63

Note: "/" indicates that the data is unavailable due to incomplete droplet size distribution from measurement

ED_001324_00000687-00209

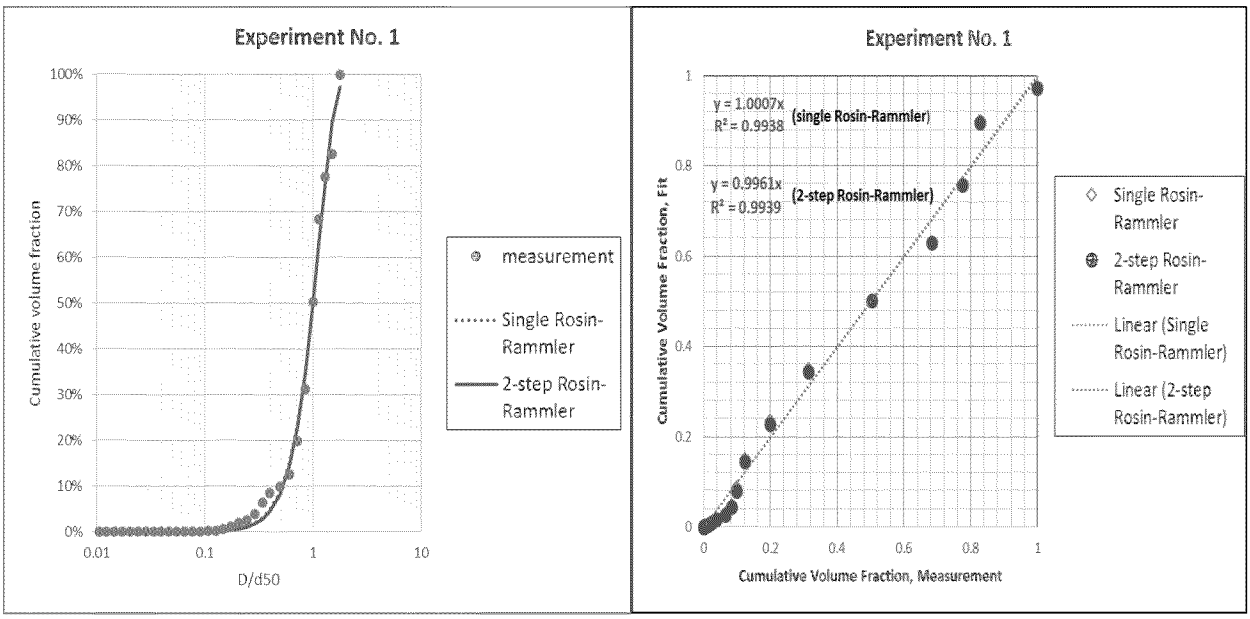
Experiment No. 1
Cumulative volume fraction
D/d50
measurement
Single Rosin-Rammler
2-step Rosin-Rammler
Experiment No. 1
y = 1.0007x
R² = 0.9938
(single Rosin-Rammler)
y = 0.9961x
R² = 0.9939
(2-step Rosin-Rammler)
Cumulative Volume Fraction, Fit
Cumulative Volume Fraction, Measurement
Single Rosin-Rammler
2-step Rosin-Rammler
Linear (Single Rosin-Rammler)
Linear (2-step Rosin-Rammler)

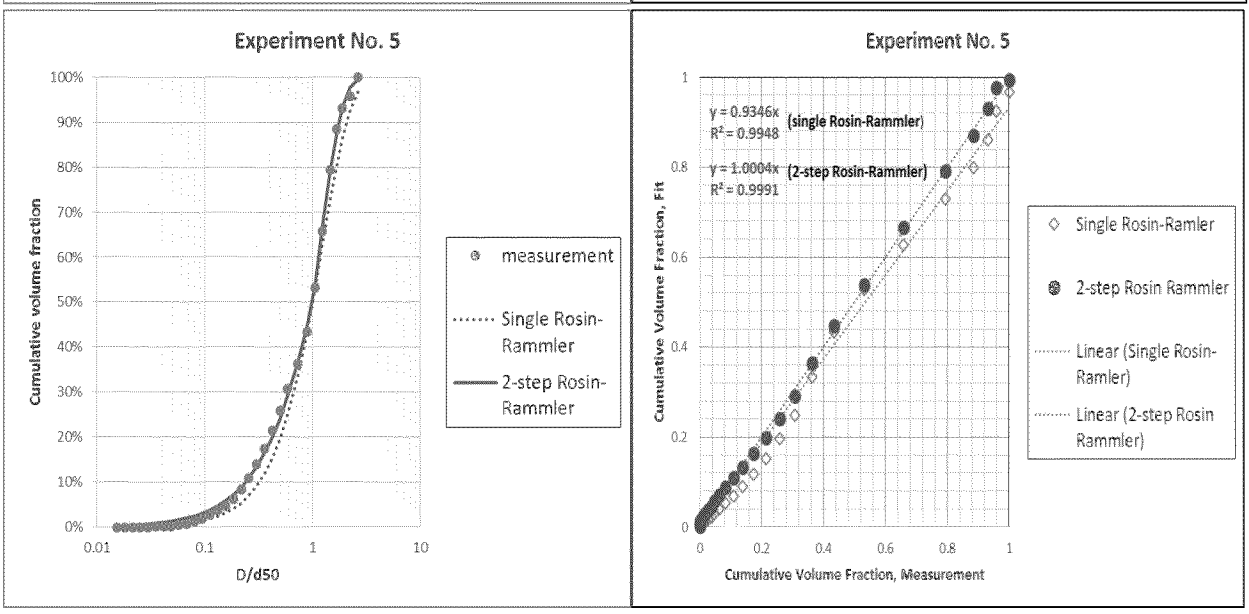
Experiment No. 5
Cumulative volume fraction
D/d50
measurement
Single Rosin-Rammler
2-step Rosin-Rammler
Experiment No. 5
y = 0.9346x
R² = 0.9948
(single Rosin-Rammler)
y = 1.0004x
R² = 0.9991
(2-step Rosin-Rammler)
Cumulative Volume Fraction, Fit
Cumulative Volume Fraction, Measurement
Single Rosin-Ramler
2-step Rosin Rammler
Linear (Single Rosin-Ramler)
Linear (2-step Rosin Rammler)

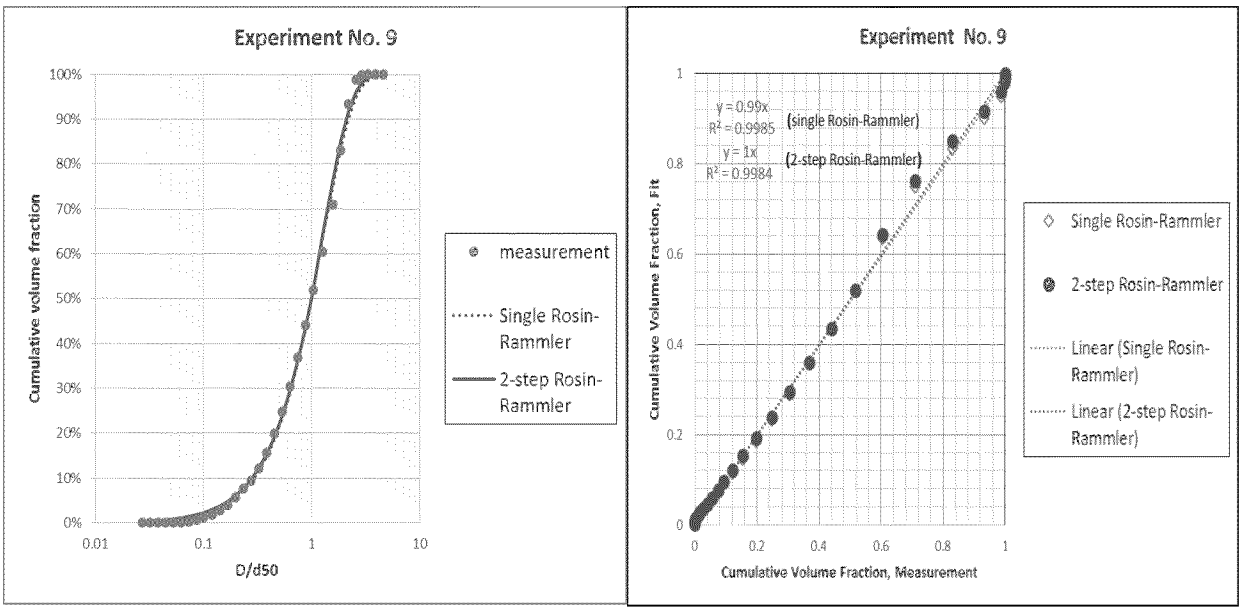

Figure 27: Cumulative distribution of d/d_{50} and regression results for IFO-120 with DOR = 0 in spring conditions

(*Note: the left figures are distributions and the right ones are regression results*)

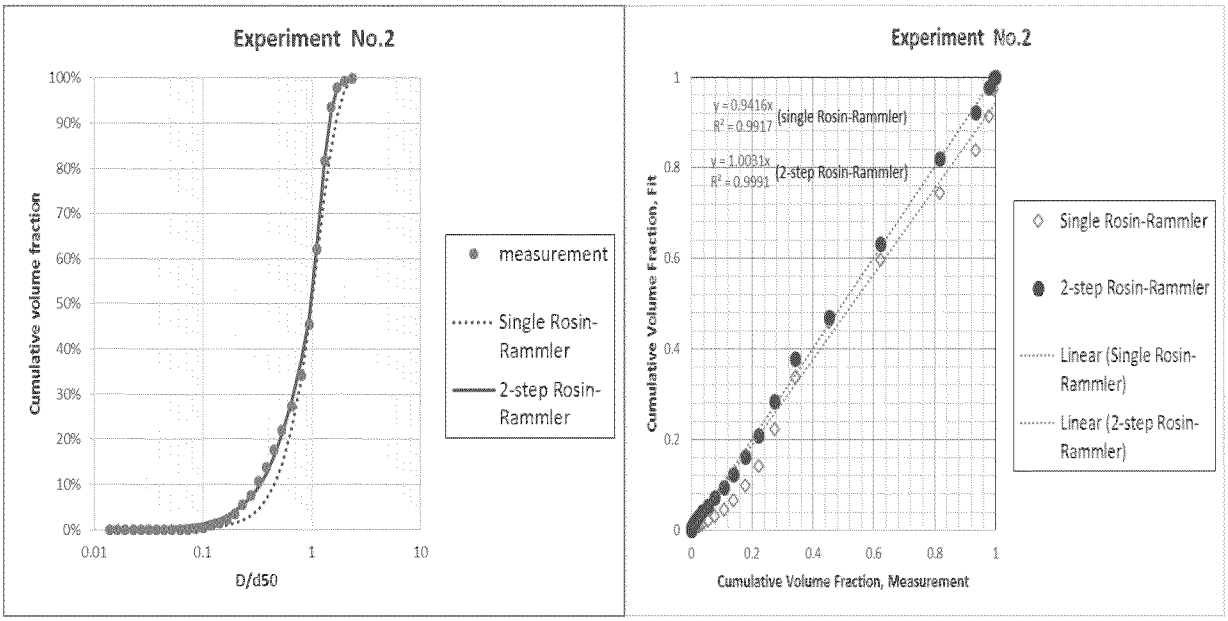

Figure 28: Cumulative distribution of d/d_{50} and regression results for IFO-120 with DOR = 1:250 in spring conditions

(*Note: the left figures are distributions and the right ones are regression results*)

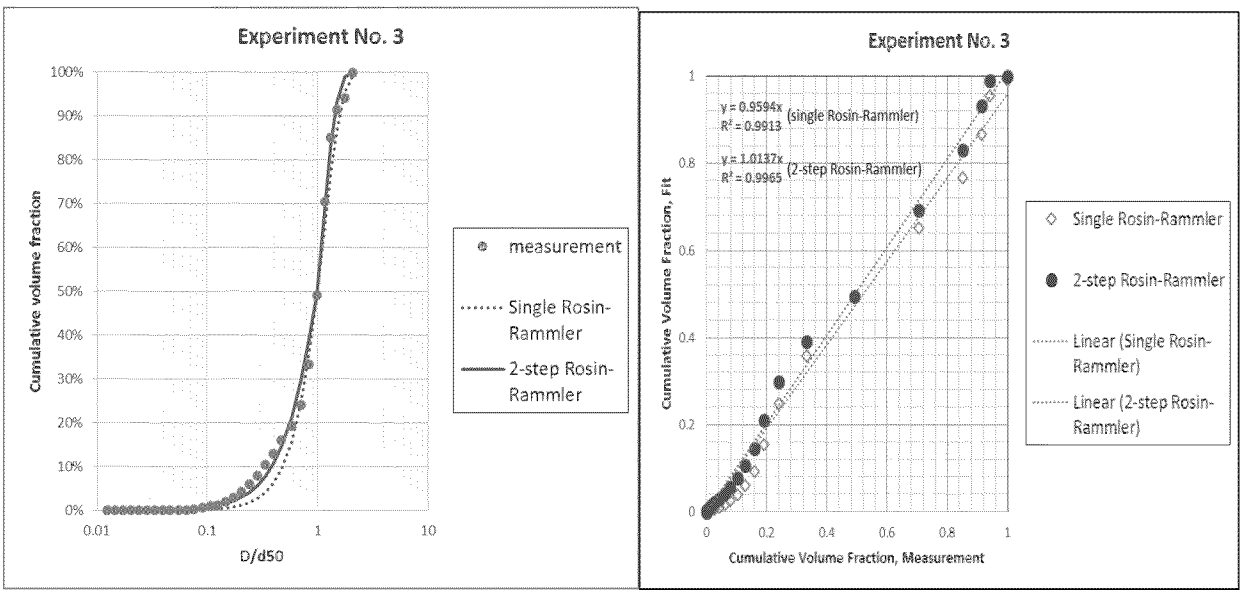

Figure 29: Cumulative distribution of d/d_{50} and regression results for IFO-120 with DOR = 1:100 in spring conditions

(*Note: the left figures are distributions and the right ones are regression results*)

ED_001324_00000687-00212

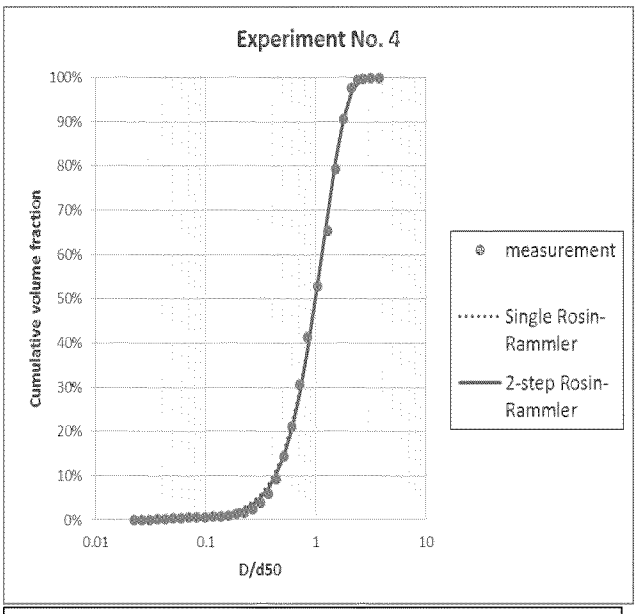

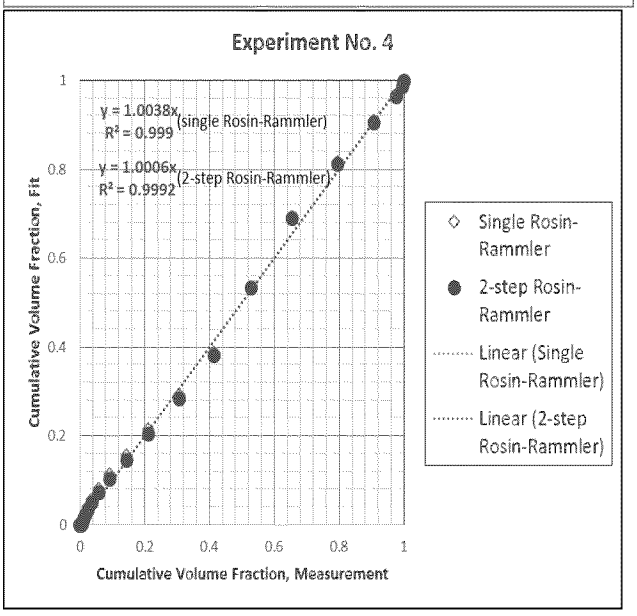

ED_001324_00000687-00213

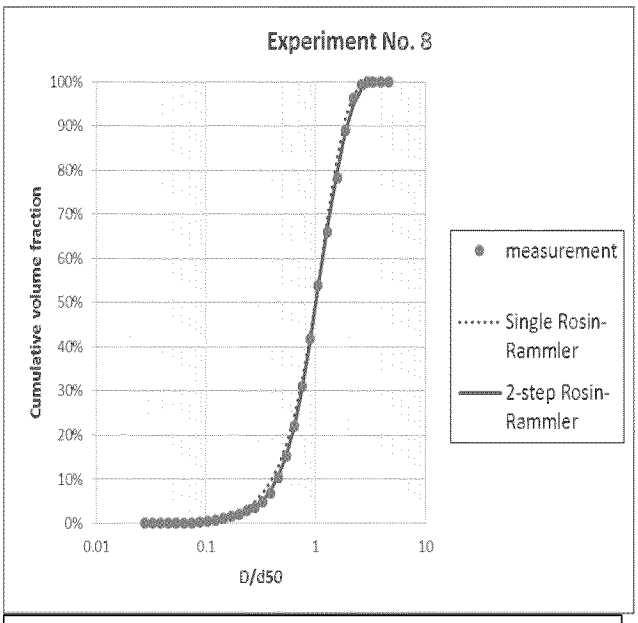

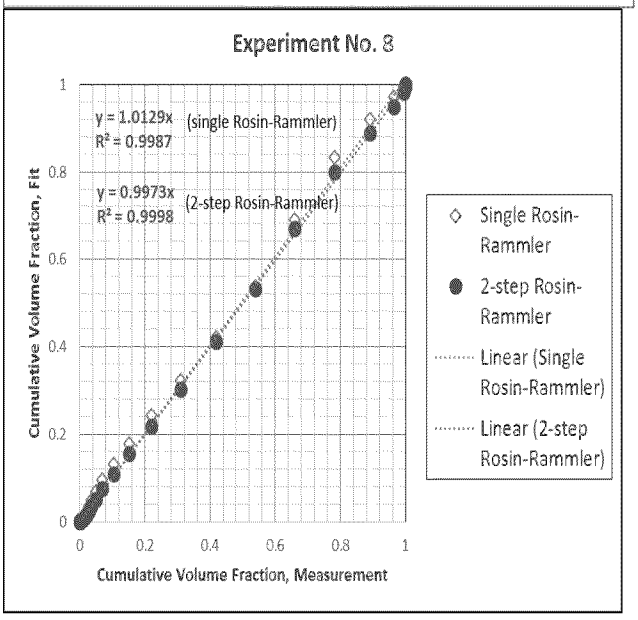

ED_001324_00000687-00214

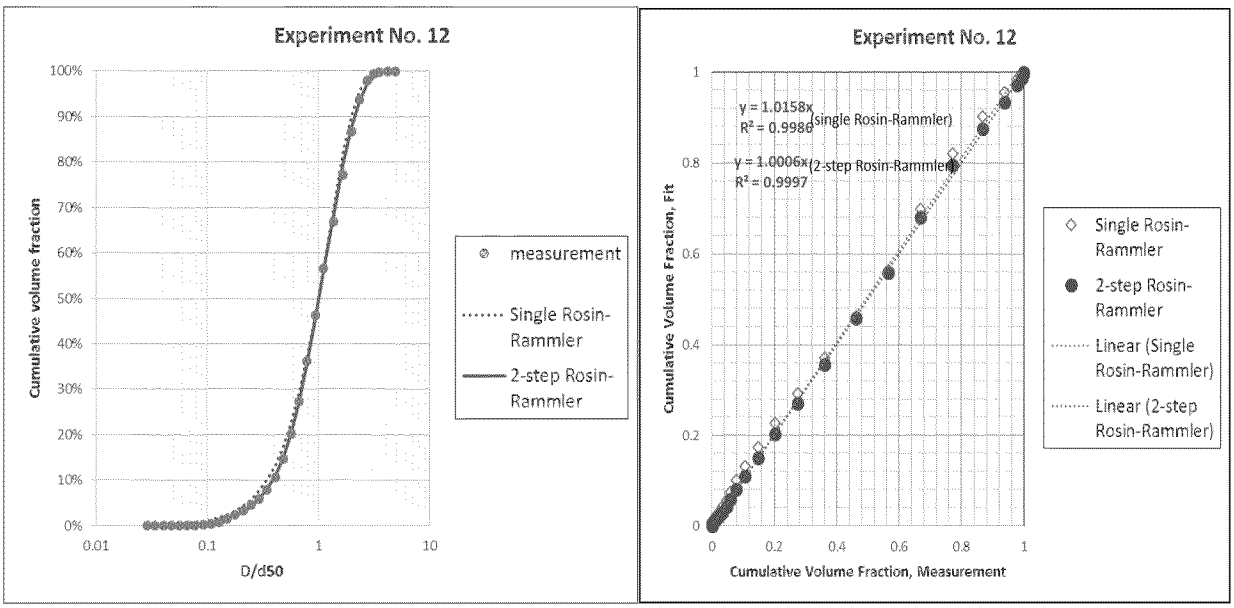

Figure 30: Cumulative distribution of d/d_{50} and regression results for IFO-120 with DOR = 1:25 in spring conditions

(*Note: the left figures are distributions and the right ones are regression results*)

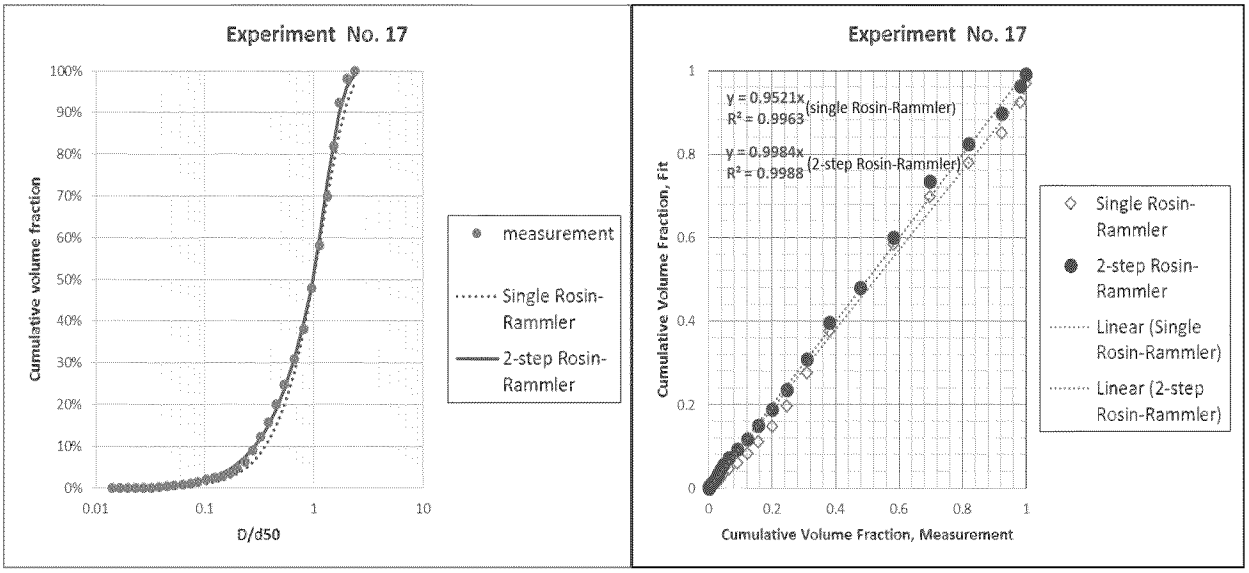

Figure 31: Cumulative distribution of d/d_{50} and regression results for IFO-120 with DOR = 0 in summer conditions

(*Note: the left figures are distributions and the right ones are regression results*)

ED_001324_00000687-00215

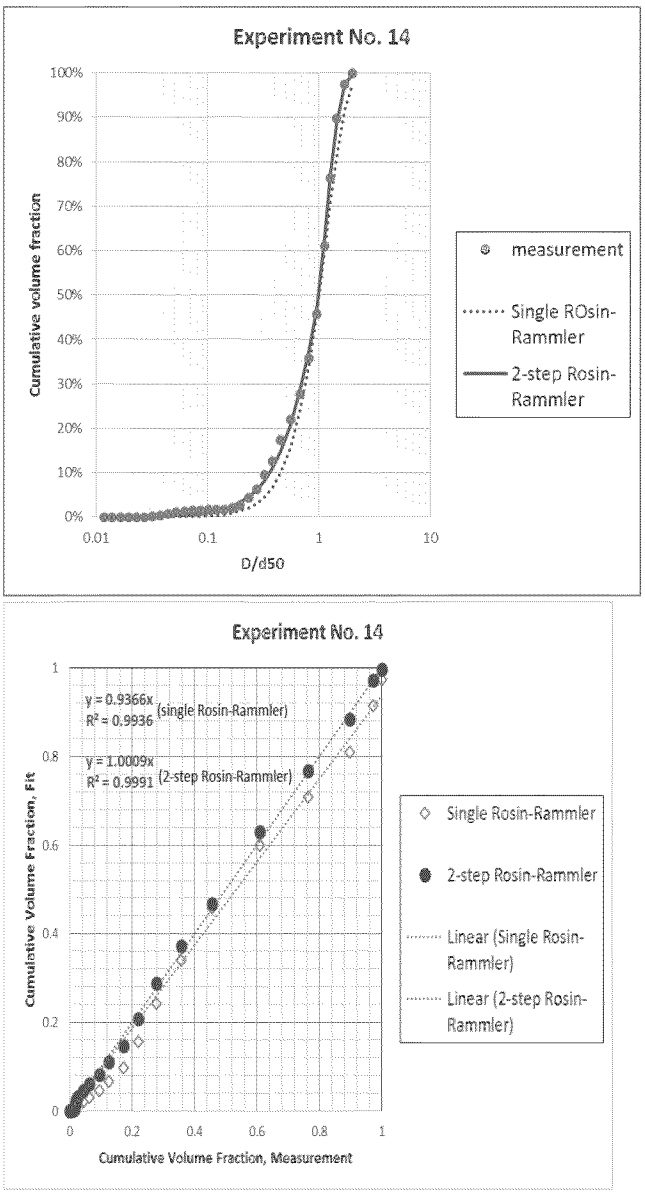

Figure 32: Cumulative distribution of d/d_{50} and regression results for IFO-120 with DOR = 1.200 in summer conditions

(*Note: the left figures are distributions and the right ones are regression results*)

ED_001324_00000687-00216

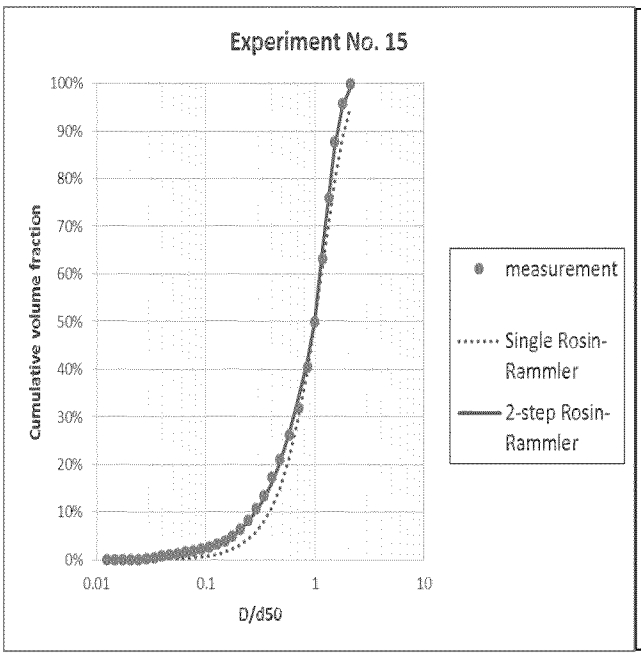

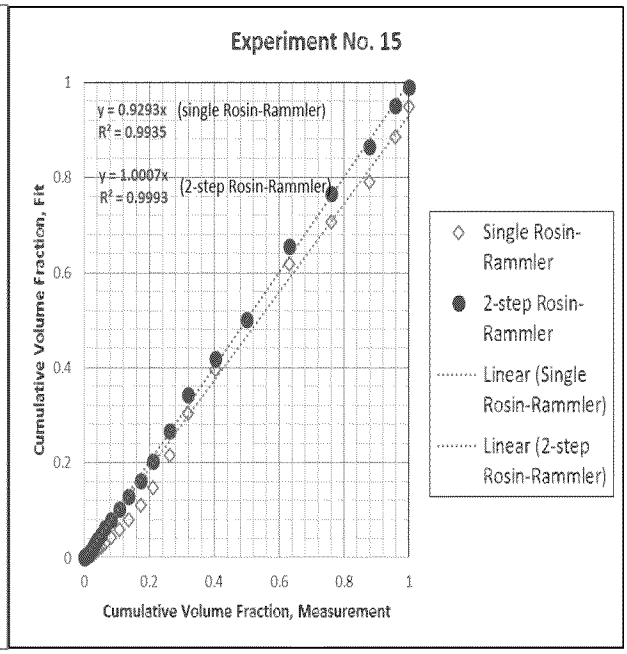

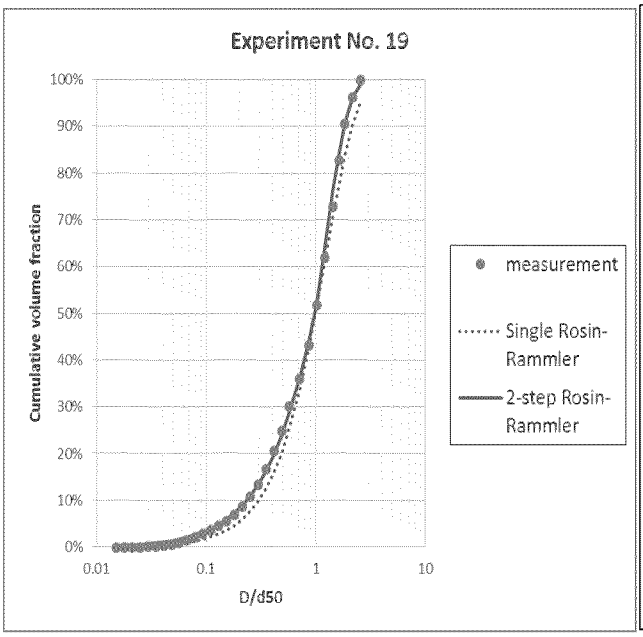

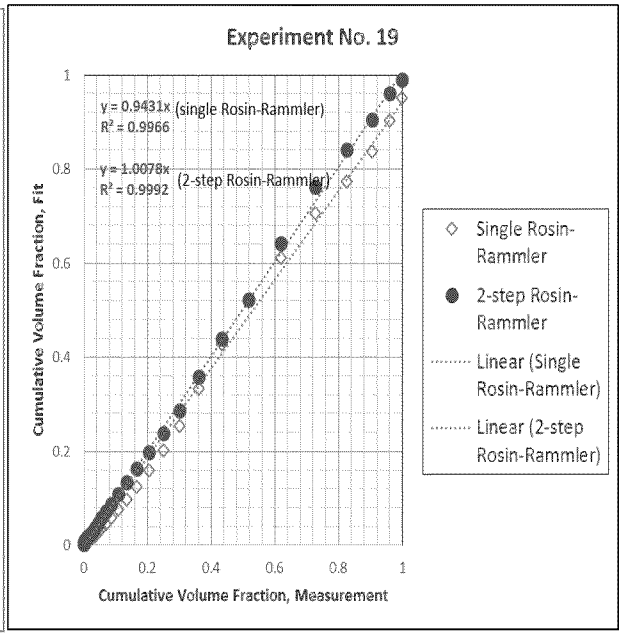

ED_001324_00000687-00217

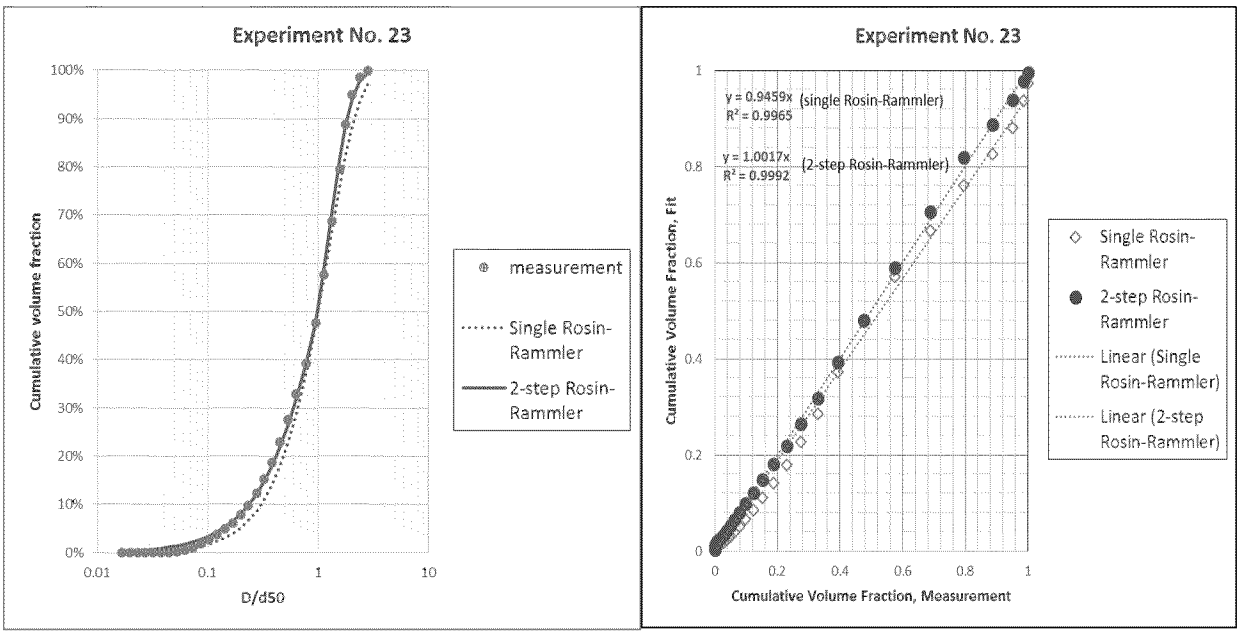

Figure 33: Cumulative distribution of d/d_{50} and regression results for IFO-120 with DOR =1: 100 in summer conditions

(*Note: the left figures are distributions and the right ones are regression results*)

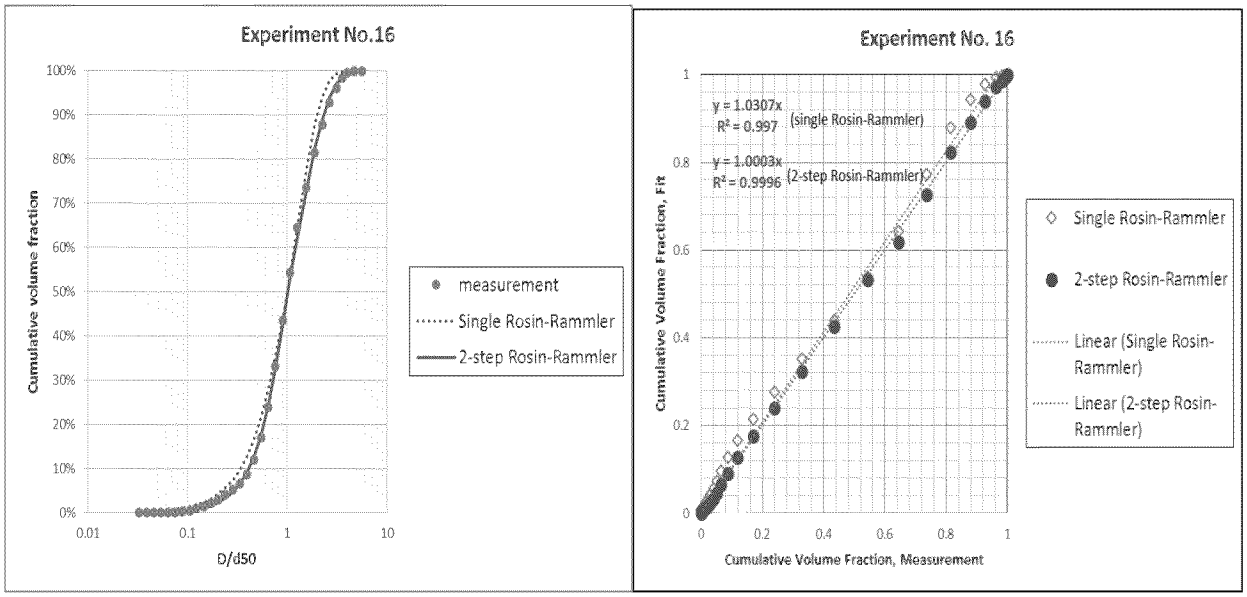

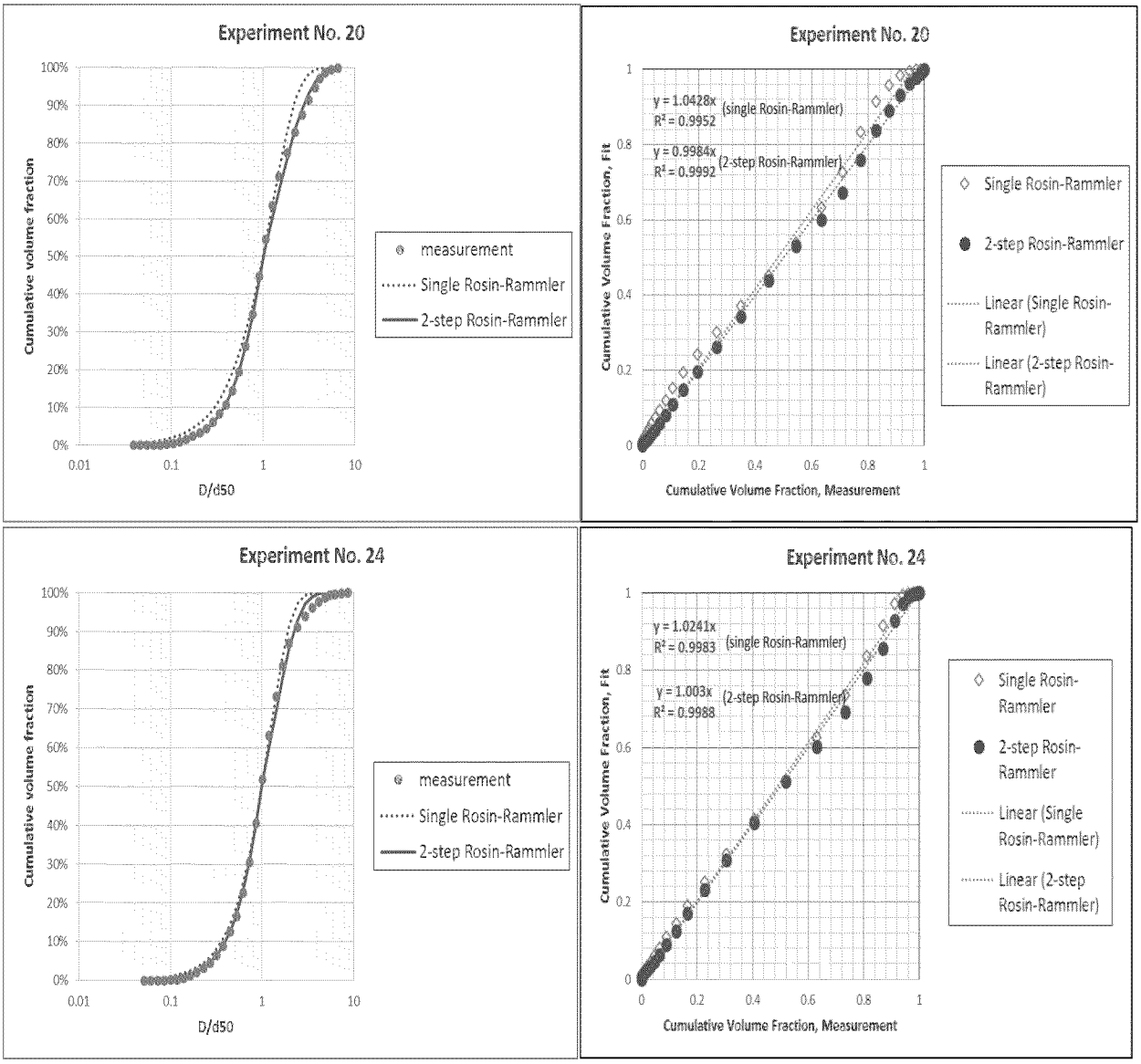

Figure 34: Cumulative distribution of d/d_{50} and regression results for IFO-120 with DOR = 1:20 in summer conditions

(*Note: the left figures are distributions and the right ones are regression results*)

ED_001324_00000687-00219

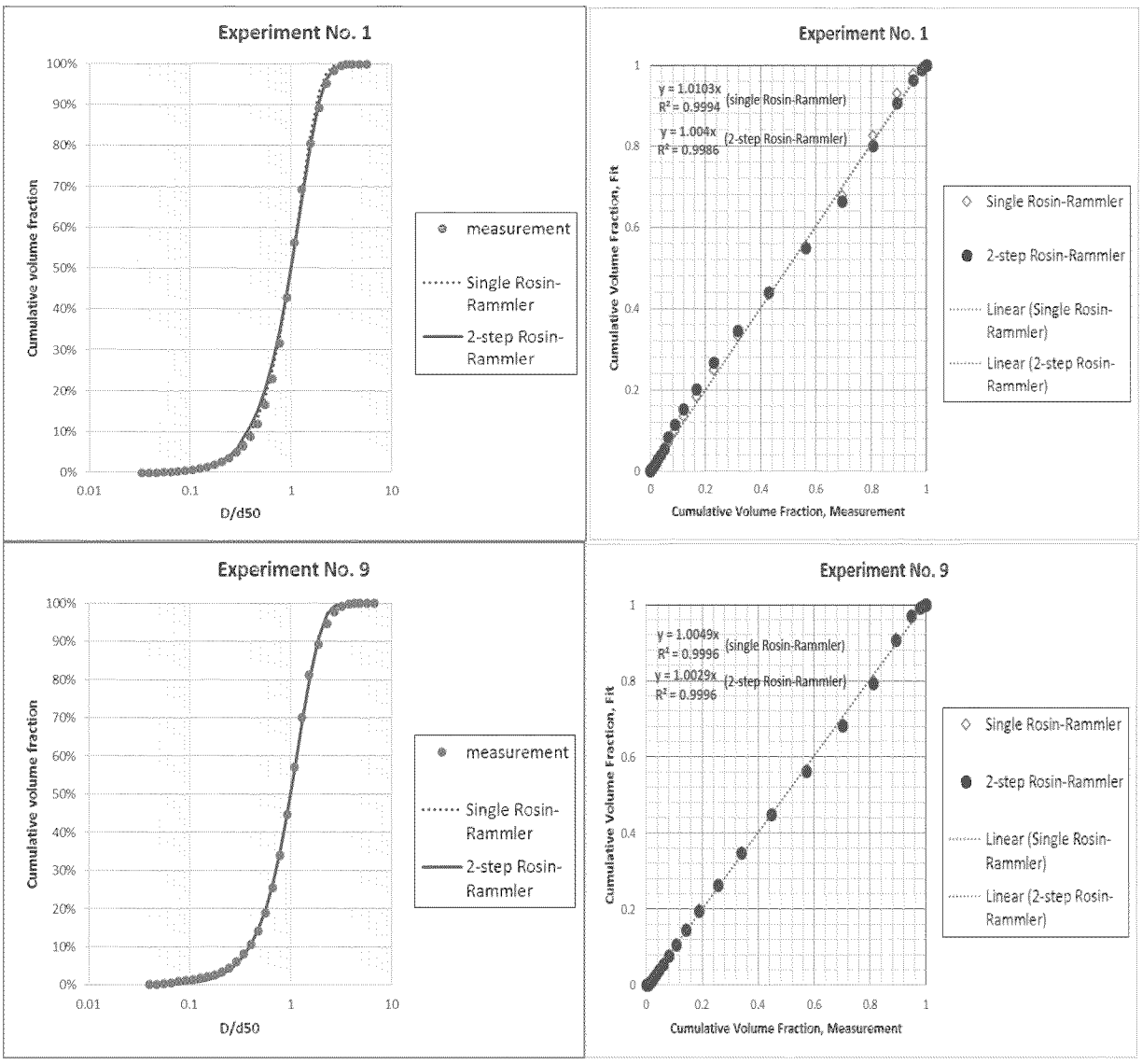

Figure 35: Cumulative distribution of d/d_{50} and regression results for ANS with DOR = 0 in spring conditions

(*Note: the left figures are distributions and the right ones are regression results*)

ED_001324_00000687-00220

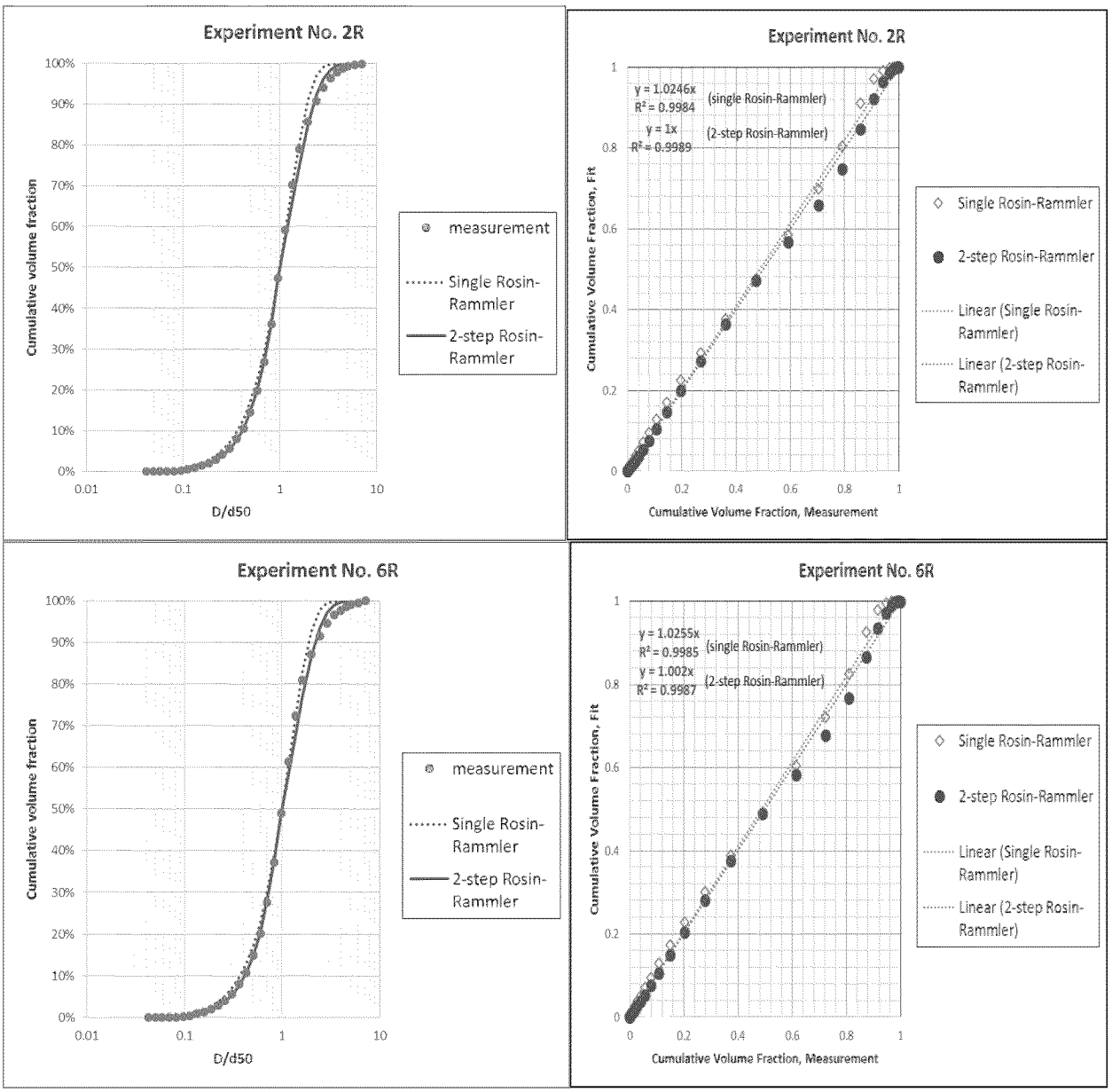

ED_001324_00000687-00221

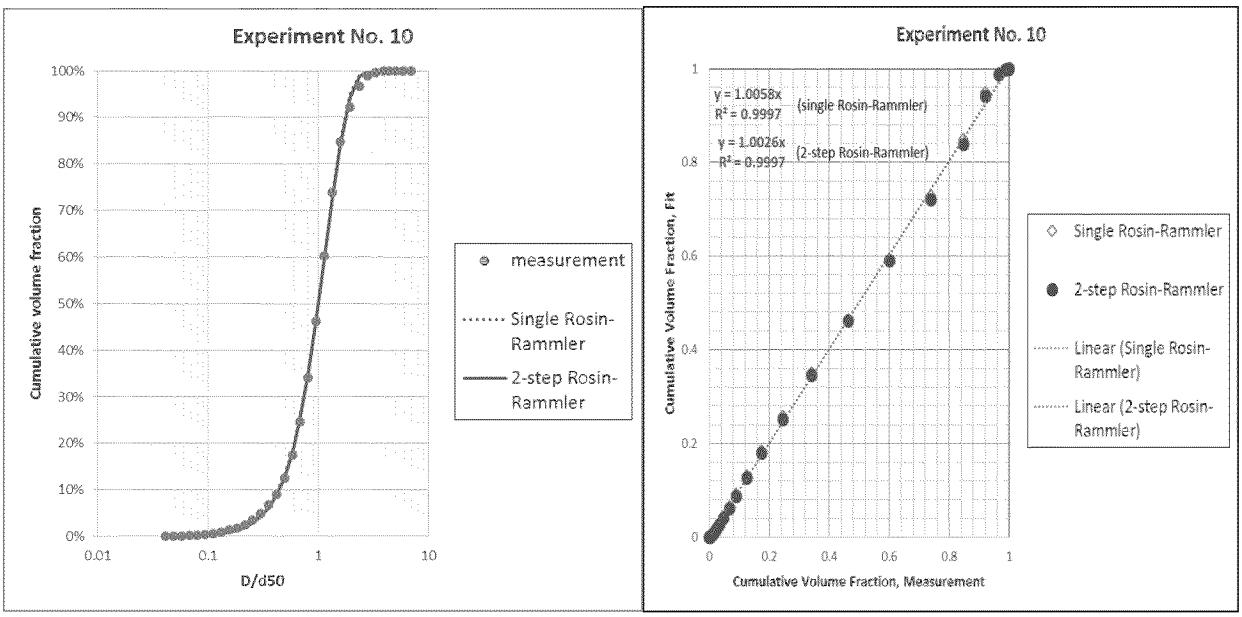

Figure 36: Cumulative distribution of d/d_{50} and regression results for ANS with DOR = 1:200 or (250) in spring conditions

(*Note: the left figures are distributions and the right ones are regression results, Experiment No. 10 is DOR=1:250*)

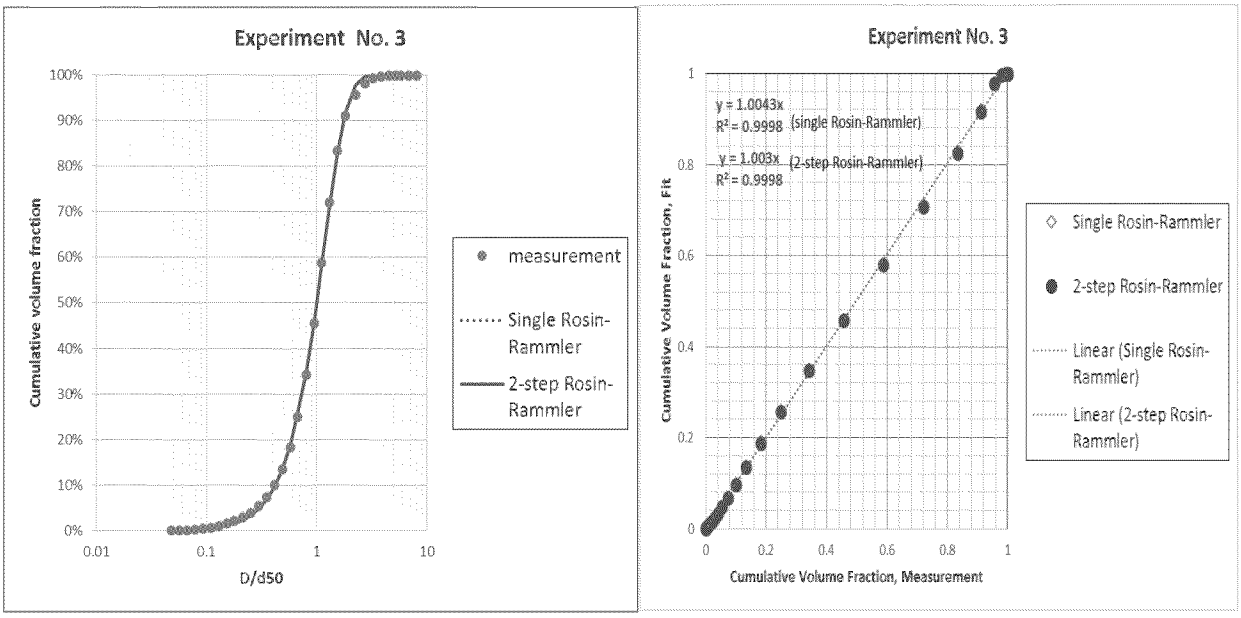

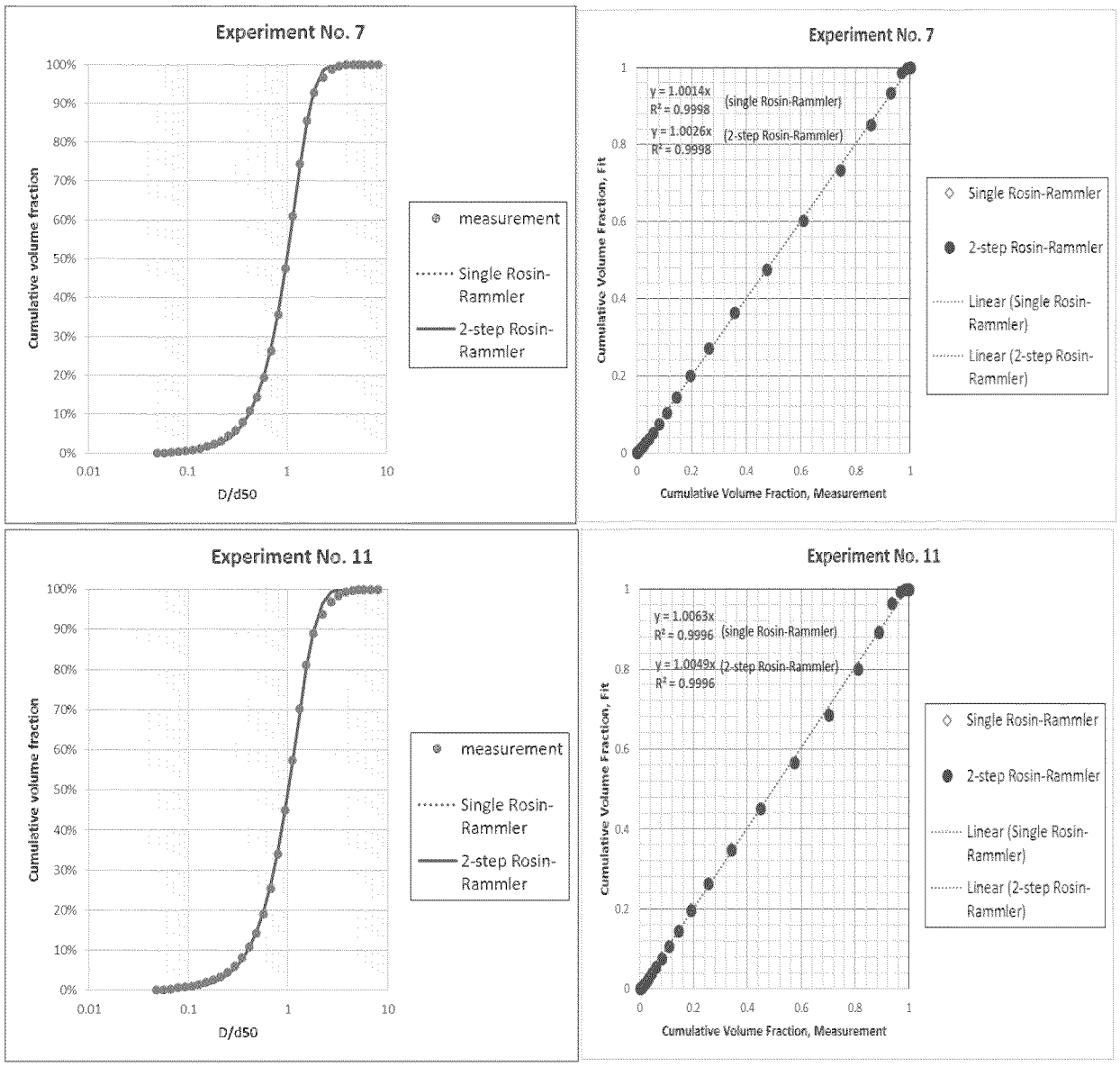

Figure 37: Cumulative distribution of d/d_{50} and regression results for ANS with DOR = 1:100 in spring conditions

(*Note: the left figures are distributions and the right ones are regression results*)

ED_001324_00000687-00223

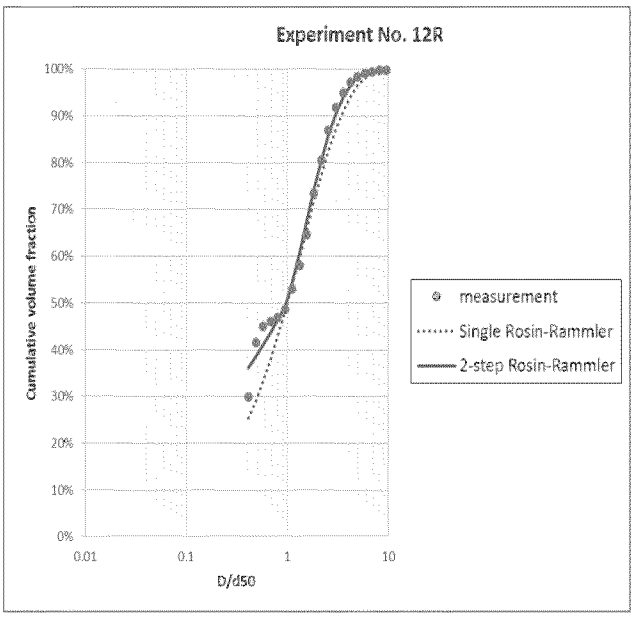

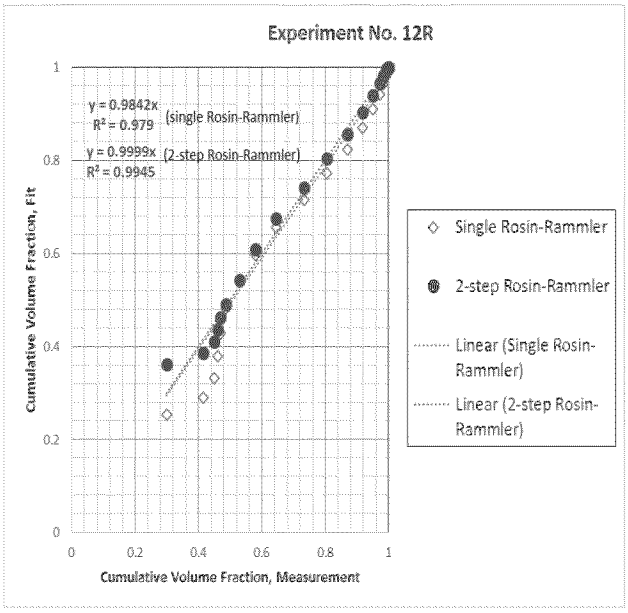

Figure 38: Cumulative distribution of d/d50 and regression results for ANS with DOR = 1:20 in spring conditions

(*Note: the left figures are distributions and the right ones are regression results*)

ED_001324_00000687-00224

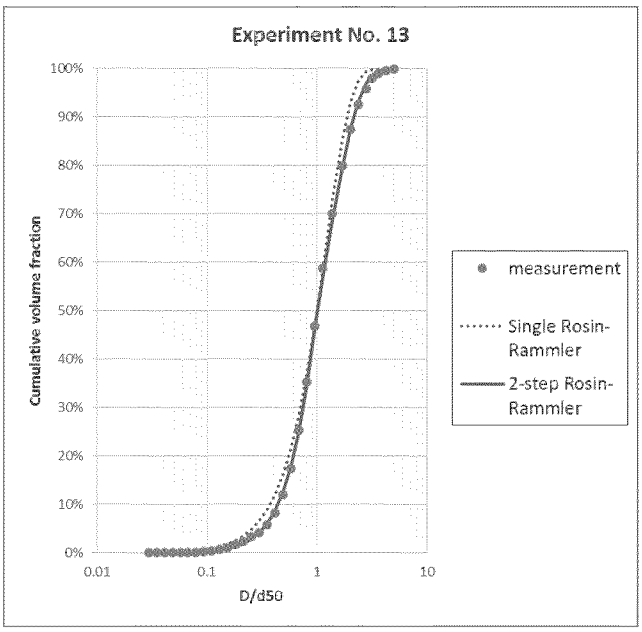

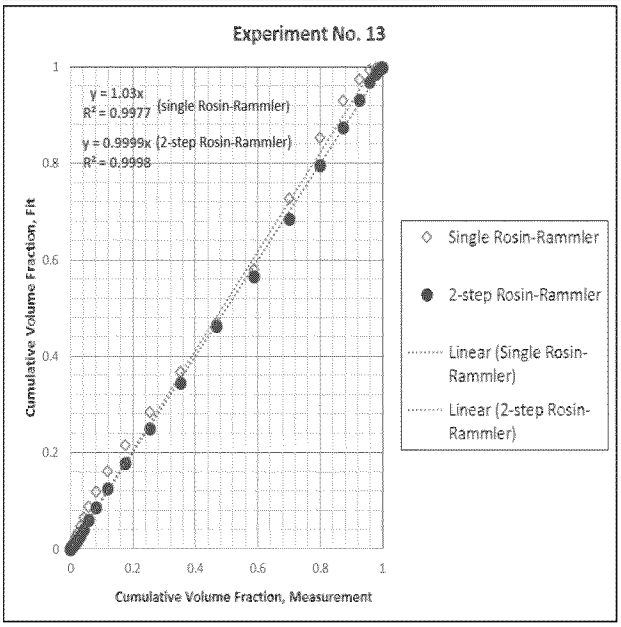

ED_001324_00000687-00225

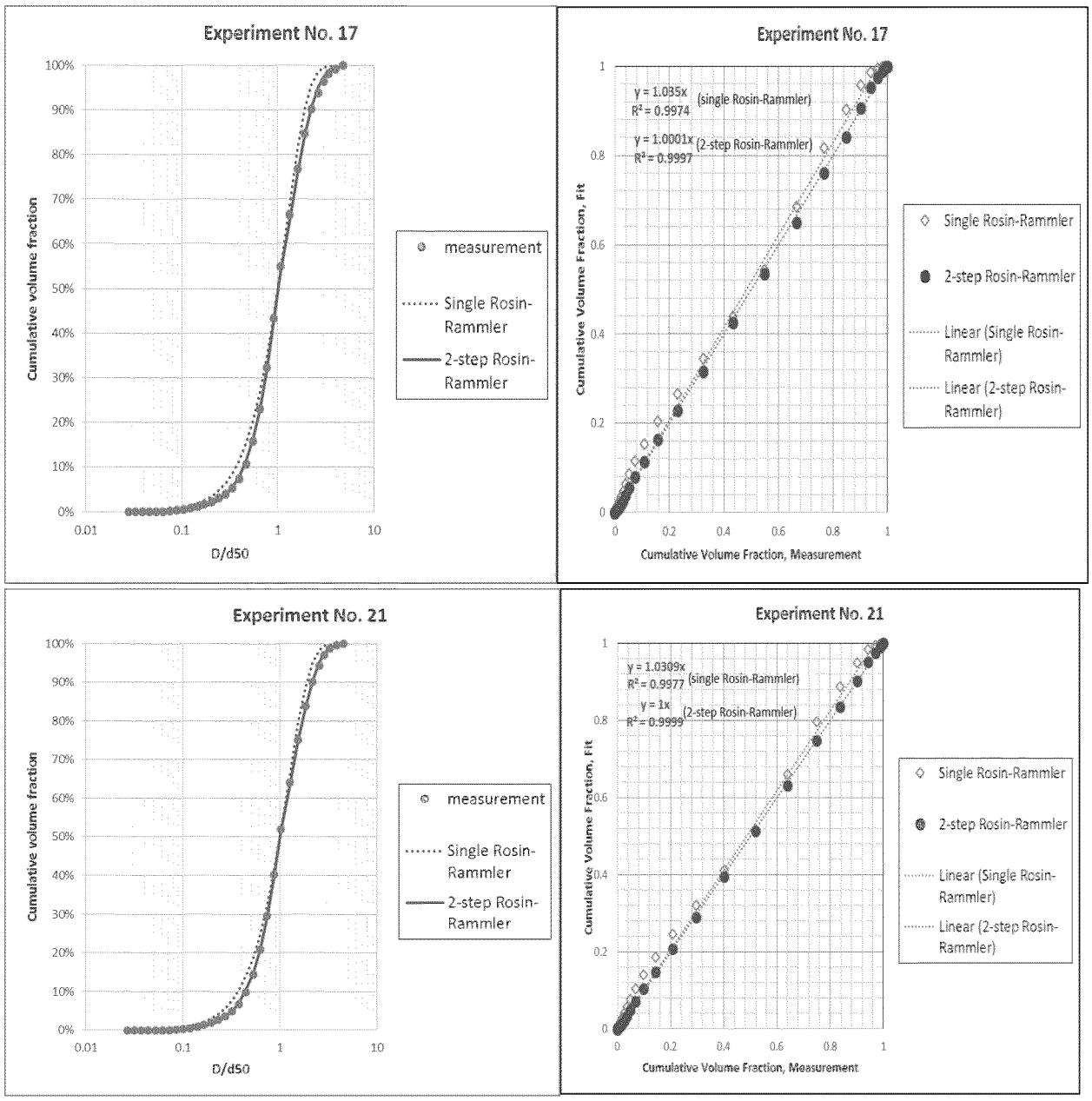

Figure 39: Cumulative distribution of d/d_{50} and regression results for ANS with DOR = 0 in summer conditions

(*Note: the left figures are distributions and the right ones are regression results*)

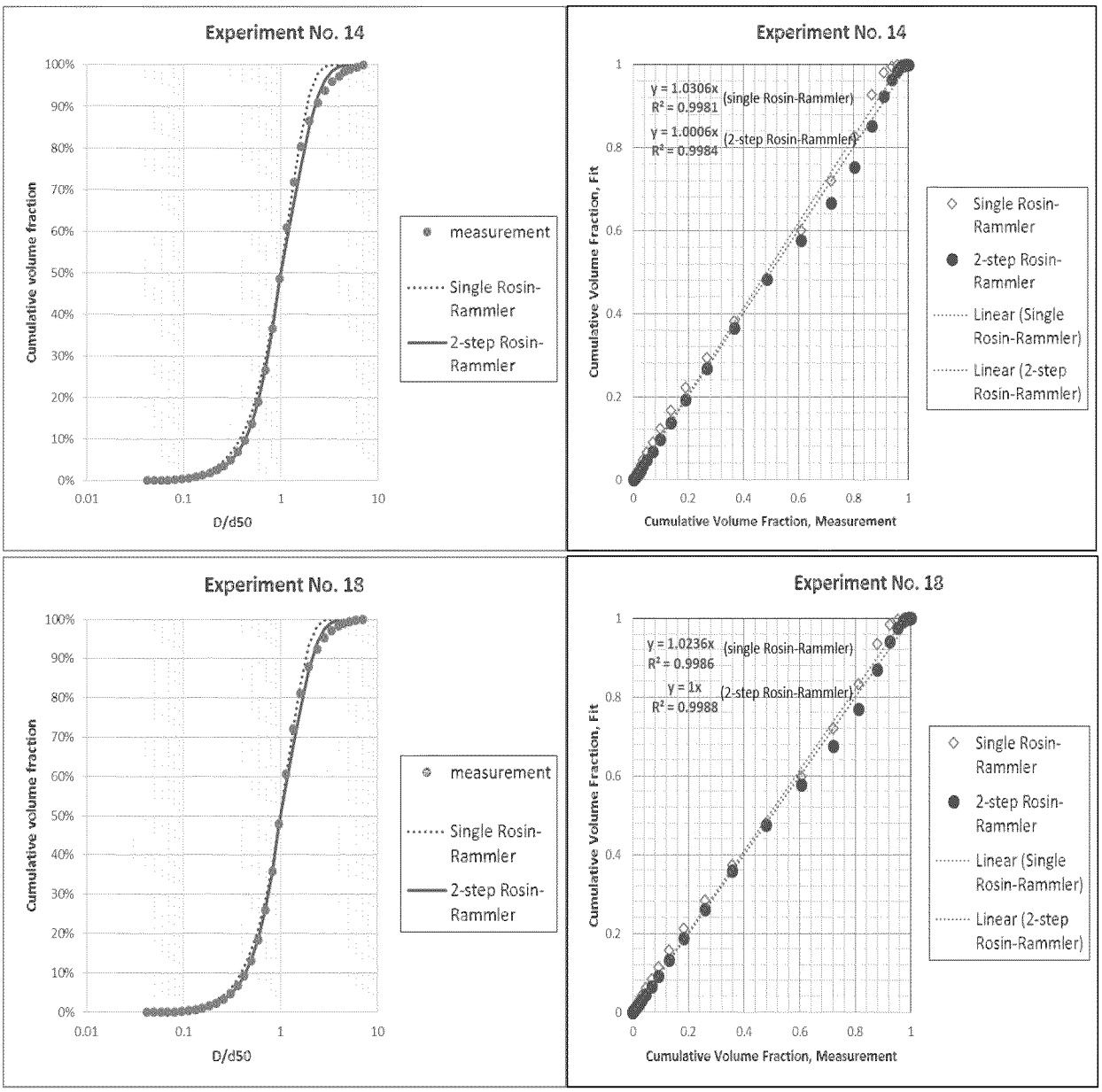
Experiment No. 14
Cumulative volume fraction
D/d50
measurement
Single Rosin-Rammler
2-step Rosin-Rammler
Experiment No. 14
y = 1.0306x (single Rosin-Rammler)
R² = 0.9981
y = 1.0006x (2-step Rosin-Rammler)
R² = 0.9984
Cumulative Volume Fraction, Fit
Cumulative Volume Fraction, Measurement
Single Rosin-Rammler
2-step Rosin-Rammler
Linear (Single Rosin-Rammler)
Linear (2-step Rosin-Rammler)
Experiment No. 18
Cumulative volume fraction
D/d50
measurement
Single Rosin-Rammler
2-step Rosin-Rammler
Experiment No. 18
y = 1.0236x (single Rosin-Rammler)
R² = 0.9986
y = 1x (2-step Rosin-Rammler)
R² = 0.9988
Cumulative Volume Fraction, Fit
Cumulative Volume Fraction, Measurement
Single Rosin-Rammler
2-step Rosin-Rammler
Linear (Single Rosin-Rammler)
Linear (2-step Rosin-Rammler)

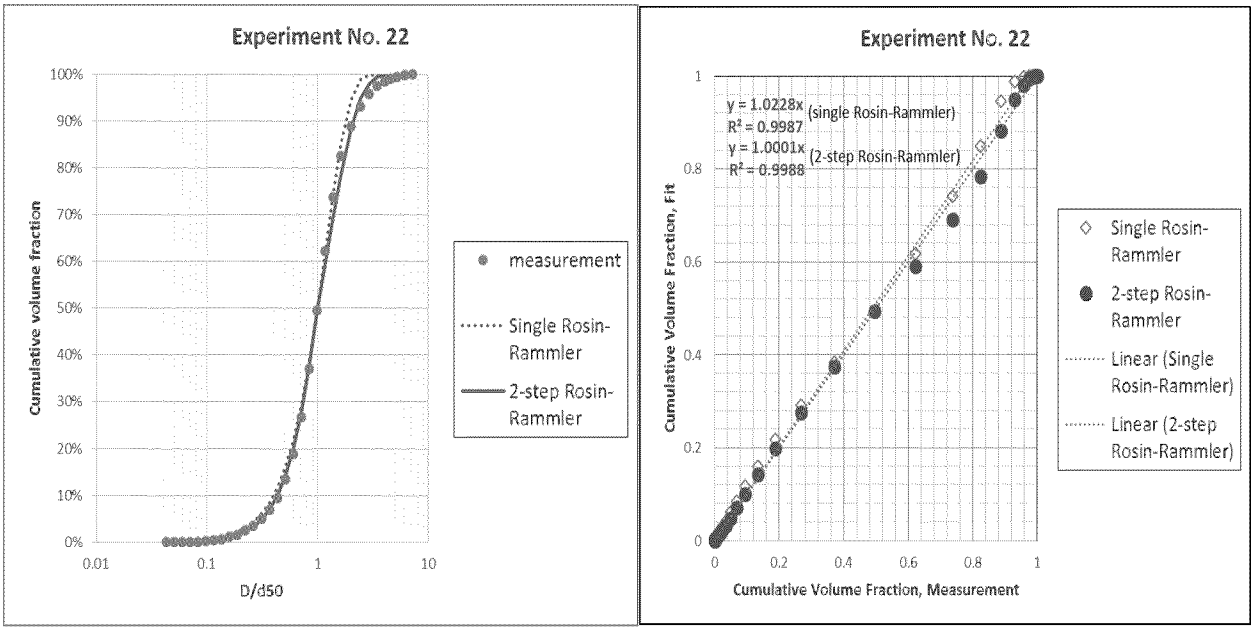

Figure 40: Cumulative distribution of d/d_{50} and regression results for ANS with DOR = 1:200 in summer conditions

(*Note: the left figures are distributions and the right ones are regression results*)

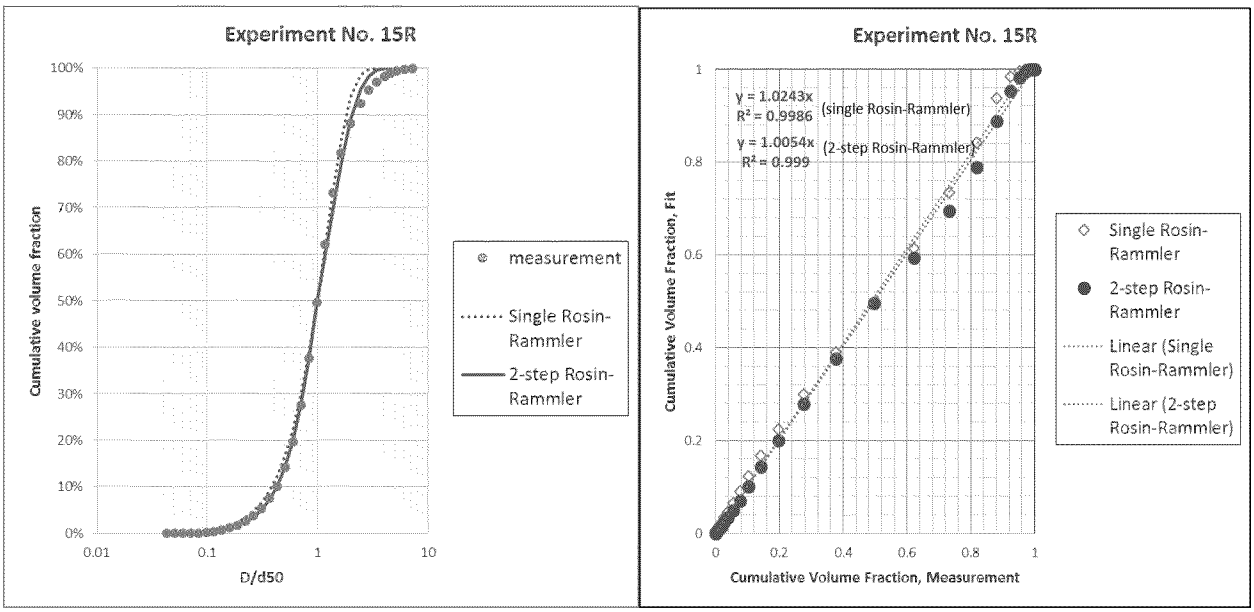

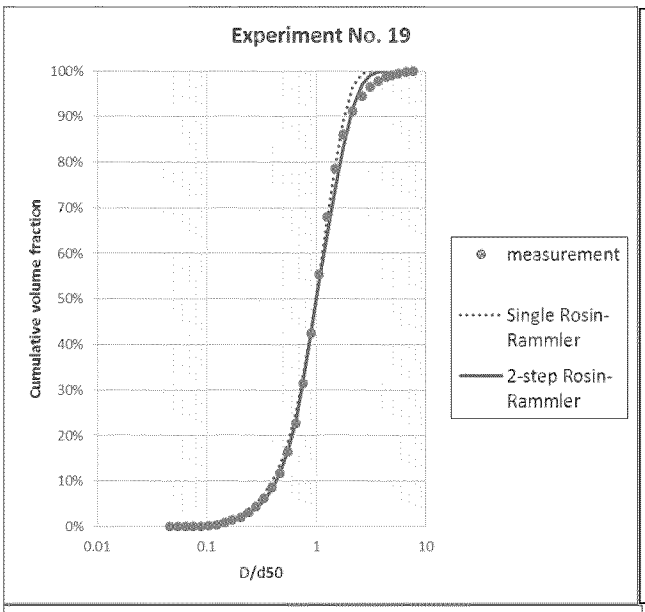

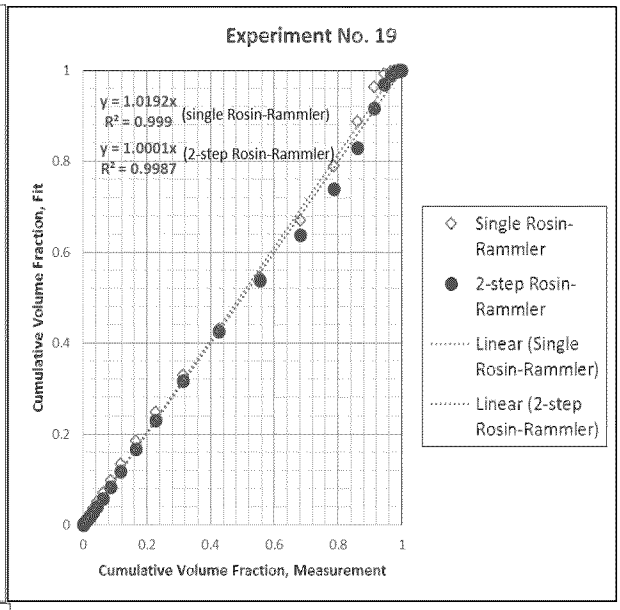

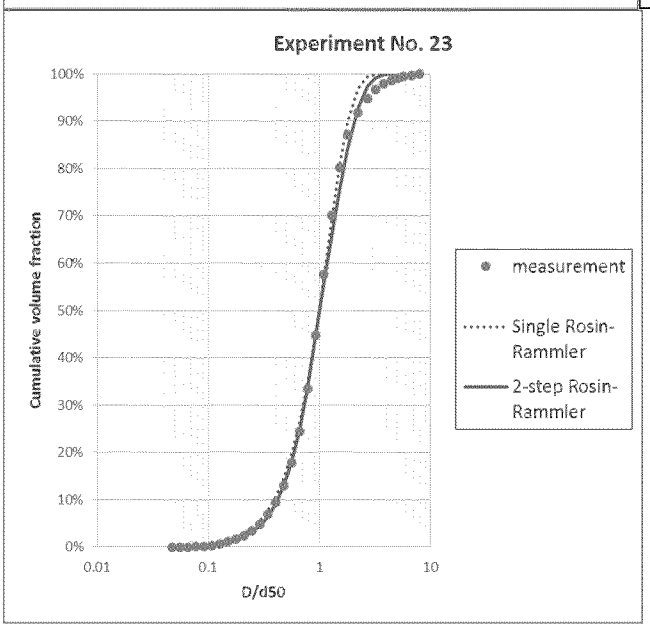

ED_001324_00000687-00229

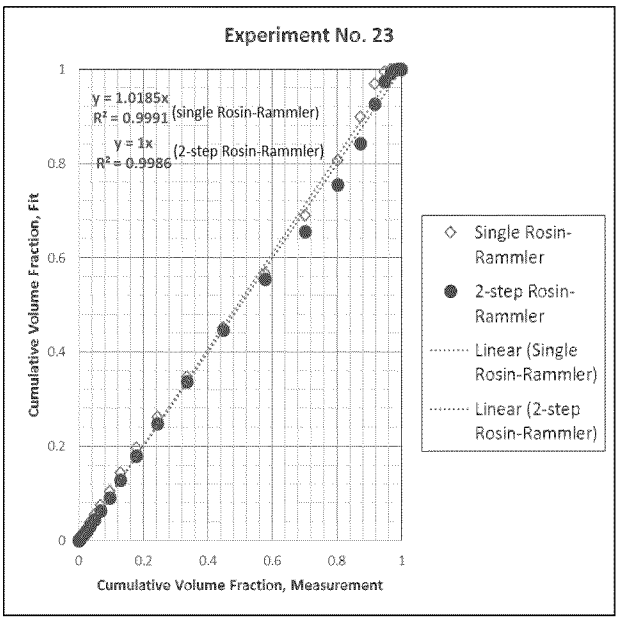

Figure 41: Cumulative distribution of d/d_{50} and regression results for ANS with DOR =1:100 in summer conditions

(*Note: the left figures are distributions and the right ones are regression results*)

ED_001324_00000687-00230

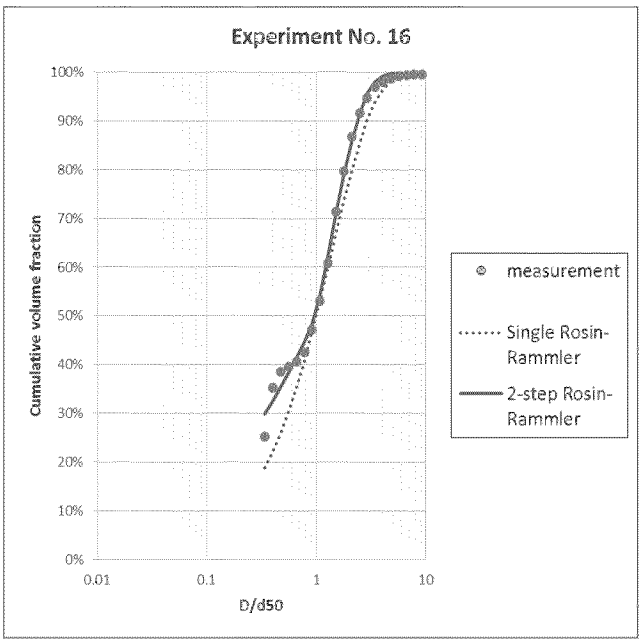

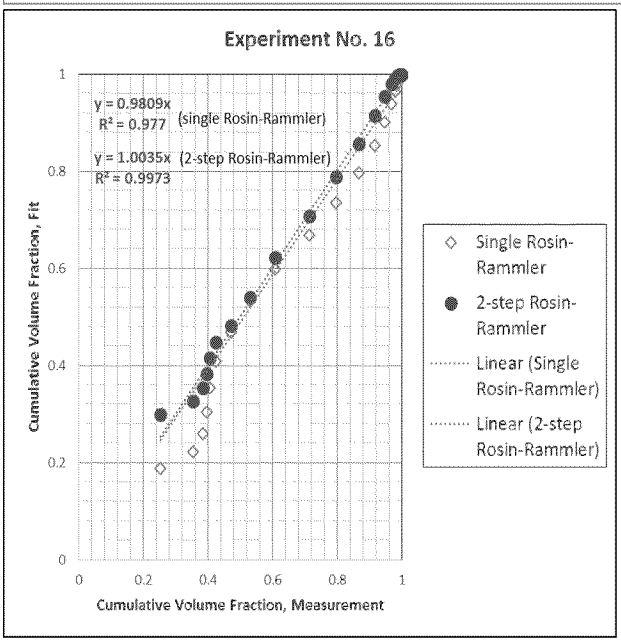

ED_001324_00000687-00231

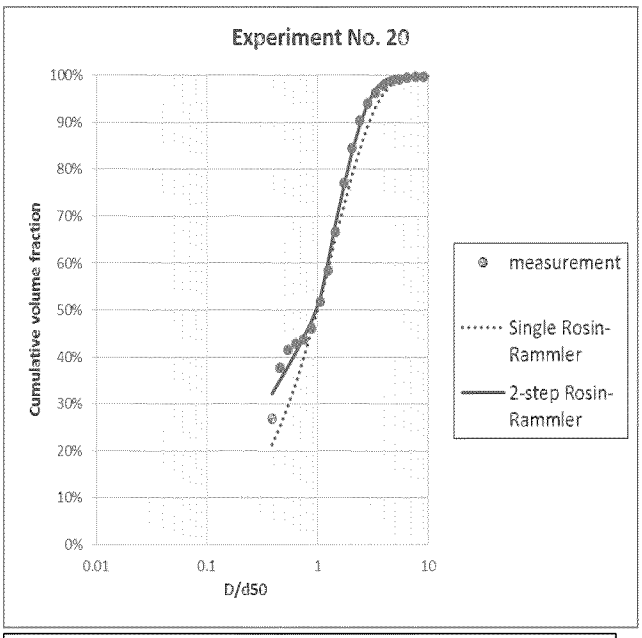

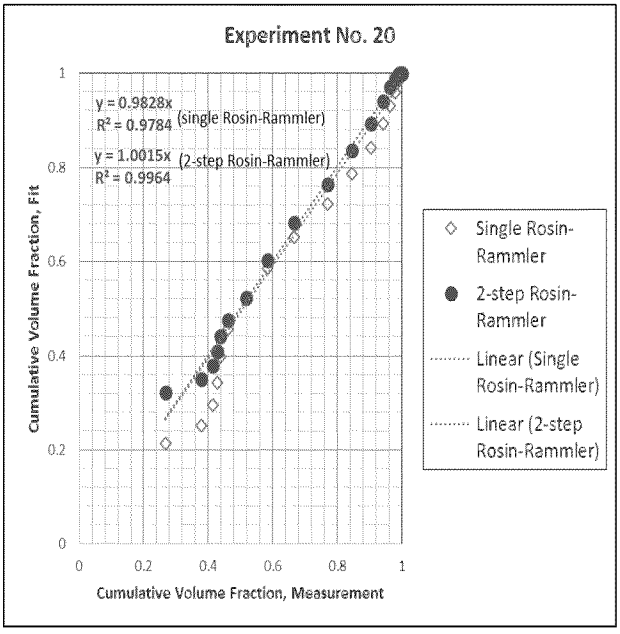

ED_001324_00000687-00232

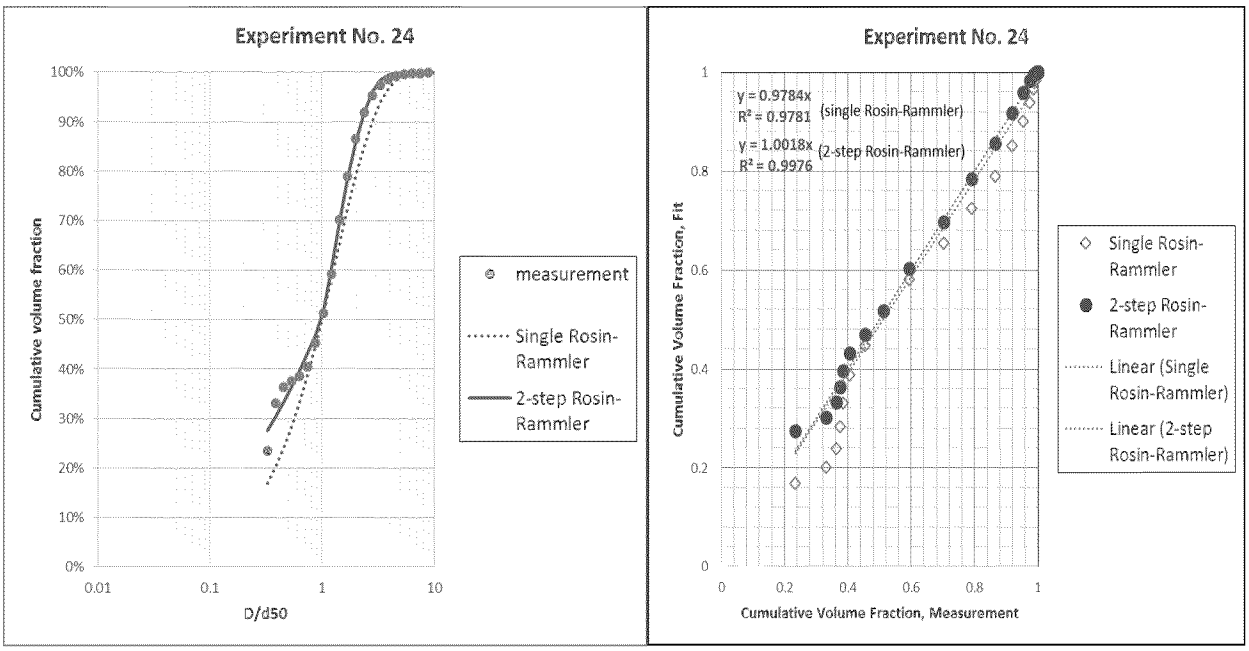

Figure 42: Cumulative distribution of d/d50 and regression results for ANS with DOR = 1:20 in summer conditions

(*Note: the left figures are distributions and the right ones are regression results*)

4 Summary

In this study, research has been conducted for the droplet size distributions of two types of oils (IFO - 120 and ANS) release from subsurface injection with/without application of chemical dispersant in different seasonal conditions (i.e., spring and summer). Firstly, a series of experiments have been conducted via wave tank experiment by COOGER in BIO to measure the droplet sizes. These data were analyzed and utilized to determine the relative volume median diameter (d_{50}) and the peak diameter (d_p). Accordingly to the droplet size distribution and the modified Weber number approach, the Weber number (*We*), as well as the additional measurements on oil viscosity and IFT, the Viscosity number (*Vi*) and Reynold number (*Re*) were calculated. In addition, the relation between the droplet size distributions and dispersant-oil-ratios (DORs) has also been analyzed. Finally, the corresponding empirical coefficients have been determined for the droplet size prediction.

Furthermore, the data analysis has also indicated that the distributions of the data with $d/d_{50} <= 1$ and $d/d_{50} > 1$ are significantly varied. Thus, it would be difficult and/or inaccurate to predict the measured IFO-120 and ANS data by only a single distribution. Therefore, a two-step Rosin-Rammler approach was introduced by advancing from the Rosin-Rammler approach proved by Johansen et al. (2013). The proposed approach uses two separate spreading coefficients: α_1 for $d/d_{50} <= 1$ and α_2 for $d/d_{50} > 1$, providing better fit of the data in all cases. The regression coefficients for the two-step Rosin-Rammler are higher than which

for the original single one in most of the case, indicating the advantage of the proposed two-step Rosin-Rammler approach.

In general, the chemical dispersant plays an importance role in reduce the droplet size of ANS no matter in spring or summer conditions. The effectiveness of dispersant in reducing droplet size is higher on ANS than which on IFO-120. There may be thresholds for the dose of chemical dispersant to some oils (e.g., IFO-120) but will need further experiments to analyze. There may also be over dose of dispersant to some oils (e.g., ANS) when the DOR is high, eventually affecting the droplet size distribution. Future experiment will also need for this particular issue.

The measured IFT for the IFO-120 and ANS with different DORs appeared significant difference compared with the ones measured from SINTEF for the modified Weber number approach. This may due to the characteristics of different oil. Further experiments will be needed to address this issue.

Acknowledgement

This study was supported by the Centre for Offshore Oil, gas, and Energy Research, Fisheries and Oceans Canada, Bedford Institute of Oceanography and US Environmental Protection Agency (US EPA).

References

Buist, I.A., W. M. Pistruzak, and D.F. Dickins, "DOME Petroleum's Oil and Gas Undersea Ice Study", in Proceedings of the Fourth Arctic Marine Oilspill Program Technical Seminar, Ottawa, ON, 1:647-686, 1981,

Brandvik, P. J., et al. (2013). "Droplet breakup in subsurface oil releases - Part 1: Experimental study of droplet breakup and effectiveness of dispersant injection." Marine Pollution Bulletin 73(1): 319-326.

Chen, F. H. and P. D. Yapa (2007). "Estimating the oil droplet size distributions in deepwater oil spills." Journal of Hydraulic Engineering-Asce 133(2): 197-207.

Chen, F. H. and P. D. Yapa (2003). "A model for simulating deepwater oil and gas blowouts - Part II: Comparison of numerical simulations with "deepspill" field experiments." Journal of Hydraulic Research 41(4): 353-365.

The Federal Interagency Solutions Group, Oil Budget Calculator Science and Engineering Team (2010). Oil Budget Calculator: Deepwater Horizon: 217.

Johansen, O., et al. (2003). "DeepSpill- Field study of a simulated oil and gas blowout in deep water." Spill Science & Technology Bulletin 8(5-6): 433-443.

Johansen, O., et al. (2013). "Droplet breakup in subsea oil releases - Part 2: Predictions of droplet size distributions with and without injection of chemical dispersants." Marine Pollution Bulletin 73(1): 327-335.

ED_001324_00000687-00234

Louis J. Thibodeaux, et al. (2011). "Marine Oil Fate: Knowledge Gaps, Basic Research, and Development Needs; A Perspective Based on the Deepwater Horizon Spill." Environmental Engineering Science 28(2): 87-93.

Lefebvre, A. H. (1989). Atomization and Sprays, Taylor & Francis, P. 421

Stephen M. Masutani and E. E. Adams (2001). Experimental Study of Multi-Phase Plumes with Application to Deep Ocean Oil Spills. Deep Spill JIP, University of Hawaii (UH) and Massachusetts Institute of Technology (MIT). 147.

Topham, D.R., Hydrodynamics of an Oilwell Blowout, Beaufort Sea Technical Report #33,Department of the Environment, Victoria, BC, 52p., 1975

Wang, C. Y. and R. V. Calabrese (1986). "Drop Breakup in Turbulent Stirred-Tank Contactors .2. Relative Influence of Viscosity and Interfacial Tension." Aiche Journal **32**(4): 667-676.

Zhao, L., et al. (2014). "Evolution of droplets in subsea oil and gas blowouts: Development and validation of the numerical model VDROP-J." Marine Pollution Bulletin 83(1): 58-69.

ED_001324_00000687-00235

Supplemental Material A. Fluorescence Analyses of 25 Oil Types at 4 Dispersant to Oil Ratios (listed in alphabetical order within oil type: Light, Intermediate, Heavy)
FWHM data in gray are estimates only as intensity did not return to half maximum before rising toward next adjacent peak.

Sample Name	API Gravity	Sulfur Content (weight %)	Point of Origin	DOR	overall maximum peak F_{Ex}^{1} (nm)	F_{Em}^{1} (nm)	F_{max}^{1} (RU)	F_{FWHM}^{1} (±4.5 nm)	Inner Filter Effect (IFE)	2nd intensity peak, lower ex/em* F_{Ex}^{2} (nm)	F_{Em}^{2} (nm)	F_{max}^{2} (RU)	F_{FWHM}^{2} (±4.5 nm)	minor peak, similar ex/higher em* F_{Ex}^{3} (nm)	F_{Em}^{3} (nm)	F_{max}^{3} (RU)	F_{FWHM}^{3} (±4.5 nm)	minor peak, higher ex/similar em* F_{Ex}^{4} (nm)	F_{Em}^{4} (nm)	F_{max}^{4} (RU)	F_{FWHM}^{4} (±4.5 nm)	$F_{281/340}$ (RU)	$F_{281/446}$ (RU)	FIR	$F_{chelsea\text{-}R}$ 239/358 (RU)	$F_{chelsea\text{-}C}$ 239/441 (RU)	F_{TriOS} 254/358 (RU)	$F_{Cyclops\text{-}R}$ 254/349 (RU)	$F_{Cyclops\text{-}C}$ 320/511 (RU)	F_{ECO} 371/460 (RU)
Arabian Light	Light (32.2°)	1.85	Saudi Arabia	0	224	335	400.4168	36.4960	1.1798	218	290	151.5028	31.7020	275	469	4.7933	248.7110	278	335	36.8206	41.0730	34.1437	4.6837	7.2898	28.8119	4.9367	16.8258	20.8790	3.5586	2.1712
				1:200	224	335	357.6249	36.4960	1.0714	218	285	148.2625	31.7020	284	478	2.6419	272.3370	275	335	33.5329	41.0730	30.9667	2.6676	11.6086	26.0505	3.8100	15.6252	19.1433	2.2830	1.3757
				1:100	224	335	426.8238	36.4960	1.2633	218	285	147.4888	31.7020	254	473	15.6626	233.8760	278	335	39.8975	41.0730	38.1081	14.1205	2.6988	36.0842	13.5018	22.3495	24.4236	12.2223	7.2024
				1:20	224	335	701.7454	41.0730	4.1859	218	290	224.3619	36.2160	236	441	236.8910	255.2810	278	335	82.6645	31.9220	78.7067	203.6622	0.3865	113.5339	231.9759	93.1478	73.9108	124.4251	53.3816
Brent	Light (38.2°)	0.40	East Shetland Basin, North Sea, UK (water depth 140 m)	0	224	335	646.1843	36.4960	1.1518	218	303	75.9188	31.7020	254	441	10.1605	144.8600	275	326	63.5367	45.6200	56.1012	7.3951	7.5863	40.2460	8.9941	31.0871	37.3653	5.6402	3.3604
				1:200	224	335	660.3712	36.4960	1.1618	221	290	63.9468	18.0940	248	432	11.6829	154.1170	275	326	65.5055	45.6200	58.2578	8.7661	6.6458	42.9915	9.3088	32.0393	38.7053	5.6408	3.7691
				1:100	221	335	708.1563	36.4960	1.3653	221	299	78.6673	27.1630	251	441	37.7209	205.3940	275	326	71.9189	50.2000	64.9403	32.8876	1.9746	58.0009	34.0570	44.3147	46.2510	22.0010	12.7049
				1:20	224	335	1098.4158	41.0730	3.0468	221	303	144.6971	22.6620	233	432	261.3387	200.2230	278	335	133.8242	36.4690	127.8678	189.0144	0.6765	173.4207	231.1604	146.2237	116.6535	85.0858	37.0050
Federated	Light (39.4°)	0.32	NW Alberta, Canada	0	224	335	574.3489	41.0730	1.1437	218	285	91.7448	27.1630	251	441	15.6750	144.7810	272	326	54.4863	50.2000	51.3190	13.8540	3.7043	68.2091	15.0958	46.4210	48.6704	9.2681	6.2912
				1:200	224	335	607.9723	41.0730	1.2130	218	290	112.8743	27.1630	248	441	30.9314	158.6540	272	326	57.8010	59.3710	55.3673	27.5293	2.0112	79.0319	29.2400	55.2828	54.6837	18.4455	12.0042
				1:100	224	335	645.2807	41.0730	1.3698	218	290	91.7746	27.1630	254	441	72.6915	181.3628	278	335	65.0589	50.2370	62.4421	66.5376	0.9384	99.7517	70.1628	71.2351	65.5325	39.0617	21.4244
				1:20	224	335	1223.1724	50.2370	4.3653	218	303	213.5284	27.1840	233	436	661.2244	226.9050	275	340	165.3826	27.3510	163.8397	460.6894	0.3556	371.8531	614.1385	289.5725	207.3393	168.2464	67.0266
Gullfaks	Light (32.7°)	0.31	North Sea, Norway (water depth 230 m)	0	221	335	937.0018	36.4960	1.2434	218	290	97.9804	22.6270	257	441	15.8195	219.6830	275	326	90.0457	41.0430	77.5575	13.4001	5.7878	44.3429	12.4754	37.0081	45.7345	10.1643	6.3561
				1:200	221	335	934.4237	36.4960	1.2715	218	290	96.3758	18.0940	251	436	18.0573	224.5310	275	326	91.9918	41.0430	80.0347	14.3665	5.5709	43.6717	14.9723	37.1213	46.3369	10.3233	8.3937
				1:100	221	335	933.0803	36.4960	1.3451	218	294	96.5534	27.1410	257	436	28.6241	219.5650	275	326	93.8404	45.6200	80.6821	24.8691	3.2443	46.8422	25.7671	39.3444	47.9996	18.4141	9.9173
				1:20	221	335	1524.2070	41.0730	3.7319	215	281	179.2527	9.0400	233	441	352.3552	200.4510	275	335	193.9621	31.9220	179.7879	253.8018	0.7084	212.7369	324.5520	187.2627	146.4968	122.7369	50.1927
Hibernia	Light (35.6°)	0.41	Newfoundland, Canada (water depth 80 m)	0	221	335	938.0775	36.4960	1.2390	218	285	173.3257	36.2160	290	492	11.2138	224.2920	275	326	87.9497	41.0430	74.9422	10.8507	6.9067	42.8229	10.5048	33.8845	44.5846	8.2628	4.5030
				1:200	221	335	951.4881	36.4960	1.3366	218	290	168.1463	36.2160	260	483	27.3287	224.2920	275	326	93.5200	45.6200	81.0861	25.1700	3.2215	48.8423	23.7015	41.7274	51.5979	22.5015	11.8736
				1:100	221	335	978.6157	36.4960	1.4740	215	281	170.8232	22.6080	254	478	55.8991	210.1160	275	326	96.1672	45.6200	85.2278	50.5145	1.6872	55.1197	50.2643	47.7291	56.0714	40.6007	19.1972
				1:20	221	335	1812.4055	41.0730	4.0175	218	290	305.6178	22.6450	225	422	567.3160	186.1020	275	335	201.2828	41.0430	182.7473	374.9851	0.4873	236.6556	480.2082	199.5141	152.8903	192.4787	68.6181
MC252 (Discoverer Enterprise)	Light (37.2°)	<0.1	Louisiana, US (water depth up to 1500 m)	0	221	335	998.4975	36.4960	1.2686	218	290	181.4689	31.6770	257	474	17.8789	224.2920	272	326	94.8271	41.0430	76.9368	15.3431	5.0144	46.3171	15.2539	40.7658	50.3429	15.0873	8.3661
				1:200	221	331	1009.1816	36.4960	1.3728	215	290	196.1398	31.7020	260	473	31.0582	214.8390	275	326	99.4748	50.1630	82.3071	26.9270	3.0567	53.4529	28.4331	45.5031	53.5737	25.1354	12.7483
				1:100	221	335	1085.5377	36.4960	1.4799	218	285	189.5899	22.6080	254	473	81.0433	228.5220	272	326	106.1992	45.6200	88.2869	72.3715	1.2199	64.3268	72.8640	55.0190	63.5313	59.5572	27.6216
				1:20	221	331	1998.5995	36.4960	4.7580	221	308	437.3233	31.7270	230	487	744.6895	200.4510	275	335	231.8561	50.2000	203.9413	527.5106	0.3866	229.0701	670.7186	200.3698	175.3657	268.1784	89.7799
MC252 (generic)	Light (35.2°)	0.21	Louisiana, US (water depth up to 1500 m)	0	221	335	857.3517	36.4960	1.2351	215	285	159.8695	22.6270	251	441	16.8587	167.7920	269	326	80.8431	45.5860	65.0029	14.7138	4.4178	36.3515	15.9277	33.1775	41.2382	10.0270	5.3895
				1:200	221	335	877.7767	41.0730	1.2462	215	303	108.8697	9.0750	254	450	26.8996	173.0670	272	326	83.4356	45.6200	68.4320	19.2422	3.5563	42.3193	21.1766	34.9381	46.2312	16.2865	9.5183
				1:100	221	335	964.0212	41.0730	1.5711	215	290	92.4174	22.5900	260	446	92.3028	218.8310	275	331	93.3841	54.7840	79.1424	83.1330	0.9520	62.4186	89.9889	56.6115	58.4282	52.7589	25.1734
				1:20	221	331	1795.1270	41.0730	4.7317	218	303	376.3732	22.6800	233	441	704.3134	204.5770	272	335	212.5289	31.8980	193.3704	483.6686	0.3998	260.6423	622.6480	217.6143	178.0065	199.9642	75.7345
Scotian Shelf Condensate	Light (51.4°)	0.02	Nova Scotia, Canada (water depth 12-20 m)	0	224	335	946.5222	41.0730	1.1527	218	303	88.8169	22.6620	--	--	--	--	275	331	95.6155	45.6200	81.6878	2.0109	40.6224	46.0174	3.3515	33.2896	45.6231	0.1522	0.0520
				1:200	221	335	1408.5872	36.4960	1.4413	218	285	595.5652	36.2160	--	--	--	--	275	331	141.1720	45.6200	118.0016	2.1982	53.6817	59.7045	3.9548	48.4607	66.0981	0.0828	0.0616
				1:100	221	335	1487.1614	41.0730	1.5326	218	285	588.8325	36.2160	--	--	--	--	275	331	151.9375	45.6200	125.7985	2.1669	58.0552	70.0388	5.2573	51.3959	74.0406	0.0638	0.1147
				1:20	221	335	1337.9812	41.0730	1.5025	218	285	565.7260	36.2160	--	--	--	--	275	331	126.3912	45.6200	104.9922	2.2033	47.6513	52.5865	5.2818	42.6106	59.2394	0.1270	0.1184
Terra Nova	Light (33.8°)	0.43	Newfoundland, Canada (water depth 90-100 m)	0	221	335	665.4964	36.4960	1.1604	218	290	124.9477	36.2160	272	511	9.1321	252.8260	275	326	62.5324	41.0430	54.4188	7.8571	6.9261	30.6780	6.8939	24.2375	30.8974	7.5572	4.6789
				1:200	221	335	719.7159	36.4960	1.2207	218	290	118.4676	31.6770	305	506	19.5982	186.5280	278	335	68.9711	45.6200	60.1640	15.8660	3.7920	37.7650	15.5717	29.9080	36.8026	14.9163	8.2815
				1:100	221	335	821.2414	36.4960	1.3653	218	290	150.9355	36.2160	269	511	52.2634	233.2450	275	335	76.9978	45.6200	67.8490	46.1358	1.4706	48.1195	45.2714	39.0681	43.5464	41.2224	20.0007
				1:20	221	335	1380.3396	41.0730	3.7647	215	303	248.2621	18.1370	230	492	486.6393	214.3630	291	335	160.6443	31.9220	149.7883	371.4435	0.4033	186.0975	438.2137	161.0352	125.2096	216.3706	73.3119
Alaska North Slope	Intermediate (29.8°)	1.09	Prudhoe Bay, Alaska, US	0	221	335	697.0711	36.4960	1.1643	218	285	131.7351	36.2160	293	473	2.6573	281.9800	275	326	66.6243	41.0430	56.0902	2.5976	21.5932	33.3178	2.3807	26.9739	34.4954	1.7365	0.8261
				1:200	221	335	715.0080	36.4960	1.1515	218	285	134.0672	36.2160	--	--	--	--	275	326	67.4011	41.0430	56.3347	1.5911	35.4051	32.4303	2.0669	26.2117	33.9454	1.3257	0.6139
				1:100	221	335	839.5968	36.4960	1.3153	218	294	148.9155	36.2160	266	497	11.7574	197.4720	272	326	79.6627	41.0430	68.4291	10.3806	6.5920	46.8092	11.2163	37.8401	44.1656	8.2902	4.5465
				1:20	221	335	1171.6320	36.4960	3.3276	218	285	196.5901	22.6270	236	446	173.1327	214.2410	275	331	126.9662	54.7840	114.5851	130.0100	0.8814	116.4722	158.2507	96.4654	90.0891	73.0147	29.5991
Alaska North Slope (10% weathered)	Intermediate (26.8°)	1.20	Prudhoe Bay, Alaska, US	0	221	335	812.9654	36.4960	1.1927	215	290	147.4303	27.1630	284	501	3.1155	226.0670	275	326	76.0907	41.0430	64.7766	2.9855	21.6973	40.3102	2.9991	31.4807	39.4282	2.2554	1.1638
				1:200	221	335	831.6980	36.4960	1.2071	215	285	151.4220	31.7020	--	--	--	--	275	326	77.5943	41.0430	64.7794	2.9855	21.6982	40.2480	4.7037	31.4551	40.9625	2.3404	1.3912
				1:100	221	335	828.0589	36.4960	1.2843	215	285	136.5127	36.2160	263	492	9.0535	230.2950	275	326	82.1870	41.0430	67.8410	7.4701	9.0817	44.5102	9.4948	37.6410	45.0597	6.3725	3.8780
				1:20	224	335	1109.5088	36.4960	3.0146	218	285	168.7047	36.2160	233	441	159.5431	186.5280	278	335	117.9003	59.3710	106.5389	117.7190	0.9050	97.2009	141.3493	86.6070	81.7803	70.4364	29.4143
Heidrun	Intermediate (28.6°)	0.46	Norwegian Sea (water depth 350 m)	0	221	335	902.6871	36.4960	1.2818	218	299	117.2393	27.1630	257	441	21.1729	219.5650	275	326	91.3695	41.0430	75.1032	16.6835	4.5016	46.6748	17.2943	37.5950	47.5629	12.6075	7.4258
				1:200	221	335	909.4710	36.4960	1.2575	218	303	120.8474	27.1840	254	432	16.4071	191.4540	275	326	93.9774	41.0430	76.8515	12.3624	6.2166	47.9185	13.4413	36.5101	46.3281	10.0746	6.6594
				1:100	221	335	964.3148	36.4960	1.3330	218	299	111.2935	27.1630	251	441	27.0994	224.1710	275	326	99.1424	41.0430	81.5684	21.8320	3.7362	57.6495	22.3738	40.8470	51.2695	17.2084	11.1786
				1:20	224	335	1098.8957	36.4960	2.1944	218	308	164.0666	22.6800	236	441	174.9308	218.8310	275	326	116.9711	50.2000	104.4772	135.8026	0.7693	103.6075	162.7506	86.9668	80.7585	74.9609	32.4840
Lago	Intermediate (27.3°)	0.30	Maracaibo Basin, Venezuela	0	221	335	352.2231	36.4960	1.0723	218	285	48.9594	22.6270	--	--	--	--	278	335	32.0908	41.0730	29.1256	2.4010	12.1308	23.5723	2.4668	17.6000	21.1205	1.7177	1.0278
				1:200	221	335	398.3964	36.4960	1.1277	218	290	51.1749	27.1630	--	--	--	--	275	335	35.8690	41.0730	32.5430	2.7752	11.7265	29.2280	3.4148	20.7464	24.3474	1.8901	1.2651
				1:100	224	335	367.7451	41.0730	1.1202	215	290	45.9607	18.0940	--	--	--	--	275	335	33.0880	41.0730	29.6885	3.3449	8.8756	26.8896	3.7673	19.4312	22.3621	2.3043	1.3997
				1:20	221	335	453.0976	41.0730	1.7484	218	299	55.7396	31.7020	236	446	63.5925	283.0880	275	335	44.7620	50.2370	41.5534	45.3767	0.9157	53.7942	57.8881	41.9449	37.3306	27.6019	12.4597
MESA	Intermediate (30.3°)	0.87	Orinoco Basin, Venezuela	0	221	335	757.8380	36.4960	1.1875	218	290	128.7504	31.6770	--	--	--	--	275	326	72.1471	50.2000	62.9403	3.4698	18.1396	47.3344	4.6808	34.9579	41.9985	2.3492	1.2833
				1:200	221	335	806.7615	36.4960	1.2196	218	290	143.3521	31.6770	--	--	--	--	275	335	74.2263	45.6200	64.0487	5.3486	11.9748	51.1556	7.1721	37.4703	42.8810	3.4450	2.1209
				1:100	221	335	745.1679	36.4960	1.2636	218	290	127.0369	31.6770	--	--	--	--	275	326	70.6516	45.6200	61.6738	9.5702	6.4443	51.2559	11.9492	37.8598	44.1276	6.6796	3.7226
				1:20	221	335	1107.0899	41.0730	2.7673	218	299	185.4842	31.6770	233	418	142.3828	181.8170	275	335	116.5099	54.7840	106.3210	102.5629	1.0366	123.4786	126.8977	95.9839	88.7799	48.8107	20.4210
Sea Rose	Intermediate	0.53	Newfoundland,	0	221	335	1145.2869	36.4960	1.2784	218	303	152.5516	31.7020	--	--	--	--	275	326	108.7189	41.0430	88.6457	9.0486	9.7967	43.5595	11.9753	40.9107	50.2525	6.7127	3.8266

(White Rose)	(29.8°)		Canada (water depth 100 m)	1:200	221	335	1223.9796	36.4960	1.3272	218	290	202.7941	27.1630	--	--	--	--	275	326	115.3793	41.0430	93.9090	12.3688	7.5924	50.1617	14.9794	42.3903	56.7183	9.6724	5.1417
				1:100	221	335	1236.6347	36.4960	1.5486	215	294	159.5234	22.6270	260	441	50.7172	205.2810	275	326	116.7994	45.6200	98.9043	45.3497	2.1809	63.0618	47.2371	54.5822	63.8962	31.4917	15.6276
				1:20	221	335	1973.5528	36.4960	3.5550	218	303	280.6617	9.0750	233	441	359.0106	171.7950	278	335	211.3166	54.7840	186.5334	261.0755	0.7145	182.6322	322.1702	163.5870	147.7333	124.8090	49.8540
Vasconia	Intermediate (26.3°)	0.56	Colombia	0	224	335	844.9348	36.4960	1.1536	215	303	100.6205	31.7020	--	--	--	--	275	326	79.9347	41.0430	68.0535	1.9690	34.5629	45.3441	4.3971	36.3864	45.3699	1.0751	0.6805
				1:200	224	335	828.3719	36.4960	1.1583	218	303	97.9280	31.7020	--	--	--	--	272	326	80.8601	41.0430	67.4266	1.5176	44.4299	44.2001	4.0596	35.4004	46.8488	0.5749	0.4581
				1:100	224	335	835.6222	36.4960	1.1724	218	290	98.3668	22.6270	--	--	--	--	275	326	80.5851	41.0430	67.9124	1.9921	34.0901	43.5892	4.6579	37.7414	46.1524	1.1150	0.6503
				1:20	221	335	935.7946	36.4960	1.6723	215	308	139.7536	27.2050	--	--	--	--	272	326	92.7718	45.6200	80.0346	23.4436	3.4139	60.3238	33.0451	52.4788	59.7833	12.6010	5.4375
Access Western Blend Dilbit	Heavy (21.3°)	3.91	Athabaska region, Alberta, Canada	0	221	335	39.5805	41.0730	1.0197	218	285	33.2874	36.2160	215	558	2.4487	56.3880	272	326	4.9297	77.4050	4.1833	0.3668	11.4056	7.2683	0.8325	4.6137	4.4813	0.1885	0.1454
				1:200	221	335	46.5153	41.0730	1.0204	215	285	38.9976	36.2160	218	567	2.9473	51.7750	272	326	5.3889	77.4050	4.6291	0.3983	11.6208	7.7770	1.0395	4.5552	4.5711	0.0901	0.0734
				1:100	221	335	49.8423	45.6200	1.0266	218	285	45.8912	36.2160	215	571	2.9107	51.7510	272	326	5.9759	77.4050	5.1332	0.6010	8.5418	8.7321	1.3962	5.2585	5.1513	0.1711	0.1227
				1:20	224	335	60.1881	45.6530	1.0777	218	285	47.3804	40.7590	233	441	13.3766	148.9860	272	326	7.8131	109.5590	7.1753	6.3520	1.1296	15.7712	11.7630	9.8247	8.5862	2.5057	0.9710
Belridge Heavy	Heavy (13.6°)	1.03	San Joaquin Valley, California, US	0	230	344	118.6885	50.2740	1.0688	221	294	25.0773	18.1090	--	--	--	--	290	353	20.8257	68.6540	17.6309	3.5970	4.9016	67.1562	7.8788	37.7229	30.6641	1.1081	0.8613
				1:200	230	344	161.7504	50.2740	1.0812	218	294	34.0575	22.6450	--	--	--	--	290	353	27.5169	68.6540	23.7155	4.5438	5.2193	88.9294	10.7576	48.5595	39.1353	1.2513	1.1570
				1:100	227	344	140.9613	50.2740	1.0744	221	308	33.8168	31.7270	--	--	--	--	290	353	25.1983	73.2570	21.4500	4.6412	4.6216	82.0319	9.3816	45.6629	36.5600	1.2524	0.9988
				1:20	227	340	147.0897	50.2740	1.1216	221	290	31.8670	18.1090	--	--	--	--	290	353	27.1402	73.2570	22.3664	6.7721	3.3027	86.7568	13.2676	50.2330	39.1433	2.4427	1.6384
Cold Lake Dilbit	Heavy (21.5°)	3.77	NE Alberta, Canada	0	224	335	120.6093	41.0730	1.0503	218	285	55.0742	36.2450	--	--	--	--	275	326	13.9909	63.8180	12.5727	0.6645	18.9218	17.8324	2.0608	11.2944	11.8179	0.2705	0.2268
				1:200	224	331	120.6515	41.0730	1.0454	218	285	50.9834	40.7590	--	--	--	--	275	326	13.4098	63.8180	12.3240	0.7111	17.3317	17.8461	1.7589	10.9085	11.6320	0.2531	0.2152
				1:100	224	335	125.8546	41.0730	1.0587	218	285	44.4385	31.7020	--	--	--	--	275	326	14.3305	63.8180	13.2762	1.1542	11.5027	21.0296	2.6073	12.3514	12.9223	0.4954	0.2521
				1:20	224	340	133.1499	41.0730	1.1657	218	285	55.7758	40.7590	233	441	15.7453	158.4750	275	326	15.3840	72.9890	14.0151	7.2938	1.9215	23.0364	13.6412	15.1511	14.9083	3.6527	1.4960
Hondo	Heavy (19.5°)	4.41	Santa Barbara Channel, California, US (water depth 260	0	221	331	283.0362	41.0730	1.0889	215	290	55.1274	31.7020	--	--	--	--	278	335	27.6105	54.7840	27.0154	1.4698	18.3809	43.2085	5.8964	26.0841	26.9209	0.4113	0.2916
				1:200	221	335	312.2745	41.0730	1.0758	218	290	62.6687	36.2160	--	--	--	--	275	335	30.6188	54.7840	29.9090	1.9443	15.3831	50.0240	6.6702	30.1853	31.3212	0.3143	0.3773
				1:100	221	335	274.7955	41.0730	1.0745	215	285	49.9639	36.2450	--	--	--	--	278	335	26.6222	54.7840	26.0164	1.4917	17.4407	39.2872	5.2774	25.4749	25.4756	0.3729	0.3969
				1:20	221	335	288.0102	41.0730	1.0747	215	285	51.1261	31.6770	--	--	--	--	278	335	27.9249	54.7840	27.6591	1.6937	16.3307	44.4916	6.3517	27.1693	27.9998	0.3853	0.3321
IFO-40	Heavy (21.9°)	2.51	unknown	0	224	335	1173.9084	41.0730	1.2005	221	303	120.4664	31.7020	--	--	--	--	275	335	114.0423	50.2000	109.7049	3.9261	27.9426	155.5248	7.4990	103.6229	111.3150	1.6747	0.8991
				1:200	221	335	1246.6349	41.0730	1.2208	218	303	130.7611	27.1630	--	--	--	--	275	335	119.5841	50.2000	115.7084	2.4241	47.7317	160.5839	6.8963	105.1693	115.5723	0.9567	0.4653
				1:100	224	335	1338.5599	41.0730	1.2469	218	303	144.2245	31.7020	--	--	--	--	278	335	128.8407	50.2000	126.7588	3.5465	35.7420	181.6527	7.1909	118.8126	128.3301	2.0773	0.8103
				1:20	224	335	1458.7885	41.0730	2.2908	218	303	168.9769	18.1230	248	520	54.9662	224.9950	278	335	151.8776	54.7840	148.7639	32.5496	4.5704	222.4382	41.1861	153.5833	156.2830	36.6263	13.9537
IFO-120	Heavy (18.4°)	2.89	unknown	0	221	335	3030.6917	36.4960	1.6769	218	299	356.9362	27.1630	--	--	--	--	275	326	288.5176	45.6200	253.8040	2.3142	109.6730	238.3292	10.3519	156.8753	198.5147	0.6383	0.7026
				1:200	221	335	2903.2101	36.4960	1.6130	221	299	284.1346	18.1230	--	--	--	--	275	335	278.0117	45.6200	245.6221	2.4122	101.8258	216.1829	14.6200	151.8306	189.2919	1.0311	0.7444
				1:100	221	335	3090.2251	36.4960	1.6501	218	303	372.9288	27.1840	--	--	--	--	275	335	289.7281	45.6200	260.1135	3.0331	85.7579	229.2055	6.2012	156.3515	190.8314	1.2379	0.4351
				1:20	221	335	2527.7304	41.0730	1.6704	215	299	362.2292	18.1230	--	--	--	--	278	326	236.1044	45.6200	215.0700	6.2661	34.3231	189.9474	15.3716	139.1934	165.5095	4.2343	1.3665
IFO-180	Heavy (14.1°)	1.54	unknown	0	224	335	1263.0471	41.0730	1.2176	221	294	93.4542	18.1090	--	--	--	--	278	335	118.9519	45.6530	115.4168	3.4277	33.6718	155.2826	9.0125	105.8880	114.2930	1.5280	0.7810
				1:200	224	335	1394.4230	41.0730	1.2311	221	303	126.8108	22.6450	--	--	--	--	278	335	131.1659	45.6530	126.7468	3.5129	36.0808	172.7134	10.4629	122.5754	123.2982	1.5977	0.8673
				1:100	224	335	1703.5484	45.6530	2.3720	218	303	158.7036	22.6620	--	--	--	--	278	335	164.8318	50.2370	158.9337	4.3777	36.3057	229.6268	43.9836	166.9271	164.3761	20.2543	7.7073
				1:20	224	335	1532.9881	41.0730	1.6277	218	303	148.5740	22.6450	--	--	--	--	275	335	149.2341	54.7840	144.6928	11.8678	12.1921	213.5766	20.6104	148.9958	150.1388	8.5394	3.8566
IFO-300	Heavy (11.9°)	1.72	unknown	0	224	335	720.5500	41.0730	1.1149	221	299	58.8131	18.1090	--	--	--	--	278	335	66.4979	45.6200	61.3247	1.0011	61.2559	58.9409	2.4890	44.3442	46.5557	0.3989	0.2483
				1:200	224	335	443.5128	41.0730	1.1449	215	303	41.1199	18.1370	--	--	--	--	275	335	42.2335	45.6200	38.6145	1.4936	25.8539	41.4059	1.6533	31.7921	32.6736	0.3091	0.2193
				1:100	224	335	465.9054	41.0730	1.0654	215	290	28.6954	18.0940	--	--	--	--	275	335	43.3745	45.6200	40.2103	0.8799	45.6987	42.1867	2.8316	32.0261	33.8555	0.3175	0.1768
				1:20	224	335	661.4977	41.0730	1.0959	221	290	44.2314	18.0940	--	--	--	--	275	335	63.3623	45.6200	58.2410	1.4631	39.8066	62.7861	3.4138	45.4621	49.9825	0.5846	0.3138
Santa Clara	Heavy (22.1°)	2.85	Ventura County, California, US	0	224	335	157.2981	41.0730	1.0544	218	290	39.5859	31.7020	--	--	--	--	278	335	15.1363	45.6530	14.2036	0.5478	25.9289	16.7196	2.0912	9.4978	10.3678	0.1712	0.1965
				1:200	224	335	147.5528	41.0730	1.0530	218	285	37.7030	40.7590	--	--	--	--	278	335	13.8842	45.6530	13.0702	0.5749	22.7335	15.6790	2.0057	8.4954	9.2278	0.1158	0.1535
				1:100	224	335	154.9767	41.0730	1.0753	218	285	39.5709	31.7020	--	--	--	--	278	335	15.3927	45.6530	14.4400	0.7907	18.2618	16.0674	2.3119	10.0251	10.3353	0.2387	0.2503
				1:20	224	335	169.3872	41.0730	1.1187	218	289	40.8290	31.6770	--	--	--	--	275	335	16.4747	45.6530	15.6909	2.2520	6.9675	20.2081	4.4623	11.7720	12.5627	1.0095	0.5811

MICROBES & OIL: WHAT'S THE CONNECTION?

Emily Maung-Douglass
Larissa Graham, Christine Hale, Stephen Sempier, Tara Skelton, LaDon Swann, Monica Wilson

Microbes may be tiny organisms, but they play a large role in removing oil from the environment. How do these microscopic organisms make large-scale impacts?

[FIGURE 1]

MICROBES & OIL

Oil can enter coastal and marine environments through natural **oil seeps** or by human activities (MacDonald et al., 2015). Once there, multiple factors break down oil, including microbes.

Microbes are single-celled living organisms. The are the oldest form of life on the planet and play critical ecological roles in the cycles of most elements and chemical compounds in our global ecosystem. . Some species of coastal bacteria and fungi naturally break down oil to eat it as part of their diet (Gutierrez et al., 2016; Simister et al., 2015). Depending on the type of oil, laboratory studies show that under ideal conditions, some microbes can degrade, or break down, up to 65 percent of oil in the water in a little more than one week(Li et al., 2013). These oil-degrading microbes live in many environments, including beaches, wetlands, mangroves, deep water, and surface waters (Kostka et al., 2011; Mahmoudi et al., 2013; Santos et al., 2011; Seidel et al., 2016; Gutierrez et al., 2016).

Because oil acts as a food source, its release into an area can increase the number of oil-eating microbes in the water. Scientists documented this in both the lab and in the Gulf of Mexico during the Deepwater Horizon (DWH) oil spill (Kostka et al., 2011; Baelum et al., 2012; Mahmoudi et al., 2013; Yang et al., 2016). They found that oil in the deep waters near the wellhead increased the numbers of microbes that eat oil. In fact, the whole community of microbes living in the area changed in response. As the number of oil-eating microbes increased, other species decreased (Yang et al., 2016). After the spill, the microbe community returned to its pre-spill state with fewer oil-degrading species.

OIL-DEGRADING MICROBES

How do they do it?

How do these microscopic forms of life break down oil? Scientists found that many species of microbes produce natural **surfactants** that help them digest oil (Qiao and Shao., 2010, Gutierrez et al., 2013). These surfactants are similar to those found in manmade **dispersants**. Multiple types of natural surfactants exist and are mixtures that can include sugars, **amino acids**, and/or **lipids** (Bookstaver et al., 2015b; Kegel et al., 2016).

Oil is made up of many types of chemicals. These include **alkanes** and **polycyclic aromatic hydrocarbons (PAHs)**. Microbes that feed on alkanes often release surfactants from their cells.

Those that consume PAHs typically move the PAHs into their cells to begin breaking down the oil (Campo et al., 2013). **Genes** determine which oil-based chemicals a microbe can break down and under which conditions (Dombrowski et al., 2016; Simister et al., 2016). For example, some species break down alkanes in high oxygen environments while others break down alkanes and PAHs better in low oxygen conditions (Simister et al., 2016).

Unexpected connections and other factors in the breakdown of oil

Conditions such as light, **nutrients**, and location affect what microbes live in an area and how quickly and thoroughly they degrade oil.

Some species of oil-degrading microbes thrive under cold water conditions, while others are found in warm waters (Baelum et al., 2012; Campo et al., 2013). Microbe species found in the warm (77° F) surface waters of the Gulf of Mexico quickly and completely break down many types of oil-based compounds. They can also break down dioctyl sodium sulfosuccinate or **DOSS**, a major component of the dispersants (**Corexit 9527A and 9500A**) used during Deepwater Horizon (Campo et al., 2013). Some species living in the deep colder (41°F) waters can also break down oil (Baelum et al., 2012; Campo et al., 2013). However, they can take up to nearly one month longer to break down the same compounds. Even then, the compounds are not broken down as completely as if they were eaten by microbes that live in warm surface waters (Campo et al., 2013).

Sunlight determines what types of microbes are present in surface waters during an oil spill (Bacosa et al., 2015a). Scientists found that exposing water samples containing crude oil to sunlight caused a change in the microbe community. The number of oil-degrading species increased as the abundance of other species decreased. These additional oil-degrading microbes in the water also caused the amount of oil-based compounds in the same area to lower (Bacosa et al., 2015a; Bacosa et al., 2015b).

Nutrient levels can determine population numbers of oil-degrading microbes. Microbes use nutrients, such as nitrogen and phosphorous, as a food source. Scientists experimentally found that adding nitrogen to systems that are heavily oiled can fuel microbes to break down oil more quickly (Bookstaver et al., 2015a). Nitrogen and phosphorous were plentiful in the Gulf of Mexico during Deepwater Horizon, which may help explain why populations of oil-degrading microbes blossomed in the Gulf during the spill (Hazen et al., 2010).

How do populations of oil-degrading microbes survive in in areas where natural oil seeps or oil spills are absent? Like many other forms of life, oil-degrading microbes exist in **symbiosis** with other species. Scientists unexpectedly discovered that one group of microbes called cyanobacteria, which do not degrade oil, actually produce alkanes like those found in oil (Figure 2) (Lea-Smith et al., 2015). The alkanes produced by cyanobacteria feed oil-degrading microbes, particularly during periods or areas where oil is scarce. Oil-degrading microbes release carbon dioxide as they break down the alkanes for nourishment. This carbon dioxide feeds the populations of cyanobacteria and the cycle continues.

INTERACTIONS WITH DISPERSANTS

Dispersants like Corexit 9500A are sometimes used during oil spills to minimize the amount of oil that reaches the shore, reducing impacts to habitats and wildlife. But how do these chemicals interact with naturally occurring, oil-degrading microbes?

Some studies indicate that the dispersants used during emergency response may discourage the natural break down of oil by microbes (Hamdan and Fulmer, 2011; Campo et al., 2013; Bookstaver et al., 2015b). For example, scientists found that Corexit 9500A can decrease the and growth and lifespan of certain species of oil-degrading microbes living in beaches and open waters (Hamdan and Fulmer, 2011; Bookstaver et al., 2015b). Scientists discovered that Corexit 9500A limits the growth of microbes on the water's surface, lowering the ability of microbes to stick to oil slicks and eventually break them down (Bookstaver et al., 2015b). Further, recent research indicates that the addition of dispersant may promote the growth of microbes that eat Corexit 9500A rather than oil-based compounds (Kleindienst et al., 2016).

Sidebar
MARINE SNOW

Marine snow is a fluffy substance that looks like snow as it drifts from the upper reaches of the water down to the seafloor (Figure 3). A common occurrence in marine waters, it can consist of a mixture of items, including bacteria, dust, dead animal fragments, and plants (NOAA, 2016). As the marine snow "falls" through the water column, it combines with oil droplets, carrying oil to the sea floor (Passow et al., 2012). Marine snow may also be eaten by tiny animals, called **zooplankton**, along the way. This oil may still be carried to the seafloor in the zooplankton's fecal pellets (Almeda et al., 2016).

Marine snow is held together by a sticky substance produced by microscopic plants and bacteria called exopolymeric substances (EPS). Scientists think the blooms of bacteria that formed during Deepwater Horizon oil spill used man-made dispersants as a food source to produce EPS, which can act as a natural dispersant to break down oil (van Eenennaam et al., 2016). While forming EPS is natural, experiments in the laboratory suggest that dispersants added during the Deepwater Horizon oil spill likely created large amounts of EPS. This in turn created large amounts of marine snow (Passow et al., 2012).

MICROBES ALONG THE SHORE

What happens when oiling takes place in coastal wetlands and beaches? Similar to open water areas, some species of microbes in beaches and wetlands break down oil as a food source (Kostka et al., 2011; Mahmoudi et al., 2013). When oil enters either marshes or beaches, it causes a shift in the microbe community in favor of oil-degrading species (Kostka et al., 2011; Beazley et al., 2012; Mahmoudi et al., 2013). Populations of oil-degrading species in wetland

soils decrease after oil is no longer detected in the environment. Additionally, oil-eating microbes in marshes naturally live around the roots of the plants and help break down oil that enters the area (Beazley et al., 2012).

The right combination of oxygen levels and nutrients, like nitrogen and iron, must be present for microbes to break down oil in coastal sand and mud (Acosta-Gonzalez and Marqués, 2016). This is because oxygen and nutrients combine to create energy for microbes. When oxygen and nutrient levels are plentiful, like in the upper sediment layers of a beach, oil-eating microbes increase in numbers and break down oil. However, this is not the case in deep sediment layers. Dispersants are applied at sea and cannot be applied within 3.45 miles of the shoreline or in areas with water depths less than 33 feet deep (U.S. Coast Guard, 2011). However, there is the potential for slower oil break down once chemically dispersed oil reaches shore. During laboratory studies, scientists found that oil treated with dispersants may carry oil deeper into beach sands than might otherwise be possible (Zuijdgeest and Huettel et al., 2012). Oil travels to depths where microbes are not in prime conditions to break down the oil, slowing down natural processes.

WHERE DO WE GO FROM HERE?

The Gulf of Mexico Research Initiative (GoMRI) and others continue to develop an understanding of microbes and their role in the breakdown of oil. To learn more about this and the research being conducted on the Deepwater Horizon spill, visit the GoMRI website at www.gulfresearchinitiative.org. Visit the Gulf Sea Grant program website at http://gulfseagrant.org/oilspilloutreach to view our other publications, about dispersants, oil, and other topics.

GLOSSARY

Alkanes — A group of compounds composed of hydrogen and carbon. These occur naturally in petroleum and natural gas, and include methane, propane, and butane. Some alkanes are produced by living organisms.

Amino acids — A collection of 22 compounds, all containing a minimum of nitrogen, oxygen, carbon, and hydrogen. Chains of amino acids make up protein. For this reason, they are sometimes referred to as the chemical building blocks of protein.

Corexit 9527A and 9500A — Dispersants approved for use in U.S. waters and those that were used to minimize the presence of surface oil slicks during the Deepwater Horizon oil spill.

Dioctyl sodium sulfosuccinate (DOSS) — A primary component of both dispersant formulas used in the Deepwater Horizon oil spill. It increases the attraction between oil and water molecules and hinders the formation of large oil slicks on the surface of the ocean. DOSS can also be found in consumer products such as detergents, cosmetics, and laxatives and, therefore, can be found in coastal waters.

Dispersants — Chemicals that are used during oil spill response efforts to break up oil slicks. Their use can limit floating oil from impacting sensitive ecosystems such as coastal habitats.

Genes — Unit of DNA that codes for a trait in an organism (e.g., coloration, size, stress response). Passed from parent to child.

Lipids — A group of compounds, including natural plant and animal oils, waxes, and fats, that do not dissolve easily in water.

Marine snow — A stringy to fluffy-looking complex of composed of live and dead bacteria, dead animals and plants, fecal matter, sand, soot, and other inorganic dust particles. Rains from upper water column to the seafloor.

Nutrients — A substance that provides nourishment essential for growth and the maintenance of life.

Oil seeps — Locations where oil and natural gas flow up naturally through cracks in the earth at a slow rate.

Polycyclic aromatic hydrocarbons (PAHs) — A group of hydrocarbons found in oil, tar, smoke from burning oil, coal, wood, (and ash from burning), car exhaust and cooked (e.g., grilled) animal fats.

Protist — Single-celled, microscopic organisms that have specialized organs and whose DNA is held together by proteins. They are considered a major herbivore of the ocean.

Surfactants — Compounds that work to break up oil. Dispersants contain surfactants that break the oil slick into smaller droplets that can more easily mix into the water column.

Symbiosis — Mutually beneficial relationship between different species of organisms living closely to one another.

Zooplankton — Very small animals, and the immature stages of larger animals, drifting in oceans, seas, and bodies of fresh water.

REFERENCES

1. MacDonald, I. R., Garcia‐Pineda, O., Beet, A., Daneshgar Asl, S., Feng, L., Graettinger, G., ... & Leifer, I. (2015). Natural and unnatural oil slicks in the Gulf of Mexico. *Journal of Geophysical Research: Oceans*, *120*(12), 8364-8380.

2. Gutierrez, T., Berry, D., Teske, A., & Aitken, M. D. (2016). Enrichment of Fusobacteria in Sea Surface Oil Slicks from the Deepwater Horizon Oil Spill. *Microorganisms*, *4*(3), 24.

3. Simister, R. L., Poutasse, C. M., Thurston, A. M., Reeve, J. L., Baker, M. C., & White, H. K. (2015). Degradation of oil by fungi isolated from Gulf of Mexico beaches. *Marine pollution bulletin*, *100*(1), 327-333.

4. Li, C., Zhou, Z. X., Jia, X. Q., Chen, Y., Liu, J., & Wen, J. P. (2013). Biodegradation of crude oil by a newly isolated strain *Rhodococcus* sp. JZX-01. *Applied Biochemistry and Biotechnology*, *171*(7), 1715-1725.

5. Kostka, J. E., Prakash, O., Overholt, W. A., Green, S. J., Freyer, G., Canion, A., ... & Huettel, M. (2011). Hydrocarbon-degrading bacteria and the bacterial community response in Gulf of Mexico beach sands impacted by the Deepwater Horizon oil spill. *Applied and Environmental Microbiology*, *77*(22), 7962-7974.

6. Mahmoudi, N., Porter, T. M., Zimmerman, A. R., Fulthorpe, R. R., Kasozi, G. N., Silliman, B. R., & Slater, G. F. (2013). Rapid degradation of deepwater horizon spilled oil by indigenous microbial communities in Louisiana saltmarsh sediments. *Environmental Science & Technology*, *47*(23), 13303-13312.

7. Santos, H. F., Carmo, F. L., Paes, J. E., Rosado, A. S., & Peixoto, R. S. (2011). Bioremediation of mangroves impacted by petroleum. *Water, Air, & Soil Pollution*, *216*(1-4), 329-350.

8. Seidel, M., Kleindienst, S., Dittmar, T., Joye, S. B., & Medeiros, P. M. (2016). Biodegradation of crude oil and dispersants in deep seawater from the Gulf of Mexico: Insights from ultra-high resolution mass spectrometry. *Deep Sea Research Part II: Topical Studies in Oceanography*, *129*, 108-118.

9. Bælum, J., Borglin, S., Chakraborty, R., Fortney, J. L., Lamendella, R., Mason, O. U., ... & Jansson, J. K. (2012). Deep‐sea bacteria enriched by oil and dispersant from the Deepwater Horizon spill. *Environmental Microbiology*, *14*(9), 2405-2416.

10. Yang, T., Nigro, L. M., Gutierrez, T., Joye, S. B., Highsmith, R., & Teske, A. (2016). Pulsed blooms and persistent oil-degrading bacterial populations in the water column during and after the Deepwater Horizon blowout. *Deep Sea Research Part II: Topical Studies in Oceanography*, *129*, 282-291.

11. Qiao, N., & Shao, Z. (2010). Isolation and characterization of a novel biosurfactant produced by hydrocarbon‐degrading bacterium *Alcanivorax dieselolei* B‐5. *Journal of Applied Microbiology*, *108*(4), 1207-1216.

12. Gutierrez, T., Berry, D., Yang, T., Mishamandani, S., McKay, L., Teske, A., & Aitken, M. D. (2013). Role of bacterial exopolysaccharides (EPS) in the fate of the oil released during the Deepwater Horizon oil spill. *PloS one*, *8*(6), e67717.

13. Bookstaver, M., Godfrin, M. P., Bose, A., & Tripathi, A. (2015a). An insight into the growth of *Alcanivorax borkumensis* under different inoculation conditions. *Journal of Petroleum Science and Engineering*, *129*, 153-158.

14. Kegel, L. L., Szabo, L., Polt, R., & Pemberton, J. E. (2016). Alkyl melibioside and cellobioside surfactants: Effect of sugar headgroup and alkyl chain length on performance. *Green Chemistry*, Advance Article. DOI: 10.1039/C6GC00436A.

15. Campo, P., Venosa, A. D., & Suidan, M. T. (2013). Biodegradability of Corexit 9500 and dispersed South Louisiana crude oil at 5 and 25 C. *Environmental Science & Technology*, *47*(4), 1960-1967.

16. Dombrowski, N., Donaho, J. A., Gutierrez, T., Seitz, K. W., Teske, A. P., & Baker, B. J. (2016). Reconstructing metabolic pathways of hydrocarbon-degrading bacteria from the Deepwater Horizon oil spill. *Nature Microbiology, 1,* 16057.

17. Simister, R. L., Antzis, E. W., & White, H. K. (2016). Examining the diversity of microbes in a deep-sea coral community impacted by the Deepwater Horizon oil spill. *Deep Sea Research Part II: Topical Studies in Oceanography, 129*, 157-166.

18. Bacosa, H. P., Liu, Z., & Erdner, D. L. (2015a). Natural sunlight shapes crude oil-degrading bacterial communities in Northern Gulf of Mexico surface waters. *Frontiers in Microbiology*, *6*, 1325.

19. Bacosa, H. P., Erdner, D. L., and Liu, Z. (2015b). Differentiating the roles of photooxidation and biodegradation in the weathering of Light Louisiana Sweet crude oil in surface water from the Deepwater Horizon site. *Marine Pollution Bulletin, 5,* 265–272. doi: 10.1016/j.marpolbul.2015.04.005

20. Hazen, T. C., Dubinsky, E. A., DeSantis, T. Z., Andersen, G. L., Piceno, Y. M., Singh, N., ... & Mason, O. U. (2010). Deep-sea oil plume enriches indigenous oil-degrading bacteria. *Science*, *330*(6001), 204-208.

21. Lea-Smith, D. J., Biller, S. J., Davey, M. P., Cotton, C. A., Sepulveda, B. M. P., Turchyn, A. V., ... & Howe, C. J. (2015). Contribution of cyanobacterial alkane production to the ocean hydrocarbon cycle. *Proceedings of the National Academy of Sciences*, *112*(44), 13591-13596.

22. Hamdan, L. J., & Fulmer, P. A. (2011). Effects of COREXIT® EC9500A on bacteria from a beach oiled by the Deepwater Horizon spill. *Aquatic Microbial Ecology*, *63*(2), 101-109.

23. Bookstaver, M., Bose, A., & Tripathi, A. (2015b). Interaction of *Alcanivorax borkumensis* with a Surfactant Decorated Oil–Water Interface. *Langmuir*, *31*(21), 5875-5881.

24. Kleindienst, S., Seidel, M., Ziervogel, K., Grim, S., Loftis, K., Harrison, S., ... & Joye, S. B. (2015). Chemical dispersants can suppress the activity of natural oil-degrading microorganisms. *Proceedings of the National Academy of Sciences*, *112*(48), 14900-14905.

25. NOAA. (2016). *What is marine snow?.* Retrieved from: http://oceanservice.noaa.gov/facts/marinesnow.html

26. Passow, U., Ziervogel, K., Asper, V., & Diercks, A. (2012). Marine snow formation in the aftermath of the Deepwater Horizon oil spill in the Gulf of Mexico. *Environmental Research Letters*, *7*(3), 035301.

27. Almeda, R., Connelly, T. L., & Buskey, E. J. (2016). How much crude oil can zooplankton ingest? Estimating the quantity of dispersed crude oil defecated by planktonic copepods. *Environmental Pollution*, *208*, 645-654.

28. van Eenennaam, J. S., Wei, Y., Grolle, K. C., Foekema, E. M., & Murk, A. J. (2016). Oil spill dispersants induce formation of marine snow by phytoplankton-associated bacteria. *Marine Pollution Bulletin*, *104*(1), 294-302.

29. Beazley, M. J., Martinez, R. J., Rajan, S., Powell, J., Piceno, Y. M., Tom, L. M., ... & Sobecky, P. A. (2012). Microbial community analysis of a coastal salt marsh affected by the Deepwater Horizon oil spill. *PloS one*, *7*(7), e41305.

30. Acosta-González, A., & Marqués, S. (2016). Bacterial diversity in oil-polluted marine coastal sediments. *Current Opinion in Biotechnology*, *38*, 24-32.

31. U.S. Coast Guard. (2011). *On Scene Coordinator Report Deepwater Horizon Oil Spill: Submitted to the National Response Team, September 2011.* Retrieved from: https://www.uscg.mil/foia/docs/DWH/FOSC_DWH_Report.pdf

32. Zuijdgeest, A., & Huettel, M. (2012). Dispersants as used in response to the MC252-spill lead to higher mobility of polycyclic aromatic hydrocarbons in oil-contaminated Gulf of Mexico sand. *PloS one*, *7*(11), e50549.

FIGURES

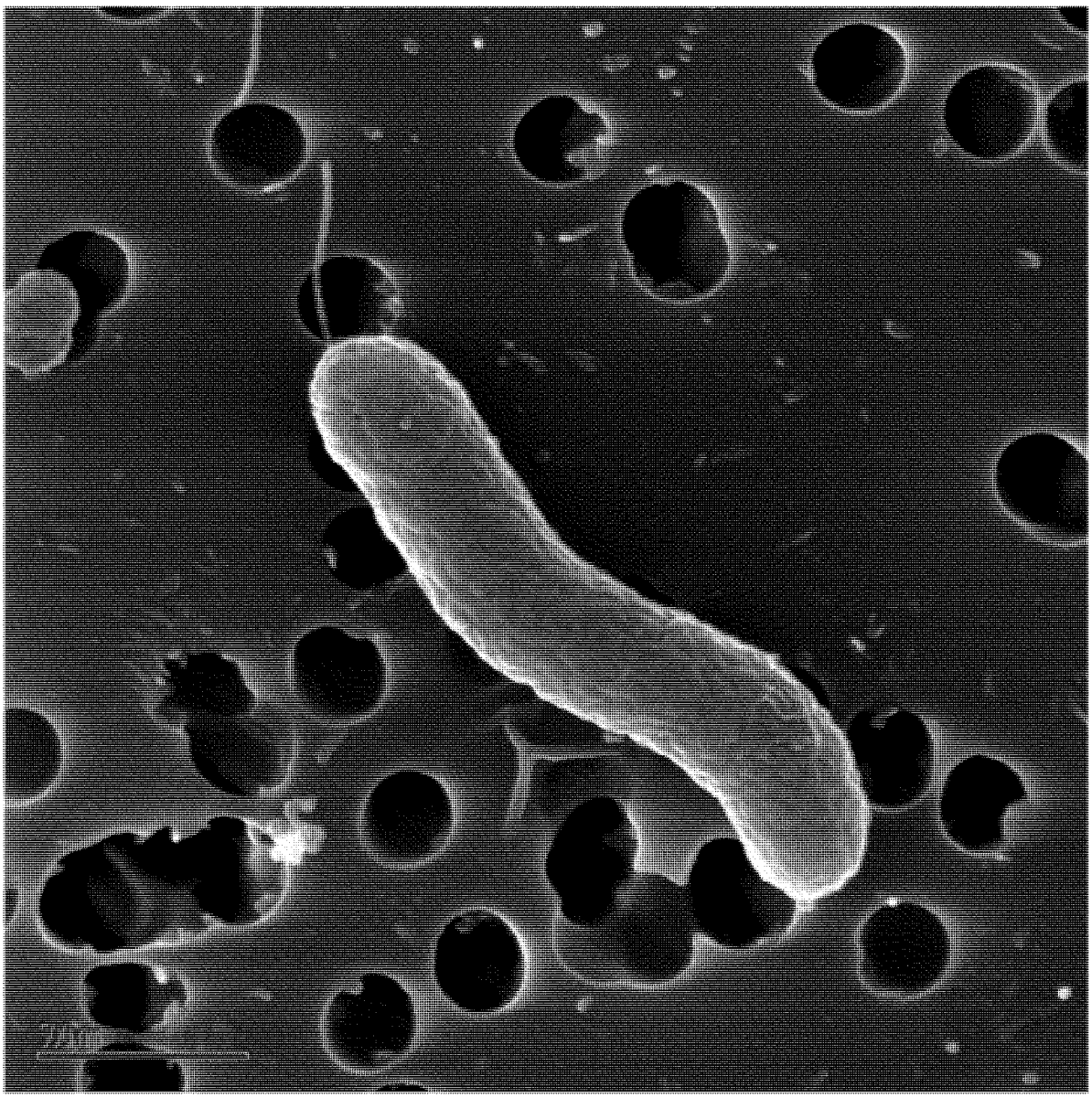

Figure 1. Microbes, like the one pictured above, break down oil that has entered the environment. The bacteria pictured above is 50 times smaller than the diameter of a human hair, yet this particular species is capable of degrading 25-60 percent of the oil it comes in contact with under cold water conditions (Baelum et al., 2012). (Reprinted from Bælum, J., Borglin, S., Chakraborty, R., Fortney, J. L., Lamendella, R., Mason, O. U., ... & Malfatti, S. A. (2012). Deep‐sea bacteria enriched by oil and dispersant from the Deepwater Horizon spill. *Environmental Microbiology*, *14*(9), 2405-2416.)

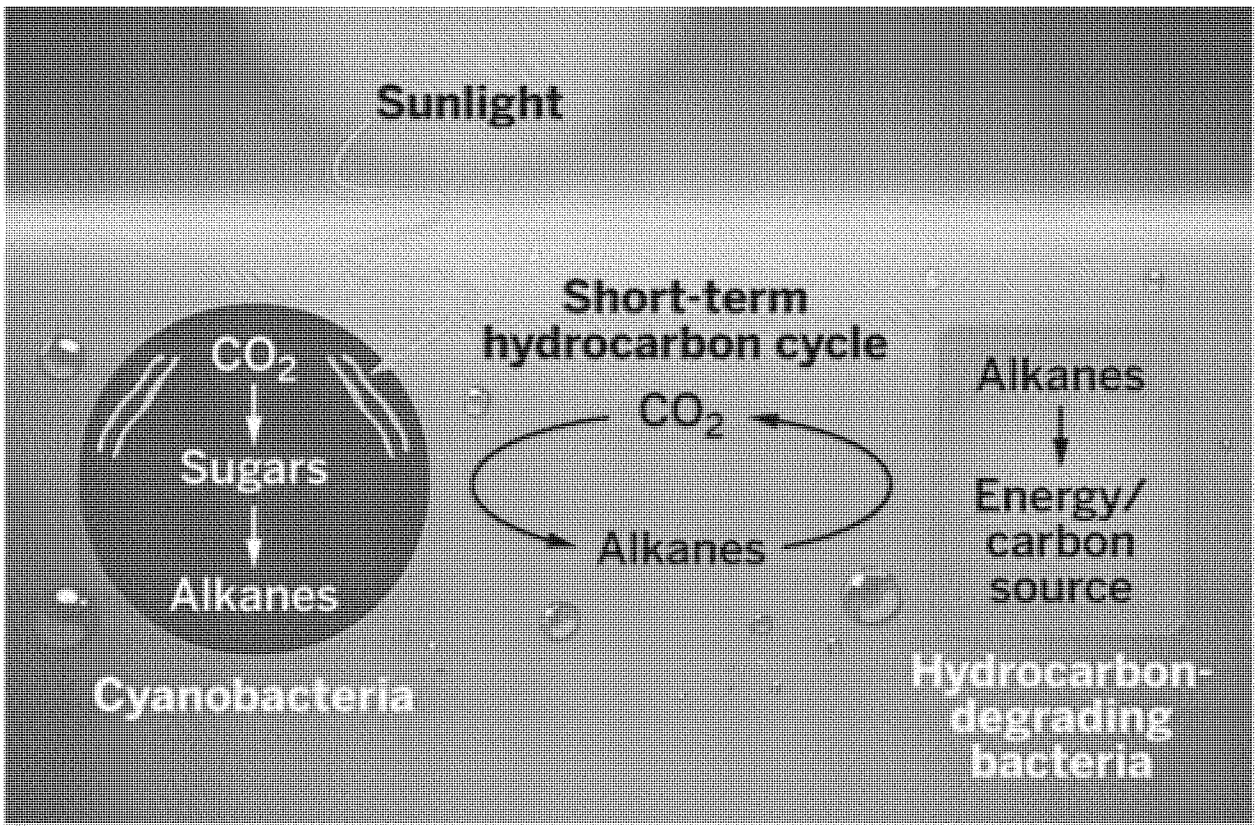

Figure 2. One type of microbe, called cyanobacteria, actually produce alkanes like those found in oil. These alkanes feed oil-degrading microbes during periods or in areas where oil is scarce. These microbes release carbon dioxide as they feed on alkanes. This carbon dioxide feeds the populations of cyanobacteria and the cycle begins again. (C&EN)

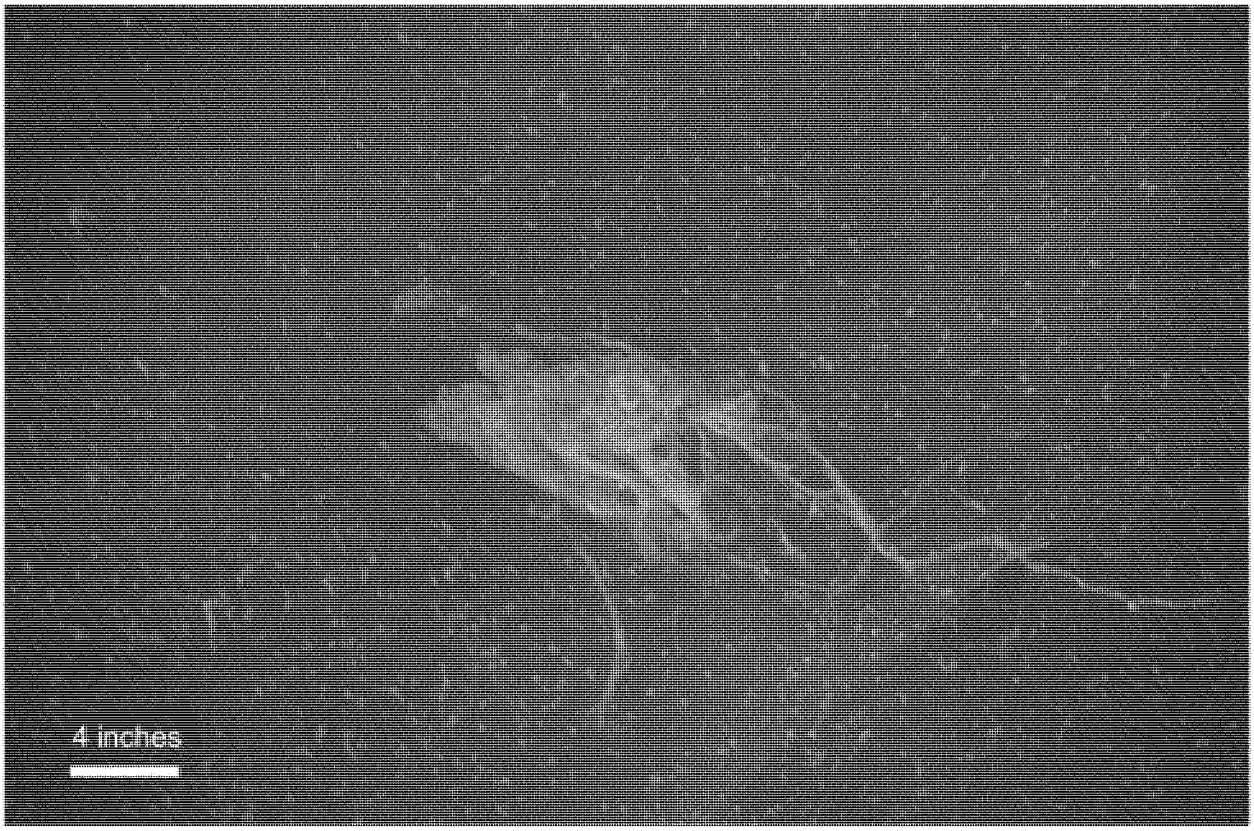

Figure 3. Marine snow (pictured above) is fluffy substance that drifts from the upper reaches of the water down to the seafloor. It is a sticky mixture made up of bacteria, dust, dead animal fragments, and plants. Oil can get trapped in marine snow and travel with the snow to the seafloor. (Reprinted from Passow, U., Ziervogel, K., Asper, V., & Diercks, A. (2012). Marine snow formation in the aftermath of the Deepwater Horizon oil spill in the Gulf of Mexico. *Environmental Research Letters*, *7*(3), 035301. doi:10.1088/1748-9326/7/3/035301)

To: Devi Sundaravadivelu[devi.sundaravadivelu@ptsied.com]; Conmy, Robyn[Conmy.Robyn@epa.gov]
Cc: Grosser, Robert[Grosser.Robert@epa.gov]; Sundaravadivelu, Devi[sundaravadivelu.devi@epa.gov]
From: Barron, Mace
Sent: Thur 10/20/2016 6:00:49 PM
Subject: RE: Tampa....
corexit 9500A 16119 REV 091616.pdf
Finasol.pdf

From: Devi Sundaravadivelu [mailto:devi.sundaravadivelu@ptsied.com]
Sent: Thursday, October 20, 2016 11:05 AM
To: Conmy, Robyn <Conmy.Robyn@epa.gov>
Cc: Barron, Mace <Barron.Mace@epa.gov>; Grosser, Robert <Grosser.Robert@epa.gov>; Sundaravadivelu, Devi <sundaravadivelu.devi@epa.gov>
Subject: Re: Tampa....

Hi Robyn,

We were able to locate Edie's copy of the Hydrosphere report for the work that was done with Dilbit (dated 3/3/16) and Endicott & Dorado (dated 7/1/16). Could you share the 3rd report for the work that was done with Finasol & Corexit from your emails.

Thanks,

Devi

Devi Sundaravadivelu, Ph.D.
Pegasus Technical Services, Inc.
On-Site Contractor to the U.S. EPA NRMRL
26 W. Martin Luther King Dr.
Cincinnati, OH 45268
Phone: (585) 732-4101

On 2016-10-19 12:52, Conmy, Robyn wrote:

Hi Mace,

Pegasus is pulling together the rest of the chem data for the dilbit tox tests. I have cc'd Devi and Bob on the message as Edie is out on medical leave for the next few weeks. I've also asked them to work on completing any remaining data analysis of the tox chem samples. Curious what you will need for the IOSC paper (extended abstracts are due Nov 30, but I've been told that it will be pushed back to mid Dec).

Devi and Bob – were you able to locate Edie's folder with the toxicity reports from Hydrosphere? If not, perhaps Mace can send to you in one email. Mine are scattered throughout emails currently.

Cheers,

Robyn

<>/<>/<>/<>/<>/<>/<>/<>/<>/<>/<>/<>/<>/<>/<>/<>/<>

Robyn N. Conmy, Ph.D.

Research Ecologist

USEPA/NRMRL/LRPCD

26 West MLK Drive

Cincinnati, Ohio 45268

513-569-7090 (office)

513-431-1970 (EPA mobile)

727-692-5333 (Personal mobile)

conmy.robyn@epa.gov

From: Barron, Mace
Sent: Tuesday, October 18, 2016 2:09 PM
To: Conmy, Robyn <Conmy.Robyn@epa.gov>
Cc: Wilson, Gregory <Wilson.Gregory@epa.gov>; Principe, Vanessa <Principe.Vanessa@epa.gov>
Subject: RE: Tampa....

Yea, we just did the TAC part, and I had thought Clean Gulf wasn't critical for me.

Could we have a call soon for update on new oils/dispersants, etc?

And chem data for the dilbits.

Let me know when you guys are available.

Mace

From: Conmy, Robyn
Sent: Tuesday, October 18, 2016 12:49 PM
To: Barron, Mace <Barron.Mace@epa.gov>; Wilson, Gregory <Wilson.Gregory@epa.gov>
Cc: Principe, Vanessa <Principe.Vanessa@epa.gov>
Subject: RE: Tampa....

Mace,

I thought oils was paying for part of your tampa trip? Was that just for the TAC portion and not clean gulf? I won't be attending any of it due to SHC BOSC review here in Cincinnati.

Cheers,

Robyn

<>/<>/<>/<>/<>/<>/<>/<>/<>/<>/<>/<>/<>/<>/<>/<>/<>/<>

Robyn N. Conmy, Ph.D.

Research Ecologist

USEPA/NRMRL/LRPCD

26 West MLK Drive

Cincinnati, Ohio 45268

513-569-7090 (office)

513-431-1970 (EPA mobile)

727-692-5333 (Personal mobile)

conmy.robyn@epa.gov

From: Barron, Mace
Sent: Tuesday, October 18, 2016 1:37 PM
To: Wilson, Gregory <Wilson.Gregory@epa.gov>
Cc: Principe, Vanessa <Principe.Vanessa@epa.gov>; Conmy, Robyn <Conmy.Robyn@epa.gov>
Subject: Tampa....

Hi Greg:

Just got your message. I did not get approval to go to Clean Gulf.

The Tampa TAC workshop starts at 4 pm on Thursday the 4th. My plan was to drive down there on Thursday morning.

I could get there Wednesday by dinner time if you wanted to catch dinner that eve? Will Robyn be there for Clean Gulf also?

Let me know your plans and I will reserve the hotel for another day.

Mace

To: chris.barker@noaa.gov[chris.barker@noaa.gov]; CJ Beegle-Krause[CJ.Beegle-Krause@sintef.no]; Conmy, Robyn[Conmy.Robyn@epa.gov]; Thomas.s.coolbaugh@exxonmobil.com[Thomas.s.coolbaugh@exxonmobil.com]; 'fingasmerv@shaw.ca'[fingasmerv@shaw.ca]; ali.khelifa@ec.gc.ca[ali.khelifa@ec.gc.ca]; jrpayne@sbcglobal.net[jrpayne@sbcglobal.net]; wspegau@pwssc.org[wspegau@pwssc.org]
From: Mandsager, Kathy
Sent: Mon 12/12/2016 10:31:45 PM
Subject: Transport & Behavior group follow-up
2016.12.09_Physical Transport and Chemical Behavior.docx

Thanks to each of you for participating on the call last week. As follow-up, please find 2 manuscripts for your review – they are listed below because they are too large to email; click on the link to view them. The Merlin paper corresponds to line 982 in the latest version of our document and the Spaulding paper corresponds to line 964.

For those of you who were not on the call last week (Jim, Tom, Chris and Ali), please review this document carefully for the changes/edits that were made especially in the Subsea Release section.

And now to schedule one final meeting for January to finish up this document. Please use this doodle poll so a date can be selected by MO 12/19: http://doodle.com/poll/wv3uatr784tvtp8f

Thank you!

Merlin F. 2014. Testing Sub-Sea Dispersant Injection At Laboratory Scale. Final Report by CEDRE. R.14.22.C/5233. 57pp.
[https://unh.app.box.com/files/0/s/merlin/1/f_34036288499]

Spaulding, M.L., Mendelsohn, D., Crowley, D., Li, Z. and Bird, A., 2015. Draft Technical Reports for Deepwater Horizon Water Column Injury Assessment: Application of OILMAP DEEP to the Deepwater Horizon Blowout. September 30, 2015; Project No, 2011-144. RPS ASA, 55 Village Square Drive, South Kingstown, RI 02879. DWH-AR0285366. See Appendix G, Development of OILMAP DEEP droplet size model.
[https://unh.box.com/s/e9l5y2pckualo0ad321tds50j50su2m7]

Kathy Mandsager

Coastal Response Research Center

Center for Spills and Environmental Hazards

220 Gregg Hall, 35 Colovos Rd

University of New Hampshire

Durham, NH 03824

603.862.1545

SINTEF

A26122- Unrestricted

FINAL report

Subsurface oil releases – Experimental Study of Droplet Distributions and Different Dispersant Injection Techniques - version 2

A scaled experimental approach using the SINTEF Tower basin

Authors
Per Johan Brandvik, Øistein Johansen, Umer Farooq, Glen Angell and Frode Leirvik

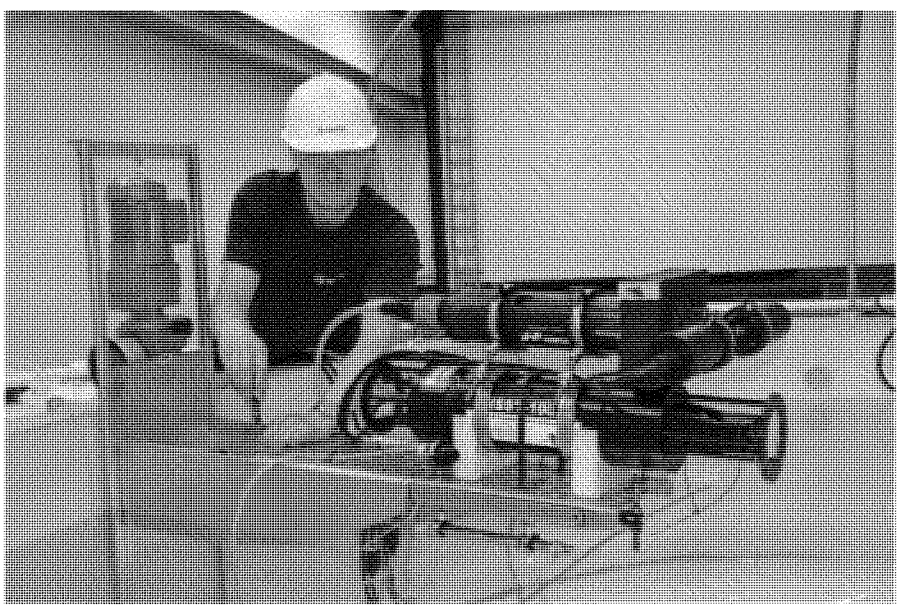

Preparing the instrumentation (LISST and in-situ camera) for monitoring of droplet size distributions in the Tower basin.

SINTEF Materials and Chemistry
Environmental Technology
2014-05-08

SINTEF

SINTEF Materials and Chemistry
Environmental Technology
2014-05-08

SINTEF

SINTEF Materialer og kjemi
SINTEF Materials and Chemistry

Address:
Postboks 4760 Sluppen
NO-7465 Trondheim
NORWAY

Telephone:+47 73593000
Telefax:+47 73597043

info.mk@sintef.no
www.sintef.no/mk
Enterprise /VAT No:
NO 948007029 MVA

KEYWORDS:
Oil spill
subsurface
release conditions
droplet size
modeling

Final report

Subsurface oil releases – Experimental Study of Droplet Distributions and Different Dispersant Injection Techniques - version 2

VERSION
FINAL Report ver. 2

DATE
2014-05-08

AUTHOR(S)
Per Johan Brandvik, Øistein Johansen, Umer Farooq, Glen Angell and Frode Leirvik

CLIENT(S)
The American Petroleum Institute – API JITF D3

CLIENT'S REF.
Patrick Twomey, EM&A

PROJECT NO.
102001616

NUMBER OF PAGES/APPENDICES:
100 + Appendices

ABSTRACT
The main objectives with this project have been to answer the following questions regarding dispersant injection during a subsea blowout.

1. How do dispersant injection method, dispersant to oil ratio (DOR) and dispersant type affect oil droplet size (Volume Median Diameter – VMD)?
2. How does the dispersant-oil mixing vary as a function of distance from the orifice for different injection methods and how does this affect oil droplet size?

The experimental work has been performed in SINTEFs Tower basin in Trondheim, Norway. This unique facility consist of a 6 meter high, 3 meter wide tank that holds 42 m^3 of natural sea water and is equipped with the latest technology for such experiments.

- A clear correlation between DOR and the shift in droplet size distribution towards smaller droplets was observed. Very limited effect was observed for the lowest concentrations (DOR 1:1000-1:500), steadily increasing up to a shift corresponding to a third of the initial VMD at the highest concentration (1:25).

- The three different injection methods tested in this project gave similar results (reduction or shift in VMD), independent of whether the dispersant was injected immediately before the outlet (simulated injection tool) or immediately after the outlet.

PREPARED BY
Per Johan Brandvik, Senior Scientist/Professor

SIGNATURE

CHECKED BY
Ivar Singsaas, Research Director, QA coordinator

SIGNATURE

APPROVED BY
for Tore Aunaas, Vice President

SIGNATURE

REPORT NO.	ISBN	CLASSIFICATION	CLASSIFICATION THIS PAGE
A26122	9788214057393	Unrestricted	Unrestricted

ED_001324_00000703-00003

Document history

VERSION	DATE	VERSION DESCRIPTION
Draft version 1	2012-08-15	First version - To be discussed with API D3 committee in Houston early in October 2012.
Draft version 2	2012-10-21	Updated version for the October meeting, now postponed to 24. October. Updates based on comments from API D3 steering committee members.
Draft version 3	2012-12-20	Updated version based on feedback and comments on and after the October meeting.
Final version	2013-03-05	Final unrestricted version implementing comments on third draft.
2nd Final version	20014-05-08	Final unrestricted version implementing additional comments.

Disclaimer:

The statements, technical information, results, conclusions and recommendations contained herein are believed to be accurate as of the date hereof. Since any use of this information is beyond our control, SINTEF expressly disclaims all liability for any results obtained or arising from any use of this report or reliance on any information in this report.

Recommended reference:

Brandvik, P.J., Johansen, Ø., Farooq, U., Angell G., and Leirvik, F. 2014 *Sub-surface oil releases – Experimental study of droplet distributions and different dispersant injection techniques- version 2. A scaled experimental approach using the SINTEF Tower basin*. SINTEF report no: A26122. Trondheim Norway 2014. ISBN: 9788214057393.

This study has been funded by the American Petroleum Institute (API) under contract 2012-106675.

ED_001324_00000703-00004

Table of contents

1 Introduction 5

2 Objectives 7

3 Deliveries 7

4 Droplet formation in turbulent flow 8

4.1 Break up regimes 8
4.2 Weber number scaling 11
4.3 Bubbly jets 11
4.4 Buoyant jets 14
4.5 Droplet size distributions 15

5 Experimental 19

5.1 Selection of oil types 19
5.2 Selection of dispersants 19
5.3 Overview SINTEF Tower basin 20
5.4 Description of a Tower basin experiment 24
5.5 Monitoring during an experiment 25
5.6 Interfacial tension measurements 32

6 Results 36

6.1 Overview of experiments 36
6.2 Initial experiments 37
6.3 Flow rate experiments 40
6.4 Dispersant-to-oil-ratio (DOR) testing 43
6.5 Experiments with dispersant injection 47
6.6 Experiments with release of warm oil 55
6.7 Modified dispersant with reduced amount of solvent 57
6.8 Comparison of the different injection techniques 58
6.9 Comparison of dispersant injection at different nozzle sizes 61
6.10 Experiments with combined releases of oil & gas (air) 63

7 Discussions 65

7.1 Initial experiment 65
7.2 Flow rate experiments - droplet sizes versus release conditions 65
7.3 Droplet sizes versus Dispersant to oil ratio (DOR) 66
7.4 Effectiveness of different dispersant injection techniques 67
7.5 Release of warm oil 69

ED_001324_00000703-00005

7.6 Modified dispersant with reduced amount of solvent 70
7.7 Comparison of the different injection techniques 71
7.8 Comparison of dispersant injection at different nozzle sizes 71
7.9 Experiments with combined releases of oil & gas (air) 71

8 Data analyses - Modelling 72
8.1 Droplet breakup model 72
8.2 Empirical model for predicting droplet sizes 72
8.3 Droplet size distributions 77
8.4 Effects of air injection 83
8.5 Up-scaling from lab to field 87

9 Conclusions 90
9.1 Dispersant dosages 90
9.2 Dispersant injection techniques 90
9.3 Experiments with warm oil 90
9.4 Experiments with different nozzle sizes to verify scaling approach 90
9.5 Data analysis – Modelling 90

10 Recommendations 92

11 References 93

APPENDICES

Appendix A: Summary overview of all Tower Basin experiments.
Appendix B: Experimental data: Numerical distributions of oil and oil/dispersant flow rates.

ED_001324_00000703-00006

1 Introduction

SINTEF received in November 2011 a request for proposal (RFP) from API called "Evaluation of subsea dispersant injection methods / equipment and effectiveness". This RFP was a part of the Joint Industry Task force (JITF) D3 and was managed by Ecosystem Management & Associates (EM&A), Maryland, USA.

API requested a proposal from SINTEF to conduct large-scale laboratory studies on the physical and chemical characterization of oil droplets associated with physically and chemically dispersed crude oil from uncontrolled well events in deep-water environments. The goal of this research is to understand droplet formation as a function of release conditions (e.g. diameter and flow rate) and oil properties (e.g. viscosity, density and interfacial tension). The important variables should be varied systematically to produce a data set suitable to calibrate and improve existing algorithms for estimation of droplet sizes. Topics of immediate interest to API include oil droplet characterizations that can be used to predict (model) the behaviour of physically and chemically dispersed oil droplets based on the oil release flow rate, configuration and size of the orifice releasing oil, and properties of the crude oil and dispersant used. For the initial research efforts, API is particularly interested in experimental work that will further increase our understanding and ability to define the dispersion process for deep water releases of crude oil with and without the use of dispersants for atomization break-up regimes, generating data to support predictive modelling of the processes with different crude oil release conditions and varying types of crude oil.

The requested experimental work from API was listed in the following prioritized order:

1) Studies of dispersant injection method
2) Studies of DOR dependence.
3) Studies of dispersant dependence

The experimental work listed above only covers parts of the overall objectives for the D3 program. The main focus of these experiments is how the dispersant injection techniques and dispersant concentrations affect the droplet size distribution.

To clarify this, SINTEF took an initiative for a meeting with the API D3 management and team members on 15th November 2011 (during SEATAC in Boston). The main conclusions from this meeting are listed below (See minutes issued by EM&A for further details):

- "Studies of dispersant injection techniques, DOR dependency and dispersant products have priority as this knowledge is needed to inform on-going development of new response equipment designed to combat deep sea releases."
- "This RFP describes the first phase of the D3 project. Later studies will focus on how release conditions and oil properties affect droplet size distribution."
- "This RFP must be regarded as a starting point of an iterative process between the D3 management and SINTEF. The project description should include inherent flexibility to change the experimental program if necessary as the project progresses and further insight is gained."

ED_001324_00000703-00007

Based on the recommendations from this meeting, this project was described as a Phase I and contains only activities covering the prioritized areas 1-3 listed above. Activities for possible Phase-II will be discussed as a part of the reporting of Phase-I.

ED_001324_00000703-00008

2 Objectives

The main objectives with this study are to answer the following questions regarding dispersant injection during a subsea blowout:

1. How do dispersant injection method, dispersant to oil ratio (DOR) and dispersant type affect oil droplet size?
2. How does the dispersant-oil mixing vary as a function of distance from the orifice for different injection methods and how does this affect oil droplet size?

3 Deliveries

According to the contract, this final report includes the following sections:

1. Description of test tank, measurement methods, etc.
2. Summary of the experiment test matrix.
3. Summary of data analysis with special emphasis on effectiveness of the different dispersant injection techniques, DOR, dispersant type and the effect on oil droplet size distribution.
4. Discussion of scaling the results from the Tower basin dispersant injection testing to field scale.
5. Summary of further research needs and opportunities.

The main findings from this study will be published in a relevant peer reviewed scientific journal focusing on the effectiveness of the different dispersant injection techniques.

ED_001324_00000703-00009

4 Droplet formation in turbulent flow

The size distribution of oil droplets formed in deep water oil and gas blowouts is known to have strong impact on the subsequent fate of the oil in the environment. Large droplets will rise relatively rapidly and come to the surface relatively close to the discharge location, while small droplets will rise more slowly and can be transported long distances from the discharge location with ambient currents before reaching the sea surface. The smallest droplets may even be kept suspended in the water masses for prolonged periods by vertical oceanic turbulent mixing, and this mechanism is the main rational for application of chemical dispersants. Releases which are predominantly producing large oil droplets (in the millimetre size range) may thus result in relatively thick surface oil slicks, while thin surface films may be expected from releases producing small droplets (micrometre range). Thin oil films are more susceptible to natural dispersion and will have distinctly shorter persistence on the sea surface than thicker oil slicks, and the possibility of oiling of adjacent shorelines may thus be strongly reduced.

Reliable predictions of the droplet size distribution in deep water blowouts will thus improve our ability to forecast the fate of oil in the environment, provide guidance for oil spill response operations and relevant information to the public. The present study was initiated to get a better understanding of the mechanisms that governs droplet break up in deep water blowouts, with and without application of chemical dispersants. In order to achieve this, we need to understand the basic mechanisms that govern droplet breakup, and empirical data to support the theoretical understanding. This chapter deals with the theoretical aspects, while the empirical findings will be presented in the subsequent chapters.

4.1 Break up regimes

Droplet breakup may be caused by different mechanisms depending on the properties of the fluid and outlet conditions, ranging from pendant droplets that separate from the nozzle when the buoyant forces outrange the interfacial tension forces, through various axial or transverse instabilities of the jet, to full atomization where droplets of a wide size range are generated almost instantaneously at the jet exit.

The full range of breakup regimes of oil jets in water was investigated in laboratory experiments reported by Masutani and Adams (2000) and Tang and Masutani (2003). Examples of the various breakup regimes of oil jets are shown in Figure 4.1. As previously observed from breakup experiments with liquid jets in air, Masutani et al. found that the breakup regimes of oil jets in water could be delimited in a Reynolds number (re) vs Ohnesorge number (Z or Oh) diagram (Figure 4.2). The two non-dimensional numbers are defined as $Re = \rho\ U\ D/\ \mu$ and $Oh = \mu/(\rho\ \sigma\ D)^{1/2}$, where U is the exit velocity, D the orifice diameter, and ρ and μ are the density and dynamic viscosity of the jet fluid. The Ohnesorge number can also be expressed as a combination of the Reynolds number and the Weber number, i.e. $Oh = We^{1/2}/Re$, where $We = \rho\ U^2\ D/\sigma$. The two boundaries which are shown in the diagram were derived from visual inspection of the breakup conditions. The broken line shows the boundary between laminar and transitional breakup, while the dashed dotted line shows the boundary between the transitional and turbulent (atomization) break regimes. Both lines were found to represent linear relationships of the form $Oh = c\ Re^{-1}$, where c is a constant of proportionality. From the definition of Ohnesorge number mentioned above, this relationship implies that both boundaries are lines for a constant Weber number, with $We = c^2$, or $We = 18 \times 18 = 324$ for the boundary between the transitional and turbulent breakup regime.

ED_001324_00000703-00010

In the present study, where the main focus will be on turbulent break up, these findings are useful as a basis for limiting the experimental conditions for the breakup experiments. Figure 4.3 shows how the Ohnesorge vs. Reynolds number diagram can be used to delimit the range of discharge conditions. The parallelogram formed grid in the diagram depicts a range of possible orifice diameters and oil flow rates that might be used in the tower tank experiments. The orifice diameters are here limited to the range from 0.5 to 20 mm, with oil flow rates in the range from 0.1 to 20 L/minute. The thick solid line drawn in the diagram shows the boundary between the transition regime and the turbulent breakup (or atomization) regime.

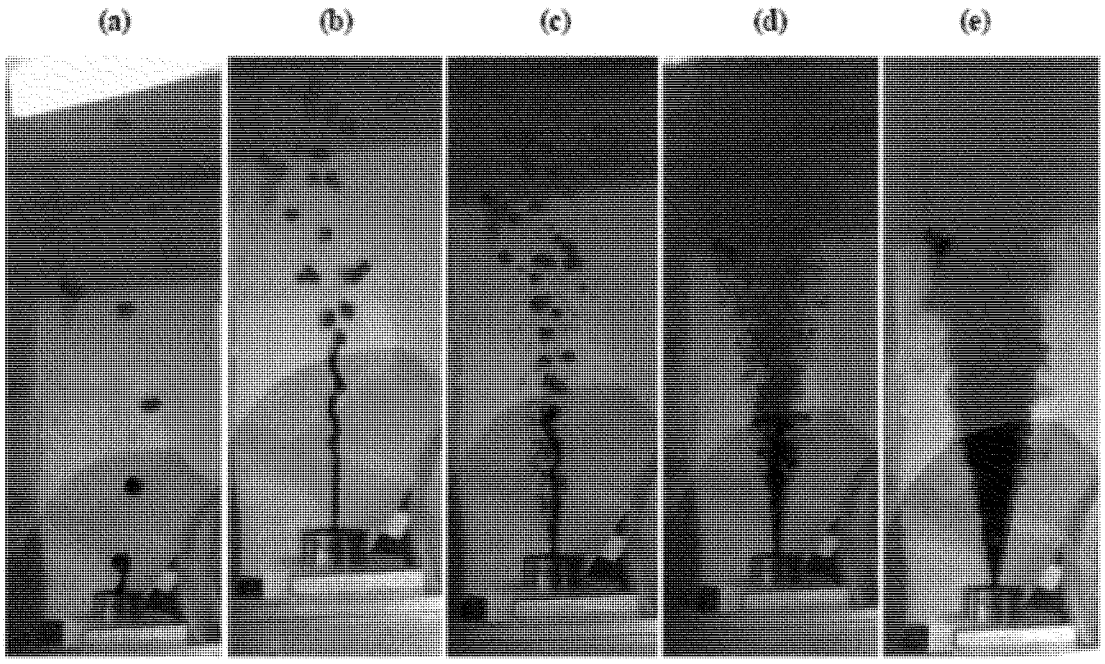

Figure 4.1: Illustration of oil jet breakup regimes from Tang and Masutani (2003). At low velocities, Rayleigh instability dominates, producing a near mono-dispersion of droplets larger than the orifice (a). As velocity is increased, the breakup location moves away from the nozzle and at some point the instability changes to a sinuous mode (b). At higher velocities, two instability mechanisms appear to operate in parallel: the surface of the jet becomes unstable to short wavelength disturbances and disintegrates close to the nozzle into fine droplets, while the core of the jet persists as a continuous fluid filament that breaks up further downstream into large droplets (c). Raising the velocity moves the breakup location of the jet core filament closer to the nozzle and also increases the fraction of fine droplets (d). Finally, atomization is attained (e).

ED_001324_00000703-00011

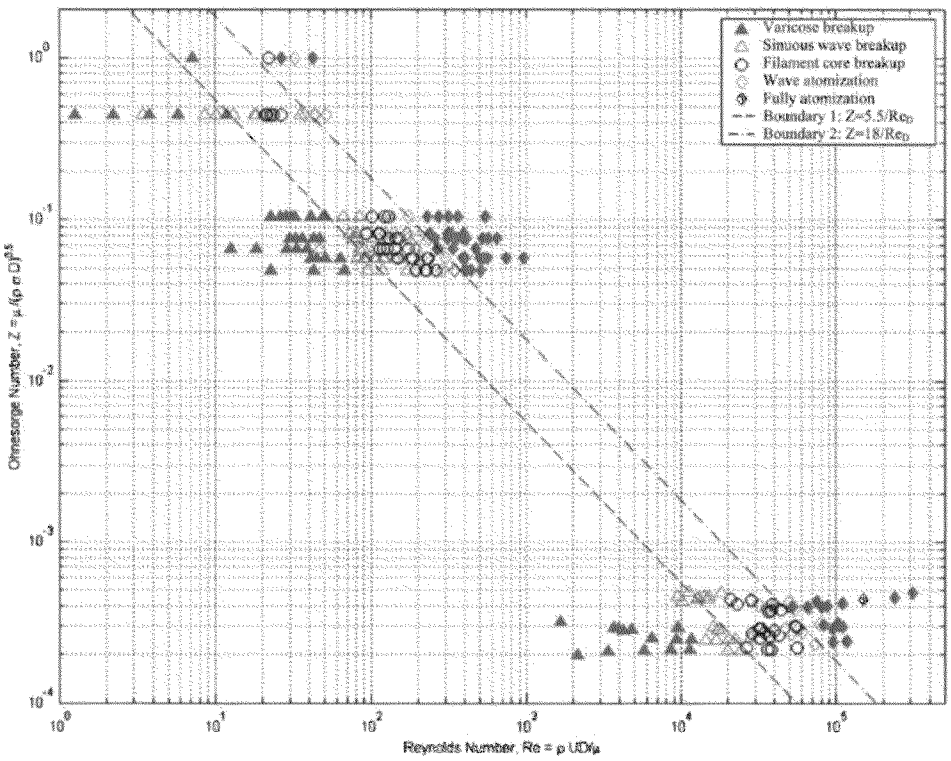

Figure 4.2: Liquid-liquid jet breakup regimes based on experiments with oil and silicone injection tests (upper two sets) and liquid CO2 injection tests (lower right hand corner). After Tang and Masutani (2003).

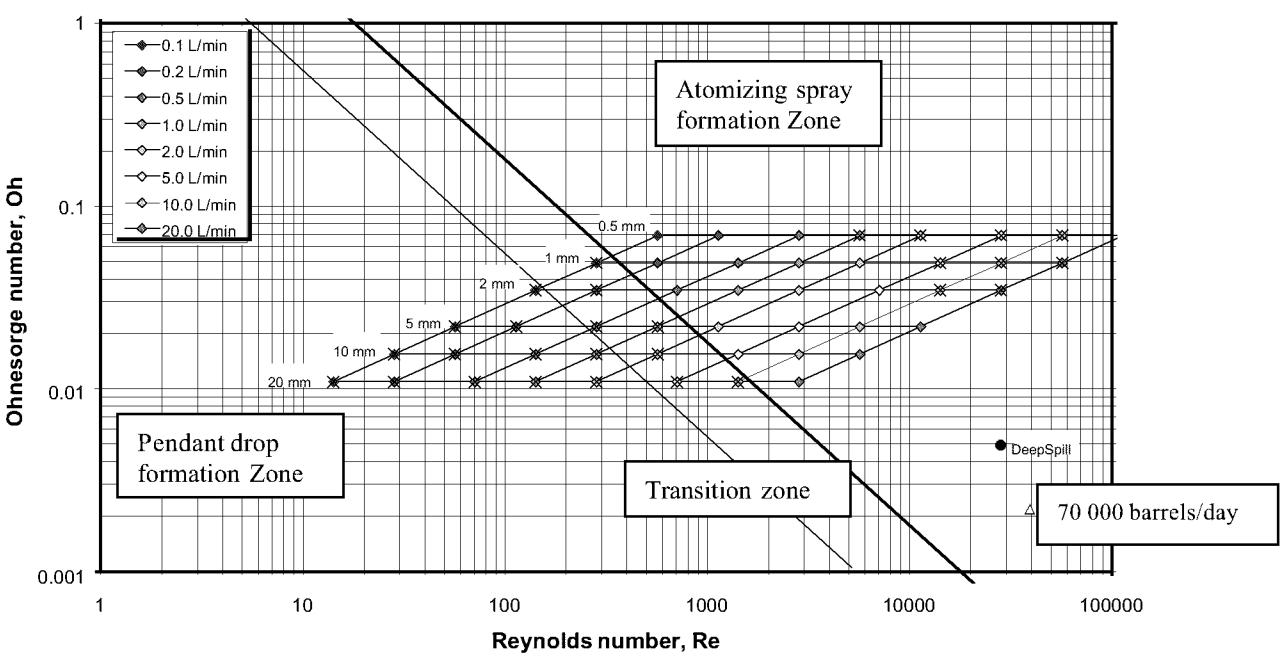

Figure 4.3: Experimental conditions plotted in an Ohnesorge vs. Reynolds number diagram. Injection rate varied from 0.1 to 20 L/min, with nozzle diameters from 0.5 to 20 mm. Oil viscosity is presumed to be 5 cP (50°C). Approximate location of the SINTEF DeepSpill experiment and a tentative large scale release are shown for comparison.

The preferred range of experimental conditions are depicted with open markers, while the cases that falls outside the turbulent regime are shown with crossed markers. Some of the cases in the turbulent breakup regime that will produce high outlet velocities (> 40 m/s) are also crossed out. These cases may be difficult to realize due to high pressure drops. The range of experimental conditions are also limited due to the size of the tank, however, nozzle sizes up to 15 mm and rates up to 100 L/min can be tested. The duration of such experiments will be limited to 10-30 seconds.

4.2 Weber number scaling

The classical theory of droplet splitting in turbulence predicts a maximum stable droplet size $d_{max} = C(\sigma/\rho)^{3/5}\varepsilon^{-2/5}$, where C is a constant of proportionality, σ is the interfacial tension (oil-water), ρ is the density of the continuous phase (water), and ε is the stationary turbulent dissipation rate (Hinze1955). However, in an oil jet emitted into water from a nozzle, the droplets will be carried downstream in the jet during the splitting process. Consequently, in a Lagrangian framework, the turbulent dissipation rate will diminish rapidly with time, and the assumption of stationary turbulence will not be applicable.

However, this theoretical model may still serve as a starting point for experimental design and development of more practical empirical equations. For example, by taking into account that the exit turbulent dissipation rate in a jet scales with the exit velocity U and diameter D, $\varepsilon \sim U^3/D$, the equation given above for d_{max} can be expressed in non-dimensional form: $d_{max}/D = A\ We^{-3/5}$, where A is a factor of proportionality, while the exit Weber number $We = \rho U^2 D/\sigma$. The factor of proportionality will depend on the flow conditions in the break up zone, and have to be determined empirically.

This scaling law is supposed to be valid when the breakup is limited by the interfacial tension of the jet liquid. However, as Hinze (1955) also pointed out, internal viscous stresses in the fluid droplets may also influence the breakup. Hinze introduced a dimensionless viscosity group N_{Vi} to account for this effect. Hinze's viscosity group is actually identical to the Ohnesorge number defined above. More recently, Wang and Calabrese (1986), proposed to replace Hinze's viscosity group by the viscosity number $Vi = \mu U/\sigma$ to account for the effect of viscous stresses. This dimensionless number is also defined as the ratio between the Weber number and the Reynolds number, i.e. Vi = We/Re.

Wang and Calabrese (1986) found that droplet breakup was governed by the Weber number scaling for small viscosity numbers ($Vi \rightarrow 0$), but that a Reynolds number scaling would apply for large viscosity number ($d_{max}/D = C\ Re^{-3/4}$, $Vi \rightarrow \infty$). For intermediate values of Vi, a combination of the two scaling laws might be applied. We will return to this relationship in the discussion of the experimental results, but it should be pointed out here that the viscosity numbers usually are small in conjunction with oil jet breakup, but large numbers may result in conjunction with application of chemical dispersant, since this can result in reductions in the interfacial tension by several orders of magnitude.

4.3 Bubbly jets

Most oil jet breakup experiments are conducted with a single fluid into water (crude oil or silicone fluid). In subsea blowouts, however, gas is in general discharged together with the oil, and the oil is quite often mixed with certain amounts of formation water. Different flow conditions can occur in

ED_001324_00000703-00013

such multiphase flows, from bubbly flow with oil as the continuous phase, via slug flow where plugs of oil and gas occupy sequential sections of the pipe, to mist flow where oil droplets are suspended in the gas flow, and some of the oil might flow along the surface of the pipe (annular flow). Bubbly flow in vertical pipes are normally associated with low to moderate gas void fractions ($0 < n < 60$ %), while mist flow is limited to very high void fractions ($n > 95\%$). However, the actual flow conditions are also influenced by the velocity of the flow, often defined by the superficial velocities of the two fluids. In the present context, we will only consider the bubbly flow condition, which in this study is of most interest because of concerns about high flow rate oil blowouts.

The main issue here is how to account for the presence of gas in the normalized variables defined above (i.e. the Reynolds, Weber and Ohnesorge numbers). For example, Neto et al. (2008) defined the nozzle Reynolds number in a series of bubbly water jet experiments in terms of the superficial water velocity $U_W = Q_W/A$, where Q_W is the volume flow of water and A is the nozzle cross section $A = \pi D^2/4$ corresponding to a nozzle diameter D, i.e. $Re_W = U_W D/\nu_W$, where ν_W is the kinematic viscosity of water.

However, this definition will not discriminate between a pure water jet and a bubbly jet with the same water flow. In order to account for this, the "water only" velocity may be substituted with an "effective" water velocity U_E derived from the principle of conservation of momentum flux. In the following, M is the exit momentum flux of the bubbly water jet, while M_E is the momentum flux of an "equivalent" pure water jet. The effective water velocity is then defined as the velocity of a pure water jet producing the same momentum flux as the bubbly water jet:

$$M = (\rho_W Q_W + \rho_G Q_G) U_{W+G},$$

$$M_E = \rho_W Q_E U_E, \text{ where } Q_E = A U_E$$

If we neglect the contribution of the gas to the momentum flux (due to the much smaller density of the gas), $M_E = M$ will imply $U_E = U_{WO}/(1 - n)^{1/2}$.

Since we now have defined the Reynolds number is in terms of the continuous phase, it is reasonable to do the same for the Weber and the Ohnesorge numbers. We then get the following definitions of the non-dimensional variables:

$$Re = \rho U_E D/\mu, \; We = \rho U_E D^2/\sigma \text{ and } Oh = \mu/(\rho \sigma D)^{1/2}$$

In the following, when we consider a system with oil and gas (instead of water and gas), oil properties will be substituted for water properties, and the subscripts will be dropped in the density and viscosity terms (implicitly implying oil).

Figure 4.4 shows a Re vs. Oh plot based on these definitions with results from the bubbly water jet experiments reported by Neto et al. (2008), covering gas volume fractions in the range from approximately 5 to 80 %. Experiments where atomization is observed are represented by filled markers, while open markers represent the transition regime. The thick red line depicts the

ED_001324_00000703-00014

transition to full atomization based on the liquid only experiments of Tang and Masutani 2003 (with oil or liquid CO_2).

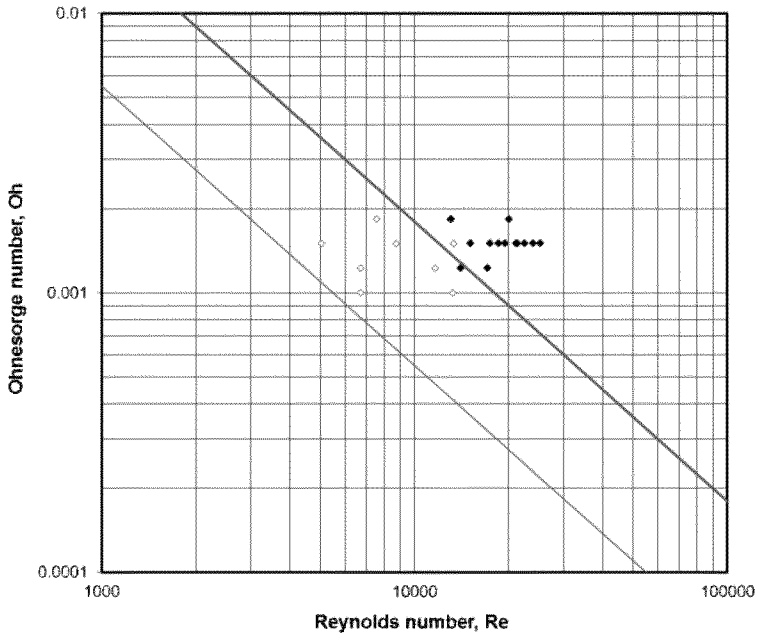

Figure 4.4: Ohnesorge – Reynolds number plot of data from bubbly water jet experiments reported by Neto et al. 2008. Filled diamonds represent cases with atomization, while the open diamonds are cases in the transition regime. The thick red line depicts the transition to full atomization based on liquid only experiments of Tang and Masutani 2003.

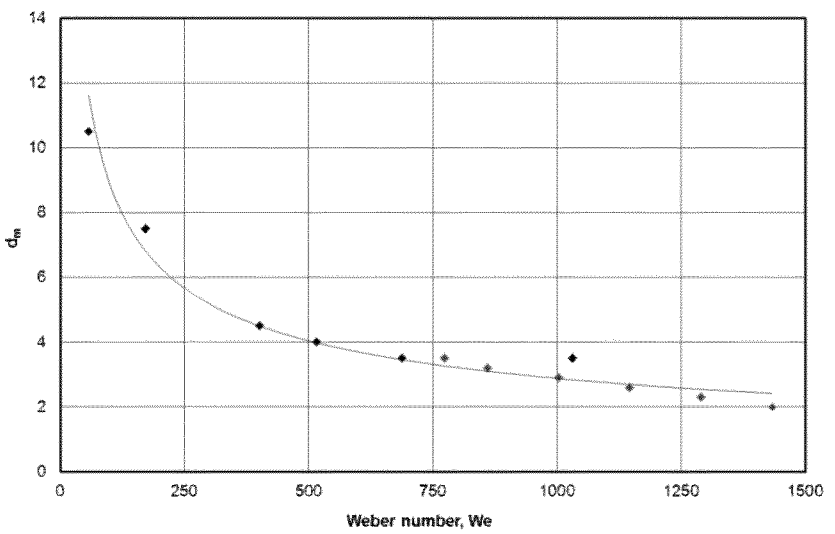

Figure 4.5: Volumetric mean bubble diameter plotted as a function of the Weber number computed from the equivalent liquid velocity U_{LE} defined above. The results shown here were obtained by Neto et al. 2008 with a 6 mm nozzle, with water only velocities in the range from about 0.5 to 3 m/s and gas volume fractions in the range from 7 to 80%. The red markers represent experiments with a fixed water only velocity (U_{LO} = 2.95 m/s), but with gas volume fraction varied from 7 to 50 %.

Figure 4.5 shows a plot of the mean bubble diameter reported by Neto et al. for a set of experiments with a 6 mm nozzle. The gas volume fractions varies in a range from about 7 up to about 80 %, while the water only velocities are in the range from about 0.5 to 3 m/s. It is promising that the transition line derived from single liquid flows also applies to bubbly jets when we use the definitions given above of the non-dimensional numbers. The same can be said for the quite systematic variation observed in Figure 2 of the mean bubble size with our definition of the Weber number. In conjunction with the planned oil experiments, these findings seem to imply that a situation with a gas volume fraction n and an oil volume flow $Q^{(n)}$ might be represented by an oil only experiment with an adjusted oil volume flow $Q = Q^{(n)}/(1-n)^{1/2}$.

4.4 Buoyant jets

The gas fraction in a bubbly jet will also contribute to the buoyancy flux of the discharge. The buoyancy flux is defined as $B = g' Q$, where Q is the total exit volume flow and $g' = g (\rho_w - \rho)/ \rho_w$ is the reduced gravity, where g is the acceleration of gravity, ρ_w is the density of water, and ρ is the density of the mixture of liquid and gas. Papanicolaou and List (1988) made an experimental investigation of the dynamics of round vertical buoyant jets, and found that buoyant jets differs from momentum jets in many aspects. While most experiments of droplet breakup in oil jets are made with jet-like outlet flow conditions due to restriction in volumetric flow rates and nozzle diameters, the conditions in deep water blowouts with large volume flows and large outlet diameters may tend to be more plume-like.

Papanicolaou and List (1988) found that the transition from jet-like to plume-like behavior in buoyant plumes is defined by a characteristic length $l_M = M^{3/4}/ B^{1/2}$. They conducted experimental studies with buoyant plumes and showed that the flow behaves like a jet at distances $z < l_M$, and like a plume for $z > 5\ l_M$. The relative distance l_M/D may indicate whether droplet splitting will take place in the jet-like or plume-like section of the buoyant plume. By insertion of the expressions for Q, B and M in this equation, this ratio is found to correspond to the exit Froude number, $Fr = U/(g'D)^{1/2}$. Exit conditions (defined by the exit velocity and the orifice diameter) that give high exit Froude numbers will thus imply that droplet splitting will occur in jet-like flow, while low exit Froude number implies buoyant plume flow in the breakup zone.

The authors also showed that in jet-like flow, the centerline velocity w_c at a distance z downstream from the exit will scale with the exit velocity, i.e. $w_c \sim U z/D$. In plume-like flow, the buoyancy flux will be the primary factor that determines the velocity development, i.e. $w_c \sim (B/z)^{1/3}$. This implies that in plume-like conditions, the exit velocity will not be a characteristic velocity for droplet breakup. From the scaling law for plume like flow, we find that at a distance $z = 5\ l_M$ where the flow shifts to plume-like behavior, the centerline velocity will be $w_c \sim (g'D)^{1/2}$. Thus, we may define a modified characteristic velocity $U' = U (1 + b\ Fr^{-1})$,where b is a factor of proportionality in the order of 1, to account for both jet-like and plume-like breakup conditions. The last term will vanish for large exit Froude numbers (i.e. $U' \approx U$ for jet-like flow), while for small Froude numbers (plume-like flow), the modified velocity will approach $U' = b\ Fr^{-1} = b\ (g'D)^{1/2}$, corresponding to the velocity at the transition to plume-like behavior. The factor of proportionality b should be determined from droplet breakup studies with buoyant flow conditions, but b = 1 could be used as a provisional estimate.

ED_001324_00000703-00016

4.5 Droplet size distributions

In the previous section, we have focused on models for prediction of the characteristic droplet size, e.g. defined as the volume median droplet diameter, d_{50}. However, we also need to consider the statistical distribution of the droplet sizes around the characteristic diameter. Of the many available options, two distribution functions are most commonly found in the literature on droplet breakup; the lognormal distribution and the Rosin-Rammler distribution (Lefebvre1989).

The former can be understood as a normal distribution of the logarithms of the droplet sizes, i.e. a normal distribution of $x = \ln(d)$, with a mean value $M = \langle x \rangle$, and a standard deviation σ_x based on x. The mean value M is also equal to the logarithm of the median droplet diameter, $M = \ln(d_{50})$. Thus, the lognormal distribution is defined by two parameters, M and σ_x.

The Rossin-Rammler distribution is also a two-parameter distribution function, defined in terms of a characteristic diameter d_i corresponding to a certain cumulative volume fraction V_i (e.g. 50%), and a spreading parameter n. The cumulative volume distribution function is given as:

$V(d) = 1 - \exp[- k_i (d/d_i)^n]$, where $k_i = - \ln(1-V_i)$

For $V_i = 50\%$, d_i is the median diameter, and $k_i = -\ln(0.5) = 0.693$.

A third option is the Upper Limit lognormal distribution (UL), which is based on the lognormal distribution, but truncated at an upper limit diameter d_{max}. The cumulative probability function for the Upper Limit lognormal distribution is simply $V_U(d) = V(d)/V(d_{max})$ for $d < d_{max}$ and $V_U(d) = 1$ elsewhere, where $V_U(d)$ corresponds to the upper limit distribution and V(d) corresponds to the lognormal distribution. This distribution function will also be skewed, as shown in Figure 4.6. Figure 4.6 shows examples of distributions for the three distribution functions, with cumulative distributions shown in the top graph and frequency distributions in the bottom graph. Both graphs are presented in terms of relative droplet diameters d/d_{50}. The spreading parameter n = 1.8 in the Rosin-Rammler distribution is chosen to give an approximate fit to the lognormal distribution with the chosen standard deviation (here $\sigma_x = 0.78$ in natural logarithmic units). The UL distribution has the same nominal median and standard deviation, but is truncated at $d/d_{50} = 3$. The top graph shows that the lognormal distribution is symmetric on a logarithmic x-axis, while both the Rossin-Rammler distribution and the UL distribution is skewed with a shortened high-end tail ($d/d_{50} > 1$). However, at the low-end ($d/d_{50} < 1$), the three distributions have almost the same shape.

The same tendency is found in the bottom graph. This graph is made by binning the diameters in equal logarithmic intervals, corresponding to the data obtained from the LISST instrument. In the output from that instrument, the top value of each bin d_n is 1.18 times the top value of the previous bin D_{n-1}, and the same increment is used here, i.e $d_n = 1.18\ d_{n-1}$. The values given on the x-axis in the bottom frame are median diameters in each bin, i.e. $d_M = (d_{n-1}\ d_n)^{1/2}$. The height of the columns represent the volume fraction contained in each bin, i.e. $\Delta V = V_n - V_{n-1}$. A close inspection of the bottom chart shows that the maximum bin volume fraction falls in the bin centered near $d/d_{50} = 1$ for all distributions, but with a slightly higher value for the Rosin-Rammler distribution ($d/d_{50} = 1.3$). However, for larger values of the spreading parameter, the peak diameter of the Rosin-

ED_001324_00000703-00017

Rammler distribution is found to approach the median diameter: with n = 2.5, the peak diameter is found to fall in the bin centered at $d/d_{50} = 1.1$.
While the arithmetic mean for a normal distribution is known to coincide with the median value, for a lognormal distribution, the arithmetic mean is given as $E = \exp(M + \sigma_x^2/2)$, where M is the logarithmic mean and σ_x is the logarithmic standard deviation. With the given parameters, M = 0 and $\sigma_x = 0.78$, this gives E = 1.36. We have estimated the arithmetic mean value for the Rosin-Rammler distribution from the binned distribution as $E = \Sigma\, d_i\, \Delta V_i$, summarized over all bins. With n =1.8, the arithmetic mean diameter was found to be $d/d_{50} = 1.09$, while for larger values of n, the arithmetic diameter was found to be closer to $d/d_{50} = 1$: with n = 2.5, the arithmetic mean was found at $d/d_{50} = 1.03$. The same method gave an arithmetic mean at $d/d_{50} = 1.34$ for the lognormal distribution, which is close to the theoretical value given above.

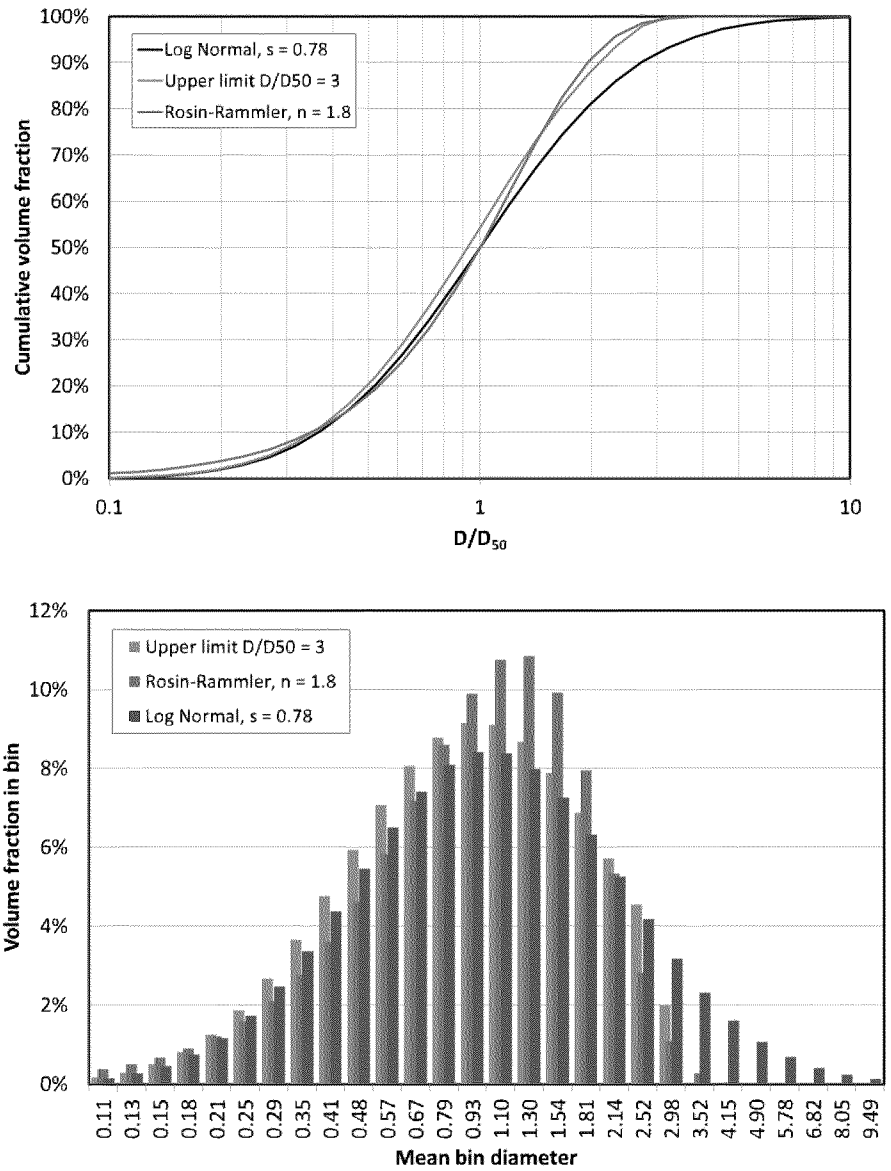

Figure 4.6: Comparison of lognormal and Rosin-Rammler distributions. Top: Cumulative distributions, bottom: Frequency distributions. The latter is based on data binned in equal logarithmic intervals, comparable to results from the LISST-instrument (see text).

The lognormal distribution may be linearized by plotting the number of standard deviations S that corresponds to a given cumulative probability V against x = ln(d) (see Figure 4.7, upper graph). The value of S(d) is computed from the given cumulative probability V(d), presuming that the distribution follows a lognormal distribution. In algorithmic notation, this can be expressed as S(x) = Norm.Inv(V(x), 0, 1), where Norm.Inv represents a function that returns the inverse of a normal distribution with a mean value M = 0 and standard deviation $\sigma_x = 1$. If the data are from a true lognormal distribution, the data points will then fall on a straight line y = a x, where the coefficient of proportionality will be $a = 1/\sigma_x$. By plotting an observed distribution in this way, we may thus assess whether the data follows a lognormal distribution, and if that is the case, determine the standard deviation of the distribution from the slope of the line.

The Rosin-Rammler distribution can be linearized in a similar way by plotting the variable –ln[1-V(d)] versus the diameter (see bottom graph in Figure 4.7). If the data follows a Rosin-Rammler distribution, the data will follow a power law function $y = b\ d^p$, where the exponent p = n and the coefficient $b = k/d_{50}^n$. This implies that by plotting an observed distribution in this way, we may assess whether the data follows a Rosin-Rammler distribution, and if that is the case, determine the median diameter d_{50} and the spreading parameter n of the distribution.

The examples shown in Figure 4.7 demonstrate the point, but also show that the Upper Limit distribution may look like a lognormal distribution at the lower end ($d/d_{50} < 1$), and as a Rosin-Rammler distribution at the upper end ($d/d_{50} > 1$).

We may also conclude that the peak diameter of the logarithmic binned distributions will coincide closely with the median diameter when the data fits a lognormal distribution. The same assumption may be made when the data fits a Rosin-Rammler distribution, but in that case, the median diameter may be slightly overestimated.

ED_001324_00000703-00019

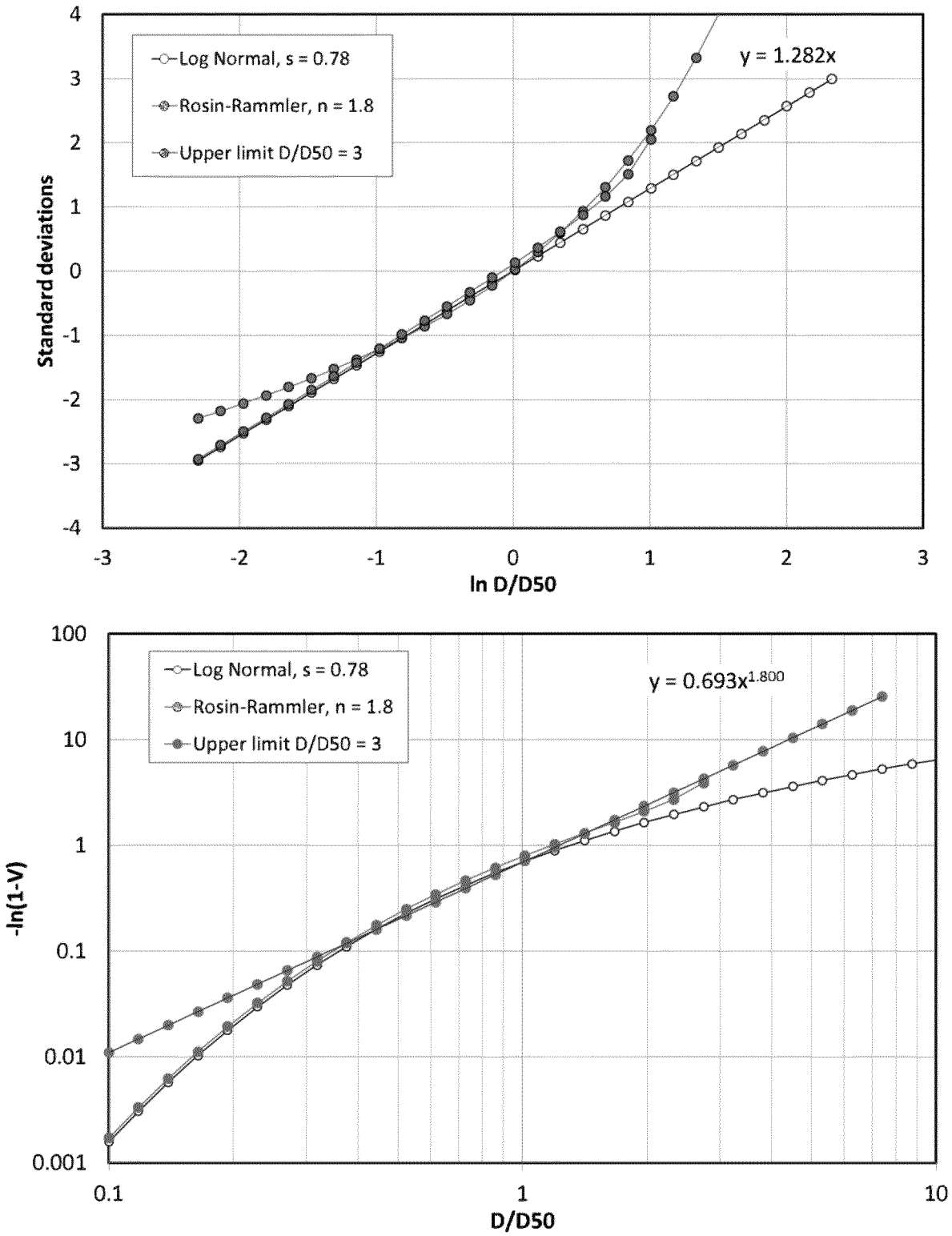

Figure 4.7: Linearization of lognormal and Rossin-Rammler distributions. Top: Log normal linearization. Bottom: Rosin-Rammler linearization.

5 Experimental

This section contains a description of the experimental methods and the experimental work performed in this project.

5.1 Selection of oil types

The experiments in this study are performed with the Norwegian Oseberg blend. Oseberg is a light paraffinic crude with high evaporative loss and is a representative candidate for a deep water high flow rate blow out scenario. However, the chemical composition and properties for such light oils can vary significantly and influence droplet sizes and dispersant effectiveness. Table 5.1 presents details for Oseberg Blend and MC252. The data for both oil types is from earlier weathering studies at SINTEF.

Table 5.1: Properties of MC252 and Oseberg blend.

	Macondo MC252 (ID 2012-0347)	**Oseberg blend** (ID 2012-0347)
Specific gravity (kg/l)	0.833	0.832
Pour Point (°C)	-27	-6
Viscosity (mPas at shear rate 10 s^{-1} and 40°C)	4	5
Asphaltene (wt%)	0.2	0.3
Waxes (wt%)	1.6	3.2
150°C – Evaporative loss (vol%)	27	22
200°C – Evaporative loss (vol%)	39	34
250°C – Evaporative loss (vol%)	50	45

Properties for different batches of Oseberg blend can vary. This batch had some higher wax content and slightly higher pour point compared to earlier batches. However, the same batch of oil is used for all experiments in this study. The oil was received from the Sture oil terminal in January 2012 and given the SINTEF ID 2012-0347. The oil IDs were tracked during the experimental work in the Tower Basin and each experiment is linked to this ID.

5.2 Selection of dispersants

Corexit 9500 was selected for this study since it was the main dispersant used during the Macondo incident and it is stored worldwide as a part of operational oil spill contingency. Two different varieties of Corexit c9500 are used in this study; Corexit EC9500A and Corexit EC9500A with reduced content of solvent (approx. double concentration of surfactants).

The first was labelled "CXIL0004" from Nalco and received in March 2012 (SINTEF ID: 2012-0062). The second was received from Nalco in June 2012 with the label "VX10612" and given SINTEF ID: 2012-0224. The dispersant was used as received and IDs were tracked during the experimental work in the Tower Basin and each experiment with dispersant is linked to a dispersant ID.

ED_001324_00000703-00021

5.3 Overview of SINTEF Tower basin

The basin tower was constructed and built in 2005, but was not assembled or tested before it was used in this project. An outline of the tower basin mounted into SINTEFs ice basin is presented in Figure 5.1. The mounted tower basin during the first filling with water is seen in Figure 5.2 and Figure 5.3 and a drawing showing the scaffolding/railing around the tower basin together with the ventilated hood and oil collecting system is shown in Figure 5.4. More details can also be found in Brandvik et al., 2013.

The assembling of the basin shell, the rebuilding of the hall to fit these type of experiments and the preparation of the necessary HSE arrangements demanded more resources than initially anticipated. The following activities were part of this preparation.

a. Mounting the different parts of the tower basin and making it leak proof
b. Establishing the necessary arrangements/procedures for filling and emptying the tower basin
c. Establishing the necessary HSE arrangements for this new type of large-scale experiments
   - scaffolding/railing around the tower and a staircase to reach the top section for inspection and sampling
   - ventilated hood to prevent light hydrocarbons / vapors from entering the laboratory hall. This allowed operators to avoid working with external air masks or other breathing protection.
   - overflow system to collect or skim off surfacing oil from the top of the tower
   - disposal system/procedure for the used oil and the large volumes (42 m^3) of water containing small oil droplets. The dispersion experiments create very small droplets with very long rising/settling times.

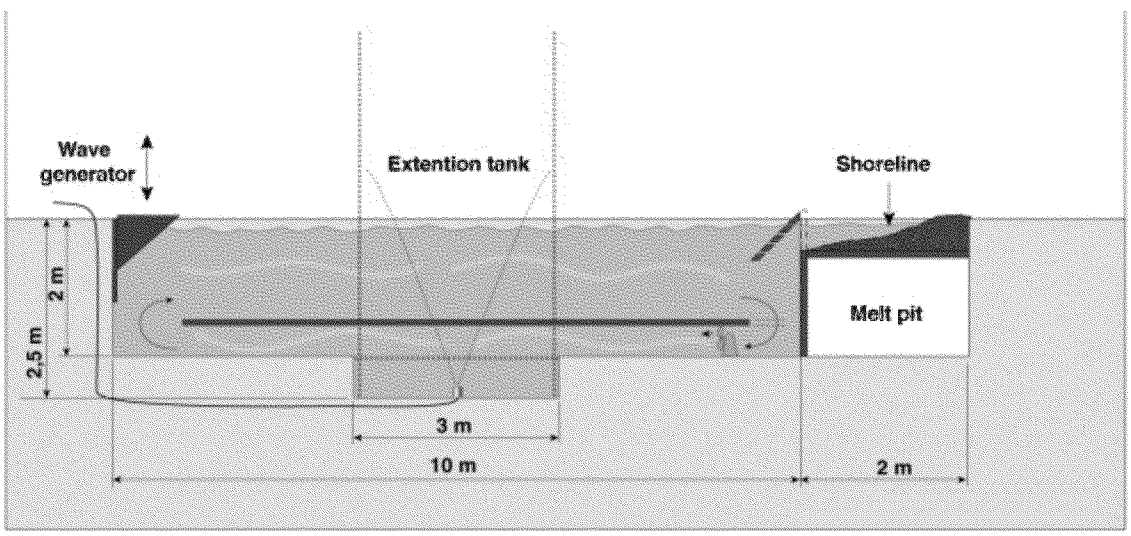

Figure 5.1: Overview of the tower basin inserted into the ice basin.

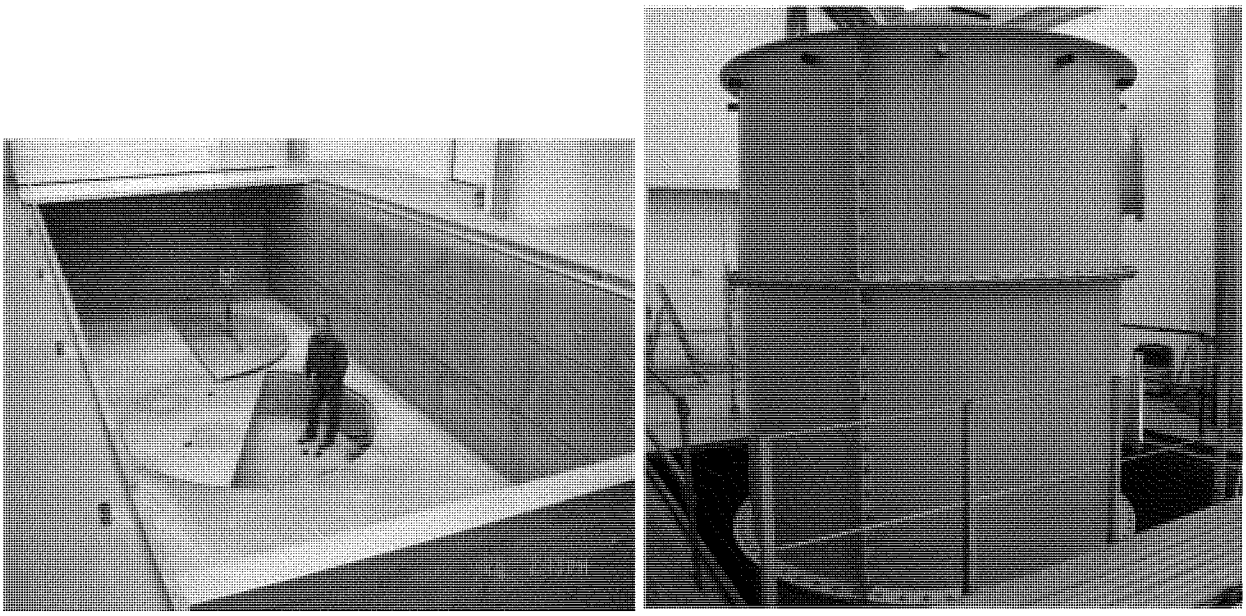

Figure 5.2: Ice basin without propellers and other equipment used for circulation showing the fundament for the Tower basin (left) and the initial mounting of the Tower basin (right).

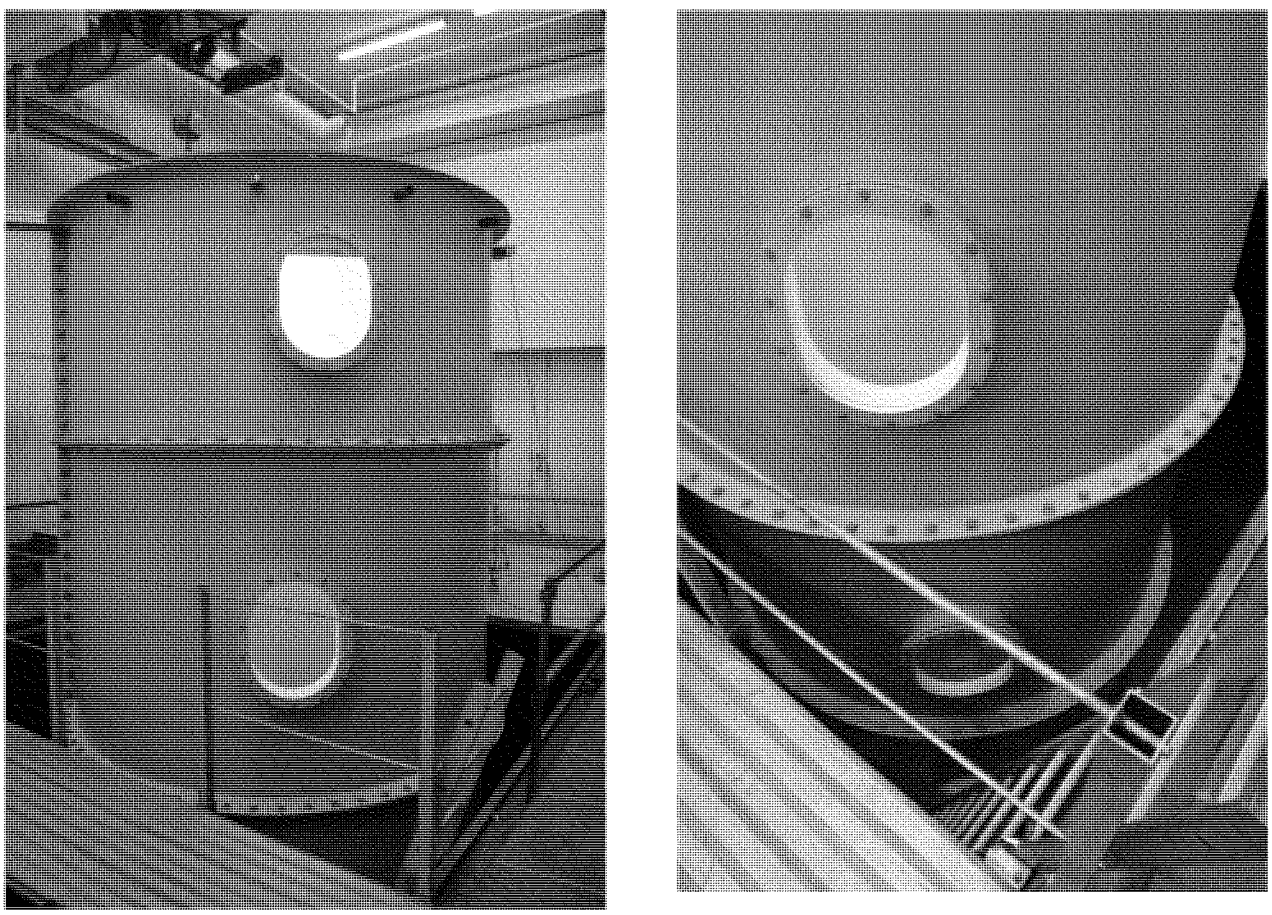

Figure 5.3: First filling of water in the SINTEF Tower Basin, January 2011.

ED_001324_00000703-00023

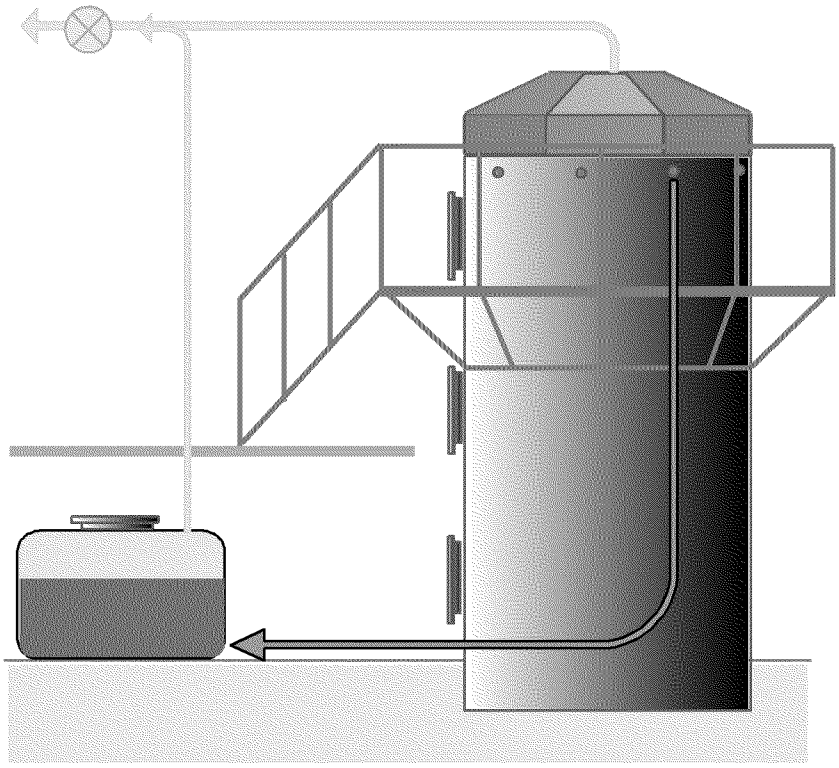

Figure 5.4: Principles for the scaffolding/railing around the tower, ventilated hood and overflow system to collect surface oil from the top of the tower.

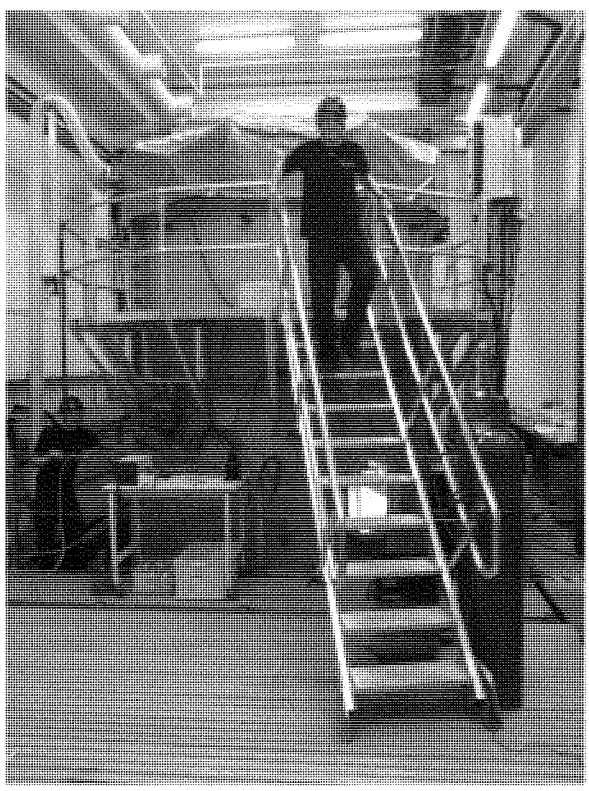

Figure 5.5: The Tower basin per March 2012 showing the ventilated hood, scaffolding, staircase and the railings to ensure safe working conditions.

Trying to fully simulate a deep water, large-scale oil and gas blow out in a 6 meter high basin is not possible. Therefore, we have focused on some important aspects and scaled down and simulate these. The main objectives have been to study oil droplet size distribution as a function of:

1. Oil release conditions (release diameter and release rates).
2. Dispersant to oil ratio (DORs).
3. Different dispersant application techniques.

The droplets are formed by turbulent droplet splitting immediately after the release nozzle where the oil/gas/water plume will quickly stabilize with respect to droplet size distribution. The plume will rise mainly due to the buoyancy of gas (air) bubbles and oil droplets. It is in this zone in the middle of the tank, approximate 3 meters above the release nozzles, where the droplet size distribution measurements are performed. The distance from the nozzle is based on dilution of the oil plume from the turbulent zone. Due to instrument limitations, this dilution should approximately be 100. This distance will also depend on the release rates.

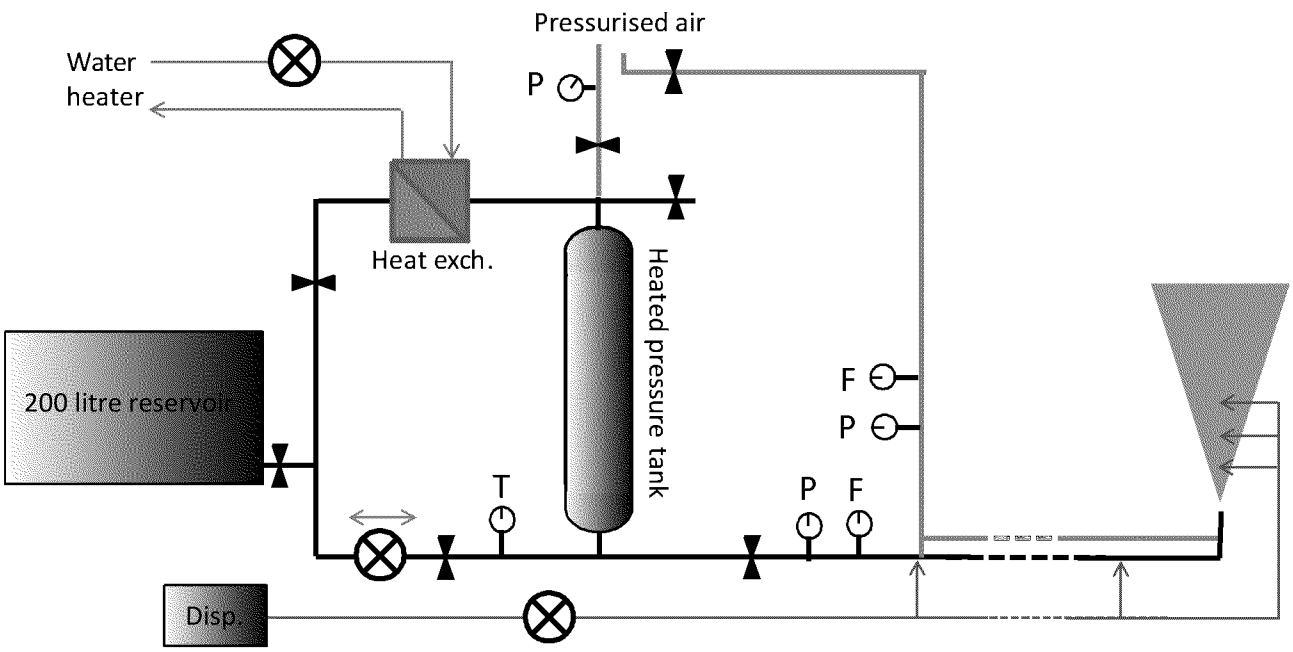

Figure 5.6: Principle overview of the set-up showing how oil, gas and dispersant are released during the experiments. The oil flow is controlled by regulating pressurized air (P) with a mass flow controller (F). The oil temperature (10-95 °C) is controlled by a heat exchanger. The dispersant is delivered by a high precision piston pump to several alternative injection points. Gas flow is controlled by pressure (P) and a mass flow controller (F).

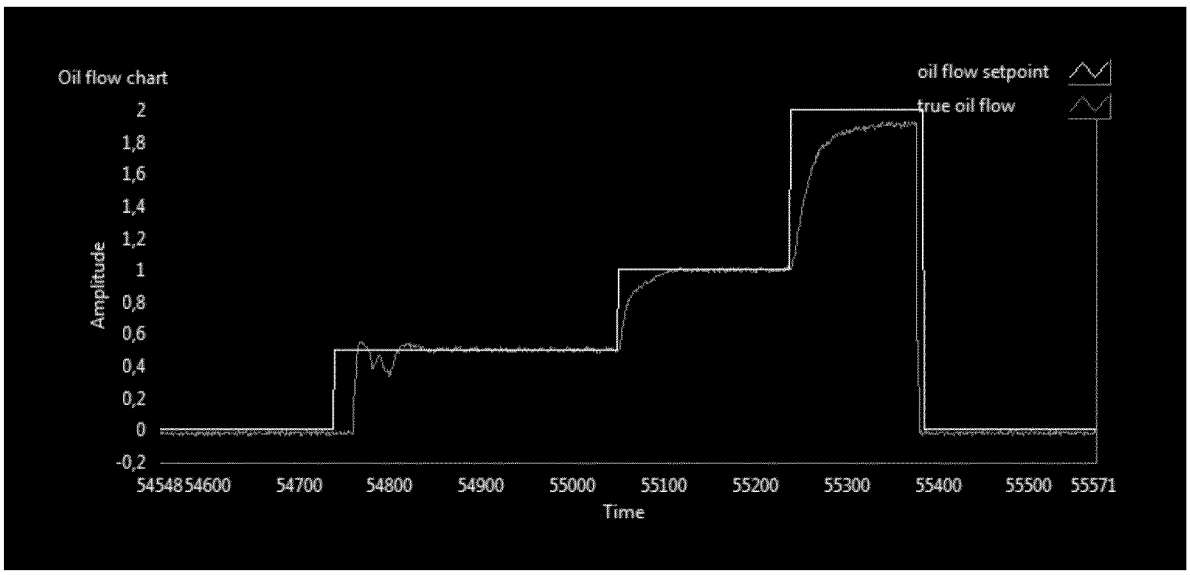

Figure 5.7: Oil flow rate (L/min) as a function of time during one Tower basin experiment. Both the set point (white) and the obtained values (red) are monitored and logged.

5.4 Description of a Tower basin experiment

A more specific procedure for operating the tower basin is described in operational procedures (Lab. procedure 507). This procedure is a part of SINTEFs general QA system for laboratory procedures.

A short version of the procedure for a blow-out experiment in the tower basin can be summarized like this:

a. Fill tower basin with water and check for leaks.
b. Install and test all release and monitoring equipment.
c. Check background values (particle/oil concentration, droplet size distribution, temperature, and pictures/video).
d. Determine and set test conditions (oil type and rate of gas (air)/oil).
e. Check and confirm status on monitoring and release equipment.
f. Prepare for experiment, background monitoring (three radial positions at approximately 3 meters above release nozzle)
g. Initiate experiment, start release of oil/gas (air)/dispersant (dependent of experiment type)
h. Monitoring of plume (3 x 3 minutes in three radial or horizontal positions)
   - Video cameras (3 to 6 cameras)
   - Oil droplet size distribution (LISST 100X, particle visual microscope (PVM) and macro camera/laser).
   - In-situ UVF monitoring of oil content/dissolved components and water sampling
   - Water temperature
i. Stop release
j. Settling of oil droplets and removal/skimming of surface oil
k. Emptying/disposal of used water containing small oil droplet and dissolved oil components according to lab. procedure
l. Cleaning and control of equipment.
m. Collection and initial quality control of monitoring data.

In general it takes 1-2 days to prepare for a Tower basin experiment, depending on the type of experiment. The experiment itself takes only 1-2 hours. After the experiments are finished, the cameras are recovered and the oil is left to settle overnight. The surface oil is skimmed off and the oily water is rinsed (if necessary, oil content < 50 ppm) by an oil-ware separator. Surface oil is collected and later delivered as hazardous waste, while the oily water is injected into the local sewer system according to SINTEFs discharge permit (low rates and oil concentration). Recovery and pre-treatment of data, cleaning the tank and equipment, rinsing of water and discharge usually takes 1-2 days.

Performing one Tower basin experiment a week has been the normal procedure in the project. From March to the end of May 2012 totally 16 experiments were performed. See Appendix A for an overview of all experiments.

5.4.1 Calibration of oil mass regulators

The following two oil mass regulators (see Figure 5.6) are used in this project.

Table 5.2 Mass regulators used in the project

Type	Range (L/min)	Period (experiments)
Digimesa FHK	0,1-5 l/min	March-April 2012 (Exp. 1 - 3)
Burkert S020 D8	0,8-30 l/min	April-June 2012 (Exp. 4 - 16)

The calibration data for the different regulators are presented in Chapter 6.2.4. Experiment numbers can be found in Appendix A.

5.5 Monitoring during an experiment

This chapter contains the description of the different monitoring techniques used during the blow-out simulation experiments. The monitoring was performed in the centre of the plume approximately 3 metres above the release point to ensure sufficient dilution of the oil & gas (air) plume. A suit of instrumentation was mounted on a piston operated platform which is inserted into the plume. The platform was mounted on a slide on the inner wall of the basin and its vertical position could be continuously changed.

Since documentation of oil droplet size distribution is central in this project, three different approaches are used to measure droplet size distribution of the rising oil droplets. The presence of a wide range of gas (air) bubbles in the plume complicates the measurements of the oil droplet.

a. The LISST-100X instrument is a laser difractometer for in-situ observations of particle size distribution and volume concentration. It also records the optical transmission, pressure and temperature. The instrument used in this project is a shorter version more suitable for laboratory work in confined areas.
b. Particle visual microscope (PVM)
c. High resolution camera and two green lasers defining a focal plane.

ED_001324_00000703-00027

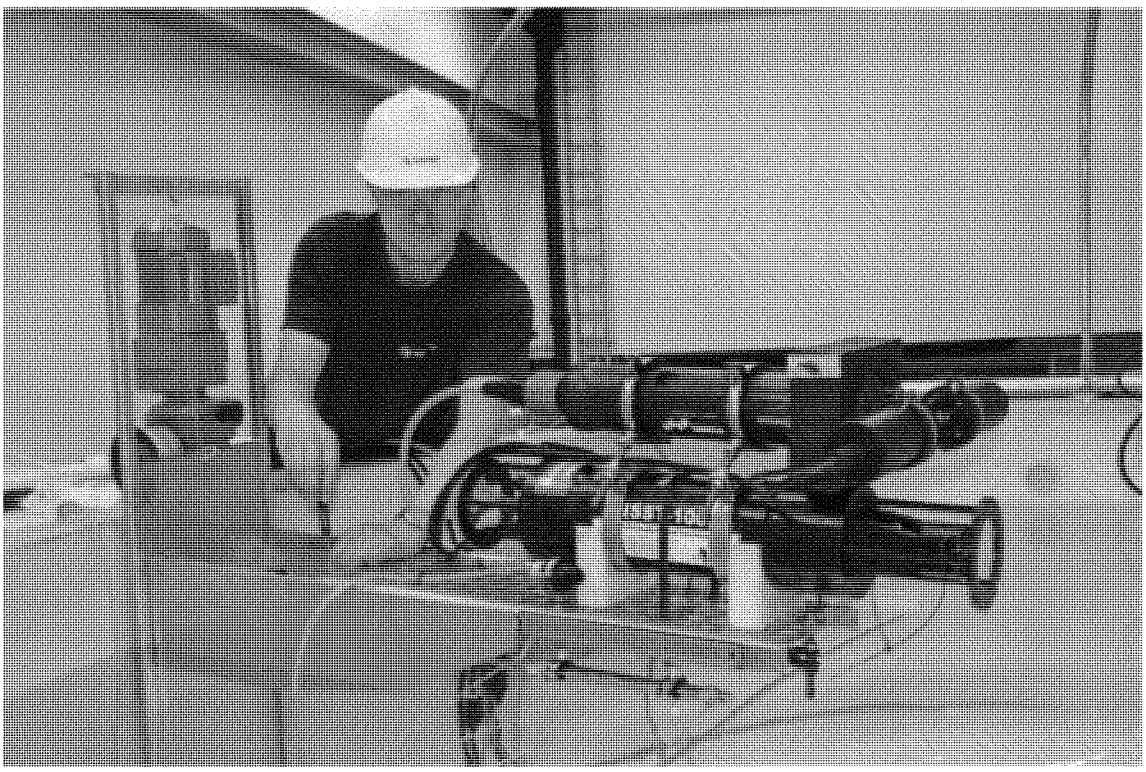

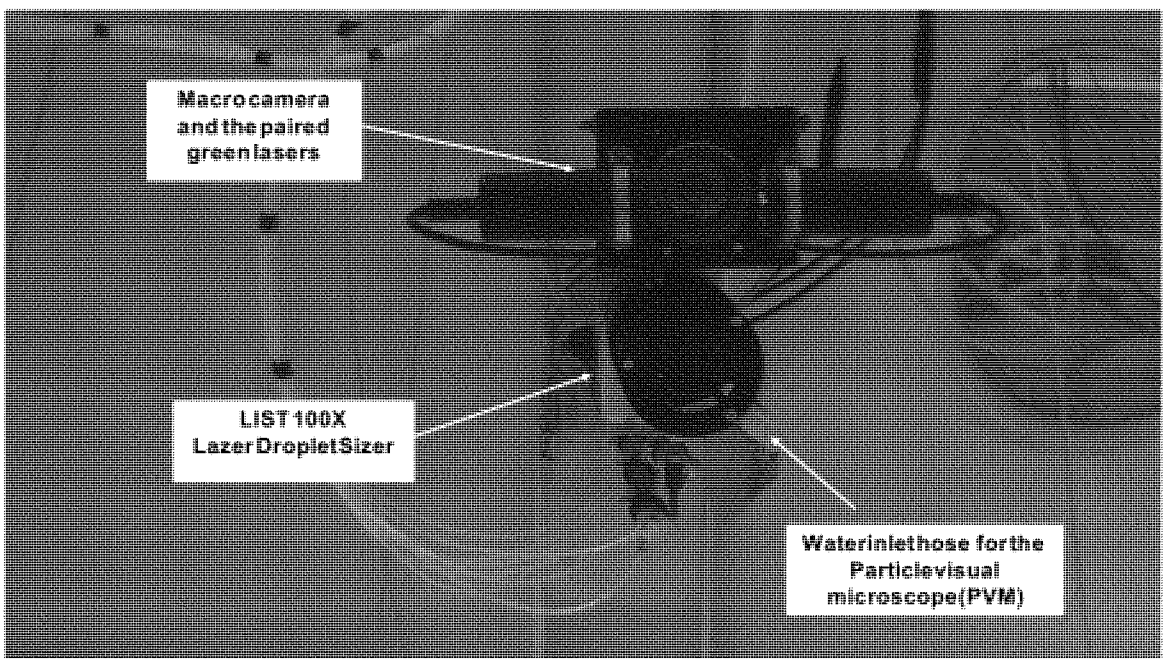

Figure 5.8: The three systems for monitoring droplet size distribution shown during adjustment over the water surface and submerged.

ED_001324_00000703-00028

5.5.1 In-situ macro camera

Specifications of the 5-megapixel Sony macro camera (GC2450) are given below:

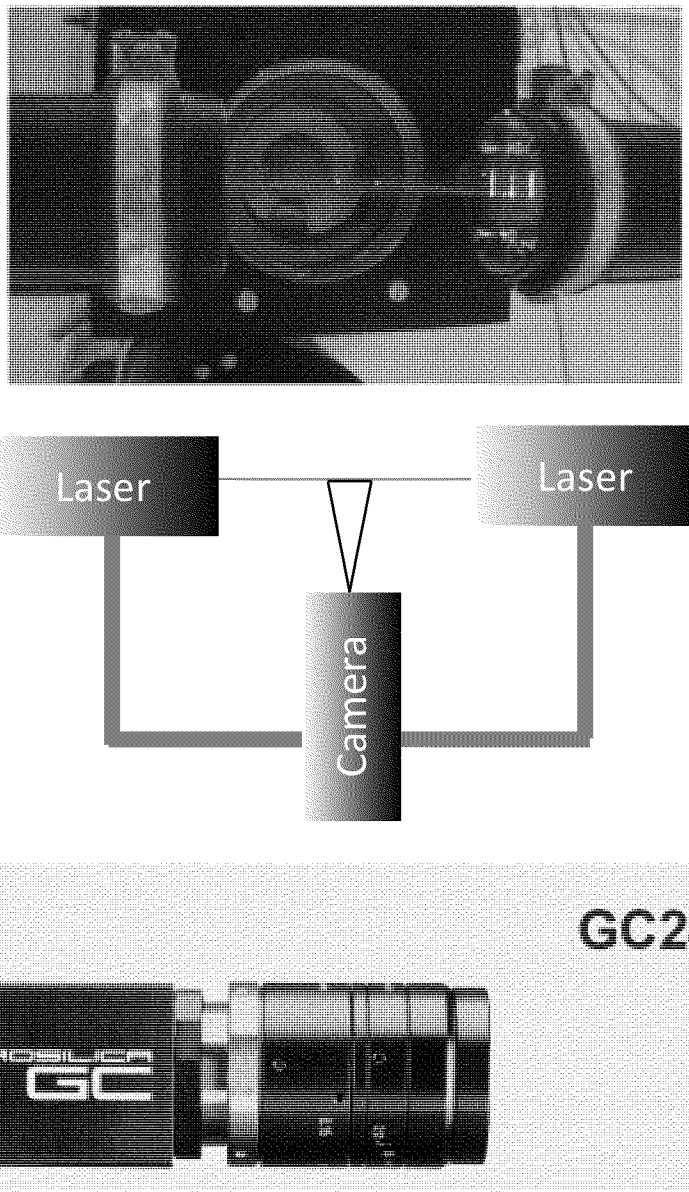

Figure 5.9: Close-up photo, a principle drawing of the macro camera and the green laser focusing plane and a picture of the camera module.

The built-in camera has the following specifications:

- Ultra-compact high resolution CCD camera - 5 Megapixels, 15 fps
- The 5-megapixel GC2450 is a very high-resolution CCD camera with Gigabit Ethernet output (GigE Vision®). The GC2450 has a frame rate of 15 fps at 2448x2050 resolution.
- The sensor used in the GC2450 is the high-quality Sony ICX625 CCD image sensor that provides high image quality, high sensitivity, and low noise.
- 5 Megapixels (2448x2050)
- Models used: GC2450, 2448x2050, 15 fps, CCD, mono

5.5.2 External Particle Visual Microscope – PVM V819

The PVM is a miniature version of the in-situ macro camera and is mounted as a probe in a water stream coming out of the tower basin. The water is not pumped, but flows out due to the ambient pressure at 3 meter depth in the Tower basin.

Figure 5.10: Illustration of the PVM probe and image analyser.

The Particle Visual Microscope has the following specifications:

- Illuminations Class 1M laser product
- Sources: 6 pulsed laser diodes
- Wavelength: 808nm
- Energy: 39µJ (at window), 6.5µJ (3mm beyond window)
- Imaging Field of view (nominal): 1075mm x 825mm
- Resolution: 2 µm
- Focus Adjustment: Manual
- Pressure Standard: Vacuum to 150psi (10bar)
- Probe Head Length: 163mm
- Diameter: 69mm

5.5.3 Light scattering sensor – LISST 100X

This method determines size distribution of an ensemble of particles, as opposed to counting type devices that size one particle at a time. The reason that laser diffraction is unaffected by composition of particles is that the scattering of laser light is observed at multiple, small forward angles. At these small angles, light scattering is determined almost entirely by light diffracted by the particle. The light transmitted through the particle makes only a weak contribution to the measured scattering. Since the light transmitted through the particle would experience the composition of the particle, i.e. its refractive index, and since it makes only a weak contribution to the observed scattering, the method of laser diffraction is mostly independent of particle composition. In the aquatic sciences, particle refractive index is poorly known. Thus, except for shape effects, laser diffraction offers an excellent method for size-distribution estimation. Shape effects are a matter of continuing research and no definite generalized guidelines are available to account for them by any method. Consequently, laser diffraction methods deliver the equivalent-spheres size distribution. By

calibrating for concentration with ISO standard natural particles, shape effects are empirically included.

The instrument is calibrated, both with a flow through cell and in the tower tank with a mono-disperse particle standard containing particles over a range of 6 – 346 microns.

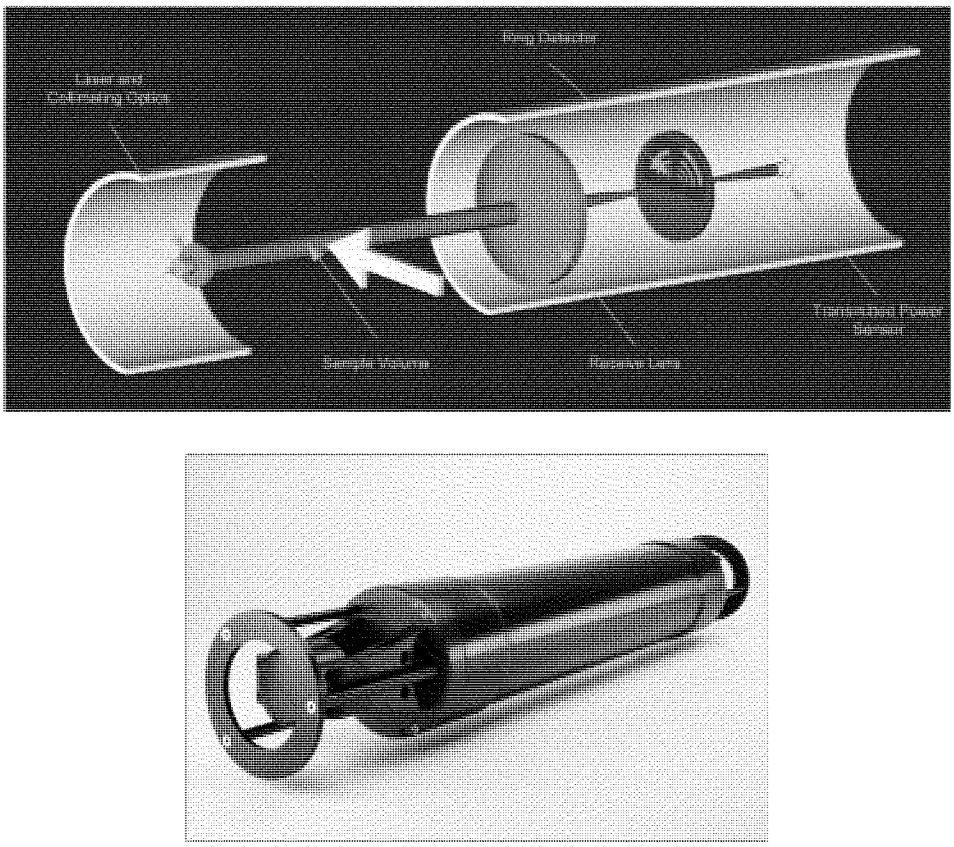

Figure 5.11: Principle drawing and close-up of the LISST

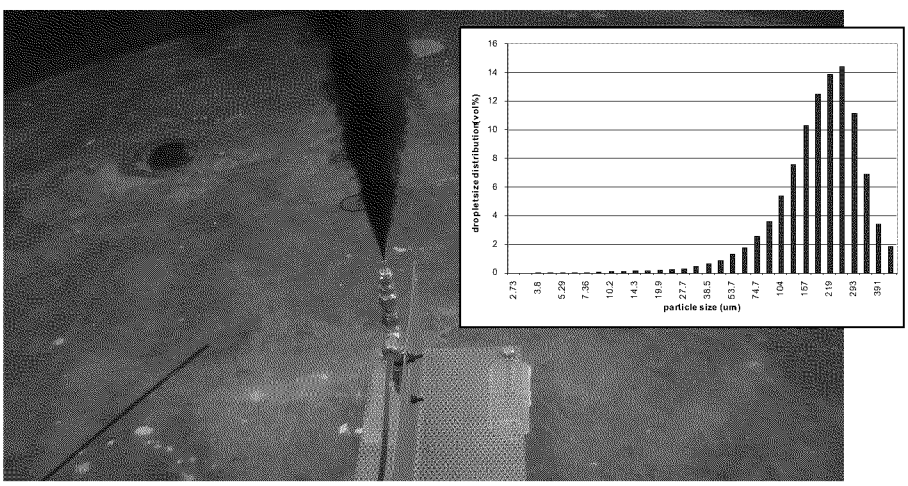

Figure 5.12: Initial release of model oil and an example of measured droplet size distribution (LIST 100X system).

5.5.4 Image analysis to produce droplet size distributions

The images from the in-situ macro camera or the Particle Visual Microscope are via image analysis, particle identification and diameter identification used to produce a droplet size distribution, see Figure 5.13. This process is performed with a program utilizing the Visual Basic procedures in LabView.

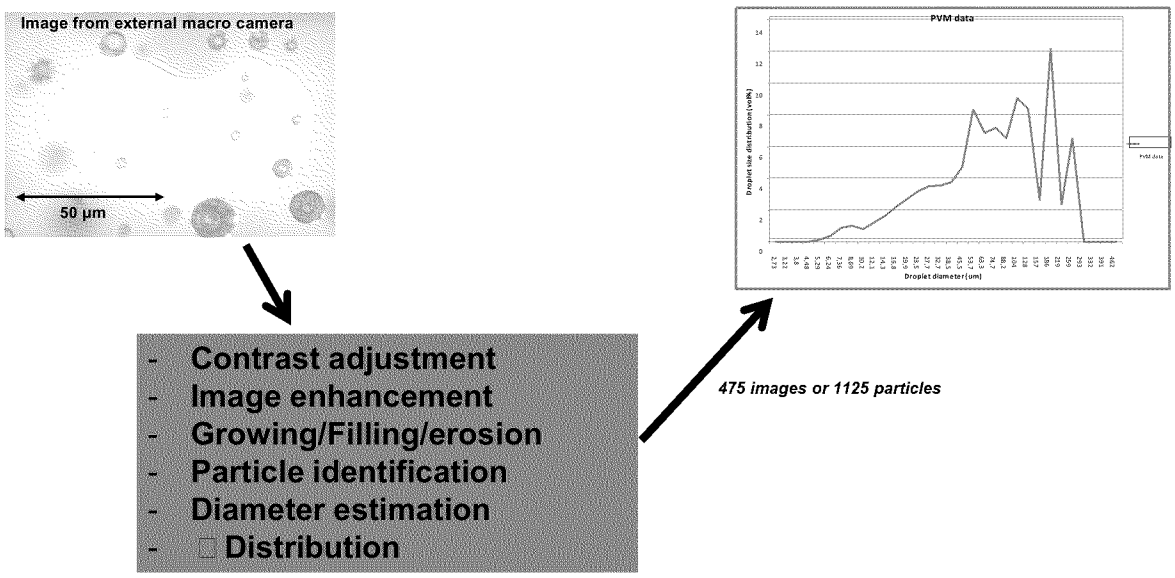

Figure 5.13: Principles for the image analysis producing a droplet size distribution from the in-situ macro camera or the particle Visual microscope.

5.5.5 Calibration of droplet size measurement

The LISST instrumentation was calibrated in a container with natural sea water (900 Litres). Different standards of polyethylene mono disperse with different size (6 – 346 microns) were injected into the experimental container used for the verification.

Commercial standard material in the size range of interest is not available. The needed standards were for this reason synthesised by SINTEFs Materials and Chemistry, Department of Synthesis and Properties, Research team: Polymer Particles and Surface Chemistry.

Table 5.3: Mono disperse standards used in LISST verification

STD ID	STD micron	STD Volume	STD Conc. weight%	mL added	ppm (900L)	Relative conc. weight%
1A	6	1000	1	240	2.7	0.5
2B	20	1000	2	240	5.3	1.0
3	38	1000	1	1000	11.1	2.0
4B	80	1000	4	1000	44.4	7.9
6	165	1000	42	120	56.0	10.0
8	346	2000	37.5	130	27.1	4.8

ED_001324_00000703-00032

The corresponding droplet size distribution was recorded by the LISST instruments (see Figure 6.3).

Figure 5.14: Verification of the LISST instrument in a 900 Litre container injecting batches of mono disperse particles.

A particle standard is also injected in front of the LISST instrument before a Tower basin experiment was initiated as a part of the general quality assurance procedure.

5.5.6 Water sampling

Water samples were taken in the same position in the tank as droplets sizes are measured. The water was sampled through a short flexible hose located on the moving sampling platform. The water samples were analyzed for oil content by solvent extraction (dichloromethane) and UV adsorption spectroscopy. See SINTEF laboratory procedures for further details.

5.5.7 In-situ measurement of oil in water (UVF cell)

The overflow hose (no pumping) used for water sampling above was also used for monitoring of oil-in-water content (droplets and dissolved components). This was done by ultraviolet fluorescence (UVF) with an UviLux flow-through cell. The water flows through this cell before being sampled. The set up used to calibrate the UVF instrument involved pumping a solution with a known concentration of dispersed oil through the cell as shown in Figure 5.15.

ED_001324_00000703-00033

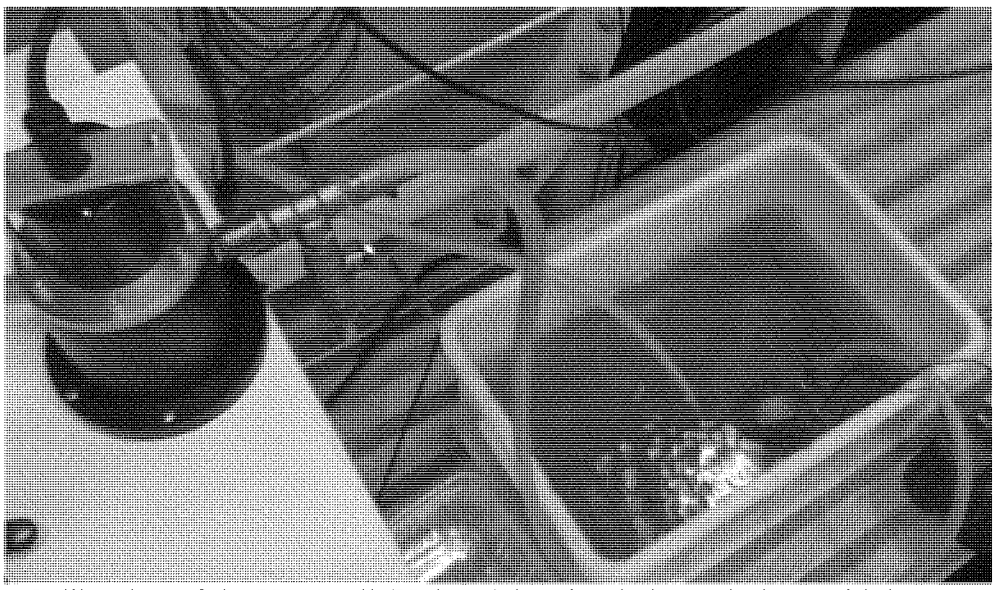

Figure 5.15: Calibration of the UVF cell (UviLux) by circulating solutions with known oil concentrations.

5.5.8 Oil sampling

Oil sampling was performed from two different locations. One is located together with the LISST and in-situ camera and used for water sampling. The other is located 1.5 meter above the nozzle and is used for more concentrated oil samples (more oil, less water). The oil that was sampled from this location was used for interfacial tension analysis (when dispersants are applied).

5.5.9 Video documentation

Three to nine HD video cameras (1280 x 960 pixels) were used to document the conditions during a Tower basin experiment. The cameras were mounted to monitor the following locations:

a. Conditions around the release nozzle (dispersant injection into the oil/gas(air)/water stream)
b. Nature of the rising plume
c. Downward looking camera from the top section of the tank giving an overview of the experiment

5.6 Interfacial tension measurements

Crude oil - sea water interfacial tension (IFT) plays a key role in the process of oil droplet formation during oil spills. Addition of dispersants reduces the interfacial tension between oil and sea water (brine) that subsequently promotes the formation of a larger number of small oil droplets when surface waves entrain oil into the water column. The effectiveness of chemical dispersion is known to depend on the specific combination of oil type, dispersant composition, dispersant concentration (dispersant-to-oil ratio), and the environmental conditions (temperature, waves, pressure etc) under which dispersion occurs. Depending on different dispersant to oil ratios and types of crude oils, the IFT between oil/brine/dispersant interfaces ranges from 28.5mN/m to an ultra-low value of 0.0002 mN/m (Khelifa and So., 2011).

Numerous methodologies have been developed for the measurements of interfacial tensions. But all different approaches have certain limitations. Oil/water IFT measurements are generally based on

drop methods e.g. spinning drop and pendant drop (Miller et al., 2001). These methods can also be used to measure oil/water IFT when dispersants are used. At ambient conditions, relatively high values of IFT (> 1mN/m) are traditionally being measured by using a pendant drop technique and ultra-low values (< 0.1mN/m) are measured with a spinning drop method (Zhang et al., 2001). We used the spinning drop method for the IFT measurements of oil/water/dispersant system in this project.

5.6.1 Spinning drop method

In the spinning drop method [SDM], two immiscible fluids are placed in a capillary tube, which is rotated, as shown in Figure 5.16. Fluid A (oil droplet) is the less dense fluid, while fluid B (sea-water) is the more dense fluid. The centrifugal field generated by rotation forces keeps the less dense fluid in the centre of the capillary tube where it forms an elongated drop. The configuration of the drop is determined by the balance of the centrifugal force and interfacial tension force. The centrifugal force elongates the drop, while the IFT suppresses this elongation to minimize the interfacial area. In the pendant drop method, gravity forces are applied for drop deformation, while SDM employs centrifugal forces (Liu, 2007). Determination of interfacial tension is related only to the diameter and does not require measurement of the drop volume.

This method is perfectly suitable for measurement of ultra-low tensions and the measurable values of IFT may range from 0.0005 to 0.5 mN/m (Zhang et al., 2001). Oil/sea-water/surfactant interfaces for ultra-low IFTs values are commonly measured by spinning drop technique (Khelifa and So., 2011), (Liu, 2007), (Zhu et al., 2008) and (Standness and Austad., 2000).

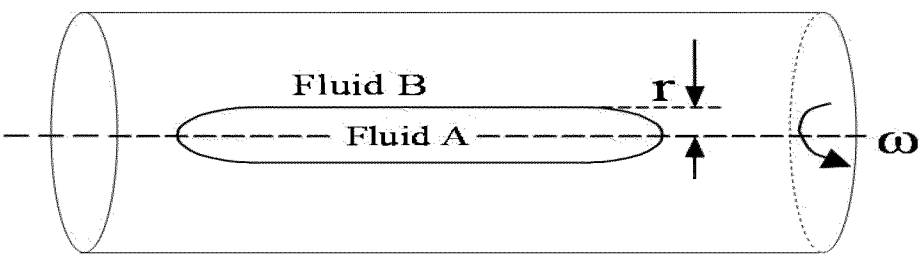

Figure 5.16: Schematic of the spinning drop method

For the interfacial tension measurements by spinning drop method, the Dataphysics Spinning Drop Tensiometer SVT-20N with control and calculation software SVTS 20 IFT was used (Figure 5.16). The Julabo F12-ED Refrigerated and Heating Circulator was used for temperature control. Disposable 1ml plastic syringes were used to inject the oil sample into the SVT 20N capillary tube.

ED_001324_00000703-00035

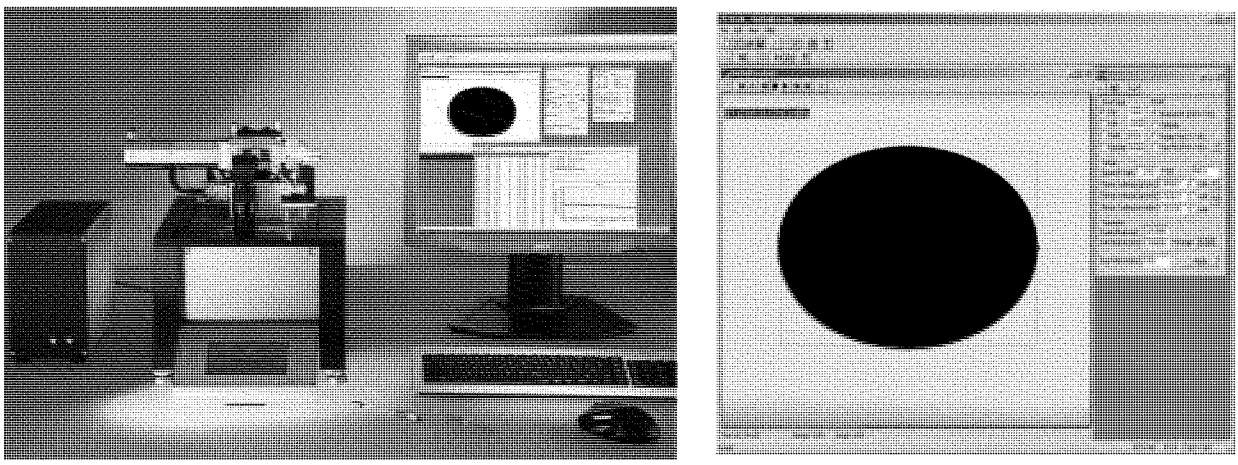

Figure 5.17: The Dataphysics Spinning Drop Tensiometer SVT-20N and its software used to measure small interfacial tension values of oil/water/dispersant interfaces.

Prior to each measurement, the capillary tube was rinsed three times with dichloromethane (DCM), acetone and deionized water, dried with nitrogen gas, and then rinsed three times with the sea-water. The capillary was carefully filled with the sea-water (outer phase liquid) to ensure the absence of air bubbles (Figure 5.18A). After the filling of capillary with sea-water, the open side of the capillary (Figure 5.18B) was closed and inserted into the measuring cell.

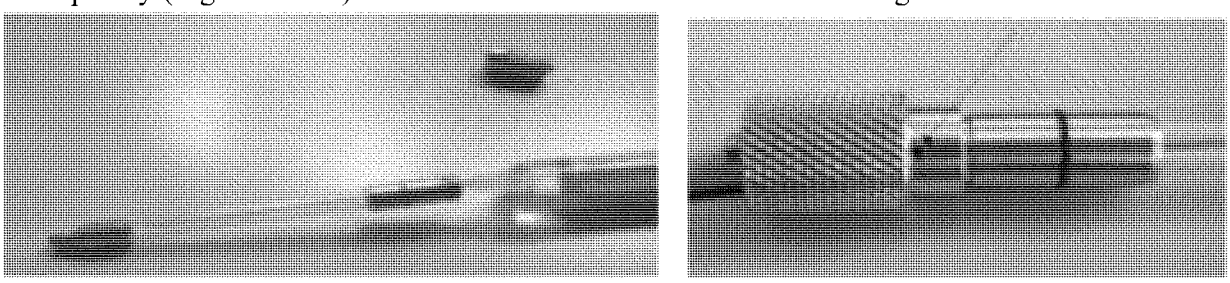

Figure 5.18 A-B: Filling of capillary with the sea-water (outer-phase) and closed capillary with septa holder

After closing the quick lock on the motor mounted the plastic protection cover on the measuring cell. The injection of a drop of the oil sample (inner phase) into the filled capillary was done by use of the 1 ml syringe with a long needle. Depending on the oil sample, the capillary may be stationary or rotating when the drop of oil is injected and the rotation speed may also vary. Measurements of IFT were taken as soon as the drop elongation was stable. Depending on the interfacial tension, different oil samples have different volumes of droplet. Parent oil and their mixture with low DOR formed relatively big droplets while oil with high DOR formed very small droplets, Figure 5.19A, B, C and D. Each measurement was run for 30-60 minutes and repeated at least two times. The reported IFT values were the mean IFT of different droplets measured during first 50-150 seconds.

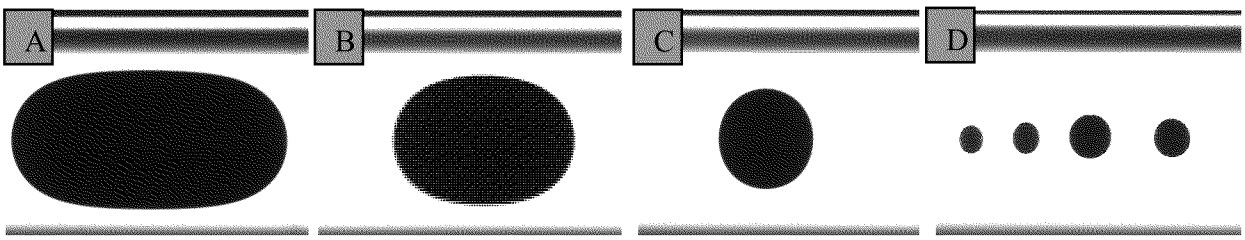

Figure 5.19: Oil droplets with different DOR; A) Oil alone, B) DOR: 1:500, C) 1:250, D) 1:50

5.6.2 Oil sampling for IFT measurements

During different injection sequences of dispersants into the oil, oil/water samples were taken 1.5 meters above the nozzle after 60 seconds of each dispersant injection. Each oil/water sample was collected in a 1 litre, long-necked measuring flask. Oil appeared as droplets depending on the DOR and method of application. Oil settled as a layer in the narrow neck of the bottle and was collected for IFT measurements after 24 hours. The settling time was important for collecting the smaller droplets in experiments with high dispersant effectiveness. The collected oil samples were stored in a dry and cool place overnight. No homogenization or heating was done before the IFT measurements.

ED_001324_00000703-00037

6 Results

6.1 Overview of experiments

The Tower Basin experiments reported from this study were performed from March to June 2012. Totally, 16 experiments were performed in this period. Each experiment usually takes a week, consisting of two days of preparation, one day for performing the experiment and another two days for cleaning and post processing of data. A summary overview of the experiments is given in Appendix A. The experiments were divided into the following groups or phases.

1. **Initial experiments** (Experiments 1, 2 and 15): Initial testing to document calibration of monitoring equipment and find suitable conditions (nozzle size and flow rate) for the later experiments. Experiments with oil:air and water:air.
2. **Flow rate experiments** (Experiments 5-7 and 14): Droplet sizes as a function of three flow rates and three nozzle sizes (0.5, 1.5, and 3 mm). Experiments marked with red circles in Figure 6.1.
3. **DOR testing** (Experiments 3, 11 and 16): Droplet sizes as a function Dispersant to oil ratio (1:1000-1:25) and interfacial tension. Experiments with premixed dispersant (Corexit 9500). Blue experiments and, to some degree, blue centre point in Figure 6.1.
4. **Dispersant injection techniques** (Experiments 5, 10, 12 and 13): Droplet sizes as a function of different dispersant injection techniques (simulated insertion tool, wand and injection into the oil jet). Blue centre point in Figure 6.1.
5. **Testing with warm oil** (Experiment 13): Experiment with cold/warm oil and different DORs. Heater used to raise temperature of the oil before injection. (Experiments 22, 23, 27).
6. **Testing with an alternative dispersant** (Experiment 16): Testing with Corexit 9500A with reduced solvent content at different DORs (centre point in Figure 6.1).

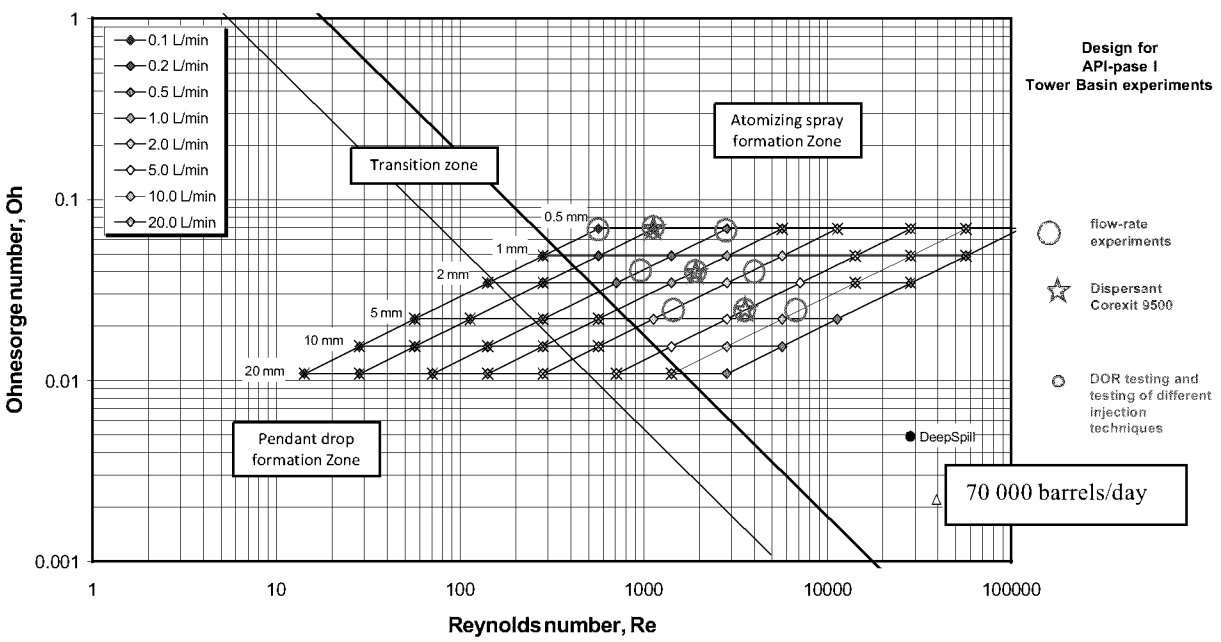

Figure 6.1: The different types of Tower basin experiments performed in the second part of this project plotted in the Ohnesorge vs. Reynolds number diagram (see Figure 4.3 for details).

ED_001324_00000703-00038

The background or basic theory for the initial experiments (rate and turbulence levels) is based on earlier tank experiments in smaller scale described in Chapter 4 Droplet formation in turbulent flow (see Figure 4.3). This figure presents the release conditions based on Ohnesorge vs. Reynolds number and has been used in this study to find a suitable starting point for the initial testing and to determine the total design of this study. The solid lines drawn in an Ohnesorge vs. Reynolds number in Figure 4.3 indicates the different droplet formation regimes for oil jets in water (without air/gas). Three different zones are indicated; Pendant drop, Atomizing and a transition zone. The experiments in this project were all performed in the Atomization regime in Figure 4.3.

6.2 Initial experiments

The main objectives with the initial experiments were to test and verify the main components of the tower basin (release and monitoring equipment). These experiments were also needed to see how often it was needed to change the water and to determine the time/resources needed for each experiment.

6.2.1 Ultra Violet Fluorescence sensor

The initial experiments were used to test and verify the sensors used to quantify the oil concentrations in the oil/gas (air) plume during a tower tank experiment. Water samples were taken 3 meters above the release in the same position as the LISST and were directed through the UVF cell.

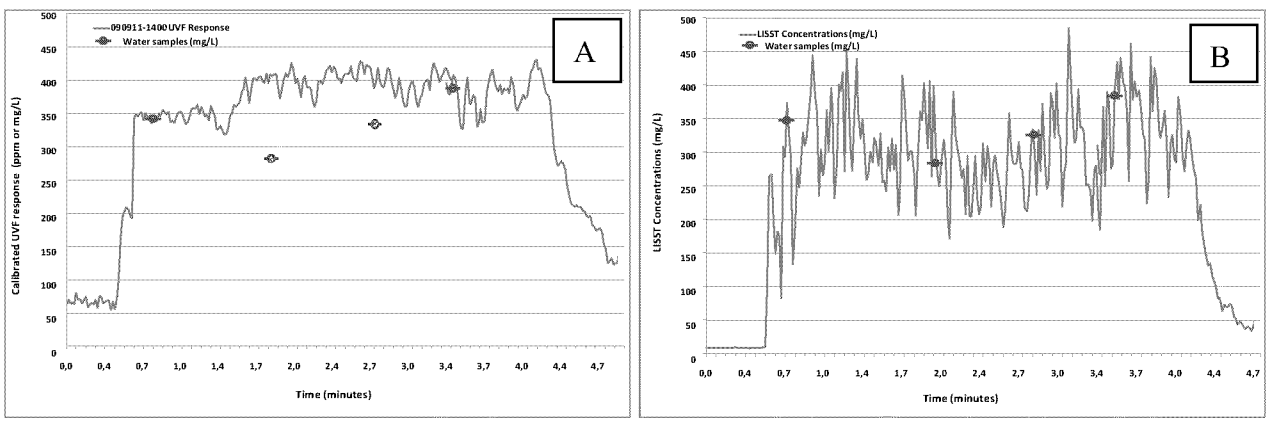

Figure 6.2: Comparison of measured oil concentration (red circles – quantified from water samples) with oil concentrations measured in-situ with UVF cell (A) and LISST (B). Vertical axes are measured oil concentration (ppm) and horizontal axes are time (minutes).

Results from the initial experiments, see example in Figure 6.2, showed that the measured oil concentration from the LISST (B) correlated better with the measured values from the water samples than the UVF sensor (A). This was as expected since the concentrations were high (50-350 ppm) and there was a variation in droplet sizes, which influences the UVF sensor.

The high oil concentrations are also above the linear response range for the UVF cell, indicating that a more thorough calibration of the UVF cell would be useful. The wide range of droplet sizes during the Tower basin experiments is also a challenge for the UVF cell. Fluorescence is a surface phenomenon and the difference in total surface is strongly dependant of droplet sizes. A shift from

ED_001324_00000703-00039

230 µm to 70 µm gives a very large increase in surface area and a large increase in response from the UVF cell even if the concentration is constant. The oil concentrations from the LISST are calculated from the measured concentration of droplets in the different size groups or bins. This gives concentration readings from the LISST that are not biased in relation to droplet sizes. This is also seen in Figure 6.2 (right). However, oil concentrations in the rising oil and gas (air) plume is not a critical parameter to fulfil the objectives of this project since they can be calculated from the release rates and dilution factors.

6.2.2 Verification of droplet size measurements

The droplet size measurements from the LISST instrument were verified with a mixture of polystyrene particle standards (6, 20, 38, 80, 165 and 346 µm). Comparison of the LISST measurements and the calculated distribution of the standard mixture are shown in Figure 6.3, see chapter 5.5.5 Calibration of droplet size measurement for details.

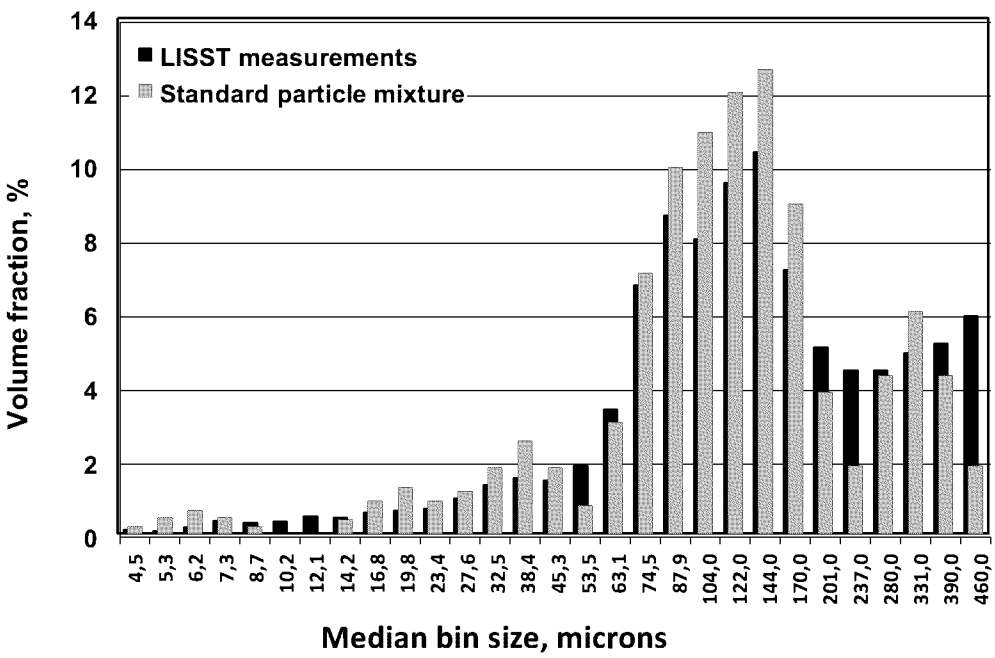

Figure 6.3: Droplet size distributions from the calibration experiments with the LISST instrument comparing measured and real distribution of the standard particle mixture.

A particle standard (80 and 346 micron) was also injected in front of the LISST instrument before Tower basin experiments were initiated as a part of the general quality assurance procedure.

6.2.3 Quantification of droplet sizes by image analysis

The data obtained from the two image based techniques (In-situ macro camera and the external PVM) contained very limited information regarding sizes of the large droplets in most experiments. This is probably due to the small focusing area of these macro methods (mm range) combined with the short time for data acquisition (usually 30 seconds). During this period a very limited number of large droplets were captured and quantified on the images.

Due to this limitation the images were only analysed and used for the large nozzle experiments (3 mm) and low flow rates (5 and 8 L/min). In these experiments the maximum peak of the distributions were not visually identified in the 2-500 micron range obtained by the LISST.

6.2.4 Verification of mass flow regulators

The mass flow regulators used in this study have been calibrated and the results are shown in the table below.

Table 6.1: Mass flow regulator verification

Type	Low		Medium		High	
	Setting	Measured	Setting	Measured	Setting	Measured
Digimesa FHK	0.10	0.12	1.5	1.49	3.0	2.96
Burkert S020 D8			1.5	1.20	2.5	2.50

6.2.5 Reproducibility within and between experiments

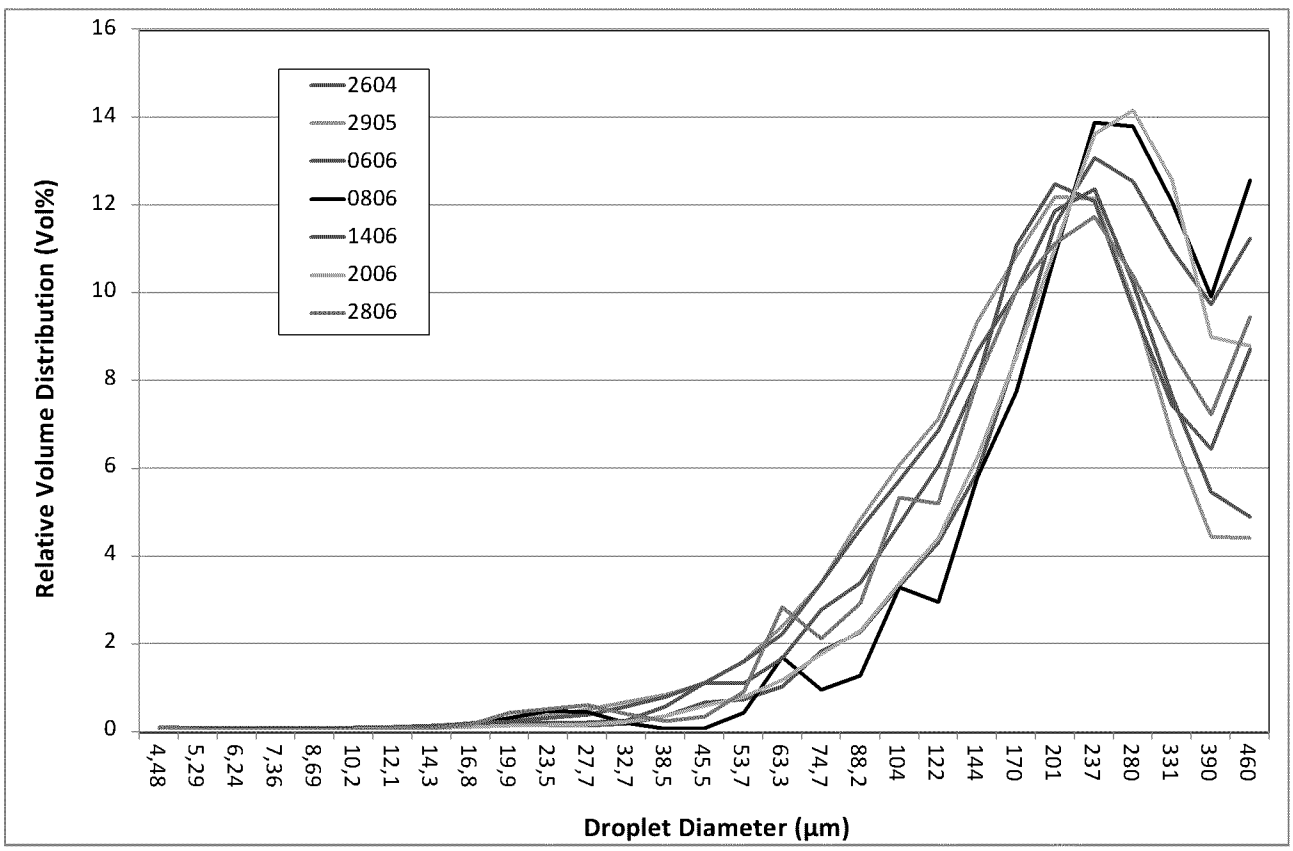

Figure 6.4: Variation in Tower basin experiments between experiments (April – June 2012). Relative droplet size distribution (volume %) for 7 individual experiments with the same experimental conditions (1.5 mm nozzle and 1.5 L/min) measured with LISST instrumentation in SINTEF Tower Basin.

ED_001324_00000703-00041

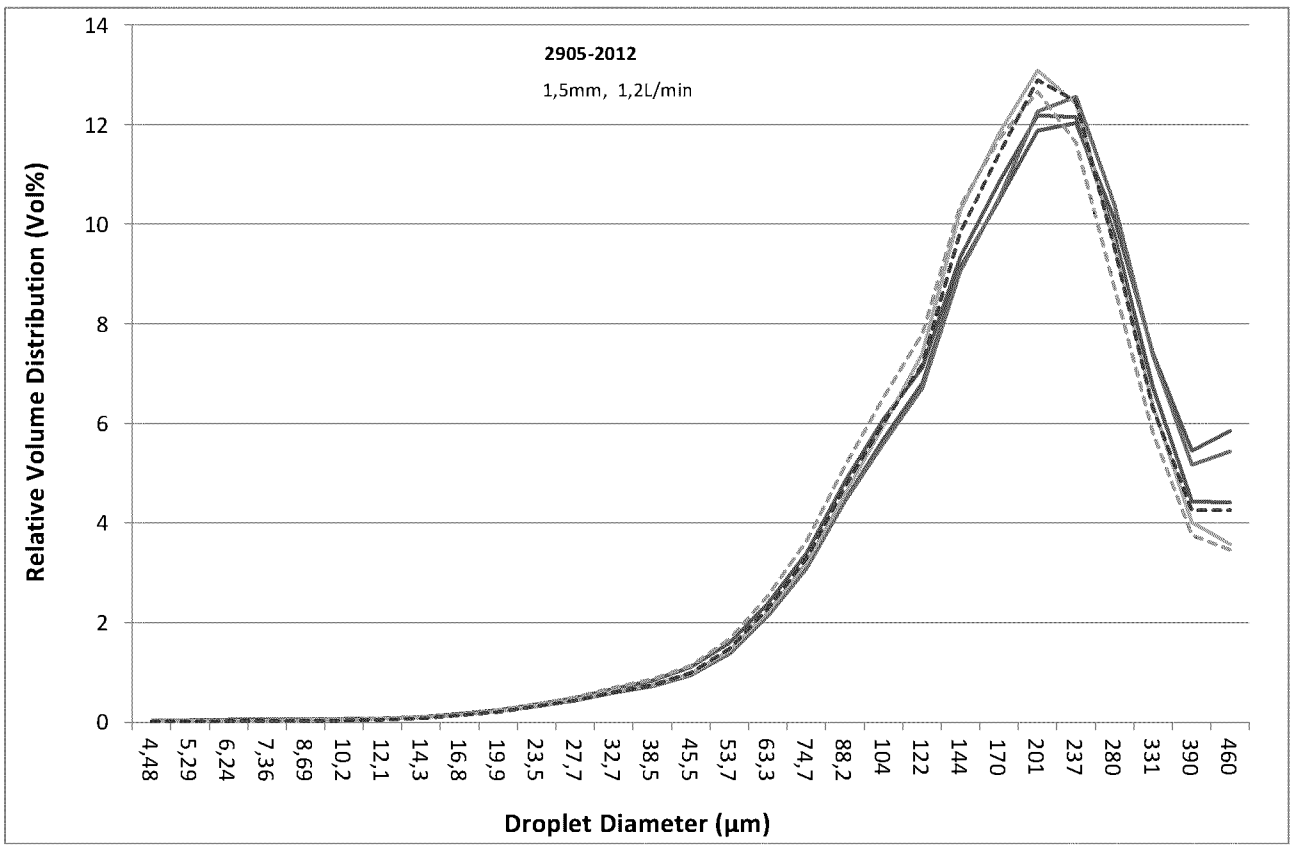

Figure 6.5: Variation within one Tower basin experiment (29. May 2012). Relative droplet size distribution (volume %) for 6 different experimental periods (90 seconds) within one Tower basin experiment with the same experimental conditions (1.5 mm nozzle and 1.2 L/min) measured with LISST instrumentation in SINTEF Tower Basin.

6.3 Flow rate experiments

The data generated in this activity are used to verify and further develop the algorithms used to estimate droplet size distributions as a function of flow rate, nozzle size and oil type (Weber number estimation or scaling), see chapter 4.2 Weber number scaling for details.The following table describes the main part of the experimental work.

Table 6.2: Experimental conditions for the flow rate experiments

Nozzle diameter:	0.5, 1.5 and 3 mm
Flow rates:	0,1 - 8 L/min
Gas-oil-ratio:	Only oil

These experiments (3 nozzle sizes and 3 flow rates for each nozzle) were performed with oil alone with no gas (air) present. The main reason for this approach was that the instrumentation for measuring oil droplet sizes cannot distinguish between oil droplet and gas bubbles. However, some initial experiments were performed with oil and gas (air) and injection of dispersants.

The results from the three nozzles 0.5, 1.5 and 3 mm are presented in Figure 6.6 and Table 6.3. The figure presents the relative volume distributions and the median bin size for each bin is used on the logarithmic x-axes.

Since the LISST is detecting noise or "non-oil" particles in the water in the three smallest bins (2,7, 3,2 and 3,8 microns), these bins are excluded from the relative distributions. Including this noise would introduce a systematic shift in the calibrating data set towards smaller volume median droplet sizes (VMD).

The histograms from the droplet size distributions in this study are presented as graphs in this report. This is not strictly correct since the data are discrete and not continuous. However, graphs were used since projecting several histograms on top of each other is visually difficult to interpret.

The graphs presenting the droplets size distributions are usually averages of 30 individual LISST measurements measured over 30 seconds. For the smallest droplets each bin represents thousands of droplets, while for the largest droplets each bin usually represents an average of 5-20 droplets.

The volume median droplet sizes (VMD) were calculated from both the relative volume distributions (maximum peak) and the cumulative distributions (50% volume). If the assumption that the data can be approximated with a log normal distribution is valid, the difference between these two measures of VMD should be very small. However, for some of the distributions, especially with high VMDs e.g. with the 3 mm nozzle in Figure 6.6, the complete distribution is NOT covered by the distribution. For these distributions the cumulative VMD will be underestimated.

ED_001324_00000703-00043

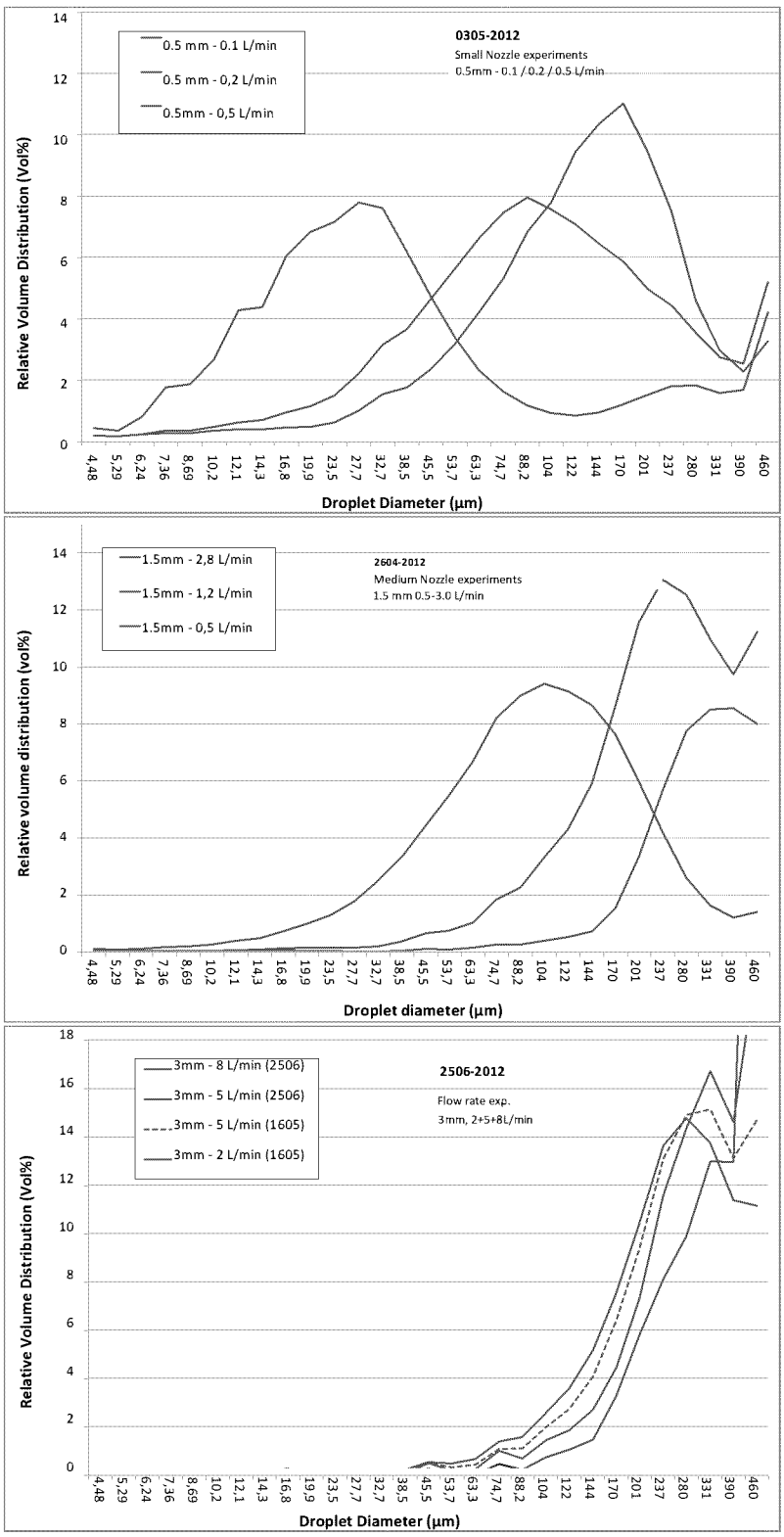

Figure 6.6: Relative droplet size distribution (volume %) as a function of nozzle size (0.5, 1.5 and 3 mm) and flow rate (0.1 – 8 L/min) for the Oseberg oil measured with LISST instrumentation in the SINTEF Tower Basin.

Table 6.3: VMD as a function of nozzle size (0.5, 1.5 and 3 mm) and flow rate (0.1 – 8 L/min) for the Oseberg oil measured with LISST instrumentation in the SINTEF Tower Basin.

Based on maximum peak

0.5 mm		**1.5 mm**		**3 mm**	
Flow rate (L/min)	VMD (µm)	Flow rate (L/min)	VMD (µm)	Flow rate (L/min)	VMD (µm)
0.1	186	0.5	391	2	460*
0.2	88.2	1.2	259	5	332
0.5	27.7	2.8	104	8	293

Based on cumulative distribution (50% volume)

0.5 mm		**1.5 mm**		**3 mm**	
Flow rate (L/min)	VMD (µm)	Flow rate (L/min)	VMD (µm)	Flow rate (L/min)	VMD (µm)
0.1	134	0.5	301	2	450*
0.2	90.7	1.2	243	5	299
0.5	27.5	2.8	93	8	262

* Based on analysis of PVM images

Experiments with oil & gas (air) for one selected nozzle size and flow rates (three experiments) were performed to validate our assumption that "oil alone" experiments could be used to generate data also valid for oil & gas (air) experiments, see Figure 6.24 and Figure 6.25.

6.4 Dispersant-to-oil-ratio (DOR) testing

To be able to evaluate the effectiveness of the different injection techniques, it is important to know the reduction in interfacial tension (IFT) and the resulting effect on droplet size distribution at different DORs. Experiments were performed in the SINTEF Tower basin with premixed dispersants to reduce uncertainty due to the injection methods. The dispersant was injected into the oil stream 3 meters (or 2000 release diameters) before the nozzle (see Figure 5.6). The dispersant is injected into the oil stream via Teflon tubing with an inner diameter of 4 mm. With an oil flow rate of 1,2-1,5 L/min, the residence time of the oil/dispersant blend from the injection point to the nozzle is in the range of 1,5 to 1,9 seconds. The intention was that this would ensure sufficient mixing of the oil/dispersant before oil was released through the nozzle (premixed).

Ideally the dispersant should have been blended into the oil in the pressure tank before injection, but this would demand thorough cleaning between experiments and probably introduce other uncertainties. However, this "premixed mode" could also be regarded as a "deep down-hole or upstream injection".

Table 6.4: Experimental conditions for the DOR experiments

Nozzle diameter:	One – 1,5 mm
Flow rate:	two – 1,2 and 1,5 L/min
Gas-oil-ratio:	Oil alone
Number of replicate experiments:	None
Dispersant application technique:	Upstream injection (Premixed)
Dispersant:	two - Corexit 9500A and a version of C9500A reduced solvent content
Oil type:	Oseberg
DORs	1:25, 50, 100, 250, 500 and 1000

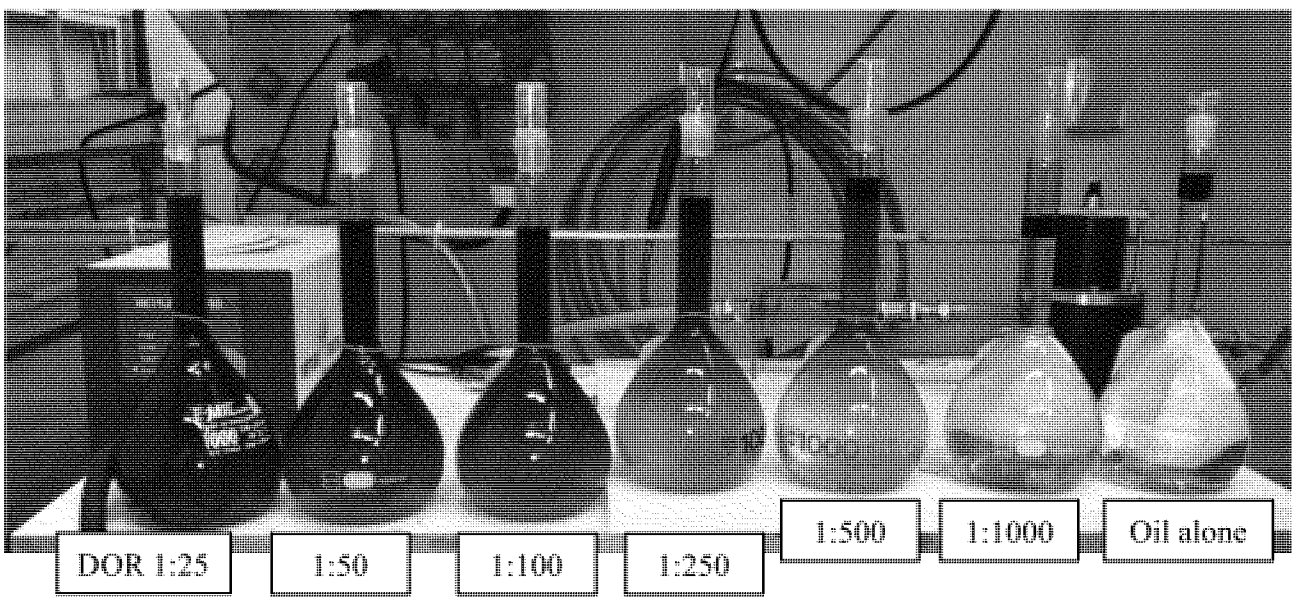

Figure 6.7: Samples of oil and water taken from the Tower basin for IFT measurements on 8. June 2012. The picture is taken after approximate 15 minutes of settling. The large droplets have already risen and formed a surface layer in the neck of the bottles. The colour of the samples reflects the concentration and droplet sizes of the remaining dispersed oil. Dispersant used is C9500. The labels represent the DORs.

ED_001324_00000703-00046

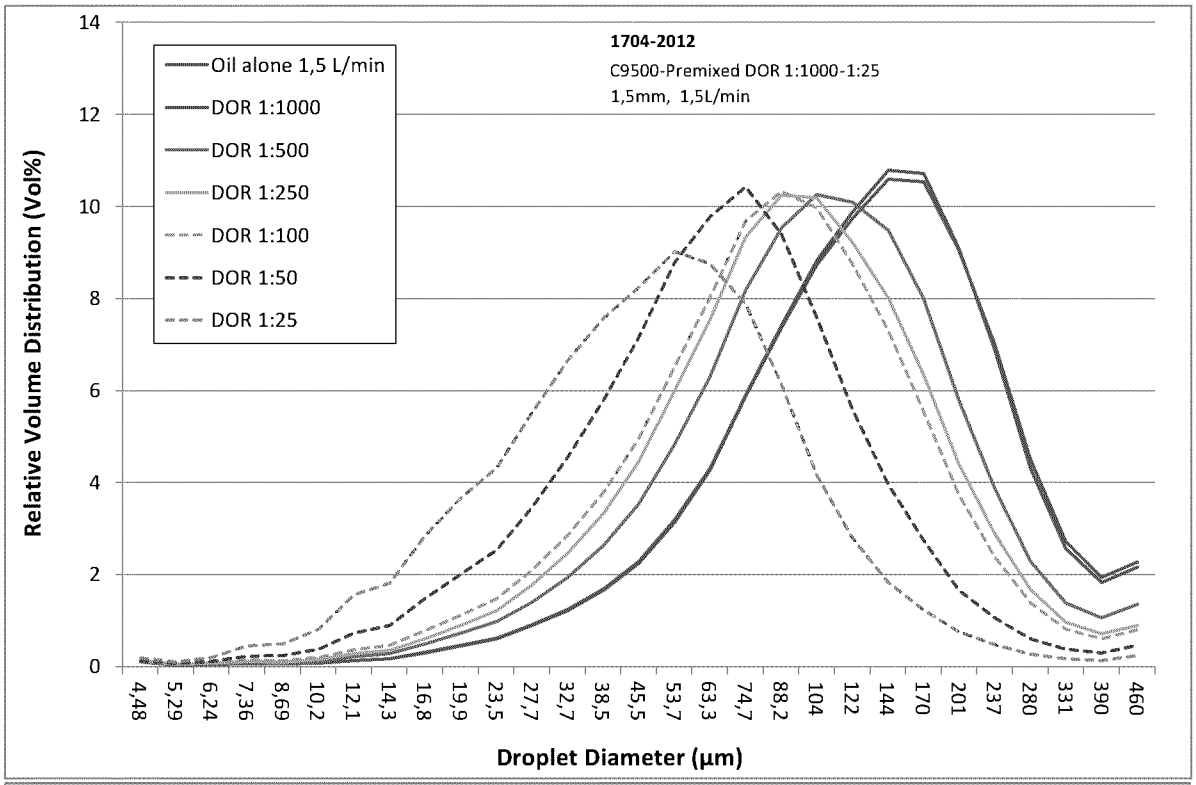

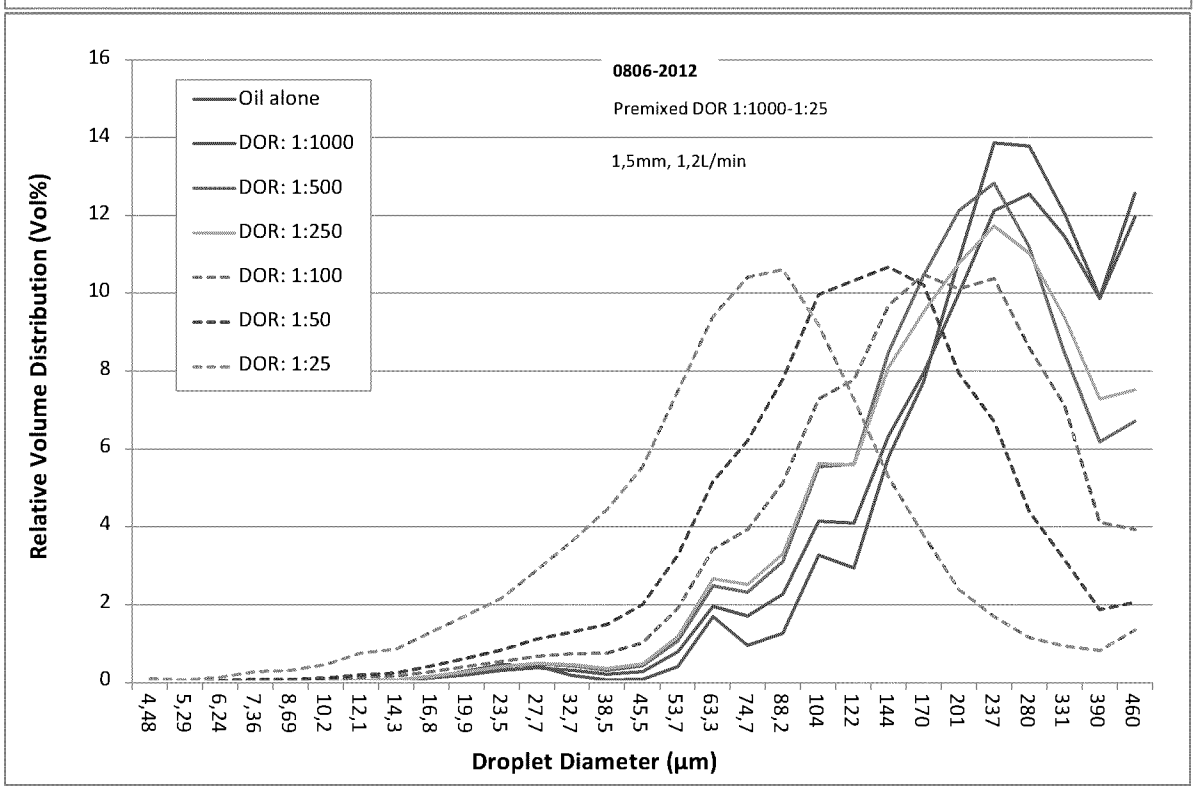

Figure 6.8: Relative droplet size distribution (volume %) as a function of Dispersant to Oil Ratio (DOR) with the Oseberg oil measured with the LISST in the SINTEF Tower Basin. Release conditions 1,5 mm and 1,2 and 1,5 L/min. Dispersant used is C9500.

Table 6.5: DOR experiment with premixed dispersant (1704): VMD as a function of Dispersant to oil ratio (DOR) for premixed dispersant. Nozzle size 1.5 mm and flow rate 1.5 L/min for the Oseberg oil measured with LISST instrumentation in the SINTEF Tower Basin. Interfacial tension measured on oil samples collected in-situ from the oil plume in the Tower basin.

DOR	Maximum peak VMD (µm)	Relative shift in VMD	Cumulative 50% VMD (µm)	Relative shift in VMD	Interfacial tension – Initial (mN/m)	Interfacial tension 30 min (mN/m)
No disp	157	1	130	1	16.5	13.2
1000	157	1	129	1	14.7	11.7
500	104	0.66	97.4	0.75	13.2	9.5
250	88.2	0.57	85.6	0.66	4.5	2.6
100	88.2	0.57	80.3	0.62	1.5	1.2
50	74.7	0.47	61.2	0.46	0.002	0.08
25	53.7	0.34	45.2	0.34	0.07	0.05

Table 6.6: DOR experiment Premixed dispersant (0806): VMD as a function of Dispersant to oil ratio (DOR) for premixed dispersant. Nozzle size 1.5 mm and flow rate 1.2 L/min for the Oseberg oil measured with LISST instrumentation in the SINTEF Tower Basin. Interfacial tension measured on oil samples collected from the oil plume in the Tower basin.

DOR	Maximum peak VMD (µm)	Relative shift in VMD	Cumulative 50% VMD (µm)	Relative shift in VMD	Interfacial tension - Initial (mN/m)	Interfacial tension 30 min (mN/m)
No disp	259	1	255	1	19.6	15.1
1000	293	1.13	246	0.96	9.5	5.0
500	259	1	207	0.81	2.9	1.5
250	259	1	211	0.83	1.3	0.8
100	186	0.72	171	0.67	0.7	0.3
50	157	0.66	123	0.48	0.07	0.008
25	88.2	0.34	71	0.28	0.08	0.07

ED_001324_00000703-00048

6.5 Experiments with dispersant injection

This section presents results from tank tests using dispersant injection techniques similar to those used during the Macondo deep water release. Tank injection equipment was designed after the techniques shown in photos in Figure 6.9, taken from the Macondo incident. These techniques were evaluated as they offer the potential for effective subsea dispersants injection.

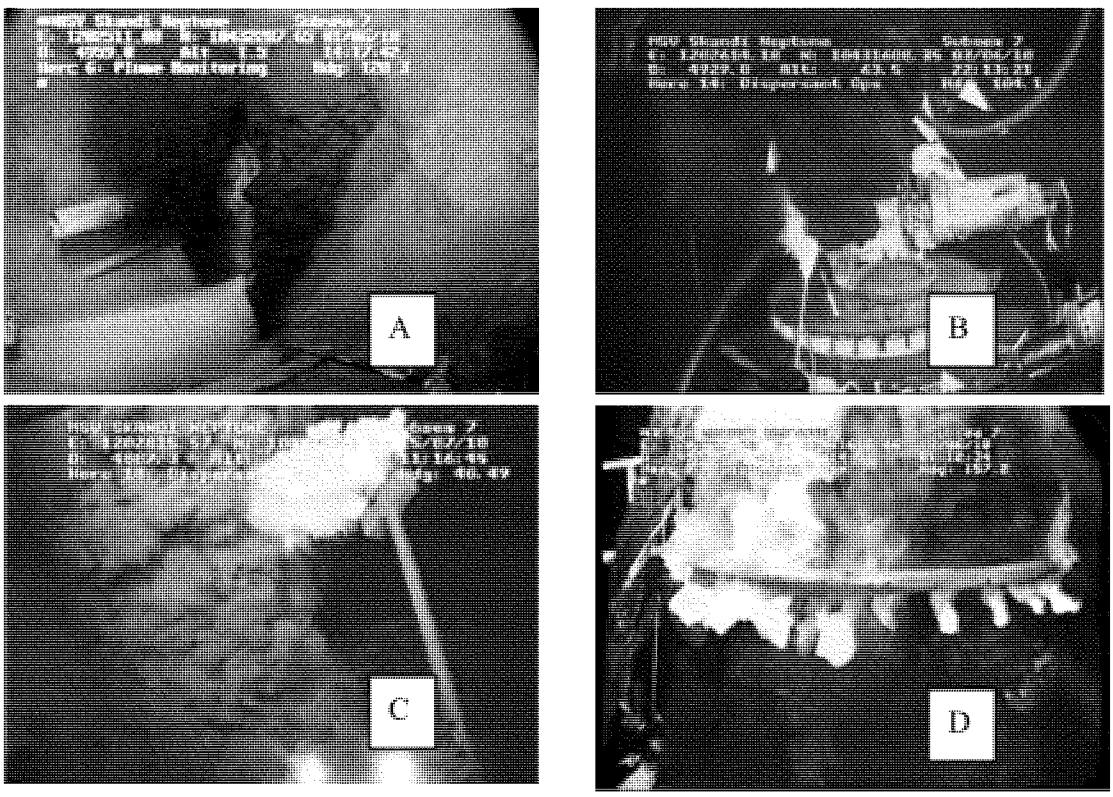

Figure 6.9: Images from the streaming video captured during the DWH deep water oil release showing different methods for injecting dispersant into the oil plume. The insertion tool (A) the wand (B and C) and the dispersant application ring (D).

Table 6.7: Experimental conditions for the dispersant injection experiments

Nozzle diameter:	One – 1.5 mm
Flow rate:	One – 1.2 L/min
Gas-oil-ratio:	No gas (air)
Dispersant application techniques	Three
Dispersant:	One - Corexit 9500A
Number of replicate experiments:	None
Oil type:	One – Oseberg

These experiments were performed with the same nozzle and flow rate used in the DOR experiments (1,2 L/min) and with the same oil type and dispersant (Oseberg/C9500A).

The application techniques tested in this study are (three different techniques):

a. Simulated insertion tool (injected 6 nozzle diameters before the nozzle outlet). See Figure 6.10-A1.
b. Injected above nozzle in the centre of the jet/plume – simulated "Wand" (different distances above nozzle), See Figure 6.10-A2
c. Horizontal injected from the side of the plume 6 diameters above the nozzle (different distances), See Figure 6.11-B.

In these down-scaled laboratory experiments, scaling from field conditions was done by using the release diameter as a scaling factor. The "distances" referred to in the bulleted list above (b, and c) are relative to nozzle diameter of 1,5 mm.

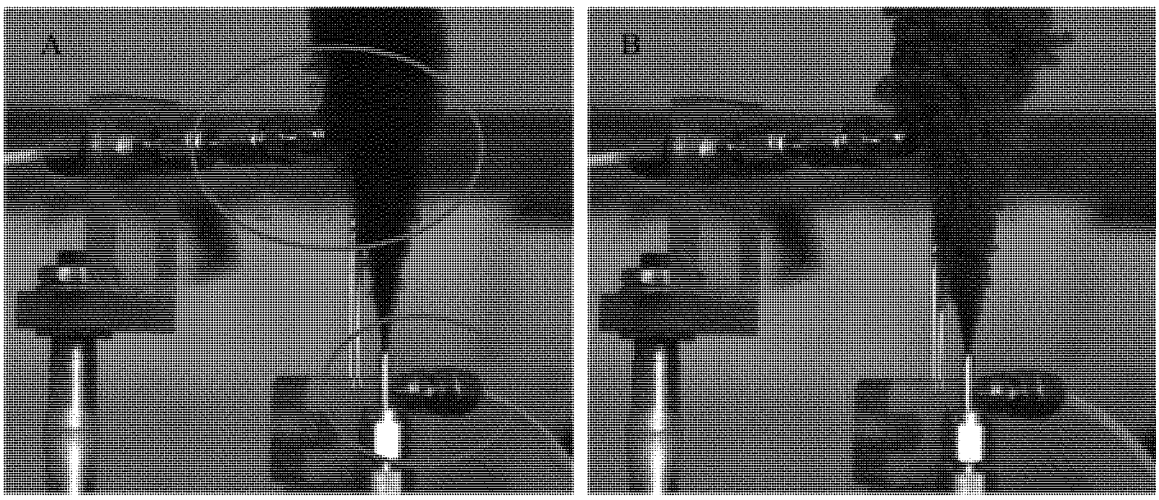

Figure 6.10: Release arrangement (1.5 mm nozzle) with options for injection of dispersant by the "Simulated insertion tool" (1) and "injection in the oil above the nozzle" (2). A: Oil released alone, no dispersant, B: Dispersant injected with the "Simulated Insertion tool" (DOR: 1:25).

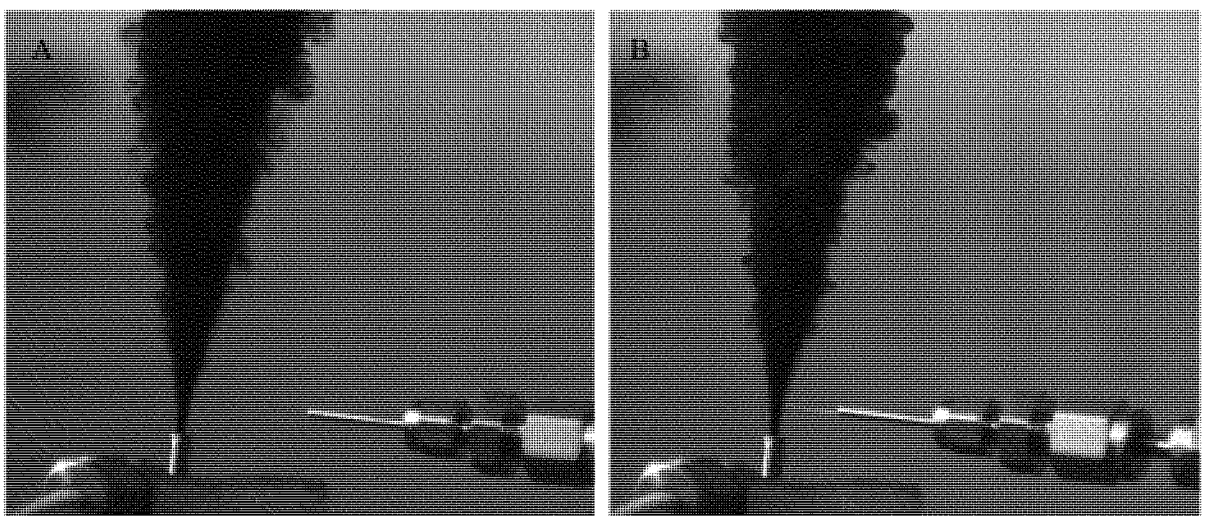

Figure 6.11: Release arrangement (1.5 mm nozzle) with options for injection dispersant horizontally into the oil. A: Oil released alone, no dispersant, B: Dispersant injected at DOR: 1:100.

ED_001324_00000703-00050

6.5.1 Simulated injection tools

This section presents the results from the testing with the "Simulated insertion tool".

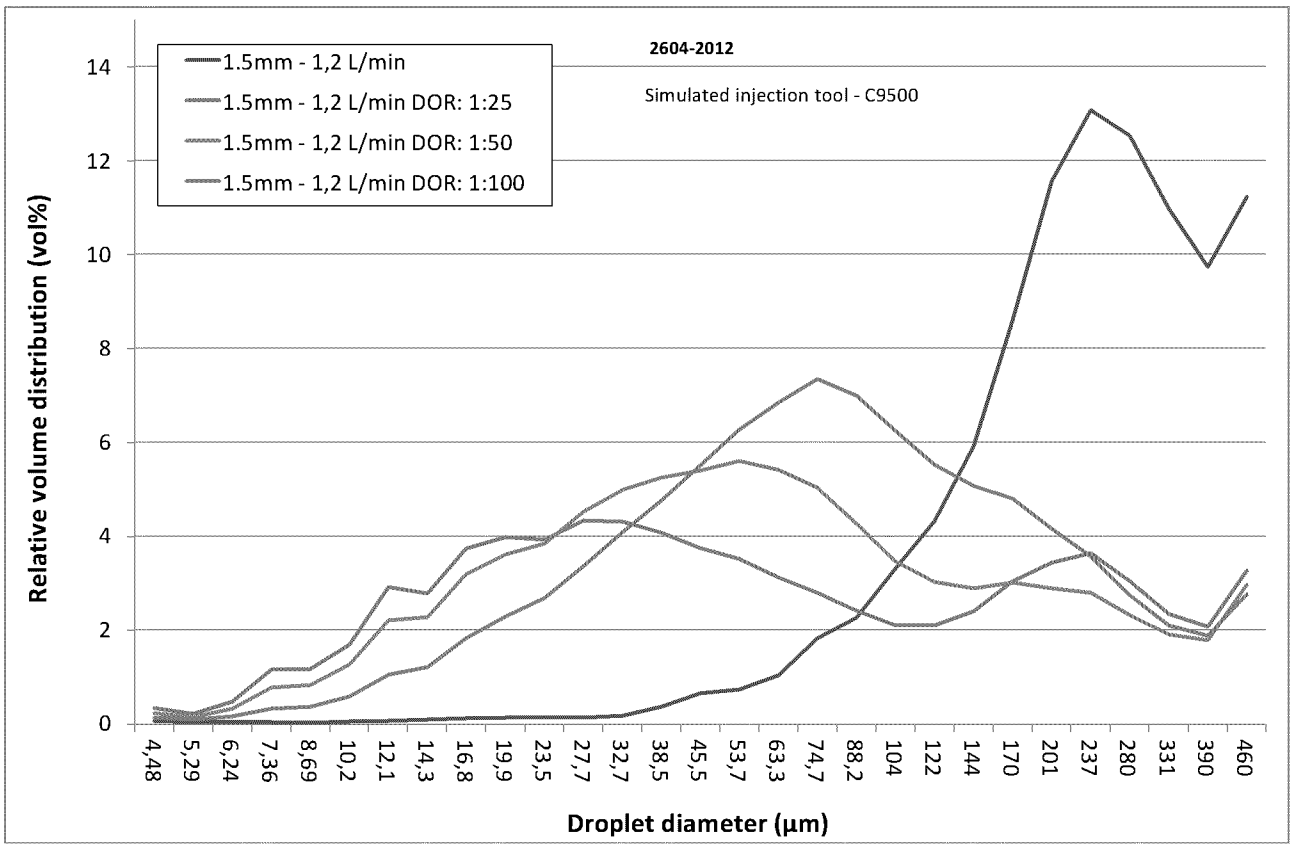

Figure 6.12: Relative droplet size distribution (volume %) with the simulated insertion tool with different Dispersant to Oil Ratio (DOR: 100, 50 and 25) on the Oseberg oil measured with LISST instrumentation in the SINTEF Tower Basin. Release conditions 1,5 mm and 1,2 L/min.

Table 6.8: VMD as a function of Dispersant injection by the "simulated insertion tool" with three different dispersant to oil ratio (1:100, 50 and 25). Nozzle size 1.5 mm and flow rate 1.2 L/min for the Oseberg oil measured with LISST instrumentation in the SINTEF Tower Basin.

DOR	Maximum peak VMD (µm)	Relative shift in VMD	Cumulative 50% VMD (µm)	Relative shift in VMD
No disp	259		243	
100	74	0.29	72	0.30
50	54	0.21	52	0.21
25	28	0.11	46	0.19

6.5.2 Injection into the oil jet above the nozzle

This section presents the results from the Tower basin experiments where the dispersant was injected into the oil at different distances above the nozzle.

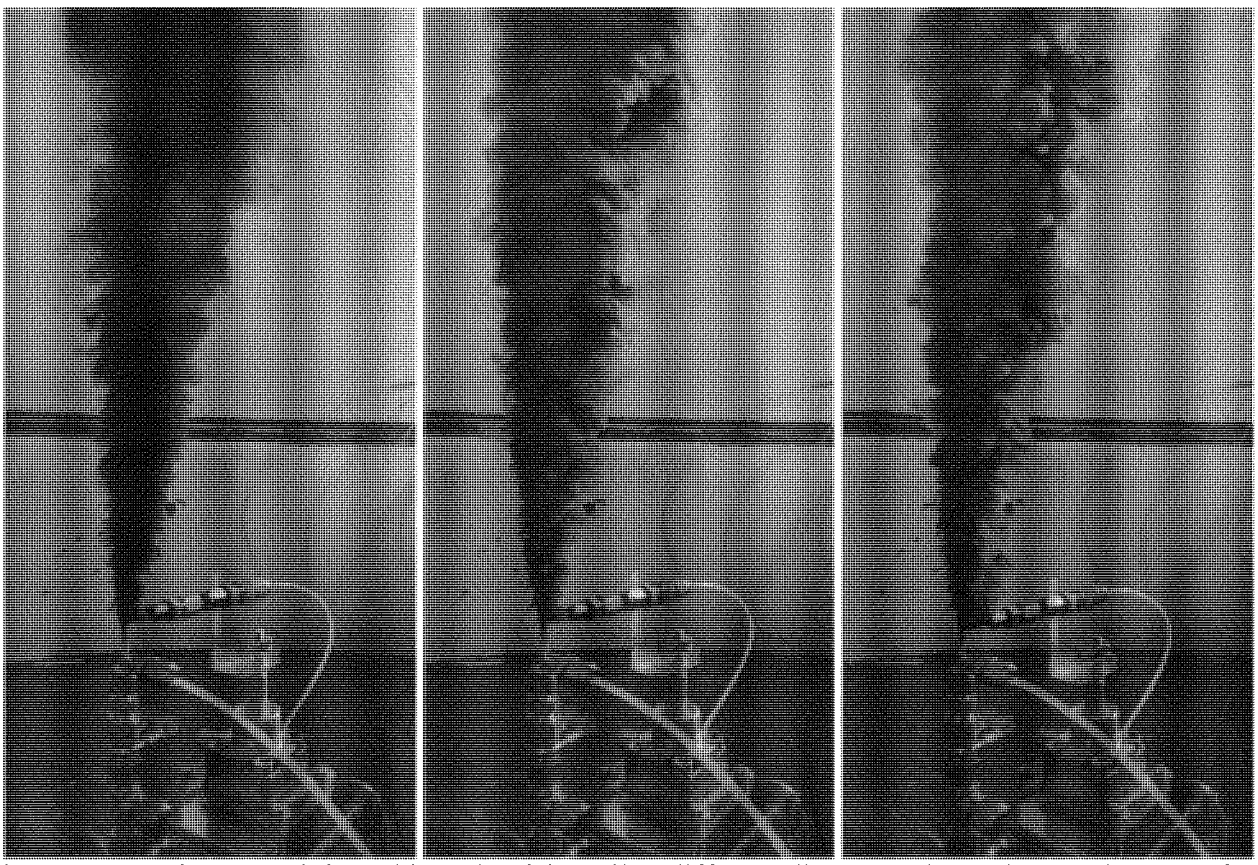

Figure 6.13: Dispersant injected into the rising oil at different distances above the nozzle. A: Before dispersant injection (blue dotted line in Figure 6.15). B: Injection at 8 mm above nozzle (yellow dotted line in Figure 6.17). C: Injection at 1,5 mm above nozzle (light blue dotted line in Figure 6.17).

ED_001324_00000703-00052

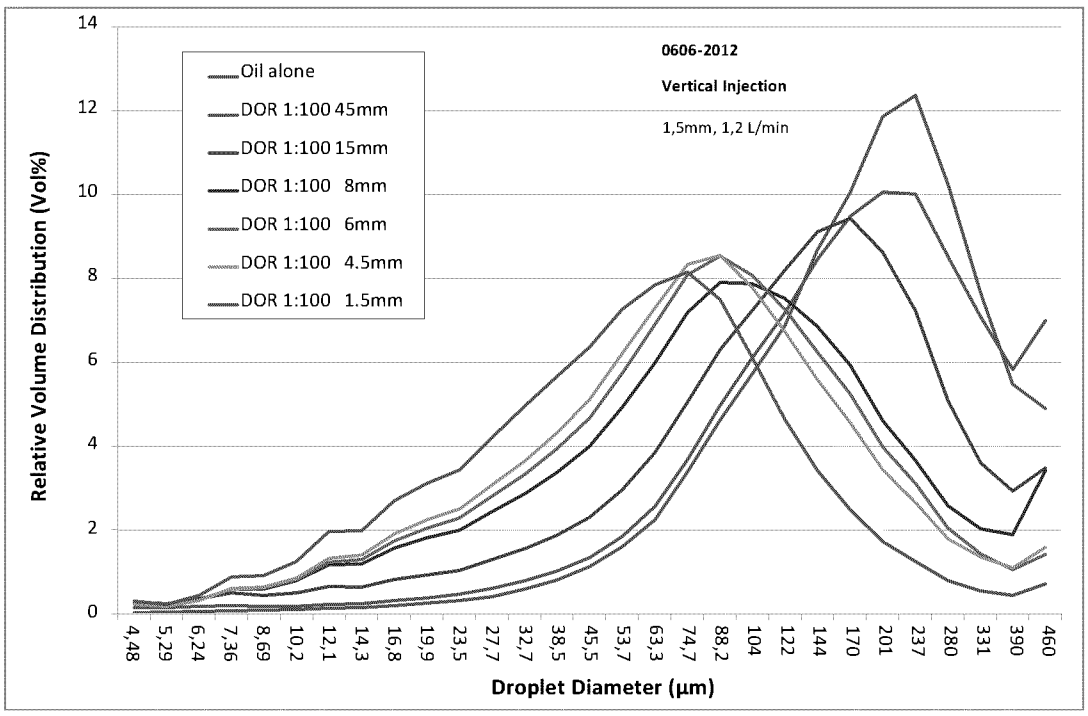

Figure 6.14: Relative droplet size distribution (volume %) with dispersant injected into the rising oil at different distances above the nozzle at DOR 1:100 with the Oseberg oil measured with LISST instrumentation in the SINTEF Tower Basin. Release conditions 1,5 mm and 1,2 L/min.

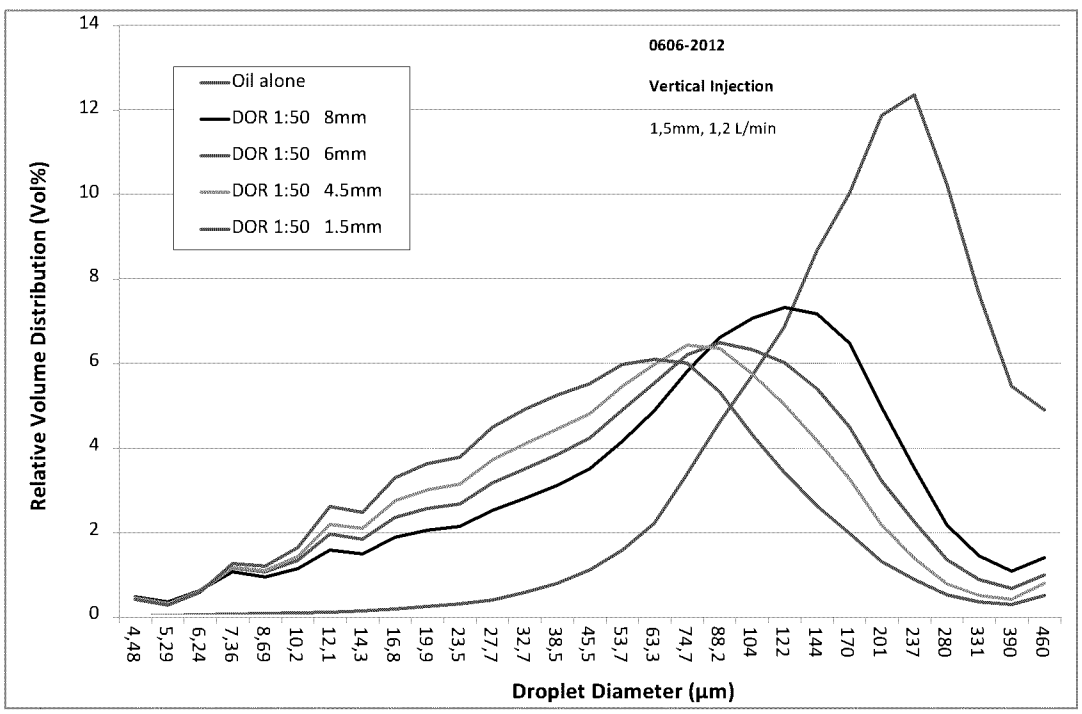

Figure 6.15: Relative droplet size distribution (volume %) with dispersant injected into the rising oil at different distances above the nozzle at DOR 1:50 with the Oseberg oil measured with LISST instrumentation in the SINTEF Tower Basin. Release conditions 1,5 mm and 1,2 L/min.

Table 6.9: Injection above nozzle (0606): VMD for dispersant injected into the oil plume at different distances above the nozzle (DOR 1:100). Nozzle size 1.5 mm and flow rate 1.2 L/min for the Oseberg oil measured with LISST instrumentation in the SINTEF Tower Basin. Interfacial tension measured on oil samples from the oil plume in the Tower basin.

Distance	Maximum peak VMD (µm)	Relative shift in VMD	Cumulative 50% VMD (µm)	Relative shift in VMD	Interfacial tension - Initial (mN/m)	Interfacial tension 30 min (mN/m)
Oil alone	259	1	193	1	18.2	15.5
45	219	0.85	183	0.95	1.4	1.4
15	186	0.72	132	0.68	0.8	0.2
8	88.2	0.34	85.8	0.46	0.7	0.8
6	88.2	0.34	75.9	0.39	0.6	0.3
4.5	88.2	0.34	71.2	0.37	1.3	1.2
1.5	74.7	0.29	53.7	0.28	0.5	0.5

Table 6.10: Injection above nozzle (0606): VMD for dispersant injected into the oil plume at different distances above the nozzle (DOR 1:50). Nozzle size 1.5 mm and flow rate 1.2 L/min for the Oseberg oil measured with LISST instrumentation in the SINTEF Tower Basin. Interfacial tension measured on oil samples from the oil plume in the Tower basin.

Distance	Maximum peak VMD (µm)	Relative shift in VMD	Cumulative 50% VMD (µm)	Relative shift in VMD	Interfacial tension - Initial (mN/m)	Interfacial tension 30 min (mN/m)
8	128	0.49	83.5	0.23	0.1	0.03
6	88.2	0.34	65.8	0.31	0.05	0.009
4.5	74.7	0.29	55.5	0.29	0.04	0.006
1.5	63.3	0.24	44.4	0.17	0.001	0.004

ED_001324_00000703-00054

6.5.3 Horizontal injection from the side into the oil jet

This section presents the results from the horizontal injection of dispersants.

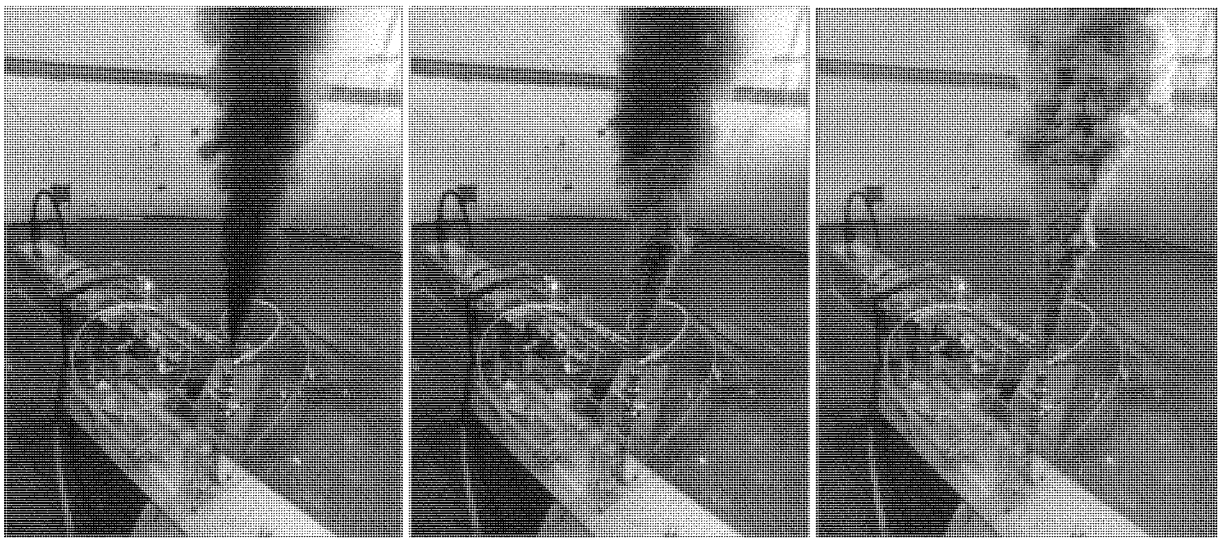

Figure 6.16: Dispersant injected horizontally 4.5 mm (3 release diameters) into the rising oil plume at DOR 1:50 in the SINTEF Tower Basin. A: Before dispersant injection (similar to blue solid line in Figure 6.17). B: Immediately after injection started. C: 30 seconds after injection started (similar to green solid line in Figure 6.17). Release conditions 1,5 mm and 1,2 L/min.

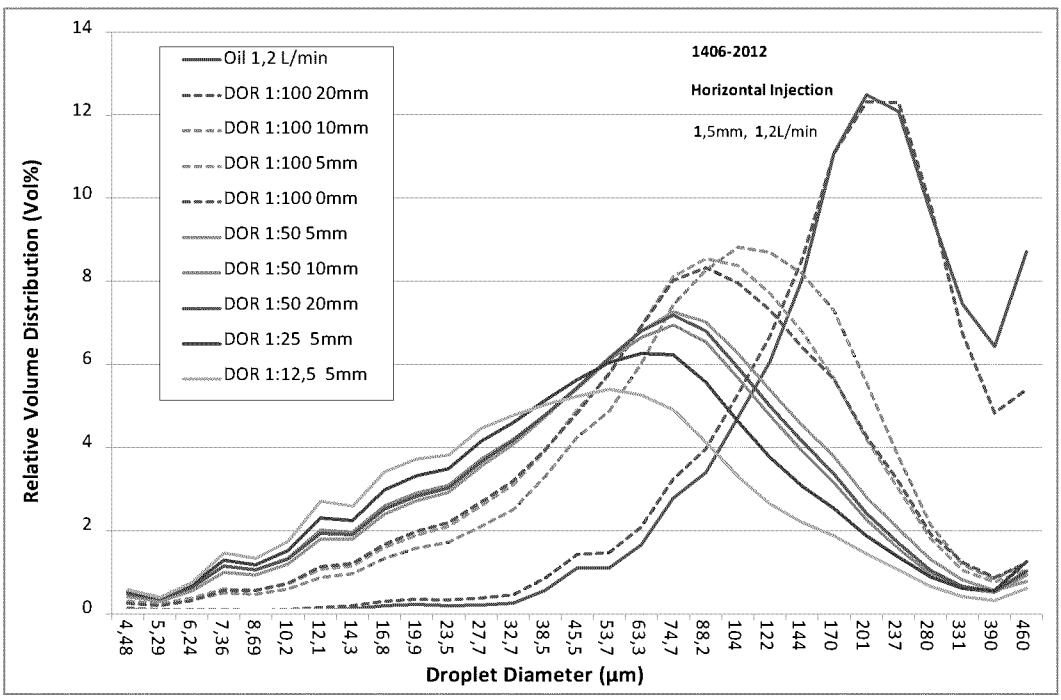

Figure 6.17: Relative droplet size distribution (volume %) with dispersant injected into the rising oil plume from the side at different distances and DORs with the Oseberg oil measured with LISST instrumentation in the SINTEF Tower Basin. Release conditions 1,5 mm and 1,5 L/min.

ED_001324_00000703-00055

Table 6.11: Horizontal injection from beside the oil jet (3 diameters above) nozzle (1406): VMD for dispersant injected into the oil plume at different distances above the nozzle (DOR 1:100). Nozzle size 1.5 mm and flow rate 1.2 L/min for the Oseberg oil measured with LISST instrumentation in the SINTEF Tower Basin. Interfacial tension measured on oil samples from the oil plume in the Tower basin.

Distance	Maximum peak VMD (µm)	Relative shift in VMD	Cumulative 50% VMD (µm)	Relative shift in VMD	Interfacial tension - Initial (mN/m)	Interfacial tension 30 min (mN/m)
Oil alone	219	1	205	1	12.4	10
20	219	1	191	0.93	3.7	2.5
10	104	0.48	88.1	0.43	1.8	1.4
5	88.2	0.40	77.0	0.37	1.9	1.0
0	88.2	0.40	76.4	0.34	*	*

*: No sample taken for IFT measurements

Table 6.12: Horizontal injection from beside the oil jet (3 diameters above) nozzle (1406): VMD for dispersant injected into the oil plume at different distances above the nozzle (DOR 1:50, 25 and 12,5). Nozzle size 1.5 mm and flow rate 1.2 L/min for the Oseberg oil measured with LISST instrumentation in the SINTEF Tower Basin. Interfacial tension measured on oil samples from the oil plume in the Tower basin.

Distance	Maximum peak VMD (µm)	Relative shift in VMD	Cumulative 50% VMD (µm)	Relative shift in VMD	Interfacial tension - Initial (mN/m)	Interfacial tension 30 min (mN/m)
20	74,7	0,34	57,3	0,28	1,6	1,4
10	74,7	0,34	55,6	0,27	0,04	0.03
5	74,7	0,34	60,3	0,27	0,03	0.01
5**	63,3	0,28	49,0	0,22	0,05	0.009
5***	53,7	0,24	40,3	0,18	*	*

*: No sample taken for IFT measurements
**: Experiment performed with DOR: 1:25
***: Experiment performed with DOR: 1:12.5

ED_001324_00000703-00056

6.6 Experiments with r elease of warm oil

In case of a subsurface release of oil, the oil would in most cases have a higher temperature than the oil released in the Tower basin experiments (room temperature 15°C). How the temperature shift from e.g. 70 to 15°C influence the droplet distribution can be estimated by existing algorithms (Weber scaling). However, how elevated temperature influences the dispersant physically mixing with the oil, surfactant interaction with the oil/water and finally the IFT and dispersant effectiveness are more complex to incorporate in algorithms for predicting droplet size distributions.

To get a first idea of the temperature effect, one experiment with elevated temperature was performed. The goal was to perform an experiment with a release temperature out of the nozzle of 60°C. This was also obtained during testing with the heat-exchanger (hot water – oil) used with the Tower basin. However, during the experiment only 51 °C was obtained, probably due to the heat lost to cold piping/hoses in the relatively short experiment. The experiment was first run with ordinary "Cold oil" (15 °C) and then the oil was run through the heater for the "Warm oil" experiment, see figure below. The temperature is measured at the release nozzle.

Simulated insertion tool was used as the injection method to ensure that the dispersant was injected into the warn oil before it entered into the cold water (10 °C).

The results from the "warm oil" experiments are compared in the next two figures with both "cold oil results" obtained in the same run as the "warm oil" experiments and with results from an earlier experiment with cold oil and the Simulated insertion tool.

ED_001324_00000703-00057

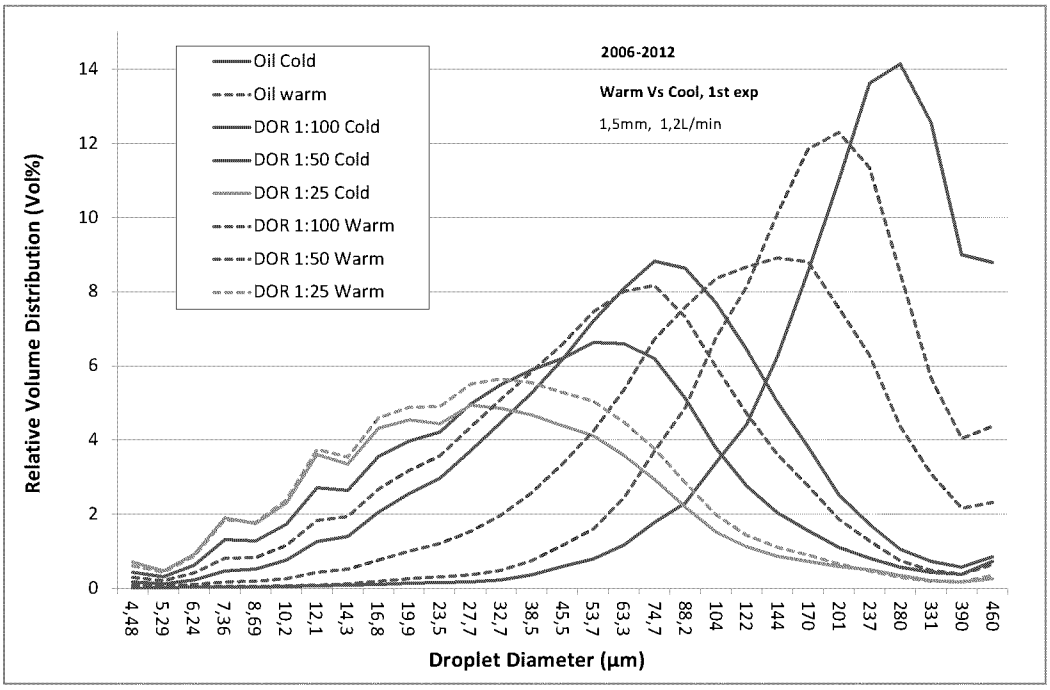

Figure 6.18: Relative droplet size distribution (volume %) as a function of temperature (cold versus warm – 15-51°C) at DOR: 1:100, 50 and 25 with the Oseberg oil measured with LISST instrumentation in the SINTEF Tower Basin. Release conditions 1,5 mm and 1,2 L/min.

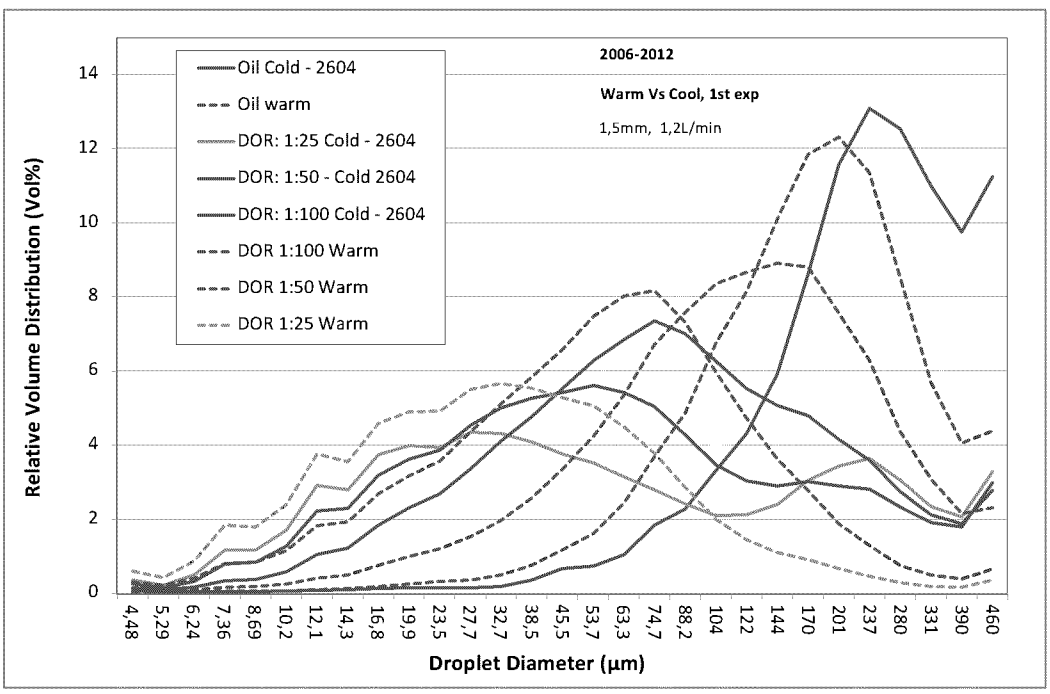

Figure 6.19: Relative droplet size distribution (volume %) as a function of temperature (cold versus warm – 15-51°C) at DOR: 1:100, 50 and 25 with the Oseberg oil measured with LISST instrumentation in the SINTEF Tower Basin. Release conditions 1,5 mm and 1,2 L/min. Warm experiment compared to earlier "cold experiment" performed 2604.

6.7 Modified dispersant with reduced amount of solvent

To study the effect of using a more concentrated dispersant (less solvent), a modified version of Corexit 9500A was used. The dispersant that was tested by "upstream injection" was used as supplied by Nalco.

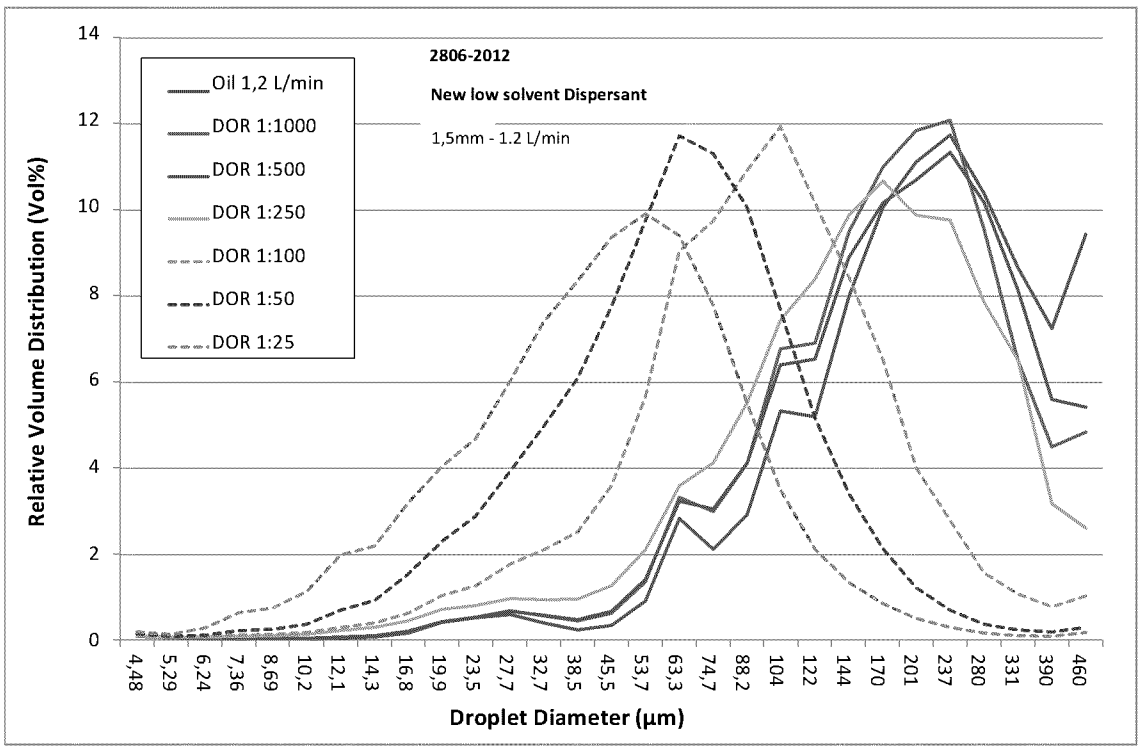

Figure 6.20: Relative droplet size distribution (volume %) with premixed low solvent version of C9500A as a function of Dispersant to Oil Ratio (DOR) with the Oseberg oil measured with LISST instrumentation in the SINTEF Tower Basin. Release conditions 1.5 mm and 1.2 L/min.

Table 6.13: DOR experiment with premixed (upstream injection) low solvent version of C9500A (2806): VMD as a function of nozzle size Dispersant to oil ratio (DOR) for premixed dispersant. Nozzle size 1.5 mm and flow rate 1.2 L/min for the Oseberg oil measured with LISST instrumentation in the SINTEF Tower Basin. Interfacial tension measured on oil samples collected from the oil plume in the Tower basin.

DOR	Maximum peak VMD (µm)	Relative shift in VMD	Cumulative 50% VMD (µm)	Relative shift in VMD	Interfacial tension - Initial (mN/m)	Interfacial tension – 30 min (mN/m)
No disp	259	1	212	1	18,1	11,8
1000	259	1	185	0,87	7,5	2,9
500	259	1	191	0,90	2,4	1,4
250	186	0,72	160	0,75	0,7	0,8
100	104	0,40	87,3	0,41	0,09	0,04
50	63,3	0,24	58,8	0,28	0,07	0,05
25	53,7	0,21	42,3	0,20	0,05	0,007

6.8 Comparison of the different injection techniques

The following figures and tables summarize the data for the different injection techniques and can be used to compare the different injection techniques.

ED_001324_00000703-00060

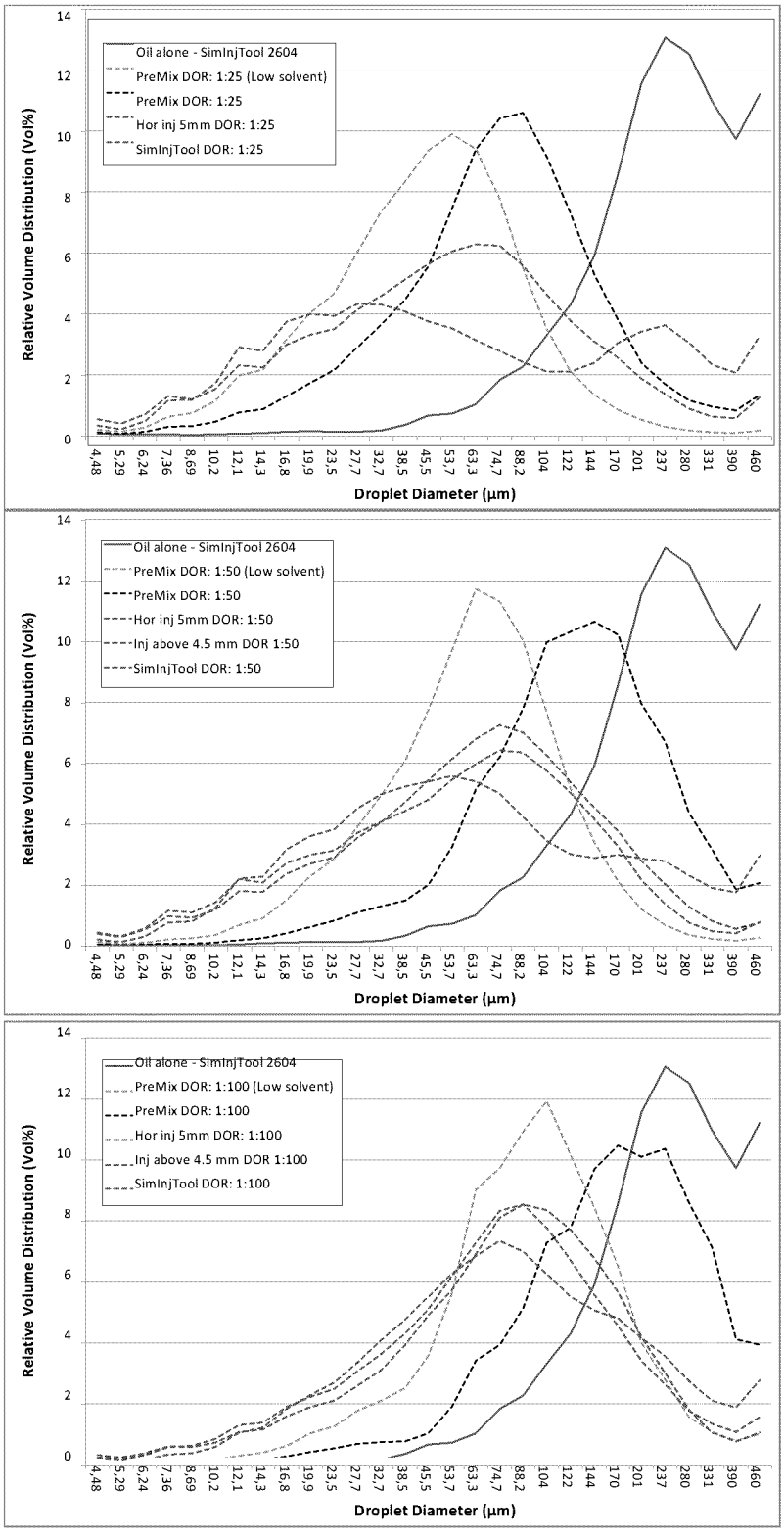

Figure 6.21: Relative droplet size distribution (volume %) for all the injection methods at Dispersant to Oil Ratio (DOR) 1:100/50/25 with the Oseberg blend. Oil alone is also included as a reference. Release conditions 1,5 mm and 1,2 L/min.

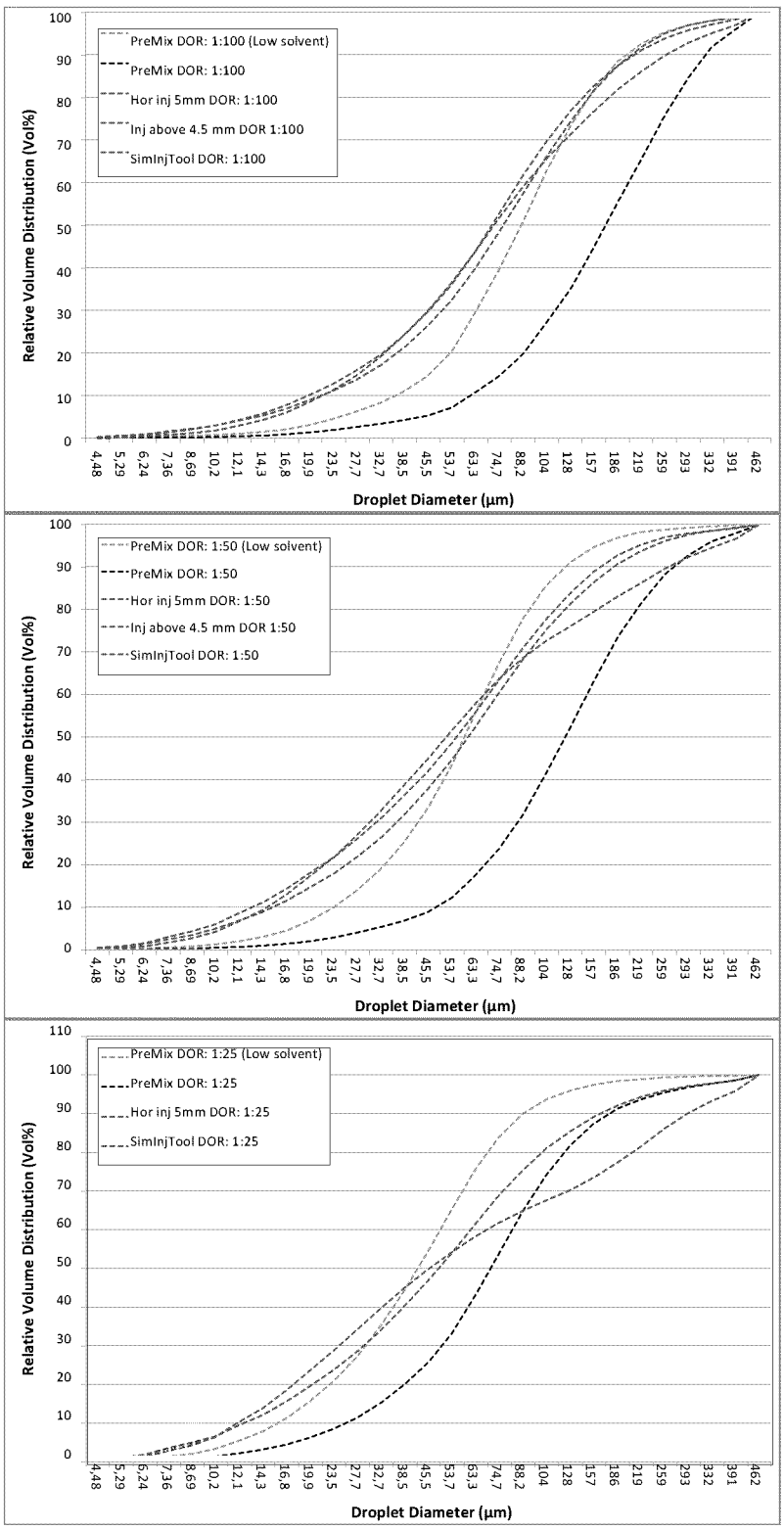

Figure 6.22: Cumulative droplet size distribution (volume %) for all the injection methods at Dispersant to Oil Ratio (DOR) 1:100/50/25 with the Oseberg oil measured with the LISST in the SINTEF Tower Basin. Release conditions 1,5 mm and 1,2 L/min.

6.9 Comparison of dispersant injection at different nozzle sizes

The down-scaling of the Tower basin experiments compared to field conditions and the strategy behind the design of the injection experiments are both based on using the release diameter as a scaling factor. To compare one of the injection methods (Injection above nozzle) with different nozzle sizes, experiments were performed with 0.5, 1.5 and 3 mm nozzle. The dispersant was injected 3 release diameters above the nozzle in each experiment, see figures on next page.

ED_001324_00000703-00063

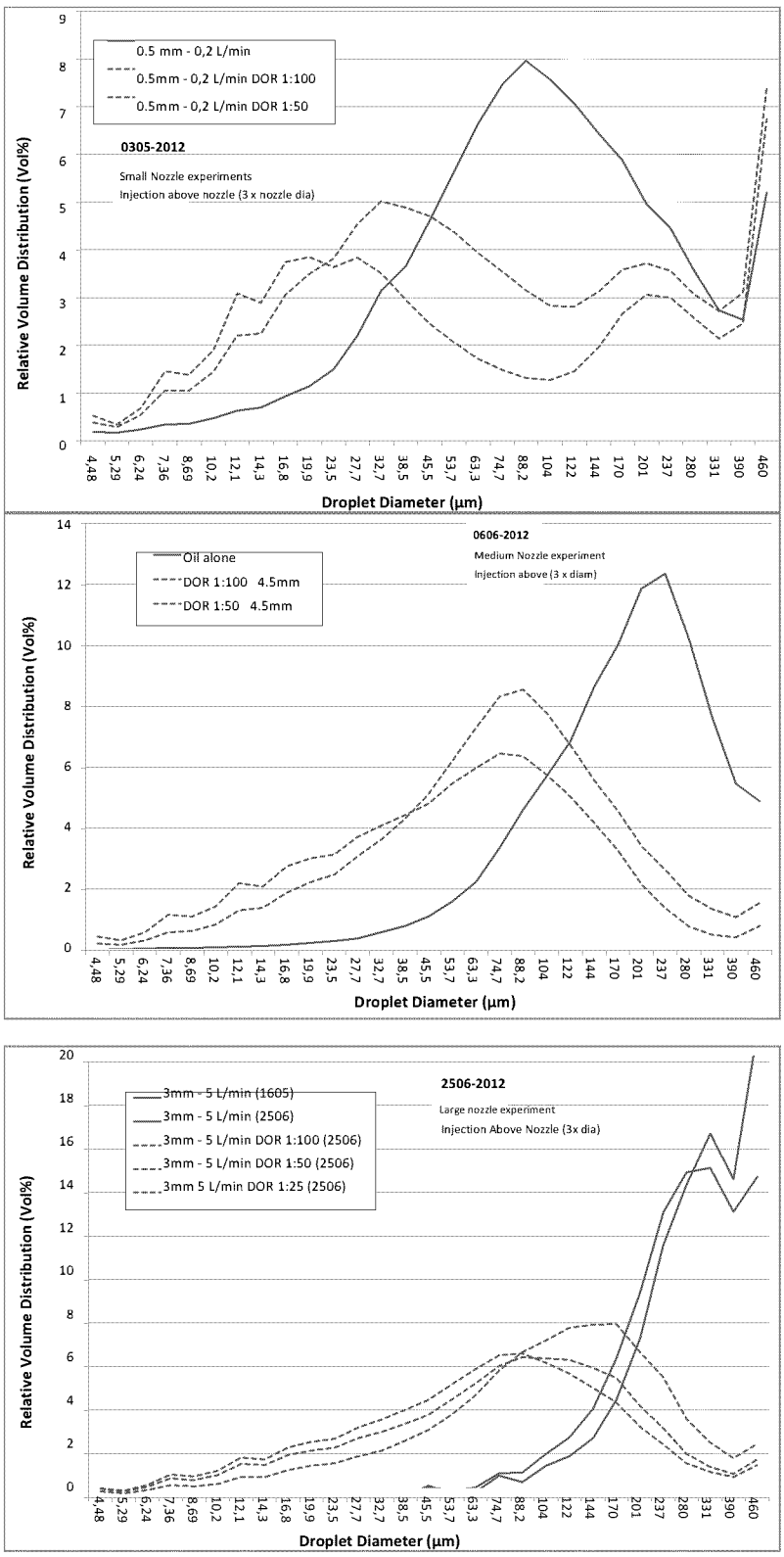

Figure 6.23: Relative droplet size distribution (volume %) with the simulated insertion tool with different Dispersant to Oil Ratio (DOR: 100, 50 and 25) on the Oseberg oil measured with LISST instrumentation in the SINTEF Tower Basin. Release conditions nozzle size: 0.5, 1.5 and 3.0 mm and release rate: 0.2, 1.5 and 5 L/min.

Table 6.14: VMD as a function of nozzle size (0.5, 1.5 and 3 mm) and dispersant injected 3 nozzle diameters above release (DOR: 1:100, 50 and 25) for the Oseberg oil measured with LISST instrumentation in the SINTEF Tower Basin.

Dispersant	**0.5 mm – 0.5 L/min**		**1.5 mm – 1.2 L/min**		**3 mm – 5 L/min**	
DOR	VMD (µm)	Relative shift in VMD	VMD (µm)	Relative shift in VMD	VMD (µm)	Relative shift in VMD (µm)
Oil alone	88,2	1	259	1	332	1
1:100	32,7	0,34	88,2	0,34	128	0,38
1:50	23,5	0,28	74,7	0,29	104	0,31
1:25					74,7	0,23

6.10 Experiments with combined releases of oil & gas (air)

This section presents the initial experiments that were performed with oil, gas (air) and dispersants.

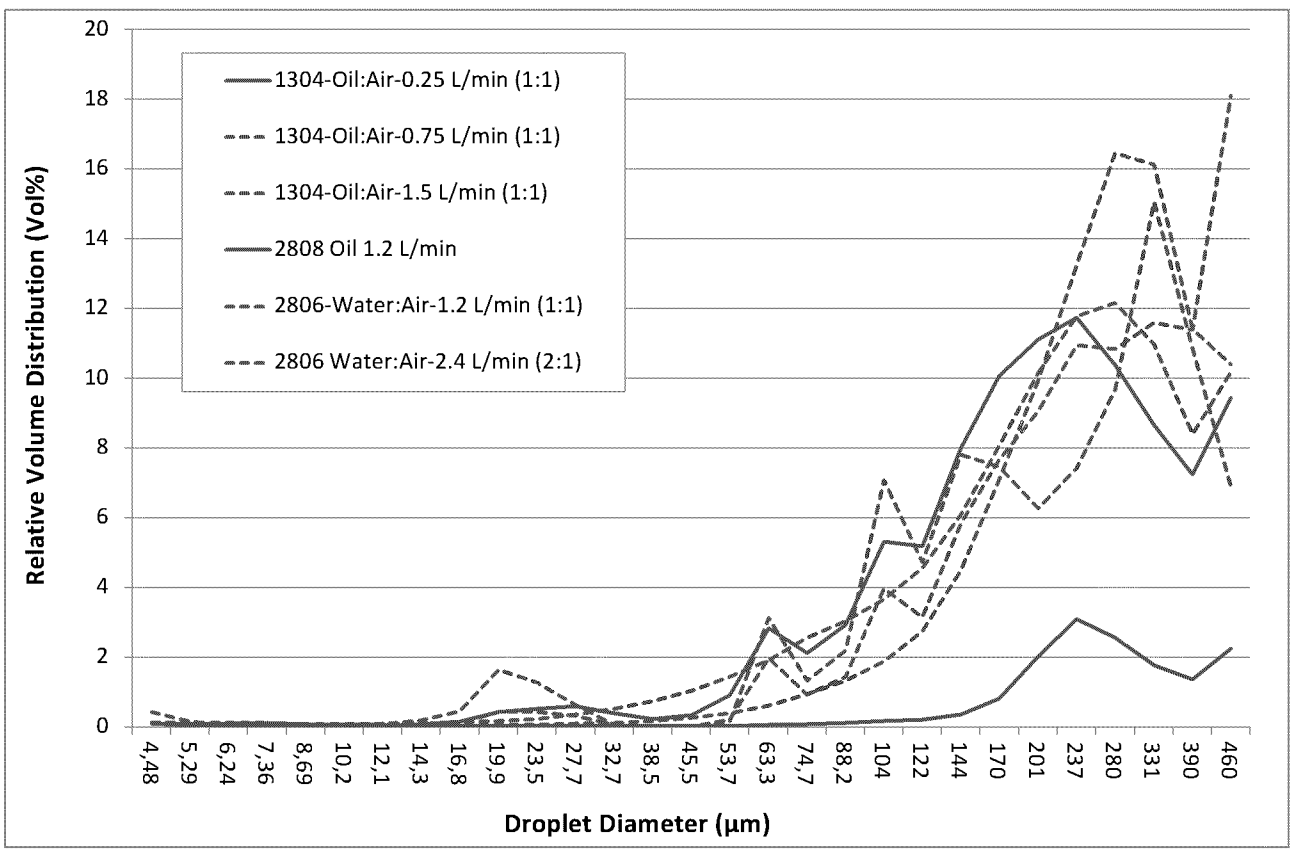

Figure 6.24: Relative droplet size distribution (volume %) with and without gas (air). Nozzle size (1.5 mm) and total flow rate (both oil and gas) of 0.25 to 2.4 L/min) for water and Oseberg blend measured with LISST instrumentation in the SINTEF Tower Basin.

ED_001324_00000703-00065

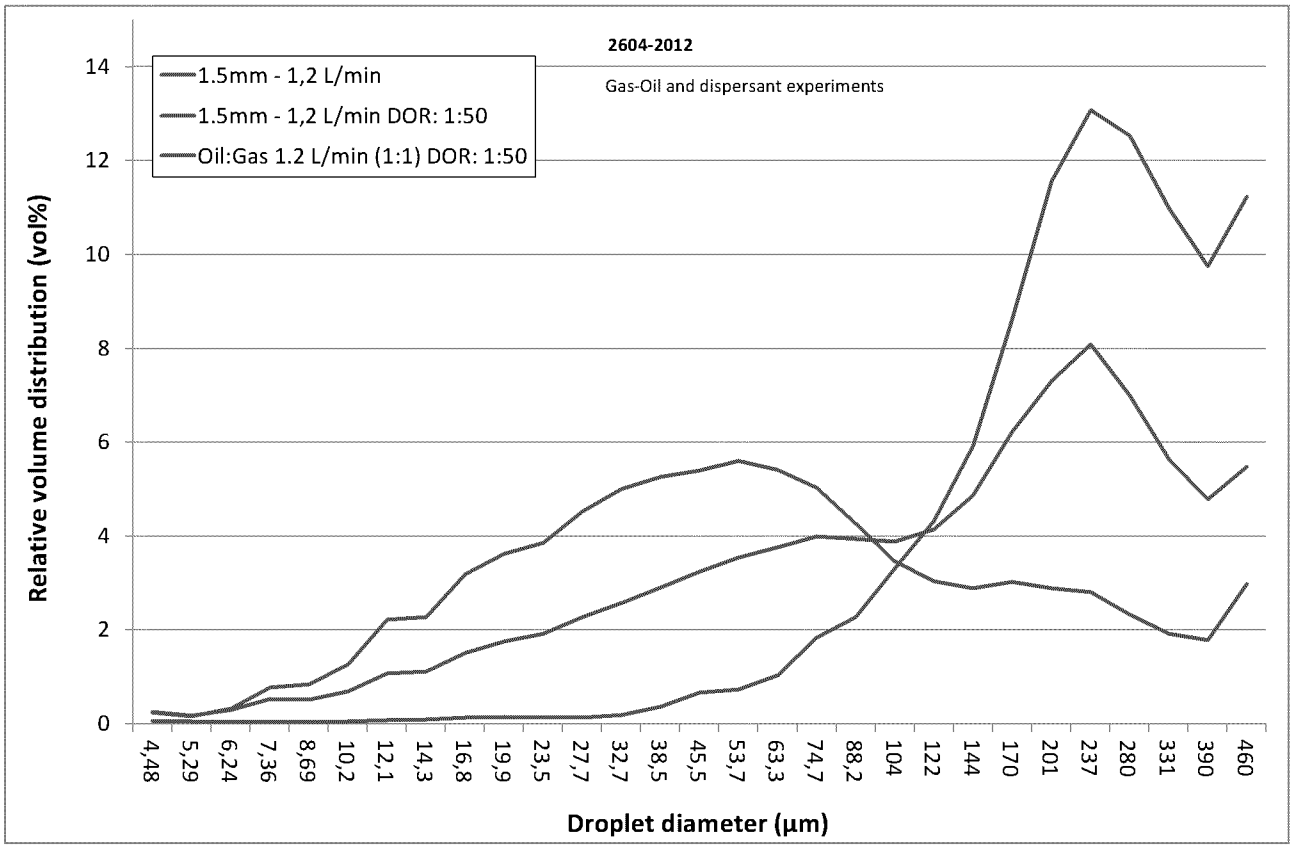

Figure 6.25: Relative droplet size distribution (volume %) with and without gas (air) and dispersant (DOR: 1:50). Nozzle size (1.5 mm) and total flow rate (both oil and gas) of 1.2 L/min for water and Oseberg blend measured with LISST instrumentation in the SINTEF Tower Basin.

7 Discussions

This chapter contains the discussion of the results presented in Chapter 6.

7.1 Initial experiment

7.1.1 Measurement of oil concentrations

In the initial experiment, both the UniLux UVF sensor and the LISST instrument were used to monitor oil concentrations. The latter gave results that best correlated with the concentrations measured in the water samples. The LISST also had a larger linear range and was able to report droplet size distributions. However, the oil concentration in the rising plume is not critical and can be calculated from the release rate and dilution factor.

7.1.2 Verification of droplet distributions measured with the LISST instrument

Droplet size distributions measured with the LISST instrument and sizes of mono disperse particle standards are presented in Figure 6.3. This calibration experiment showed a very good fit between the standard particles and the distribution reported from the LISST.

7.1.3 Verification of mass flow regulators

The set values and the obtained flow rate values for the three different mass flow regulators are presented in Table 6.1. There are some minor deviations for some of the settings (low values for Digimesa or high values for the Burkert 5-100). However, as long as the deviations are small and the real flow rates are used in the calculations, these deviations are not regarded as a problem. Each Tower basin experiment also had a separate flow rate log, where the actual flow rate from each part of the experiment can be calculated.

7.1.4 Reproducibility within and between experiments

The ability of the control and monitoring system in the Tower basin to reproduce droplet size distributions at the most frequent used conditions (1.5 mm nozzle and oil rate 1.2 L/min) is presented in Figure 6.4 and Figure 6.5. The first figure presents variations between 7 different Tower basin experiments performed over a two month period. We can see from the figure that three of these experiments have a slightly larger VMD than the others (VMD of 237 compared to 201 microns). This is probably caused by a slightly lower release rate (approximately 1.1 compared to 1.2 L/min). However, this can be compensated for in the calculations in chapter 8 using the correct flow from the flow rate logs that were recorded for each experiment.

The second figure shows the droplet distributions for the different experimental periods (90 seconds) within one Tower basin experiment. This showed very little variation of droplet size distributions (and flow rate) within one experiment.

7.2 Flow rate experiments - droplet sizes versus release conditions

The droplet size data for the different release experiments utilizing three nozzle sizes (0.5, 1.5 and 3) and three different flow rates for each nozzle (0,1 – 8 L/min) are presented in Figure 6.6. An overview of all the Volume Median Diameters (VMD) for these experiments is also given in Table 6.3.

Most of the data are from the LISST instrumentation, which is used as the main sensor for droplet size measurements. The data obtained from the two image based techniques (In-situ macro camera and the external PVM) contained very limited information regarding sizes of the large droplets in most experiments. This is probably due to the small focusing area of these macro methods (mm range) combined with the short time for data acquisition (usually 30 seconds). During this period a very limited number of large droplets were captured and quantified on the images.

Due to this limitation, the images were only analysed and used for the large nozzle experiments (3 mm) and low flow rates (5 and 8 L/min). In these experiments the maximum peak of the distributions was not visually identified in the 2-500 micron range obtained by the LISST. For these experiments, droplet data is provided by image analysis of the PVM images, see legends in Table 6.3.

Assuming a log normal distribution, both the peak value from the relative volume distributions and the 50% from the cumulative distribution should give similar estimates of VMD. However, use of the cumulative distribution assumes that we actually have data for the complete range of droplets. This is not the case for distributions with a significant amount of droplets above the LISST range of 500 microns. However, since the Relative droplet distributions have a limited resolution (30 bins) and the cumulative distributions can be used to interpolate between the bins exactly, the same numerical values cannot be expected. When comparing these two measures of VMD in Table 6.3, we observe that the values based on the cumulative distributions are generally slightly smaller compared to their counterparts.

The experiments give a consistent data set with droplet sizes as expected based on the earlier used algorithm for Weber number scaling of droplet sizes. These data will be used to verify earlier published work (Johansen et al., 2013) to improve existing algorithms for predicting droplet size distributions for different release conditions (modified Weber scaling). See section 8 for further details.

7.3 Droplet sizes versus Dispersant to oil ratio (DOR)

To study the influence on dispersant to oil ratio (DOR) on the interfacial tension and the droplet size distributions, experiments were performed with a wide range of DORs. The relative distributions for two different experiments are presented in Figure 6.8, Table 6.5 and Table 6.6. The only difference between these two experiments is the flow rate of the oil. The second experiment is performed with a lower flow rate (1.2 L/min opposed to 1.5 L/min in the first experiment).

The dispersant (C9500A) was injected into the oil stream 3 meters or 2000 nozzle diameters upstream of the nozzle. It is assumed that the dispersant blends into the oil along this distance upfront of the nozzle. For this reason, this method of upstream dispersant injected is regarded as premixing of dispersant. The residence time of the dispersant/oil from the injection point to the nozzle is less than 2 seconds (1.2 L/min).

The lower figure (1.2 L/min) show that the lowest concentrations (1:1000-500-250) have a very limited effect on the droplet size distributions. It is very difficult to visually see any difference on these three droplet size distributions. However, the three highest concentrations (1:100, 50 and 25)

ED_001324_00000703-00068

give a shift towards smaller droplets. The upper figure with a higher flow rate (1.5 L/min) shows some effect of the dispersant at low dosage rates (1:500 and 1:250).

The lack of shift in droplet size distribution with the lowest dosages of dispersant is surprising since the Interfacial tension (oil-water) is lowered (see Table 6.5 and Table 6.6.). The relatively large bin sizes could mask small shifts in droplet size distribution. However, a more probable explanation could be insufficient mixing of the dispersant into the oil despite the 2000 release diameters between injection of the dispersant and the release nozzle. At the lowest dispersant dosages, the injection of the dispersant into the 4 mm oil tubing is probably too small compared to the turbulence level to give sufficient mixing of dispersant and oil before release into the Tower basin. The combinations of flow and oil properties used in these experiments give a Reynolds number (Re) of 1000-1300. A Re lower than 2000 is usually taken as an indication of tubular flow which gives low turbulence and reduced mixing during this short residence time (< 2 seconds). The fact that increased oil flow rate (1.5 versus 1.2 L/min) gives better mixing (higher effectiveness at 1:500/250) supports this hypothesis.

In future DOR experiments, a "mixing-chamber" should be installed to locally raise Re and ensure sufficient turbulence and mixing of oil and dispersants, especially at low dispersant treatment rates (DOR 1:1000 – 1:250).

7.4 Effectiveness of different dispersant injection techniques

Three different dispersant injection techniques were tested in this project;

1. Simulated insertion tool, injection of dispersant 6 nozzle diameters before the outlet
2. Injection in the centre of the rising plume at different heights above the nozzle
3. Horizontal Injection into the plume from outside at different distances

The effectiveness of these injection techniques, evaluated by the relative shift in droplet size distribution, was compared with the premixed results from the previous chapter.

7.4.1 Simulated insertion tool

During the Macondo deep water dispersant injection in the Gulf of Mexico in 2010, dispersant was injected with an "insertion tool". This was a nozzle on the tip of an approximately 2-3 meter long tube which was inserted into the broken riser. In our case this was not possible to simulate directly because inserting some device into these small nozzles (0.5 – 3 mm) would reduce the diameter and restrict the flow. For this reason the dispersant was injected into a separate tube attached orthogonal to the outlet 6 diameters before the nozzle opening.

The results from the simulated insertion tool are presented in Figure 6.12 and the VMD are summarized in Table 6.8. The observed shifts in droplet size distributions are consistent with the dispersant concentrations. This means that an increased dispersant concentration reduces the droplets (VMD). The experiments give systematic shifts in droplet sizes from 259 microns (oil alone), to 75 microns (1:100), 54 microns (1:50) and finally 24 for the 1:25. This is the same trend as for the premixed experiments, but the measured droplet sizes are significant smaller for the simulated inserted tool. No oil samples have been collected for IFT analysis during this type of experiment.

ED_001324_00000703-00069

For the highest dispersant treatment, a bimodal distribution can be seen in Figure 6.12, indicating that the dispersant is not completely mixed into the oil stream and that some of the oil is not treated.

7.4.2 Injection at different heights above the nozzle

To simulate the injection of dispersant with the "wand" during the Macondo deep water dispersant injection, dispersant was injected into the rising oil plume at different heights above the nozzle. The results from this dispersant injection are presented in Figure 6.14 and Figure 6.15 (relative droplet distribution - DOR 1:50 and 1:100) and in Table 6.9 and Table 6.10.

These figures show that to be effective in our Tower basin, the dispersant has to be injected rather close to the nozzle. There was a significant difference in droplet size distribution between the experiments where the dispersant was injected close to the nozzle (1.5 to 8 mm or 1 to 6 nozzle diameters) compared to injecting higher above the nozzle. Both the experiments at DOR 1:50 and 1:100 show this trend.

A liquid jet from a nozzle will form a solid cone up to 4-6 nozzle diameters (Or et al., 2011). This is called the zone of flow establishment (ZFE). Above this zone the solid cone will break up and form a spray of droplets (zone established flow – ZEF). Injecting the dispersant in ZFE seems to be most efficient. Then the dispersant is injected directly into the oil cone and mixed into the oil, lowering the IFT before the oil enters the more turbulent ZEF, where the droplets are formed. See illustration in Figure 7.1.

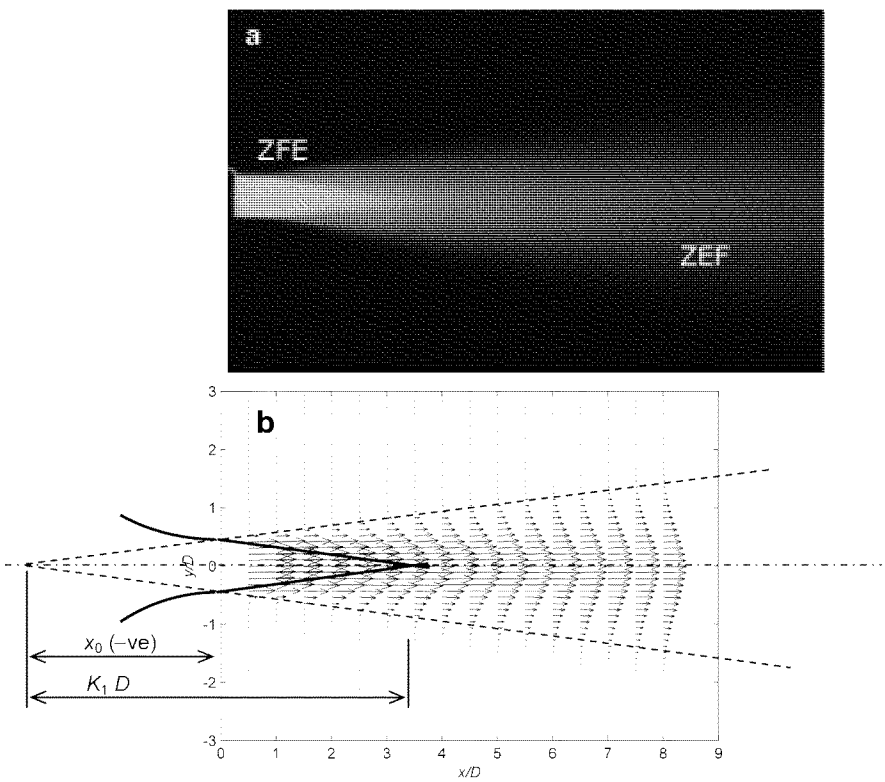

Figure 7.1: Mean concentration field of a jet shown as a grey-level image (a) and mean velocity fields for a simple jet (B). x_0 is the virtue origin and K_1 is a decay constant (Or et al., 2011).

ED_001324_00000703-00070

The shear forces in ZEF are much higher compared to further above the nozzle. Injecting the dispersant in and above ZEF is less effective due to reduced mixing (loss of dispersant due to injection into the water instead of into oil cone) and less turbulent conditions. The reduced effectiveness can be seen in the red lines for 15mm (10D) and 45mm (30D) in Figure 6.14. This reduced effectiveness of the dispersant injection high above the nozzle can be explained by;

1. the droplets are already formed
2. reduced turbulence/shear forces in this zone compared to closer to the nozzle
3. further splitting into smaller droplets demands higher turbulence
4. less effective use of dispersant, since some is injected into the water phase instead of the oil

This can also be seen from the measured IFT from oil samples collected in the Tower basin during experiments Table 6.9 and Table 6.10 where the oil samples collected close to the nozzle have significantly lower IFT and corresponding smaller VMDs.

When the dispersant is injected directly into an oil cone in the zone of established flow (e.g. 4.5 mm or 3D) it looks like there is a limited effect of increasing the dispersant dosage (DOR) from 1:100 to 1:50. The shift in VMD from 1:100 to 1:50 is only from 88 to 75 microns.

7.4.3 Injection horizontally into the plume

These experiments were originally designed to study dispersant released on the side of the rising plume and then drawn into the plume. However, the tube or nozzle used for dispersant injection was so small that instead of releasing the dispersant into the water it had sufficient release velocity to be injected into the zone of flow establishment (4.5 mm or three release diameters) of the rising oil (see Figure 6.11 and Figure 6.16).

Injection experiments were performed with two dispersant treatment ratios (DOR: 1:100 and 1:50) and a series of different injection distance (0 – 20 mm). Single experiments were also performed at DOR: 1:25 and 1:12.5 with a distance of 5 mm (see Figure 6.17, Table 6.11 and Table 6.12).

The horizontal distance has limited effect on the shift in droplet size distribution in our Tower basin, as long as the dispersant beam enters directly into the oil cone close to the release nozzle (4.5 mm or 3 nozzle diameters). The differences in VMD versus dispersant treatment ratios are (at a horizontal distance of 5 mm) for DOR: 1:100/50/25 and 12.5; 88, 75, 63 and 54 microns.

This means that doubling the dispersant volume from DOR 1:100 to 1:50 in our Tower basin, will only lower the VMD from 88 to 75 or 0.40 to 0.34 relative to oil alone (219 microns), see Table 6.11and Table 6.12.

7.5 Release of warm oil

This experiment was not a part of the original experimental design, but was included later in the process, since we omitted some dispersant injection experiments (dispersant ring).

The dispersant was injected with the simulated insertion tool to ensure good contact and mixing of the dispersant into the warm oil before release.

ED_001324_00000703-00071

Not all the experimental data presented in Figure 6.17 and Figure 6.18 was as initially expected. The "cold" and "warm" oil distributions show slightly smaller droplets for the warm oil due to lower viscosity. For the oil treated with dispersants the opposite trend can be seen. For all three treatment ratios (1:100, 1:50 and 1:25) the warm oil gives distributions with slightly larger droplets compared to the cold oil.

This was not as initially expected, and possible factors that might explain this behaviour are listed below:

1. Cooling effect from the injected dispersant could reduce the effect of the warm oil
2. Increased viscosity difference between warm (low viscous) oil and more viscose dispersant give less efficient mixing
3. The critical micelle concentrations (CMC) for the surfactants and the resulting IFT (water/oil) could change at elevated oil temperatures.

Since the treatment ratio is in the range of 1-4%, the cooling effect from the cold dispersant should be minimal (1). Regarding viscosity (2), reduced mixing due to increased difference in viscosity is difficult to justify. It should actually be the other way around with increased mixing since the continuous phase (the oil) is warm and less viscous. The heat from the warm oil should also quickly warm the injected dispersant and lower its viscosity.

Concerning the third point, some studies (Rewick et al., 1984 and Mohajeri & Noudeh, 2012) indicate that CMC of surfactants could decrease with increased temperature. A possible temperature sensitivity of the CMC could also be different for the main groups of surfactants in most dispersants (sorbitan esters, etoxylated sorbitanesters, sulfosuccinate sodiumsalts and branched octanols). This difference could change the internal ratio of the surfactants available for the oil-water interphase, which could increase the IFT and reduce effectiveness of the dispersant.

Measurement at SINTEF on samples from the Tower basin and premixed oil samples (DOR 1:50) show that the IFT increase in the range of 2-10 times going from 10 and 50°C. The significance of this increase in IFT (from ultralow to low) should be verified in both small-scale (spinning drop) and in the Tower basin. This is suggested as an important topic for a possible phase-II study.

7.6 Modified dispersant with reduced amount of solvent

A modified version of Corexit 9500A with reduced amount of solvent was tested with "upstream injection" at varying DOR (1:1000 – 1:25), see Figure 6.19 and Table 6.13. When comparing the shift in droplet sizes as a function of varying DORs for the new product compared to the ordinary version of C9500A (Figure 6.8, Table 6.5 and Table 6.6.) the modified version is significantly more effective.

At a DOR of 1:100 the VMD of the ordinary C9500A is 186 microns and with the modified product 104 microns. At DOR 1:50 and 1:25, the corresponding values are 157 versus 63 and 88 versus 54 microns. This means that the relative shift in VMD at DOR 1:100 is 0.72 for ordinary C9500A and 0.40 for the modified product.

It is difficult to evaluate the significance of this effect (0.72 versus 0.40) without evaluating the exact increased surfactant content in the modified product, since the DOR are similar for the two tests.

7.7 Comparison of the different injection techniques

To easier compare the effectiveness of the different injection techniques, the resulting droplet size distributions are presented in Figure 6.21 and Figure 6.22. The comparison is made for the same nozzle and flow rate (1.5 mm and 1.2 L/min).

The main conclusions from these summary figures are as long as the dispersant is injected close to the nozzle, in the zone of flow establishment before the droplets are formed, all three injection methods (simulated insertion tool, horizontal injection and injection above the nozzle) produce similar droplet size distributions at DOR 1:100.

At DOR 1:50 and 1:25 the insertion tool produces slightly smaller droplets compared to the other injection methods.

7.8 Comparison of dispersant injection at different nozzle sizes

Dispersant was injected above the nozzle at three different nozzle diameters (0.5, 1.5 and 3 mm). The dispersant was in all cases injected 3 nozzle diameters above the nozzles. The droplet distributions for three different DORs (1:100, 1:50 and 1:25) are given in Figure 6.23 and Table 6.14.

The nozzle diameter is a main scaling parameter for the design of the experiments in the SINTEF Tower basin. In the three series of experiments that range over a relatively large range of nozzle diameters (the largest nozzle was six times larger than the smallest) the dispersant was injected in the same position relatively to the nozzle size.

It is not easy to see the strong similarities between the graphs in Figure 6.23, but it is easier comparing the relative shift in droplet sizes (VMD) in Table 6.14. For all three nozzles, a dispersant treatment of DOR 1:100 gives a relative reduction in VMD of 0.34-0.38. This means that for all three nozzle sizes, the droplets (VMD) are reduced to a third at DOR 1:100.

The results from these experiments are very supportive for the basic idea behind SINTEFs down-scaled Tower basin approach. The fact that scaled dispersant experiments gave consistent results is very encouraging for utilizing these results in operational oil spill models.

7.9 Experiments with combined releases of oil & gas (air)

The experiments with oil, gas (air) and dispersants are discussed in section 8.4.

ED_001324_00000703-00073

8 Data analyses - Modelling

8.1 Droplet breakup model

The present understanding is that the characteristic droplet size generated by a turbulent oil jet injected into water will follow a Weber number scaling. With the characteristic droplet size represented by the median droplet diameter d_{50}, this implies:

$$d_{50}/D = A\ We^{-3/5} \tag{8.1}$$

where D is the diameter of the exit, A is an empirical coefficient, and We is the exit Weber number, $We = \rho\ U^2\ D/\sigma$, where ρ is the density of the oil, σ is the interfacial tension between oil and water (IFT), and U is the exit velocity. This relationship is valid for interfacial tension limited breakup, but under certain conditions, viscous forces may be of importance (Wang and Calabrese 1986). If these forces are dominant, the characteristic droplet size will instead be related to the exit Reynolds number

$$d_{50}/D = C\ Re^{-3/4} \tag{8.2}$$

where C is an empirical coefficient and the Reynolds number is $Re = \rho\ U\ D/\mu$, where μ is the dynamic viscosity of the oil. Wang and Calabrese (1986) derived a semi-empirical equation for the intermediate case, where both interfacial tension and viscous forces are influencing droplet breakup:

$$d_{50}/D = A\ We^{-3/5}\ (1 + B\ Vi\ (d_{50}/D)^{1/3})^{3/5} \tag{8.3}$$

where B is an empirical coefficient and Vi is the Viscosity number, $Vi \equiv We/Re = \mu\ U/\sigma$.
For large values of the viscosity number, $Vi >> 1$, Eq. 8.3 can be approximated by the equation

$$(d_{50}/D)^{4/5} = A\ We^{-3/5}\ (B\ Vi\ )^{3/5} \tag{8.4}$$

By taking into account that the viscosity number is the ratio between the Weber number and the Reynolds number, Eq. 8.4 can also be expressed in terms of the Reynolds number:

$$(d_{50}/D)^{4/5} = A\ B^{3/5}\ Re^{-3/5},\ \text{or}\ d_{50}/D = A^{5/4}\ B^{3/4}\ Re^{-3/4} \tag{8.5}$$

This implies that the coefficient C in Eq. 8.2 is $C = A^{5/4}\ B^{3/4}$. Wang and Calabrese's equation (Eq. 8.3) thus changes smoothly from a Weber number scaling to a Reynolds number scaling when the viscosity number increases and eventually becomes very large ($Vi >> 1$). This condition can be met for high exit velocities, high oil viscosities, or for low interfacial tensions. The latter may result from injection of a chemical dispersant into the oil, which may reduce IFT by a factor of 100 or more.

8.2 Empirical model for predicting droplet sizes

We have used Wang and Calabrese's model (Eq. 8.3) as the basis for developing a new algorithm for prediction of droplet sizes in oil jets. The values that were used are obtained from experiments with untreated oil, and experiments with dispersants injected upstream in the oil line in different

ED_001324_00000703-00074

dispersant to oil ratios (DOR), and in addition, results from experiments where the dispersants were injected a short distance before the outlet (simulated injection tool) and a short distance after the outlet (vertical injection 1.5 mm above the outlet). The main results are summarized in **Table 8.1**, which also include the test conditions (nozzle size and volume flow rate, and various derived variables, such as exit velocity, Weber number and viscosity number). For the cases with dispersants, the interfacial tension values were measured on oil samples taken from the plume.
In some cases with low DOR (i.e in the range 1:1000 to 1:250, marked with grey shading in **Table 8.1**), we have noted that the peak droplet size is practically insensitive to the observed variations in the reported IFT values. This discrepancy might indicate that the dispersant has been inefficiently mixed into the oil line before the exit nozzle, and thus having limited effect on oil droplet breakup. However, during handling and storage of the samples, oil and dispersants would have been blended in the sampling flasks, causing a significant reduction in the measured IFT values. Due to this uncertainty, we have excluded these tests from the data analyses.

Table 8.1: Data from tower tank tests. Grey shading indicates tests that have been excluded from the analyses due to uncertainties in the recorded IFT values (see text). Here, D is the nozzle size; Q the oil flow rate; DOR the dispersant to oil ratio; We the Weber number; U the exit velocity; Vi the viscosity number and d_p the peak droplet diameter obtained from the LISST droplet size measurements. IFT data in bold are estimated as mean values from other experiments with same DOR.

Date	D, mm	Q, L/min	DOR	IFT, mN/m	U, m/s	We	Vi	d_p, um
17.04 2012	1.5	1.5	-	16.5	14.1	1.53E+04	9	144.0
	1.5	1.5	1:1000	14.7	14.1	1.72E+04	10	144.0
	1.5	1.5	1:500	13.2	14.1	1.91E+04	11	104.0
	1.5	1.5	1:250	4.5	14.1	5.60E+04	31	88.2
	1.5	1.5	1:100	1.5	14.1	1.68E+05	94	88.2
	1.5	1.5	1:50	0.002	14.1	1.26E+08	70 736	74.7
	1.5	1.5	1:25	0.07	14.1	3.60E+06	2 021	53.7
26.04 2012	1.5	0.5	-	15	4.7	1.87E+03	3	391.0
	1.5	1.2	-	15	11.3	1.08E+04	8	237.0
	1.5	2.8	-	15	26.4	5.86E+04	18	104.0
Simulated	1.5	1.2	1:100	**0.66**	11.3	2.45E+05	172	74.7
inj. tool	1.5	1.2	1:50	**0.056**	11.3	2.88E+06	2021	53.7
	1.5	1.2	1:25	**0.055**	11.3	2.93E+06	2058	27.7
03.05 2012	0.5	0.1	-	15	8.5	2.02E+03	6	170.0
	0.5	0.2	-	15	17.0	8.07E+03	11	88.2
	0.5	0.5	-	15	42.4	5.04E+04	28	27.6
Injection	0.5	0.2	-	0.658	17.0	1.84E+05	258	32.7
above	0.5	0.2	-	0.056	17.0	2.16E+06	3032	19.9
06.06 2012	1.5	1.2	-	18.2	11.3	8.87E+03	6	237.0
Injection	1.5	1.2	1:100	0.5	11.3	3.23E+05	226	74.5
1.5 mm ab.	1.5	1.2	1:50	0.001	11.3	1.61E+08	113177	63.3

Date	D, mm	Q, L/min	DOR	IFT, mN/m	U, m/s	We	Vi	d_p, um
28.06 2012	1.5	1.2	-	18.1	11.3	8.92E+03	6	237.0
	1.5	1.2	1:1000	7.5	11.3	2.15E+04	15	237.0
	1.5	1.2	1:500	2.4	11.3	6.72E+04	47	237.0
	1.5	1.2	1:250	0.7	11.3	2.31E+05	162	170.0
	1.5	1.2	1:100	0.09	11.3	1.79E+06	1 258	104.0
	1.5	1.2	1:50	0.07	11.3	2.31E+06	1 617	63.3
	1.5	1.2	1:25	0.05	11.3	3.23E+06	2 264	53.7

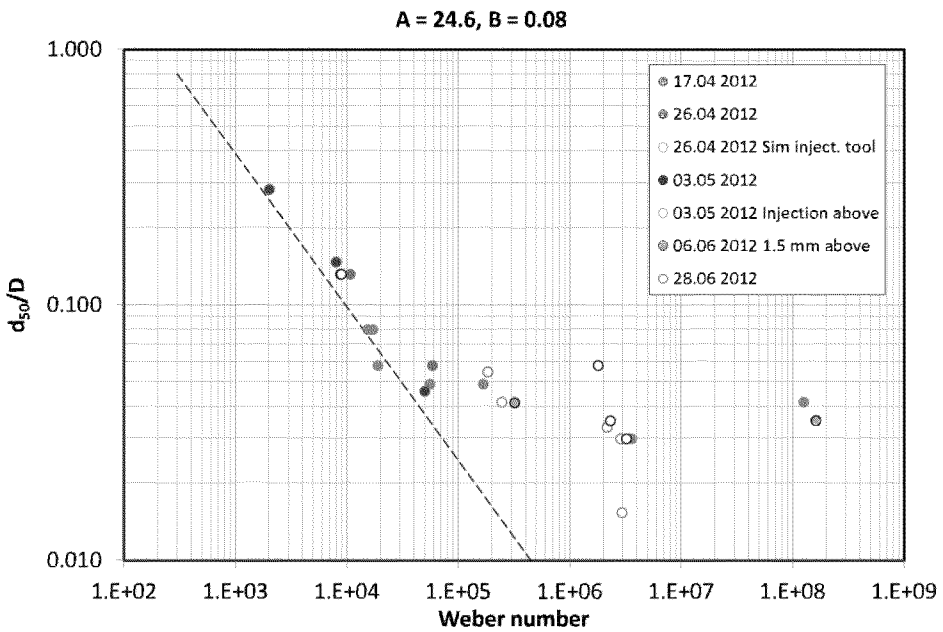

Figure 8.1 shows a plot of the relative median droplet size (d_{50}/D) vs. the exit Weber number for untreated oil and oil with premixed dispersants. The median droplet size is derived from the peak droplet diameter by assuming $d_{50} = d_p/1.2$, where the factor 1.2 is based on a presumed Rosin Rammler type droplet size distribution (Johansen et al. in press). The graph shows clearly that the Weber number scaling does not hold for a large number of the cases. As expected, the largest deviations were found for cases with premixed dispersants. Figure 8.2 shows the same results versus the outlet Reynolds number.

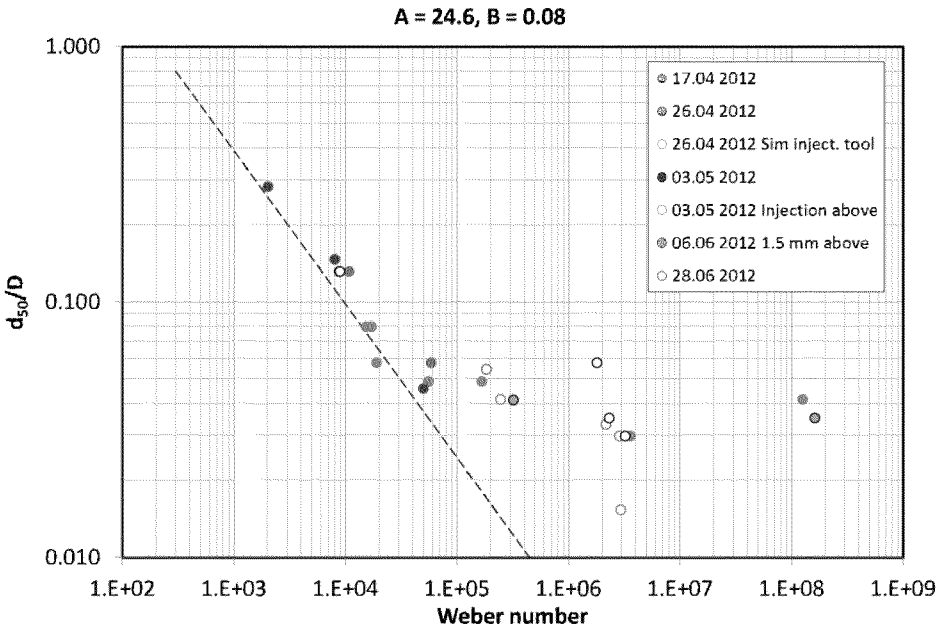

Figure 8.1: Weber number plot of median droplet size data for Oseberg Blend – results with no treatment and with dispersants. The broken line shows the Weber number scaling model (Eq. 8.1).

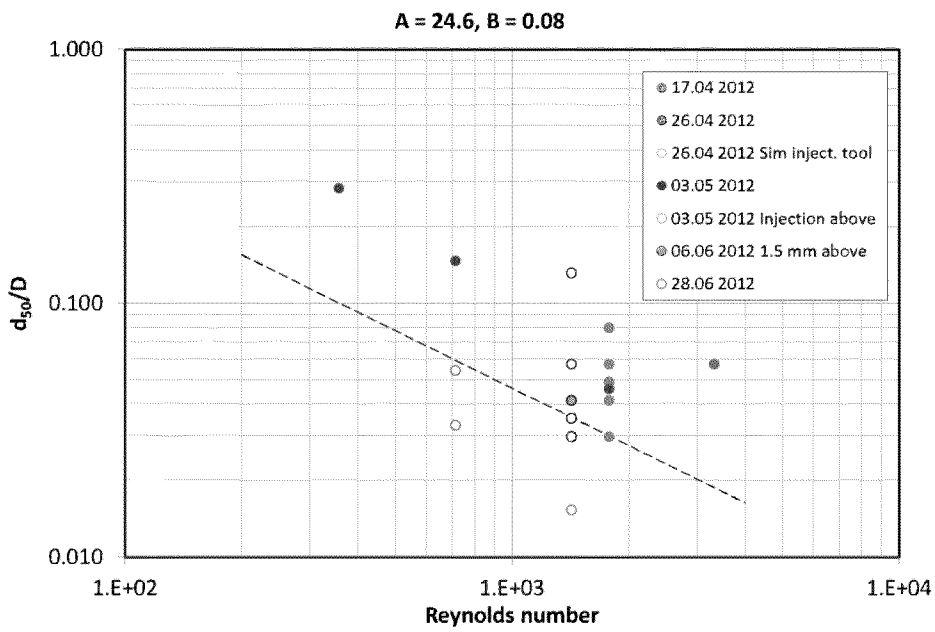

Figure 8.2: Reynolds number plot of median droplet size data for experiments with no treatment and with dispersants. The broken line shows the Reynolds number scaling model (Eq. 8.2).

Figure 8.3 shows a plot of the same results based on Wang and Calabrese's model, with coefficients A and B determined by best fit for all data. Figure 8.4 shows the best fit correlation (computed vs. measured values of d_{50}/D).

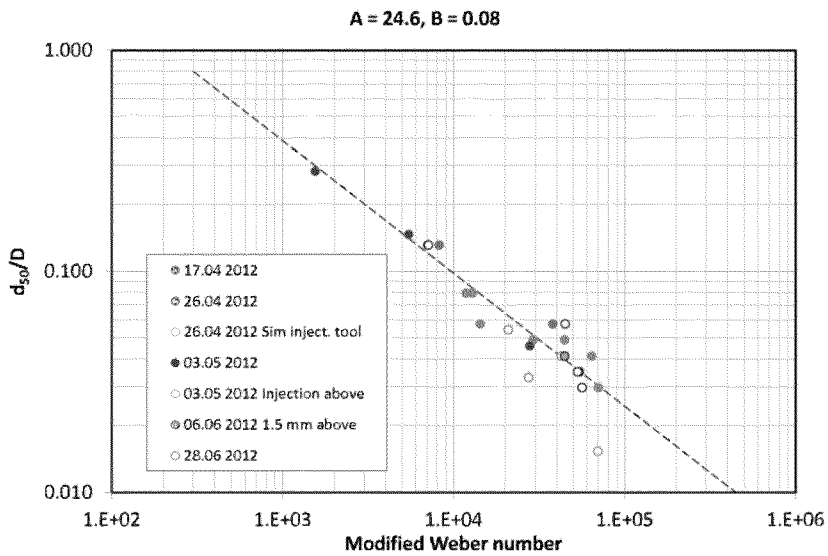

Figure 8.3: Modified Weber number plot of median droplet size data for experiments with no treatment and with dispersants. The modified Weber number includes the correction for the viscosity effect, and is defined as $We^* = We/[1 + B\ Vi\ (d_{50}/D)^{1/3}]$. The broken line represents the Wang and Calabrese model with coefficients A = 24.6 and B = 0.08.

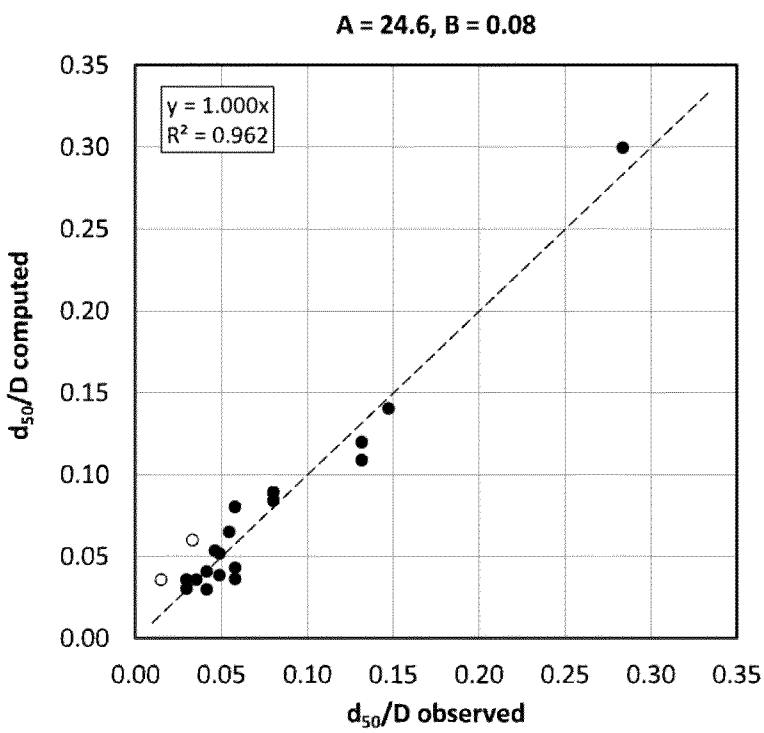

Figure 8.4: Measured and computed relative median droplet sizes d_{50}/D from all experiments. The computed values are determined with the Wang and Calabrese model with best fit coefficients A = 24.8 and B = 0.08. The data points with open markers are excluded from the correlation (see text).

In order to demonstrate the implications of the modified Weber number model, we have used results from the April 17 experiments (Figure 8.5). The figure shows measured median droplet diameters as a function of the corresponding viscosity number Vi = μ U/σ, where μ is the dynamic viscosity of the oil, U is the exit velocity and σ is the interfacial tension. Since the oil viscosity and the exit velocity are constant in these experiments, increasing values of Vi is caused by reduced interfacial tension due to injection of dispersants with increasing DOR. The computed line shows an asymptotic behavior with increasing values of Vi, with the median droplet diameter approaching a lower limiting value (broken line), determined by the exit Reynolds number (Eq. 8.5). The measured median droplet diameters follow a comparable trend, with deviations most probably related to uncertainties in the determination of the interfacial tension. Further details can be found in Johansen et al., 2013.

This demonstration has two important implications:

- Below a certain DOR, further increase in DOR will have minor effect on the median droplet size
- The achievable minimum droplet size will be limited by the exit Reynolds number

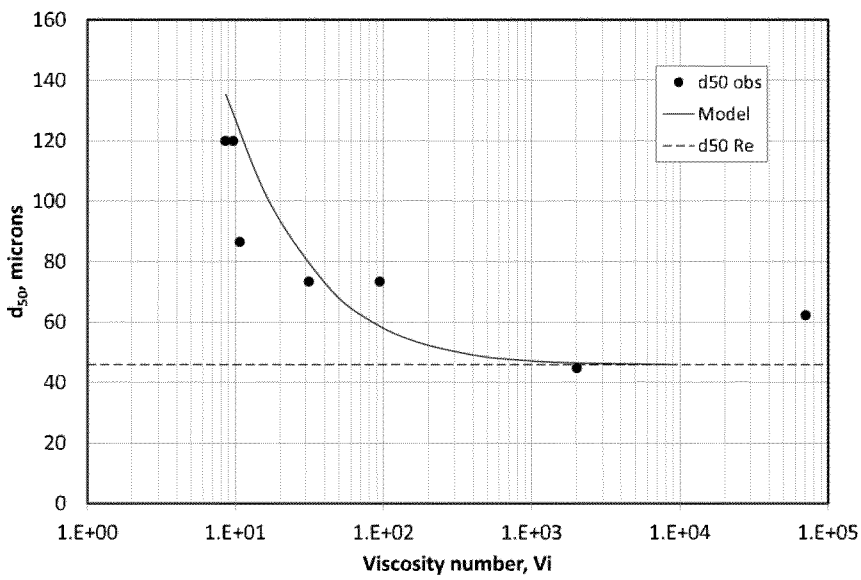

Figure 8.5: Measured and computed median droplet sizes d_{50} from the April 17 experiment with 1.5 mm nozzle diameter and 1.5 l/min oil flow rate. The viscosity number increases due to reduced IFT caused by injection of dispersants with increasing DOR. The computed values (marked "Model") are determined with the Wang and Calabrese model with the coefficient A and B as found above. The broken line marked "d50 Re" represent the lowest achievable median droplet size for the given Reynolds number (Eq. 6.5).

8.3 Droplet size distributions

The analysis above provides a method for estimating the median droplet size depending on outlet conditions and IFT, but in order to predict the actual droplet size distribution, an appropriate size distribution function and its parameters must be known. Here, we will consider to distribution functions commonly used for representing droplet and particle size distribution; the lognormal distribution and the Rosin Rammler distribution.

ED_001324_00000703-00079

The lognormal distribution is in principle a normal distribution based on the logarithm of the observed droplet sizes, and may be expressed as Normdist(x, mean, stdev) where x = ln(d), mean = arithmetic mean of x and stdev is the standard deviation of the x-values. The Rosin Rammler distribution is expressed by the equation $V = 1 - \exp[k (d/d_{50})^{\alpha}]$, where V is the cumulative volume fraction, the coefficient k = 0.693, d_{50} is the volume median droplet size, and α is the spreading parameter. The validity of a chosen distribution function can be tested by linearization. If the observations fall on a straight line after certain transformations of the variables, the chosen distribution function applies, and the parameters for the distribution can be determined.
For the lognormal distribution, linearization is obtained by plotting normalized deviations from the mean as a function of the logarithm of the droplet size. The normalized deviations S are expressed in units of standard deviations, and may be determined from the cumulative probabilities P by the function S = NormInv(P, mean = 0, stdev = 1). The Rosin Rammler distribution can be linearized by plotting the logarithm of Y = -ln(1-V) as a function of the logarithm of the droplet size. When several data sets are involved, it is convenient to rather use a relative measure of the droplet size, i.e. $\delta = d/d_{50}$, where d_{50} is the volume median droplet diameter.

We have applied this approach to two series of experiments – the series from April 14 2012 with upstream injection of dispersants in a wide range of DOR, and the vertical dispersant injection experiments conducted on July 6 2012. The cumulative distributions that were obtained from the LISST data are shown in Figure 8.6. Note that the distributions are limited upwards by the 500 microns upper detection limit of the LISST instrument. The cumulative volume fraction at the detection limit is estimated from the observed peak diameter – presumed to corresponding to 50% by volume – and a best fit logarithmic standard deviation for the whole set. The graphs show a clear left-hand shift in the droplet distributions with increasing DOR values and decreasing injection heights, while the shape of the distributions seems to be more or less unchanged. Figure 8.7 and Figure 8.8 show the same distributions in linearized form.

Figure 8.7 indicates distinct differences between the two tests series. To the extent that a lognormal distribution applies to the data, the vertical injection tests from June 6 implies a significantly larger standard deviation than the upstream injection test series from April 17 (stdev = 1.1 vs. 0.7). Moreover, the April 17 series gives a good fit to a lognormal distribution for S-values down to -2, corresponding to a cumulative volume fraction of 2%. The data from the June 6 test series also shows a reasonably good fit to a lognormal distribution, even while the data deviates more from a straight line. However, these deviations may to some extent be due to variations in the standard deviations between the different tests.

The Rosin Rammler plot in Figure 8.8 indicates that the data from the April test series gives the best fit to the Rosin Rammler distribution in the low to medium range of the distribution. Distinct deviations from a straight line are seen for Y-values below 0.01 and above 2.3, corresponding to cumulative volume fractions of respectively 1% and 90%. For the June 6 test series, the results indicate significant variations in the spreading parameter of the Rosin Rammler distribution. A good fit is found with $\alpha = 1.8$ for the whole range of the oil only data, but to the extent that the Rosin Rammler function applies, data from the injection tests implies smaller values of the spreading parameter.

ED_001324_00000703-00080

In total, these findings point in favour of the lognormal distribution, but with the implication of possible variations in the standard deviations depending of the injection method. For the upstream injection tests, the best fit overall to the lognormal was obtained with stdev = 0.7, while a larger standard deviation (stdev = 1.1) was found for the vertical injection tests.

ED_001324_00000703-00081

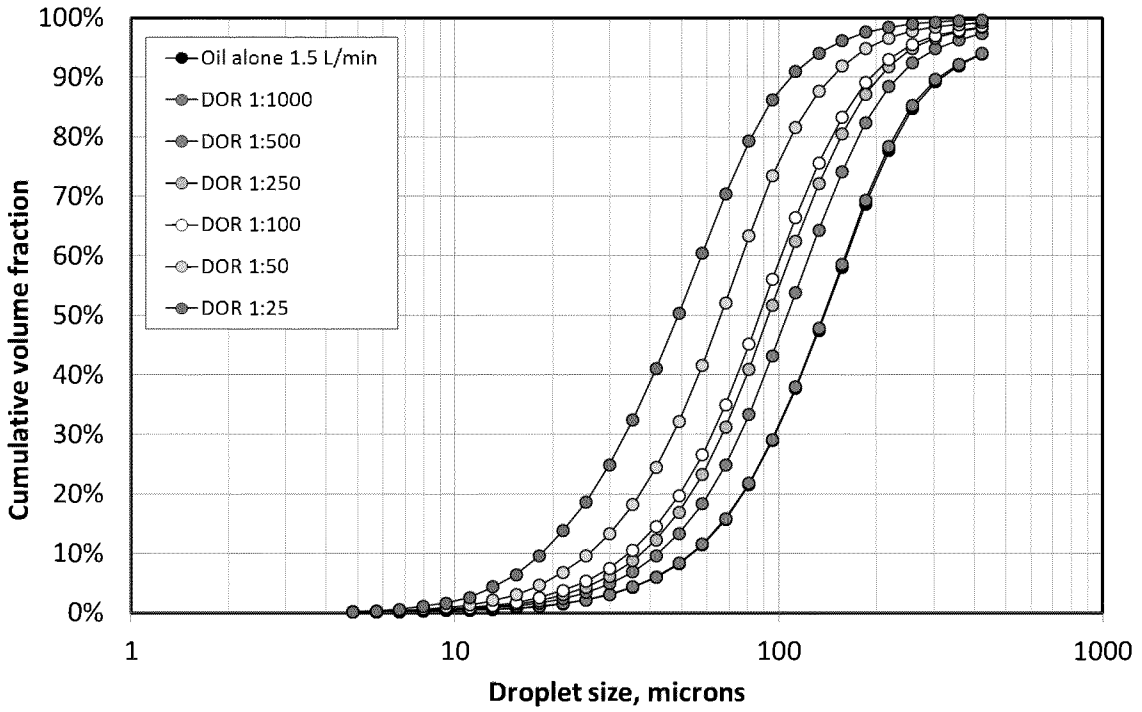

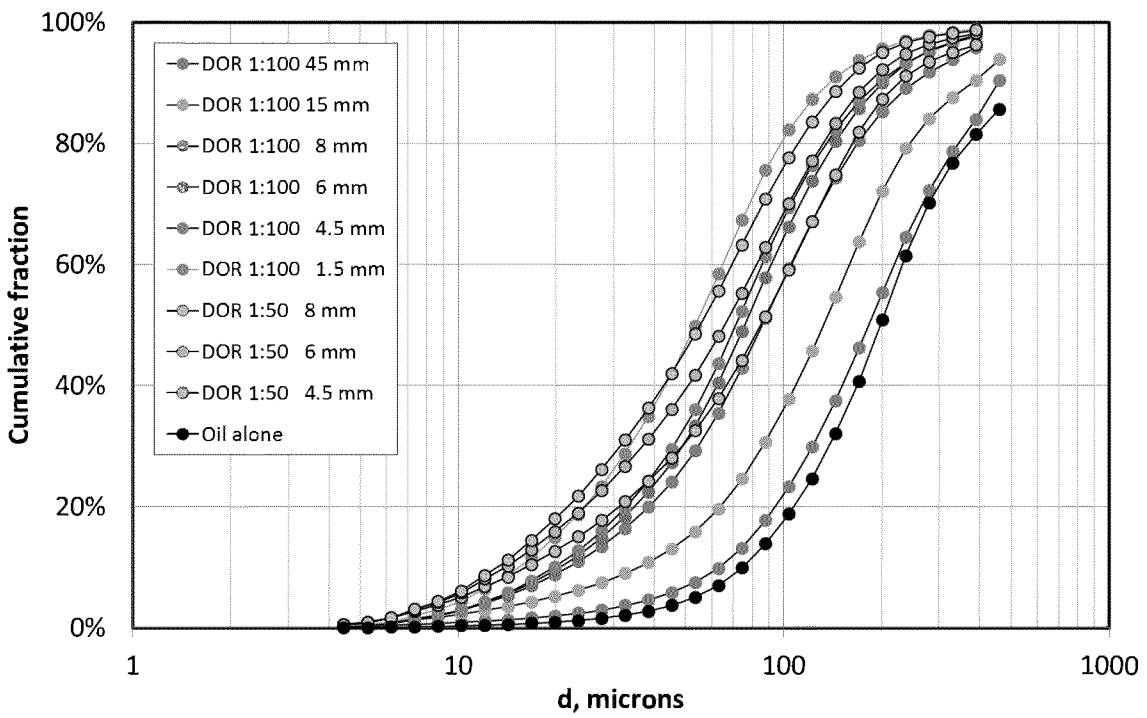

Figure 8.6: Measured droplet size distributions from the April 17 experiments with upstream injection of dispersants (top) and the June 6 experiments with injection of dispersants at various heights above the nozzle (bottom). Corresponding DOR values and heights are given in the legend. Note that the distributions are limited upwards by the 500 microns upper detection limit of the LISST instrument. See text for more details.

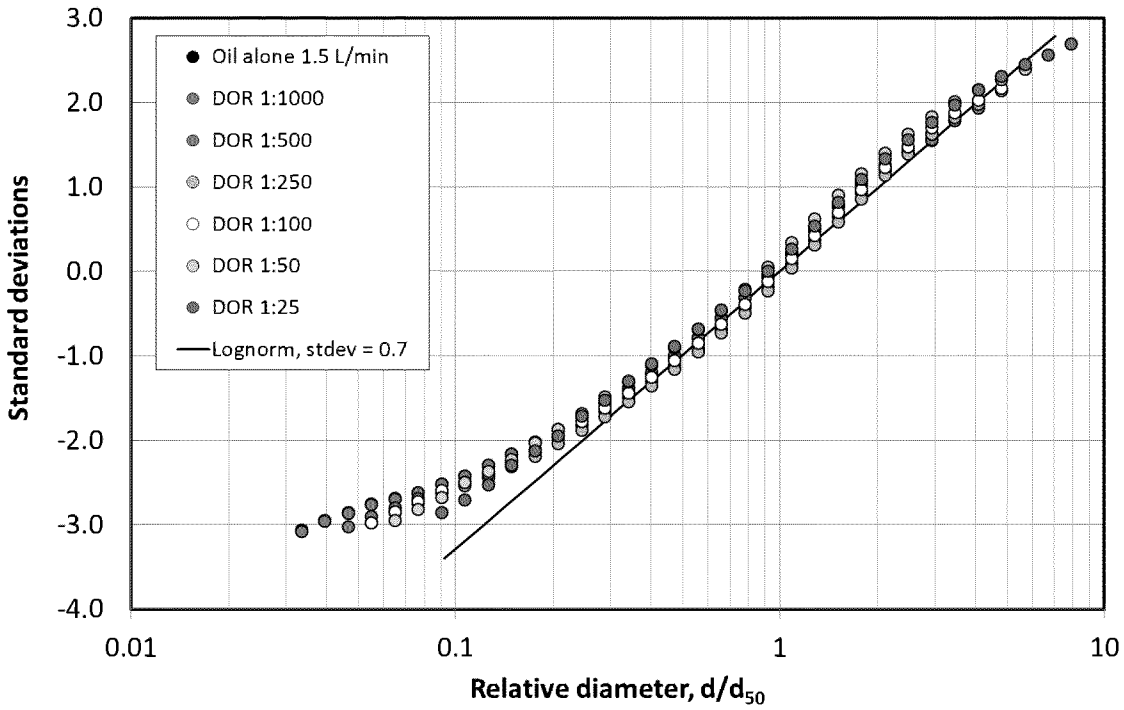

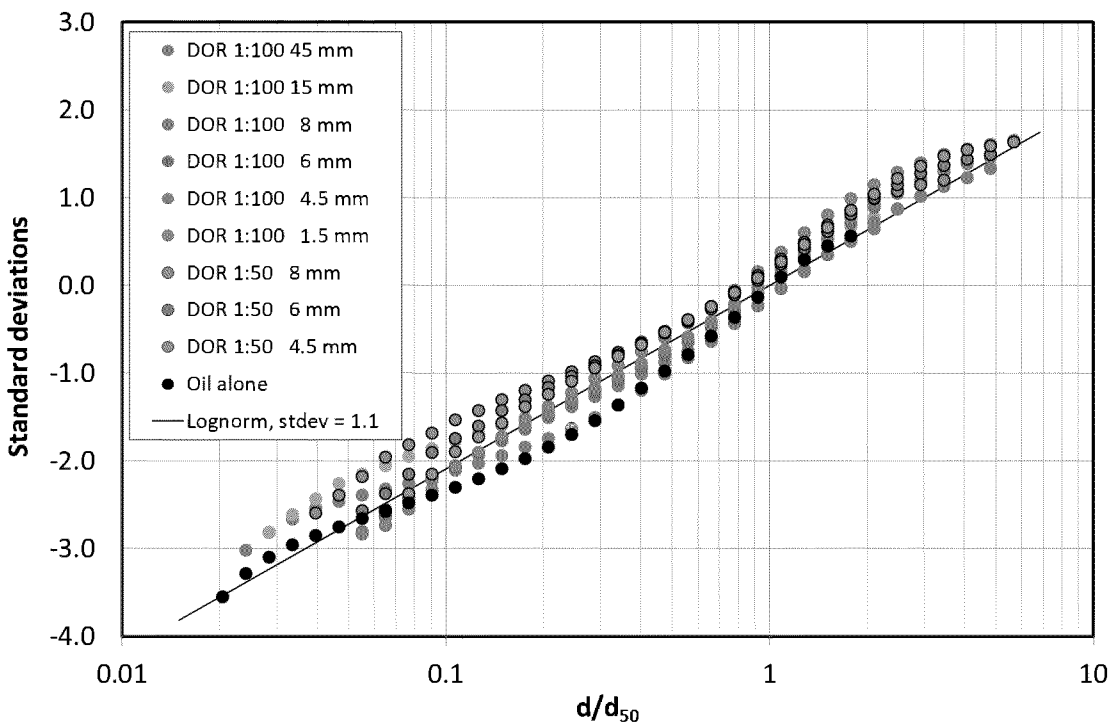

Figure 8.7: Lognormal linearized droplet size distributions from the April 17 experiments and the June 6 experiments. Corresponding DOR values and heights are given in the legend. Note that the distributions are limited upwards by the 500 microns upper detection limit of the LISST instrument. See text for more details.

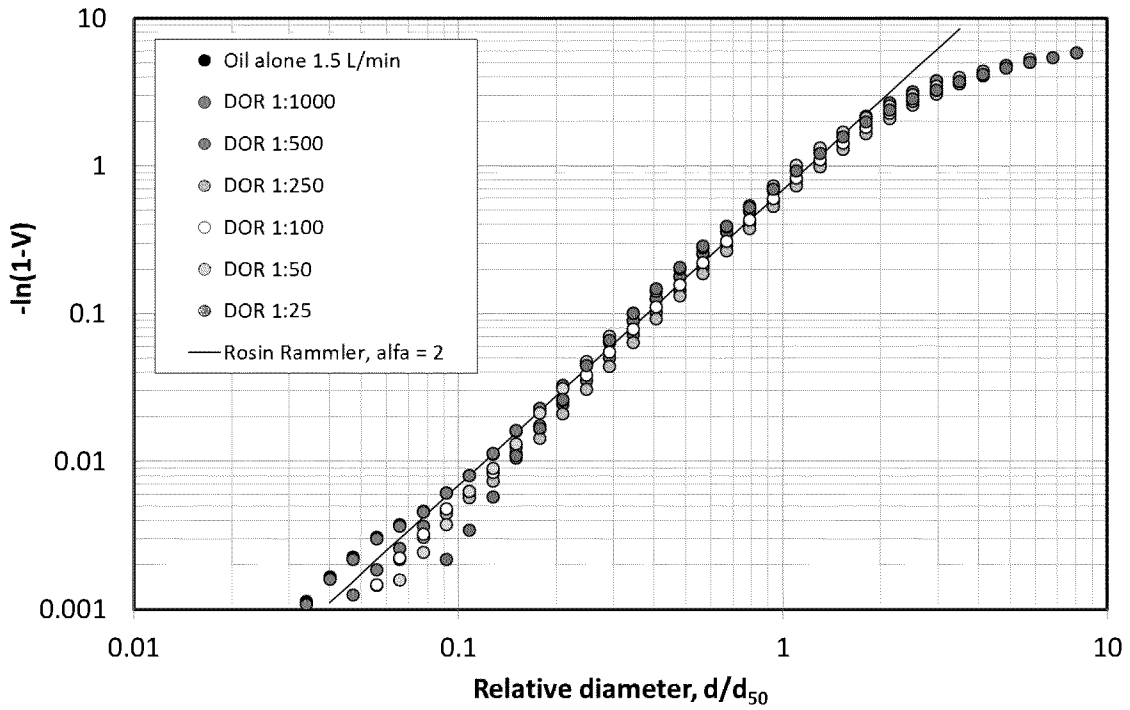

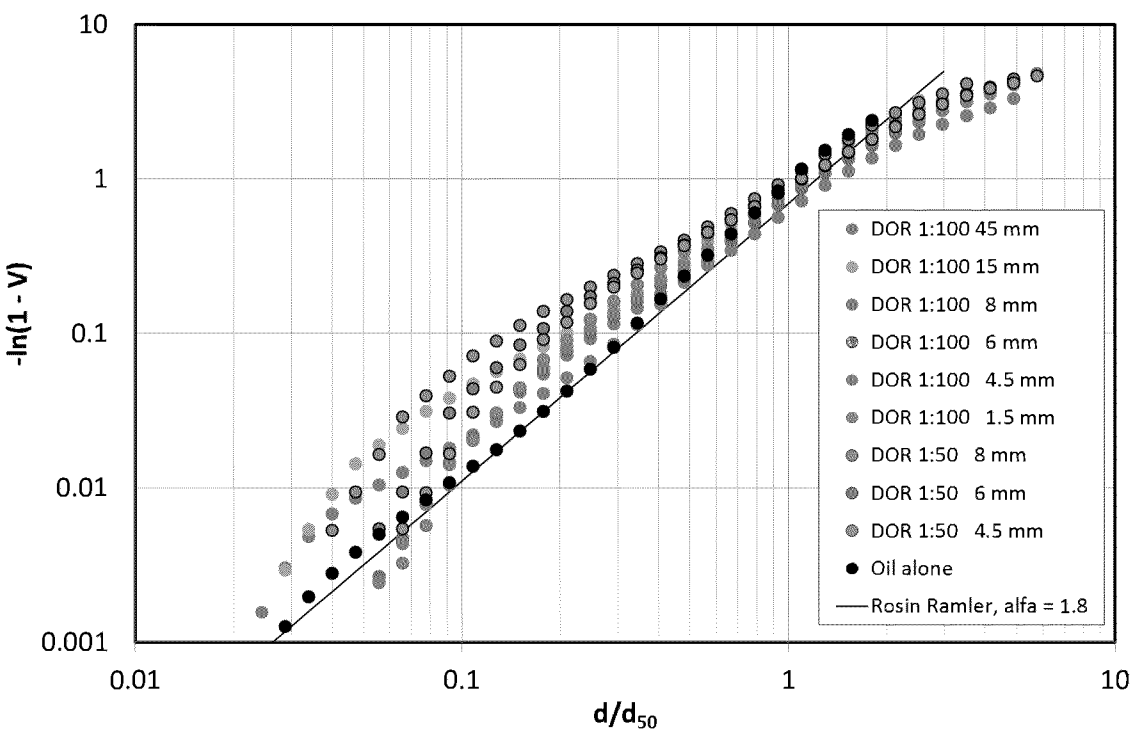

Figure 8.8: Rosin Rammler linearized droplet size distributions from the April 17 experiments and the June 6 experiments. Corresponding DOR values and heights are given in the legend. Note that the distributions are limited upwards by the 500 microns upper detection limit of the LISST instrument. See text for more details.

8.4 Effects of air injection

In the chapter on the theory of droplet breakup in turbulent jets (Chapter 3), we found that the effect of gas released together with oil could be accounted for in terms of an efficient exit velocity expressed by the equation $U_e = U_{oil} (1 - n)^{-1/2}$, where U_{oil} is the oil only exit velocity (i.e. the oil volume flow rate divided by the nozzle cross section), and n is the gas void fraction in the exit flow. Due to the fact that the LISST instrument does not discriminate between gas bubbles and oil droplets, the present experimental setup makes it difficult to test this assumption directly. However, in this section, we will make an attempt to separate gas bubbles from oil droplets on a theoretical basis. For this purpose, we have selected two experiments with injection of dispersants at a DOR of 1:50 with the simulated injection tool. The first experiment was conducted with oil only, while in the second experiment, air was injected together with oil at a 1:1 ratio. Figure 8.9 shows the droplet size distributions obtained with the LISST instrument in both cases. The nozzle diameter was 1.5 mm, and the total flow rate was 1.2 L/min in both cases, but made up of equal volume parts of air and oil in the second case, corresponding to a gas void fraction of 50%.

The oil only experiment has a peak droplet diameter of 53.5 microns, while the peak diameter is shifted to 237 microns in the second experiment. However, the second distribution seems to be bimodal, with a secondary peak at about 75 microns. This secondary peak coincides reasonably well with the expected shift in the median droplet size due to the mixed oil and gas flow: with equal total flow rate, but a void fraction of 50%, the effective exit velocity will be reduced by a factor of 1.4 (square root of two). With a Reynolds number correlation for the median droplet size with an exponent of -3/4, this implies an increase in the median droplet size with a factor of 1.3, i.e. from 53.5 to 69.3 microns.

Assuming that the bimodal distribution reflects a sum of the distributions of oil droplets and gas bubbles, the main peak will be related to the peak diameter of the gas bubble distribution. Figure 8.10 shows an attempt to explain the total distribution in terms of two distinct distributions, one representing oil droplets, and one representing gas bubbles. Both distributions are presumed to be log-normal distributions, defined be the median droplet/bubble diameter and the logarithmic standard deviation.

ED_001324_00000703-00085

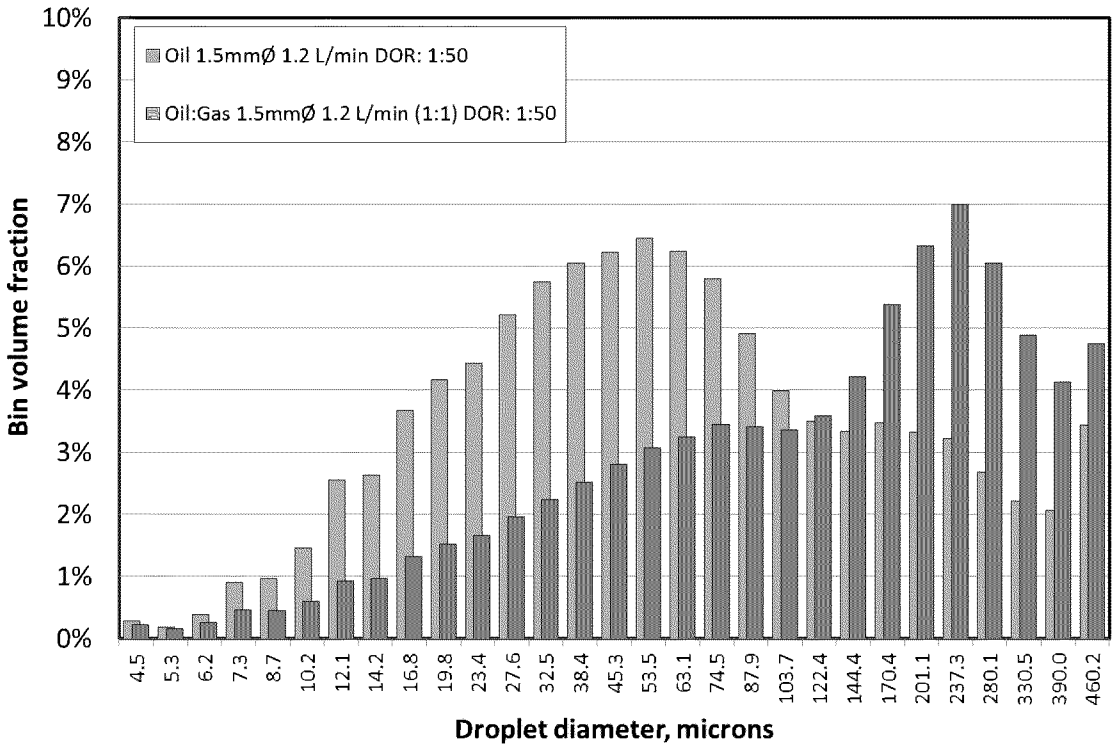

Figure 8.9: Droplet size distributions obtained with the LISST instrument for two experiments with injection of dispersants, one with oil only and one with gas together with oil (see legend).

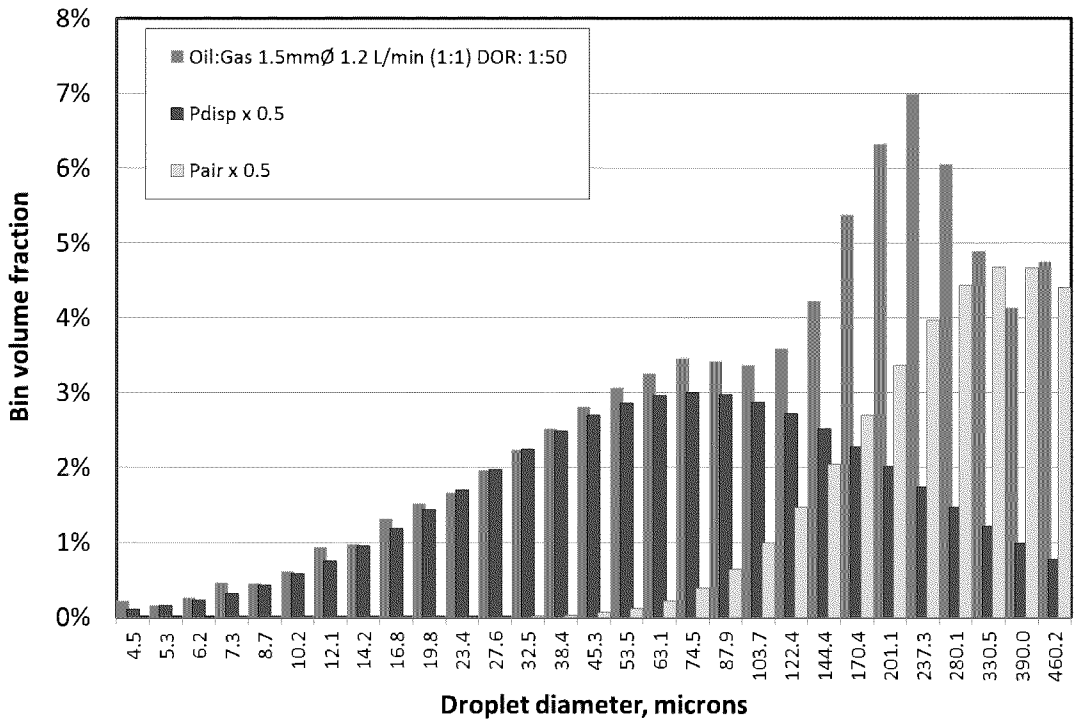

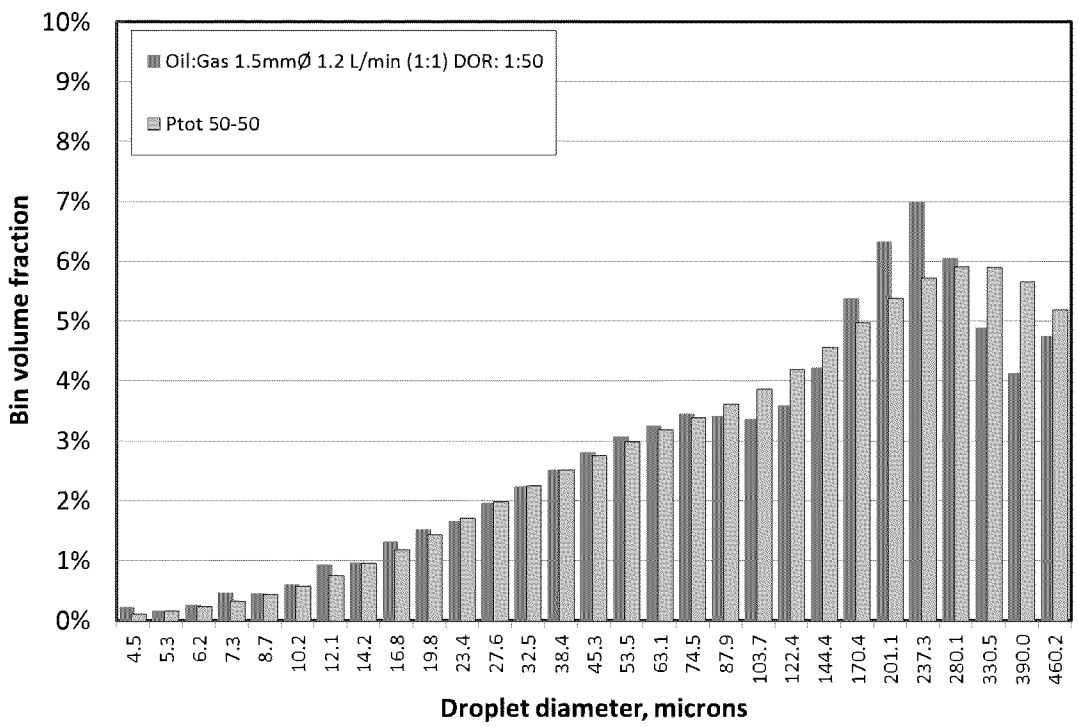

Figure 8.10: Bimodal droplet size distributions composed of equal amounts of oil and gas. The top graph shows the presumed distributions for oil droplets and gas bubbles (each reduced by a factor of 0.5) on the background of the observed bimodal distribution (grey columns). The bottom graph shows the combined distribution on the background of the observed distribution (grey).

The median diameter for the oil droplet distribution is taken as 70 microns, according to the assumption above on the effect of a 50% void fraction, while the standard deviation is chosen as 1.1 in natural log units based on the observed distribution (see top graph in Figure 8.10). For the air bubble distribution, the standard deviation was set to 0.7 in natural log units, and the median air bubble diameter was chosen as 330 microns. The latter is larger than the observed main peak at 237 microns, but is meant to account for the left-hand shift in the visible peak due to the superposition of the droplet size distribution. However, the median bubble size of 330 microns also corresponds to the peak diameter observed in a parallel experiment with 1:1 flow rates of water and air, where the nozzle size and the total flow rate was the same as in the oil-air experiments, but with water replacing oil. Figure 8.10 shows that the bimodal character of the distribution is less pronounced in the computed composite distribution, but when presented in cumulative form, the correspondence between the observed and computed distributions is striking, as shown in Figure 8.11.

Thus, in total, the present analysis of the results from the experiment with dispersant injection in a mixed oil and air flow is found to provide a plausible explanation of the observed increase in the peak droplet size as an effect of the presence of gas bubbles. Secondly, it also gives support to the assumption of the momentum related effect of gas on the median droplet size.

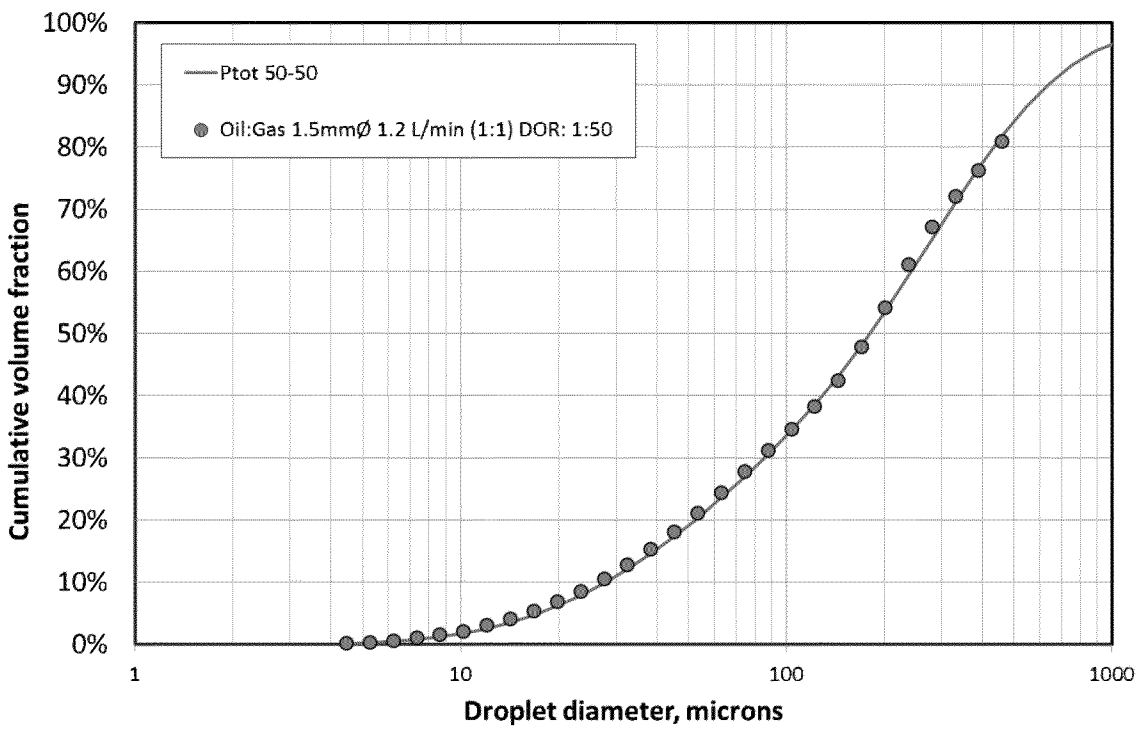

Figure 8.11: Cumulative droplet size distributions composed of equal amounts of oil and gas. The markers show the observed cumulative distribution from the experiment discussed above with dispersant injection with DOR 1:50 in a mixed (1:1) oil and air flow. The solid line shows the computed distribution composed of separate oil droplet and gas bubble distributions.

ED_001324_00000703-00088

8.5 Up-scaling from lab to field

Up-scaling of the results from the tower tank experiments to full scale conditions may in principle be based on a Weber number scaling. By assuming a certain full scale outlet diameter D, we can determine the oil flow rate Q that corresponds to a Weber number in one of the laboratory experiments. From the expression for the outlet volume flow $Q = \pi/4\ D^2\ U$ we can eliminate the outlet velocity U and get an expression for the Weber number in terms of volume flow:

$$We = (\rho/\sigma)\ (4/\pi)^2\ Q^2/D^3 \tag{8.6}$$

Solving for Q gives us an expression for the equivalent oil volume flow Q_{eq} for a given outlet diameter and Weber number:

$$Q_{eq} = \pi/4\ We^{1/2}\ (\sigma/\rho)^{1/2}\ D^{3/2} \tag{8.7}$$

The corresponding oil only outlet velocity will be:

$$U = Q/\ (\pi/4\ D^2) \tag{8.8}$$

For releases with both gas and oil, we must also apply the void fraction adjustment as described in Chapter 3. For large volume flows which might be buoyancy dominated, an exit Froude number adjustment must also be applied, also described in Chapter 3:

Adjustment for void fraction:

$$U_n = U/(1 - n)^{1/2}, \tag{8.9}$$

where U is the oil only outlet velocity and n is the gas void fraction at the exit.

Adjustment for buoyancy (large volume flows):

$$U' = U_n\ (1 + Fr^{-1}), \tag{8.10}$$

where $Fr = U_n\ /(g'\ D)^{1/2}$ with $g' = g\ [\rho_w - \rho_{oil}\ (1 - n)]/\rho_w$.

The adjusted velocity U′ is used in the Weber and Reynolds numbers to get respectively $We' = \rho\ U'^2\ D/\sigma$ and $Re' = \rho\ U'\ D/\mu$, and these corrected non-dimensional numbers are then used in the modified Weber number correlations to predict the volume median droplet size.

Table 8.2 shows two examples where these principles have been applied to up-scaling. The different variables in the table are explained in the following.

Table 8.2: Up-scaling from tower tank tests to field test and full scale conditions. Variables are explained in the text.

	D, mm	Q_{oil}	Void	U_{oil}, m/s	U', m/s	We'	Re'	d_{50} oil	d_{50} disp
Lab. exp.	1.5	1.5 L/mn	0 %	14.1	14.1	15 283	1 783	133 µm	45 µm
Field exp.	120	64 m^3/h	50 %	1.6	2.5	38 273	25 230	5.4 mm	0.5 mm
Full scale	400	392 m3/h	50%	0.9	2.7	153 670	92 300	7.7 mm	0.76 mm

The equivalent oil flow rate Q_{oil}, is determined from the Weber number and the chosen up-scaled outlet diameter D by use of Eq. 8.7. The corresponding oil only outlet velocity U_{oil} is computed from Eq. 8.8. This velocity is adjusted for gas void fraction (Eq. 8.9) and Froude number (Eq. 8.10) to get the adjusted velocity U'. The volume median droplet sizes d_{50} are computed from the modified Weber number model (Eq. 8.3) for untreated oil (d_{50} oil) and treated oil (d_{50} disp), with

ED_001324_00000703-00089

dispersant injection presumed to cause a reduction in IFT by a factor of 200. Two up-scaled diameters are shown – one representing the DeepSpill field experiment with an outlet diameter of 120 mm, and one full scale corresponding to a diameter consistent with a blow-out scenario with an outlet diameter of 400 mm.

The resulting droplet size distributions are shown in Figure 8.12. The distributions are based on the volume median diameters shown in Table 8.2. Lognormal distributions with a standard deviation of 0.7 are used for treated oil and untreated oil for lab conditions. For the field experiment conditions and the full scale condition lognormal distributions with the same standard deviation are used for treated oil, while Rosin Rammler distributions with a spreading parameter of 1.8 are used for untreated oil.

Compared to the laboratory conditions, the results for the field experiment and the full scale conditions show considerably larger median droplet sizes, but at the same time, a larger shift is found in the median droplet size from untreated to treated oil. The first effect is due to increased outlet diameters as expected by the Weber number scaling: $d_{50} = D\ A\ We^{-3/5}$, implying $d_{50} \sim D$ for constant We. However, it should be noted that the computed increase in the median droplet will be much less than proportional to the increase in diameter when the effects of void fraction and buoyancy is taken into account. Keeping in mind that the median droplet size for treated oil may be expected to follow a Reynolds number correlation, the increased relative effect on treatment for the field experiment and full scale conditions may be related to the large increase in the Reynolds number caused by the increased outlet diameters: assuming constant Weber number and increasing outlet diameter, the Reynolds number will increase in proportion to the square root of the diameter. In addition, since the adjustment for void fraction and buoyancy will cause an increase in the effective outlet velocity, a further increase in the Reynolds number will follow, as shown in Table 8.2.

ED_001324_00000703-00090

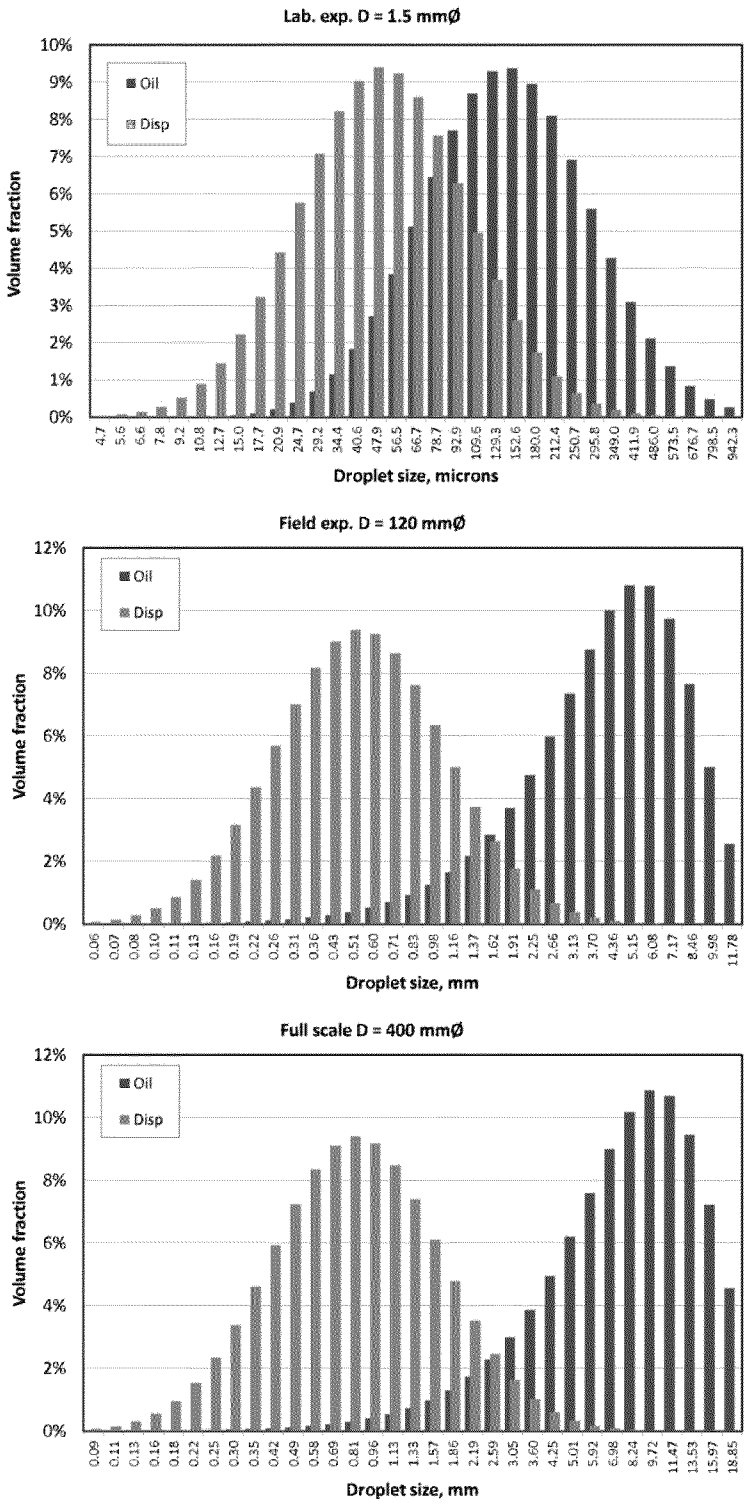

Figure 8.12: Droplet size distributions for laboratory scale (top), field scale (middle) and full scale discharges (bottom), with oil only flow rates computed from the Weber number corresponding to the experimental conditions. Blue columns represent treated oil (labeled "Disp"), while brown columns represent untreated oil (labeled "Oil").

9 Conclusions

The major findings from the discussions are summarized in this chapter.

9.1 Dispersant dosages

The dosage experiments were performed with varying dispersant to oil ratios (DOR) from 1:1000 (0.1%) to 1:25 (4%). Two experiments were performed with Corexit 9500 and one with a reduced solvent version of C9500 (giving approximate 100% more active material).

- A clear correlation between DOR and the shift in droplet size distribution towards smaller droplets was observed. Very limited effect was observed for the lowest concentrations, steadily increasing up to shift corresponding to a third of the initial VMD at the highest concentration.
- The effect of the more concentrated version of Corexit gave shifts in MVD that corresponded to the increased content of active material (double concentration) and corresponding reduction in IFT.

9.2 Dispersant injection techniques

Three different injection techniques were tested; Simulated insertion tool, injection above nozzle into the rising oil and sidewise injection into the rising oil.

- The tested injection methods gave similar results (reduction or shift in VMD), independent of whether the dispersant was injected immediately before the outlet (simulated injection tool) or immediately after the outlet.
- An oil jet sprayed from a nozzle, like in a subsurface blow-out or in our down-scaled experiments, will form a solid oil cone up to approximately 6 nozzle diameters. Injecting the dispersant into this solid oil cone seems to be most efficient. With this approach the dispersant will mix into the oil and reduce the IFT before the oil enters the highly turbulent zone where the droplets are formed.

9.3 Experiments with warm oil

An initial experiment with warm oil (58 °C) was performed. The results indicated a reduced effect of dispersant injection, since larger droplets (VMDs) were measured compared to experiments with lower oil temperature (11 °C). However, the validity of this single initial experiment is uncertain and the effect of oil temperature will be studied more in detail in Phase-II of this project.

9.4 Experiments with different nozzle sizes to verify scaling approach

The nozzle diameter is a main scaling parameter for the design of the experiments in the SINTEF Tower basin. The following experiments were performed to verify the validity of this approach:

- A series of experiments with varying nozzle size (0.5, 1.5 and 3mm)
- Dispersant was injected in the same position relatively to the nozzle size (3 D above).

Dispersant treatment with all three nozzles sizes gave a similar relative reduction in VMD, e.g. 0.34-0.38 for DOR 1:100. This means that for all three nozzle sizes, the diameter of the droplets (VMD) are reduced to a third when using a DOR 1:100.

The results from these experiments are very supportive for the basic idea behind SINTEFs down-scaled Tower basin approach. The fact that scaled dispersant experiments gave consistent results is very encouraging for utilizing these results in operational oil spill models. These models can then be

ED_001324_00000703-00092

used both for contingency planning, environmental risk assessments and guidance for operative subsurface releases including dispersant injection (see next chapter).

9.5 Data analysis – Modelling

The major findings from the analysis of the experimental data may be summarized as follow:

Droplet size model:

- The analysis of the results from the tower tank experiment with and without dispersant injection gives support to a modified Weber number model with coefficients A ≈ 25 and B ≈ 0.08. For cases with injection of dispersants at high DOR, this correlation tends to change into a Reynolds number scaling. Further details can be found in Johansen et al., 2013.
- The droplet size distributions for treated oils tend to follow lognormal distributions, while the Rosin Rammler distribution may provide a better fit for untreated oils.

Mixed oil and gas flows:

- The effect of mixed oil and gas flows is difficult to assess directly because the LISST instrument does not discriminate between oil droplets and gas bubbles. However, we have made an indirect assessment by considering droplet size distribution data obtained from two tower tank experiments with upstream injection of dispersants, one with and one without air mixed into the oil line.
- The apparent increase in the peak droplet size with mixed oil and air flows has been explained as an effect of a gas bubble distribution superimposed on an oil droplet size distribution.
- This case study also gives support to the assumption of the momentum related effect of gas on the median droplet size.

Up-scaling from lab to full scale:

- Up-scaling from lab to full scale can occur by choosing a representative full scale outlet diameter and keeping the Weber number constant. On this basis an equivalent oil flow rate can be computed for the full scale conditions.
- Calculations of oil droplet size distributions for up-scaled conditions with untreated oil show an increase in the volume median droplet size with increasing outlet diameters, but when adjustments are made for void fraction and buoyancy flux, this increase is considerably less than expected from a simple Weber number scaling.
- For up-scaled conditions with dispersant injection, a larger relative shift in droplet size is found than in the lab tests. This is explained by the observation that the median droplet size will be expected to follow a Reynolds number correlation for treated oils. Assuming constant Weber number and increasing outlet diameter, the Reynolds number will increase in proportion to the square root of the diameter. In addition, since the adjustment for void fraction and buoyancy will cause an increase in the effective outlet velocity, a further increase in the Reynolds number will follow.

ED_001324_00000703-00093

10 Recommendations

The following questions or topics have been identified during the discussion of this report and should be evaluated for further studies:

1. How does the temperature of the released oil influence the droplet size distribution of the oil, both with and without injection of dispersants? The preliminary results from this study should be verified with additional experiments.

2. Does the presence of gas (air), released together with oil, influence the droplet size distribution of the oil, both with and without injection of dispersants? The results obtained so far have been difficult to interpret since the main instrumentation (LISST) cannot distinguish between oil droplets and gas bubbles. Other methods to quantify size of gas bubbles should be evaluated.

3. How does dispersant effectiveness, measured by shift in droplet size distribution, vary as a function of oil properties (different oil types), dispersant type (commercial available products) and dispersant dosage? Several, carefully selected, oil types and dispersants should be tested.

4. How does the deep water pressure (100-300 bars) influence droplet formation and effect of dispersant injection? How can this be studied in pressurized tanks under controlled conditions similar to the SINTEF Tower basin?

5. How does "live oil" influence the formation of droplets and the effect of dispersant injection? How will the release of gas (degassing), precipitation of waxes and asphaltenes, hydrate formation etc. during the release influence oil droplet formation? Can such experiments be performed in pressured tanks as indicated above? Can also additional natural gas be added in these experiments?

6. How do different release or turbulence conditions for the oil release influence droplet formation? Experiments should also be studied with significantly less turbulence, not only in the "Atomizing range", but also in the "Transition" and "Pendant drop" zone.

7. The upper limit for nozzle size and flow rates should be explored. It should be possible to do short term experiments (30-120 seconds?) in the SINTEF Tower Basin with significant higher flow rates (10-15 mm nozzle and 100-200 L/min).

8. How does dispersant treatment influence possible coalescence and droplet splitting in the plume after the initial droplet sizes are formed? Experiments with multiple instruments (LISST at different heights?) could be performed.

9. As an alternative to the resource demanding experiments in the SINTEF Tower basin (42 m^3), bench-scale testing in the new MiniTower (80 L) should be evaluated and compared.

11 References

Brandvik, P.J., Johansen, Ø., Leirvik,F., Farooq, U., and Daling, P.S. 2013. Droplet breakup in sub-surface oil releases – Part 1: Experimental study of droplet breakup and effectiveness of dispersant injection. Mar. Pollut. Bull. 2013 Volume 73, Issue 1, 15 2013, pp. 319-326.

Khelifa and So. (2011). Effects of chemical dispersants on oil-brine interfacial tension and droplet formation. *34th AMOP Technical seminar on environmental contamination and response.* Alberta.

Liu, S. (2007). Alkaline surfactant polymer enhanced oil recovery process. Rice University, USA: PhD Thesis.

Miller et al., R. F. (2001). Characterization of water/oil interfaces. I J. Sjoblom, *Encyclopedic handbook of emulsion technology* (ss. 1-41). New York: Marcel Dekker, Inc.

Standness and Austad. (2000). Wettability alteration in chalk: 2. Mechanism for wettability alteration from oil-wet to water-wet using surfactants. *JPSE, 28*, 123-148.

Zhang et al. (2002). Studies of synergism/antagonism for lowering dynamic interfacial tensions in surfactant/alkali/acidic oil systems 1. synergism/antagonism in surfactant/model oil systems. *J. Colloid Interface Sci., 249*, 187–193.

Zhang et al., H. B. (2001). Determination of low interfacial tension with a laser light scattering technique and a comparative analysis with drop shape methods. *J. Colloid Interface Sci., 237*, 11-20.

Zhu et al., Y. X. (2008). Production of ultra-low interfacial tension between crude oil and mixed brine solution of Triton X-100 and its oligomer Tyloxapol with cetyltrimethylammonium bromide induced by hydrolyzed polyacrylamide. *Colloids Surf. A., 332*, 90-97.

Or, C.M., Lam, K.M. and Liu, P. 2011: Potential core lengths of round jets in stagnant and moving envirionments. Journal of Hydro-environment Research, Vol. 5, pp. 81-91.

Mohajeri, E and Noudeh, G.D. 2012: Effect of temperature on the critical micelle concentration and micellization Thermodynamic of non-ionic surfactants: Polyoxyethylene sorbitan fatty acid esters. www.ejchem.net E-Journal of Chemistry. 2012, 9(4) 2268-2274. ISSN: 0973-4945.

Hinze, J.O., 1955: Fundamentals of the hydrodynamic mechanism of splitting in dispersion processes. A.I.Ch.E. Journal, Vol. 1, pp. 289-295.

Masutani, S.M. and E.E. Adams, 2000: Experimental study of multiphase plumes and application to deep ocean oil spills. Final report to the U.S. Department of Interior, Minerals Management Service, contract No. 1435-01-98-CT-30946.

Neto, I.E.L., D.Z. Zhu and N. Rajaratnam, 2008: Bubbly jets in stagnant water. International Journal of Multiphase Flow, 34, pp. 1130-1141.

L. Tang and S.M. Masutani, 2003: Laminar and Turbulent Flow Liquid-liquid Jet Instability and Breakup. Proceedings of the Thirteenth International Offshore and Polar Engineering Conference, Honolulu, Hawaii, USA, pp. 317-324.

Hinze, J.O., 1955: Fundamentals of the hydrodynamic mechanism of splitting in dispersion processes. A.I.Ch.E. Journal, Vol. 1, pp. 289-295.

Johansen, Ø., Brandvik, P.J., and Farooq, U. 2013. Droplet breakup in sub-surface oil releases – Part 2: Predictions of droplet size distributions with and without injection of chemical dispersants. Mar. Pollut. Bull. 2013 Volume 73, Issue 1, 15 2013, pp. 327-335.

Lefebvre, AH, 1989: Atomization and Sprays, Taylor & Francis, 421 pp.

Masutani, S.M. and E.E. Adams, 2000: Experimental study of multiphase plumes and application to deep ocean oil spills. Final report to the U.S. Department of Interior, Minerals Management Service, contract No. 1435-01-98-CT-30946.

Neto, I.E.L., D.Z. Zhu and N. Rajaratnam, 2008: Bubbly jets in stagnant water. International Journal of Multiphase Flow, 34, pp. 1130-1141.

Papanicolaou, P.N. and E.J. List, 1988: Investigation of round vertical turbulent buoyant jets. J. Fluid Mech. Vol. 195, pp. 341-391.

Tang L., and S.M. Masutani, 2003: Laminar and Turbulent Flow Liquid-liquid Jet Instability and Breakup. Proceedings of the Thirteenth International Offshore and Polar Engineering Conference, Honolulu, Hawaii, USA, pp. 317-324.

Wang, C.Y. and R.V. Calabrese, 1986: Drop Brekup in Turbulent Stirred-Tank Contractors. Part II: Relative Influence of Viscosity and Interfacial Tension. AIChE Journal, Vol. 32, pp. 667-676.

ED_001324_00000703-00096

Appendix A:
Summary overview of all Tower Basin experiments.

ED_001324_00000703-00097

API D3 - Tower basin experiments – Summary log for all experiments (March – June 2012)

Exper no	Date	Nozzle size (mm)	Type of experiment					
			Rate (L/min)	Oil	Gas	Disp GOR Injection	Comments	ws
1	210312	1.5	0.5/1.5/3	OB	N	1:50	Initial experiment and testing of acoustic sensors (Paul Panetta) Problems with flow regulations (low flows). Acoustic data was good and LISST data on 1.5 and 3 L/min. Water sampling	6
2	130412	1.5	0.5/1.5/3	W OB	Yes	No	Experiments with: water/gas, oil/gas and oil only. Constant total flow. No water sampling Oil alone and Water: Air data were bad Oil alone: Air data is good	
3	170412	1.5	1.5	OB	N	DOR	DOR experiments (Upstream injection) Water sampling (IFT) Good LISST data, very good IFT measurements and Cam/Still data	7
4	190412	1.5	0.5/1.5/3	OB	N		New test with oil alone + Sim Insertion tool injection. Not meaningful droplet distributions? Probably polluted/dirty LISST lenses.	10
5	260412	1.5	0.5/1.2/3	OB		SimInjTool	New round with Oil alone 0.5/1.2/3 Regulators OK/Calibrated.	0
6	030512	0.5	0.1/0.2/0.5	OB	N	Rate exp + Inj above nozzle	Problems with autoregulation of flow. Operated manually □ OK	0
7	160512	3.0	2 + 5	OB	N	Rate exp + Inj above nozzle	Problems with autoregulation of flow. Operated manually □ OK Samples for IFT analysis. Injection too high above nozzle (30 mm)	4

8	290512	1.5	1.2	OB	N	Vert. Inject. DOR 1:50/100	Flow operated manually OK. Samples for IFT analysis (PJ). Problems with particle in dispersant tube, causing overpressure and rapture of tube. No dispersant injected. Very nice replicate experiments with no dispersant injection.	7
9	010612	1.5	1.2	OB	N	Vert. Inject. DOR 1:50/100	Flow operated manually OK. Samples for IFT analysis. Problems with LISST instrument No data saved..!	7
10	060612	1.5	1.2	OB	N	Vert. Inject. DOR 1:50/100	Flow operated manually OK. Samples for IFT analysis. Injection centered with support rods (se video). Moved UW light and installed extra "Diver lights". Very nice video and LISST data	9
11	080612	1.5	1.2	OB	N	DOR 1:1000-1:25	Flow operated manually OK. New DOR experiment at reduced flow rate (1.2 L/min) to produce slightly larger and comparable droplet distributions. Very good video/Still (only nozzleCam/still) and LISST data	7
12	140612	1.5	1.2	OB	N	Horzontal inj DOR 1:50/100	Very successful experiment. Nice pictures with new macro still/video camera.	8
13	200612	1.5		OB	N	Sim inj. tool DOR: 1:100/50/25	Warm vs. cold oil, first experiment, problems with heater only 58C	
14	250612	3.0	2 + 5 + 8	OB	N	Rate exp + Inj above nozzle	New flow rate experiment with 3 mm nozzle. Dispersant injected 9 mm (3 x dia) above nozzle. "Problems" with dispersant pump overpressure at highest disp rate.	
15	280612	1.5	0.5/1.2/3	W	Yes		Water:air Experiment (repeated from experiment 21.03)	8
16	280612	1.5	1.2	OB	N	DOR 1:1000-25	Alternative dispersant (C9500 with less solvent). Viscous disp, but no problems at these low rates. Tried also Sim.inj. Tool but run out of oil..?	

Red: Not successful experiment
Yellow: Partly successful experiment
Green: Completely successful experiment

WS: Water samples (oil analysis, surfactant analysis or IFT measurements)

Appendix B:
Experimental data: Numerical distributions of oil and experimental conditions.

ED_001324_00000703-00101

ED_001324_00000703-00102

SINTEF

1704-2012

Date 1704-2012

Date: DDMM-YYYY of experiment – Used to identify each experiments in the report

Conditions C9500-Premixed DOR 1:1000-1:25
Comments DOR experiment
Nozzle size 1,5mm, 1,5L/min

This field is used to define the experimental conditions and the purpose or type of experiment

Name Oil alone 1,5 L/min
Average start 550 15:51:58
Average stop 600 15:52:48
Number of records 50

One experiments contains many runs with different flow rates, injection techniques and/or dispersant to oil ratios (DORs). This section identifies each run or data segment.
Name: Used as identifier (legends) in many of the figures in the report.
Start/Stop and **Number of records** identifies the data records averaged and used to represent this run or data segment.

Bins	2,73	3,22	3,8	4,48	5,29	6,24	7,36	8,69	10,2	12,1	14,3	16,8	19,9	23,5	27,7	32,7	38,5	45,5	53,7
	63,3	74,7	88,2	104	122	144	170	201	237	280	331	390	460						
Average conc	5,28	2,17	0,72	0,22	0,11	0,12	0,16	0,13	0,17	0,30	0,37	0,63	0,93	1,27	1,84	2,53	3,42	4,63	
	6,46	8,75	12,05	15,10	17,90	20,00	21,71	21,60	18,56	14,36	9,23	5,60	4,00	4,67					
Stdev conc	0,74	0,31	0,11	0,04	0,02	0,03	0,05	0,04	0,07	0,12	0,16	0,26	0,38	0,49	0,69	0,94	1,25	1,68	
	2,27	2,97	3,90	4,75	5,59	6,30	7,08	7,36	6,63	5,18	3,32	2,02	1,60	2,38					

Bins: Midpoint in microns for each of the 32 log distributed bins. These are not given for each of the data sets.

Average conc: Averaged concentration in ppm (10 measurements per second/record, usually 300-500 measurements) for all droplets within each bin.
Stdev conc: Standard deviation in concentration for all droplets within each bin. Reflects both experimental variation and the size variation within each bin.

ED_001324_00000703-00103

Date 0305-2012
Conditions Small Nozzle experiments
Comments Injection above nozzle (3 x nozzle dia)
Nozzle size 0.5mm - 0.1 / 0.2 / 0.5 L/min
Name 0.5 mm - 0.1 L/min

Average start	348	15:12:8																	
Average stop	402	15:13:2																	
Number of records	54																		
Average conc	0,35	0,23	0,15	0,10	0,10	0,13	0,16	0,15	0,20	0,23	0,22	0,26	0,27	0,36	0,57	0,88	1,00	1,34	
	1,82	2,41	3,03	3,88	4,44	5,38	5,91	6,29	5,39	4,28	2,61	1,69	1,30	1,87					
stdev	0,03	0,02	0,01	0,01	0,01	0,01	0,01	0,01	0,02	0,03	0,04	0,05	0,06	0,08	0,13	0,21	0,26	0,34	0,46
	0,59	0,77	0,97	1,15	1,45	1,97	2,62	2,70	2,39	1,58	1,11	1,10	2,26						

Name 0.5 mm - 0,2 L/min

Average start	1259	15:51:42																	
Average stop	1289	15:52:12																	
Number of records	30																		
Average conc	0,62	0,38	0,23	0,14	0,13	0,19	0,27	0,28	0,37	0,49	0,54	0,73	0,89	1,17	1,72	2,46	2,85	3,62	
	4,40	5,17	5,82	6,20	5,90	5,51	5,02	4,58	3,87	3,46	2,76	2,14	1,97	4,06					
stdev	0,10	0,06	0,03	0,02	0,02	0,03	0,04	0,05	0,06	0,10	0,12	0,17	0,23	0,29	0,40	0,55	0,67	0,84	1,04
	1,25	1,50	1,70	1,74	1,67	1,48	1,13	0,77	0,69	0,79	1,00	1,45	4,51						

Name 0.5mm - 0,5 L/min

Average start	1427	15:54:30																	
Average stop	1457	15:55:0																	
Number of records	30																		
Average conc	11,54	4,69	1,62	0,65	0,54	1,20	2,63	2,81	4,03	6,39	6,56	9,01	10,20	10,68	11,62	11,35	9,24	7,08	
	5,05	3,46	2,43	1,75	1,37	1,27	1,44	1,82	2,27	2,71	2,73	2,36	2,51	6,30					
stdev	5,36	1,84	0,50	0,15	0,11	0,28	0,75	0,82	1,20	2,01	1,91	2,49	2,60	2,47	2,56	2,35	1,90	1,43	1,03
	0,69	0,46	0,31	0,23	0,19	0,21	0,25	0,38	0,58	0,63	0,50	0,68	2,73						

Name	0.5mm - 0,2 L/min DOR 1:100																		
Average start		1697	15:59:0																
Average stop		1727	15:59:30																
Number of records			30																
Average conc		7,22	2,98	1,05	0,42	0,32	0,59	1,15	1,15	1,58	2,41	2,45	3,34	3,81	4,18	4,96	5,47	5,33	5,13
	4,78	4,29	3,87	3,44	3,09	3,06	3,41	3,91	4,06	3,88	3,35	2,96	3,39	8,06					
stdev	5,34	1,88	0,53	0,16	0,11	0,21	0,49	0,48	0,67	1,11	1,06	1,43	1,54	1,53	1,66	1,56	1,34	1,06	0,91
	0,87	0,93	0,96	0,88	0,78	0,68	0,64	0,68	0,66	0,56	0,66	1,17	3,99						

Name	0.5mm - 0,2 L/min DOR 1:50																		
Average start		1787	16:0:30																
Average stop		1817	16:1:0																
Number of records			30																
Average conc		27,14	8,92	2,35	0,69	0,45	0,89	1,89	1,78	2,44	3,98	3,73	4,84	4,97	4,70	4,95	4,53	3,83	3,16
	2,66	2,22	1,92	1,71	1,64	1,88	2,53	3,44	3,94	3,87	3,31	2,78	3,17	8,69					
stdev	16,67	4,01	0,61	0,10	0,07	0,10	0,24	0,25	0,46	1,09	1,06	1,53	1,56	1,36	1,39	1,15	0,90	0,67	0,53
	0,40	0,30	0,21	0,17	0,18	0,21	0,32	0,46	0,48	0,44	0,47	0,73	2,85						

Date 2604-2012
Type of experiment Medium Nozzle experiments
Injection medods Simulated injection tool - C9500
Flow and Nozzle size 1.5 mm 0.5-3.0 L/min

Name 1.5mm - 0,5 L/min
Average start 359 13:46:50
Average stop 389 13:47:20
Number of records 30

Average conc	0,71	0,39	0,18	0,08	0,04	0,03	0,03	0,03	0,04	0,07	0,09	0,11	0,09	0,05	0,04	0,04	0,09	0,20	
	0,17	0,23	0,41	0,40	0,64	0,85	1,15	2,41	5,27	8,90	12,20	13,37	13,42	12,57					
stdev	0,02	0,01	0,01	0,01	0,00	0,00	0,00	0,00	0,00	0,01	0,01	0,01	0,01	0,00	0,00	0,00	0,01	0,02	0,02
	0,03	0,07	0,08	0,13	0,18	0,26	0,56	1,14	1,71	2,36	2,78	4,00	6,42						

Name 1.5mm - 1,2 L/min
Average start 474 13:48:45
Average stop 504 13:49:15
Number of records 30

Average conc	0,71	0,50	0,33	0,21	0,15	0,13	0,14	0,13	0,16	0,23	0,30	0,41	0,45	0,42	0,42	0,56	1,09	1,97	
	2,20	3,10	5,47	6,76	9,86	12,85	17,61	25,60	34,40	38,90	37,30	32,67	28,99	33,43					
stdev	0,05	0,04	0,05	0,05	0,05	0,05	0,05	0,04	0,05	0,07	0,08	0,12	0,14	0,16	0,18	0,25	0,44	0,75	0,91
	1,28	2,13	2,64	3,69	4,82	6,48	8,37	10,25	12,46	12,84	12,08	11,86	16,39						

Name 1.5mm - 2,8 L/min
Average start 609 13:51:00
Average stop 639 13:51:30
Number of records 30

Average conc	4,72	2,43	1,15	0,57	0,41	0,58	0,90	0,93	1,28	1,98	2,38	3,61	4,87	6,38	8,77	12,24	16,40	21,72	
	26,98	32,79	40,34	44,09	46,13	44,80	42,50	37,48	29,27	20,58	12,77	7,96	5,95	6,94					
stdev	2,95	1,20	0,40	0,13	0,09	0,18	0,37	0,41	0,60	1,02	1,17	1,80	2,38	3,07	4,22	5,67	6,94	8,43	10,33
	11,85	13,44	14,12	13,87	12,93	11,65	9,37	6,50	4,02	2,25	1,42	1,34	2,14						

Name 1.5mm - 1,2 L/min DOR: 1:100
Average start 1239 14:1:30
Average stop 1269 14:2:0
Number of records 30

Average conc	10,18	4,00	1,34	0,48	0,31	0,54	1,09	1,21	1,87	3,32	3,87	5,80	7,25	8,50	10,62	12,93	15,02	17,39	
	19,79	21,62	23,19	22,07	19,73	17,43	16,00	15,13	13,13	11,28	8,66	6,68	5,95	8,77					
stdev	5,78	1,85	0,44	0,11	0,06	0,16	0,45	0,52	0,86	1,63	1,81	2,70	3,28	3,72	4,65	5,54	6,12	6,75	7,69
	8,21	8,52	7,99	6,77	5,46	4,22	2,95	1,69	0,97	0,77	0,82	1,03	2,29						

Name 1.5mm - 1,2 L/min DOR: 1:50
Average start 1329 14:3:00
Average stop 1359 14:3:30
Number of records 30

Average conc	25,73	8,61	2,30	0,67	0,43	0,91	2,14	2,28	3,45	6,03	6,19	8,66	9,84	10,46	12,30	13,56	14,27	14,68	
	15,23	14,70	13,67	11,59	9,43	8,25	7,86	8,20	7,85	7,61	6,33	5,21	4,86	8,10					
stdev	16,79	5,25	1,30	0,36	0,22	0,49	1,21	1,29	1,98	3,55	3,58	5,00	5,61	5,87	6,85	7,47	7,79	7,93	8,20
	7,87	7,27	6,11	4,90	4,23	3,98	4,12	3,95	3,85	3,23	2,70	2,62	4,64						

Name 1.5mm - 1,2 L/min DOR: 1:25
Average start 1416 14:4:27
Average stop 1417 14:4:28
Number of records 1 (single measurements due to saturation of LISST due high concentration of small droplets)

Average conc	41,23	13,31	3,37	0,93	0,60	1,31	3,13	3,14	4,57	7,81	7,48	10,03	10,69	10,53	11,62	11,56	10,94	10,06	
	9,43	8,39	7,49	6,46	5,62	5,65	6,43	8,17	9,19	9,75	8,17	6,27	5,55	8,76					
stdev	5,18	1,24	0,18	0,02	0,01	0,06	0,23	0,23	0,37	0,75	0,65	0,85	0,78	0,64	0,65	0,65	0,63	0,56	0,50
	0,31	0,13	0,02	0,08	0,13	0,12	0,16	0,05	0,21	0,31	0,24	0,31	0,42						

Name	Oil:Gas 1.2 L/min (1:1) DOR: 1:50																		
Average start		1598	14:7:29																
Average stop		1628	14:7:59																
Number of records			30																
Average conc		8,42	3,67	1,36	0,54	0,38	0,63	1,12	1,11	1,48	2,28	2,37	3,21	3,72	4,07	4,81	5,47	6,16	6,86
	7,50	7,95	8,45	8,35	8,23	8,78	10,31	13,15	15,45	17,09	14,79	11,95	10,11	11,60					
stdev	2,57	0,97	0,29	0,10	0,07	0,14	0,29	0,29	0,39	0,61	0,59	0,78	0,87	0,92	1,09	1,19	1,21	1,19	1,23
	1,19	1,09	0,96	0,82	0,78	0,79	0,93	1,06	1,29	1,49	1,88	2,35	3,53						

Date 2506-2012
Conditions Flow rate exp.
Comments Injection above Nozzle (3x dia)
Nozzle size 3mm, 2+5+8L/min

Name 3mm - 8 L/min (2506)
Average start 264 12:56:30
Average stop 294 12:57:0
Number of records 30

Average conc	0,01	0,01	0,02	0,04	0,08	0,12	0,14	0,16	0,20	0,28	0,39	0,51	0,48	0,33	0,23	0,31	0,89	2,02	
	1,81	2,49	5,09	5,79	9,46	13,17	18,98	27,54	38,15	49,80	53,96	50,22	41,55	40,73					
stdev	0,01	0,01	0,02	0,04	0,06	0,08	0,07	0,06	0,07	0,09	0,13	0,15	0,17	0,16	0,14	0,20	0,44	0,79	0,86
	1,17	2,08	2,56	4,07	5,61	7,88	10,73	14,29	18,40	20,73	21,56	21,85	27,31						

Name 3mm - 5 L/min (2506)
Average start 704 13:3:50
Average stop 734 13:4:20
Number of records 30

Average conc	0,00	0,00	0,01	0,02	0,05	0,07	0,06	0,06	0,08	0,11	0,23	0,32	0,15	0,04	0,02	0,02	0,13	0,95	
	0,32	0,44	1,79	1,25	2,60	3,37	4,90	8,02	13,09	20,80	25,75	29,98	26,22	38,37					
stdev	0,00	0,00	0,01	0,03	0,05	0,05	0,04	0,04	0,04	0,05	0,08	0,11	0,05	0,04	0,02	0,02	0,09	0,43	0,19
	0,26	0,71	0,58	1,01	1,45	2,18	3,45	5,04	7,48	9,77	11,76	12,79	25,95						

Name 3mm - 5 L/min DOR 1:100 (2506)
Average start 780 13:5:5
Average stop 810 13:5:35
Number of records 30

Average conc	13,02	5,45	1,96	0,77	0,55	0,90	1,56	1,43	1,79	2,68	2,68	3,58	4,09	4,41	5,33	6,12	7,36	8,82	
	10,82	13,30	16,53	18,89	20,46	22,09	22,50	22,66	18,89	15,64	10,29	7,14	5,10	6,97					
stdev	12,58	4,43	1,25	0,38	0,23	0,43	0,87	0,79	1,04	1,68	1,62	2,22	2,54	2,74	3,36	3,79	4,28	4,85	6,06
	7,27	8,60	9,51	9,82	10,44	10,73	11,05	9,34	7,97	5,57	4,20	3,41	5,97						

Name	3mm - 5 L/min DOR 1:50 (2506)																		
Average start	839	13:6:4																	
Average stop	869	13:6:34																	
Number of records	30																		
Average conc	23,87	9,19	2,94	1,02	0,69	1,22	2,29	2,08	2,65	4,03	3,84	5,06	5,62	5,92	7,07	7,82	8,78	9,89	
	11,73	13,58	15,68	16,70	16,61	16,43	15,50	14,26	10,93	8,29	5,19	3,61	2,84	4,51					
stdev	18,86	6,76	1,99	0,65	0,43	0,77	1,51	1,38	1,79	2,80	2,64	3,50	3,86	4,04	4,81	5,29	5,86	6,52	7,72
	8,89	10,22	10,87	10,80	10,63	10,04	9,27	7,23	5,68	3,78	2,93	2,85	6,18						

Name	3mm 5 L/min DOR 1:25 (2506)																		
Average start	894	13:6:59																	
Average stop	924	13:7:29																	
Number of records	30																		
Average conc	14,75	5,94	2,04	0,77	0,57	1,04	1,92	1,75	2,21	3,30	3,15	4,14	4,61	4,86	5,77	6,43	7,23	8,09	
	9,38	10,59	11,75	11,88	11,11	10,24	9,07	7,90	5,86	4,38	2,85	2,11	1,70	2,65					
stdev	14,84	5,47	1,70	0,60	0,43	0,79	1,54	1,42	1,82	2,81	2,65	3,49	3,85	4,02	4,77	5,26	5,82	6,42	7,44
	8,37	9,24	9,32	8,72	8,14	7,39	6,62	5,15	4,14	3,07	2,78	2,77	5,32						

Date 1605-2012
Conditions Flow rate experiment
Comments Injection above nozzle (3 x nozzle dia)
Nozzle size 3mm, 2 + 5 ml/min

Name 3mm - 2 L/min (1605)
Average start 472 15:41:56
Average stop 502 15:42:26
Number of records 30

Average conc	0,04	0,03	0,02	0,01	0,02	0,02	0,01	0,01	0,02	0,04	0,08	0,12	0,03	0,00	0,00	0,00	0,01	0,12	
	0,02	0,03	0,19	0,09	0,32	0,44	0,61	1,38	2,42	3,37	4,12	5,40	5,39	17,21					
stdev	0,03	0,02	0,01	0,01	0,01	0,01	0,01	0,01	0,03	0,03	0,02	0,05	0,01	0,00	0,00	0,00	0,01	0,08	0,01
	0,02	0,14	0,06	0,20	0,27	0,32	0,76	1,65	2,23	2,70	4,31	4,10	15,22						

Name 3mm - 5 L/min (1605)
Average start 601 15:44:5
Average stop 631 15:44:35
Number of records 30

Average conc	0,00	0,00	0,01	0,01	0,03	0,06	0,07	0,09	0,13	0,18	0,28	0,38	0,31	0,17	0,11	0,14	0,52	1,60	
	1,08	1,45	3,56	3,64	6,41	8,88	13,19	20,62	30,28	42,24	48,09	48,81	42,27	47,46					
stdev	0,01	0,01	0,01	0,02	0,03	0,06	0,05	0,05	0,06	0,07	0,09	0,14	0,12	0,11	0,08	0,11	0,27	0,69	0,53
	0,76	1,32	1,60	2,39	3,19	4,86	7,70	11,84	16,51	19,58	18,84	18,83	30,57						

Name 3mm - 5 L/min DOR: 1:100 (1605)
Average start 1242 15:54:46
Average stop 1272 15:55:16
Number of records 30

Average conc	7,17	2,87	1,00	0,40	0,29	0,48	0,82	0,75	0,95	1,43	1,44	1,94	2,22	2,39	2,89	3,36	4,08	4,96	
	5,98	7,32	9,15	10,70	12,20	13,92	15,92	17,98	17,82	17,17	14,44	11,84	10,34	13,48					
stdev	13,48	4,81	1,41	0,45	0,29	0,52	0,99	0,91	1,19	1,90	1,86	2,56	2,95	3,19	3,93	4,49	5,20	6,11	7,49
	9,08	11,05	12,81	14,16	15,89	17,98	20,30	20,28	19,20	15,30	12,08	10,79	14,36						

Name 3mm - 5 L/min DOR: 1:50 (1605)
Average start 1131 15:52:55
Average stop 1161 15:53:25
Number of records 30

Average conc		15,73	5,72	1,71	0,56	0,36	0,64	1,19	1,06	1,36	2,12	2,03	2,72	3,03	3,20	3,83	4,25	4,76	5,41
	6,50	7,64	8,87	9,53	9,56	9,58	9,15	8,47	6,56	5,06	3,37	2,45	2,08	3,19					
stdev	21,54	7,47	2,11	0,66	0,42	0,74	1,43	1,28	1,66	2,64	2,51	3,40	3,78	3,97	4,76	5,24	5,82	6,56	7,87
	9,22	10,66	11,41	11,38	11,37	10,85	10,06	7,79	6,00	3,97	2,90	2,63	4,64						

Name 3mm - 5 L/min DOR: 1:25 (1605)
Average start 1267 15:55:11
Average stop 1297 15:55:41
Number of records 30

Average conc		0,31	0,19	0,11	0,07	0,06	0,08	0,10	0,09	0,10	0,14	0,15	0,19	0,16	0,10	0,07	0,08	0,16	0,30
	0,25	0,33	0,59	0,63	0,94	1,23	1,67	2,27	2,55	2,94	3,34	3,52	3,55	5,25					
stdev	0,15	0,10	0,07	0,06	0,05	0,07	0,09	0,07	0,08	0,09	0,08	0,08	0,08	0,08	0,08	0,09	0,11	0,13	0,15
	0,19	0,25	0,32	0,41	0,47	0,54	0,66	0,90	1,50	2,33	2,95	3,53	6,82						

Date 1704-2012
Conditions C9500-Premixed DOR 1:1000-1:25
Comments High flowrate experiment
Nozzle size 1,5mm, 1,5L/min

Name DOR 1:1000
Average start 597 15:52:45
Average stop 627 15:53:15
Number of records 30

Average conc	5,58	2,31	0,77	0,24	0,12	0,13	0,18	0,15	0,20	0,35	0,43	0,74	1,09	1,48	2,14	2,94	3,98	5,39	
	7,49	10,09	13,84	17,39	20,70	23,17	25,30	25,13	21,33	16,16	10,11	6,02	4,29	5,10					
stdev	0,71	0,30	0,11	0,04	0,02	0,03	0,04	0,04	0,06	0,11	0,15	0,25	0,36	0,48	0,67	0,91	1,21	1,61	2,18
	2,85	3,75	4,59	5,42	6,16	6,79	6,73	5,87	4,56	2,90	1,77	1,39	2,02						

Name DOR 1:500
Average start 672 15:54:0
Average stop 702 15:54:30
Number of records 30

Average conc	6,24	2,50	0,80	0,25	0,12	0,14	0,21	0,19	0,26	0,47	0,59	1,03	1,50	2,02	2,90	4,00	5,41	7,28	
	9,95	12,94	16,81	19,60	21,07	20,74	19,47	16,42	11,89	7,96	4,72	2,87	2,20	2,79					
stdev	0,98	0,37	0,12	0,04	0,02	0,03	0,06	0,06	0,09	0,17	0,23	0,38	0,54	0,69	0,96	1,29	1,69	2,23	2,97
	3,75	4,70	5,33	5,61	5,35	4,89	4,10	3,06	2,12	1,36	0,94	0,81	1,10						

Name DOR 1:250
Average start 747 15:55:15
Average stop 777 15:55:45
Number of records 30

Average conc	6,65	2,65	0,85	0,26	0,13	0,16	0,25	0,22	0,31	0,56	0,69	1,18	1,73	2,34	3,40	4,74	6,40	8,54	
	11,48	14,43	17,89	19,61	19,50	17,65	15,33	12,13	8,44	5,53	3,22	1,88	1,38	1,74					
stdev	2,08	0,77	0,23	0,07	0,04	0,07	0,13	0,13	0,20	0,38	0,47	0,80	1,12	1,47	2,05	2,77	3,57	4,56	5,82
	6,99	8,24	8,75	8,65	7,93	6,95	5,57	4,09	2,84	1,74	1,04	0,75	0,94						

Name	DOR 1:100																		
Average start		812	15:56:20																
Average stop		842	15:56:50																
Number of records			30																
Average conc		7,41	2,95	0,95	0,30	0,15	0,20	0,32	0,30	0,44	0,80	1,01	1,70	2,42	3,18	4,50	6,15	8,14	10,62
	13,97	17,19	20,75	22,13	21,36	18,72	15,64	11,88	8,00	5,12	2,97	1,76	1,32	1,73					
stdev	1,44	0,52	0,16	0,05	0,03	0,05	0,10	0,10	0,16	0,30	0,38	0,63	0,87	1,10	1,51	2,01	2,57	3,25	4,11
	4,87	5,64	5,80	5,46	4,73	3,97	3,06	2,18	1,55	1,06	0,74	0,65	0,93						

Name	DOR 1:50																		
Average start		882	15:57:30																
Average stop		912	15:58:0																
Number of records			30																
Average conc		12,34	4,41	1,26	0,36	0,19	0,30	0,58	0,60	0,94	1,82	2,22	3,65	4,97	6,25	8,55	11,26	14,29	17,64
	21,65	24,09	25,69	23,16	18,72	13,79	9,75	6,78	4,13	2,64	1,50	0,96	0,74	1,16					
stdev	5,27	1,64	0,40	0,10	0,06	0,11	0,27	0,31	0,51	1,03	1,24	1,99	2,59	3,11	4,08	5,12	6,09	7,06	8,21
	8,70	8,86	7,67	5,81	4,14	2,80	1,91	1,21	0,82	0,51	0,36	0,31	0,58						

Name	DOR 1:25																		
Average start		1006	15:59:34																
Average stop		1030	15:59:58																
Number of records			24																
Average conc		25,45	8,45	2,22	0,60	0,34	0,64	1,45	1,59	2,56	4,93	5,70	8,97	11,52	13,59	17,35	20,89	23,81	25,88
	28,33	27,48	24,75	19,26	13,11	8,79	5,76	3,90	2,38	1,53	0,88	0,56	0,46	0,78					
stdev	8,48	2,36	0,49	0,11	0,06	0,16	0,44	0,51	0,88	1,77	1,93	2,94	3,51	3,82	4,63	5,23	5,63	5,79	6,01
	5,68	4,92	3,76	2,54	1,70	1,16	0,81	0,56	0,40	0,26	0,17	0,14	0,24						

Name	Oil alone 1,5 L/min																		
Average start		550	15:51:58																
Average stop		600	15:52:48																
Number of records			50																
Average conc		5,28	2,17	0,72	0,22	0,11	0,12	0,16	0,13	0,17	0,30	0,37	0,63	0,93	1,27	1,84	2,53	3,42	4,63
	6,46	8,75	12,05	15,10	17,90	20,00	21,71	21,60	18,56	14,36	9,23	5,60	4,00	4,67					
stdev	0,74	0,31	0,11	0,04	0,02	0,03	0,05	0,04	0,07	0,12	0,16	0,26	0,38	0,49	0,69	0,94	1,25	1,68	2,27
	2,97	3,90	4,75	5,59	6,30	7,08	7,36	6,63	5,18	3,32	2,02	1,60	2,38						

Date 0806-2012
Conditions Premixed DOR 1:1000-1:25
Comments Reduced flow rate exp.
Nozzle size 1,5mm, 1,2L/min

Name DOR: 1:1000
Average start 308 15:42:35
Average stop 338 15:43:5
Number of records 30

Average conc	0,25	0,15	0,09	0,05	0,04	0,04	0,04	0,04	0,04	0,07	0,10	0,19	0,34	0,51	0,59	0,49	0,35	0,46
1,23	2,97	2,60	3,43	6,26	6,18	9,53	11,98	15,03	18,20	18,86	17,23	14,84	17,95					
stdev	0,05	0,03	0,03	0,02	0,02	0,02	0,02	0,02	0,02	0,03	0,04	0,06	0,09	0,12	0,18	0,22	0,21	0,27	0,55
0,95	1,10	1,49	2,30	2,59	3,52	4,28	5,21	6,70	7,37	8,08	9,01	15,49						

Name DOR: 1:500
Average start 375 15:43:42
Average stop 405 15:44:12
Number of records 30

Average conc	0,28	0,16	0,09	0,05	0,03	0,04	0,05	0,04	0,05	0,07	0,10	0,20	0,36	0,53	0,65	0,58	0,44	0,58
1,43	3,28	3,07	4,12	7,31	7,41	11,19	13,79	15,98	16,92	14,74	11,16	8,16	8,85					
stdev	0,04	0,02	0,02	0,02	0,02	0,02	0,02	0,02	0,03	0,03	0,04	0,06	0,09	0,14	0,19	0,24	0,24	0,32	0,61
1,01	1,23	1,64	2,41	2,77	4,03	5,23	5,99	6,46	5,85	4,65	4,05	6,63						

Name DOR: 1:250
Average start 453 15:45:0
Average stop 483 15:45:30
Number of records 30

Average conc	0,32	0,17	0,09	0,04	0,03	0,03	0,04	0,04	0,05	0,08	0,12	0,23	0,40	0,58	0,69	0,63	0,51	0,67
1,61	3,57	3,37	4,42	7,50	7,46	10,78	12,67	14,33	15,62	14,68	12,49	9,71	10,03					
stdev	0,05	0,02	0,02	0,02	0,02	0,02	0,02	0,02	0,02	0,04	0,05	0,08	0,11	0,15	0,21	0,27	0,29	0,39	0,73
1,20	1,43	1,80	2,47	2,90	4,13	5,30	6,28	6,58	6,55	6,77	6,97	10,34						

Name DOR: 1:100
Average start 543 15:46:30
Average stop 573 15:47:0
Number of records 30

Average conc		0,71	0,39	0,19	0,10	0,07	0,09	0,13	0,13	0,17	0,27	0,35	0,56	0,81	1,06	1,33	1,44	1,49	1,98
	3,68	6,54	7,51	9,78	13,87	14,83	18,45	19,95	19,24	19,76	16,37	13,55	7,85	7,52					
stdev		0,21	0,11	0,06	0,03	0,02	0,03	0,04	0,04	0,06	0,10	0,12	0,19	0,26	0,35	0,48	0,64	0,79	1,07	1,72
	2,64	3,54	4,47	5,62	6,23	7,47	8,26	7,94	8,30	7,03	6,47	4,86	6,71						

Name DOR: 1:50
Average start 633 15:48:0
Average stop 663 15:48:30
Number of records 30

Average conc		1,14	0,58	0,27	0,12	0,09	0,12	0,18	0,18	0,24	0,40	0,50	0,82	1,19	1,56	2,07	2,42	2,79	3,71
	6,04	9,50	11,42	14,33	18,32	18,96	19,59	18,77	14,62	12,32	8,08	5,83	3,47	3,81					
stdev		0,49	0,22	0,09	0,04	0,03	0,04	0,07	0,08	0,11	0,17	0,21	0,33	0,45	0,60	0,83	1,11	1,41	1,87	2,65
	3,55	4,87	6,20	7,35	8,30	8,35	8,10	6,20	4,82	2,99	2,21	1,78	2,65						

Name DOR: 1:25
Average start 723 15:49:30
Average stop 753 15:50:0
Number of records 30

Average conc		4,49	1,85	0,67	0,26	0,18	0,33	0,67	0,73	1,06	1,74	1,95	2,94	3,90	4,90	6,53	8,19	10,04	12,45
	16,78	21,10	23,36	23,79	20,57	16,35	11,85	8,50	5,37	3,82	2,62	2,14	1,90	3,05					
stdev		3,32	1,15	0,32	0,10	0,07	0,15	0,37	0,43	0,65	1,12	1,20	1,78	2,21	2,56	3,28	4,08	5,12	6,21	7,79
	9,28	10,34	10,23	8,43	6,82	4,80	3,19	1,88	1,28	0,95	0,91	1,12	2,99						

Name	Oil alone																		
Average start		184	15:40:31																
Average stop		191	15:40:38																
Number of records			7	(reduced number of measurements due to noisy signals in initiation of experiments)															
Average conc		0,29	0,12	0,04	0,02	0,01	0,01	0,01	0,01	0,01	0,02	0,04	0,10	0,21	0,31	0,29	0,13	0,05	0,06
	0,28	1,12	0,64	0,85	2,16	1,94	3,82	5,10	7,15	9,13	9,07	7,94	6,52	8,27					
stdev	0,07	0,01	0,02	0,01	0,01	0,01	0,01	0,01	0,01	0,01	0,01	0,02	0,03	0,05	0,09	0,07	0,04	0,05	0,15
	0,38	0,30	0,40	0,78	0,83	1,40	2,02	3,74	5,80	6,32	5,36	4,80	7,96						

Date 0606-2012
Conditions Vertical Injection
Comments DOR 1:100 and DOR 1:50
Nozzle size 1,5mm, 1,2 L/min

Name DOR 1:100 45mm
Average start 589 15:7:15
Average stop 619 15:7:45
Number of records 30

Average conc	0,44	0,33	0,24	0,19	0,18	0,22	0,24	0,21	0,22	0,27	0,29	0,38	0,46	0,56	0,73	0,96	1,23	1,63	2,23
	3,09	4,44	6,01	7,37	8,67	10,23	11,45	12,16	12,10	10,28	8,56	7,05	8,44						
stdev	0,33	0,23	0,15	0,10	0,09	0,11	0,12	0,10	0,11	0,13	0,13	0,16	0,20	0,24	0,32	0,41	0,53	0,69	0,96
	1,31	1,75	2,24	2,81	3,27	3,74	4,61	5,31	5,39	4,79	4,65	5,28	9,11						

Name DOR 1:100 15mm
Average start 669 15:8:35
Average stop 699 15:9:5
Number of records 30

Average conc	2,79	1,52	0,75	0,40	0,33	0,50	0,72	0,63	0,71	0,93	0,91	1,16	1,32	1,47	1,84	2,21	2,66	3,27	4,20
	5,47	7,20	8,96	10,30	11,66	12,98	13,42	12,28	10,29	7,23	5,12	4,15	4,95						
stdev	1,57	0,76	0,33	0,15	0,11	0,17	0,27	0,23	0,26	0,35	0,33	0,42	0,47	0,52	0,66	0,78	0,94	1,15	1,47
	1,87	2,37	2,86	3,30	3,79	4,24	4,39	4,20	4,29	3,63	2,73	2,38	3,41						

Name DOR 1:100 8mm
Average start 759 15:10:5
Average stop 789 15:10:35
Number of records 30

Average conc	3,69	1,73	0,72	0,33	0,26	0,46	0,82	0,83	1,08	1,60	1,63	2,17	2,50	2,75	3,35	3,95	4,64	5,51	6,78
	8,23	9,89	10,88	10,84	10,37	9,45	8,18	6,36	5,05	3,54	2,79	2,59	4,71						
stdev	1,80	0,76	0,28	0,11	0,08	0,16	0,31	0,31	0,41	0,62	0,60	0,79	0,90	0,98	1,21	1,42	1,64	1,92	2,31
	2,77	3,34	3,70	3,83	4,00	4,10	4,14	3,66	3,31	2,47	2,16	3,21	10,41						

Name DOR 1:100 6mm
Average start 826 15:11:12
Average stop 856 15:11:42
Number of records 30

Average conc	3,63	1,71	0,72	0,33	0,25	0,43	0,77	0,80	1,06	1,59	1,66	2,24	2,64	2,94	3,62	4,28	5,06	6,02	
	7,40	8,88	10,41	10,99	10,38	9,36	8,04	6,74	5,13	4,01	2,63	1,83	1,34	1,82					
stdev	2,53	1,06	0,38	0,15	0,11	0,20	0,39	0,39	0,52	0,81	0,81	1,09	1,27	1,41	1,75	2,06	2,41	2,83	3,49
	4,14	4,71	4,72	4,29	3,86	3,41	3,12	2,57	2,31	1,71	1,39	1,26	1,96						

Name DOR 1:100 4.5mm
Average start 929 15:12:55
Average stop 959 15:13:25
Number of records 30

Average conc	3,35	1,53	0,62	0,28	0,22	0,39	0,72	0,75	1,02	1,57	1,66	2,26	2,67	2,97	3,66	4,33	5,13	6,08	
	7,38	8,67	9,90	10,16	9,25	7,99	6,64	5,43	4,08	3,16	2,12	1,61	1,30	1,88					
stdev	2,67	1,07	0,36	0,13	0,09	0,18	0,38	0,39	0,54	0,85	0,87	1,19	1,39	1,54	1,91	2,27	2,66	3,08	3,74
	4,30	4,80	4,84	4,48	4,01	3,40	2,89	2,31	1,93	1,30	1,08	1,02	1,78						

Name DOR 1:100 1.5mm
Average start 1038 15:14:44
Average stop 1068 15:15:14
Number of records 30

Average conc	8,42	3,32	1,13	0,43	0,33	0,63	1,29	1,33	1,82	2,86	2,90	3,94	4,56	5,03	6,18	7,27	8,29	9,33	
	10,65	11,48	11,95	10,99	8,96	6,80	4,99	3,63	2,53	1,81	1,16	0,80	0,65	1,05					
stdev	8,99	2,83	0,70	0,19	0,12	0,27	0,70	0,70	1,02	1,77	1,69	2,32	2,57	2,66	3,19	3,55	3,89	4,18	4,70
	4,89	4,89	4,29	3,36	2,57	1,89	1,39	0,98	0,78	0,56	0,39	0,33	0,66						

Name DOR 1:50 8mm
Average start 1814 15:27:40
Average stop 1844 15:28:10
Number of records 30

Average conc		8,11	3,63	1,42	0,62	0,48	0,83	1,39	1,24	1,49	2,07	1,95	2,46	2,67	2,80	3,30	3,66	4,07	4,58
	5,42	6,37	7,58	8,61	9,22	9,56	9,35	8,44	6,46	4,60	2,83	1,89	1,42	1,84					
stdev	7,48	2,88	0,91	0,31	0,21	0,38	0,71	0,61	0,74	1,09	0,99	1,27	1,38	1,43	1,71	1,85	2,02	2,21	2,60
	3,00	3,43	3,69	3,80	4,05	4,18	4,11	3,26	2,50	1,67	1,35	1,28	1,93						

Name DOR 1:50 6mm
Average start 1882 15:28:48
Average stop 1912 15:29:18
Number of records 30

Average conc		17,34	6,99	2,38	0,90	0,65	1,20	2,25	2,06	2,58	3,78	3,54	4,54	4,95	5,16	6,11	6,74	7,40	8,16
	9,43	10,64	11,94	12,50	12,17	11,59	10,38	8,65	6,19	4,33	2,63	1,71	1,31	1,93					
stdev	9,64	3,23	0,84	0,23	0,13	0,25	0,56	0,50	0,67	1,12	1,02	1,36	1,45	1,45	1,72	1,80	1,92	2,04	2,35
	2,64	2,91	2,86	2,49	2,24	2,11	2,12	1,92	1,56	1,06	0,79	0,66	1,09						

Name DOR 1:50 4.5mm
Average start 1969 15:30:15
Average stop 1999 15:30:45
Number of records 30

Average conc		20,42	7,78	2,49	0,88	0,63	1,17	2,28	2,15	2,79	4,24	4,06	5,31	5,83	6,08	7,19	7,91	8,58	9,31
	10,55	11,55	12,43	12,29	11,11	9,72	8,06	6,31	4,22	2,71	1,52	0,98	0,82	1,55					
stdev	15,77	5,02	1,22	0,32	0,18	0,36	0,82	0,77	1,08	1,84	1,72	2,32	2,50	2,51	2,92	3,09	3,20	3,36	3,74
	3,95	4,09	3,80	3,21	2,66	2,18	1,89	1,45	1,03	0,66	0,66	0,92	2,88						

Name	DOR 1:50 1.5mm																		
Average start		2104	15:32:30																
Average stop		2134	15:33:0																
Number of records			30																
Average conc		27,97	9,93	2,88	0,92	0,63	1,29	2,76	2,65	3,58	5,68	5,40	7,18	7,89	8,23	9,77	10,70	11,42	12,01
	13,00	13,27	13,05	11,57	9,38	7,44	5,72	4,30	2,88	1,95	1,17	0,79	0,65	1,11					
stdev	13,94	4,25	0,99	0,25	0,14	0,27	0,67	0,64	0,93	1,66	1,53	2,10	2,24	2,23	2,57	2,67	2,73	2,80	3,06
	3,07	2,92	2,44	1,82	1,35	1,06	0,93	0,82	0,79	0,61	0,50	0,49	0,91						

Name	Oil alone																		
Average start		450	15:4:56																
Average stop		500	15:5:46																
Number of records			50																
Average conc		0,01	0,01	0,01	0,02	0,04	0,05	0,06	0,07	0,09	0,11	0,13	0,17	0,21	0,27	0,34	0,50	0,68	0,96
	1,37	1,91	2,90	3,96	4,91	5,89	7,44	8,60	10,17	10,60	8,77	6,56	4,69	4,20					
stdev	0,01	0,01	0,01	0,01	0,02	0,02	0,02	0,02	0,03	0,04	0,05	0,06	0,08	0,10	0,13	0,20	0,30	0,44	0,61
	0,87	1,33	1,85	2,51	3,21	4,18	5,11	6,14	6,85	6,20	4,73	3,75	3,99						

Date 1406-2012
Conditions Horizontal Injection
Comments DOR 1:25/50/100
Nozzle size 1,5mm, 1,2L/min

Name DOR 1:100 20mm
Average start 248 15:50:10
Average stop 278 15:50:40
Number of records 30

Average conc	0,36	0,25	0,17	0,12	0,09	0,10	0,10	0,08	0,09	0,13	0,17	0,25	0,30	0,29	0,32	0,39	0,72	1,19
1,23	1,74	2,69	3,29	4,36	5,52	7,04	9,16	10,19	10,17	8,13	5,58	4,00	4,47					
stdev	0,09	0,06	0,04	0,03	0,03	0,03	0,03	0,03	0,03	0,05	0,06	0,09	0,12	0,14	0,17	0,21	0,32	0,46	0,55
0,77	1,15	1,55	1,98	2,40	2,98	3,55	3,65	3,55	3,09	2,79	3,18	4,31						

Name DOR 1:100 10mm
Average start 308 15:51:10
Average stop 338 15:51:40
Number of records 30

Average conc	1,68	0,88	0,42	0,22	0,17	0,24	0,35	0,33	0,41	0,60	0,66	0,92	1,08	1,18	1,43	1,71	2,25	2,89
3,31	4,10	5,05	5,62	5,99	5,92	5,57	4,96	3,78	2,57	1,45	0,80	0,58	0,84					
stdev	1,64	0,71	0,27	0,11	0,08	0,14	0,25	0,24	0,32	0,48	0,49	0,67	0,79	0,91	1,15	1,37	1,61	1,88	2,31
2,79	3,32	3,72	3,74	3,40	2,77	2,10	1,59	1,29	0,91	0,59	0,51	0,89						

Name DOR 1:100 5mm
Average start 388 15:52:30
Average stop 418 15:53:0
Number of records 30

Average conc	2,77	1,39	0,63	0,30	0,23	0,37	0,58	0,55	0,70	1,03	1,11	1,54	1,82	2,02	2,50	2,99	3,78	4,72
5,53	6,65	7,80	8,21	8,04	7,41	6,52	5,44	4,04	2,89	1,74	1,02	0,73	1,02					
stdev	1,13	0,54	0,23	0,10	0,08	0,13	0,21	0,20	0,25	0,36	0,36	0,49	0,58	0,66	0,84	1,01	1,20	1,41	1,74
2,09	2,38	2,48	2,42	2,32	2,01	1,54	1,25	1,23	0,92	0,63	0,56	0,88						

Name DOR 1:100 0mm
Average start 468 15:53:50
Average stop 498 15:54:20
Number of records 30

Average conc		4,66	2,16	0,88	0,39	0,29	0,48	0,84	0,83	1,09	1,67	1,79	2,47	2,91	3,22	3,96	4,69	5,80	7,08
	8,48	10,13	11,74	12,19	11,66	10,71	9,42	8,27	6,25	4,66	2,83	1,83	1,28	1,79					
stdev	2,14	0,82	0,26	0,09	0,06	0,12	0,26	0,26	0,36	0,59	0,59	0,81	0,94	1,04	1,31	1,55	1,80	2,09	2,55
	3,01	3,39	3,56	3,46	3,23	2,88	2,57	2,18	2,06	1,68	1,35	1,09	1,81						

Name DOR 1:50 5mm
Average start 530 15:54:52
Average stop 560 15:55:22
Number of records 30

Average conc		8,09	3,45	1,28	0,53	0,40	0,69	1,23	1,16	1,49	2,23	2,23	2,97	3,36	3,62	4,39	5,04	5,86	6,73
	7,60	8,40	8,97	8,66	7,74	6,65	5,62	4,68	3,46	2,53	1,61	1,01	0,71	0,97					
stdev	7,06	2,49	0,70	0,21	0,14	0,29	0,64	0,59	0,78	1,24	1,15	1,52	1,66	1,73	2,08	2,31	2,45	2,58	2,89
	3,00	3,04	2,82	2,36	1,90	1,67	1,65	1,42	1,17	0,75	0,47	0,40	0,68						

Name DOR 1:50 10mm
Average start 588 15:55:50
Average stop 618 15:56:20
Number of records 30

Average conc		11,48	4,66	1,63	0,64	0,47	0,83	1,51	1,40	1,78	2,67	2,60	3,43	3,83	4,07	4,90	5,54	6,30	7,12
	8,03	8,75	9,15	8,61	7,48	6,29	5,17	4,15	2,98	2,08	1,27	0,81	0,69	1,24					
stdev	9,92	3,45	0,94	0,26	0,16	0,35	0,80	0,73	0,99	1,60	1,47	1,96	2,13	2,19	2,64	2,90	3,11	3,35	3,85
	4,14	4,29	4,03	3,41	2,81	2,22	1,74	1,31	1,10	0,80	0,63	0,69	1,55						

Name DOR 1:50 20mm
Average start 628 15:56:30
Average stop 658 15:57:0
Number of records 30

Average conc		8,52	3,71	1,40	0,58	0,44	0,76	1,34	1,23	1,54	2,26	2,22	2,94	3,30	3,54	4,26	4,85	5,57	6,34
	7,17	7,92	8,36	7,92	6,89	5,81	4,83	3,92	2,83	1,99	1,22	0,77	0,65	1,20					
stdev		6,03	2,28	0,72	0,25	0,18	0,33	0,65	0,59	0,75	1,13	1,06	1,40	1,54	1,64	1,98	2,22	2,47	2,69	3,16
	3,44	3,54	3,30	2,75	2,20	1,66	1,22	0,86	0,71	0,51	0,48	0,69	1,55						

Name DOR 1:50 5mm
Average start 688 15:57:30
Average stop 718 15:58:0
Number of records 30

Average conc		6,29	2,82	1,10	0,47	0,36	0,60	1,02	0,94	1,17	1,70	1,69	2,23	2,51	2,70	3,25	3,72	4,36	5,08
	5,73	6,44	7,01	6,92	6,35	5,59	4,78	4,01	3,01	2,12	1,27	0,75	0,59	1,00					
stdev		5,62	2,29	0,79	0,29	0,20	0,36	0,67	0,61	0,76	1,12	1,06	1,38	1,54	1,66	2,03	2,31	2,55	2,80	3,27
	3,63	3,96	3,97	3,56	2,99	2,35	1,81	1,32	0,92	0,60	0,42	0,40	0,88						

Name DOR 1:25 5mm
Average start 743 15:58:25
Average stop 773 15:58:55
Number of records 30

Average conc		9,18	3,68	1,28	0,50	0,36	0,65	1,18	1,08	1,39	2,10	2,05	2,72	3,02	3,18	3,77	4,19	4,67	5,12
	5,50	5,70	5,68	5,07	4,21	3,42	2,81	2,32	1,71	1,25	0,82	0,57	0,52	1,15					
stdev		8,70	2,80	0,77	0,25	0,17	0,32	0,66	0,61	0,81	1,32	1,24	1,66	1,81	1,87	2,23	2,40	2,47	2,49	2,63
	2,50	2,29	1,93	1,45	1,07	0,79	0,61	0,47	0,44	0,38	0,37	0,55	1,78						

Name DOR 1:12,5 5mm

Average start	791	15:59:13																	
Average stop	821	15:59:43																	
Number of records	30																		
Average conc	17,41	6,30	1,90	0,65	0,45	0,83	1,61	1,46	1,91	2,97	2,82	3,73	4,07	4,18	4,87	5,22	5,50	5,72	
	5,89	5,74	5,36	4,51	3,61	2,90	2,41	2,05	1,58	1,17	0,73	0,46	0,37	0,68					
stdev	16,35	4,78	1,05	0,26	0,15	0,30	0,68	0,63	0,87	1,52	1,42	1,93	2,06	2,03	2,33	2,33	2,22	2,06	2,04
	1,85	1,62	1,27	0,91	0,66	0,53	0,48	0,43	0,36	0,26	0,19	0,18	0,39						

Name Oil alone 1,2 L/min

Average start	133	15:48:15																	
Average stop	163	15:48:45																	
Number of records	30																		
Average conc	0,24	0,18	0,14	0,10	0,08	0,07	0,07	0,05	0,06	0,08	0,11	0,17	0,19	0,17	0,18	0,21	0,48	0,93	
	0,91	1,38	2,31	2,81	3,92	5,02	6,65	9,16	10,33	10,00	7,98	6,16	5,33	7,21					
stdev	0,03	0,02	0,02	0,02	0,02	0,02	0,02	0,01	0,02	0,02	0,03	0,05	0,06	0,06	0,07	0,09	0,17	0,31	0,35
	0,53	0,89	1,13	1,53	1,95	2,75	4,05	5,15	5,77	5,04	4,40	5,65	9,95						

Date 2006-2012
Conditions Sim.Inj.Tool, DOR 1:100/50/25
Comments Warm Vs. Cold oil, 1st experiment
Nozzle size 1,5mm, 1,2L/min

Name DOR 1:100 Cold
Average start 300 15:43:31
Average stop 330 15:44:1
Number of records 30

Average conc	5,02	2,10	0,76	0,30	0,22	0,40	0,81	0,90	1,31	2,17	2,42	3,53	4,39	5,12	6,38	7,69	9,07	10,58
	12,42	13,94	15,18	14,86	13,25	11,07	8,64	6,56	4,35	2,97	1,81	1,24	0,98	1,45				
stdev	3,43	1,26	0,38	0,12	0,08	0,17	0,40	0,43	0,65	1,12	1,18	1,70	2,05	2,31	2,86	3,33	3,76	4,22	4,90
	5,30	5,55	5,32	4,60	3,88	3,18	2,67	2,01	1,50	1,01	0,81	0,76	1,36					

Name DOR 1:50 Cold
Average start 461 15:46:12
Average stop 470 15:46:21
Number of records 9

Average conc	16,06	6,15	1,96	0,68	0,49	0,98	2,02	1,97	2,66	4,17	4,07	5,46	6,11	6,47	7,64	8,42	9,03	9,51
	10,17	10,13	9,53	7,87	5,82	4,25	3,13	2,40	1,70	1,27	0,87	0,67	0,60	1,12				
stdev	3,81	1,48	0,50	0,18	0,12	0,20	0,34	0,31	0,40	0,62	0,61	0,83	0,91	0,98	1,14	1,17	1,16	1,11	1,11
	1,10	1,13	1,05	0,86	0,72	0,57	0,48	0,46	0,48	0,45	0,40	0,38	0,84					

Name DOR 1:25 Cold
Average start 548 15:47:39
Average stop 549 15:47:40
Number of records 1 (saturation of LISST due to high concentration of small droplets)

Average conc	27,49	9,60	2,70	0,84	0,55	1,08	2,24	2,07	2,73	4,28	3,97	5,11	5,37	5,26	5,83	5,74	5,54	5,19
	4,87	4,22	3,47	2,60	1,80	1,33	1,02	0,87	0,70	0,60	0,41	0,26	0,20	0,32				
stdev	21,08	6,27	1,32	0,25	0,11	0,29	0,85	0,80	1,17	2,09	1,90	2,53	2,58	2,43	2,68	2,61	2,54	2,33	2,08
	1,52	1,06	0,71	0,44	0,27	0,19	0,12	0,05	0,05	0,08	0,09	0,09	0,11					

Name DOR 1:100 Warm
Average start 1005 15:55:16
Average stop 1035 15:55:45
Number of records 30

Average conc	1,29	0,64	0,30	0,15	0,12	0,18	0,30	0,32	0,45	0,72	0,87	1,30	1,69	2,07	2,62	3,35	4,38	5,70
7,21	9,12	11,41	12,88	14,21	14,73	15,12	14,95	12,86	10,68	7,42	5,25	3,66	3,93					
stdev	1,52	0,65	0,24	0,09	0,06	0,11	0,22	0,25	0,37	0,63	0,73	1,08	1,39	1,67	2,14	2,66	3,25	3,89	4,74
5,47	6,14	6,24	5,73	5,40	5,61	6,39	6,26	5,63	4,35	3,57	2,87	3,23						

Name DOR 1:50 Warm
Average start 1060 15:56:10
Average stop 1090 15:56:40
Number of records 30

Average conc	6,70	2,83	1,03	0,41	0,30	0,56	1,10	1,15	1,59	2,51	2,64	3,67	4,36	4,90	5,98	6,99	8,00	9,02
10,24	11,00	11,20	10,04	8,20	6,47	4,96	3,80	2,56	1,76	1,03	0,67	0,54	0,89					
stdev	4,27	1,64	0,53	0,19	0,13	0,25	0,54	0,56	0,79	1,27	1,29	1,77	2,05	2,24	2,70	3,05	3,32	3,52	3,82
3,82	3,61	2,99	2,18	1,72	1,50	1,36	1,04	0,75	0,43	0,37	0,42	0,89						

Name DOR 1:25 Warm
Average start 1136 15:57:26
Average stop 1160 15:57:50
Number of records 24

Average conc	16,00	5,84	1,75	0,58	0,41	0,83	1,76	1,70	2,29	3,59	3,39	4,39	4,68	4,70	5,27	5,41	5,31	5,06
4,83	4,29	3,61	2,73	1,91	1,37	1,06	0,87	0,63	0,44	0,28	0,18	0,17	0,34					
stdev	16,58	5,59	1,54	0,48	0,33	0,68	1,47	1,41	1,92	3,06	2,86	3,71	3,92	3,89	4,34	4,42	4,31	4,07	3,88
3,44	2,90	2,20	1,55	1,12	0,87	0,72	0,53	0,40	0,27	0,19	0,19	0,48						

Name	Oil Cold																		
Average start		194	15:41:45																
Average stop		224	15:42:15																
Number of records			30																
Average conc		0,00	0,00	0,01	0,01	0,03	0,04	0,05	0,06	0,07	0,09	0,11	0,15	0,18	0,21	0,22	0,30	0,47	0,75
	1,01	1,50	2,26	2,92	4,29	5,60	7,93	10,85	13,96	17,27	17,95	15,94	11,41	11,15					
stdev	0,00	0,01	0,01	0,01	0,02	0,03	0,04	0,04	0,04	0,04	0,05	0,06	0,08	0,09	0,10	0,13	0,20	0,33	0,46
	0,72	1,08	1,41	1,91	2,37	3,41	4,73	6,44	8,53	10,04	10,83	9,11	10,94						

Name	Oil warm																		
Average start		937	15:54:8																
Average stop		967	15:54:38																
Number of records			30																
Average conc		0,07	0,06	0,05	0,06	0,06	0,08	0,09	0,09	0,11	0,15	0,19	0,29	0,39	0,47	0,55	0,73	1,11	1,72
	2,39	3,63	5,45	7,20	9,97	12,02	14,91	17,49	18,16	16,75	12,55	8,40	5,98	6,46					
stdev	0,02	0,01	0,02	0,02	0,03	0,03	0,03	0,03	0,04	0,04	0,05	0,07	0,11	0,15	0,18	0,27	0,43	0,70	1,02
	1,55	2,37	3,24	4,57	5,63	6,98	7,93	8,24	8,10	6,75	5,29	4,85	6,06						

Date 2806-2012
Conditions DOR 1:1000-1:25
Comments New low solvent Dispersant & Water-air experiment
Nozzle size 1,5mm - 1.2 L/min

Name 2806-Water:Air-1.2 L/min (1:1)
Average start 594 14:5:1
Average stop 624 14:5:31
Number of records 30

Average conc	0,30	0,23	0,14	0,07	0,03	0,01	0,01	0,01	0,01	0,02	0,03	0,07	0,25	0,19	0,10	0,01	0,00	0,00	0,03
0,47	0,20	0,33	1,06	0,71	1,17	1,12	0,94	1,11	1,45	2,25	1,62	1,03							
stdev	0,02	0,01	0,00	0,00	0,00	0,00	0,00	0,00	0,00	0,00	0,00	0,00	0,00	0,01	0,01	0,00	0,00	0,00	0,01
0,09	0,04	0,05	0,17	0,20	0,48	0,66	0,66	0,80	1,06	1,50	1,93	1,49							

Name 2806 Water:Air-2.4 L/min (2:1)
Average start 1000 14:11:47
Average stop 1030 14:12:17
Number of records 30

Average conc	0,19	0,18	0,15	0,09	0,05	0,02	0,01	0,01	0,01	0,02	0,03	0,07	0,27	0,26	0,20	0,05	0,01	0,02	0,13
1,18	0,56	0,86	2,35	1,87	3,46	4,54	5,36	6,48	6,42	6,86	6,74	10,71							
stdev	0,06	0,03	0,01	0,01	0,01	0,01	0,00	0,00	0,00	0,00	0,00	0,01	0,02	0,03	0,04	0,02	0,01	0,01	0,06
0,31	0,21	0,36	0,87	0,81	1,53	2,14	2,78	3,33	3,28	4,14	4,78	9,71							

Name DOR 1:1000
Average start 1802 14:29:19
Average stop 1832 14:29:49
Number of records 30

Average conc	0,36	0,28	0,21	0,13	0,08	0,06	0,06	0,05	0,05	0,08	0,12	0,22	0,50	0,62	0,79	0,65	0,51	0,72	1,56
3,82	3,45	4,72	7,78	7,94	10,92	12,65	13,63	13,90	10,98	7,49	5,17	5,56							
stdev	0,07	0,05	0,05	0,05	0,05	0,04	0,04	0,04	0,04	0,05	0,07	0,12	0,19	0,26	0,40	0,50	0,53	0,75	1,25
2,08	2,54	3,34	4,40	4,86	6,37	8,02	9,86	11,14	9,19	6,19	4,27	4,43							

Name	DOR 1:500																		
Average start		1883	14:30:40																
Average stop		1913	14:31:10																
Number of records			30																
Average conc		0,40	0,30	0,22	0,14	0,09	0,07	0,07	0,07	0,08	0,12	0,18	0,31	0,64	0,78	0,98	0,86	0,69	1,00
	2,08	4,74	4,48	6,04	9,36	9,56	13,03	14,87	15,64	16,59	14,90	11,92	8,19	7,93					
stdev	0,07	0,04	0,03	0,02	0,02	0,02	0,03	0,02	0,03	0,05	0,06	0,10	0,14	0,18	0,23	0,28	0,29	0,41	0,67
	1,01	1,29	1,79	2,50	3,00	4,16	5,00	5,58	6,33	6,20	5,70	5,06	7,74						

Name	DOR 1:250																		
Average start		1962	14:31:59																
Average stop		1992	14:32:29																
Number of records			30																
Average conc		1,33	0,81	0,45	0,24	0,15	0,16	0,22	0,23	0,29	0,48	0,64	0,98	1,54	1,72	2,06	2,00	2,04	2,70
	4,47	7,65	8,79	11,75	15,86	17,86	21,03	22,70	21,05	20,80	16,73	13,84	6,78	5,57					
stdev	0,50	0,25	0,12	0,06	0,04	0,05	0,06	0,06	0,08	0,13	0,15	0,24	0,35	0,47	0,66	0,80	0,97	1,30	1,99
	2,94	3,71	5,01	6,45	7,60	8,30	8,77	8,38	8,88	7,29	7,23	4,48	4,73						

Name	DOR 1:100																		
Average start		2052	14:33:29																
Average stop		2082	14:33:59																
Number of records			30																
Average conc		1,16	0,67	0,35	0,17	0,11	0,11	0,15	0,16	0,21	0,35	0,47	0,73	1,21	1,48	2,05	2,44	2,91	4,16
	6,54	10,46	11,27	12,63	13,80	11,76	9,76	7,54	4,63	3,21	1,82	1,25	0,90	1,19					
stdev	0,54	0,26	0,11	0,05	0,03	0,04	0,07	0,08	0,11	0,18	0,23	0,35	0,50	0,68	1,02	1,42	1,88	2,59	3,60
	4,68	5,86	6,40	6,16	5,68	4,63	3,94	2,58	1,75	1,06	0,78	0,75	1,57						

Name	DOR 1:50																		
Average start		2143	14:35:0																
Average stop		2173	14:35:30																
Number of records			30																
Average conc		3,33	1,53	0,61	0,24	0,15	0,22	0,38	0,42	0,62	1,14	1,52	2,49	3,75	4,68	6,38	8,06	9,87	12,58
	15,81	19,03	18,36	16,31	12,45	8,39	5,54	3,46	1,97	1,14	0,62	0,39	0,32	0,49					
stdev	1,74	0,70	0,24	0,09	0,05	0,08	0,17	0,20	0,32	0,60	0,76	1,19	1,58	1,95	2,59	3,38	4,27	5,23	6,13
	6,66	6,76	5,82	4,26	2,93	1,92	1,26	0,76	0,45	0,28	0,22	0,22	0,38						

Name	DOR 1:25																		
Average start		2228	14:36:25																
Average stop		2258	14:36:55																
Number of records			30																
Average conc		11,36	4,22	1,32	0,45	0,31	0,61	1,42	1,64	2,48	4,33	4,78	6,95	8,85	10,22	13,16	16,12	18,21	20,44
	21,61	20,52	16,99	12,01	7,64	4,62	2,94	1,87	1,13	0,68	0,39	0,25	0,22	0,42					
stdev	7,82	2,48	0,62	0,17	0,11	0,25	0,67	0,77	1,26	2,35	2,51	3,66	4,33	4,78	5,91	6,98	7,62	8,07	8,14
	7,32	6,14	4,34	2,79	1,82	1,30	0,95	0,64	0,42	0,26	0,19	0,18	0,42						

Name	Oil 1,2 L/min																		
Average start		1596	14:25:54																
Average stop		1626	14:26:24																
Number of records			30																
Average conc		0,32	0,25	0,17	0,10	0,06	0,04	0,04	0,03	0,03	0,05	0,08	0,16	0,40	0,49	0,57	0,37	0,23	0,32
	0,86	2,65	1,98	2,73	4,97	4,85	7,46	9,38	10,37	10,94	9,69	8,08	6,75	8,80					
stdev	0,04	0,02	0,02	0,03	0,03	0,02	0,02	0,02	0,02	0,03	0,04	0,07	0,11	0,16	0,24	0,26	0,21	0,30	0,61
	1,26	1,38	1,93	2,95	3,09	4,32	5,62	6,95	8,58	9,64	9,80	9,08	12,92						

SINTEF

Technology for a better society
www.sintef.no

From: "Saved by Internet Explorer 11"
Subject: BIODISPERS | Emergency Response | US EPA

Jump to main content
<iframe src="//www.googletagmanager.com/ns.html?id=GTM-L8ZB" height="0" width="0" style="display:none;visibility:hidden"></iframe>

EPA United States Environmental Protection Agency

EPA

United States Environmental Protection Agency

Search Search

- Emergency Response
- Share
  - Facebook
  - Twitter
  - Google+
  - Pinterest
- Contact Us

BIODISPERS

TECHNICAL PRODUCT BULLETIN #D-9
USEPA, OEM REGULATIONS IMPLEMENTATION DIVISION
ORIGINAL LISTING DATE: JUNE 28, 2002
REVISED LISTING DATE:
"BIODISPERS"
(formerly PETROBIODISPERS)

I. NAME, BRAND, OR TRADEMARK

BIODISPERS
Type of Product: Dispersant

II. NAME, ADDRESS, AND TELEPHONE NUMBER OF MANUFACTURER/CONTACT

Petrotech America Corporation
130 William Street, Suite 802

New York, NY 10038
Phone: (212) 933-9071, ext. 7001
Fax: (877) 226-4028
Email: info@helpenvironmental.com
(Mr. Lawrence Gallo)

III. NAME, ADDRESS, AND TELEPHONE NUMBER OF PRIMARY DISTRIBUTORS

Petrotech America Corporation
130 William Street, Suite 802
New York, NY 10038
Phone: (212) 933-9071, ext. 7001
Fax: (877) 226-4028
Email: info@helpenvironmental.com
(Mr. Lawrence Gallo)

Manufacturing Plant:
Clariant Corp.
Charlotte, NC

H.E.L.P. Environmental
926 3rd Avenue
Brooklyn, NY 11232

IV. SPECIAL HANDLING AND WORKER PRECAUTIONS FOR STORAGE AND FIELD APPLICATION

1. Flammability:
Non-flammable
2. Ventilation:
Use general ventilation to minimize exposure to vapor or mist.
3. Skin and eye contact; protective clothing; treatment in case of contact:
Skin contact - immediately flush with copious amounts of water. Remove and wash contaminated clothing and shoes. If irritation persists, see a doctor. Eye contact - may cause eye irritation. In case of contact, immediately flush eyes with plenty of water. If irritation persists, immediately see a doctor. Hygienic practices - wear safety glasses. Wear gloves in accordance with routine laboratory safety precautions.
4.a. Maximum storage temperature: >70°C
4.b. Minimum storage temperature: -25°C
4.c. Optimum storage temperature range:
4.d. Temperatures of phase separations and chemical changes: No phase or chemical separation observed.

V. SHELF LIFE

The product has unlimited shelf life.

VI. RECOMMENDED APPLICATION PROCEDURE

1. Application Method:
Recommended application is by aircraft, fireboat monitors or similar apparatus.
2. Concentration/Application Rate:

Concentration varies with spilled material - solvents at 5%, light oils at 10%, medium oils at 10%, and heavy oils at 10%.
3. Conditions for Use:
Data is for water temperature of 40°F to 65°F. There are no known application restrictions.

VII. TOXICITY AND EFFECTIVENESS

a. Toxicity:

Material Tested	Species	LC50 (ppm)
BIODISPERS	Menidia beryllina Mysidopsis bahia	13.46 96-hr 78.90 48-hr
No. 2 Fuel Oil	Menidia beryllina Mysidopsis bahia	12.42 96-hr 2.82 48-hr
BIODISPERS & No. 2 Fuel Oil (1:10)	Menidia beryllina Mysidopsis bahia	5.95 96-hr 2.66 48-hr
Reference Toxicant (SDS)	Menidia beryllina Mysidopsis bahia	11.84 96-hr 21.81 48-hr

b. Effectiveness:
SWIRLING FLASK DISPERSANT EFFECTIVENESS TEST WITH SOUTH LOUISIANA (S/L) AND PRUDHOE BAY (P/B) CRUDE OILS

Oil	Effectiveness (%)
Prudhoe Bay Crude	51.0
South Louisiana Crude	63.0
Average of Prudhoe Bay and South Louisiana Crudes	57.0

VIII. MIROBIOLOGICAL ANALYSIS

NA

IX. PHYSICAL PROPERTIES

1. Flash Point, ASTM Method D56: 193°F
2. Pour Point, ASTM Method D97: -26°F
3. Viscosity at 40°C, ASTM Method D445: Initial boil point 104.2°C, at 50 mL 109°C, at 70mL 111°C, at 80 mL 113.7°C, final temperature 307.1°C
4. Specific Gravity: 0.965
5. pH: 7
6. Surface Active Agents: CONFIDENTIAL
7. Solvents: Water
8. Additives: None
9. Solubility: Product is 100% soluble in water.

X. ANALYSIS FOR HEAVY METALS, CYANIDE, AND CHLORINATED HYDROCARBONS

Compound	Concentration (ppm)
Arsenic	<2.50
Cadmium	<0.75

Chromium	
Copper	<0.50
Lead	<5.00
Mercury	N/D
Nickel	<1.20
Zinc	<0.50
Cyanide	3.90*
Chlorinated Hydrocarbons	<5.00

N/D = Not detected
*During the analysis of cyanide on sample #V202057-01 (Petrotech Dispersant) analyst encountered interferences due to the matrix of sample. Soapy residue created a false positive for cyanide. Sample showed no traces of cyanide. Value related to the soap film turbidity.

Top of Page

Contact Us to ask a question, provide feedback, or report a problem.

Main menu

- Learn the Issues
  - Air
  - Chemicals and Toxics
  - Climate Change
  - Emergencies
  - Greener Living
  - Health and Safety
  - Land and Cleanup
  - Pesticides
  - Waste
  - Water
- Science & Technology
  - Air
  - Climate Change
  - Ecosystems
  - Health
  - Land, Waste and Cleanup
  - Pesticides
  - Substances and Toxics
  - Sustainable Practices
  - Water
- Laws & Regulations
  - By Business Sector
  - By Topic

- Compliance
- Enforcement
- Laws and Executive Orders
- Policy and Guidance
- Regulations

- About EPA
  - Administrator Gina McCarthy
  - Current Leadership
  - Organization Chart
  - Staff Directory
  - Planning, Budget and Results
  - Jobs and Internships
  - Headquarters Offices
  - Regional Offices
  - Labs and Research Centers

Secondary menu

- Español
- 中文: 繁體版
- 中文: 简体版
- Tiếng Việt
- 한국어

- EPA Home
- Privacy and Security Notice
- Accessibility

Last updated on December 31, 2014

- Hotline
- News
- Blog
- Apps
- Widgets

Social sites:

- Twitter
- Facebook
- YouTube
- Flickr
- Instagram

More social media at EPA »

<iframe src="//www.googletagmanager.com/ns.html?id=GTM-L8ZB" height="0" width="0" style="display:none;visibility:hidden"></iframe>

EPA

United States Environmental Protection Agency

DISPERSIT SPC 1000™

TECHNICAL PRODUCT BULLETIN #D-5
USEPA, OEM REGULATIONS IMPLEMENTATION DIVISION
ORIGINAL LISTING DATE: APRIL 22, 1999
REVISED LISTING DATE:
"DISPERSIT SPC 1000™"
(a/k/a SEACARE E.P.A. (ECOSPERSE™ POLLUTION ABATEMENT))

I. NAME, BRAND, OR TRADEMARK

DISPERSIT SPC 1000™
Type of Product: Dispersant (Water Based)

II. NAME, ADDRESS, AND TELEPHONE NUMBER OF MANUFACTURER/CONTACT

U.S. Polychemical Corp.
584 Chestnut Ridge Road
Chestnut Ridge, NY 10977
Phone: (845) 356-5003
Fax: (845) 356-6656
Email: bruceg@uspoly.com

(Mr. Bruce Gebhardt)

III. NAME, ADDRESS, AND TELEPHONE NUMBER OF PRIMARY DISTRIBUTORS

Maritime Solutions, Inc.
17 Battery Pl. Suite 913
New York, NY 10004
Phone: (201) 541-0939
(212) 747-9044
Fax: (212) 747-9240
(Mr. Chris Constantine / Mr. Richard Fredricks)

IV. SPECIAL HANDLING AND WORKER PRECAUTIONS FOR STORAGE AND FIELD APPLICATION

1. Flammability:
IMO: Non-flammable
DOT: Non-hazardous
2. Ventilation:
None normally required. Adequate to maintain fume levels below the TLV.
3. Skin and eye contact:
Avoid prolonged contact with skin and eyes. Flush eyes with plenty of water for at least 15 minutes. Get medical attention. Wear long sleeve shirt, chemical resistant gloves, and chemical protective goggles in case of exposure to mist.
4.a. Maximum storage temperature: 180ºF
4.b. Minimum storage temperature: -25ºF
4.c. Optimum storage temperature range: 40ºF to 140ºF
4.d. Temperatures of phase separations and chemical changes: None

V. SHELF LIFE

The shelf life of Dispersit SPC 1000™ is unlimited in unopened containers. Containers must be kept closed when not in use to prevent contamination.

VI. RECOMMENDED APPLICATION PROCEDURE

1. Application Method:
The dispersant may be applied by any conventional methods such as 1) aerial spraying and 2) boat spraying to accommodate weather conditions.
2. Concentration/Application Rate:
A dispersant to oil ratio ranging from 1 part dispersant to 50 parts oil to 1 part dispersant to 10 parts oil; or an application rate of about 2-10 gallons (7.6 liters- 37.9 liters) per acre (4840 square meters) is suggested. These rates will be dependent on the type of oil, degree of weathering, temperature and extent of oil slick.
3. Conditions for Use:
Timely application ensures the highest degree of successful dispersion of the oil spill.

VII. TOXICITY AND EFFECTIVENESS

a. Toxicity

Material Tested	Species	LC50 (ppm)
	Menidia	3.5 96-hr

DISPERSIT SPC 1000™	beryllina Mysidopsis bahia	16.6 48-hr
No. 2 Fuel Oil	Menidia beryllina Mysidopsis bahia	11.6 96-hr 11.7 48-hr
DISPERSIT SPC 1000™ & No. 2 Fuel Oil (1:10)	Menidia beryllina Mysidopsis bahia	7.9 96-hr 8.2 48-hr
Reference Toxicant (SDS)	Menidia beryllina Mysidopsis bahia	6.3 96-hr 11.7 48-hr

b. Effectiveness:
SWIRLING FLASK DISPERSANT EFFECTIVENESS TEST WITH SOUTH LOUISIANA (S/L) AND PRUDHOE BAY (P/B) CRUDE OIL

Oil	**Effectiveness (%)**
Prudhoe Bay Crude	40%
South Louisiana Crude	105%
Average of Prudhoe Bay and South Louisiana Crudes	73%

VIII. MIROBIOLOGICAL ANALYSIS

Not applicable

IX. PHYSICAL PROPERTIES

1. Flash Point, ASTM D-56-87: 208ºF
2. Pour Point, ASTM D-97-87: < -20ºC
3. Viscosity, ASTM D-445-88: 144CPS, @ 68ºF
4. Specific Gravity, ASTM D-1298-85(90): 0.995, @ 68ºF
5. pH, ASTM D-1293-84(90): 10.0
6. Surface Active Agents: Anionic and non-ionic, proprietary, surfactants
7. Solvents: Proprietary, non-petroleum based
8. Additives: None
9. Solubility in Water: Complete

X. ANALYSIS FOR HEAVY METALS, CYANIDE, AND CHLORINATED HYDROCARBONS

Compound	**Concentration (ppm)**
Arsenic	< 1.00
Cadmium	< 2.00

Chromium	
Copper	< 2.00
Lead	< 1.00
Mercury	< 0.04
Nickel	< 10.00
Zinc	< 2.00
Cyanide	< 2.00
Chlorinated Hydrocarbons	< 5.00

Top of Page

Contact Us to ask a question, provide feedback, or report a problem.

Main menu

- Learn the Issues
  - Air
  - Chemicals and Toxics
  - Climate Change
  - Emergencies
  - Greener Living
  - Health and Safety
  - Land and Cleanup
  - Pesticides
  - Waste
  - Water
- Science & Technology
  - Air
  - Climate Change
  - Ecosystems
  - Health
  - Land, Waste and Cleanup
  - Pesticides
  - Substances and Toxics
  - Sustainable Practices
  - Water
- Laws & Regulations
  - By Business Sector
  - By Topic
  - Compliance
  - Enforcement
  - Laws and Executive Orders
  - Policy and Guidance

- Regulations
- About EPA
  - Administrator Gina McCarthy
  - Current Leadership
  - Organization Chart
  - Staff Directory
  - Planning, Budget and Results
  - Jobs and Internships
  - Headquarters Offices
  - Regional Offices
  - Labs and Research Centers

Secondary menu

- Español
- 中文: 繁體版
- 中文: 简体版
- Tiếng Việt
- 한국어

- EPA Home
- Privacy and Security Notice
- Accessibility

Last updated on December 31, 2014

- Hotline
- News
- Blog
- Apps
- Widgets

Social sites:

- Twitter
- Facebook
- YouTube
- Flickr
- Instagram

More social media at EPA »

From: "Saved by Internet Explorer 11"
Subject: FFT-SOLUTION® | Emergency Response | US EPA

Jump to main content
<iframe src="//www.googletagmanager.com/ns.html?id=GTM-L8ZB" height="0" width="0" style="display:none;visibility:hidden"></iframe>

EPA United States Environmental Protection Agency

EPA

United States Environmental Protection Agency

Search Search

- Emergency Response
- Share
  - Facebook
  - Twitter
  - Google+
  - Pinterest
- Contact Us

FFT-SOLUTION®

TECHNICAL PRODUCT BULLETIN #D-17
USEPA, OEM REGULATIONS IMPLEMENTATION DIVISION
ORIGINAL LISTING DATE: NOVEMBER 01, 2011
"FFT-SOLUTION®"

I. NAME, BRAND, OR TRADEMARK

FFT-SOLUTION®
Type of Product: Dispersant

II. NAME, ADDRESS, AND TELEPHONE NUMBER OF MANUFACTURER/CONTACT

Fog Free Technologies, LLC
4365 Dorchester Road
Building 300, Suite 301
North Charleston, SC 29405
Product Management

Office Phone: (843) 735-6626
Mobile: (478) 697-2588
E-mail: doc@fogfreetechnologies.com
Website: http://www.fogfreetechnologies.com/ Exit
(Mr. William H. Knight)

III. NAME, ADDRESS, AND TELEPHONE NUMBER OF PRIMARY DISTRIBUTORS

Fog Free Technologies, LLC
4365 Dorchester Road
Building 300, Suite 301
North Charleston, SC 29405
Product Management
Office Phone: (843) 735-6626
Mobile: (478) 697-2588
E-mail: doc@fogfreetechnologies.com
Website: http://www.fogfreetechnologies.com/ Exit
(Mr. William H. Knight)

IV. SPECIAL HANDLING AND WORKER PRECAUTIONS FOR STORAGE AND FIELD APPLICATION

1. Flammability: IMO: Non-Flammable, DOT: Non-Hazardous
2. Ventilation: Lowest level of skin protection is acceptable, but no special ventilation is required.
3. Skin and eye contact; protective clothing; treatment in case of contact: Lowest level of skin protection is acceptable. Avoid eye contact. In case of eye contact, immediately flush eyes with large amounts of water for at least 15 minutes. Avoid contact with skin. In case of skin contact, immediately flush with water and soap if available. For open systems where contact is likely, wear long sleeve shirt, chemical resistant gloves and chemical goggles.
4.a. Maximum storage temperature: 170°F
4.b. Minimum storage temperature: 30°F
4.c. Optimum storage temperature range: 40°F to 105°F
4.d. Temperatures of phase separations and chemical changes: None

V. SHELF LIFE

The shelf life of unopened drums of FFT-SOLUTION® is limited to 60 months. Storage should be in a semi-controlled warehouse, out of direct sunlight.

VI. RECOMMENDED APPLICATION PROCEDURE

1. Application Method: Aerial Spraying – Aircraft provide the most rapid method of applying dispersants to an oil spill and a variety of aircraft can be used for spraying. For aerial spraying, FFT-SOLUTION® is applied undiluted. Typical application altitudes of 30 to 50 feet have been used, although higher altitudes may be effective under certain conditions. Actual effective altitudes will depend upon application equipment, weather, and aircraft. Careful selection of spray nozzles is critical to achieve desired dose levels, since droplet size must be controlled. Many nozzles used for agricultural spraying are of low capacity and product fine a spray. A quarter-inch open pipe may be all that is necessary if the aircraft travels at 120 mph (104 knots) or more, since the air shear at these speeds will be sufficient to break the dispersant into the proper sized droplets. Optimal temperatures for application are between 33°F and 105°F.

Boat Spraying – FFT-SOLUTION® may also be applied by workboats equipped with spray booms mounted on the stern of the vessel. (Mounting boom on the stern prevents any over spray from making contact with boat operators.) The preferred and most effective method of application from a workboat is to use a low-volume, low-pressure pump so the chemical can be applied undiluted. Standard agriculture spray equipment is designed to make dosage adjustments or provide different spray tips that effect dosage rates. Natural wave or boat wake action usually provides adequate mixing energy to disperse the oil. A typical agriculture spray boom can be mounted to the stern to get wide coverage. The booms on shrimp boats also can be retrofitted to cover a much wider path during applications. The manufacturer also recommends that in lieu of spray tips on the booms, spray tips be changed into solid tubing for injection of FFT-SOLUTION® 3 to 5 feet below the water surface. This will get the thicker crude slicks injected faster and with better results. FFT-SOLUTION® should be applied as droplets, not fogged or atomized.

2. Concentration/Application Rate: A treatment rate of about 2 to 10 U.S. gallons per acre, or dispersant to oil ration of 1:50 to 1:10 is recommended. This rate varies depending on the type of oil, degree of weathering, temperature, and thickness of the slick.

3. Conditions for Use: FFT-SOLUTION® can be applied to weathered oil as well as light, medium, or heavy oils. Early treatment even at reduced treatment rates, can also counter the foaming tendencies of the spilled oil in turbulent waters. FFT-SOLUTION® can be used on any type oil spills in salt water.

VII.TOXICITY AND EFFECTIVENESS

a. Toxicity:

Material Tested	Species	LC50 (ppm)
FFT-SOLUTION®	Menidia beryllina Mysidopsis bahia	5.34 96-hr 2.72 48-hr
No. 2 Fuel Oil	Menidia beryllina Mysidopsis bahia	40.80 96-hr 5.19 48-hr
FFT-SOLUTION® & No. 2 Fuel Oil (1:10)	Menidia beryllina Mysidopsis bahia	5.14 96-hr 2.75 48-hr
Reference Toxicant (SDS)	Menidia beryllina Mysidopsis bahia	2.42 96-hr 6.97 48-hr

b. Effectiveness:

SWIRLING FLASK DISPERSANT EFFECTIVENESS TEST WITH SOUTH LOUISIANA (S/L) AND PRUDHOE BAY (P/B) CRUDE OIL

Oil	Effectiveness (%)
Prudhoe Bay Crude	49.97%
South Louisiana Crude	48.87%
Average of Prudhoe Bay and South Louisiana Crudes	49.42%

VIII. MICROBIOLOGICAL ANALYSIS

NA

IX. PHYSICAL PROPERTIES

1. Flash Point: 170°F
2. Pour Point: 23°F
3. Viscosity: 450 SUS @100°F
4. Specific Gravity: 1.0302 @60°F
5. pH: 9.96
6. Surface Active Agents: CONFIDENTIAL
7. Solvents: None
8. Additives: None
9. Solubility: Product is 100% soluble in water

X. ANALYSIS FOR HEAVY METALS, CYANIDE, AND CHLORINATED HYDROCARBONS

Compound	Concentration (ppm)
Arsenic	ND
Cadmium	ND
Chromium	ND
Copper	ND
Lead	ND
Mercury	ND
Nickel	ND
Zinc	ND
Cyanide	ND
Chlorinated Hydrocarbons	ND

Top of Page

Contact Us to ask a question, provide feedback, or report a problem.

Main menu

- Learn the Issues
  - Air
  - Chemicals and Toxics
  - Climate Change
  - Emergencies
  - Greener Living
  - Health and Safety
  - Land and Cleanup

- Pesticides
- Waste
- Water

- Science & Technology
  - Air
  - Climate Change
  - Ecosystems
  - Health
  - Land, Waste and Cleanup
  - Pesticides
  - Substances and Toxics
  - Sustainable Practices
  - Water
- Laws & Regulations
  - By Business Sector
  - By Topic
  - Compliance
  - Enforcement
  - Laws and Executive Orders
  - Policy and Guidance
  - Regulations
- About EPA
  - Administrator Gina McCarthy
  - Current Leadership
  - Organization Chart
  - Staff Directory
  - Planning, Budget and Results
  - Jobs and Internships
  - Headquarters Offices
  - Regional Offices
  - Labs and Research Centers

Secondary menu

- Español
- 中文: 繁體版
- 中文: 简体版
- Tiếng Việt
- 한국어

- EPA Home
- Privacy and Security Notice
- Accessibility

Last updated on December 31, 2014

- Hotline
- News
- Blog
- Apps
- Widgets

Social sites:

- Twitter
- Facebook
- YouTube
- Flickr
- Instagram

More social media at EPA »

The Effectiveness of Dispersants on Oil Encapsulated in Ice for Extended Periods

Tim Nedwed (ExxonMobil Upstream Research Company)
Victoria Broje (Shell Exploration & Production Company)
Stéphane Le Floch (CEDRE Research Department Manager)

Oil spill response in ice-prone regions requires access to all response tools because of the multiple challenges that ice produces. Oil spilled in ice can become rapidly encapsulated into the ice during the ice-growth season. This encapsulation minimizes marine organisms contactwith oil, but also restricts / eliminates access to the oil for response. Encapsulation also prevents oil slick evaporation, dispersion and emulsification to any significant degree and allows responders to track the oil through the winter and respond to the released oil during the spring melt.

This paper describes research to determine if oil encapsulated in ice for long periods remains dispersible after ice melt. In 2015 the Arctic Response Technology Joint Industry Programme (JIP) executed a unique, long-term mesocosm experiment to improve the scientific knowledge of the fate and biodegradation of oil and oil spill response residues in ice, as well as the environmental effects to ice associated ecology. Several mesocosms were installed in the sea ice of the Van Mijenfjorden in Svea, Svalbard in February and remained in place until May. Oil was introduced into two mesocosms and allowed to freeze in without any treatment. In two other mesocosms oil pre-mixed with dispersant was introduced and was allowed to freeze in. Ice cores were collected from all mesocosms at periods of 1, 2, and 3 months. These ice cores were subsequently melted in the CEDRE laboratory to simulate spring ice melt and the release of oil into open water. Effectiveness of dispersion was tested with untreated oil, oil treated with dispersants after the melt and oil pre-mixed with dispersant prior to being frozen into ice.

Results of this study provide valuable information for planning dispersant operations for oil spills in ice-covered waters.

1 Introduction

Arctic oil production both onshore and offshore has produced greater than 25 billion barrels of oil (IHS International E&P Database as of September 3, 2014). Oil production in the Arctic began almost 100 years ago with Norman Wells field in Canada's Northwest Territories. Offshore Arctic exploration began over 40 years ago and has led to the completion of approximately 440 wells (IHS International E&P Database as of September 3, 2014).

A distinguishing feature of the Arctic is the presence of ice for all or part of the year. The extent, thickness, and duration of ice vary throughout the Arctic and from year to year. During the summer and fall many areas are ice free for significant periods. In the near term, offshore oil exploration will likely occur during these ice-free periods. Therefore, any oil spill response planning for these operations will include developing strategies for these open water periods. However, robust contingency planning will include scenarios where oil could become entrapped in ice.

The dynamic nature of the Arctic (ice cover, low temperatures, remoteness, and extended

periods of darkness) causes some unique challenges for Arctic activities including oil spill response. These challenges are well known and often described. However, one benefit of ice cover and subsequent encapsulation of spilled oil is the significant benefit of extending response times (Sørstrøm et al. 2010). Rapid response is often necessary for spills to open water because of the dynamic nature of spilled oil – slicks are rapidly spreading, breaking into smaller slicks, moving, emulsifying, and ultimately stranding on shorelines. In fact, depending on where an offshore oil spill occurs, oil spilled in open water could strand on shorelines before significant response activities can even start. Oil spilled in significant ice cover has the potential to contain oil in a much smaller area than in open water as illustrated by two experimental releases of Sture Blend crude oil in 1989 and 1993 (Vefsnmo and Johannessen, 1994). The 1989 experiment released 30 m^3 of oil into open water while the 1993 experiment released 26 m^3 of oil in 70 – 90% concentrations of broken ice. After 10 hours of spreading the thickest portion of the open water slick covered an area of 2 km x 50 m (100,000 m2) with a 13 km sheen "tail." After 10 hours the spill in broken ice covered only 100 m2. Concentrated ice cover also minimizes wave motion and hence slick dispersion and emulsification rates. Low temperatures, smaller slick areas and greater thickness reduce volatilization rates. As a result, oil remains fresh, burnable and dispersible for a longer period of time than under otherwise similar scenarios in open waters of a temperate region. Further, land-fast ice will prevent oil spilled offshore from reaching shorelines until the spring / summer melt and allow collection of oil concentrated against the ice edge. All of these advantages provide responders additional time to plan for and implement an effective response to at least partly offset challenges caused by Arctic remoteness and conditions.

In 2009, three oil industry trade associations (IPIECA, International Oil and Gas Producers, and American Petroleum Institute) formed a committee to review Arctic oil spill response capabilities and to identify potential technology enhancements and research needs. This resulted in a joint report describing this effort (Potter et al., 2012). In 2012, nine international oil and gas companies began a joint industry project (JIP) to conduct research designed to enhance Arctic oil spill response capabilities based on recommendations from the 2009 study. This effort developed into multiple working groups to further advance various aspects of oil spill response. The Dispersants working group was focused on enhancing industry's understanding on the use of dispersants in the Arctic and Environmental Effects working group was focused on increasing the understanding of the effects of oil and response techniques in the Arctic.

The JIP Environmental Effects working group coordinated and oversaw placement of several mesocosms in the sea ice of the Van Mijenfjorden in Svea, Svalbard from February to May 2015. These mesocosm were installed to study oil weathering, natural biodegradation, and the sensitivity / resiliency of sea ice communities (IOGP-ART, 2017). One potential scenario that the mesocosm allowed study of is a subsea blowout during the ice growth season where dispersants are applied to the oil at the release point. This oil will be fresh when the dispersant is applied and at least a portion of the oil could rise under the ice where it could become encapsulated until spring melt.

The Dispersants working group used the mesocosm study as an opportunity to collect ice cores containing either crude oil alone or oil crude oil premixed with dispersant to conduct dispersant effectiveness study. The objective of the study was to evaluate the potential for dispersion of encapsulated crude oil released from melting ice. This paper describes the results of dispersion effectiveness testing performed on the oil samples from the ice cores after the cores

were melted to release the oil and illustrate 3 scenarios:

- Dispersion of untreated oil released from melted ice without addition of dispersant
- Dispersion of untreated oil released from melted ice treated with new dispersant after the melt
- Dispersion of oil pre-treated with dispersant prior to freeze in. No additional dispersant added after the melt.

2 Materials and Methods

Eight 1.6 m diameter mesocosms were installed in late February 2015 into the sea ice of a fjord near Svea, Svalbard (IOGP-ART, 2017). A conceptual drawing of a mesocosm is shown in Figure 1.

To install a mesocosm, an opening was cut into the ice in January and the 1.6 m mesocosm was placed in the opening. The mesocosm contained buoyancy that allowed them to float with about 25 cm of freeboard. Oil was placed on the surface of the water inside the central area of the mesocosm and allowed to freeze in place. Variable snow accumulation in the mesocosm caused 10 – 20 cm of accumulation that packed to a relatively solid slush. Between 34 – 37 cm of ice grew below the oil. Two of the mesocosms contained oil only; two contained dispersant mixed with oil at a dose rate of 1:20; two contained crude oil burn residue, and two were controls with no oil. In the mesocosm with crude oil, 20 liters of oil was put in place to produce an oil layer approximately 1 cm thick. In the mesocosm with burn residue, the residue from 20 liters of oil was put in place. For this study, cores were only used from the mesocosms with crude oil and crude oil plus dispersant.

The oil used in the mesocosms was from the Kobbe field in the North Sea offshore of Norway. The Kobbe oil has the properties shown in Table 1.

Table 1. Properties of Kobbe Oil used in the Mesocosm Studies

Density (g/ml)	0.797
Pour Point (°C)	-36
Viscosity (cP at 13°C and 100 s^{-1} shear)	3
Asphaltene (weight %)	0.03
Waxes (weight %)	3.4

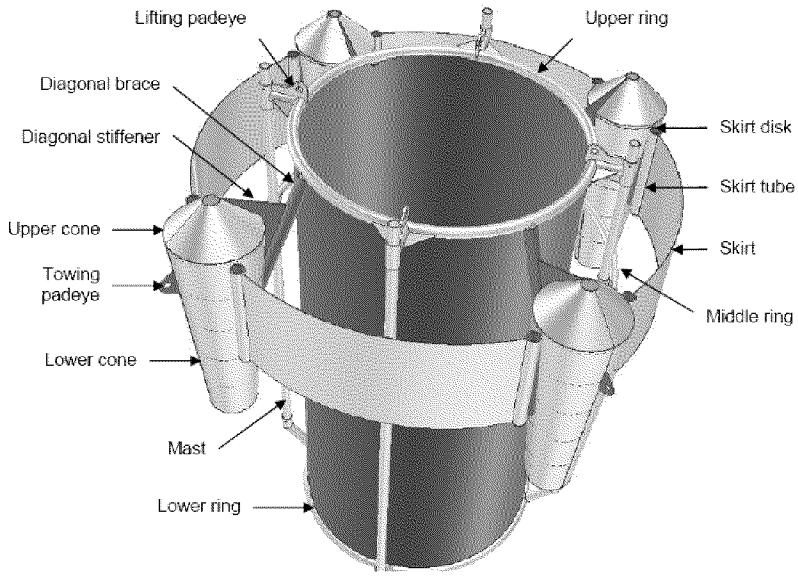

Figure 1. Conceptual drawing of a mesocosm (IOGP-ART, 2017).

Cores for this study were collected using a 9-cm diameter corer from each of the four mesocosms 1 month (T1), 2 months (T2), and 3 months (T3) after beginning of the experiment. The corer was cleaned after taking each core. Then, ice cores were cut in 3 or 4 sections: packed **Snow** of variable thickness –when present; **Top** ice section which contained the main oil layer – oil slick; **Middle** ice section; and **Bottom** ice section which was the ice - water interface. Ice sections were immediately placed in a bag containing 500 mL of 3°C filter-sterilized (0.2 µm filter) seawater and put into a refrigerator at 2-3°C to melt. Once melted, an oil sample from each core was collected from the surface of the melt water, stored in a single amber bottle for each core and shipped to the CEDRE laboratory in Brest, France where they were stored for 6 months at minus 80°C. Figure 2 shows a photograph of a core collected from a crude oil plus dispersant mesocosm at 3 months (T3). These samples were then split into triplicate prior to dispersant effectiveness testing to allow three tests per mesocosm per sampling time.

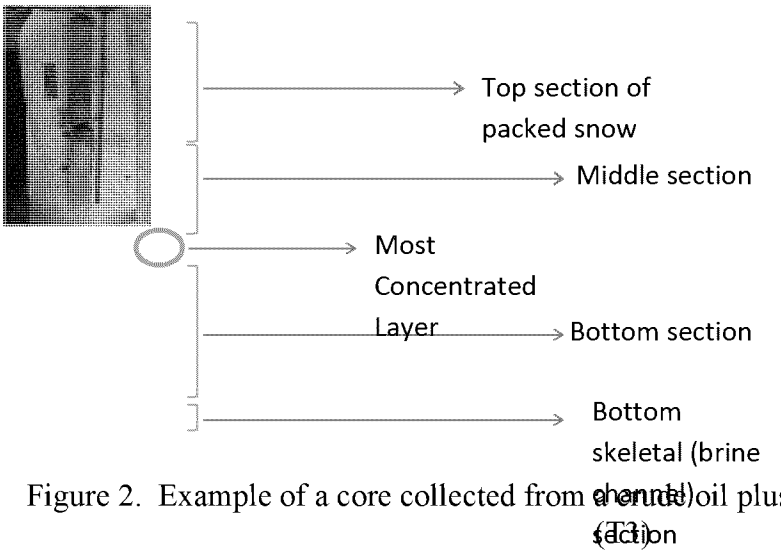

Figure 2. Example of a core collected from a crude oil plus dispersant mesocosm at 3 months (T3).

The triplicate samples from each core at each sampling time underwent dispersant efficiency testing using a Field Test protocol developed previously (Fiocco et al., 1999). The dispersant used for the lab testing and in the mesocoms was FINASOL® OSR 52 dispersant. The protocol was adapted to account for storage of the samples and the use of brackish water as follows:

1. Oil samples were placed in a thermoregulated room at 10°C for one night (from 6 PM to 8 AM);
2. A volume of 5 liters of brackish water (salinity of 20 ppt) was prepared and, also, placed in the thermo-regulated room at 10°C for one night;
3. The testing procedure was as follows:
    a. A 100 mL volumetric cylinder was filled with 80 mL of brackish water;
    b. 1.5 mL of oil was added gently on the water surface by using a glass syringe;
    c. For the samples requiring addition of new dispersant, 6 drops (~60 μL) of dispersant was evenly distributed around the entire oil surface in the volumetric cylinder. The dispersant-treated oil did not have additional dispersant added.
    d. The oil and the dispersant in the cylinder were allowed to sit undisturbed for 1 min.
    e. The glass cylinder was then gently turned upside down (corresponding to approx. 30 rpm) for 1 min;
    f. The visual estimation criteria provided by the protocol (below) were used to assess the oil dispersibility. Pictures were taken at T0 (immediately after stopping the agitation), T+1min (after 1 min of rest / settling), T+5min (after 5 min of rest) and T+15min (after 15 min of rest).

Criteria for dispersibility estimation:

Good dispersibility: Formation of brown **dispersion** (oil droplets). The oil droplets will slowly rise to the surface at a standstill. This dispersibility was given a rating of 10.

Reduced dispersibility: Formation of dark/black, large oil droplets. Fast rise of droplets to the surface. This dispersibility was given a rating of 5.

Bad dispersibility: Little/ no difference from reference oil (untreated) cylinder. Fast rise of large oil droplets (at a standstill). This dispersibility was given a rating of 1.

Table 2 shows the samples that were tested. A control dispersant effectiveness test was performed on the fresh Kobbe oil that had not been placed in a mesocosm.

Table 2. List of Samples that Underwent Dispersant Effectiveness Testing

		T0	T1	T2	T3
Original Kobbe oil	without dispersant	1 test			

	with dispersant	1 test			
Untreated Kobbe Mescosm oil	without dispersant		1 test	1 test	1 test
	with fresh dispersant		3 tests	3 tests	3 tests
Pre-treated Kobbe Mesocosm oil	without fresh dispersant		3 tests	3 tests	3 tests

3 Results and Discussion

The fresh Kobbe crude oil (oil that was not placed in a mesocosm) did not disperse without adding dispersant. It took less than 1 min of settling for the oil to rise the surface without adding any dispersant. The dispersion was stable when dispersants were added with little oil resurfacing after 15 minutes of settling as illustrated in Figure 3. Untreated fresh Kobbe crude oil was classified as having "bad dispersibility" while treated fresh Kobbe crude oil was classified as having "good dispersibility" even after 15 minutes of settling time.

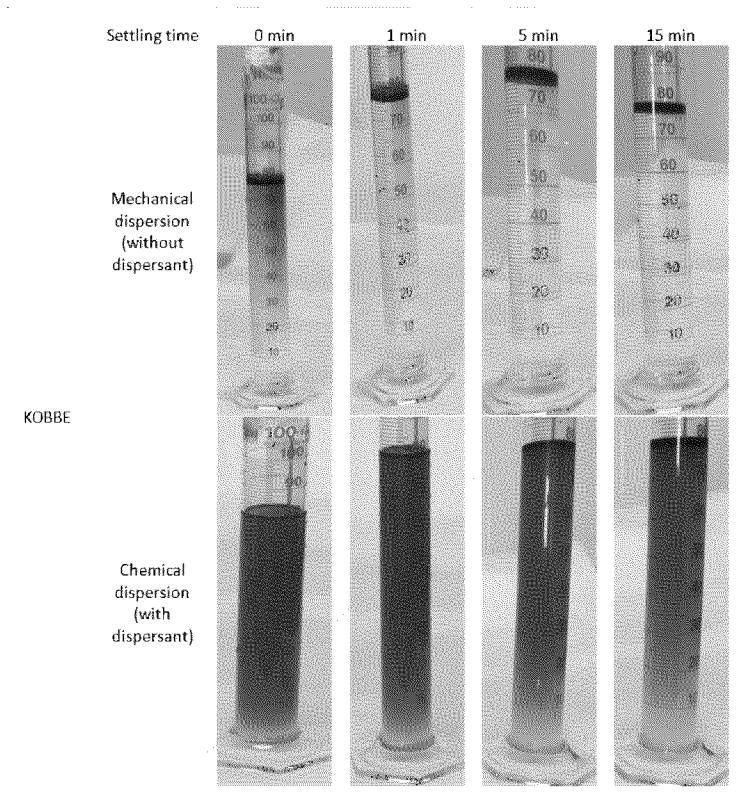

Figure 3. Photographs of the graduated cylinders containing brackish water and fresh Kobbe crude oil taken at 0, 1, 5, and 10 minutes after the 1 minute of mixing time specified for the test.

Table 3 provides the results for the mesocosm samples. The mesocosm oil that was not treated with dispersant before or after the cores were collected was classified as "bad dispersibility" for all three coring periods – 1 month to 3 months. After less than 1 minute of settling time the oil had risen to the surface. The appearance of the cylinders after the mixing time was very similar to those shown for mechanical dispersion in Figure 3.

The oil pretreated with dispersant prior to placement in the mesocosms (pre-treated oil)

collected at 1 month was classified as having "good dispersion" for the total 15 minutes of settling time. The same pretreated oil was classified as having "good dispersion" after 1 minute of settling but "reduced dispersion" at 5 and 15 minutes of settling for the cores collected after 2 and 3 months. Figure 4 shows the photos of a cylinder after mixing taken after 0, 1, 5, and 15 minutes of settling for the pre-treated oil from a core collected after 3 months in the mesocosm.

Dispersants are known to leach from oil to water over time with faster leaching rates for lower salinity water (Knudsen et al., 1994). This is because dispersants contain a mix of hydrophilic and oleophilic surfactants. The melting process required to collect the oil from the cores for this testing may have allowed leaching of the hydrophobic surfactants from the oil to the water; however, it is possible that surfactants leached from the oil onto the ice while the mesocosms were in place. This could have caused the reduced dispersion after 1 minute of settling time.

Table 3 : Dispersibility of the oil collected from the mesocosms.

	Treatment	No settling	1 min settling	5 min settling	15 min settling	Average Rating
1 month (T1)	Untreated oil	B / 1	B / 1	B /1	B / 1	1
	Pre-treated oil	G /10	G /10	G /10	G /10	10
	Post-treated oil	G /10	G /10	G /10	G /10	10
2 months (T2)	Untreated oil	B / 1	B / 1	B / 1	B / 1	1
	Pre-treated oil	G /10	G /10	R / 5	R / 5	7.5
	Post-treated oil	G /10	G /10	G /10	G /10	10
3 months (T3)	Untreated oil	B / 1	B / 1	B / 1	B / 1	1
	Pre-treated oil	G /10	G /10	R / 5	R / 5	7.5
	Post-treated oil	G /10	G /10	G /10	G /10	10

G = Good dispersibility / rating 10, R = Reduced dispersibility / rating 5, and B = Bad dispersibility / rating 1

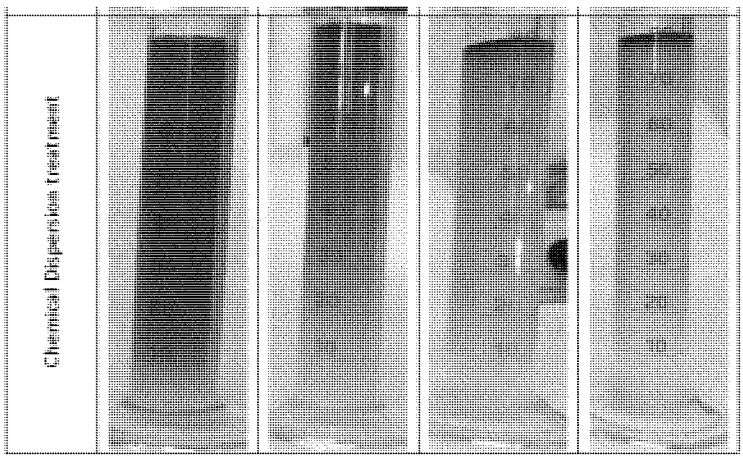

Figure 4. Photographs of the graduated cylinders containing brackish water and Kobbe crude oil pretreated with dispersant prior to placement in the mesocosm and tested without additional dispersant. The core was collected at 3 months. Photos were taken at 0, 1, 5, and 10 minutes after the 1 minute of mixing time specified for the test.

The oil that was treated with dispersants only after the cores were collected and melted

(post-treated oil) showed the best dispersant effectiveness. This oil was classified as "good dispersion" for cores collected at 1, 2, and 3 months even after 15 minutes of settling time (Table 3). This oil was as dispersible as the fresh Kobbe oil that had not been placed in a mesocosm. This indicates that the oil frozen into the mesocosms remained relatively fresh even after 3 months.

Figure 5 shows that average rating for all the dispersant efficiency testing. The average rating was determined for each sample by averaging the rating at each settling time period as shown in Table 3.

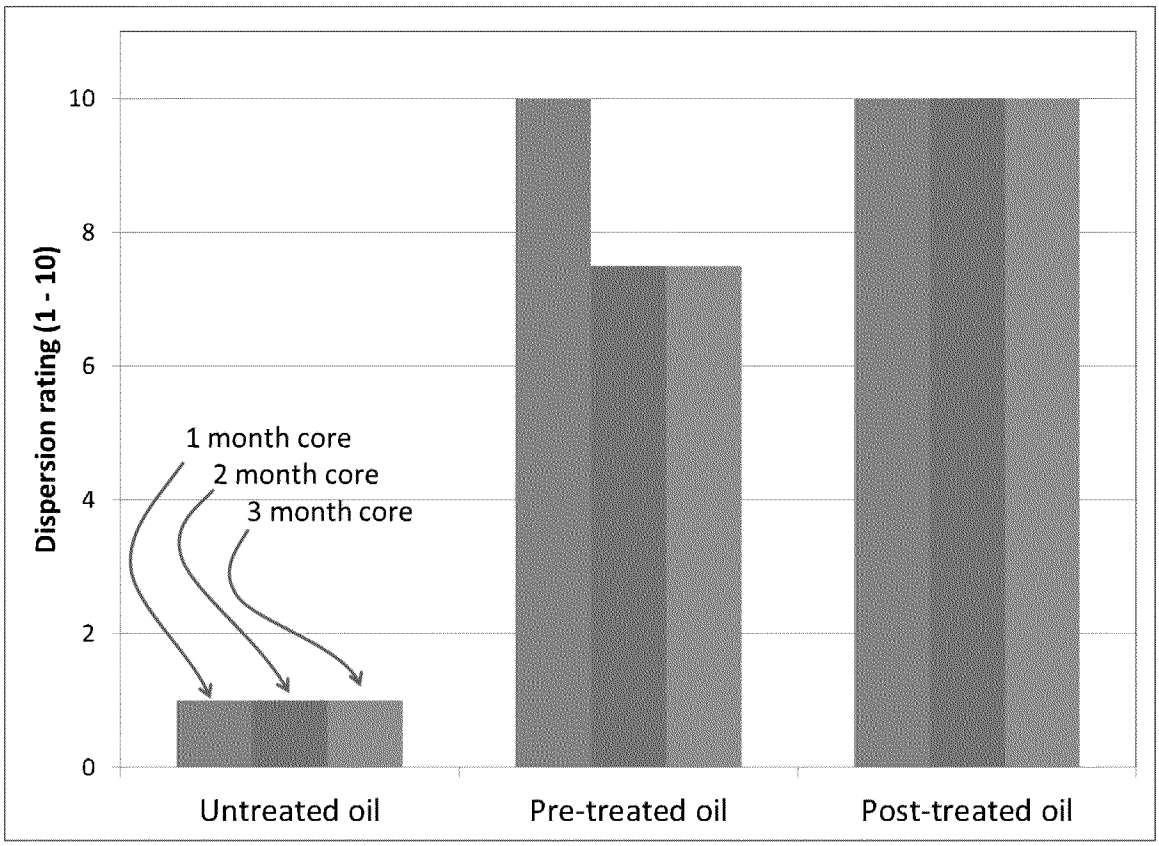

Figure 5. Graph of average dispersion rating for each core collection time and for each treatment.

4 Conclusions

A low density and viscosity crude oil (Kobbe) was frozen into sea ice in a fjord near Svea, Svalbard from February through May 2015. Cores that contained the frozen crude oil were collected at 1 month intervals over this period. The cores were melted to release crude oil samples that were then tested for dispersibility using a field effectiveness test.

The crude oil that was frozen into the ice and treated with dispersant after the core collection and melting maintained "good dispersion" even after 3 months frozen into the ice. In fact, this oil was as dispersible as fresh Kobbe crude oil.

The crude oil that was pre-treated with dispersant prior to freezing into the ice was still dispersible but less so than the oil that was post-treated with dispersant. The melt process used to collect samples and partitioning of surfactants from the oil to ice in the mesocosms may have

allowed leaching into the water of some of the surfactants in these oil samples causing the reduced dispersion.

This study indicates that oil trapped in sea ice over the winter could remain dispersible for at least 3 months. Dispersion can happen if the oil is pre-treated with dispersants, but dispersant efficiency may be higher if the oil is treated with dispersants after it is released from the ice after a melt.

Thus, application of dispersants could be a viable option for oil found in ice leads before it has a chance to significantly weather and emulsify either during the ice growth season or during the ice melt. Further, oil found in melt pools on top of ice and freshly released into water could be treated with dispersant and disperse when exposed to wave action after the ice breaks up. One potential scenario is a subsea blowout during the ice growth season where dispersants are applied to the oil at the release point. This oil will be fresh when the dispersant is applied and at least a portion of the oil could rise under the ice where it could become encapsulated until spring melt. The findings of this study indicate that the oil could disperse when this oil is released during the spring melt.

5 References

Fiocco, R.J., Daling, P.S., DeMarco, G., & Lessard, R.R., Advancing Laboratory / Field Dispersant Effectiveness Testing, in *Proceedings of the 1999 International Oil Spill Conference*, March 8-11, Seattle, WA.

IOGP-ART, 2017. Long Term Ice Exposure Studies for Enhancing Arctic Neba Science Base, In *Proceedings of the 2017 International Oil Spill Conference* (in press).

Knudsen, O.Ø., Brandvik, P.J., and Lewis, A., 1994. Treating Oil Spill with W/O Emulsion Inhibitors – A Laboratory Study of Surfactant Leaching from the Oil to the Water Phase. In *Proceedings of the Seventeenth Arctic and Marine Oil Spill Program (AMOP) Technical Seminar.* Environment Canada, June 8-10, 1994, Vancouver, British Columbia.

Potter, S., I. Buist, K. Trudel, D. Dickins and E. Owens. 2012. Spill Response in the Arctic Offshore. Prepared for the American Petroleum Institute and the Joint Industry Programme on Oil Spill Recovery in Ice, D. Scholz (ed.). American Petroleum Institute, Washington.

Sørstrøm, S. E., P.-J. Brandvik, I. Buist, P. Daling, D. Dickins, L.-G. Faksness, S. Potter, J. F. Rasmussen and I. Singsaas (2010). Joint Industry Program on Oil Spill Contingency for Arctic and Ice-covered Waters: Summary Report. Oil in Ice JIP. Tronheim, Norway, Sintef.

Vefsnmo, S. and Johannessen, B. O. 1994. Experimental oil spill in the Barents Sea. Drift and spread of oil in broken ice. Sintef Technical Paper 199515, Norway.

Comparative Study to Determine the Biodegradability of Dispersants at Environmentally Relevant Concentrations

Yu Zhang[1], Mobing Zhuang[1], Pablo Campo[2], Ruta Suresh Deshpande[3], Devi Sundaravadivelu[3], Robyn N. Conmy[4] and Jorge W. Santo Domingo[4]

1. Department of Biomedical, Chemical and Environmental Engineering, University of Cincinnati, 2901 Woodside Drive, Cincinnati, OH 45221, USA
2. Cranfield Water Science Institute, Cranfield University, Cranfield MK43 0AL, UK
3. Pegasus Technical Services Inc., 46 E Hollister Street, Cincinnati, OH 45219, USA
4. U.S. Environmental Protection Agency, National Risk Management Risk Laboratory, 26 W. MLK Drive Cincinnati, OH 45268, USA

ABSTRACT

Chemical dispersant agents reduce the interfacial tension between oil and water, and increase the surface area to volume ratio of oil droplets thus facilitating the biodegradation of spilled oil. Dispersants are composed of surface active molecules known as surfactants and various commercial products contain Dioctyl Sulfosuccinate (DOSS) as the active ingredient. Since previous laboratory studies including the BFT were conducted at oil and dispersant concentrations significantly higher (~0.7 g/L oil with DOR of 1:25) than those typically found in field conditions, experiments were conducted at low levels of oil and dispersant (28 μg/L oil with DOR of 1:25) in order to determine the degradation trends at environmentally relevant concentrations. Experiments were conducted using two crude oils (Alaskan North Slope and Endicott) and two dispersant products (Corexit 9500 and Finalsol OSR 52) to study the biodegradation of dispersants and dispersed oil and oil alone samples were used as controls. Two

oil degrading cultures, isolated from the surface (meso) and deep sea (cryo) of the Gulf of Mexico, were enriched on crude oil at 25 and 5 °C and were used as the inocula. The biodegradation experiments were performed at 5 °C for 56 days and at 25 °C for 48 days using sterile GP2 artificial seawater as the media. The time series concentration of DOSS, the primary surfactant in the dispersants was monitored using LC-MS/MS in addition to the oil concentration which was measured using GC-MS/MS. Although the initial concentration of DOSS in Finasol OSR 52 was 20% higher than in Corexit 9500, over 95% of the anionic surfactant fraction was metabolized for both types of dispersant products by the end of the experiment at 25 °C while it persisted at 5 °C. The effect of dispersant and oil type on microbial community structure was also analyzed using PCR analysis. Results indicated that the abundance of *Thalassospira* correlated well with hydrocarbon degradation trends. The results from this study significantly expands on our understanding of biodegradation of DOSS, dispersed, and non-dispersed oil and also provides information regarding bacterial community composition.

Keywords: biodegradation, oil spills, dispersant, crude oil, RNA

INTRODUCTION

First generation chemical dispersants (industrial detergents) were primarily used in marine oil spills after the first major tanker catastrophe, the *Torrey Canyon* oil spill, in which large amount of alkylphenol surfactants were delivered to the contaminated area (Clayton, 1993; Committee on Effectiveness of Oil Spill Dispersants, 1989). The addition of dispersant lowered the interfacial tension between spilled oil and water, accelerated the breakdown of oil slicks, and prevented the resurfacing of small droplets (European Maritime Safety Agency, 2010). Moreover, discussions regarding dispersant utilization in deep-sea condition has come to the forefront after the GOM oil spill in 2010.

Corexit 9500, a well-known formula capable of dispersing heavy and weathered oils, is listed on the U.S. EPA National Contingency Plan Product Schedule and stockpiled around the world (Lessard and Demarco, 2010). Finasol OSR 52, another product that is widely stockpiled in Europe and European Free Trade Association countries, has not been completely evaluated for its toxicity and biodegradability. However, the pressing demand for deep-sea drilling requires continuing assessment of biodegradability of dispersants and dispersed oil (Zhuang et al. 2016).

In the aquatic environment, biodegradation is one of the predominant oil removal mechanisms in which bacteria utilize the spilled oil as a carbon source and thus degrade the oil components. While chemical dispersants increase the bioavailability of the oil to the microbes, the degradation of the dispersants themselves can be a challenge for the microbial community. Several studies assessed the biodegradation of C9500, while only Bergueiro-Lopez et al. (1997) examined the metabolism of Finasol OSR 52 by employing a mixture of bacteria called BIOLEN

IG 30. To date, the biodegradability of various crude oils dispersed with C9500 have been assessed in laboratory experiments, such as Prude Bay crude oil (Venosa and Holder, 2007), Macondo crude oil (Wang et al., 2016), and South Louisiana crude oil (Campo et al., 2013). Results varied due to the differences in oil properties and microbial community structure. Only a limited number of studies have been conducted where the biodegradability of dispersed Endicott crude oil was evaluated, and with only one publication evaluating the biodegradation by monitoring total petroleum hydrocarbon concentration under anaerobic conditions (Personna et al., 2014).

In order to characterize the biodegradation of DOSS and hydrocarbons, experiments were set up to study the degradation of two crude oils (ANS and Endicott), two dispersants (C9500 and Finasol) and three dispersed oils (ANS dispersed by C9500, ANS dispersed by Finasol and Endicott dispersed by C9500) under two temperature conditions which represented the surface (25 °C) and deep water (5 °C) environments, respectively.

METHODS

Cultures and Medium

Two mixed cultures of oil degrading bacteria were provided by EPA's Gulf Ecology Division at Gulf Breeze, FL. The mixed cultures were collected at a depth of 1240 m (cryo) and 5 m (meso) near the Macondo well at the GOM, enriched using crude oil and preserved in 10% glycerol until use. Sterilized GP2 artificial seawater was used as the media in this experiment and was prepared by dissolving several mineral salts in deionized water (Bidwell and Spotte, 1985).

Treatments

Dispersed oil treatment: The dispersed oil treatment was prepared in a 2 L baffled flask by adding the crude oil and the dispersant to 1.5 L of GP2 at a volumetric dispersant-to-oil ratio of 1:24 (10 μL dispersant: 240 μL oil). The baffled flask was shaken at 200rpm for 10-minutes, followed by a 10-minute settling period to allow the undispersed oil to rise to the top. After settling, 1 L of the dispersion was drained without disturbing the undispersed oil slick on the water surface. This procedure was repeated two more times which yielded 3 L of total dispersed oil and it was diluted into 12 L of GP2 (Panels A, B and C of Figure). Subsequently, a series of 250 mL silanized shaker flasks were filled with 100 mL aliquots of the dispersed oil.

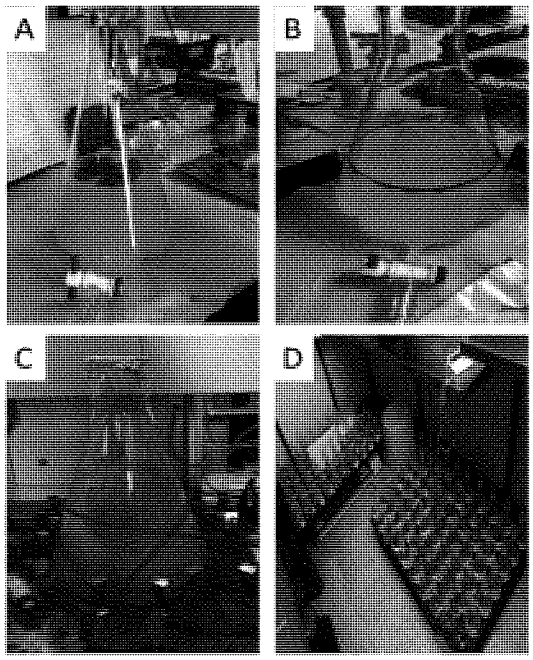

Figure Dispersed Oil Preparation (A, B and C) and Experiment Unit loading (D)

Non-dispersed oil treatment: To evaluate the biodegradation of crude oil alone,

approximately 4 μL crude oil was directly pipetted into each shake flask containing 100 mL sterile GP2. The final concentration of oil in the samples was approximately 28 μg/L, which was almost the same as the dispersed oil treatment.

Dispersant alone treatment: The dispersant alone treatments were prepared by spiking 20 μL of dispersant into 14 L of GP2 under continuous mixing, to yield a concentration similar to the dispersed oil treatment. After 30 minutes of continuously mixing, 100 mL of the solution was added into 250 mL silanized shaker flasks.

The dispersed oil, non-dispersed oil and dispersant alone treatments were then spiked with 0.5 mL of inoculum per flask with the cryo and meso cultures for the 5 and 25 °C experiments, respectively. After preparation, all the shaker flasks were placed on the orbital shakers in corresponding constant temperature rooms (5 or 25 °C) for the duration of the experiment (Panel D of Figure).

Oil component and DOSS analysis

DOSS and oil samples were prepared as described in Campo (2013). According to the ASTM D7730 Standard Method (ASTM D7730, 2011), DOSS was measured by using a 1200 series liquid chromatograph coupled with a 6410 tandem mass spectrometer (LC-MS/MS) from Agilent (Palo Alto, CA). Analysis of oil components was performed on an Agilent (Palo Alto, CA) 7890A GC coupled with an Agilent 7000 mass selective detector triple quadrupole and an Agilent 7693 series auto sampler. It was equipped with a DB-5 capillary column by J&W Scientific (30 m X 0.25 mm, and 0.25 μm film thickness) to achieved chromatographic separation of the alkanes and aromatics. A modified method based on EPA Method 8270D

(2007) was followed.

RESULTS AND DISCUSSION

Biodegradation of DOSS

Table 1 summarizes the initial concentration, biodegradation rates and removal extents of DOSS, the active anionic surfactant in C9500 and Finasol, with and without crude oils at 25 °C. Although the initial concentration of primary surfactant (DOSS) in Finasol was around 20% higher than in C9500, over 95% of the anionic surfactant fraction was metabolized for both types of dispersant products by the end of the experiment at 25 °C while it persisted at 5 °C. Thus, the low temperature condition greatly inhibited the microbial uptake of DOSS.

At 25 °C, biodegradation was fast in the replicates with or without ANS. 96% and 98% of DOSS were degraded for dispersant alone and dispersed oil treatment for two dispersants by the end of experiment, respectively. The presence of ANS remarkably favored the biodegradation first order rate of C9500 by approximately 2.4-fold, but no such effect was observed for the experiment with Finasol and ANS. Besides, DOSS uptake occurred after an acclimation period of 2 days, and removal extents surpassed 98% by day 48 in the presence of Endicott.

Table 1 Summary of Biodegradability of Two Dispersants at 25 °C

Treatments	Initial DOSS Concentration (μg/L)	Degradation rate (d^{-1})	Removal extent (%)
C9500 alone	203.97 ± 6.98	- 0.07 ± 0.009	96
C9500 + ANS	228.16 ± 11.94	- 0.16 ± 0.015	98
Finasol Alone	280.87 ± 21.19	- 0.060 ± 0.008	96
Finasol + ANS	234.11 ± 5.38	- 0.068 ± 0.006	98
C9500 + Endicott	206.96 ± 4.28	- 0.077 ± 0.007	98

Biodegradation of total alkanes

Table 2 presents the hopane-normalized concentration of total alkanes in dispersed oils. All the targets compounds were normalized by hopane concentration since it was unchanged through the whole experiments in all the treatments. The initial hopane-normalized concentration for 5 °C was almost twice as that of 25 °C because of the oil present in the enrichments. This was confirmed by analyzing the cryo and meso biomass alone, without the addition of any oil. The biodegradation of total alkanes occurred without any lag phase at 25 °C, regardless of the type of dispersed oil, while a 4-day acclimation period was observed at 5 °C. Over 90% of the total alkanes was metabolized by the meso culture by the end of experiment in all the cases.

Table 2 Biodegradability of Hopane-Normalized Total Alkanes in Dispersed Oils at 5 and 25 °C

Temperature	Treatments	Initial Concentration (mg total Alkanes / mg Hopane)	Lag Phase Period (d)	Removal extent (%)
25 °C	ANS + C9500	106.61 ± 3.64	0	92
	ANS + Finasol	113.17 ± 3.69	0	90
	Endicott + C9500	142.91 ± 3.33	0	94
5 °C	ANS + C9500	209.79 ± 7.72	4	85
	ANS + Finasol	220.56 ± 4.30	4	93
	Endicott + C9500	178.42 ± 1.77	4	94

At 5 °C, the presence of Finasol considerably favored the removal of alkanes than C9500 (93% vs. 85%) with ANS. Although, ANS and Endicott crude oil are both medium oil (Table 3), the percentage of total alkanes in Endicott is much higher than ANS crude oil, especially for light alkanes. The remove extent of dispersed Endicott is higher than that of dispersed ANS due to the easier metabolism of short chain alkanes.

Table 3 Physical Properties of ANS and Endicott *

Property	ANS	Endicott
Density, ρ (g/mL)	0.8733	0.8838
Dynamic Viscosity, μ (cP, at 15 °C)	35	120
Kinematic Viscosity, ν (cSt, at 15 °C)	40	134
API gravity	28.24	23.00
Total Alkanes Concentration (mg total Alkanes / mg Crude Oil)	35.52	110.38
of Total PAHs Concentration (mg total PAHs / mg Crude Oil)	20.63	37.46

* General crude oil categories: Heavy (API < 22.3°), Medium (22.3° ≤ API < 31.1°), and Light (API ≥ 31.1°).
* Source: SL Ross Environmental Research, 2010.

Biodegradation of total PAHs

Table 4 presents total PAH degradation for all the dispersed oil treatments at two temperatures. Similar to alkanes, the hopane-normalized total PAH concentration at 5 °C was higher than at 25 °C because of the higher hopane content from the meso cultures. At 25 °C, a notable decline in total PAHs was observed after an acclimation period of 2 days, and, subsequently degraded up to 82% by day 48 in ANS + C9500 treatment. For the other two dispersed oils, PAHs persisted until the end of experiment. Such contrary and unexpected findings is explained in more detail under the microbial community structure section.

At 5 °C, a 12-day lag phase occurred before observable degradation ensued in dispersed ANS treatments, while the cryo culture began degrading PAHs after 32 days for dispersed Endicott. Similar to the alkanes, higher temperature considerably favored the biodegradation of ANS dispersed by C9500 by shortening the lag phase period. At the last sampling event, 21%,

28% and 15% of the initial loaded concentration persisted for ANS + C9500, ANS + Finasol and Endicott + C9500 treatment, respectively. Although Endicott contains more PAHs than ANS (as shown in Table 3), dispersed Endicott was easier to remove owing to the higher percentage of 2-ring compounds which biodegraded faster than 3- and 4- ring PAHs.

Table 4 Biodegradability of Hopane-Normalized Total PAHs in Dispersed Oils at 5 and 25 °C

Temperature	Treatments	Initial Concentration (mg total PAHs / mg Hopane)	Lag Phase Period (d)	Removal extent (%)
25 °C	ANS + C9500	44.38 ± 1.54	2	82
	ANS + Finasol	61.08 ± 2.33	48	3
	Endicott + C9500	53.81 ± 0.14	48	19
5 °C	ANS + C9500	51.17 ± 0	12	79
	ANS + Finasol	63.57 ± 2.25	12	71
	Endicott + C9500	58.55 ± 0.38	32	85

Microbial community structure

As mentioned previously, meso cultures showed significant differences in PAHs uptake between ANS + C9500 and ANS + Finasol experiments which were performed under the same conditions, except for the dispersant product. PCR analysis of these bacterial consortia provided a clearer understanding of the microbial makeup and an in-depth explanation for the inconsistent result.

Table 5 displays the significant species in the active community including *Alcanivorax, Pseudoidiomarina* and *Thallassospira* which were abundant in the C9500 experiment but not in the Finasol experiment. In the active community, *Alcanivorax,* one of the predominant

hydrocarbon-degrading bacteria in the contaminated seawater, (Cappello et al, 2007; Harayama et al, 2004; Wang et al, 2014) increased from 0.74% to a maximum of 69.3% of total abundance in the C9500 experiment. *Alcanivorax* is a ubiquitous bacteria that was found in the GOM during the DWH oil spill (Kostka et al., 2016). However, the same species in the Finasol experiment was consistently lower at around 20%. Moreover, a similar trend was observed by comparing *Pseudoidiomarina* and *Thallassospira* (Moghadam et al., 2014). Hence, it is reasonable to infer this loss of active community could contribute to the unusual persistence of aromatics at 25 °C.

Table 5 Significant active genes of meso cultures in ANS alone treatment of ANS + C9500 (A) and ANS + Finasol (B) experiments

Species	Experiment	Initial Percentage (%)	Maximum Percentage (%)
Alcanivorax	A	33.13 ± 15.19	69.34 ± 2.10
	B	10.74 ± 3.39	20.58 ± 6.51
Pseudoidiomarina	A	0.15 ± 0.15	21.88 ± 3.88
	B	12.75 ± 1.49	14.93 ± 1.22
Thallassospira	A	0.02 ± 0.03	26.28 ± 2.99
	B	3.92 ± 0.83	0.82 ± 0.69

CONCLUSION

The goal of this work was to evaluate the effect of temperature on the biodegradability of dispersants and dispersed oils by using two oils (ANS crude oil and Endicott) and two dispersants (C9500 and Finasol OSR 52). This research not only evaluated the effect of dispersant type (Finasol and C9500) on ANS biodegradation, but also analyzed the biodegradation potential of two types of crude oil (ANS and Endicott) when dispersed with C9500.

DOSS disappeared promptly at 25 °C, while it persisted throughout the experiments at 5 °C. Additionally, the length of the acclimation period and removal extent were highly impacted by the addition of the dispersant. Similar to DOSS degradation, temperature affected the biodegradation of total alkanes significantly in both acclimation period and removal extent. Around 80% of the PAHs degraded at 5 °C whereas most PAHs persisted at 25 °C in ANS+Finasol and Endicott+C9500 treatment, which possibly resulted from the loss of several oil degrading microbial species such as *Alcanivorax, Pseudoidiomarina* and *Thallassospira.* Although the composition of Endicott considerably differs from ANS, especially the short chain paraffin and 2-ring PAHs, the degradation trends were similar to dispersed ANS, which indicated that the effect of C9500 on the two oils were similar. Since the PAHs persisted at 25 °C, and low activity of critical degrading species in meso cultures was observed, it is recommended that different cultures should be evaluated under the same test conditions in future experiments.

ACKNOWLEDGEMENTS

We acknowledge Jan Kurtz and Diane Yates from EPA's Gulf Ecology Division (GED) at Gulf Breeze, FL, who collected the water samples in the GOM and performed the enrichments and provided them for the experiments. The research was a product of the U.S. Environmental Protection Agency's National Risk Management Research Laboratory (NRMRL) and was partially funded by EPA, NRMRL, Cincinnati, OH, under Pegasus Technical Services, Inc. Contract EP-C-11-006.

REFERENCES

1. ASTM D7731-11e1, 2011. Standard test method for determination of

dipropyleneglycol monobutyl ether and ethylene glycol monobutyl ether in sea water by liquid chromatography/tandem mass spectrometry (LC/MS/MS). *ASTM International*, West Conshohocken, PA. *www.astm.org*

2. Bergueiro-Lopez J.R., Moreno-Garcia-Luengo S., Serra-Socias F., Fuertes- Perez A., Perez-Navarro-Gomez A., Morales-Correas N., Domingez-Laseca, F., 1997. FINASOL OSR 52 Active Components Biodegradation by Using the Biological Activator BIOLEN IG 30. *Spill Science & Technology Bulletin* 3(4), 269-272. doi: 10.1016/S1353-2561(97)00026-1
3. Bidwell J.P., and Spotte S., 1985. Artificial Seawaters: Formulas and Methods. Jones and Bartlett Publishers, Inc., Boston, Ma.
4. Campo P., Venosa A.D., Suidan M.T., 2013. Biodegradability of Corexit 9500 and Dispersed South Louisiana Crude Oil at 5 and 25 °C. *Environmental Science & Technolology* 47(4), 1960-1967. doi: 10.1021/es303881h
5. Cappello S., Denaro R, Genovese M., Giuliano P., Yakimov M.M., 2007. Predominant growth of Alcanivorax during experiments on "oil spill bioremediation" in mesocosms. *Microbiological Research* 162(2), 185-190. doi: http://dx.doi.org/10.1016/j.micres.2006.05.010
6. Clayton, John R., 1992. Oil Spill Dispersants: Mechanisms of Action and Laboratory Tests. 9-23.
7. Committee on Effectiveness of Oil Spill Dispersants, 1989. Using Oil Spill Dispersants on the Sea. 6-7.
8. European Maritime Safety Agency, 2010. Manual on the Applicability of Oil Spill Dispersants - Version 2. *www.emsa.europa.eu*
9. HarayamA S., Kasai Y., Hara A., 2004. Microbial communities in oil-contaminated seawater. *Current Opinion in Biotechnology* 15(3), 205-214. doi: http://dx.doi.org/10.1016/j.copbio.2004.04.002
10. Kostka, J. E., Prakash, O., et al., 2011. Hydrocarbon-degrading bacteria and the bacterial community response in Gulf of Mexico beach sands impacted by the Deepwater Horizon oil spill. *Applied and Environmental Microbiology* 77(22), 7962-7974.

doi: 10.1128/AEM.05402-11

11. Lessard P.R., Demarco G., 2000. The Significance of Oil Spill Dispersants. *Spill Science & Technolology Bulletin* 6(1), 59-68.
doi: http://dx.doi.org/10.1016/S1353-2561(99)00061-4

12. Moghadam M.S., Ebrahimipour G., Abtahi B., Ghassempour A., Hashtroudi M.S., 2014. Biodegradation of polycyclic aromatic hydrocarbons by a bacterial consortium enriched from mangrove sediments. *Journal of Environmental Health Science and Engineering* 12(1).
doi: 10.1186/s40201-014-0114-6

13. Personna Y.R., Boufadel M.C., Zhang S., 2014. Assessing weathered Endicott oil biodegradation in brackish water. *Marine Pollution Bulletin* 86, 102-110.
doi: http://dx.doi.org/10.1016/j.marpolbul.2014.07.037

14. SL Ross Environmental Research, 2010. Comparison of large scale (Ohmsett) and small scale dispersant effectiveness test results. *Report for U.S. Department of the Interior*, Minerals Management Service, Herndon, Va.

15. United State Environmental Protect Agency, 2007. Method 8270D Semivolatile Organic Compounds by Gas Chromatography/Mass Spectrometry (GC-MS). *https://www3.epa.gov/*

16. Venosa, A.D., Holder, E.L., 2007. Biodegradability of dispersed crude oil at two different temperatures. *Marine Pollution Bulletin* 54, 545-553.
doi: http://dx.doi.org/10.1016/j.marpolbul.2006.12.013

17. Wang J., Sandoval K., Ding Y., Stoeckel D.,1, Minard-Smithc A., Andersen G., Dubinsky E., Atlas R., Gardinali P., 2016. Biodegradation of dispersed Macondo crude oil by indigenous Gulf of Mexico microbial communities. *Science of the Total Environment* 557-558, 453-468.
doi: http://dx.doi.org/10.1016/j.scitotenv.2016.03.015

18. Wang W., Zhong R., Shan D., Shao Z., 2014. Indigenous oil-degrading bacteria in crude oil-contaminated seawater of the Yellow Sea, China. *Applied Microbiology and Biotechnology* 98(16), 7253-7269.
doi: 10.1007/s00253-014-5817-1

19. Zhuang M., Abulikemub G., Campo P., Platten W.E., Suidan M.T., Venosa A.D.,

Conmy R.N., 2016. Effect of dispersants on the biodegradation of South Louisiana crude oil at 5 and 25 °C. *Chemosphere* 144, 767-774.
doi: http://dx.doi.org/10.1016/j.chemosphere.2015.08.040

To: Conmy, Robyn[Conmy.Robyn@epa.gov]
From: Mike Fulton - NOAA Federal
Sent: Fri 7/10/2015 1:17:01 PM
Subject: Re: dispersant

Hi Robin,
We do have both. I suspect we have enough to share. I'll check and let you know early next week. One caveat...we'd have to the pull the material for you from a larger container. We didn't receive separate aliquots. Can that work?
Mike

On Fri, Jul 10, 2015 at 9:00 AM, Conmy, Robyn <Conmy.Robyn@epa.gov> wrote:

Hi Mike,

I couldn't recall if you said your lab has finasol and corexit in stock for testing? If so, would you have any to share with us? We are running low and trying secure a liter or 2 of each.

Thanks,

Robyn

<>/<>/<>/<>/<>/<>/<>/<>/<>/<>/<>/<>/<>/<>/<>/<>/<>/<>/<>

Robyn N. Conmy, Ph.D.

Research Ecologist

USEPA/NRMRL/LRPCD

26 West MLK Drive

Cincinnati, Ohio 45268

513-569-7090 (office)

513-431-1970 (EPA mobile)

727-692-5333 (Personal mobile)

conmy.robyn@epa.gov

--
Dr. Michael H. Fulton-Estuaries and Land Use Branch Chief
Center for Coastal Environmental Health and
Biomolecular Research (CCEHBR)
USDOC/NOAA/NOS/NCCOS
219 Fort Johnson Road
Charleston, SC 29412-9110
voice: (843) 762-8576 fax: (843) 762-8700
e-mail: mike.fulton@noaa.gov http://www.chbr.noaa.gov

Land Remediation and Pollution Control Division

Quality Assurance Activity Review

QA Activity Project:	Biodegradability of Dispersants and Dispersed Oil at Two Temperatures		
QA Activity Number:	G-LRPCD-0015045-SP-1-0		
QA Activity:	Symposium/Conference Paper	Date Received:	2017-01-12
Project Lead:	Conmy, Robyn	Project Branch:	ESMB
QA Activity POC:	Conmy, Robyn	POC Branch:	ESMB
Reviewer:	Voit, Jim	LCO Tracking No.:	
Date Reviewed:	2017-02-08	Date Approved:	2017-02-08
QA Activity Title:	Comparative Study to Determine the Biodegradability of Dispersants at Environmentally Relevant Concentration		

QUALITY ASSURANCE MANAGER RECOMMENDATION

Approved - All aspects reviewed are acceptable.

X Approved with minor revisions -
This work needs minor corrections, but does not require additional QA review. The PI/PO should respond to each QA review comment and return the response write-up or a corrected version of text to the QA office.

Not Approved revisions required -
This work contains major errors or there are QA findings that require major re-writes. An additional QA review of the corrected text is required, along with the PI/PO's written response to each QA comment.

QA requirements are not applicable

Comments

please see the attached review

Voit, Jim

Quality Assurance Manager

***Supporting Information**

Biodegradability of Different Initial Concentrations of Alaska North Slope Crude Oil Dispersed with Corexit C9500

Mobing Zhuang[1], Gulizhaer Abulikemu[2], Pablo Campo[3]*, William Platten III[4], Makram T. Suidan[5], Albert D. Venosa (retired)[4]and Robyn N. Conmy[4]

1 Department of Biomedical, Chemical and Environmental Engineering, University of Cincinnati, 2901 Woodside Drive, Cincinnati, OH 45221, USA

2 Pegasus Technical Services Inc., 46 E Hollister St, Cincinnati, OH 45219 USA

3 Cranfield Water Science Institute, Cranfield University, Cranfield, Beds, MK43 0AL, UK

4 U.S. Environmental Protection Agency, NRMRL, 26 W. MLK Drive Cincinnati, OH, 45268, USA

5 Faculty of Engineering and Architecture, American University of Beirut, Bechtel Engineering Bldg. - 3rd flr. - Room 308 P.O. Box: 11-0236 Riad El Solh 1107 2020, Beirut, Lebanon

*Corresponding author: Pablo Campo
Tel: +44 (0)1234 754332
E-mail address: p.campo-moreno@cranfield.ac.uk

ED_001324_00000728-00001

Table S1. Summary of Experimental Layout for High Concentration Experiment.

Test	Temperature	Treatment	Sampling Events	Sample Replicates	Total Experimental Units (EU)
1	5 °C	C9500 alone	11	3	33
2	5 °C	ANS dispersed by C9500	11	3	33
3	5 °C	alone	11	3	33
4	5 °C	Killed ANS control	1	3	3
5	5 °C	Killed C9500 control	11	3	33
6	5 °C	Killed ANS+C9500 control	11	3	33
				Subtotal EU's	**168**
7	25 °C	C9500 alone	9	3	27
8	25 °C	ANS dispersed by C9500	9	3	27
9	25 °C	ANS alone	9	3	27
10	25 °C	Killed ANS control	1	3	3
11	25 °C	Killed C9500 control	9	3	27
12	25 °C	Killed ANS+ C9500 control	9	3	27
				Subtotal EU's	**138**
			Total EU's for High Concentration Experiment		**306**

ED_001324_00000728-00002

Table S2. Summary of Experimental Layout for Low Concentration Experiment.

Test	Temperature	Treatment	Sampling Events	Sample Replicates	Total Experimental Units (EU)
13	5 °C	C9500 alone	11	3	33
14	5 °C	ANS+C9500	11	3	33
15	5 °C	ANS alone	11	3	33
16	5 °C	Killed ANS control	1	3	3
17	5 °C	Killed C9500 control	11	3	33
18	5 °C	Killed (ANS+C9500) control	11	3	33
19	5 °C	Killed (ANS+C9500) +Protease	6	3	18
				Subtotal EU's	**186**
20	25 °C	C9500 alone	10	3	30
21	25 °C	ANS+C9500	10	3	30
22	25 °C	ANS alone	10	3	30
23	25 °C	Killed ANS control	1	3	3
24	25 °C	Killed C9500 control	10	3	30
25	25 °C	Killed (ANS+C9500) control	10	3	30
26	25 °C	Killed (ANS+C9500) +Protease	6	3	18
				Subtotal EU's	**181**
		Total EU's for Low Concentration Experiment			**357**

ED_001324_00000728-00003

Table S3. First-order biodegradation rate coefficients and standard deviations (sd) of individual alkanes in the high concentration experiment.

Compound	5 °C ANS alone		25 °C ANS alone		5 °C ANS+C9500		25 °C ANS+C9500	
	rate (d^{-1})	sd (d^{-1})	rate (d^{-1})	sd (d^{-1})	rate (d^{-1})	sd (d^{-1})	rate (d^{-1})	sd (d^{-1})
C10	0.19	0.02	1.34	0.18	0.63	0.03	2.00	0.34
C11	0.15	0.01	1.16	0.15	0.40	0.02	1.30	0.09
C12	0.12	0.01	1.02	0.14	0.29	0.03	0.96	0.06
C13	0.11	0.01	0.94	0.14	0.27	0.03	0.91	0.05
C14	0.11	0.01	0.92	0.14	0.25	0.03	0.82	0.04
C15	0.11	0.01	0.95	0.14	0.24	0.03	0.84	0.05
C16	0.11	0.01	1.01	0.15	0.24	0.03	0.92	0.05
C17	0.11	0.01	1.08	0.16	0.24	0.03	0.97	0.06
PR	0.15	0.03	0.45	0.11	0.07	0.01	0.39	0.04
C18	0.11	0.01	1.06	0.14	0.22	0.02	0.96	0.05
PH	0.15	0.03	0.46	0.12	0.08	0.01	0.43	0.04
C19	0.11	0.01	1.05	0.14	0.22	0.02	0.97	0.06
C20	0.11	0.01	0.99	0.14	0.21	0.02	0.93	0.05
C21	0.10	0.01	0.97	0.14	0.20	0.02	0.91	0.05
C22	0.10	0.01	0.88	0.13	0.19	0.02	0.84	0.04
C23	0.09	0.01	0.84	0.13	0.18	0.02	0.79	0.04
C24	0.09	0.01	0.84	0.14	0.17	0.02	0.79	0.04
C25	0.09	0.01	0.81	0.13	0.15	0.02	0.81	0.03
C26	0.08	0.01	0.81	0.14	0.12	0.02	0.78	0.04
C27	0.08	0.01	0.74	0.13	0.11	0.01	0.71	0.05
C28	0.12	0.02	0.75	0.12	0.12	0.02	0.60	0.09
C29	0.12	0.02	0.81	0.15	0.12	0.02	0.81	0.07
C30	0.10	0.01	0.83	0.14	0.12	0.02	0.74	0.04
C31	0.09	0.01	0.81	0.14	0.09	0.01	0.61	0.05
C32	0.10	0.01	0.81	0.14	0.09	0.01	0.60	0.06
C33	0.09	0.01	0.68	0.09	0.07	0.01	0.56	0.06
C34	0.08	0.01	0.60	0.09	0.05	0.01	0.54	0.05
C35	0.07	0.01	0.53	0.09	0.04	0.01	0.58	0.04

.

ED_001324_00000728-00004

Table S4. First-order biodegradation rate coefficients and standard deviations (sd) of individual alkanes in low concentration experiment.

Compound	5 °C ANS alone		25 °C ANS alone		5 °C ANS+C9500		25 °C ANS+C9500	
	rate (d^{-1})	sd (d^{-1})	rate (d^{-1})	sd (d^{-1})	rate (d^{-1})	sd (d^{-1})	rate (d^{-1})	sd (d^{-1})
C10	0.47	0.03	0.93	0.16	0.63	0.04	NA1	NA1
C11	0.25	0.02	0.57	0.07	0.25	0.03	0.47	0.02
C12	0.20	0.01	0.38	0.06	0.23	0.02	0.24	0.03
C13	0.18	0.01	0.42	0.06	0.21	0.02	NA2	NA2
C14	0.13	0.01	0.28	0.04	0.15	0.01	NA2	NA2
C15	0.14	0.01	0.35	0.04	0.15	0.01	NA2	NA2
C16	0.14	0.01	0.37	0.04	0.15	0.02	NA2	NA2
C17	0.13	0.01	0.36	0.04	NA2	NA2	NA2	NA2
PR	NA2	NA2	0.04	0.01	NA2	NA2	NA2	NA2
C18	NA2	NA2	0.35	0.04	NA2	NA2	NA2	NA2
PH	NA2	NA2	0.03	0.01	NA2	NA2	NA2	NA2
C19	NA2	NA2	0.32	0.04	NA2	NA2	NA2	NA2
C20	NA2	NA2	0.30	0.04	NA2	NA2	NA2	NA2
C21	NA2	NA2	0.29	0.04	NA2	NA2	NA2	NA2
C22	NA2	NA2	0.17	0.03	NA2	NA2	NA2	NA2
C23	NA2	NA2	NA2	NA2	NA2	NA2	NA2	NA2
C24	NA2	NA2	NA2	NA2	NA2	NA2	NA2	NA2
C25	NA2	NA2	NA2	NA2	NA2	NA2	NA2	NA2
C26	NA2	NA2	NA2	NA2	NA2	NA2	NA2	NA2
C27	NA2	NA2	NA2	NA2	NA2	NA2	NA2	NA2
C28	NA2	NA2	NA2	NA2	NA2	NA2	NA2	NA2
C29	NA2	NA2	NA2	NA2	NA2	NA2	NA2	NA2
C30	NA2	NA2	NA2	NA2	NA2	NA2	NA2	NA2
C31	NA2	NA2	NA2	NA2	NA2	NA2	NA2	NA2
C32	NA2	NA2	NA2	NA2	NA2	NA2	NA2	NA2
C33	NA2	NA2	NA2	NA2	NA2	NA2	NA2	NA2
C34	NA2	NA2	NA2	NA2	NA2	NA2	NA2	NA2
C35	NA2	NA2	NA2	NA2	NA2	NA2	NA2	NA2

NA1: Rate not calculated because of excessively rapid removal after acclimation.
NA2: Rate not calculated because noted compounds were persisted during the experiment.

ED_001324_00000728-00005

Table S5. First-order degradation rate coefficients and standard deviations (sd) of individual PAHs in high concentration experiment.

Compound	5 °C ANS alone		25 °C ANS alone		5 °C ANS+C9500		25 °C ANS+C9500	
	rate (d^{-1})	sd (d^{-1})	rate (d^{-1})	sd (d^{-1})	rate (d^{-1})	sd (d^{-1})	rate (d^{-1})	sd (d^{-1})
nap	0.44	0.04	0.68	0.05	0.71	0.02	1.94	0.02
C1-nap	0.23	0.02	0.60	0.04	0.41	0.03	1.84	0.04
C2-nap	0.17	0.02	0.38	0.07	0.26	0.02	0.61	0.03
C3-nap	0.27	0.02	0.35	0.10	0.20	0.02	0.40	0.05
C4-nap	0.13	0.02	0.29	0.10	0.16	0.02	0.35	0.05
phe	0.19	0.01	0.37	0.09	0.26	0.02	0.46	0.05
C1-phe	0.12	0.01	0.34	0.12	0.19	0.02	0.37	0.06
C2-phe	0.05	0.01	0.21	0.07	0.19	0.03	0.27	0.04
C3-phe	0.00	0.00	0.00	0.00	0.00	0.00	0.00	0.00
C4-phe	0.00	0.00	0.00	0.00	0.00	0.00	0.00	0.00
flu	0.19	0.02	0.37	0.10	0.26	0.02	0.44	0.05
C1-flu	0.15	0.02	0.35	0.11	0.21	0.02	0.39	0.06
C2-flu	0.05	0.01	0.20	0.07	0.11	0.01	0.27	0.04
C3-flu	0.00	0.00	0.00	0.00	0.00	0.00	0.00	0.00
dbt	0.25	0.01	0.43	0.08	0.44	0.02	0.77	0.03
C1-dbt	0.13	0.01	0.32	0.10	0.22	0.02	0.41	0.04
C2-dbt	0.04	0.01	0.17	0.06	0.11	0.01	0.26	0.04
C3-dbt	0.00	0.00	0.00	0.00	0.00	0.00	0.00	0.00
nbt	0.00	0.00	0.00	0.00	0.00	0.00	0.00	0.00
C1-nbt	0.00	0.00	0.00	0.00	0.00	0.00	0.00	0.00
C2-nbt	0.00	0.00	0.00	0.00	0.00	0.00	0.00	0.00
C3-nbt	0.00	0.00	0.00	0.00	0.00	0.00	0.00	0.00
pyr*	--	--	--	--	--	--	--	--
C1-pyr	0.00	0.00	0.00	NA	NA	0.00	NA	NA
C2-pyr	0.00	0.00	0.00	0.00	0.00	0.00	0.00	0.00
cry	0.00	0.00	0.00	0.00	0.00	0.00	0.00	0.00
C1-cry	0.00	0.00	0.00	0.00	0.00	0.00	0.00	0.00
C2-cry	0.00	0.00	0.00	0.00	0.00	0.00	0.00	0.00
C3-cry	0.00	0.00	0.00	0.00	0.00	0.00	0.00	0.00
C4-cry	0.00	0.00	0.00	0.00	0.00	0.00	0.00	0.00

NA: Rate not calculated because noted compounds were persisted during the experiment.
* Not detected in any samples.

ED_001324_00000728-00006

Table S6. First-order degradation rate coefficients and standard deviations (sd) of individual PAHs in low concentration experiment.

Compound	5 °C ANS alone		25 °C ANS alone		5 °C ANS+C9500		25 °C ANS+C9500	
	rate (d^{-1})	sd (d^{-1})	rate (d^{-1})	sd (d^{-1})	rate (d^{-1})	sd (d^{-1})	rate (d^{-1})	sd (d^{-1})
nap	NA	NA	0.29	0.05	0.43	0.09	0.36	0.03
C1-nap	NA	NA	0.24	0.03	0.44	0.09	0.28	0.03
C2-nap	NA	NA	0.17	0.04	0.40	0.09	0.21	0.04
C3-nap	NA	NA	0.18	0.04	0.31	0.06	0.20	0.04
C4-nap	NA	NA	0.13	0.03	0.15	0.02	0.14	0.02
phe	NA	NA	NA	NA	NA	NA	0.19	0.03
C1-phe	NA	NA	NA	NA	0.18	0.03	0.20	0.03
C2-phe	0.25	0.01	0.14	0.03	0.11	0.01	NA	NA
C3-phe	0.02	0.01	0.02	0.00	0.00	0.00	0.00	0.00
C4-phe	0.00	0.00	0.00	0.00	0.00	0.00	0.00	0.00
flu	NA	NA	NA	NA	0.29	0.06	NA	NA
C1-flu	NA	NA	NA	NA	0.15	0.02	0.00	0.00
C2-flu	0.29	0.03	0.14	0.03	0.21	0.01	0.00	0.00
C3-flu	0.02	0.00	0.03	0.00	0.00	0.00	0.02	0.00
dbt	NA	NA	0.00	0.00	0.31	0.11	0.00	0.00
C1-dbt	NA	NA	NA	NA	0.23	0.05	0.29	0.06
C2-dbt	0.00	0.00	0.00	0.00	0.00	0.00	0.00	0.00
C3-dbt	0.00	0.00	0.00	0.00	0.00	0.00	0.00	0.00
nbt	0.00	0.00	NA	NA	0.00	0.00	0.31	0.11
C1-nbt	0.00	0.00	0.00	0.00	0.00	0.00	0.00	0.00
C2-nbt	0.00	0.00	0.00	0.00	0.00	0.00	0.00	0.00
C3-nbt	0.00	0.00	0.00	0.00	0.00	0.00	0.00	0.00
pyr*	--	--	--	--	--	--	--	--
C1-pyr	0.00	0.00	0.00	0.00	0.00	0.00	0.27	0.07
C2-pyr	0.00	0.00	0.00	0.00	0.00	0.00	0.00	0.00
cry	0.00	0.00	0.00	0.00	0.00	0.00	0.00	0.00
C1-cry	0.00	0.00	0.00	0.00	0.00	0.00	0.00	0.00
C2-cry	0.00	0.00	0.00	0.00	0.00	0.00	0.00	0.00
C3-cry	0.00	0.00	0.00	0.00	0.00	0.00	0.00	0.00
C4-cry	0.00	0.00	0.00	0.00	0.00	0.00	0.00	0.00

NA: Rate not calculated because of excessively rapid removal after acclimation.
*Not detected in any samples.

ED_001324_00000728-00007

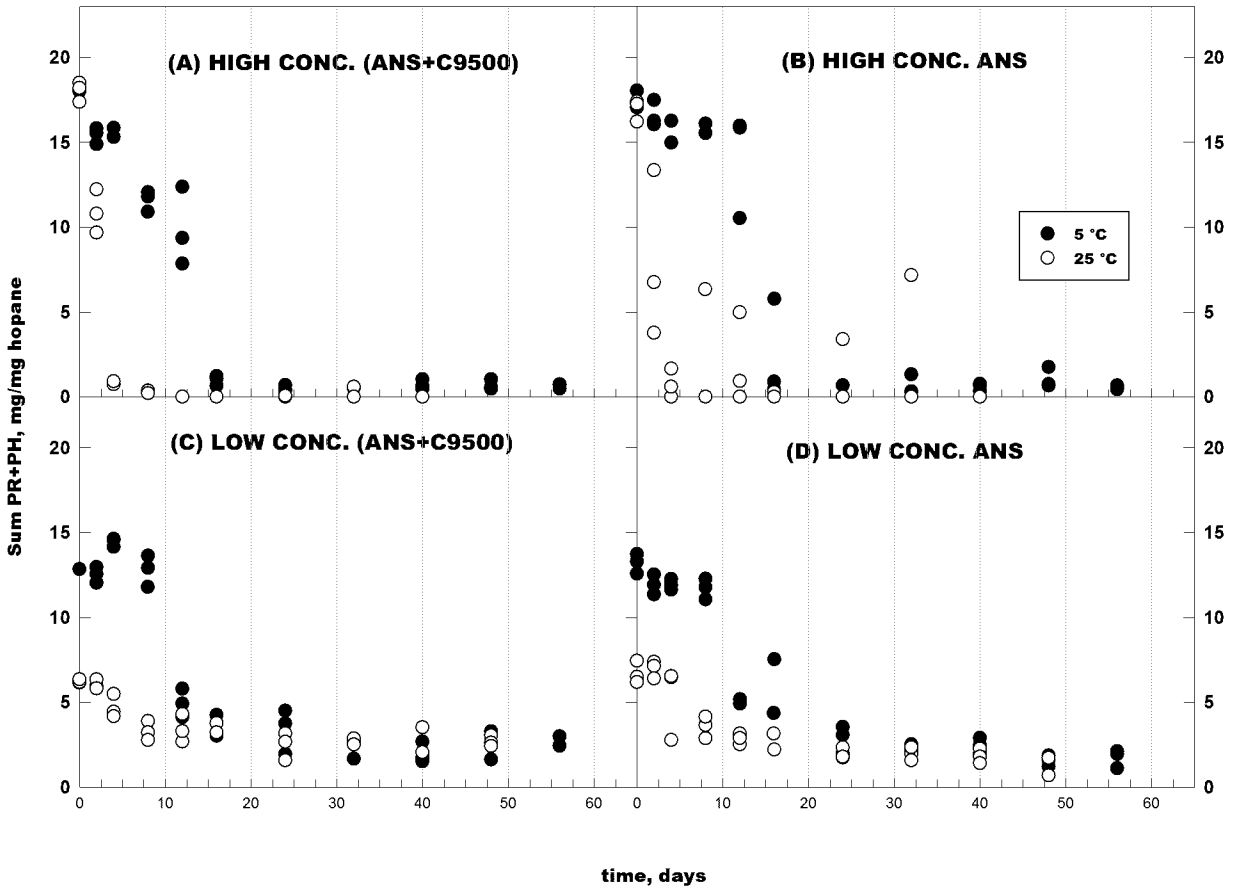

Figure S1. Biodegradation of branched alkanes in the presence (A, C) and absence (B, D) of C9500 at 5 °C and 25 °C. High concentration treatments are in panel A and B, whereas low concentration treatments are in panels C and D.

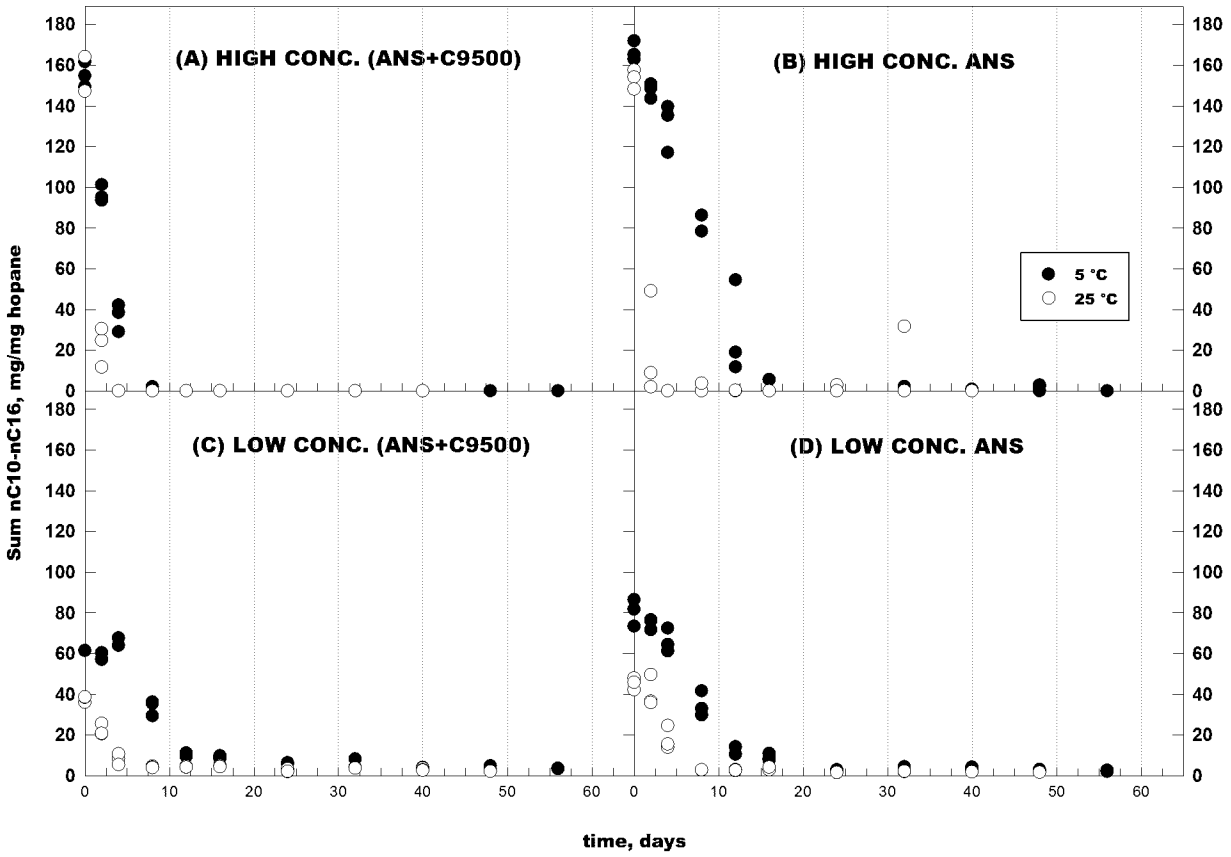

Figure S2. Biodegradation of n-alkanes (nC10-nC16) in the presence (A, C) and absence (B, D) of C9500 at 5 °C and 25 °C. High concentration treatments are in panel A and B, whereas low concentration treatments are in panels C and D.

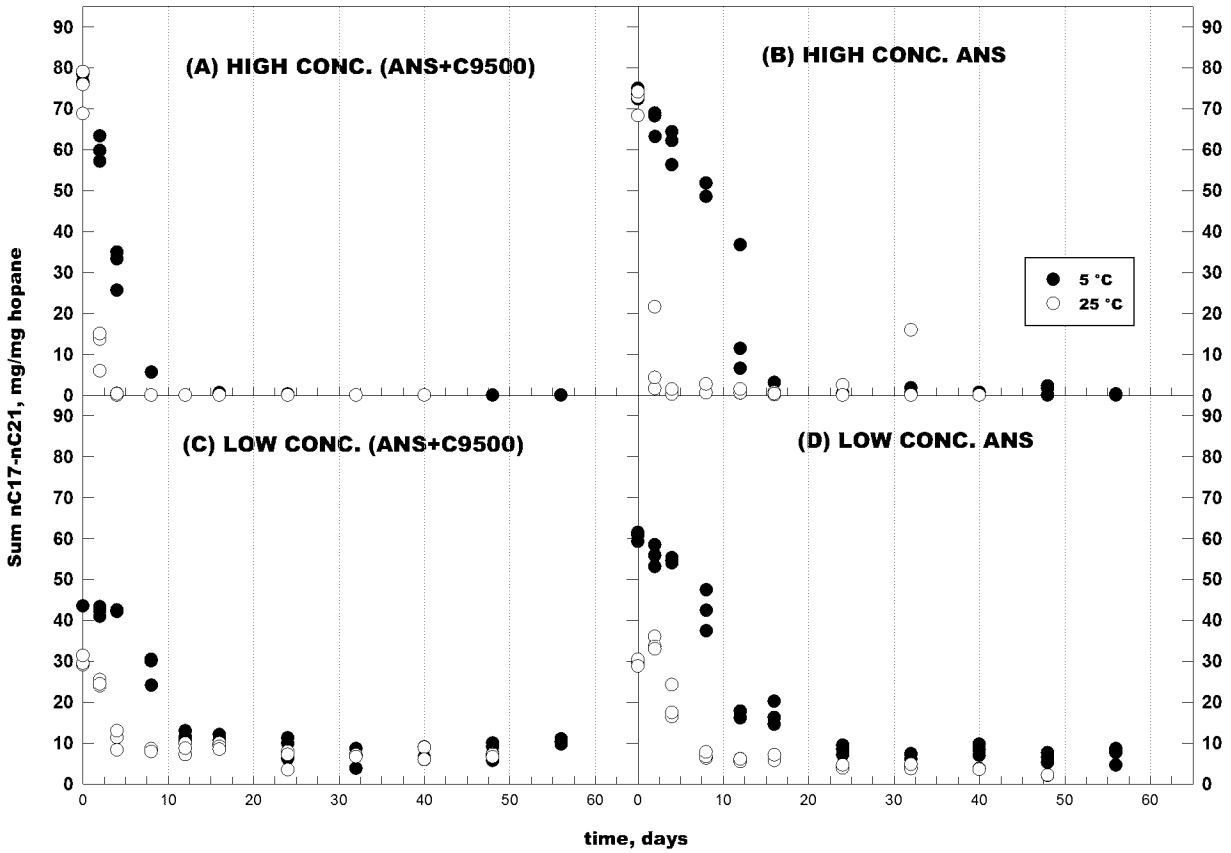

Figure S3. Biodegradation of n-alkanes (nC17-nC21) in the presence (A, C) and absence (B, D) of C9500 at 5 °C and 25 °C. High concentration treatments are in panel A and B, whereas low concentration treatments are in panels C and D.

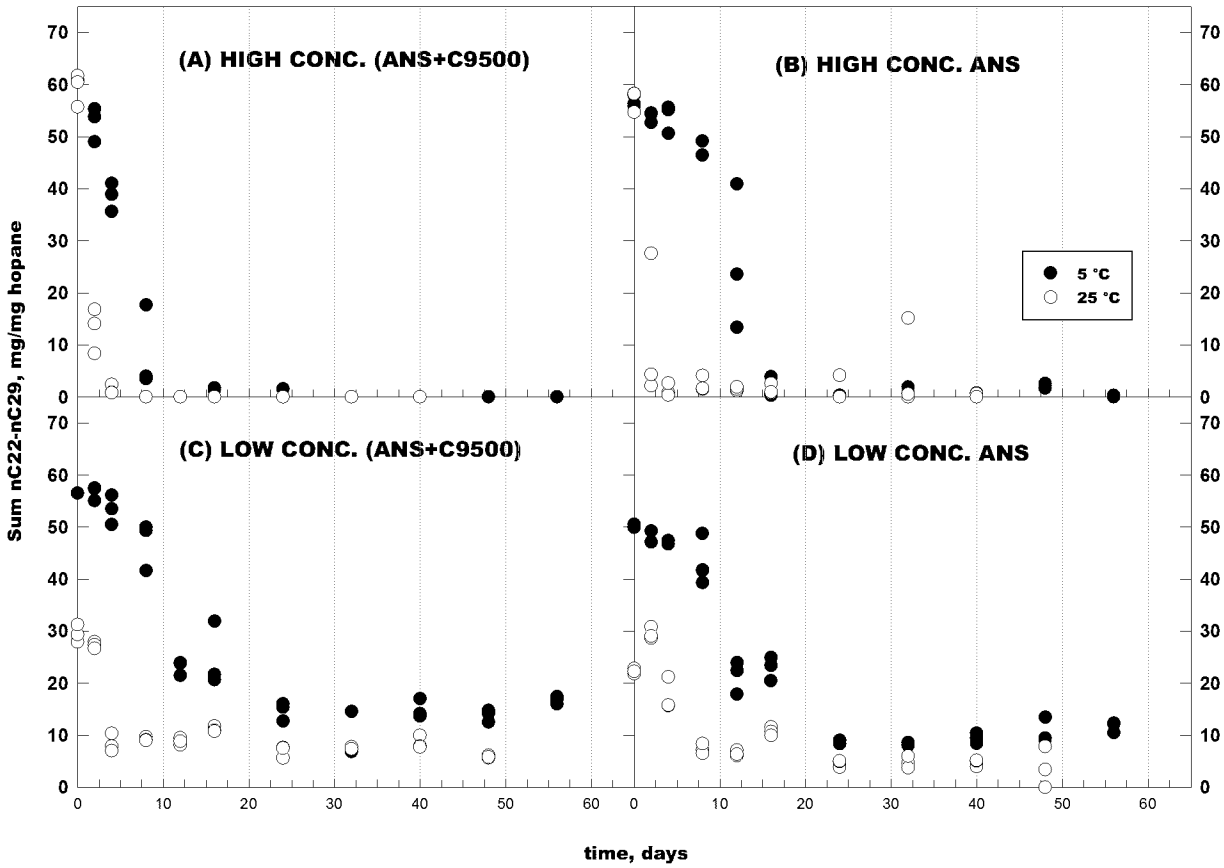

Figure S4. Biodegradation of n-alkanes (nC22-nC29) in the presence (A, C) and absence (B, D) of C9500 at 5 °C and 25 °C. High concentration treatments are in panel A and B, whereas low concentration treatments are in panels C and D.

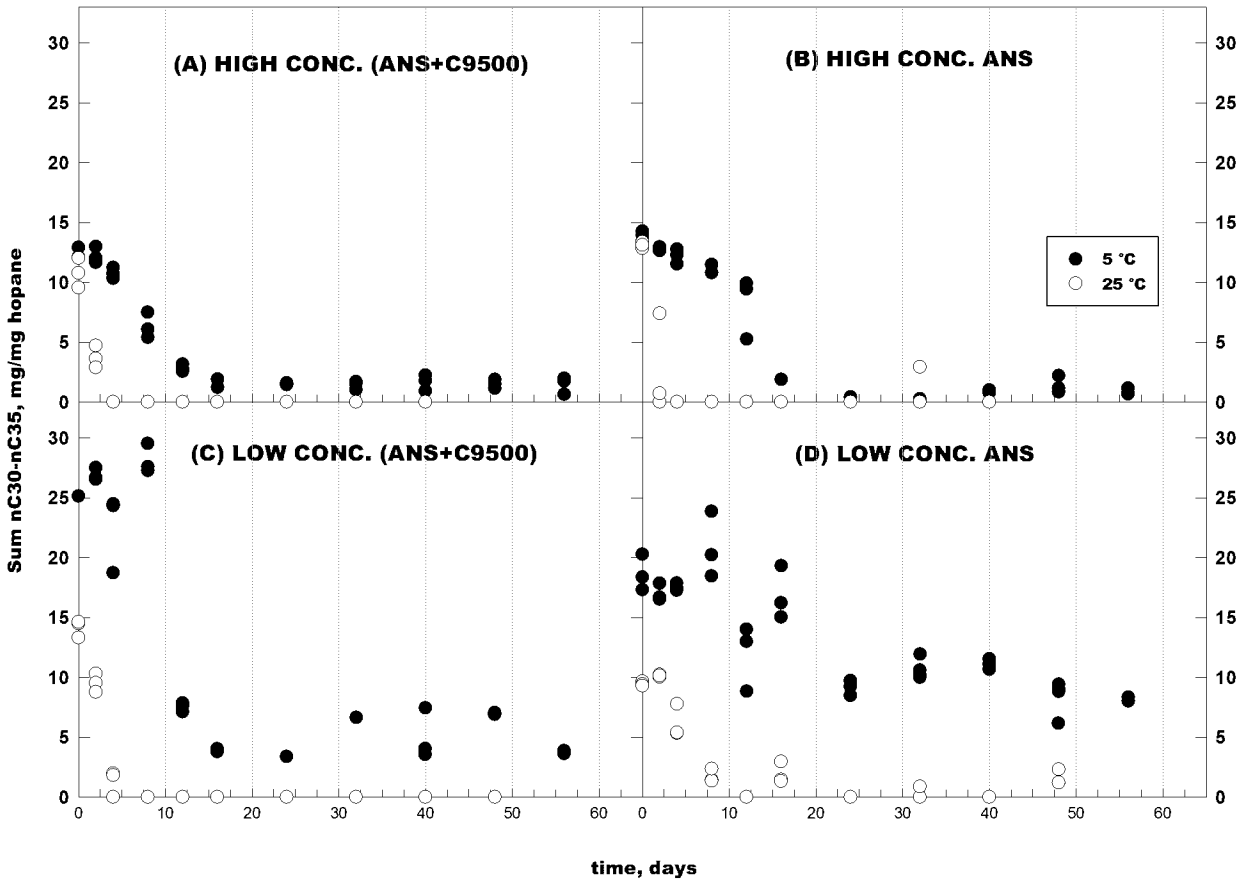

Figure S5. Biodegradation of n-alkanes (nC30-nC35) in the presence (A, C) and absence (B, D) of C9500 at 5 °C and 25 °C. High concentration treatments are in panel A and B, whereas low concentration treatments are in panels C and D.

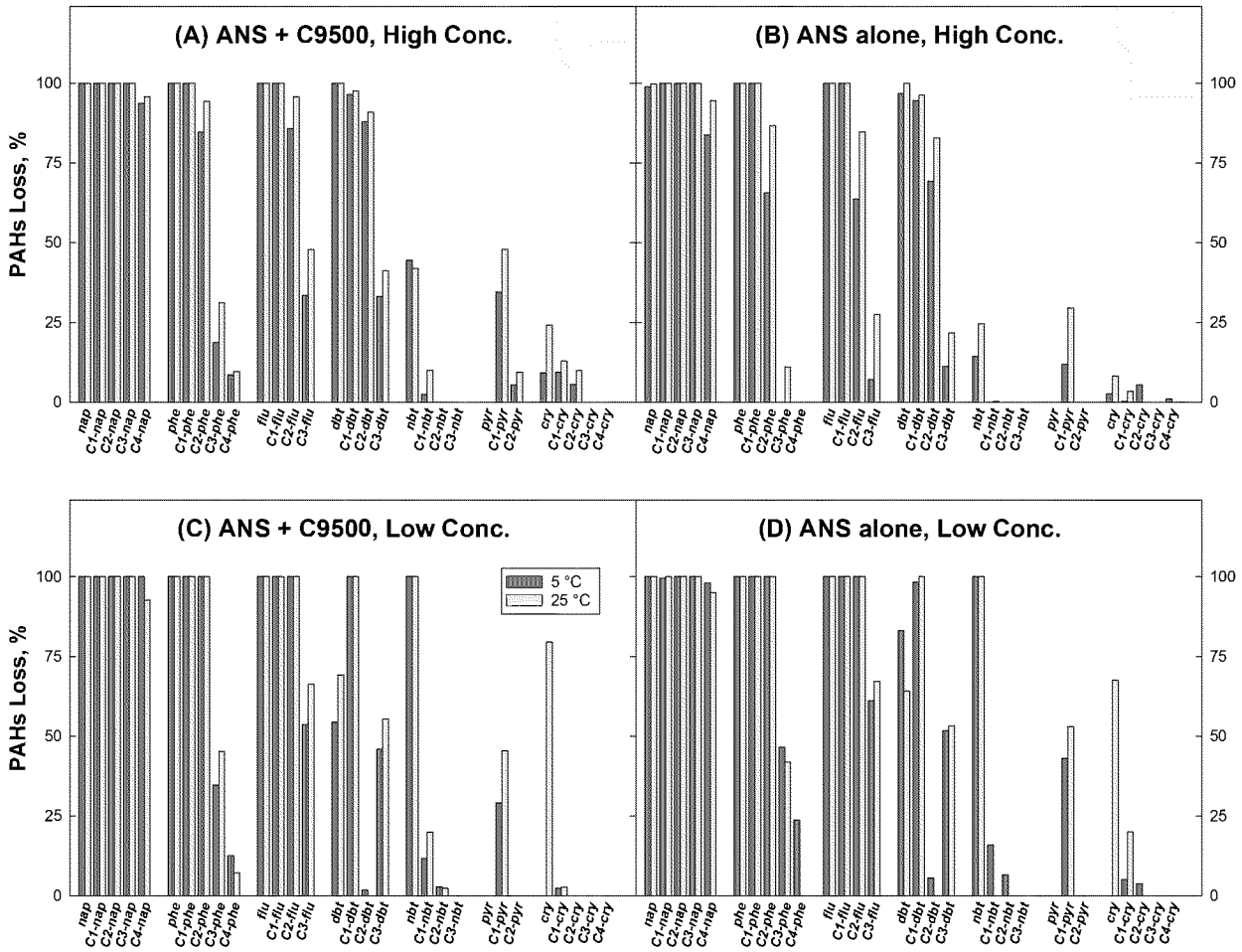

Figure S6. Average loss percentage of individual PAH in the presence (A, C) and absence (B, D) of C9500 at 5 °C and 25 °C in high concentration (A, B) and low concentration (C, D) experiment.

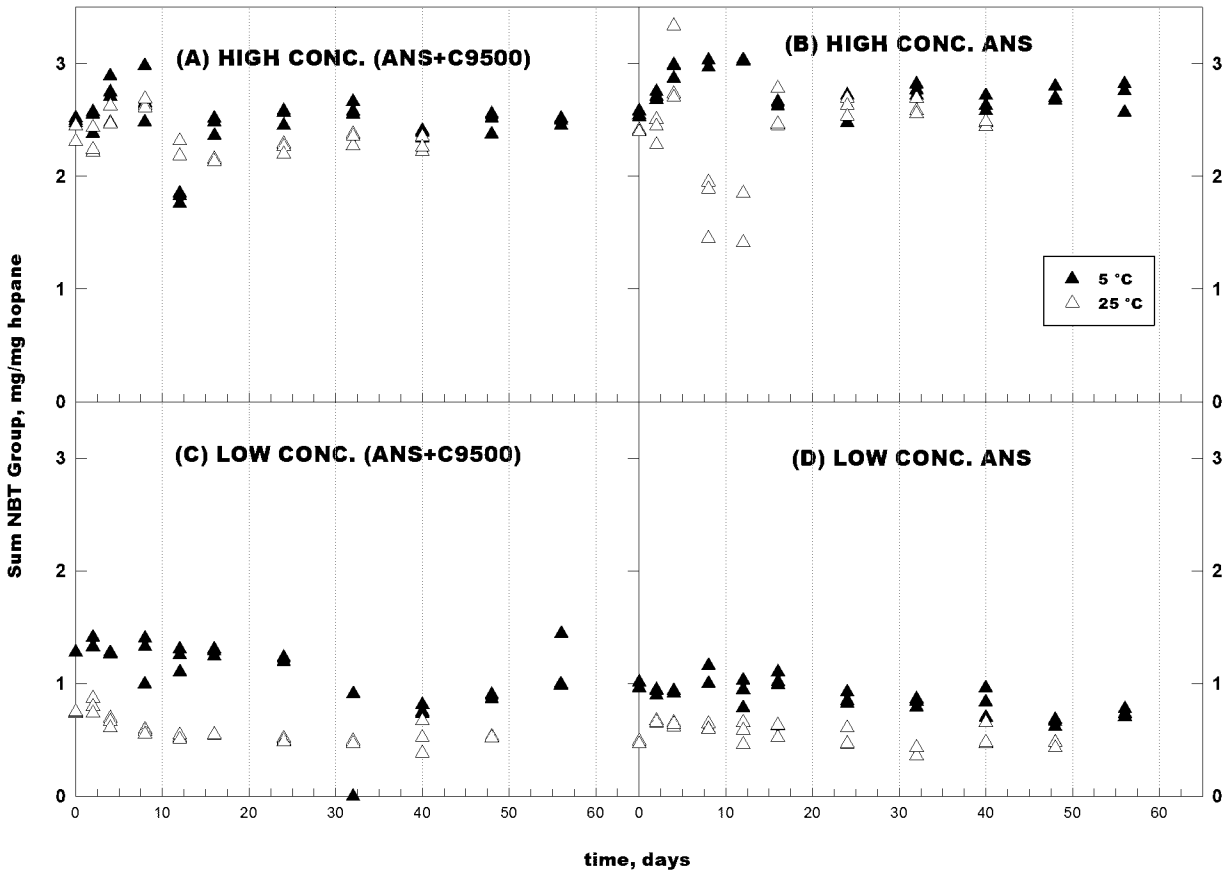

Figure S7. Biodegradation of naphthobenzothiophene homologues in the presence (A, C) and absence (B, D) of C9500 at 5 °C and 25 °C. High concentration treatments are in panel A and B, whereas low concentration treatments are in panels C and D.

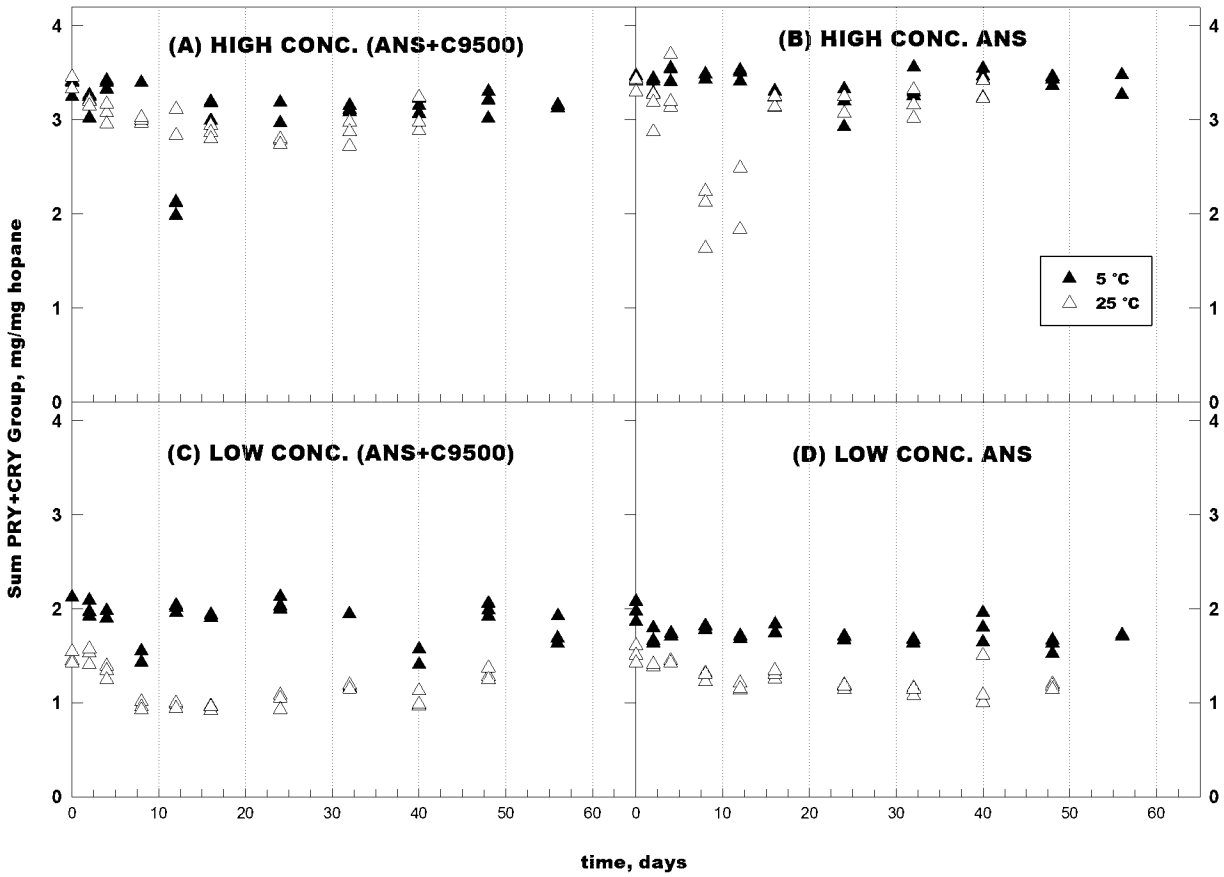

Figure S8. Biodegradation of pyrene homologues + chrysene homologues in the presence (A, C) and absence (B, D) of C9500 at 5 °C and 25 °C. High concentration treatments are in panel A and B, whereas low concentration treatments are in panels C and D.

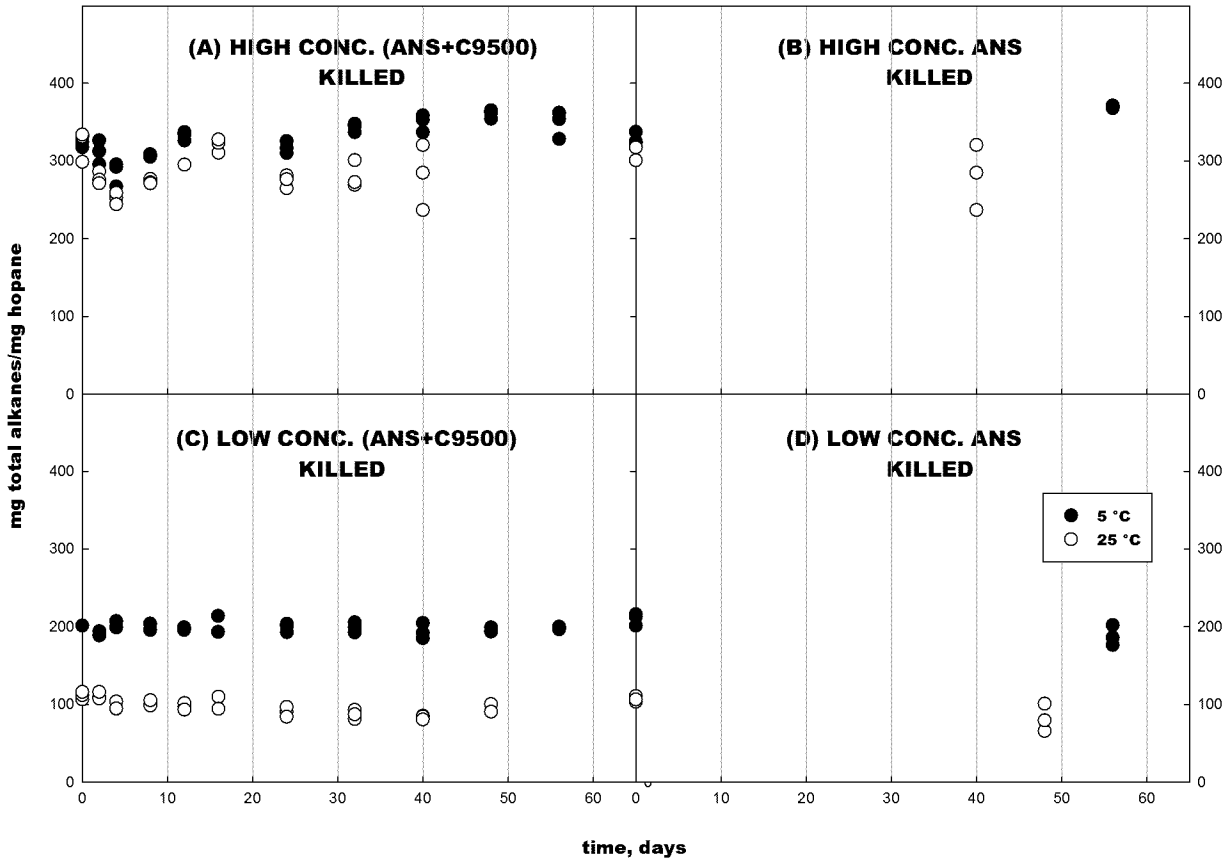

Figure S9. Biodegradation of hopane-normalized total alkanes at both temperatures in high concentration treatments (A, B) and low concentration treatments (C, D) in killed control samples.

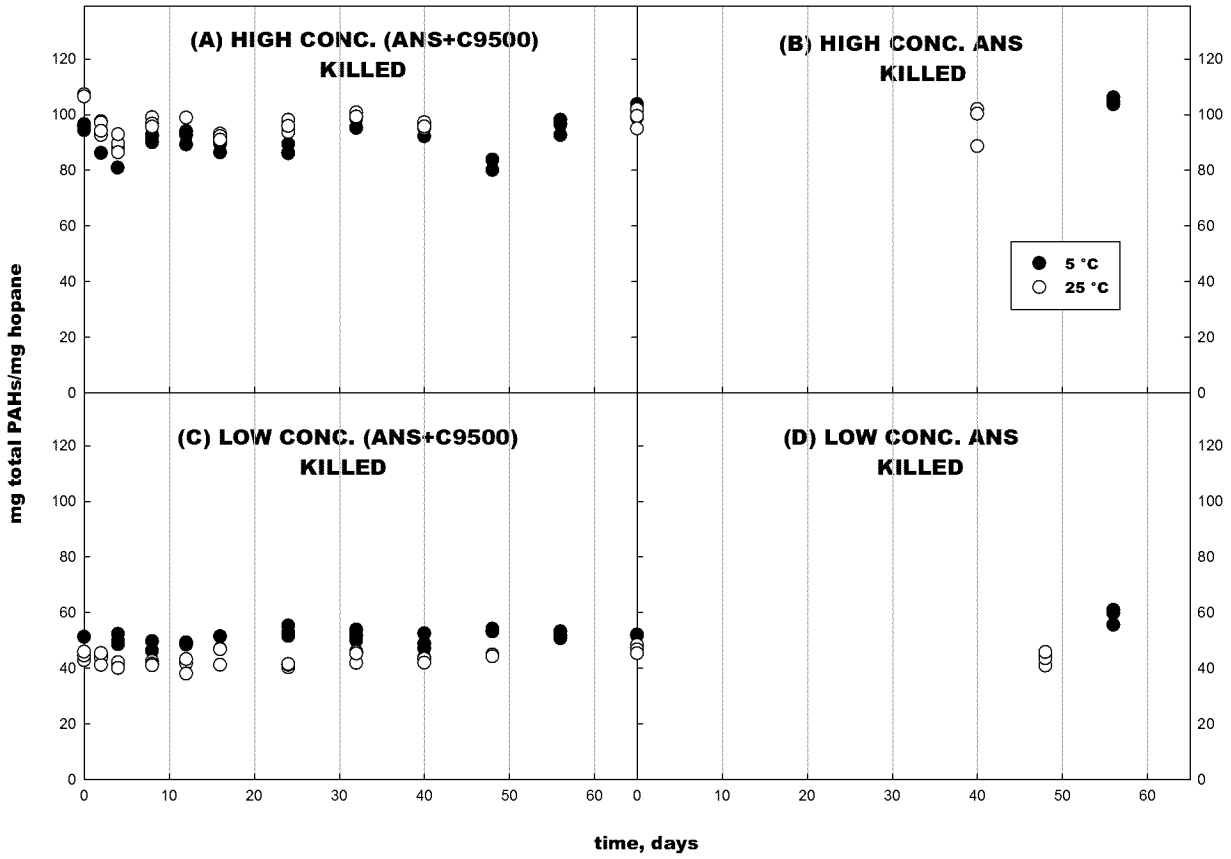

Figure S10. Biodegradation of hopane-normalized total PAHs at both temperatures in high concentration treatments (A, B) and low concentration treatments (C, D) in killed control samples.

Biodegradability of Different Initial Concentrations of Alaska North Slope Crude Oil Dispersed with Corexit C9500

Mobing Zhuang[1], Gulizhaer Abulikemu[2], Pablo Campo[3*], William Platten III[4], Makram T. Suidan[5], Albert D. Venosa (retired)[4], and Robyn N. Conmy[4]

1 Department of Biomedical, Chemical and Environmental Engineering, University of Cincinnati, 2901 Woodside Drive, Cincinnati, OH 45221, USA

2 Pegasus Technical Services Inc., 46 E Hollister St, Cincinnati, OH 45219 USA

3 Cranfield Water Science Institute, Cranfield University, Cranfield, Beds, MK43 0AL, UK

4 U.S. Environmental Protection Agency, NRMRL, 26 W. MLK Drive Cincinnati, OH, 45268, USA

5 Faculty of Engineering and Architecture, American University of Beirut, Bechtel Engineering Bldg. - 3rd flr. - Room 308 P.O. Box: 11-0236 Riad El Solh 1107 2020, Beirut, Lebanon

*Corresponding author: Pablo Campo
Tel: +44 (0)1234 754332
E-mail address: p.campo-moreno@cranfield.ac.uk

ED_001324_00000729-00001

ABSTRACT

In-situ concentrations of dispersant and crude oil observed during the Deepwater Horizon oil spill were lower than typically studied. To better understand biodegradation of the low oil and dispersant concentrations observed, laboratory experiments were conducted with Alaska North Slope crude oil (ANS) and the dispersant Corexit 9500 (C9500) to evaluate the removal of selected chemicals including: dioctyl sodium succinate (DOSS) which is an anionic surfactant in C9500, alkanes, and polycyclic aromatics hydrocarbons (PAHs). The study considered the biodegradability of ANS alone, ANS dispersed with C9500 at a dispersant-to-oil ratio of 1:25, and C9500 alone. Oil loads of 1,000 and 40 μL/L were compared at two temperatures with microbial cultures acclimated to the temperature 25 (meso culture) and 5 (cryo culture) °C. The biodegradation rate of DOSS, by the meso culture (25 °C) was approximately an order of magnitude faster in the high concentration experiment than in the low concentration experiment. At the lower temperature, the deep-water culture cryo (5 °C) had limited ability to metabolize DOSS regardless of the initial concentrations. Biodegradation of oil components was favored by the presence of dispersant as C9500 shortened lag phases and enhanced biodegradation rates. Alkanes and PAHs were degraded more rapidly in the high concentration samples. In the low concentration experiment, the percentage of alkanes persisting was higher than in the high concentration experiment (8-18% vs below 1%). No significant lag period in PAH biodegradation was observed in the high oil concentration experiment compared to the low oil concentration experiment where a lag period of 12 to 16 d was observed. The extent of biodegradation of some of the less soluble aromatic compounds increased by 4-86% under low oil concentration conditions.

ED_001324_00000729-00002

KEYWORDS

Corexit 9500, biodegradation, initial oil concentration

ED_001324_00000729-00003

INTRODUCTION

To minimize the impact of oil spills, responders adopt the Net Environmental Benefit Analysis, this is, any response technique should decrease the environmental costs rather than increase them (API, 2013). When mechanical recovery or in situ burning cannot achieve the goal of protecting shorelines from oil, the impact of using dispersants is likely favored by the benefits, which include keeping oil from sensitive areas and speeding up biodegradation by breaking an oil slick into small droplets (Prince, 2015). Thus, it is important to study the biodegradability of dispersants and dispersed oil under various conditions for better informed use in future applications.

In the aftermath of the Deepwater Horizon blowout in the Gulf of Mexico (GOM), comprehensive monitoring of the dispersant Corexit 9500 (C9500) and hydrocarbons in both surface and subsurface environments took place. In samples collected near the Macondo well, concentrations of dioctyl sodium sulfosuccinate (DOSS), an anionic surfactant present in C9500, ranged from 0.4 to 12 μg/L (Kujawinski et al., 2011). After the spill, DOSS was detected in subsurface waters at concentrations below 40 μg/L at different locations in the GOM, while in one surface water sample close to the wellhead concentration exceeded 200 μg/L (Gray et al., 2014). The combination of turbulence at the GOM surface and the dispersant application could rapidly decrease oil concentrations to below 100 mg/L, dropping even further over time (Lee et al., 2013). Hence, these researchers recommended that biodegradation tests of dispersed oil should be conducted under more dilute concentrations to mimic real conditions.

Most studies published on biodegradation of oil and dispersants prior to the Deepwater incident had been conducted at concentrations well-above the reported in situ levels (Operational

ED_001324_00000729-00004

Science Advisory Team, 2010; Prince, 2015). Several studies assessing biodegradation of oil dispersed by C9500 used initial oil and dispersant concentrations from 100 to 4,500 mg/L, with dispersant-to-oil ratios (DOR) of 1:10, 1:20, or 1:25 (Campo et al., 2013; Lindstrom and Braddock, 2002; Zahed et al., 2010). A few studies were published on oil biodegradation with initial oil and dispersant concentrations below 100 μL/L (Brakstad et al., 2015; Prince et al., 2013; Venosa and Holder, 2007).

Our objective was to determine how the initial amounts of oil and dispersant affect their biodegradation. Thus, we conducted high (1000 μL/L) and low oil concentration (40 μL/L) biodegradation experiments with Alaska North Slope crude oil (ANS) and C9500 at 5 and 25 °C. C9500 is a dispersant included in the National Contingency Plan Product Schedule and was applied to both the surface and submarine environment in the GOM (Operational Science Advisory Team, 2010). Performance, evaluated by measuring time-varying DOSS, and oil chemicals in high and low concentration experiments at 5 and 25 °C are reported in this paper.

MATERIALS AND METHODS

Chemicals and Reagents

The U.S. Environmental Protection Agency (EPA) provided the ANS and the dispersant C9500 (Nalco Naperville, IL) used in this study. Standards for DOSS and its deuterated surrogate (D_{17}-DOSS) were obtained from Aldrich (St. Louis, MO) and Isotec (Miamisburg, OH), respectively. Acetonitrile, deionized ultra-filtered water, and mineral salts were purchased from Fisher Scientific (Pittsburgh, PA). Dichloromethane (DCM) was obtained from Tedia (Fairfield, OH). Sylon CT (Sigma-Aldrich, St. Louis, MO) was used for the deactivation of the glassware to prevent adherence of oil and biomass to the sides of the flasks. The protease

ED_001324_00000729-00005

cocktail for inhibiting enzymatic activity was also acquired from Sigma-Aldrich (St. Louis, MO).

Protease Solution Preparation

Following the instruction provided with the protease cocktail, 5 mL dimethyl sulfoxide (DMSO) was added to 1,075 mg lyophilized powder, which was previously stored unopened at 20 °C. The solution was vortexed for ten minutes before the addition of 20 mL deionized water. The resulting solution was clear. The reconstituted protease solution contained the following inhibitors: 4-(2-aminoethyl) benzenesulfonyl fluoride hydrochloride (23 mM), ethylenediaminetetraacetic acid (100 mM), bestatin (2 mM), pepstatin A (0.3 mM), and E-64 (0.3 mM).

Artificial Seawater

The salts in the GP2 medium, dissolved in DI water, were (expressed in g/L) NaCl (21.03), $MgCl_2 \cdot 6H_2O$ (9.5), Na_2SO_4 (3.52), $CaCl_2 \cdot 2H_2O$ (1.32), KCl (0.61), KBr (0.088), $NaB_4O_7 \cdot 10H_2O$ (0.034), $SrCl_2 \cdot 6H_2O$ (0.02), $NaHCO_3$ (0.17) $FeCl_3 \cdot 6H_2O$ (0.05), $Na_5P_3O_{10}$ (0.297) and KNO_3 (2.89). The GP2 pH was ≈ 7.5. The GP2 medium was autoclaved at 121 °C for 30 min and then used as the sterile matrix in this study (Spotte et al., 1984).

Microbial Cultures

The meso culture was originally isolated from the surface water of the GOM in the vicinity of the Macondo well. The cryo culture was isolated from water close to the plume location at a depth of 1,240 m near the wellhead . Both cultures were isolated by EPA's Gulf Breeze, FL research laboratory. Enriched inocula were prepared as follows: in 2-L shake flasks, 2.5 mL South Louisiana crude oil (SLC) were added to 500 mL of the original unfiltered GOM

ED_001324_00000729-00006

seawater supplemented with 2.8 g/L KNO_3, 0.55 g/L NaP_3O_{10}. The flasks were rotated (400 rpm) at 5 °C (cryo culture) and 25 °C (meso culture). Thegrowth times were 7 d for the meso culture and 17 d for the cryo culture. After these periods, cells were harvested by centrifugation (6,000 × g for 30 min at 4 °C) and the pellets preserved in 10% glycerol at -70 °C. Before shipping to EPA-Cincinnati, 1 mL of each thawed culture were added to shake flasks containing 500 mL GP2 medium fortified with 2.5 mL of SLC. The cultures used in this study were grown at EPA (Cincinnati, OH) by transferring the original cultures from EPA's Gulf Breeze to GP2 medium supplemented with SLC. The meso culture was harvested after 3 weeks of growth and the cryo culture after 5 weeks. The harvested culture was processed in the same fashion as mentioned previously: centrifugation (6,000 × g for 30 min at 4 °C) and the pellets preserved in 10% glycerol at -70 °C. For use in experiments, the cultures were defrosted at room temperature, washed with 0.85% saline solution to remove glycerol, centrifuged, and brought back up to the frozen volume.

Experimental Design

A summary of the experimental design is shown in Tables S1 and S2 for the high and low oil concentration experiments, respectively. For the high concentration experiments, 6 treatments were tested at 5 and 25 °C in triplicate: C9500 dispersant alone, ANS oil alone, ANS dispersed with C9500, and the corresponding killed controls (KCs). The 5 °C experiment required 11 sampling events in triplicate (0, 2, 4, 8, 12, 16, 24, 32, 40, 48 and 56 d), while 9 events were used for the 25 °C (0, 2, 4, 8, 12, 16, 24, 32 and 40 d). At each sampling event, triplicate shake flasks of each treatment along with KCs were sacrificed, except for the ANS alone KCs which were analyzed at the beginning and end of the experiment.

ED_001324_00000729-00007

The same treatments were included in the low concentration experiment, but both oil and dispersant concentrations were prepared at 4% of the initial loads used in the high concentration experiment. Additionally, a seventh treatment involved the use of triplicate KCs containing the enzyme protease (0.5 mL) to neutralize the enzymatic DOSS hydrolysis. This treatment was included only in the low concentration experiment. The sampling events were conducted similarly to the high concentration experiment with the exception of the protease treatment, which was sampled at 0, 12, 24, 35, 46 and 56 d and 0, 8, 18, 28, 38 and 48 d for the 5 and 25 °C experiments, respectively.

After all treatments were prepared, the appropriate cultures were spiked (0.5 mL) and the flasks were placed on orbital shakers. The shakers were operated at 200 rpm and kept in the appropriate constant temperature rooms until the expected sampling events. All KCs were sterilized by adding 1 mL sodium azide stock (50 g/L) into the 100 mL of GP2 medium.

High Concentration Treatments

To evaluate the biodegradation of dispersed oil, 2 L baffled beakers were used in which 40 µL of C9500 and 1,000 µL of ANS were added to 1,200 mL of GP2 to achieve a volumetric DOR of 1:25. Subsequently, the beaker containing the mixture was shaken at 200 rpm for 10 minutes and then left stationary for an additional 10 min, then the dispersion was transferred to a 20-L continuously mixed carboy. The stationary time was to allow undispersed oil to rise to the top layer of water and draining the dispersion into carboy should be carefully done (not disturbing the top layer of undispersed oil). The above procedure was repeated until the volume in the carboy reached 14 L. Subsequently, 100 mL aliquots of the mixtures were transferred to the shake flasks.

ED_001324_00000729-00008

The second treatment was for the evaluation of oil as the only substrate. ANS (100 μL) was added directly to shake flasks containing 100 mL sterile GP2 medium, which yielded an estimated oil concentration of 1,000 μL/L. To evaluate the degradation of dispersant alone, 480 μL of C9500 was added to 14 L of sterile GP2 medium in a continuously mixed carboy; after 30 min, 100 mL aliquots of this mixture were dispensed into shake flasks for this treatment.

Low Concentration Treatments

To prepare the low concentration dispersed oil, a single batch of 1,200 mL GP2 was spiked with 200 μL ANS onto the water surface followed by addition of 8 μL C9500 onto the oil slick, which yielded a volumetric DOR of 1:25 in a 2 L baffled beaker. The beaker was placed on a shaker and agitated for 20 minutes. The shaker was started at a very slow speed and was ramped up to 200 rpm gradually. After mixing, the beaker remained stationary for 10 minutes and, subsequently, the dispersion was carefully drained into a 20 L continuously mixing carboy. The above procedure was repeated until the volume in the carboy reached 3 L, and then 12 L of sterile GP2 was added to dilute the mixture. The shaker was started at a very slow speed and was ramped up to 200 rpm gradually. The beaker was placed on a shaker for 20 min and then remained stationary for 10 minutes. Subsequently, 3 L of the dispersion were poured into a 20 L carboy under continuous mixing and 12 L of sterile GP2 was added for dilution purposes. Overall, the oil and dispersant amounts in this treatment were approximately 4% of that in the high concentration experiment. Finally, shake flasks were filled with 100 mL aliquots of the diluted dispersed oil. Low concentration ANS alone was prepared by spiking 4 μL of oil into shake flasks containing 100 mL sterile GP2, which yields an oil concentration of 40 μL/L (i.e., 4% of the high concentration oil alone experiment). The low concentration dispersant alone

ED_001324_00000729-00009

treatment was prepared in a single batch of sterile GP2 (14 L) spiked with approximately 20 μL of C9500. The batch was mixed for 30 minutes and, subsequently, 100 mL aliquots were transferred into the shake flasks.

Oil Components and Dispersant Analysis

To monitor C9500 degradation, DOSS was measured using liquid chromatography tandem mass spectrometry (LC-MS/MS) following the Standard method ASTM D7730−11 (2011). For the high concentration experiment, oil analysis was conducted with a 6890 GC coupled with a 5973 mass spectrometry from Agilent (Palo Alto, CA). In the low concentration experiment, an Agilent (Palo Alto, CA) 7000 GC Triple Quad system was used. The quantification range for the single quad and triple quad mass spectrometry are 1-30 μg/L and 0.5-10 μg/L, respectively. The same column, a DB-5MS column (30m × 0.25mm, 0.25μm film thickness), was used to achieve chromatographic separation of analytes in both instruments. The method was a modification based on EPA Method 8270D (2007). Details of sample preparation methods and oil extraction by DCM can be found elsewhere (Campo et al., 2013). The targeted oil components were pristane (PR), phytane (PH), normal paraffins (n-C_{10-35}) and 2-, 3- and 4-ring PAH compounds and their alkylated homologues (C_{0-4}-naphthalenes, C_{0-3}-fluorenes , C_{0-3}-dibenzothiophenes, C_{0-4}-phenanthrenes/anthracenes, C_{0-4}-napthbenzthiophenes, C_{0-2}-pyrenes, C_{0-4}-chrysenes). The concentrations of these analytes were normalized to the concentration of hopane present in the oil (Prince et al., 1994).

Statistical Analysis

Statistical analysis was performed with Graphpad Prism 6 software. Lag phases were determined by two-way ANOVA followed by Tukey's test among different sampling events. First-order rate

ED_001324_00000729-00010

coefficients were calculated by least squares. To detect significant difference between two treatments, extra sum-of-square F test (for first order mechanism) and an equivalent form (Jerrold, 1984) of analysis of covariance (for zero order mechanism) were conducted. The Student *t*-test was used when comparing two groups of values (i.e. concentration values of two sampling events). In all the aforementioned tests, a significance level $\alpha = 0.05$ was used.

RESULTS AND DISCUSSION

Removal of DOSS

High Concentration Experiment. Biologically active samples revealed a rapid removal rate of DOSS at 25 °C (Fig. 1A-B, open symbols) with extents of transformation exceeding 95% after 2 d in dispersed oil (Fig. 1B) and 4 d in C9500 alone (Fig. 1A). The first order rate coefficients were -1.82 ± 0.25 d^{-1} (ANS+C9500) and -0.71 ± 0.024 d^{-1} (C9500 alone). The presence of oil enhanced the DOSS biodegradation rate constant by a factor of approximately 2.6. Disappearance of DOSS was also observed in KCs at 25 °C, with zero order rates of -138 ± 7 and -221 ± 11 $\mu g\ L^{-1}\ d^{-1}$ for C9500 alone (Fig. 1C) and dispersed oil (Fig. 1D), respectively. As monooctyl sulfosuccinate (MOSS) was found in KCs, Campo et al. (2013) explained this abiotic loss in terms of hydrolysis which was confirmed by (Batchu et al., 2014). The presence of oil significantly enhanced DOSS removal in KCs ($p < 0.0001$).

In contrast with the rapid removal rates observed for DOSS at 25 °C, the biotic and abiotic processes at 5 °C were much slower. DOSS persisted for 40 d before its concentration decreased in all treatments. The difference in DOSS concentration between live samples and parallel KCs in the dispersed oil treatment was statistically insignificant at days 48 ($p = 0.078$) and 56 ($p = 0.726$). In the C9500 alone treatment, DOSS was significantly lower in live samples

ED_001324_00000729-00011

than in KCs at days 48 ($p = 0.0015$) and day 56 ($p = 0.023$). These results point to biotransformation as the predominant DOSS removal mechanism as opposed to hydrolysis.

ED_001324_00000729-00012

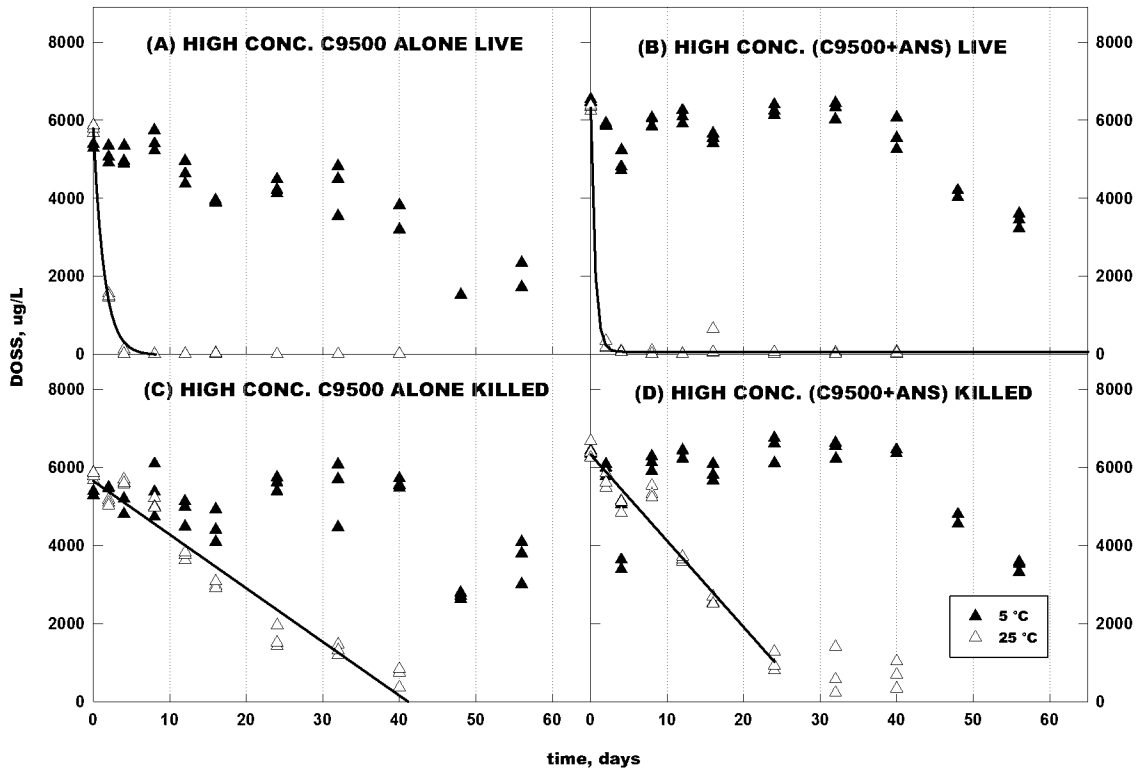

Figure 1. Disappearance of DOSS in high concentration experiment in the absence (A, C) and Presence (B, D) of ANS at 5 °C and 25 °C. Live samples are in panel A and B, whereas killed controls are in panels C and D.

Low Concentration Experiment. At 25 °C and for the dispersed oil treatment, no lag period was observed in DOSS uptake, which showed a first-order constant rate of -0.16 ± 0.015 d^{-1} (Fig. 2B). In the absence of oil (Fig. 2A), we observed an acclimation period of 2 d followed by DOSS biodegradation (-0.07 ± 0.009 d^{-1}). The presence of oil favored DOSS removal as was observed in the high concentration experiment. Removal extents over 95% for DOSS required 32 and 48 d in the presence and absence of oil, respectively. In the corresponding KCs, DOSS concentrations decreased following zero-order kinetics, with constant rates of -4.1 ± 0.3 μg L^{-1} d^{-1} (C9500 alone, Fig. 2C) and -5.1 ± 0.4 μg L^{-1} d^{-1} (C9500 and ANS, Fig. 2D).

For the high concentration experiment at 25 °C and regardless of the presence of oil, the

time series concentration of DOSS in the live samples rapidly declined to zero and clearly separated from the values measured in the corresponding KCs. In the low concentration experiment, it appeared that DOSS disappearance with time in both treatments, C9500 alone and dispersed ANS, overlapped with the abiotic losses observed in the KCs (Fig. 2). To differentiate between microbial activity and hydrolysis, we compared by a *t*-test ($\alpha = 0.05$) the average DOSS concentrations measured in live samples with those values found in the parallel KCs. Live samples significantly departed from the controls after 4 d ($p = 0.0227$) and 16 d ($p = 0.0053$) in the presence and absence of ANS, respectively. At early stages in the experiment, we could not identify the predominant removal mechanism for DOSS but, eventually, microbial uptake prevailed as the main process in terms of rate and extent.

DOSS biodegradation was at both the higher initial concentration and temperature ??????????. Nevertheless, based on our low concentration results, it is reasonable to infer that biodegradation of DOSS at the surface of GOM might not happen as rapidly since dilution and emulsification can attenuate the concentration of dispersant. In this fashion, DOSS was detected with a reporting limit of 0.25 $\mu g\ L^{-1}$ and a highest concentration of 229 ±16 $\mu g\ L^{-1}$ in surface water samples collected 1-2 months after the spill near the Macondo well (Gray et al., 2014).

DOSS concentration remained unchanged (ANOVA followed by Tukey's test among all sampling events in each treatment) in live samples and KCs under 5 °C and low oiling conditions (Fig. 2, closed symbols). Such finding agreed with studies by Kujawinski et al. (2011) and Gray et al. (2014) who concluded that subsurface degradation of DOSS was minimal. Campo et al. (2013) observed no hydrolysis or biodegradation of DOSS in SLC at 5 °C within 42 d.

ED_001324_00000729-00014

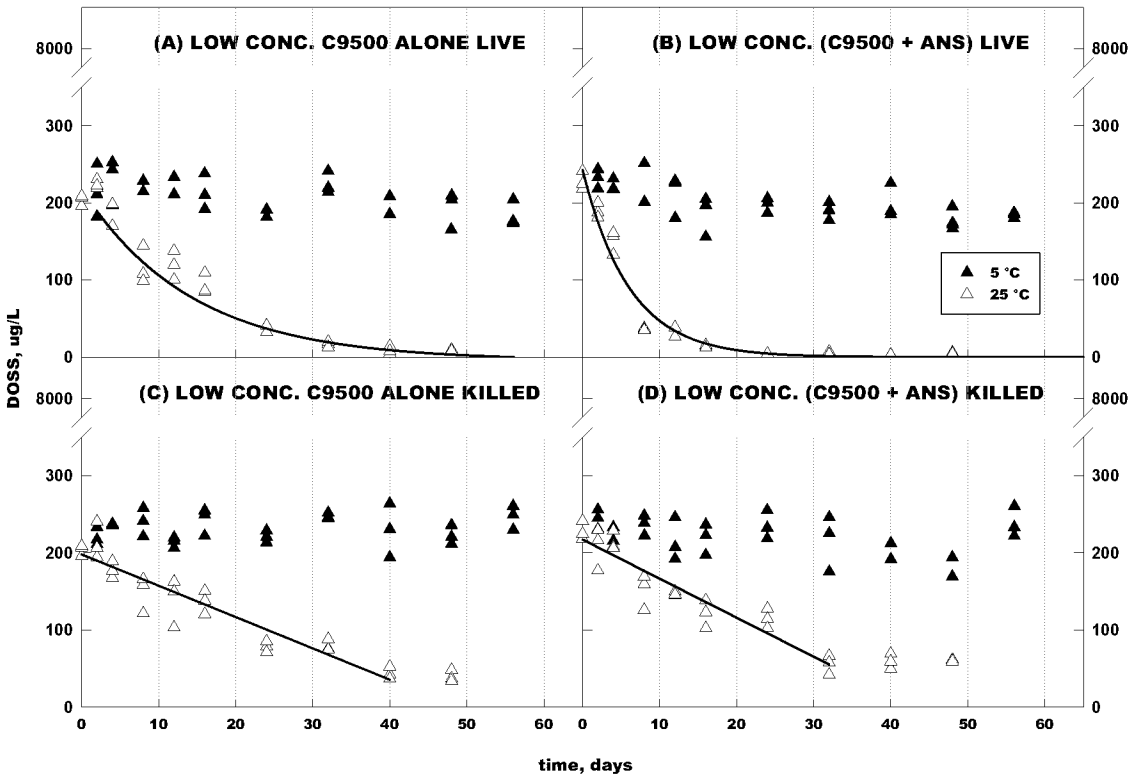

Figure 2. Disappearance of DOSS in low concentration experiment in the absence (A, C) and Presence (B, D) of ANS at 5 °C and 25 °C. Live samples are in panel A and B, whereas killed controls are in panels C and D.

We also included a series of dispersed oil KCs containing a protease cocktail (Fig. 3A), which inhibits enzymatic activity to clarify the abiotic DOSS disappearance. At 25 °C, the addition of inhibitor clearly slowed down the hydrolysis process as the zero-order rate constant in the protease KCs was -3.7 ± 0.4 μg L^{-1} d^{-1} (Fig. 3A) as opposed to -5.1 ± 0.4 μg L^{-1} d^{-1} (Fig. 3B) obtained for the regular KCs (p = 0.021). Such finding confirms the enzymatic nature of DOSS hydrolysis. Nevertheless, different enzymes may be involved in the process so that the protease cocktail could not block all of them. In the protease controls at 5 °C, DOSS persisted throughout the experiment as observed in the regular KCs for that temperature. This indicates that either the lower temperature attenuated DOSS breakdown, the cryo culture lacked the

required enzymes, or a combination of both causes???????????.

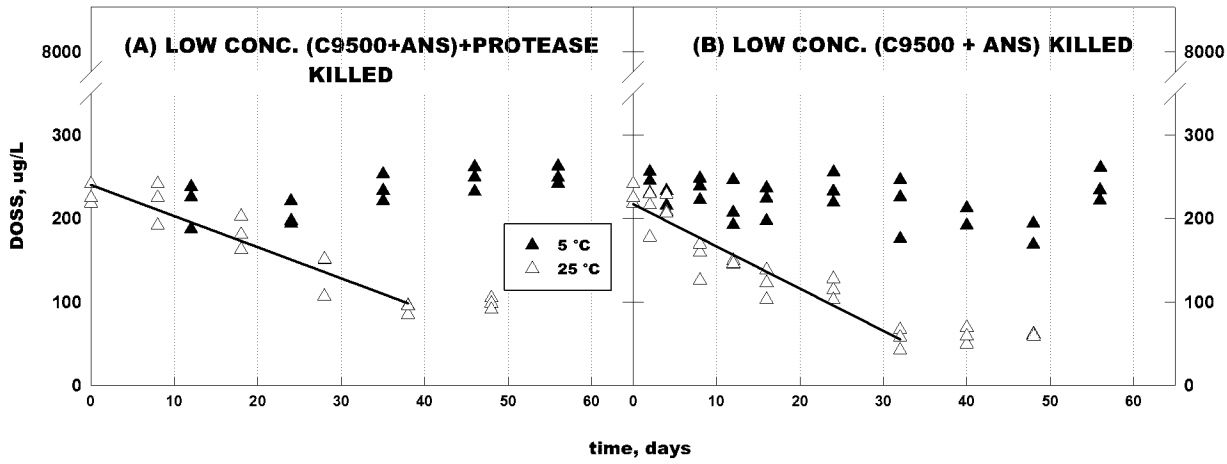

Figure 3. Disappearance of DOSS in low concentration dispersed oil killed controls in the presence (A) and absence (B) of protease at 5 and 25 °C.

Total Alkane Degradation

High Concentration Experiment. Total alkanes at both temperatures are presented in Fig. 4 A-B. At 25 °C, the meso culture metabolized the aliphatic fraction with a first-order rate constants of -0.91 ± 0.10 and -0.85 ± 0.04 d^{-1} in the absence and presence of C9500, respectively. For both treatments, the extent of removals reached 99% after 4 days. As expected, aliphatics degraded slower at 5 °C. In the dispersed oil treatment, this fraction followed first order kinetics (-0.24 ± 0.01 d^{-1}) while, for the oil alone samples, alkanes exhibited a linear decay during the first 8 d followed by first order kinetics of similar rate (-0.25 ± 0.03 d^{-1}). After days 16 (dispersed oil) and 24 (oil alone), the alkane extent of removal was 99% for the lower temperature.

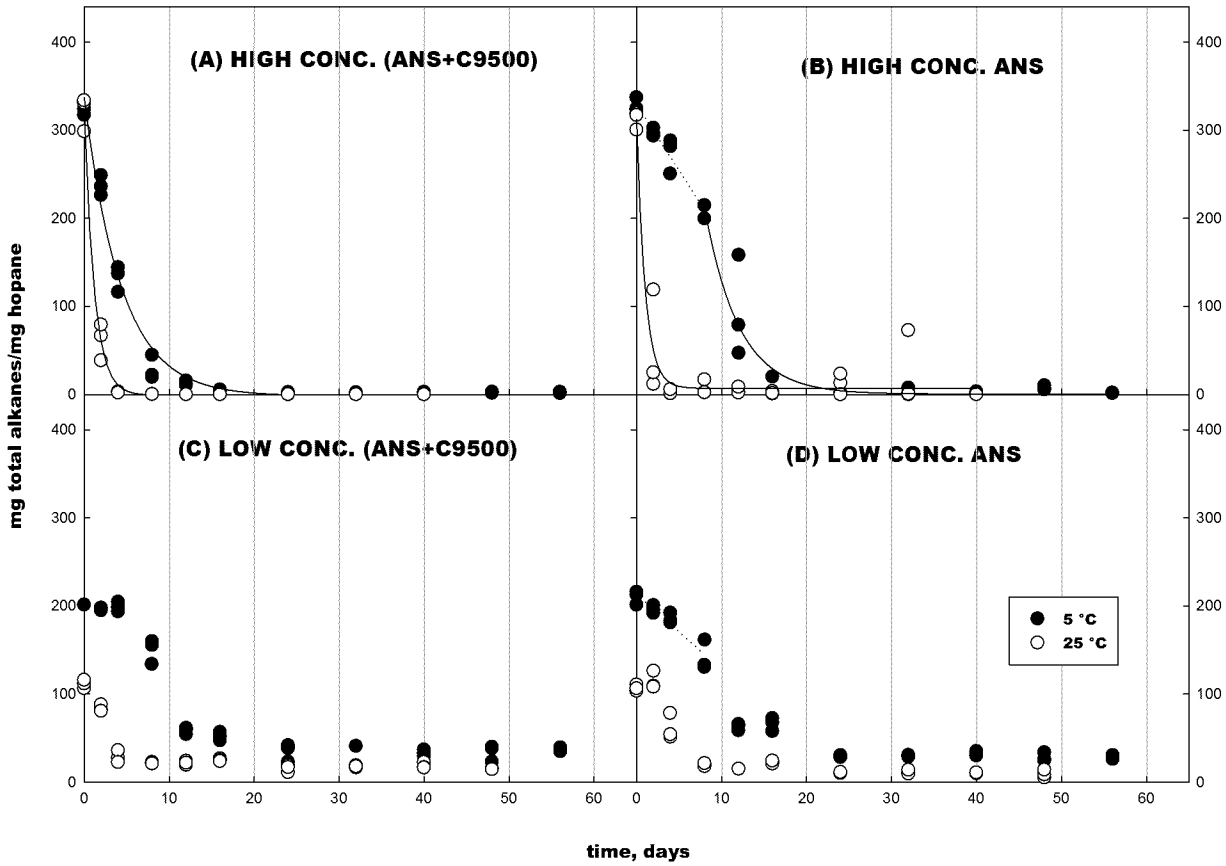

Figure 4. Biodegradation of hopane-normalized total alkanes at both temperatures in high concentration treatments (A, B) and low concentration treatments (C, D).

Low Concentration Experiment. In this experiment, the initial total alkane concentrations were considerably different at 5 and 25 °C (Fig. 4 C and D). The meso culture showed background concentrations of PAHs and hopane, the conservative biomarker to which all the target analytes concentrations are normalized. The hopane background levels were comparable to those measured in the initial oil added to the flasks. Hence, at time zero, the total alkane concentration normalized to hopane at 25 °C were almost half of the corresponding value at 5 °C.

At 25 °C, the alkane residual concentrations ranged from 8 to 18% of the initial values (Fig. 4 A and B). In the oil alone treatment, alkane biodegradation started after a lag phase of 2 d, while these chemicals were promptly metabolized in the dispersed oil treatment. At 5 °C, the cryo culture required 4 d for acclimation in the dispersed oil. In the absence of dispersant, after a slow and steady linear decay, fast disappearance of alkanes occurred between days 8 and 12. This suggests that C9500 reduced the length of the acclimation phase for alkane uptake.

Table 1 summarizes the actual concentrations of total alkanes (not normalized to hopane) for the first and last sampling event for both the high and low concentration experiments. It is noteworthy that a higher alkane residual amount was observed in the low concentration experiment than the high concentration one.

Table 1. Average and standard deviations (sd) of total alkanes and PAHs concentration in the high and low concentration experiment at first and last sampling event.

			5 °C		25 °C		5 °C		25 °C	
Samples			**ANS alone**		**ANS alone**		**ANS+C9500**		**ANS+C9500**	
			average (µg/L)	**sd**	**average (µg/L)**	**sd**	**average (µg/L)**	**sd**	**average (µg/L)**	**sd**
High Conc.										
	Alkanes	**First**	47,400	604	43,300	9,390	24,600	973	27,200	126
		Last	201	26	36	42	186	52	BDL	BDL
	PAHs	**First**	14,500	110	13,700	3,090	7,310	323	8,790	94
		Last	3,040	281	2,470	300	1,300	74	1,270	158
Low Conc.										
	Alkanes	**First**	2,010	202	1,740	149	1,420	72	1,130	39
		Last	216	21	83	75	225	13	142	4
	PAHs	**First**	482	53	773	25	330	12	453	14
		Last	71	5	88	5	58	10	80	4

ED_001324_00000729-00018

Degradation of Individual Alkanes

High Concentration Experiment. Table S3 summarizes the first-order biodegradation coefficients for individual alkanes. At 25 °C, among all the compounds monitored only n-C_{10} biodegraded faster (-2.00 vs. -1.34 d^{-1}) with the addition of dispersant. Branched alkanes exhibited similar rates regardless of the presence of C9500, although higher variability among triplicates was observed in the oil alone samples (Fig. S1 A and B). At 5 °C, consistently higher rates for n-C_{10-27} were observed in the dispersed oil treatment when compared to the oil alone treatment. Also, no lag period for the biodegradation of branched alkanes occurred when C9500 was added, whereas an 8-day lag period occurred in the absence of dispersant.

Low Concentration Experiment. As depicted in Figs. S1-5 (panels C and D), only n-C_{10-16} ?????was completely removed at both temperatures in the low concentration experiment. In this case,a more qualitative approach was used by comparing the disappearance time. At 25 °C in the low oil concentration experiment, n-C_{10} was degraded faster in the presence of dispersant, disappearing completely before day 2, whereas in the absence of C9500, its depletion was only achieved after day 8. The biodegradation of n-C_{10} was also accelerated when C9500 was present at 5 °C, as shown in Table S4 (-0.47 vs -0.63 d^{-1}). At both temperatures, branched alkanes were not degraded faster in the presence of dispersant, as shown in Table S4 and Fig. S1 C-D.

The major mechanism of uptake of water-insoluble substrates (i.e., alkanes) is generally recognized as direct interaction between microbes and the hydrophobic substance (Rojo, 2009; Wentzel et al., 2007) and the effects of surfactant on such process are inconclusive (Bredholt et al., 2002; Bruheim et al., 1999; Tang et al., 1998). Both conducive and inhibitory effects of dispersant on oil biodegradation have been reported (Lindstrom and Braddock, 2002; Prince et

ED_001324_00000729-00019

al., 2013; Venosa and Holder, 2007). In this study, C9500 exhibited positive effects on the biodegradation of alkanes in the high and low concentration experiments. Such effects included enhancement of biodegradation rates and shortening of lag periods. Rate enhancements were more notable in the high concentration experiment, whereas C9500 clearly shortened lag phases in the lower concentration tests.

The application of dispersants to an oil slick promotes the formation of small oil droplets by decreasing the interfacial tension between oil and water (Jasper et al., 1978; Li et al., 2009; Lunel, 1995). Consequently, the total interfacial area of oil droplets for microbes to interact with is increased. In the high concentration experiment, exposure of substrates to the microbes is enough that biodegradation can initiate soon after inoculation. In this case, it is likely that dispersants assisted degradation mainly by increasing interfacial area for microbes to interact with oil. For the low concentration experiment, the observed long acclimation phase at both temperatures was possibly due to limited exposure of alkanes to the microorganisms in the beginning. Since the oil load, appearing as an iridescent sheen, is so low, the mixing energy in the flasks could be high enough to produce similar droplet size distribution in the oil alone and dispersed oil treatments.

Total Aromatics Degradation

High Concentration Experiment. Fig. 5A-B presents total PAH biodegradation data for the high concentration experiment at both temperatures. Aromatics removals of 42 and 24% occurred by day 2 in the dispersed oil and the oil alone treatment, respectively. This difference in extent was significant ($p < 0.0001$), which indicates a positive effect of the dispersant. At 5 °C, the time for attaining maximum level of PAHs removal in non-dispersed treatment took twice as

ED_001324_00000729-00020

long as in dispersed oil treatment 16 days vs. 8 days (solid symbols in Fig. 5B and 5A, respectively). The overall PAHs removals in the presence and absence of dispersant were 86% and 82%, respectively.

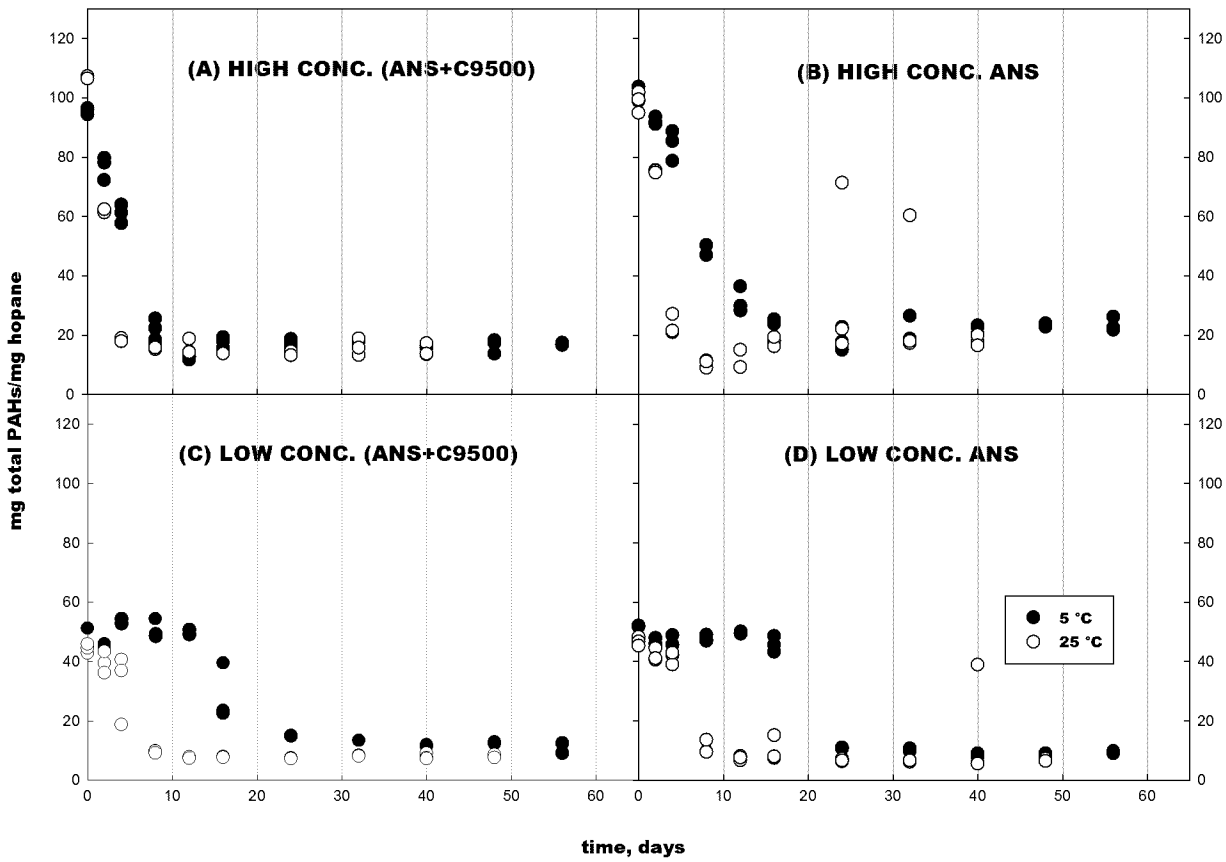

Figure 5. Biodegradation of hopane-normalized total PAHs at both temperatures in high concentration treatments (A, B) and low concentration treatments (C, D).

Low Concentration Experiment. As shown in Fig. 5C-D, when comparing the two low concentration treatments at 25 °C (open symbols), the only difference was in one replicate of dispersed oil on day 4, which had significantly lower total PAH concentration than the parallel diluted oil alone samples. At the high temperature (open symbols), the patterns of PAH degradation were similar in the absence and presence of C9500, regardless of initial concentration. The treatment without dispersant exhibited higher variability. The lag period at

the low temperature (closed symbols) was longer than at 25 °C; it lasted 12 and 16 days for dispersed oil and oil alone, respectively. For the sampling event on day 16, the extent of PAH removal was 20 to 50% in the replicates of dispersed oil sample, while it was negligible in the treatment without dispersant.

Transport of compounds from non-aqueous phase to aqueous phase is often the most rate-limiting step in the biodegradation of PAHs. Surfactants can enhance the dissolution of PAHs by increasing interfacial area of oil droplet and subsequently increase the bioavailability of PAHs to microorganisms (Haritash and Kaushik, 2009; Mrozik et al., 2003). The effect of C9500 on the biodegradation of total PAHs was less pronounced in the low concentration experiment than in the high concentration experiment, as this effect was observed only in one or more replicates in a single sampling event. This finding is consistent with our previous assumption about low concentration experiment: droplet size distribution in the oil alone and dispersed oil treatments are similar. Dispersion in the oil alone microcosms might have been efficient enough even without the addition surfactant, considering the mixing energy was sufficient (Kaku, 2006) and the initial presence of oil was an iridescent rainbow-colored sheen. Clearly, the comparison between our low concentration dispersed oil samples and oil alone samples indicates that dispersants had little effect on the concentration of PAHs. Nevertheless, most toxicity studies on dispersed oil conclude that the presence of dispersant increased environmental risk for aquatic organisms living in the water column (Milinkovitch et al., 2011; Ramachandran et al., 2004), which is possibly due to their relatively high concentration of oil (4.75 g/L and 100 mL/L, respectively) and dispersant (0.25g/L and 5 mL/L, respectively) in the laboratory tests.

Individual Aromatics Degradation

ED_001324_00000729-00022

High Concentration Experiment. A first-order model could be used to fit the biodegradation of the individual PAHs that had a negligible fraction persisting by the end of the high concentration experiment. At both temperatures, the biodegradation rates of naphthalene, phenanthrene, fluorine, and dibenzothiophene and their homologues in the high concentration experiment were consistently higher in the presence of dispersant (Table S5). The greatest enhancement was observed with naphthalene at 25 °C, which was 2.9-fold higher than at 5 °C (-1.94 d^{-1} vs. -0.68 d^{-1}). The surfactant likely assisted the transfer of more soluble compounds from the oil phase to the aqueous phase through the formation of small oil droplets and the resultant increase in interfacial area. Because the bio-uptake of aromatics is mostly from aqueous phase (Haritash and Kaushik, 2009; Mrozik et al., 2003), C9500 promoted the biodegradation of PAHs by increasing their bioavailability in water.

Low Concentration Experiment. Among the low concentration individual PAHs, the time-varying concentration of specific aromatics could be fitted to a first-order kinetics model (rates shown in Table S6), and the results revealed reduced rates in low concentration treatments, especially when C9500 was present (i.e. naphthalene: -0.36 d^{-1} v -1.94 d^{-1}). However, we could not fit a first-order model for the other PAH compounds in the low concentration experiments because of the long lag period and the immediate and nearly complete removal after biodegradation started. As mentioned before, the impact of C9500 in the low concentration experiment was difficult to assess, because different PAH concentrations in parallel dispersed oil and oil alone samples was observed only at one or more replicates in a single sampling event (25 °C: day 4, 5 °C: day 16). In the low concentration experiment, the starting PAH concentrations (330-773 **μg/L**) were below the remaining residual found in the high concentration experiment (1270-3040 **μg/L**), but the cultures were able to degrade the aromatic compounds to an even

ED_001324_00000729-00023

lower level, as shown in Table 1. C_4-naphthalene, C_{2-4}-phenanthrene, C_{2-3}-fluorene, and naphthobenzothiophene were removed at higher extent in the low rather than in the high concentration samples (Fig. S6). The increase in removal extent for the aforementioned aromatics were 6-14%, 4-47%, 14-54%, and 55-86% respectively. Zahed et al. (2010) also observed similar enhancement of crude oil removal extent in low oiling experiments. Taking C_2-phenanthrene as an example, it was fully degraded in the low concentration experiment, whereas its removal extent ranged from 66% to 94% when the initial oil concentration was high. The enhancement in the extent of removal under diluted conditions was more remarkable at low temperature, which contributed to our conclusion that solubility was the limiting factor for those compounds to be biodegraded. Whether oil concentration is high or low, pyrene, chrysene and naphthobenzothiophene homologues persisted until the last sampling event at both temperatures, as depicted in Figs. S7 and S8. The heavy PAHs, such as chrysene, are likely to be retained on a beach for several years, according to Yin et al. (2015), who conducted research that monitors the submerged oil mats and surface residual oil balls off Alabama's beach affected by the 2010 DWH incident.

ED_001324_00000729-00024

ACKNOWLEDGMENTS

We thank Jan Kurtz and Diane Yates from EPA's Gulf Ecology Division (GED) at Gulf Breeze, FL, who collected the water samples in the GOM and performed the enrichments and provided them for our experiments. The research was a product of the U.S. Environmental Protection Agency's National Risk Management Research Laboratory (NRMRL) and was partially funded by EPA, NRMRL, Cincinnati, OH, under Pegasus Technical Services, Inc. Contract EP-C-11-006.

REFERENCES

2007. U.S. Environmental Protection Agency, EPA 8270D Semivolatile organic compounds by gas chromatography/mass spectrometry (GC/MS), 3rd. ed, Washington, D.C.

API, 2013. Net Environmental Benefit Analysis for effective oil spill preparedness and response. 2013. http://www.api.org/~/media/Files/EHS/Clean_Water/Oil_Spill_Prevention/NEBA/NEBA-Net-Environmental-Benefit-Analysis-July-2013.pdf.

Batchu, S.R., Ramirez, C.E., Gardinali, P.R., 2014. Stability of dioctyl sulfosuccinate (DOSS) towards hydrolysis and photodegradation under simulated solar conditions. Sci. Total. Environ. 481, 260-265.

Bateman, J.N., Speer, B., Feduik, L., Hartline, R.A., 1986. Naphthalene association and uptake in Pseudomonas putida. J. Bacteriol. 166, 155-161.

Brakstad, O.G., Nordtug, T., Throne-Holst, M., 2015. Biodegradation of dispersed Macondo oil in seawater at low temperature and different oil droplet sizes. Marine pollution bulletin 93, 144-152.

Bredholt, H., Bruheim, P., Potocky, M., Eimhjellen, K., 2002. Hydrophobicity development, alkane oxidation, and crude-oil emulsification in a Rhodococcus species. Can. J. Microbiol. 48, 295-304.

Bruheim, P., Bredholt, H., Eimhjellen, K., 1999. Effects of surfactant mixtures, including Corexit 9527, on bacterial oxidation of acetate and alkanes in crude oil. Appl. Environ. Microbiol. 65, 1658-1661.

Campo, P., Venosa, A.D., Suidan, M.T., 2013. Biodegradability of Corexit 9500 and dispersed South Louisiana crude oil at 5 and 25 degrees C. Environ. Sci. Technol. 47, 1960-1967.

D7730−11, A., 2011. Standard Test Method for Determination of Dioctyl Sulfosuccinate in Sea Water by Liquid Chromatography/Tandem Mass Spectrometry (LC/MS/MS). ASTM International 2011. ASTM International.

Gray, J.L., Kanagy, L.K., Furlong, E.T., Kanagy, C.J., McCoy, J.W., Mason, A., Lauenstein, G., 2014. Presence of the Corexit component dioctyl sodium sulfosuccinate in Gulf of Mexico waters after the 2010 Deepwater Horizon oil spill. Chemosphere 95, 124-130.

Haritash, A.K., Kaushik, C.P., 2009. Biodegradation Aspects of Polycyclic Aromatic Hydrocarbons (PAHs): A review. J. Hazard. Mater. 169, 1-15.

Jasper, W.L., Kim, T.L., Wilson, M.P., 1978. Droplet size distributions in a treated oil–water system., in: McCarthy, L.T., Lindblom, G.P., Walter, H.F. (Eds.), Chemical Dispersants for the Control of Oil Spills. American Society for Testing and Materials, Philadelphia, PA.

Jerrold, H.Z., 1984. Chapter 4, Biostatistical Analysis (4th Edition). Prentice Hall.

Kaku, V.J., Boufadel, M.C., Venosa, A.D., 2006. Evaluation of mixing energy in laboratory flasks used for dispersant effectiveness testing. J. Environ. Eng. Div. ASCE 132, 93-101.

Kujawinski, E.B., Kido Soule, M.C., Valentine, D.L., Boysen, A.K., Longnecker, K., Redmond, M.C., 2011. Fate of dispersants associated with the deepwater horizon oil spill. Environ. Sci. Technol. 45, 1298-1306.

Lee, K., Nedwed, T., Prince, R.C., Palandro, D., 2013. Lab tests on the biodegradation of chemically dispersed oil should consider the rapid dilution that occurs at sea. Mar. Pollut. Bull. 73, 314-318.

Li, Z., Lee, K., King, T., Boufadel, M.C., Venosa, A.D., 2009. Evaluating Chemical Dispersant Efficacy in an Experimental Wave Tank: 2—Significant Factors Determining In Situ Oil Droplet Size Distribution. 26, 1407-1418.

Lindstrom, J.E., Braddock, J.F., 2002. Biodegradation of petroleum hydrocarbons at low temperature in the presence of the dispersant Corexit 9500. Mar. Pollut. Bull. 44, 739-747.

Lunel, T., 1995. Understanding the mechanism of dispersion through oil droplet size measurements at sea., in: P. Lane (Ed.), The Use of Chemicals in Oil Spill Response. American Society for Testing and Materials, Philadelphia, PA.

Milinkovitch, T., Kanan, R., Thomas-Guyon, H., Le Floch, S., 2011. Effects of dispersed oil exposure on the bioaccumulation of polycyclic aromatic hydrocarbons and the mortality of juvenile Liza ramada. Sci. Total. Environ. 409, 1643-1650.

Mrozik, A., Piotrowska-Seget, Z., Labuzek, S., 2003. Bacterial Degradation and Bioremediation of Polycyclic Aromatic Hydrocarbons. Pol. J. Environ. Stud. 12, 15-25.

Operational Science Advisory Team, 2010. Summary report for sub-sea and sub-surface oil and dispersant detection: sampling and monitoring. Prepared for Paul F. Zukunft, U.S. Coast Guard.

Prince, R.C., 2015. Oil spill dispersants: boon or bane? Environmental science & technology 49, 6376−6384.

Prince, R.C., Elmendorf, D.L., Lute, J.R., Hsu, C.S., Halth, C.E., Senius, J.D., Dechert, G.J., Douglas, G.S., Butler, E.L., 1994. 17α(H),21β(H)-hopane as a conserved internal marker for estimating the blodegradation of crude oil. Environ. Sci. Technol. 28, 142-145.

Prince, R.C., McFarlin, K.M., Butler, J.D., Febbo, E.J., Wang, F.C., Nedwed, T.J., 2013. The primary biodegradation of dispersed crude oil in the sea. Chemosphere 90, 521-526.

Ramachandran, S.D., Hodson, P.V., Khan, C.W., Lee, K., 2004. Oil dispersant increases PAH uptake by fish exposed to crude oil. Ecotox. Environ. Safe. 59, 300-308.

Rojo, F., 2009. Degradation of Alkanes by Bacteria. Environ. Microbiol. 11, 2477-2490.

Spotte, S., Adams, G., Bubucis, P.M., 1984. GP2 medium is an synthetic seawater for culture or maintenance of marine organisms. . Zoo Biol. 3, 229-240.

Tang, W.C., White, J.C., Alexander, M., 1998. Utilization of sorbed compounds by microorganisms specifically isolated for that purpose. Appl. Microbiol. Biotechnol. 49, 117-121.

Venosa, A.D., Holder, E.L., 2007. Biodegradability of dispersed crude oil at two different temperatures. Mar. Pollut. Bull. 54, 545-553.

Wentzel, A., Ellingsen, T.E., Kotlar, H.K., Zotchev, S.B., Throne-Holst, M., 2007. Bacterial metabolism of long-chain n-alkanes. Appl. Microbiol. Biotechnol. 76, 1209-1221.

Word, J.Q., Clark, J.R., Word, L.S., 2014. Comparison of the Acute Toxicity of Corexit 9500 and Household Cleaning Products. Human Ecol. Risk Assess. 21, 19.

Yin, F., John, G.F., Hayworth, J.S., Clement, T.P., 2015. Long-term monitoring data to describe the fate of polycyclic aromatic hydrocarbons in Deepwater Horizon oil submerged off Alabama's beaches. The Science of the total environment 508, 46-56.

Zahed, M.A., Aziz, H.A., Isa, M.H., Mohajeri, L., 2010. Effect of initial oil concentration and dispersant on crude oil biodegradation in contaminated seawater. Bull. Environ. Contam. Toxicol. 84, 438-442.

Biodegradability of Different Initial Concentrations of Alaska North Slope Crude Oil Dispersed with Corexit C9500

Mobing Zhuang[1], Gulizhaer Abulikemu[2], Pablo Campo[3*], William Platten III[4], Makram T. Suidan[5], Albert D. Venosa (retired)[4] and Robyn N. Conmy[4]

1 Department of Biomedical, Chemical and Environmental Engineering, University of Cincinnati, 2901 Woodside Drive, Cincinnati, OH 45221, USA

2 Pegasus Technical Services Inc., 46 E Hollister St, Cincinnati, OH 45219 USA

3 Cranfield Water Science Institute, Cranfield University, Cranfield, Beds, MK43 0AL, UK

4 U.S. Environmental Protection Agency, NRMRL, 26 W. MLK Drive Cincinnati, OH, 45268, USA

5 Faculty of Engineering and Architecture, American University of Beirut, Bechtel Engineering Bldg. - 3rd flr. - Room 308 P.O. Box: 11-0236 Riad El Solh 1107 2020, Beirut, Lebanon

*Corresponding author: Pablo Campo
Tel: +44 (0)1234 754332
E-mail address: p.campo-moreno@cranfield.ac.uk

ED_001324_00000731-00001

ABSTRACT

Laboratory experiments were conducted using Alaska North Slope crude oil (ANS) and the dispersant Corexit 9500 (C9500) to study the biodegradability of ANS alone, ANS dispersed with C9500 at a dispersant-to-oil ratio of 1:25. To determine the role that substrate concentration plays in biodegradation kinetics, oil loads of 1,000 and 40 ppm (v:v) were compared at 25 and 5 °C. The biodegradation rate of dioctyl sodium sulfosuccinate (DOSS), which is an anionic surfactant in C9500, by the meso culture (25 °C) was approximately an order of magnitude faster in the high concentration experiment than in the low concentration experiment. At the lower temperature, the deep-water culture cryo (5 °C) had limited ability to metabolize DOSS regardless of the initial concentrations. Uptake of oil components was favored by the presence of dispersant as C9500 shortened lag phases and enhanced biodegradation rates. Alkanes and PAHs were degraded more rapidly in the high concentration samples. In the low concentration experiment, the percentage of alkanes persisting was higher than in the high concentration experiment (8-18% vs. below 1%). No significant lag period in PAH biodegradation was observed in the high oil concentration experiment compared to the low oil concentration experiment where a lag period of 12 to 16 d was observed. The extent of biodegradation of some of the less soluble aromatics increased by 4-86% under low oil concentration conditions.

KEYWORDS

Corexit 9500, biodegradation, initial oil concentration

ED_001324_00000731-00002

INTRODUCTION

To minimize the impact of oil spills, responders adopt the Net Environmental Benefit Analysis, this is, any response technique should decrease the environmental costs rather than increase them (API, 2013). When mechanical recovery or in situ burning cannot achieve the goal of protecting shorelines from oil, the impact of using dispersants is likely outweighed by the benefits, which include keeping oil from sensitive areas and speeding up biodegradation by breaking an oil slick into small droplets (Prince, 2015). Thus, it is important to study the biodegradability of dispersants and dispersed oil under various conditions for better informed use in future applications.

Makes it sound like the BCA is already foregone conclusion.

In the aftermath of the Deepwater Horizon blowout in the Gulf of Mexico (GOM), comprehensive monitoring of dispersant Corexit 9500 (C9500) and hydrocarbons in both surface and subsurface environments took place. In samples collected near the Macondo well, concentrations of dioctyl sodium sulfosuccinate (DOSS), an anionic surfactant present in C9500, ranged from 0.4 to 12 μg/L (Kujawinski et al., 2011). After the spill, Gray et al. (2014) sampled at GOM different locations and detected DOSS in subsurface waters at concentrations below 40 μg/L, while in one surface water sample close to the wellhead the value exceeded 200 μg/L. In terms of oil concentration, Lee et al. (2013) pointed out that the combination of turbulence on the GOM surface and the dispersant application could rapidly decrease oil concentrations to below 100 mg/L, dropping even further over time. Hence, these researchers recommended that biodegradation tests of dispersed oil should be conducted under more dilute concentrations to mimic real conditions.

ED_001324_00000731-00003

64 Most studies published on biodegradation of oil and dispersants prior to the Deepwater
65 incident had been conducted at concentrations well-above the reported in situ levels (Operational
66 Science Advisory Team, 2010; Prince, 2015). Several studies assessing biodegradation of oil
67 dispersed by C9500 used initial oil and dispersant concentrations from 100 to 4,500 mg/L, with
68 a dispersant-to-oil ratios (DOR) of 1:10, 1:20, or 1:25 (Campo et al., 2013; Lindstrom and
69 Braddock, 2002; Zahed et al., 2010). To our knowledge, few studies have been published on oil
70 biodegradation with initial oil and dispersant concentrations below 100 ppm (Brakstad et al.,
71 2015; Prince et al., 2013; Venosa and Holder, 2007). Thus our objective was to determine how
72 the initial amounts of oil and dispersant affect their biodegradation. We conducted high and low
73 oil concentration biodegradation experiments with Alaska North Slope crude oil (ANS) and
74 C9500 at 5 and 25 °C. C9500 is a dispersant included in the National Contingency Plan Product
75 Schedule and was applied to both the surface and submarine environment in the GOM
76 (Operational Science Advisory Team, 2010). The biodegradation of DOSS, dispersed ANS, and
77 ANS alone in high and low concentration experiments at 5 and 25 °C are reported in this paper.

78 MATERIALS AND METHODS

79 **Chemicals and Reagents**

80 The U.S. Environmental Protection Agency (EPA) provided the ANS and the dispersant
81 C9500 (Nalco Naperville, IL) used in this study. Standards for DOSS and its deuterated
82 surrogate (D_{17}-DOSS) were obtained from Aldrich (St. Louis, MO) and Isotec (Miamisburg,
83 OH), respectively. Acetonitrile, deionized ultra-filtered water, and mineral salts were purchased
84 from Fisher Scientific (Pittsburgh, PA). Dichloromethane (DCM) was obtained from Tedia
85 (Fairfield, OH). Sylon CT (Sigma-Aldrich, St. Louis, MO) was used for the deactivation of the

ED_001324_00000731-00004

glassware to prevent adherence of oil and biomass to the sides of the flasks. The protease cocktail for inhibiting enzymatic activity was also acquired from Sigma-Aldrich (St. Louis, MO).

Protease Solution Preparation

Following the instruction provided with the protease cocktail, 5 mL dimethyl sulfoxide (DMSO) was added to 1,075 mg lyophilized powder, which was previously stored unopened at -20 °C. The solution was vortexed for ten minutes before the addition of 20 mL deionized water. The resulting solution was clear. The reconstituted protease solution contained the following inhibitors: 4-(2-aminoethyl) benzenesulfonyl fluoride hydrochloride (23 mM), ethylenediaminetetraacetic acid (100 mM), bestatin (2 mM), pepstatin A (0.3 mM), and E-64 (0.3 mM).

Artificial Seawater

? define

GP2 medium was autoclaved at 121 °C for 30 min and then used as the sterile matrix in this study (Spotte et al., 1984). The salts in the GP2 medium, dissolved in DI water, were (expressed in g/L) NaCl (21.03), $MgCl_2 \cdot 6H_2O$ (9.5), Na_2SO_4 (3.52), $CaCl_2 \cdot 2H_2O$ (1.32), KCl (0.61), KBr (0.088), $NaB_4O_7 \cdot 10H_2O$ (0.034), $SrCl_2 \cdot 6H_2O$ (0.02), $NaHCO_3$ (0.17) $FeCl_3 \cdot 6H_2O$ (0.05), $Na_5P_3O_{10}$ (0.297) and KNO_3 (2.89). The GP2 pH was ≈ 7.5.

Microbial Cultures

The original cultures were isolated from the surface water of the GOM (meso) in the vicinity of the Macondo well and water close to the plume location at a depth of 1,240 m near the wellhead (cryo) by EPA's Gulf Breeze, FL research laboratory. Enriched inocula were procured

ED_001324_00000731-00005

as follows: in 2-L shake flasks, 2.5 mL SLC were added to 500 mL of the original unfiltered GOM seawater supplemented with 2.8 g/L KNO_3, 0.55 g/L NaP_3O_{10}. The flasks were rotated (400 rpm) at 5 °C (cryo culture) and 25 °C (meso culture). The adequate growth times were 7 d for the meso culture and 17 d for the cryo culture. After these periods, cells were harvested by centrifugation (6,000 × g for 30 min at 4 °C) and the pellets preserved in 10% glycerol at -70 °C. Before shipping to EPA-Cincinnati, 1 mL of each thawed culture were added to shake flasks containing 500 mL GP2 medium fortified with 2.5 mL of SLC. The meso culture was harvested after 6 days of growth and the cryo culture after 29 days. The cultures used in the experiments of this study were grown at EPA (Cincinnati, OH) by transferring the original cultures from EPA's Gulf Breeze to GP2 medium supplemented with South Louisiana crude oil (SLC). The meso culture was harvested after 3 weeks of growth and the cryo culture after 5 weeks. The harvested culture was processed in the same fashion as mentioned previously: centrifugation (6,000 × g for 30 min at 4 °C) and the pellets preserved in 10% glycerol at -70 °C. Upon use in experiments, the cultures were defrosted at room temperature, washed with 0.85% saline solution to remove glycerol, centrifuged, and brought back up to the frozen volume.

Experimental Setup and Sampling

You never actually discuss how much inoculum you add to each 100 mL flask.

A summary of the experimental setup is shown in Tables S1 and S2 for the high and low oil concentration experiments, respectively. For the high concentration experiments, 6 treatments were tested at 5 and 25 °C in triplicate: C9500 dispersant alone, ANS oil alone, ANS dispersed with C9500, and the corresponding killed controls (KCs). The 5 °C experiment required 11 sampling events in triplicate (0, 2, 4, 8, 12, 16, 24, 32, 40, 48 and 56 d), while 9 events were conducted at 25 °C (0, 2, 4, 8, 12, 16, 24, 32 and 40 d). At each sampling event, triplicate shake

ED_001324_00000731-00006

128 flasks of each treatment along with KCs were sacrificed, except for the ANS alone KCs which
129 were analyzed at the beginning and end of the experiment.

130 The same treatments were included in the low concentration experiment, but both oil and
131 dispersant concentrations were prepared at 4% of the initial loads used in the high concentration
132 experiment. Additionally, a seventh treatment involved the use of triplicate KCs containing the
133 enzyme protease (0.5 mL) to neutralize the enzymatic DOSS hydrolysis. This treatment was
134 included only in the low concentration experiment. The sampling events were conducted
135 similarly to the high concentration experiment with the exception of the protease treatment,
136 which was sampled at 0, 12, 24, 35, 46 and 56 d and 0, 8, 18, 28, 38 and 48 d for the 5 and 25 °C
137 experiments, respectively.

138 After all treatments were prepared, the appropriate cultures were spiked (0.5 mL) and the
139 flasks were placed on orbital shakers. The shakers were operated at 200 rpm and kept in the
140 appropriate constant temperature rooms until the expected sampling events. All KCs were
141 sterilized by adding 1 mL sodium azide stock (50 g/L) into the 100 mL of GP2 medium.

142 **High Concentration Treatments**

1mL : 1200mL ? 1:25 ?

143 To evaluate the biodegradation of dispersed oil, 2 L baffled beakers were used in which
144 40 μL of C9500 and 1,000 μL of ANS were added to 1,200 mL of GP2 to achieve a volumetric
145 DOR ratio of 1:25. Subsequently, the beaker containing the mixture was shaken at 200 rpm for
146 10 minutes and then left stationary for an additional 10 min, then the dispersion was transferred
147 to a 20-L continuously mixed carboy. The above procedure was repeated until the volume in the
148 carboy reached 14 L. Subsequently, 100 mL aliquots of the mixtures were transferred to the
149 shake flasks. The second treatment was for the evaluation of oil as the only substrate. ANS (100
150 μL) was added directly to shake flasks containing 100 mL sterile GP2 medium, which yielded an

.10 mL : 100 mL → 1:1000 ratio

This is the only treatment that doesn't involve

estimated oil concentration of 1,000 ppm by volume. The oil added to the ANS alone and dispersed ANS treatments aimed to result in the same oil concentration by volume. To evaluate the degradation of dispersant alone, 480 µL of C9500 was added to 14 L of sterile GP2 medium in a continuously mixed carboy; after 30 min, 100 mL aliquots of this mixture were dispensed into shake flasks for this treatment.

Low Concentration Treatments

.2 mL : 1200 mL ≟ 1:25 ?

To prepare the low concentration dispersed oil, a single batch of 1,200 mL GP2 was spiked with 200 µL ANS onto the water surface followed by addition of 8 µL C9500 onto the oil slick, which yielded a volumetric DOR of 1:25 in a 2 L baffled beaker. The shaker was started at a very slow speed and was ramped up to 200 rpm gradually. The beaker was placed on a shaker for 20 min and then remained stationary for 10 minutes. Subsequently, 3 L of the dispersion were poured into a 20 L carboy under continuous mixing and 12 L of sterile GP2 was added for dilution purposes. Overall, the oil and dispersant amounts in this treatment were approximately 4% of that in the high concentration experiment. Finally, shake flasks were filled with 100 mL aliquots of the diluted dispersed oil. Low concentration ANS alone was prepared by spiking approximately 4 µL of oil into shake flasks containing 100 mL sterile GP2, which yields an oil concentration of 40 ppm by volume (i.e., 4% of the high concentration oil alone experiment). The low concentration dispersant alone treatment was prepared in a single batch of sterile GP2 (14 L) spiked with approximately 20 µL of C9500. The batch was mixed for 30 minutes and, subsequently, 100 mL aliquots were transferred into the shake flasks.

already on it.

shaken for

I only have 1.2 L Assume you made many batches

no stationary phase?

Oil components and Dispersant Analysis

.004 mL : 100 mL

4:100 000 = 4×10^{-5}

$\frac{.2\ mL\ ANS}{1.2\ L\ H_2O}$ $\frac{3\ L\ H_2O}{(3+12)\ L\ H_2O}$ = 3.3×10^{-5}

To monitor C9500 degradation, DOSS was measured by liquid chromatography tandem mass spectrometry (LC-MS/MS) following the Standard method ASTM D7730−11 (2011). The targeted oil components were pristane (PR), phytane (PH), normal paraffins (n-C_{10-35}) and 2-, 3- and 4-ring PAH compounds and their alkylated homologues (C_{0-4}-naphthalenes, C_{0-3}-fluorenes, C_{0-3}-dibenzothiophenes, C_{0-4}-phenanthrenes/anthracenes, C_{0-4}-napthbenzthiophenes, C_{0-2}-pyrenes, C_{0-4}-chrysenes). The concentrations of these analytes were normalized to hopane present in the oil (Prince et al., 1994). Details of oil extraction by DCM and sample preparation methods can be found elsewhere (Campo et al., 2013). For the high concentration experiment, oil analysis was conducted with a 6890 GC coupled with a 5973 mass spectrometry from Agilent (Palo Alto, CA). In the low concentration experiment, an Agilent (Palo Alto, CA) 7000 GC Triple Quad system was used. The quantification range for the single quad and triple quad mass spectrometry are 1-30 μg/L and 0.5-10 μg/L, respectively. In the case that the concentration of oil hydrocarbons is below the range, we used the quantification results as an estimation of the actual amount. The same column, a DB-5MS column (30m × 0.25mm, 0.25μm film thickness), was used to achieve chromatographic separation of analytes in both instruments. The method was a modification based on EPA Method 8270D (2007).

1)

2)

RESULTS AND DISCUSSION

Degradation of DOSS

High Concentration Experiment. Live samples revealed an extremely fast removal rate of DOSS at 25 °C (Fig. 1A-B, open symbols) with extents exceeding 95% after 2 d in dispersed oil (Fig. 1B) and 4 d in C9500 alone (Fig. 1A). The first order rate coefficients were -1.82 ± 0.25 d^{-1} (ANS+C9500) and -0.71 ± 0.024 d^{-1} (C9500 alone). The presence of oil enhanced DOSS

typically in my field rate constants are always positive. ~~It is a rate constant, not~~

ED_001324_00000731-00009

194 biodegradation by a factor of approximately 2.6. Disappearance of DOSS was also observed in

195 KCs at 25 °C, with zero order rates of -138 ± 7 and -221 ± 11 μg L^{-1} d^{-1} for C9500 alone (Fig.

196 1C) and dispersed oil (Fig. 1D), respectively. As monooctyl sulfosuccinate (MOSS) was found in

197 KCs, Campo et al. (2013) explained this abiotic loss in terms of hydrolysis which was confirmed

198 by (Batchu et al., 2014). The presence of oil significantly enhanced DOSS removal in KCs ($p <$

199 0.0001).

200 In contrast with the rapid removal of DOSS at 25 °C, the biotic and abiotic processes at 5

201 °C were much slower. DOSS persisted for 40 d before its concentration decreased in all

202 treatments. The difference in DOSS concentration between live samples and parallel KCs in the

203 dispersed oil treatment was statistically insignificant at days 48 ($p = 0.078$) and 56 ($p = 0.726$).

204 In the C9500 alone treatment, DOSS was significantly lower in live samples than in KCs at days

205 48 ($p = 0.0015$) and day 56 ($p = 0.023$). These results point to biodegradation as the predominant

206 DOSS removal mechanism as opposed to hydrolysis.

ED_001324_00000731-00010

If you are analyzing as a first-order loss, you should plot as ln C -v- t, or ln C/Co -v- t. to allow the reader to really see the goodness of fit.

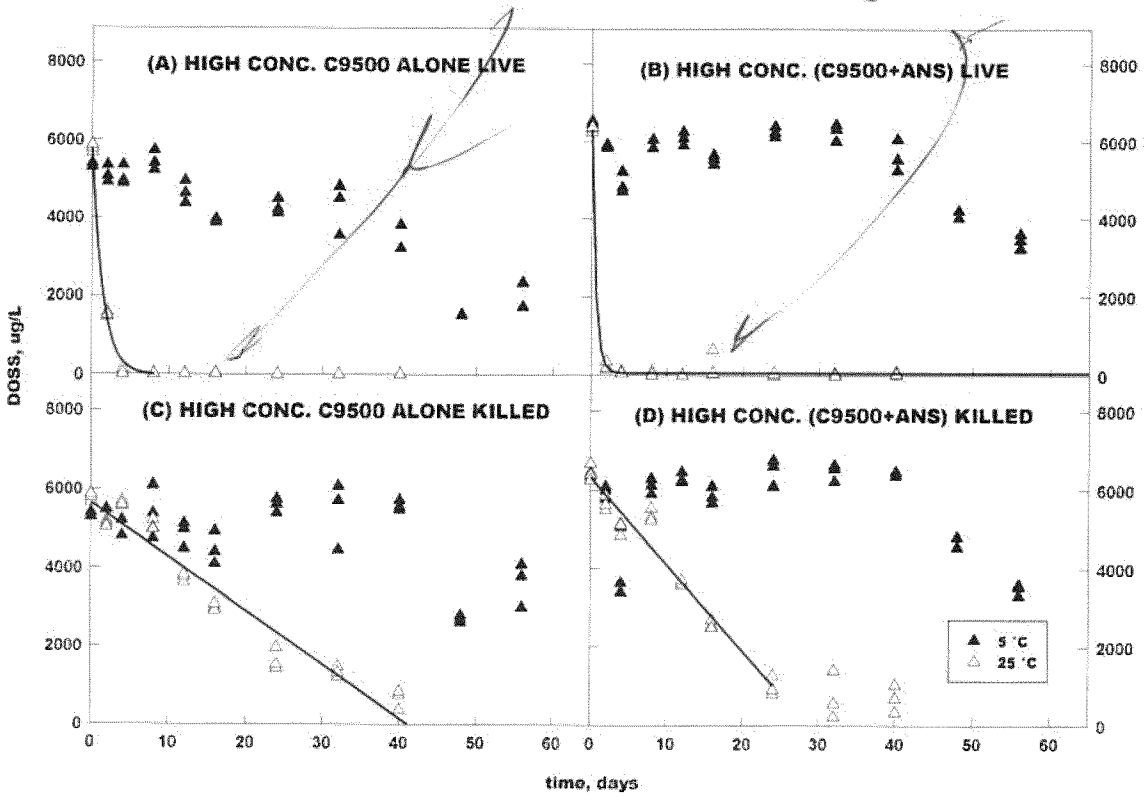

Figure 1. Disappearance of DOSS in high concentration experiment in the absence (A, C) and Presence (B, D) of ANS at 5 °C and 25 °C. Live samples are in panel A and B, whereas killed controls are in panels C and D.

Low Concentration Experiment. At 25 °C and for the dispersed oil treatment, no lag period was observed in DOSS uptake, which showed a first-order constant rate of -0.16 ± 0.015 d^{-1} (Fig. 2B). In the absence of oil (Fig. 2A), we observed an acclimation period of 2 d followed by DOSS biodegradation (-0.07 ± 0.009 d^{-1}). The presence of oil favored DOSS removal as was observed in the high concentration experiment . Removal extents over 95% for DOSS required 32 and 48 d in the presence and absence of oil, respectively. In the corresponding KCs, DOSS concentrations decreased following zero-order kinetics, with constant rates of -4.1 ± 0.3 μg L^{-1} d^{-1} (C9500 alone, Fig. 2C) and -5.1 ± 0.4 μg L^{-1} d^{-1} (C9500 and ANS, Fig. 2D).

How did you conclude this? There seems to be some anomalies w/ the initial point even w/ll KCs.

For the high concentration experiment at 25 °C and regardless of the presence of oil, the time series concentration of DOSS in the live samples rapidly declined to zero and clearly

separated from the values measured in the corresponding KCs. In the low concentration experiment, it appeared that DOSS disappearance with time in both treatments, C9500 alone and dispersed ANS, overlapped with the abiotic losses observed in the KCs (Fig. 2). To differentiate between microbial activity and hydrolysis, we compared by a *t*-test ($\alpha = 0.05$) the average DOSS concentrations measured in live samples with those values found in the parallel KCs. Live samples significantly departed from the controls after 4 d ($p = 0.0227$) and 16 d ($p = 0.0053$) in the presence and absence of ANS, respectively. At early stages in the experiment, we could not identify the predominant removal mechanism for DOSS but, eventually, microbial uptake prevailed as the main process in terms of rate and extent.

DOSS presented a faster microbial uptake at both the higher initial concentration and temperature. Nevertheless, based on our low concentration results, it is reasonable to infer that biodegradation of DOSS at the surface of GOM might not happen as rapidly since dilution and emulsification can attenuate the concentration of dispersant. In this fashion, DOSS was detected with a reporting limit of 0.25 μg L^{-1} and a highest concentration of 229 ±16 μg L^{-1} in surface water samples collected 1-2 months after the spill near the Macondo well (Gray et al., 2014).

This is discussion out of place.

DOSS concentration remained unchanged in live samples and KCs under 5 °C and low oiling conditions (Fig. 2, closed symbols). Such finding agreed with studies by Kujawinski et al. (2011) and Gray et al. (2014) who concluded that subsurface degradation of DOSS was minimal. Campo et al. (2013) observed no hydrolysis or biodegradation of DOSS in SLC at 5 °C within 42 d.

ED_001324_00000731-00012

Is the broken scale necessary?

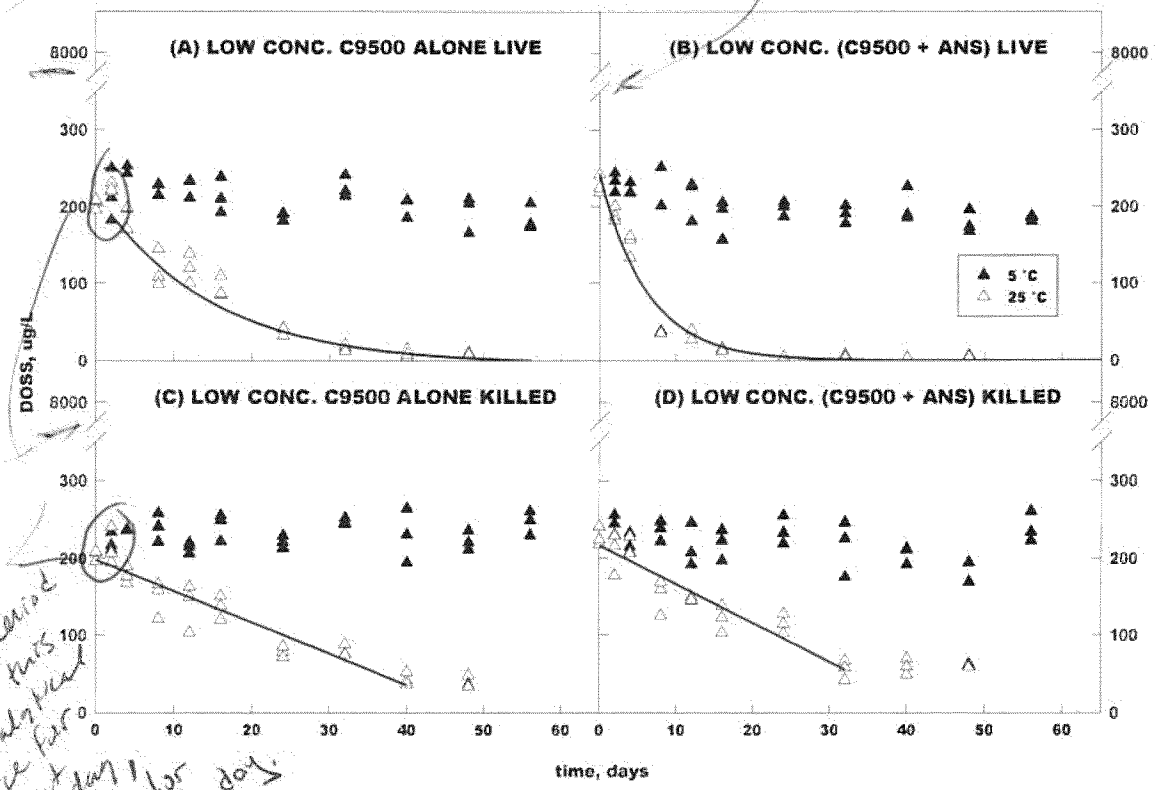

was there really an abiotic acclimation period too? Or is this analytical noise for that day? Or for 0-day?

Figure 2. Disappearance of DOSS in low concentration experiment in the absence (A, C) and Presence (B, D) of ANS at 5 °C and 25 °C. Live samples are in panel A and B, whereas killed controls are in panels C and D.

We also included a series of dispersed oil KCs containing a protease cocktail (Fig. 3A), which inhibits enzymatic activity to clarify the abiotic DOSS disappearance. At 25 °C, the addition of inhibitor clearly slowed down the hydrolysis process as the zero-order rate constant in the protease KCs was -3.7 ± 0.4 μg L^{-1} d^{-1} (Fig. 3A) as opposed to -5.1 ± 0.4 μg L^{-1} d^{-1} (Fig. 3B) obtained for the regular KCs ($p = 0.021$). Such finding suggests the enzymatic nature of DOSS hydrolysis. Nevertheless, different enzymes may be involved in the process so that the protease cocktail could not block all of them. In the protease controls at 5 °C, DOSS persisted throughout the experiment as observed in the regular KCs for that temperature. This indicates that either the lower temperature attenuated DOSS breakdown, the cryo culture lacked the required enzymes, or a combination of both causes.

ED_001324_00000731-00013

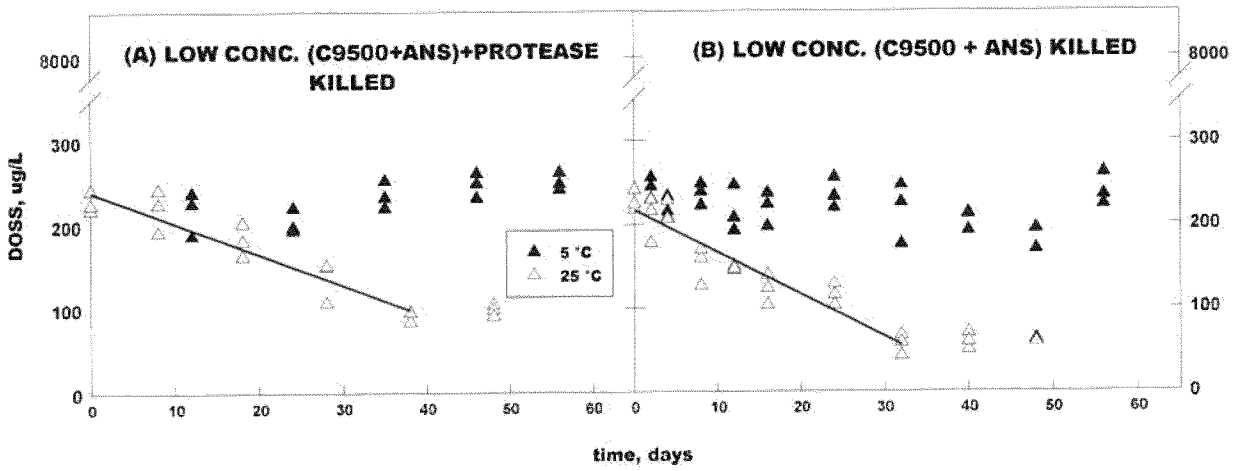

Figure 3. Disappearance of DOSS in low concentration dispersed oil killed controls in the presence (A) and absence (B) of protease at 5 and 25 °C.

Total Alkane Degradation

High Concentration Experiment. Total alkanes at both temperatures are presented in Fig. 4 A-B. At 25 °C, the meso culture metabolized the aliphatic fraction with a first-order rate constants of -0.91 ± 0.10 and -0.85 ± 0.04 d^{-1} in the absence and presence of C9500, respectively. For both treatments, the extent of removals reached 99% after 4 days. As expected, aliphatics degraded slower at 5 °C. In the dispersed oil treatment, this fraction followed first-order kinetics (-0.24 ± 0.01 d^{-1}) while, for the oil alone samples, alkanes presented a linear decay during the first 8 d followed by first order kinetics of similar rate (-0.25 ± 0.03 d^{-1}). After days 16 (dispersed oil) and 24 (oil alone), the alkane extent of removal was 99% for the lower temperature.

why was the ratio of alkanes:hopane different for the 5°C (as well)? The ratio wasn't conserved through the preparation process. If the [~] was supposed to be 4% lower for "low conc", which (alkanes or hopane) were not on target?

268

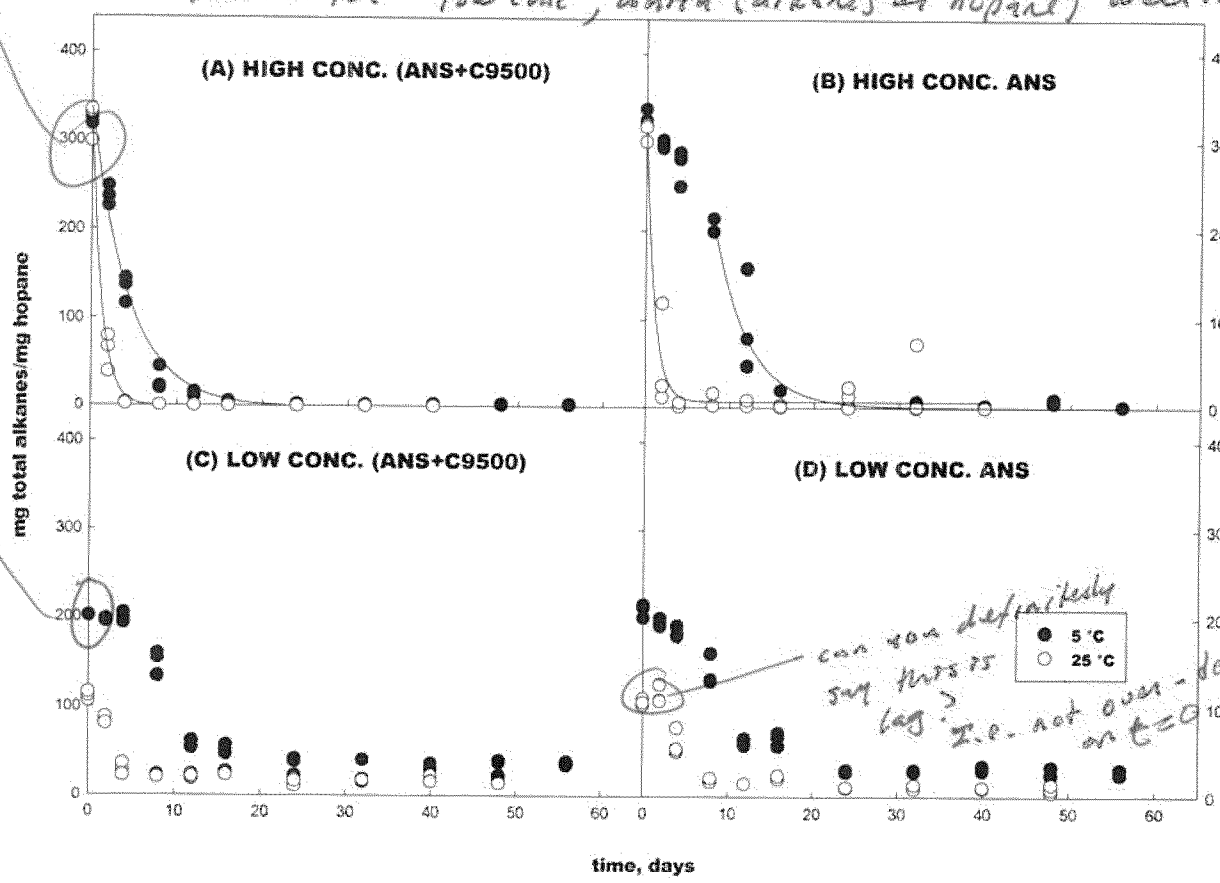

can you definitely say this is lag? I.e. not over-dependent on t=0 data?

269

270 **Figure 4. Biodegradation of hopane-normalized total alkanes at both temperatures in high**
271 **concentration treatments (A, B) and low concentration treatments (C, D).**

272 *Low Concentration Experiment.* In this experiment, the initial total alkane concentrations
273 were considerably different at 5 and 25 °C (Fig. 4 C and D). In fact, the meso culture showed
274 background concentrations of PAHs and hopane, the conservative biomarker to which all the
275 target analytes concentrations are normalized. The hopane background levels were comparable to
276 those measured in the initial oil added to the flasks. Hence, at time zero, the total alkane
277 concentration normalized to hopane at 25 °C were almost half of the corresponding value at 5
278 °C.

So [hopane] was not diluted (whether 1:25 or 1:1200, depending on which is correct) Will this raise red-flags?

279

This is not very clear. It seems that the $[hopane]_{high}$ was equal to the $[hopane]_{ANS}$ despite the ANS was diluted 1:1200, or 1:25 ...?

at what time?

At 25 °C, the alkane residual concentrations ranged from 8 to 18% of the initial values (Fig. 4 A and B). In the oil alone treatment, alkane biodegradation started after a lag phase of 2 d, while these organics were promptly metabolized in the dispersed oil treatment. At 5 °C, the cryo culture required 4 d for acclimation in the dispersed oil. In the absence of dispersant, after a slow and steady linear decay, fast disappearance of alkanes occurred between days 8 and 12. This suggests that C9500 reduced the length of the acclimation phase for alkane uptake.

see graph earlier page.

Table 1 summarizes the actual concentrations of total alkanes (not normalized to hopane) for the first and last sampling event for both the high and low concentration experiments. It is noted that a higher alkane residual amount was observed in the low concentration experiment than the high concentration one. This was especially true considering the combination of high temperature and dispersant application, where the alkane concentrations were less than the detection limit and 142 ± 4 μg L^{-1} in the last sampling event of low concentration samples. One possible explanation is that carbon and energy sources were limited in the low concentration microcosms. Fewer microorganisms provided less microbial surface for hydrophobic compounds to interact with, which resulted in less complete degradation of alkanes.

So presumably the only difference between high and low is the amount of ANS (i.e. for ANS alone). So nutrient limiting theory suggests that the the other nutrients (other than alkanes) must be present in ANS. Or was there a difference in the initial inoculum (see p 6).

I sort of assumed you inoculated all the same cells/reactor, whether high or low ANS.

Table 1. Average and standard deviations (sd) of total alkanes and PAHs concentration in the high and low concentration experiment at first and last sampling event.

Samples			5 °C ANS alone average (μg/L)	sd	25 °C ANS alone average (μg/L)	sd	5 °C ANS+C9500 average (μg/L)	sd	25 °C ANS+C9500 average (μg/L)	sd
High Conc.	Alkanes	First	47,400	604	43,300	9,390	24,600	973	27,200	126
		Last	201	26	36	42	186	52	0	0
	PAHs	First	14,500	110	13,700	3,090	7,310	323	8,790	94
		Last	3,040	281	2,470	300	1,300	74	1,270	158
Low Conc.	Alkanes	First	2,010	202	1,740	149	1,420	72	1,130	39

	Last	216	21	83	75	225	13	142	4
PAHs	First	482	53	773	25	330	12	453	14
	Last	71	5	88	5	58	10	80	4

Degradation of Individual Alkanes

High Concentration Experiment. Table S3 summarizes the first-order biodegradation coefficients for individual alkanes. At 25 °C, among all the compound monitores only n-C_{10} was biodegraded faster (-2.00 vs. -1.34 d^{-1}) with the addition of dispersant. Branched alkanes exhibited similar rates regardless of the presence of C9500, although higher variability among triplicates was observed in the oil alone samples (Fig. S1 A and B). At 5 °C, consistently higher rates for n-$C_{10\text{-}27}$ were observed in the dispersed oil treatment when compared to the oil alone treatment. Also, no lag period for the biodegradation of branched alkanes occurred when C9500 was added, whereas an 8-day lag period occurred in the absence of dispersant.

Low Concentration Experiment. As depicted in Figs. S1-5 (panels C and D), only n-$C_{10\text{-}16}$ was completely removed at both temperatures in the low concentration experiment. In this case, a more qualitative approach was used by comparing the disappearance time. At 25 °C in the low oil concentration experiment, n-C_{10} was degraded faster in the presence of dispersant, disappearing completely before day 2, whereas in the absence of C9500, its depletion was achieved only after day 8. The biodegradation of n-C_{10} was also accelerated when C9500 was present at 5 °C, as shown in Table S4 (-0.47 vs -0.63 d^{-1}). At both temperatures, branched alkanes were not degraded faster in the presence of dispersant, as shown in Table S4 and Fig. S1 C-D.

so straight-chain enhanced w/ dispersant
branched not-enhanced " "

ED_001324_00000731-00017

The major mechanism of uptake of water-insoluble substrates (i.e., alkanes) is generally recognized as direct interaction between microbes and the hydrophobic substance (Rojo, 2009; Wentzel et al., 2007) and the effects of surfactant on such process are inconclusive (Bredholt et al., 2002; Bruheim et al., 1999; Tang et al., 1998). Both conducive and inhibitory effects of dispersant on oil biodegradation have been reported (Lindstrom and Braddock, 2002; Prince et al., 2013; Venosa and Holder, 2007). In this study, C9500 exhibited similar effects on the biodegradation of alkanes in the high and low concentration experiments. Such effects included enhancement of biodegradation rates and shortening of lag periods. Rate enhancements were more notable in the high concentration experiment, whereas C9500 clearly shortened lag phases in the lower concentration tests. ~~[illegible] I would say high and low DNS were not similar. HI: no C9500 effect on~~ quite mixed results hi/low 5°/25°. No consistency.

The application of dispersants to an oil slick promotes the formation of small oil droplets by decreasing the interfacial tension between oil and water (Jasper et al., 1978; Li et al., 2009; Lunel, 1995). Consequently, the total interfacial area of oil droplets for microbes to interact with is increased. In the high concentration experiment, exposure of substrates to the microbes is enough that biodegradation can initiate soon after inoculation. In this case, dispersants assisted biodegradation mainly by increasing interfacial area for microbes to interact with oil. For the low concentration experiment, the observed long acclimation phase at both temperatures, especially in the absence of C9500, was possibly due to limited exposure of alkanes to the microorganisms in the beginning. Since the oil load, appearing as an iridescent sheen, is so low, the mixing energy in the flasks could be high enough to produce similar droplet size distribution in the oil alone and dispersed oil treatments. Thus, C9500 may have shortened the lag phase in the low concentration experiment by promoting the attachment of microbes to the oil droplet.

not at 25°C and [High]

However, you got faster removal w/ C9500. line 307 and line 309

The largest lag-Ø in [low] was seen WITH C9500 at 5°C.

Is a given alkane molecule less likely to encounter a microbe in the [low] exp? I ~~[illegible]~~ am guessing the [microbe] is the same.

335 **Total Aromatics Degradation**

336 *High Concentration Experiment*. Fig. 5A-B presents total PAH biodegradation data for
337 the high concentration experiment at both temperatures. Aromatics removals of 42 and 24%
338 occurred by day 2 in the dispersed oil and the oil alone treatment, respectively. This difference in
339 extent was significant ($p < 0.0001$), which indicates a positive effect of the dispersant. At 5 °C,
340 the time for attaining maximum level of PAHs removal in non-dispersed treatment took twice as
341 much time as in dispersed oil treatment 16 days vs. 8 days (solid symbols in Fig. 5B and 5A,
342 respectively). The overall PAHs removals in the presence and absence of dispersant were 86%
343 and 82%, respectively.

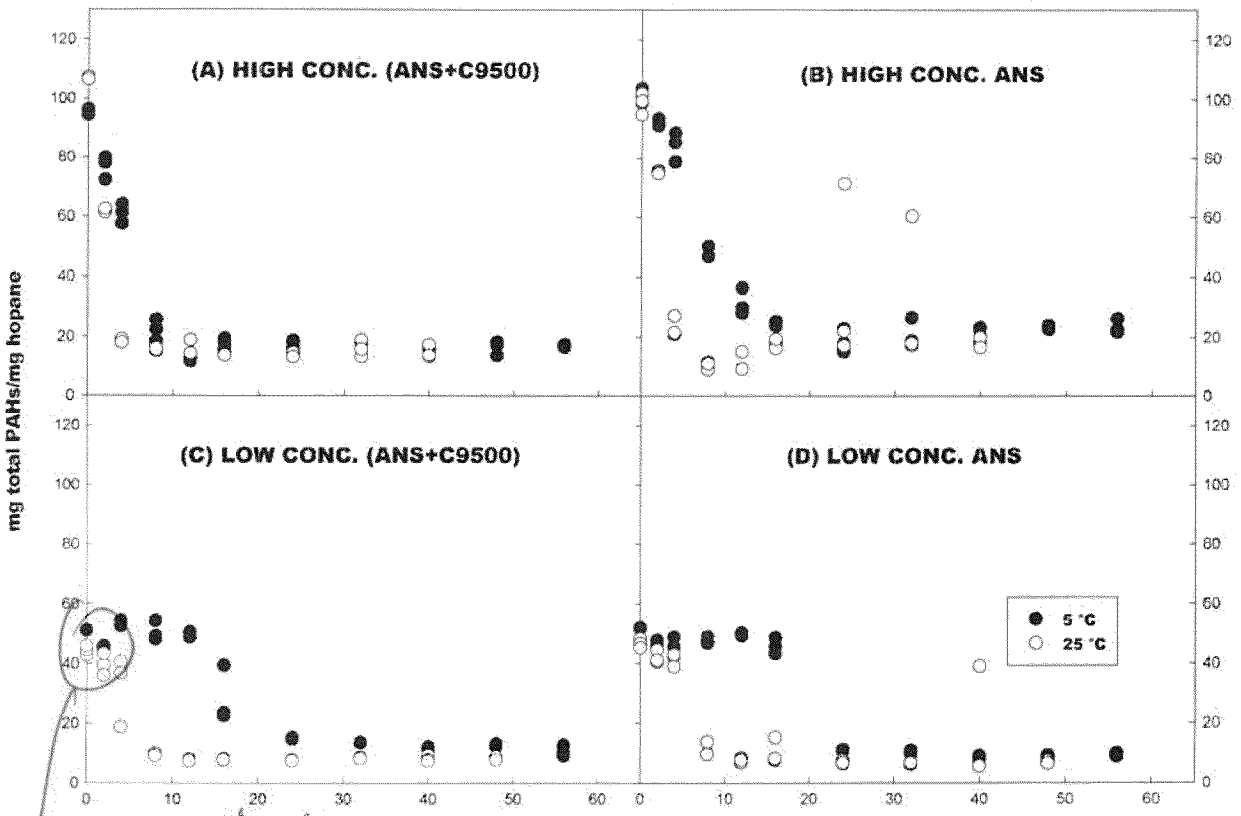

344

So while alkanes, the hopane anomalie didn't affect this initial ratio?? This suggests that [hopane] was not the problem w/ the alkanes, as the PAHs are both high, like hopane, in both 5°C 25°C.

Figure 5. Biodegradation of hopane-normalized total PAHs at both temperatures in high concentration treatments (A, B) and low concentration treatments (C, D).

Low Concentration Experiment. As shown in Fig. 5C-D, when comparing the two low concentration treatments at 25 °C (open symbols), the only difference was in one replicate of dispersed oil on day 4, which had significantly lower total PAH concentration than the parallel diluted oil alone samples. At the high temperature (open symbols), the patterns of PAH degradation were similar in the absence and presence of C9500, regardless of initial concentration. The treatment without dispersant experienced higher variability. The lag period at the low temperature (closed symbols) was longer than at 25 °C; it lasted 12 and 16 days for dispersed oil and oil alone, respectively. For the sampling event on day 16, the extent of PAH removal was 20 to 50% in the replicates of dispersed oil sample, while it was negligible in the treatment without dispersant.

Transport of compounds from non-aqueous phase to aqueous phase is often the most rate-limiting step in the biodegradation of PAHs. Surfactants can enhance the dissolution of PAHs by increasing interfacial area of oil droplet and subsequently increase the bioavailability of PAHs to microorganisms (Haritash and Kaushik, 2009; Mrozik et al., 2003). The effect of C9500 on the biodegradation of total PAHs was less pronounced in the low concentration experiment than in the high concentration experiment, because this effect was observed only in one or more replicates in a single sampling event. This finding is consistent with our previous assumption about low concentration experiment: droplet size distribution in the oil alone and dispersed oil treatments are similar. Dispersion in the oil alone microcosms might have been efficient enough even without the addition surfactant, considering the mixing energy was sufficient (Kaku, 2006) and the initial presence of oil was an iridescent rainbow-colored sheen. Clearly, the comparison

Is this a diff. effect than w/ alkanes? (lines 323-334)

ED_001324_00000731-00020

between our low concentration dispersed oil samples and oil alone samples indicates that dispersants had less enhancing effect on the bio-uptake of PAHs after dilution. Nevertheless, most toxicity studies on dispersed oil concluded that the presence of dispersant increased environmental risk for aquatic organisms living in the water column (Milinkovitch et al., 2011; Ramachandran et al., 2004), which is possibly due to their relatively high concentration of oil and dispersant in the laboratory tests.

(relative to environmental concentrations)

Individual Aromatics Degradation

?

so if there was > neg., then the first-order model didn't work. What if there was < neg at the end, but "negligible" by the next-to-last event? Could it be modeled?

High Concentration Experiment. A first-order model could be used to fit the biodegradation of the individual PAHs that had a negligible fraction persisting by the end of the high concentration experiment. At both temperatures, the biodegradation rates of naphthalene, phenanthrene, fluorine, and dibenzothiophene and their homologues in the high concentration experiment were consistantly higher in the presence of dispersant (Table S5). The greatest enhancement was observed with naphthalene at 25 °C, which was 2.9-fold higher than at 5 °C (-1.94 d^{-1} vs. -0.68 d^{-1}). The surfactant likely assisted the transfer of more soluble compounds from the oil phase to the aqueous phase through the formation of small oil droplets and the resultant increase in interfacial area. Because the bio-uptake of aromatics is mostly from aqueous phase (Haritash and Kaushik, 2009; Mrozik et al., 2003), C9500 promoted the biodegradation of PAHs by increasing their bioavailability in water.

Low Concentration Experiment. Among the low concentration individual PAHs, the time-varying concentration of specific aromatics could be fitted to a first-order kinetics model (rates shown in Table S6), and the results revealed reduced rates due to dilution (low vs. high), especially when C9500 was present (i.e. naphthalene: -0.36 d^{-1} v -1.94 d^{-1}). However, we could

This phenom defies the principle of first-order reaction. First-order reactions have rate constants that are not dependent on initial concentration

ED_001324_00000731-00021

not fit a first-order model for the other PAH compounds in the low concentration experiments because of the long lag period and the immediate and nearly complete removal after biodegradation started. As mentioned before, C9500 ~~acted less effectively~~ on the biodegradation of total PAHs in the low concentration experiment, because different PAH concentrations in parallel dispersed oil and oil alone samples was observed only at one or more replicates in a single sampling event (25 °C: day 4, 5 °C: day 16). Nevertheless, C_4-naphthalene, C_{2-4}-phenanthrene, C_{2-3}-fluorene, and naphthobenzothiophene were removed at higher extent in the low rather than in the high concentration samples (Fig. S6). The increase in removal extent for the aforementioned aromatics were 6-14%, 4-47%, 14-54%, and 55-86% respectively. Zahed et al. (2010) also observed similar enhancement of crude oil removal extent in low oiling experiments. In the low concentration experiment, the starting PAH concentrations were equal to or below the remaining residual found in the high concentration experiment, but the cultures were able to degrade the aromatic compounds to an even lower level, as shown in Table 1. The reasons are a combination of the following: (1) the alkylated structure of these compounds led to less aqueous dissolution and less susceptibility to microbial attack; (2) their aqueous uptake was primarily diffusion, for which neither energized membrane nor adenosine triphosphate was essential (Bateman et al., 1986). Taking C_2-phenanthrene for example, it was fully degraded in the low concentration experiment, whereas its removal extent ranged from 66% to 94% when the initial oil concentration was high. The enhancement in the extent of removal under diluted conditions was more remarkable at low temperature, which contributed to our conclusion that solubility was the limiting factor for those compounds to be biodegraded. Whether oil concentration is high or low, pyrene, chrysene and naphthobenzothiophene homologues persisted until the last sampling event at both temperatures, as depicted in Figs. S7 and S8. The heavy

the impact of C9500 ~~the had much less impact~~

was difficult to assess

This seems to suggest that it is just "abiotic" sorption to the cell wall, and not active uptake, or biodegradation necessarily. And since the ratio PAH: cell area is lower a [low], then voila?

PAHs, such as chrysene, are likely to be retained on a beach for several years, according to Yin et al. (2015), who conducted research that monitors the submerged oil mats and surface residual oil balls off Alabama's beach affected by the 2010 DWH incident.

417 ACKNOWLEDGMENTS

418 We thank Jan Kurtz and Diane Yates from EPA's Gulf Ecology Division (GED) at Gulf
419 Breeze, FL, who collected the water samples in the GOM and performed the enrichments and
420 provided them for our experiments. The research was a product of the U.S. Environmental
421 Protection Agency's National Risk Management Research Laboratory (NRMRL) and was
422 partially funded by EPA, NRMRL, Cincinnati, OH, under Pegasus Technical Services, Inc.
423 Contract EP-C-11-006.

424 REFERENCES

425 2007. U.S. Environmental Protection Agency, EPA 8270D Semivolatile organic compounds by
426 gas chromatography/mass spectrometry (GC/MS), 3rd. ed, Washington, D.C.

427 API, 2013. Net Environmental Benefit Analysis for effective oil spill preparedness and response.
428 2013. http://www.api.org/~/media/Files/EHS/Clean_Water/Oil_Spill_Prevention/NEBA/NEBA-
429 Net-Environmental-Benefit-Analysis-July-2013.pdf.

430 Batchu, S.R., Ramirez, C.E., Gardinali, P.R., 2014. Stability of dioctyl sulfosuccinate (DOSS)
431 towards hydrolysis and photodegradation under simulated solar conditions. Sci. Total. Environ.
432 481, 260-265.

433 Bateman, J.N., Speer, B., Feduik, L., Hartline, R.A., 1986. Naphthalene association and uptake in
434 Pseudomonas putida. J. Bacteriol. 166, 155-161.

435 Brakstad, O.G., Nordtug, T., Throne-Holst, M., 2015. Biodegradation of dispersed Macondo oil
436 in seawater at low temperature and different oil droplet sizes. Marine pollution bulletin 93,
437 144-152.

438 Bredholt, H., Bruheim, P., Potocky, M., Eimhjellen, K., 2002. Hydrophobicity development,
439 alkane oxidation, and crude-oil emulsification in a Rhodococcus species. Can. J. Microbiol. 48,
440 295-304.

441 Bruheim, P., Bredholt, H., Eimhjellen, K., 1999. Effects of surfactant mixtures, including Corexit
442 9527, on bacterial oxidation of acetate and alkanes in crude oil. Appl. Environ. Microbiol. 65,
443 1658-1661.

ED_001324_00000731-00024

Campo, P., Venosa, A.D., Suidan, M.T., 2013. Biodegradability of Corexit 9500 and dispersed South Louisiana crude oil at 5 and 25 degrees C. Environ. Sci. Technol. 47, 1960-1967.

D7730–11, A., 2011. Standard Test Method for Determination of Dioctyl Sulfosuccinate in Sea Water by Liquid Chromatography/Tandem Mass Spectrometry (LC/MS/MS). ASTM International 2011. ASTM International.

Gray, J.L., Kanagy, L.K., Furlong, E.T., Kanagy, C.J., McCoy, J.W., Mason, A., Lauenstein, G., 2014. Presence of the Corexit component dioctyl sodium sulfosuccinate in Gulf of Mexico waters after the 2010 Deepwater Horizon oil spill. Chemosphere 95, 124-130.

Haritash, A.K., Kaushik, C.P., 2009. Biodegradation Aspects of Polycyclic Aromatic Hydrocarbons (PAHs): A review. J. Hazard. Mater. 169, 1-15.

Jasper, W.L., Kim, T.L., Wilson, M.P., 1978. Droplet size distributions in a treated oil–water system., in: McCarthy, L.T., Lindblom, G.P., Walter, H.F. (Eds.), Chemical Dispersants for the Control of Oil Spills. American Society for Testing and Materials, Philadelphia, PA.

Kaku, V.J., Boufadel, M.C., Venosa, A.D., 2006. Evaluation of mixing energy in laboratory flasks used for dispersant effectiveness testing. J. Environ. Eng. Div. ASCE 132, 93-101.

Kujawinski, E.B., Kido Soule, M.C., Valentine, D.L., Boysen, A.K., Longnecker, K., Redmond, M.C., 2011. Fate of dispersants associated with the deepwater horizon oil spill. Environ. Sci. Technol. 45, 1298-1306.

Lee, K., Nedwed, T., Prince, R.C., Palandro, D., 2013. Lab tests on the biodegradation of chemically dispersed oil should consider the rapid dilution that occurs at sea. Mar. Pollut. Bull. 73, 314-318.

Li, Z., Lee, K., King, T., Boufadel, M.C., Venosa, A.D., 2009. Evaluating Chemical Dispersant Efficacy in an Experimental Wave Tank: 2—Significant Factors Determining In Situ Oil Droplet Size Distribution. 26, 1407-1418.

Lindstrom, J.E., Braddock, J.F., 2002. Biodegradation of petroleum hydrocarbons at low temperature in the presence of the dispersant Corexit 9500. Mar. Pollut. Bull. 44, 739-747.

Lunel, T., 1995. Understanding the mechanism of dispersion through oil droplet size measurements at sea., in: P. Lane (Ed.), The Use of Chemicals in Oil Spill Response. American Society for Testing and Materials, Philadelphia, PA.

Milinkovitch, T., Kanan, R., Thomas-Guyon, H., Le Floch, S., 2011. Effects of dispersed oil exposure on the bioaccumulation of polycyclic aromatic hydrocarbons and the mortality of juvenile Liza ramada. Sci. Total. Environ. 409, 1643-1650.

Mrozik, A., Piotrowska-Seget, Z., Labuzek, S., 2003. Bacterial Degradation and Bioremediation of Polycyclic Aromatic Hydrocarbons. Pol. J. Environ. Stud. 12, 15-25.

ED_001324_00000731-00025

478 Operational Science Advisory Team, 2010. Summary report for sub-sea and sub-surface oil and
479 dispersant detection: sampling and monitoring. Prepared for Paul F. Zukunft, U.S. Coast Guard.

480 Prince, R.C., 2015. Oil spill dispersants: boon or bane? Environmental science & technology 49,
481 6376–6384.

482 Prince, R.C., Elmendorf, D.L., Lute, J.R., Hsu, C.S., Halth, C.E., Senius, J.D., Dechert, G.J., Douglas,
483 G.S., Butler, E.L., 1994. 17α(H),21β(H)-hopane as a conserved internal marker for estimating the
484 blodegradation of crude oil. Environ. Sci. Technol. 28, 142-145.

485 Prince, R.C., McFarlin, K.M., Butler, J.D., Febbo, E.J., Wang, F.C., Nedwed, T.J., 2013. The
486 primary biodegradation of dispersed crude oil in the sea. Chemosphere 90, 521-526.

487 Ramachandran, S.D., Hodson, P.V., Khan, C.W., Lee, K., 2004. Oil dispersant increases PAH
488 uptake by fish exposed to crude oil. Ecotox. Environ. Safe. 59, 300-308.

489 Rojo, F., 2009. Degradation of Alkanes by Bacteria. Environ. Microbiol. 11, 2477-2490.

490 Spotte, S., Adams, G., Bubucis, P.M., 1984. GP2 medium is an synthetic seawater for culture or
491 maintenance of marine organisms. . Zoo Biol. 3, 229-240.

492 Tang, W.C., White, J.C., Alexander, M., 1998. Utilization of sorbed compounds by
493 microorganisms specifically isolated for that purpose. Appl. Microbiol. Biotechnol. 49, 117-121.

494 Venosa, A.D., Holder, E.L., 2007. Biodegradability of dispersed crude oil at two different
495 temperatures. Mar. Pollut. Bull. 54, 545-553.

496 Wentzel, A., Ellingsen, T.E., Kotlar, H.K., Zotchev, S.B., Throne-Holst, M., 2007. Bacterial
497 metabolism of long-chain n-alkanes. Appl. Microbiol. Biotechnol. 76, 1209-1221.

498 Word, J.Q., Clark, J.R., Word, L.S., 2014. Comparison of the Acute Toxicity of Corexit 9500 and
499 Household Cleaning Products. Human Ecol. Risk Assess. 21, 19.

500 Yin, F., John, G.F., Hayworth, J.S., Clement, T.P., 2015. Long-term monitoring data to describe
501 the fate of polycyclic aromatic hydrocarbons in Deepwater Horizon oil submerged off Alabama's
502 beaches. The Science of the total environment 508, 46-56.

503 Zahed, M.A., Aziz, H.A., Isa, M.H., Mohajeri, L., 2010. Effect of initial oil concentration and
504 dispersant on crude oil biodegradation in contaminated seawater. Bull. Environ. Contam.
505 Toxicol. 84, 438-442.

ED_001324_00000731-00026

***Supporting Information**

Biodegradability of Different Initial Concentrations of Alaska North Slope Crude Oil Dispersed with Corexit C9500

Mobing Zhuang[1], Gulizhaer Abulikemu[2], Pablo Campo[3], William Platten III[4], Makram T. Suidan[5]*, Albert D. Venosa (retired)[4]and Robyn N. Conmy[4]

1 Department of Biomedical, Chemical and Environmental Engineering, University of Cincinnati, 2901 Woodside Drive, Cincinnati, OH 45221, USA

2 Pegasus Technical Services Inc., 46 E Hollister St, Cincinnati, OH 45219 USA

3 Cranfield Water Science Institute, Cranfield University, Cranfield, Beds, MK43 0AL, UK

4 U.S. Environmental Protection Agency, NRMRL, 26 W. MLK Drive Cincinnati, OH, 45268, USA

5 Faculty of Engineering and Architecture, American University of Beirut, Bechtel Engineering Bldg. - 3rd flr. - Room 308 P.O. Box: 11-0236 Riad El Solh 1107 2020, Beirut, Lebanon

*Corresponding author: Makram T. Suidan
Tel: 00961-1-347952
Fax: 00961-1-744462
E-mail address: msuidan@aub.edu.lb

ED_001324_00000731-00027

Table S1. Summary of Experimental Layout for High Concentration Experiment.

Test	Temperature	Treatment	Sampling Events	Sample Replicates	Total Experimental Units (EU)
1	5 °C	C9500 alone	11	3	33
2	5 °C	ANS dispersed by C9500	11	3	33
3	5 °C	alone	11	3	33
4	5 °C	Killed ANS control	1	3	3
5	5 °C	Killed C9500 control	11	3	33
6	5 °C	Killed ANS+C9500 control	11	3	33
				Subtotal EU's	**168**
7	25 °C	C9500 alone	9	3	27
8	25 °C	ANS dispersed by C9500	9	3	27
9	25 °C	ANS alone	9	3	27
10	25 °C	Killed ANS control	1	3	3
11	25 °C	Killed C9500 control	9	3	27
12	25 °C	Killed ANS+ C9500 control	9	3	27
				Subtotal EU's	**138**
		Total EU's for High Concentration Experiment			**306**

ED_001324_00000731-00028

Table S2. Summary of Experimental Layout for Low Concentration Experiment.

Test	Temperature	Treatment	Sampling Events	Sample Replicates	Total Experimental Units (EU)
13	5 °C	C9500 alone	11	3	33
14	5 °C	ANS+C9500	11	3	33
15	5 °C	ANS alone	11	3	33
16	5 °C	Killed ANS control	1	3	3
17	5 °C	Killed C9500 control	11	3	33
18	5 °C	Killed (ANS+C9500) control	11	3	33
19	5 °C	Killed (ANS+C9500) +Protease	6	3	18
				Subtotal EU's	**186**
20	25 °C	C9500 alone	10	3	30
21	25 °C	ANS+C9500	10	3	30
22	25 °C	ANS alone	10	3	30
23	25 °C	Killed ANS control	1	3	3
24	25 °C	Killed C9500 control	10	3	30
25	25 °C	Killed (ANS+C9500) control	10	3	30
26	25 °C	Killed (ANS+C9500) +Protease	6	3	18
				Subtotal EU's	**181**
		Total EU's for Low Concentration Experiment			**357**

26

ED_001324_00000731-00029

Table S3. First-order biodegradation rate coefficients and standard deviations (sd) of individual alkanes in the high concentration experiment.

Compound	5 °C ANS alone		25 °C ANS alone		5 °C ANS+C9500		25 °C ANS+C9500	
	rate (d^{-1})	sd (d^{-1})	rate (d^{-1})	sd (d^{-1})	rate (d^{-1})	sd (d^{-1})	rate (d^{-1})	sd (d^{-1})
C10	0.19	0.02	1.34	0.18	0.63	0.03	2.00	0.34
C11	0.15	0.01	1.16	0.15	0.40	0.02	1.30	0.09
C12	0.12	0.01	1.02	0.14	0.29	0.03	0.96	0.06
C13	0.11	0.01	0.94	0.14	0.27	0.03	0.91	0.05
C14	0.11	0.01	0.92	0.14	0.25	0.03	0.82	0.04
C15	0.11	0.01	0.95	0.14	0.24	0.03	0.84	0.05
C16	0.11	0.01	1.01	0.15	0.24	0.03	0.92	0.05
C17	0.11	0.01	1.08	0.16	0.24	0.03	0.97	0.06
PR	0.15	0.03	0.45	0.11	0.07	0.01	0.39	0.04
C18	0.11	0.01	1.06	0.14	0.22	0.02	0.96	0.05
PH	0.15	0.03	0.46	0.12	0.08	0.01	0.43	0.04
C19	0.11	0.01	1.05	0.14	0.22	0.02	0.97	0.06
C20	0.11	0.01	0.99	0.14	0.21	0.02	0.93	0.05
C21	0.10	0.01	0.97	0.14	0.20	0.02	0.91	0.05
C22	0.10	0.01	0.88	0.13	0.19	0.02	0.84	0.04
C23	0.09	0.01	0.84	0.13	0.18	0.02	0.79	0.04
C24	0.09	0.01	0.84	0.14	0.17	0.02	0.79	0.04
C25	0.09	0.01	0.81	0.13	0.15	0.02	0.81	0.03
C26	0.08	0.01	0.81	0.14	0.12	0.02	0.78	0.04
C27	0.08	0.01	0.74	0.13	0.11	0.01	0.71	0.05
C28	0.12	0.02	0.75	0.12	0.12	0.02	0.60	0.09
C29	0.12	0.02	0.81	0.15	0.12	0.02	0.81	0.07
C30	0.10	0.01	0.83	0.14	0.12	0.02	0.74	0.04
C31	0.09	0.01	0.81	0.14	0.09	0.01	0.61	0.05
C32	0.10	0.01	0.81	0.14	0.09	0.01	0.60	0.06
C33	0.09	0.01	0.68	0.09	0.07	0.01	0.56	0.06
C34	0.08	0.01	0.60	0.09	0.05	0.01	0.54	0.05
C35	0.07	0.01	0.53	0.09	0.04	0.01	0.58	0.04

NA: Rate not calculated because the biodegradation of noted compounds did not follow first order kinetics.

ED_001324_00000731-00030

Table S4. First-order biodegradation rate coefficients and standard deviations (sd) of individual alkanes in low concentration experiment.

Compound	5 °C ANS alone		25 °C ANS alone		5 °C ANS+C9500		25 °C ANS+C9500	
	rate (d^{-1})	sd (d^{-1})	rate (d^{-1})	sd (d^{-1})	rate (d^{-1})	sd (d^{-1})	rate (d^{-1})	sd (d^{-1})
C10	0.47	0.03	0.93	0.16	0.63	0.04	NA1	NA1
C11	0.25	0.02	0.57	0.07	0.25	0.03	0.47	0.02
C12	0.20	0.01	0.38	0.06	0.23	0.02	0.24	0.03
C13	0.18	0.01	0.42	0.06	0.21	0.02	NA2	NA2
C14	0.13	0.01	0.28	0.04	0.15	0.01	NA2	NA2
C15	0.14	0.01	0.35	0.04	0.15	0.01	NA2	NA2
C16	0.14	0.01	0.37	0.04	0.15	0.02	NA2	NA2
C17	0.13	0.01	0.36	0.04	NA2	NA2	NA2	NA2
PR	NA2	NA2	0.04	0.01	NA2	NA2	NA2	NA2
C18	NA2	NA2	0.35	0.04	NA2	NA2	NA2	NA2
PH	NA2	NA2	0.03	0.01	NA2	NA2	NA2	NA2
C19	NA2	NA2	0.32	0.04	NA2	NA2	NA2	NA2
C20	NA2	NA2	0.30	0.04	NA2	NA2	NA2	NA2
C21	NA2	NA2	0.29	0.04	NA2	NA2	NA2	NA2
C22	NA2	NA2	0.17	0.03	NA2	NA2	NA2	NA2
C23	NA2	NA2	NA2	NA2	NA2	NA2	NA2	NA2
C24	NA2	NA2	NA2	NA2	NA2	NA2	NA2	NA2
C25	NA2	NA2	NA2	NA2	NA2	NA2	NA2	NA2
C26	NA2	NA2	NA2	NA2	NA2	NA2	NA2	NA2
C27	NA2	NA2	NA2	NA2	NA2	NA2	NA2	NA2
C28	NA2	NA2	NA2	NA2	NA2	NA2	NA2	NA2
C29	NA2	NA2	NA2	NA2	NA2	NA2	NA2	NA2
C30	NA2	NA2	NA2	NA2	NA2	NA2	NA2	NA2
C31	NA2	NA2	NA2	NA2	NA2	NA2	NA2	NA2
C32	NA2	NA2	NA2	NA2	NA2	NA2	NA2	NA2
C33	NA2	NA2	NA2	NA2	NA2	NA2	NA2	NA2
C34	NA2	NA2	NA2	NA2	NA2	NA2	NA2	NA2
C35	NA2	NA2	NA2	NA2	NA2	NA2	NA2	NA2

NA1: Rate not calculated because of excessively rapid removal after acclimation.
NA2: Rate not calculated because noted compounds were persisted during the experiment.

ED_001324_00000731-00031

Table S5. First-order degradation rate coefficients and standard deviations (sd) of individual PAHs in high concentration experiment.

Compound	5 °C ANS alone		25 °C ANS alone		5 °C ANS+C9500		25 °C ANS+C9500	
	rate (d^{-1})	sd (d^{-1})	rate (d^{-1})	sd (d^{-1})	rate (d^{-1})	sd (d^{-1})	rate (d^{-1})	sd (d^{-1})
nap	0.44	0.04	0.68	0.05	0.71	0.02	1.94	0.02
C1-nap	0.23	0.02	0.60	0.04	0.41	0.03	1.84	0.04
C2-nap	0.17	0.02	0.38	0.07	0.26	0.02	0.61	0.03
C3-nap	0.27	0.02	0.35	0.10	0.20	0.02	0.40	0.05
C4-nap	0.13	0.02	0.29	0.10	0.16	0.02	0.35	0.05
phe	0.19	0.01	0.37	0.09	0.26	0.02	0.46	0.05
C1-phe	0.12	0.01	0.34	0.12	0.19	0.02	0.37	0.06
C2-phe	0.05	0.01	0.21	0.07	0.19	0.03	0.27	0.04
C3-phe	0.00	0.00	0.00	0.00	0.00	0.00	0.00	0.00
C4-phe	0.00	0.00	0.00	0.00	0.00	0.00	0.00	0.00
flu	0.19	0.02	0.37	0.10	0.26	0.02	0.44	0.05
C1-flu	0.15	0.02	0.35	0.11	0.21	0.02	0.39	0.06
C2-flu	0.05	0.01	0.20	0.07	0.11	0.01	0.27	0.04
C3-flu	0.00	0.00	0.00	0.00	0.00	0.00	0.00	0.00
dbt	0.25	0.01	0.43	0.08	0.44	0.02	0.77	0.03
C1-dbt	0.13	0.01	0.32	0.10	0.22	0.02	0.41	0.04
C2-dbt	0.04	0.01	0.17	0.06	0.11	0.01	0.26	0.04
C3-dbt	0.00	0.00	0.00	0.00	0.00	0.00	0.00	0.00
nbt	0.00	0.00	0.00	0.00	0.00	0.00	0.00	0.00
C1-nbt	0.00	0.00	0.00	0.00	0.00	0.00	0.00	0.00
C2-nbt	0.00	0.00	0.00	0.00	0.00	0.00	0.00	0.00
C3-nbt	0.00	0.00	0.00	0.00	0.00	0.00	0.00	0.00
pyr*	--	--	--	--	--	--	--	--
C1-pyr	0.00	0.00	0.00	NA	NA	0.00	NA	NA
C2-pyr	0.00	0.00	0.00	0.00	0.00	0.00	0.00	0.00
cry	0.00	0.00	0.00	0.00	0.00	0.00	0.00	0.00
C1-cry	0.00	0.00	0.00	0.00	0.00	0.00	0.00	0.00
C2-cry	0.00	0.00	0.00	0.00	0.00	0.00	0.00	0.00
C3-cry	0.00	0.00	0.00	0.00	0.00	0.00	0.00	0.00
C4-cry	0.00	0.00	0.00	0.00	0.00	0.00	0.00	0.00

NA: Rate not calculated because noted compounds were persisted during the experiment.
* Not detected in any samples.

ED_001324_00000731-00032

Table S6. First-order degradation rate coefficients and standard deviations (sd) of individual PAHs in low concentration experiment.

Compound	5 °C ANS alone		25 °C ANS alone		5 °C ANS+C9500		25 °C ANS+C9500	
	rate (d^{-1})	sd (d^{-1})	rate (d^{-1})	sd (d^{-1})	rate (d^{-1})	sd (d^{-1})	rate (d^{-1})	sd (d^{-1})
nap	NA	NA	0.29	0.05	0.43	0.09	0.36	0.03
C1-nap	NA	NA	0.24	0.03	0.44	0.09	0.28	0.03
C2-nap	NA	NA	0.17	0.04	0.40	0.09	0.21	0.04
C3-nap	NA	NA	0.18	0.04	0.31	0.06	0.20	0.04
C4-nap	NA	NA	0.13	0.03	0.15	0.02	0.14	0.02
phe	NA	NA	NA	NA	NA	NA	0.19	0.03
C1-phe	NA	NA	NA	NA	0.18	0.03	0.20	0.03
C2-phe	0.25	0.01	0.14	0.03	0.11	0.01	NA	NA
C3-phe	0.02	0.01	0.02	0.00	0.00	0.00	0.00	0.00
C4-phe	0.00	0.00	0.00	0.00	0.00	0.00	0.00	0.00
flu	NA	NA	NA	NA	0.29	0.06	NA	NA
C1-flu	NA	NA	NA	NA	0.15	0.02	0.00	0.00
C2-flu	0.29	0.03	0.14	0.03	0.21	0.01	0.00	0.00
C3-flu	0.02	0.00	0.03	0.00	0.00	0.00	0.02	0.00
dbt	NA	NA	0.00	0.00	0.31	0.11	0.00	0.00
C1-dbt	NA	NA	NA	NA	0.23	0.05	0.29	0.06
C2-dbt	0.00	0.00	0.00	0.00	0.00	0.00	0.00	0.00
C3-dbt	0.00	0.00	0.00	0.00	0.00	0.00	0.00	0.00
nbt	0.00	0.00	NA	NA	0.00	0.00	0.31	0.11
C1-nbt	0.00	0.00	0.00	0.00	0.00	0.00	0.00	0.00
C2-nbt	0.00	0.00	0.00	0.00	0.00	0.00	0.00	0.00
C3-nbt	0.00	0.00	0.00	0.00	0.00	0.00	0.00	0.00
pyr*	--	--	--	--	--	--	--	--
C1-pyr	0.00	0.00	0.00	0.00	0.00	0.00	0.27	0.07
C2-pyr	0.00	0.00	0.00	0.00	0.00	0.00	0.00	0.00
cry	0.00	0.00	0.00	0.00	0.00	0.00	0.00	0.00
C1-cry	0.00	0.00	0.00	0.00	0.00	0.00	0.00	0.00
C2-cry	0.00	0.00	0.00	0.00	0.00	0.00	0.00	0.00
C3-cry	0.00	0.00	0.00	0.00	0.00	0.00	0.00	0.00
C4-cry	0.00	0.00	0.00	0.00	0.00	0.00	0.00	0.00

NA: Rate not calculated because of excessively rapid removal after acclimation.
*Not detected in any samples.

ED_001324_00000731-00033

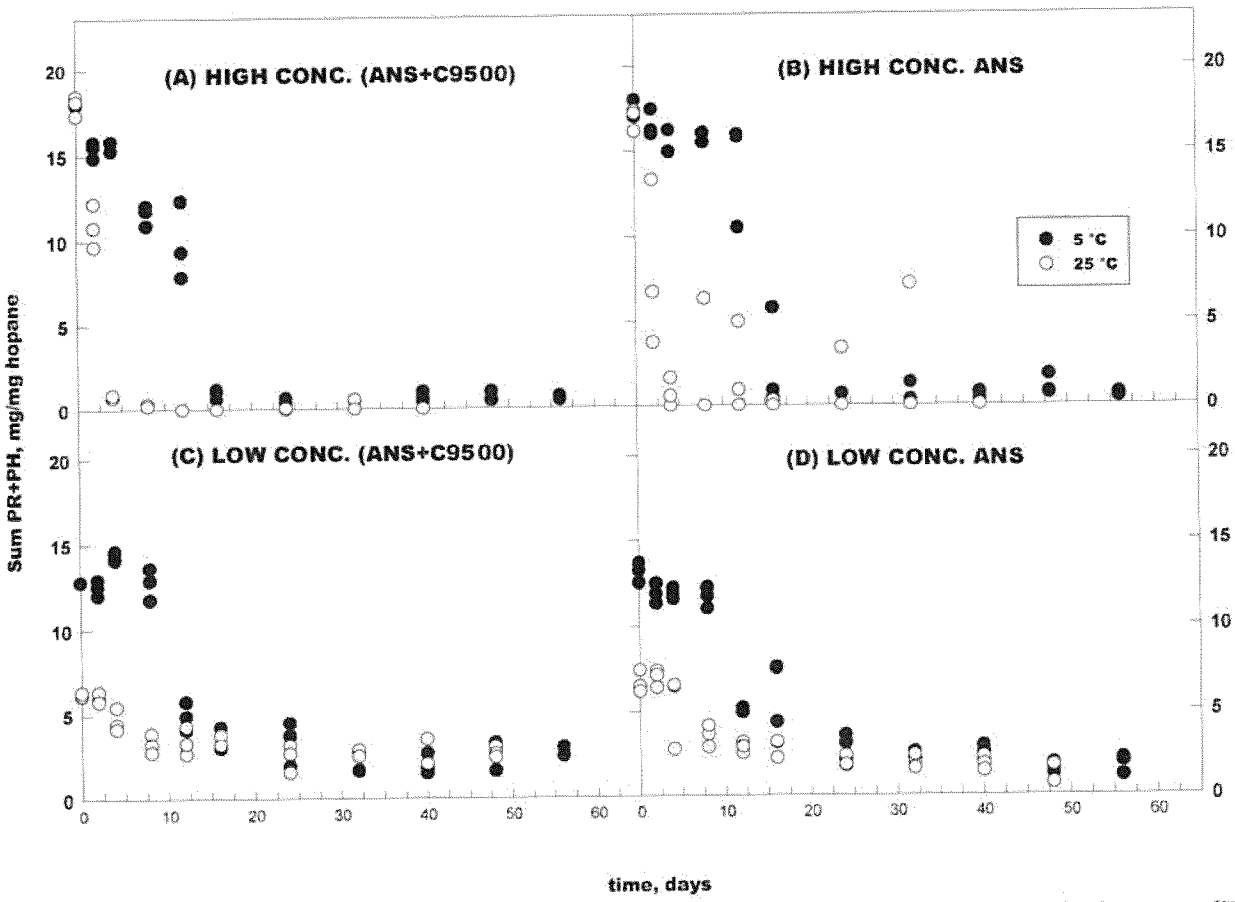

35
36 **Figure S1. Biodegradation of branched alkanes in the presence (A, C) and absence (B,**
37 **D) of C9500 at 5 °C and 25 °C. High concentration treatments are in panel A and B,**
38 **whereas low concentration treatments are in panels C and D.**

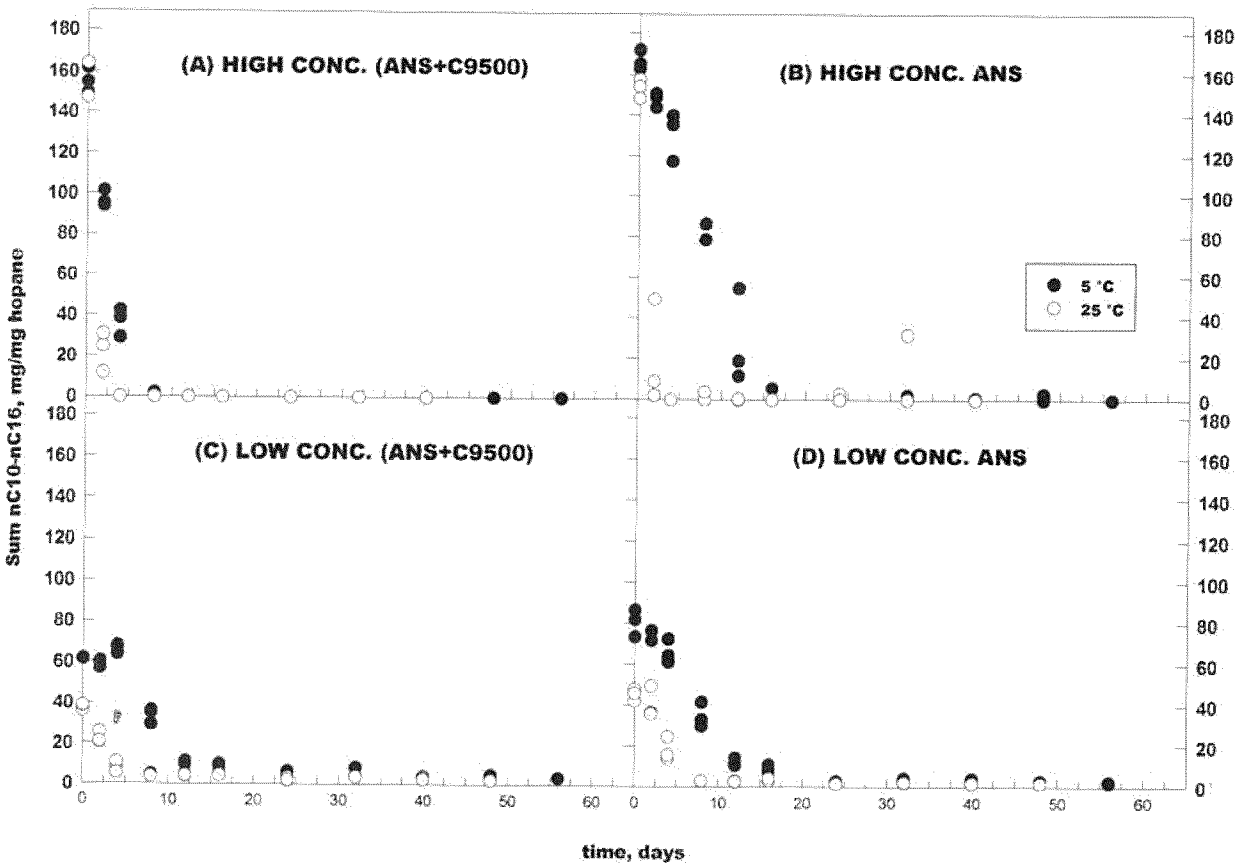

Figure S2. Biodegradation of n-alkanes (nC10-nC16) in the presence (A, C) and absence (B, D) of C9500 at 5 °C and 25 °C. High concentration treatments are in panel A and B, whereas low concentration treatments are in panels C and D.

ED_001324_00000731-00035

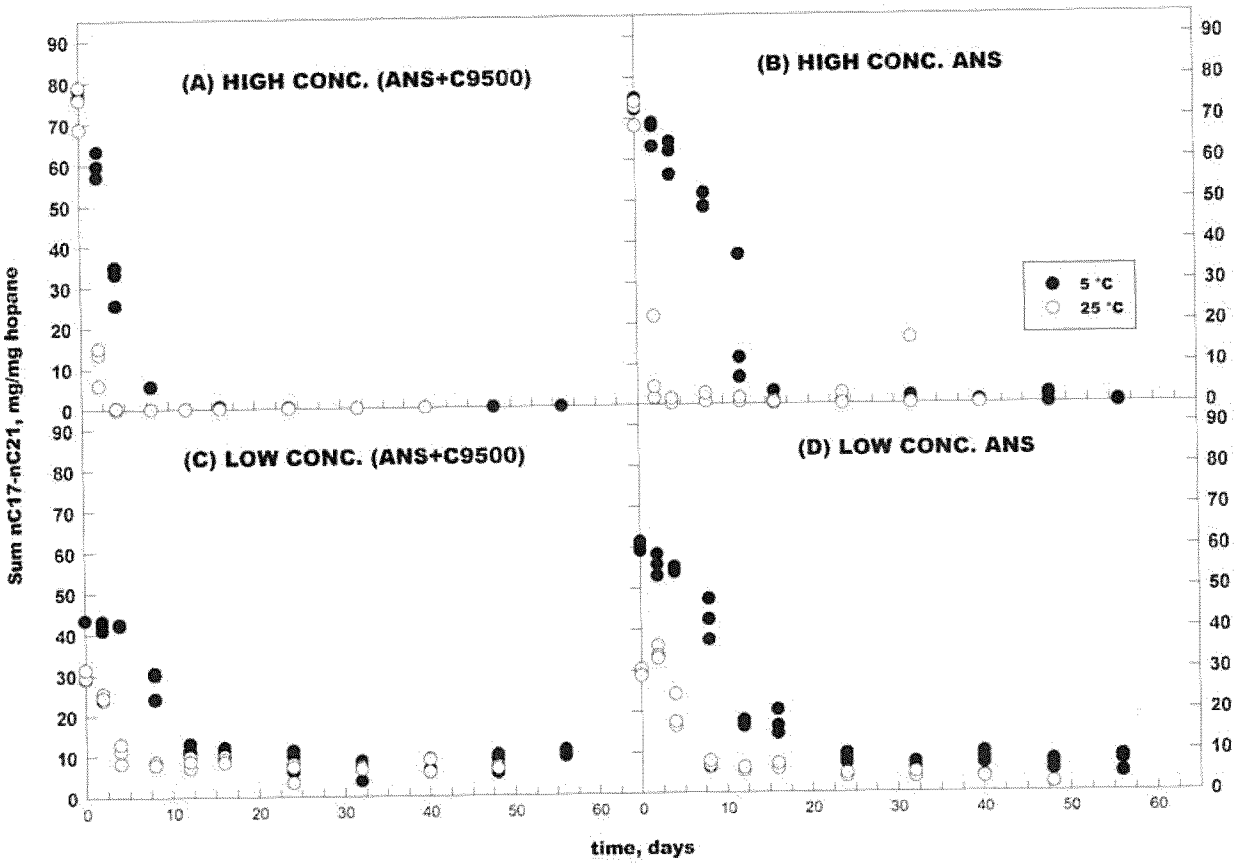

43

44 **Figure S3. Biodegradation of n-alkanes (nC17-nC21) in the presence (A, C) and**
45 **absence (B, D) of C9500 at 5 °C and 25 °C. High concentration treatments are in panel**
46 **A and B, whereas low concentration treatments are in panels C and D.**

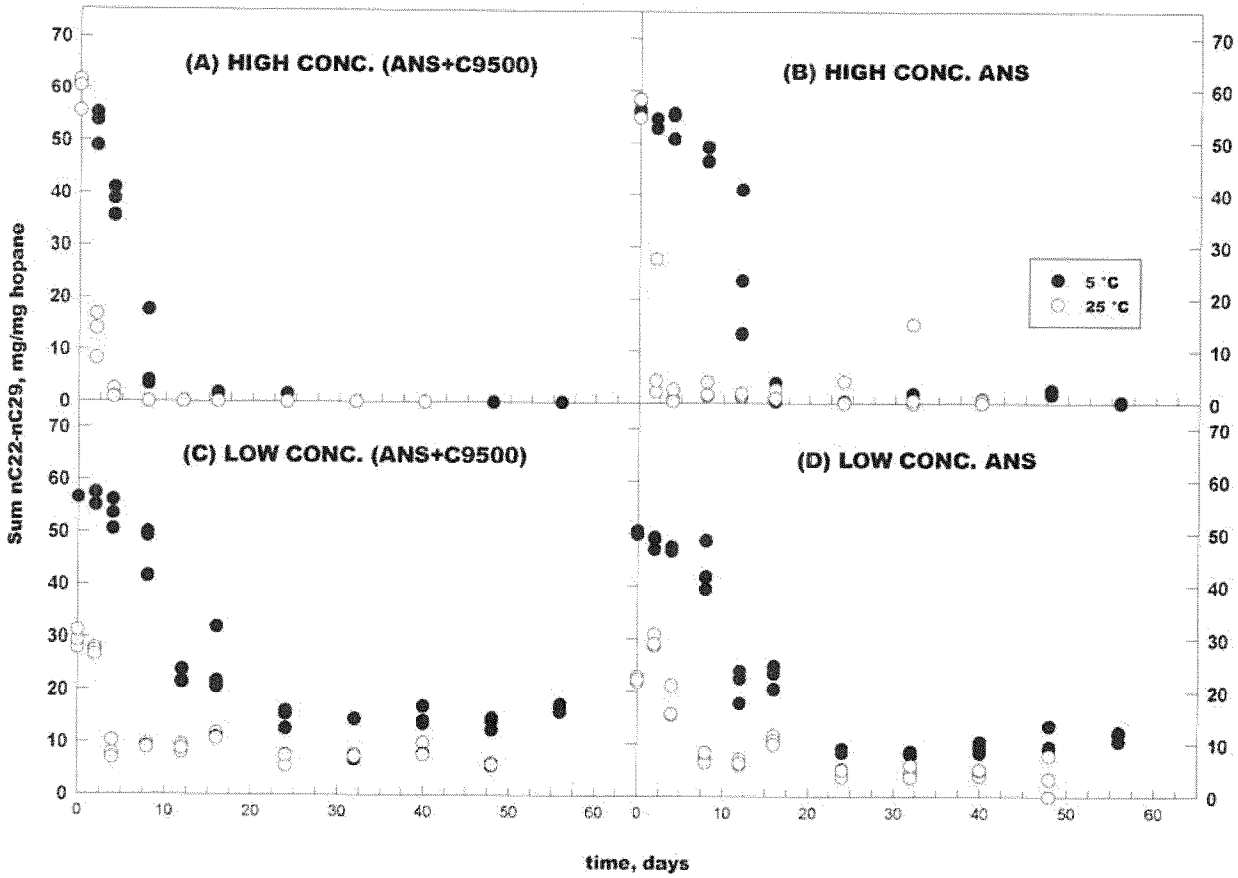

Figure S4. Biodegradation of n-alkanes (nC22-nC29) in the presence (A, C) and absence (B, D) of C9500 at 5 °C and 25 °C. High concentration treatments are in panel A and B, whereas low concentration treatments are in panels C and D.

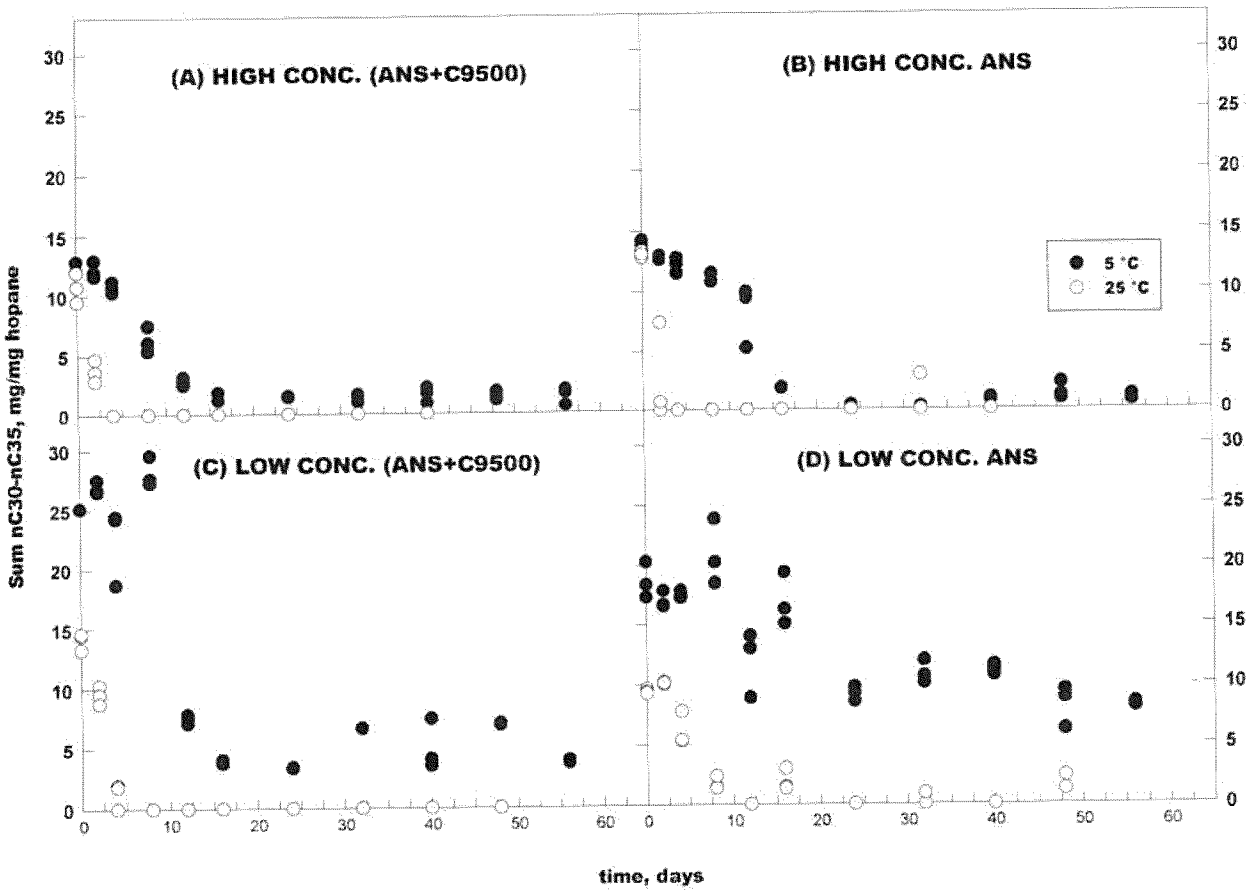

Figure S5. Biodegradation of n-alkanes (nC30-nC35) in the presence (A, C) and absence (B, D) of C9500 at 5 °C and 25 °C. High concentration treatments are in panel A and B, whereas low concentration treatments are in panels C and D.

ED_001324_00000731-00038

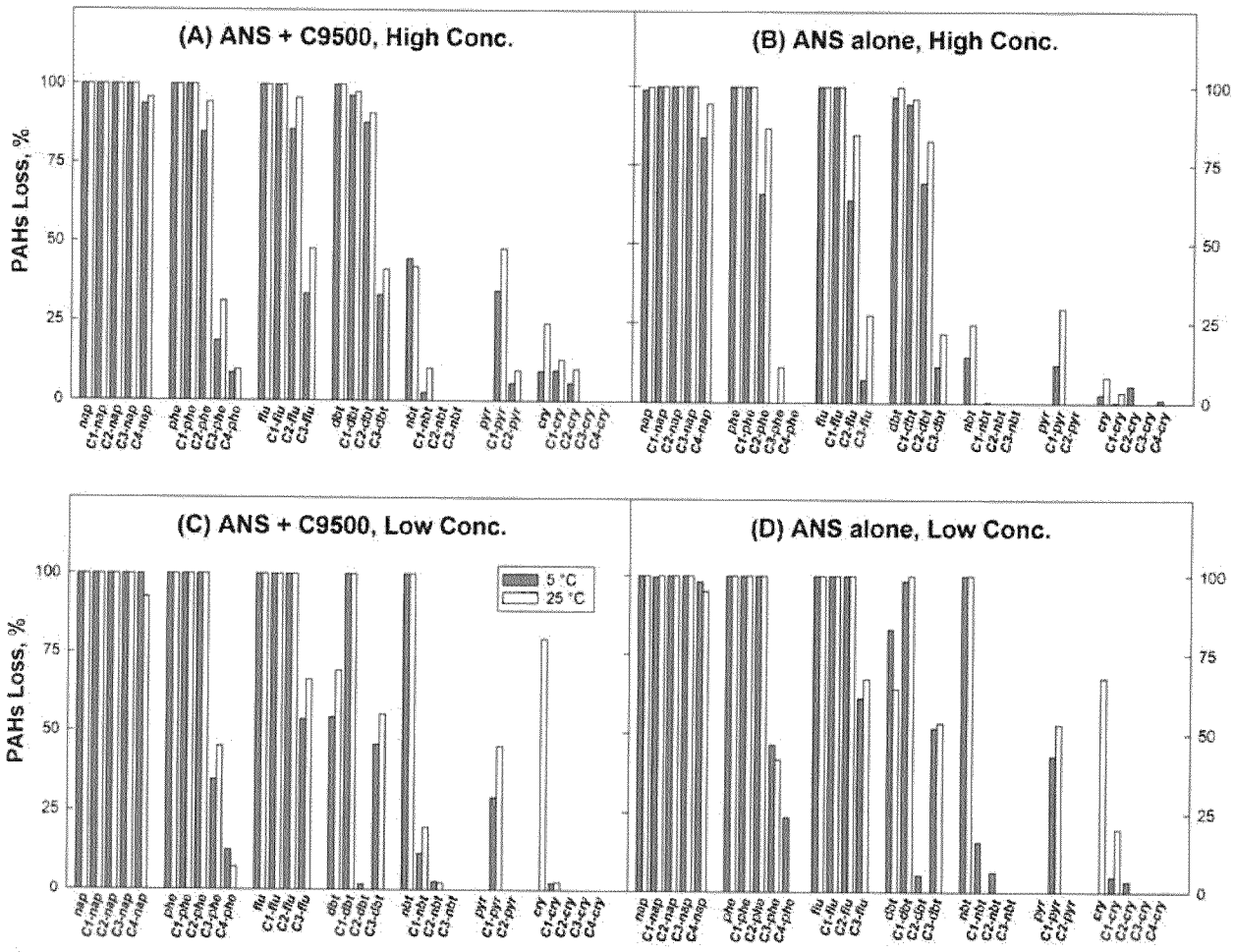

Figure S6. Loss percentage of individual PAH in the presence (A, C) and absence (B, D) of C9500 at 5 °C and 25 °C in high concentration (A, B) and low concentration (C, D) experiment.

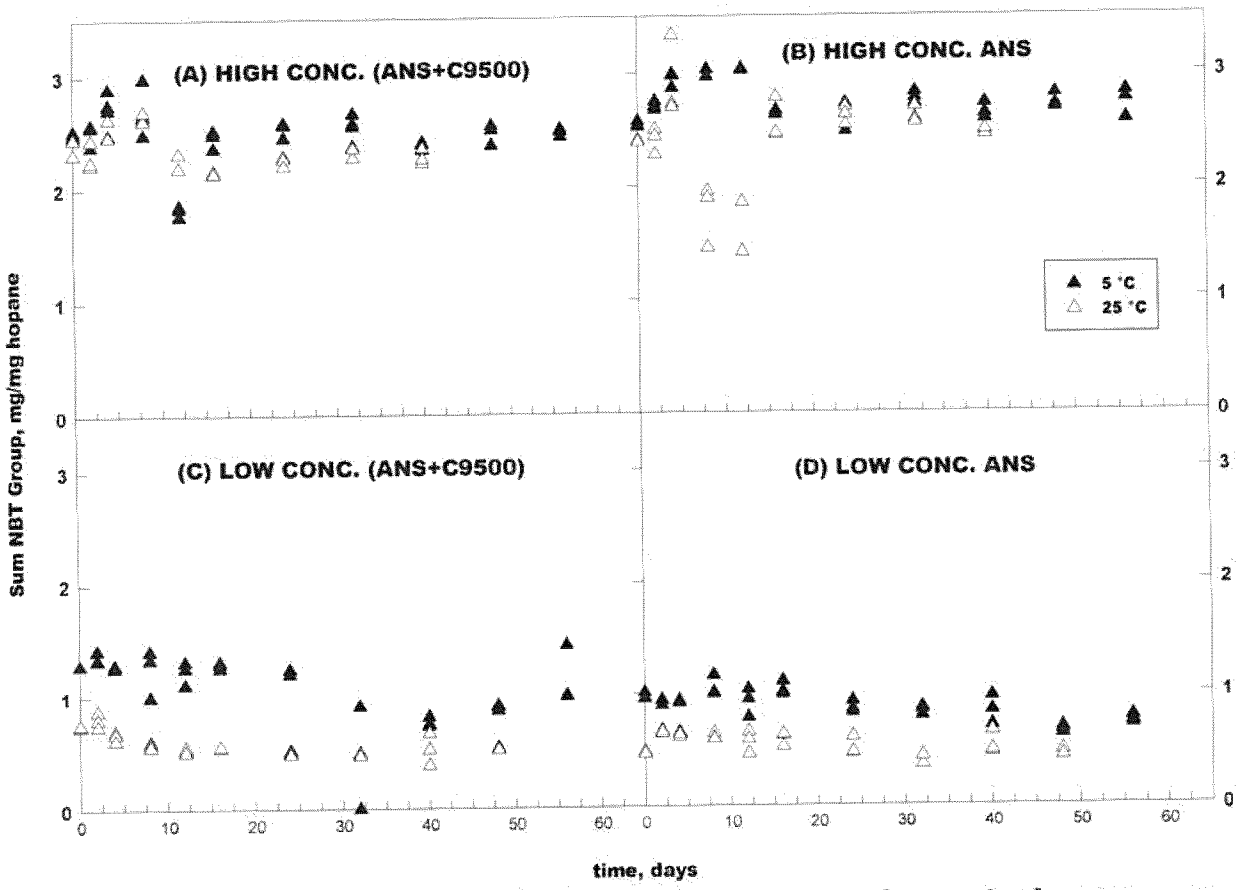

Figure S7. Biodegradation of naphthobenzothiophene homologues in the presence (A, C) and absence (B, D) of C9500 at 5 °C and 25 °C. High concentration treatments are in panel A and B, whereas low concentration treatments are in panels C and D.

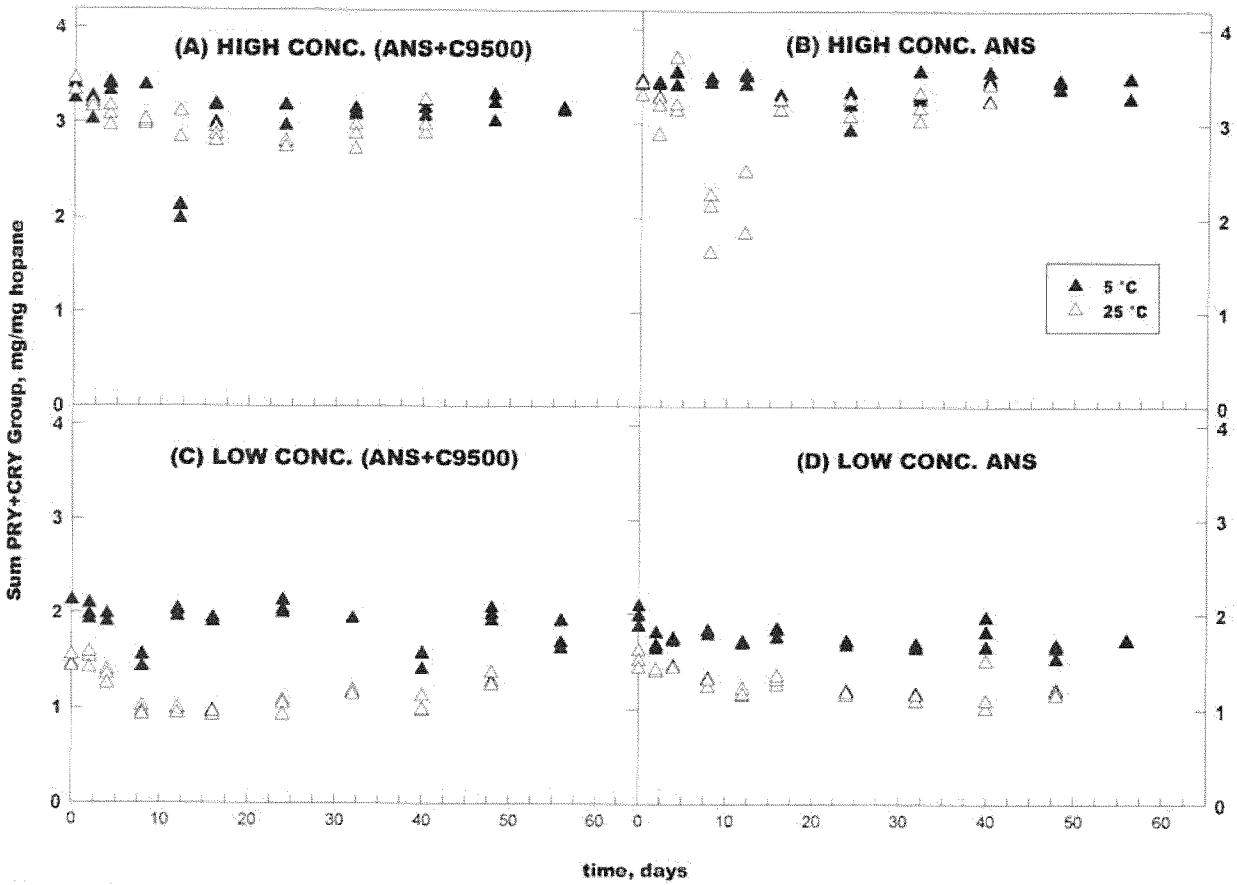

Figure S8. Biodegradation of pyrene homologues + chrysene homologues in the presence (A, C) and absence (B, D) of C9500 at 5 °C and 25 °C. High concentration treatments are in panel A and B, whereas low concentration treatments are in panels C and D.

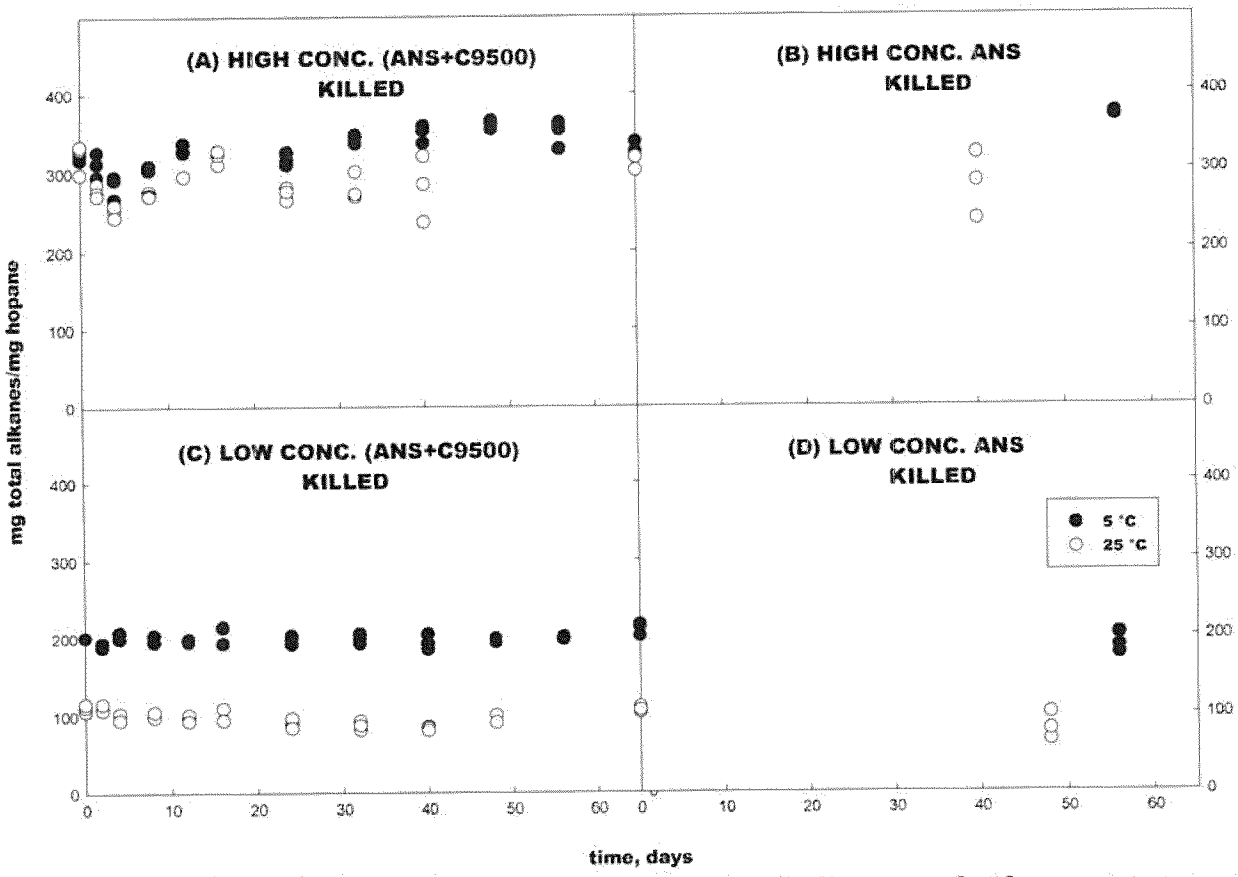

Figure S9. Biodegradation of hopane-normalized total alkanes at both temperatures in high concentration treatments (A, B) and low concentration treatments (C, D) in killed control samples.

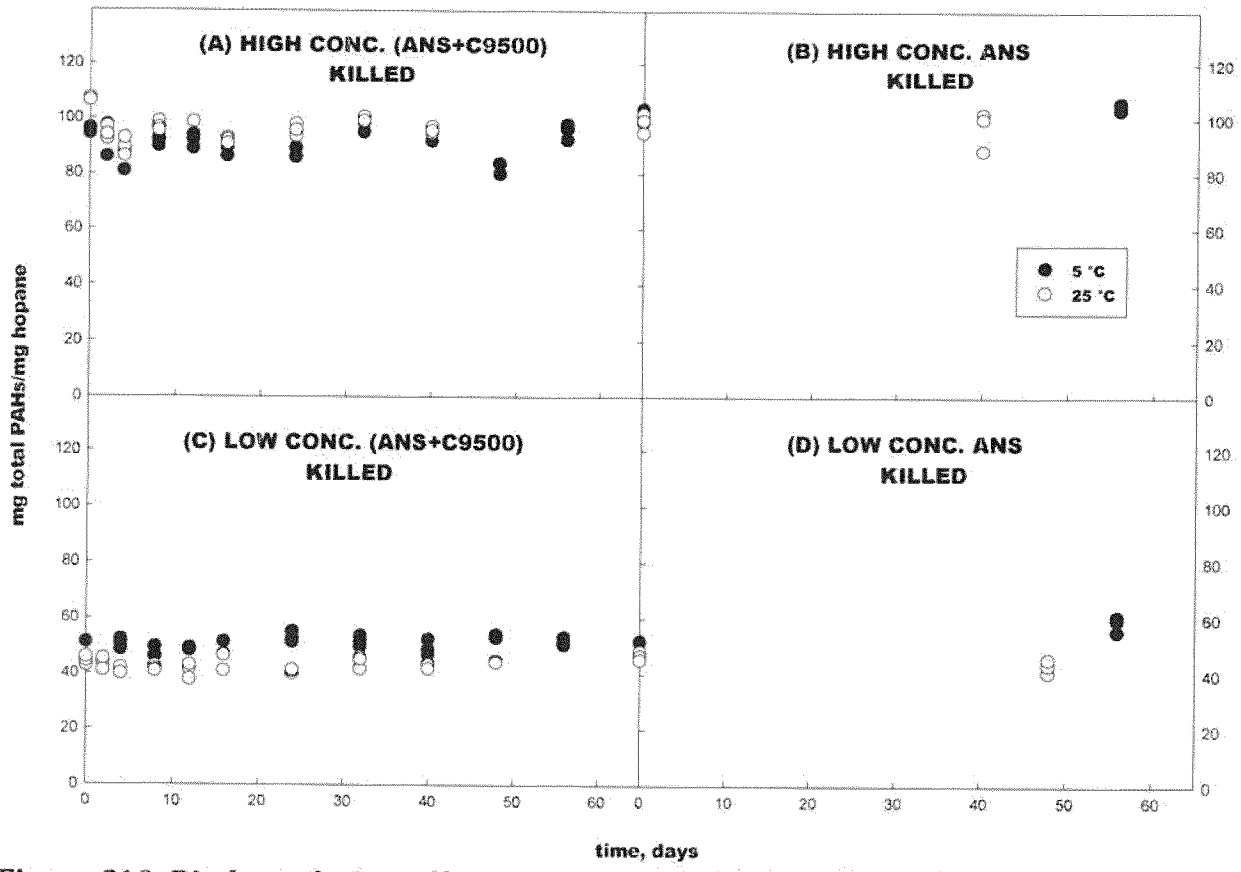

Figure S10. Biodegradation of hopane-normalized total PAHs at both temperatures in high concentration treatments (A, B) and low concentration treatments (C, D) in killed control samples.

To: Conmy, Robyn[Conmy.Robyn@epa.gov]; King, Thomas L[Tom.King@dfo-mpo.gc.ca]
From: Robinson, Brian
Sent: Thur 5/7/2015 6:46:49 PM
Subject: RE: subsea release experiments

Hi Robyn,

I was just about to send you a message about the status of the fluorometers. That is great if we will get them next week. We just opened the wave tank facility last week, and everything appears to have survived our harsh winter. We are currently running a few dilbit experiments, which will free up some time to start our subsurface injection experiments in the coming weeks. To answer your questions:

1) **VOC Paper** –I'm still working on it…I had to put it aside for a few weeks while I finished another paper based on our work the Chinese SOA. Since I hate being the hold up in getting this work out in press, next week I will send all of the data that I have prepared so far and perhaps together we can work on finishing the paper.

2) **Shimadzu** - I've been working with Mary to get the QS shipped to us. If all goes well she will be sending it out on May 11th. Once it arrives, I will have Claire prepare the solutions and run them.

3) **Start Date** - Once we have the fluorometers, we can start pretty much any time. We plan to conduct all the additional experiments, including 9 runs with Finasol and ANS, and 6 runs with MC252 and Corexit. I'm also working with Michel to co-ordinate his visit here to conduct his jet characterization measurements.

4) **Live Oil** - Unfortunately generating live oil is a much more complex process than we thought, and would require purchasing new equipment (http://goo.gl/Cwo5bU) and likely hiring someone with expertise in performing this type of work. In the no-cost BSEE extension we proposed injecting two types of gases into the tank. After speaking with Michel, he felt as though injecting a gas would produce little data of value. Therefore, instead we are proposing a series of experiments using a sample of gas condensate.

A conference call next week would be a great idea. We are free next Wed, Thursday afternoon, or Friday. Please let us know what date and time works best for you. I think Rod may join us as well since he has a few questions regarding the new BSEE proposal. I'll also see if Michel can call in.

Thanks,

Brian

From: Conmy, Robyn [mailto:Conmy.Robyn@epa.gov]
Sent: May 7, 2015 1:00 PM
To: Robinson, Brian; King, Thomas L
Subject: subsea release experiments

Hi Brian and Tom,

I have shipped the fluorometers back to you. They should arrive by Wednesday next week. If they do not, please email me and I will track them down.

In an effort to get us back on track with this project, here are some items / questions that I have:

1. What is the status of the VOC in air data and manuscript that Brian is working on? The EPA program office is eager to see what was found during the experiments?

2. How is the Shimadzu EEMS fluorometer looking? Do you have the quinine sulfate from Mary?

3. What is the start date for Spring experiments? And are a few runs with South LA crude still planned?

4. How is the preparation coming along for live oil release?

Keep in mind that our draft report to BSEE is due in August. I may plan for a trip to BIO in the beginning of July, if that works for your schedule. This way we can pull together all the data for the report.

Maybe a call for early next week would be a good idea?

Cheers,

Robyn

<>/<>/<>/<>/<>/<>/<>/<>/<>/<>/<>/<>/<>/<>/<>/<>/<>

Robyn N. Conmy, Ph.D.

Research Ecologist

USEPA/NRMRL/LRPCD

26 West MLK Drive

Cincinnati, Ohio 45268

513-569-7090 (office)

513-431-1970 (EPA mobile)

727-692-5333 (Personal mobile)

conmy.robyn@epa.gov

To: Conmy, Robyn[Conmy.Robyn@epa.gov]
Cc: Venkatapathy, Raghuraman[Venkatapathy.Raghuraman@epa.gov]; Holder, Edith[holder.edith@epa.gov]; Grosser, Robert[Grosser.Robert@epa.gov]
From: Sundaravadivelu, Devi
Sent: Tue 1/17/2017 8:18:52 PM
Subject: Toxicity WAF samples status

Hi Robyn,

This is where we are with respect to the toxicity project:

1. The first set of WAF samples from Hydrosphere (from Sep 2015 to Feb 2016), were extracted and analyzed. Out of the 81 samples, we had sent out results for 73 samples to Mace. We have resolved the issues with the last 8 samples and will be sending out the rest of the results this week. This set of sample consisted of WAFs prepared with ANS, Cold Lake and Western Canadian.

2. WAFs prepared with Endicott and Dorado (June 2016) have been extracted. Oil chemistry analysis will begin now.

3. Two hydrosphere studies (dated 9/16/2016 and 10/4/2016) were conducted with Corexit and Finasol alone. We do not have any oil chemistry analysis pending for those.

4. Accell shipped to Hydrosphere in October 2016. No oil chemistry for these too I think.

Thanks,

Devi

Devi Sundaravadivelu, Ph.D.

Pegasus Technical Services, Inc.

On-Site Contractor to the U.S. EPA

ORD/NRMRL

26 W. Martin Luther King Dr.

Cincinnati, OH 45268

(585) 732-4101 / (513) 569-7478

Oil plume simulations: Tracking oil droplet size distribution and fluorescence within high-pressure release jets

R.N. Conmy[1], **B. Robinson** [2], **T. King** [2], **M. Boufadel**[3], **S. Ryan**[2], **C. McIntyre**[2], **M. I. Abercrombie**[4], **K. Lee** [2,5]

[1]U.S. Environmental Protection Agency, Office of Research and Development, 26 MLK Drive West, Cincinnati, OH 45255, USA

[2] Bedford Institute of Oceanography, Fisheries and Oceans Canada, 1 Challenger Dr, Dartmouth, NS, B2Y 4A2, Canada

[3] New Jersey Institute of Technology, Department of Civil and Environmental Engineering, University Heights, Newark, NJ 07102, USA

[4]University of South Florida, College of Marine Science, 140 7th Ave South, St. Petersburg, FL 33701, USA

[5] Commonwealth Scientific and Industrial Research Organisation, Oceans and Atmosphere Flagship, PO Box 1130, Bentley WA 6102, Australia

ABSTRACT

Optical measurements have been used during oil spill response for more than three decades to determine oil presence in slicks and plumes. Oil surveillance approaches range from simple (human eyeball) to the sophisticated (sensors on AUVs, aircraft, satellites). *In situ* fluorometers and particle size analyzers were deployed during the Deepwater Horizon (DWH) Gulf of Mexico oil spill to track shallow and deep subsea plumes. Uncertainties regarding instrument specifications and capabilities during DWH necessitated performance testing of sensors exposed to simulated, dispersed oil plumes. Seventy-two wave tank experiments were conducted at the Bedford Institute of Oceanography. Simulated were oil releases with varying parameters such as oil release rate, oil temperature (reservoir temp ~ 80 °C), water temperature (<8 °C and >15 °C), oil type, dispersant type (Corexit 9500 and Finasol OSR52) and dispersant

ED_001324_00000745-00001

to oil ratio (DOR). Plumes of Alaskan North Slope Crude, South Louisiana Crude and IFO-120 oils were tracked using *in situ* fluorescence, droplet size distribution (DSD), total petroleum hydrocarbons (TPH) and benzene-toluene-ethylbenzene-xylene (BTEX). Results offer valuable information on the behavior and dispersibility of oils over a range of viscosity, DOR and environmental conditions. Findings have implications for fate and transport models, where DSD, chemistry and fluorescence are all impacted by release variables. This research was supported by the Bureau of Safety and Environmental Enforcement.

INTRODUCTION

The 2010 *Deepwater Horizon* (DWH) oil spill highlighted the pressing need for a better understanding of the interaction of chemical dispersants and crude oil at ocean depth. Early in the blowout release, partial emulsification of oil and heterogeneous slicks were observed as it rose to the surface from 1500-m depth (JAG report, 2010). As a countermeasure, Sub-Sea Dispersant Injection (SSDI) was used, where dispersants were injected directly at the release point as a possible means to increase dispersion efficiency and to potentially reduce the amount of dispersant needed if applied at the air-sea interface (CRRC Report, 2010). Potential advantages of this application during a continuous oil release included the fact that the fresh (un-weathered) oil was considered well suited for dispersion, operators were able to inject the dispersant directly into the oil stream thereby maximizing dispersant/oil contact, sufficient control of DOR (Dispersant-to-Oil Ratio) could be maintained, injection may minimize the need for surface application because of reduced oil surfacing, and optimized subsurface application would likely promote formation of smaller and stable oil droplets, enhancing biodegradation (Lee et al., 2009). The Unified Area Command (UAC) coordinated a large-scale environmental

ED_001324_00000745-00002

monitoring program to track and characterize dispersed subsurface oil plumes based on field data and transport modeling outputs. Oil Droplet Size Distribution (DSD) and fluorescence intensity from submersible sensors were used as an indication of Dispersion Effectiveness (DE) onboard vessels, where concentrations were monitored to evaluate oil dispersion (presence of small droplets ≤ 70 μm) based on previous studies for surface dispersant applications (Li et al., 2009a). Monitoring provided sound evidence of the presence of oil-bearing small particles both in surface waters and in the subsurface plume (JAG Report, 2010). SSDI correlated with a higher proportion of low molecular weight compounds in subsea waters compared to surface, suggesting that SSDI may have promoted the formation of small oil droplets in the deep sea and thus would have the potential for enhancing the weathering and dissolution of oil in the water column.

However, uncertainties still exist regarding the effectiveness of this application. For example, assumptions of the optimal DOR are based on empirical data mostly obtained from bench-scale experiments designed for testing at standard temperatures and pressures (STP), whereas conditions at a wellhead on the ocean floor or anywhere along a riser could be significantly different. Hence, DOR for direct injection needs to be better understood. Although theoretical analyses and experiments suggest that oil jet breakup is insensitive to the absolute value of hydrostatic pressure for incompressible liquid-liquid systems (Masutani and Adams 2000), the effects of several ambient environmental factors on SSDI, including high release pressure, high oil temperature, low water temperature, and the presence of methane and suspended sediments in the oil plume and/or surrounding water column remain to be clarified. Improved understanding on the influence of these factors and the interaction of oil and chemical

ED_001324_00000745-00003

dispersant under a range of turbulent regimes at depth is required for informed decision-making for future SSDI use.

For evaluating DE, standard laboratory tests are inherently limited in simulating operational performance under realistic environmental conditions in part due to space constraints that are critical for transport and dilution efficiency (NRC, 2005). Meso-scale tanks capable of generating waves and flume flows to simulate ocean conditions help to address this issue. One such tank facility at the Bedford Institute of Oceanography (BIO; Dartmouth, Nova Scotia) has been used previously to assess chemical dispersant effectiveness for various oil types as a function of energy dissipation rate and particle size distribution (Li et al. 2009b) and demonstrated that the effectiveness of a dispersant is strongly dependent on wave conditions, dispersant type, and oil type (Wickley-Olsen et al. 2007; Li et al. 2008; Lee et al. 2009). A strong correlation has been established between dispersion effectiveness and *in situ* DSD within the hydrodynamic regime, particularly energy dissipation rate, under a variety of wave conditions (Li et al. 2008; Li et al. 2009b), where flume mode can simulate the effects of underwater currents on dispersion and dilution of oil (Li et al. 2009a; Li et al. 2010). Experiments have also shown the reliability of fluorescence intensity as a proxy for oil concentration within oil dispersions (Conmy et al., 2014).

Presented here are results from a series of high pressure jet releases of oil within the BIO flume tank to assess the operational performance of SSDI. DSD and fluorescence intensity were used as a proxy for dispersion efficiency for treatments with (chemically-enhanced dispersion) and without (physical dispersion) chemical dispersants. The objective of this work was to evaluate the effects of water temperature and dispersant-to-oil ratio on DE of three oils at high

ED_001324_00000745-00004

reservoir temperatures. Findings help (1) to determine the applicability of existing *in situ* monitoring technologies for SSDI and (2) inform efforts to integrate DSD into deep water blowout plume formation models that enable prediction of the dispersed oil droplets under high-flow subsurface release velocities. DWH spill monitoring program DSD and fluorescence data played a significant role in supporting emergency response operations, fate and transport modeling, and impact assessment. Findings from this study have implications for efforts in support of future deep-water spill preparedness.

METHODS

Flume Tank Description - Oil dispersion experiments were conducted using Alaska North Slope crude oil (ANS), South Louisiana Crude (SLC) and Intermediate Fuel Oil 120 (IFO 120) with Corexit 9500 and Finasol OSR 52 chemical dispersants in the 32m long flow-through carbon steel flume tank (31,000 L) at BIO. Seawater was pulled from the Bedford Basin (50cm below surface) via two smaller centrifugal pumps (110 gpm), and filtered through high-flow polypropylene bag filters (5 and 25 μm) to a fiberglass holding tank (25,000 L) that supplies seawater for the system to ensure that a constant flow rate is maintained. Two high-flow centrifugal pumps (600 gpm) provided flow to generate horizontal water currents in the tank, where flow gauges on influent and effluent pipes were monitored and valve adjustments made to obtain a balanced flow rate throughout experiments. Water current velocities were measured in the tank using an ADV (Nortek Vectrino) to maintain consistent horizontal water current velocities (3.5 cm/s) at all measured depths. At the completion of experiments, oil absorbent pads removed oil from the water surface. Effluent wastewater was filtered over layers of polypropylene PomPom Oil-Mops to remove insoluble oil from the water prior to discharging, where effluent samples were collected and PomPom's were changed if oil concentrations exceed

ED_001324_00000745-00005

the minimum guidelines (10 ppm) for wastewater discharge in Canada.

Subsurface Oil Injection System - A custom subsurface oil injection system was used to generate dispersed oil plumes in the tank (Figure 1), consisting of a 2 L stainless steel pressure vessel and a series of valves and pressure gauges, fastened to the outer wall of the tank. Inside the tank, a fitting connects the outer assembly to a nozzle (2.4 mm), which extends mid-width perpendicular to the tank wall (9 m downstream from the influent pipe) and is angled at the tip to direct the discharge plume downstream and use horizontal length of the tank to capture the plume movement. For each experiment, oil or oil/dispersant premix is added to the pressure vessel in order to reduce the influence of any additional confounding factor of mixing effectiveness. Copper coil within the pressure vessel connects to a water bath to permit oil heating to 80°C, and then pressurized (40 psi for ANS and SLC; 60 psi for IFO 120) with compressed Nitrogen. A ball valve connected to the vessel controls the oil release through the subsurface nozzle into the tank. Release time and total volume (determined by mass) of oil injected are recorded. After each experiment, the subsurface injector system was cleaned by flushing with toluene, acetone and fresh water.

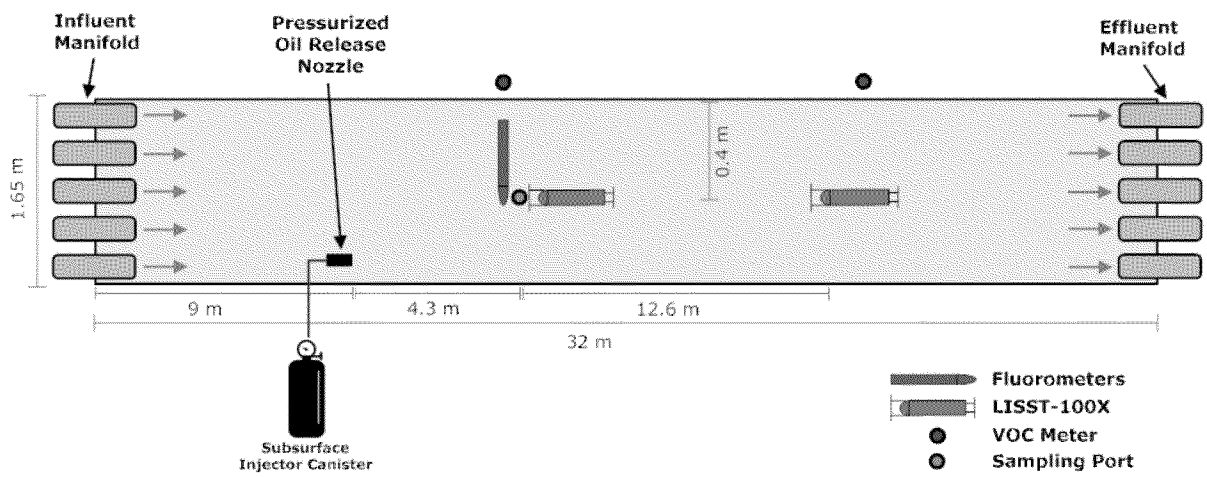

Figure 1. Schematic diagram showing the location of the subsurface injector and *in situ* instrumentation submerged within the tank.

Submersible Sensor Deployment - Sensors were mounted on an aluminum frame located 4.3 m from the oil release point with their pressure windows and at a depth of 0.4 m. The instruments were attached to a crosspiece support bar, so that they were all located the same distance downstream from the oil release point with the pressure window pointed directly towards the bottom of the tank. Data acquisition systems were used to control and collect data with real-time displays from the *in situ* fluorometers. A total of six *in situ* hydrocarbon fluorometers were evaluated during this study; Chelsea Technologies Group UV Aquatrackas - Refined and Crude models, Turner Designs Group Cyclops - Fine and Crude models, Sea Bird – Wet Labs Inc ECO-FLU, and GmBH Trios. Sampling rates and units of signal intensity varied for each instrument with one reading every 5 seconds for GmBH (μg/L PAH), every 3 seconds for Cyclops (auto-gain feature; mV), and every 1 second for the ECO and Aquatrackas (μg/L QSDE, μg/L perylene and μg/L carbazole, respectively. Oil droplet size was measured *in situ* using two LISST-100X (Laser *in-situ* Scattering and Transmissometry) particle size analyzers (Sequoia Scientific, Inc), measuring particle size from 2.5 – 500 μm. The first LISST (upstream LISST) was located immediately after the fluorometer package support frame at a distance of 5.1 m from the oil release point and the second LISST (downstream LISST) was located at 16.9 m from the oil release point and both at a depth of 0.4 m (Figure 1). Placement was informed by the numerical modeling efforts conducted previously in the tank to maximize oil droplet detection without saturating the instrument. Real-time data was provided by LISST-SOP data acquisition software (ver. 5) with a sample acquisition rate of one measurement every 3 seconds.

ED_001324_00000745-00007

Underwater video of oil droplets and the transport of the plume were captured using a GoPro Hero4 digital camera, as well as a Sony RX100 III digital camera with underwater housing.

Submersible Sensor Data Processing - LISST data files were processed using a statistically-based quality control script written using the R statistical package. This script identifies and removes "Over Range" samples (defined as 0 μL/L) and outliers. Outliers are defined as any reading that is greater than the moving mean (5 data points before and after the targeted time point) of the dataset multiplied by four times the standard deviation (over the same interval as the moving mean). Due to the potential for one or more extreme outliers to skew both the moving mean and standard deviation calculations for points around them, this outlier detection routine is run iteratively, excluding previously flagged points, until no more outliers are detected. The script then calculates the Total Particle Concentration (TPC), Volume Mean Diameter (VMD), and Particle Size Concentration (PSC). It then detects the plume curve (if present) and time-normalizes the data based on that location. Data are presented as Droplet Size Distribution (DSD). Plots presented include data 2 minutes before and 8 minutes after the start of the plume curve. Data from the Downstream LISST were normalized so that the plume began at t = 5 min in order to visually convey that the plume was detected in the tank roughly 3 min after detection by the LISST further upstream near point of injection release. Similar to the LISST data, a script was used to detect outliers in the fluorometry data. Curve detection was performed and the data was time-normalized to include 2 minutes of data before, and 8 minutes of data after the start of the plume curve. The baseline of the plume curve was calculated using data points observed in the first minute preceding the start of the curve and this baseline was subtracted from the data. Finally, factory calibration factors were applied to the data.

Experimental Design -. Seawater temperature and salinity in the tank were recorded

ED_001324_00000745-00008

using a handheld probe (YSI Incorporated, Yellow Springs, OH). Prior to experiments, the tank was operated in recirculation mode (10 minutes) to allow current flow to stabilize. Five minutes prior to oil injection, data-logging on all instruments was started and background seawater samples were collected. After oil injection, the real-time readout of the fluorometer signal was monitored for the first spike in signal intensity (usually after 2 minutes), and bottle chemistry sample collection began. The experiments ran for 12 minutes and the tank was cleaned using Big Orange Degreaser, to prevent any potential contamination between experiments. Instrument windows were cleaned using disposable alcohol wipes. Water samples were returned to the lab and stored at 4°C.

Discrete Chemistry Samples - Water samples for chemical analysis were collected at various time points throughout the experiments. Three ¼" stainless steel tubes were attached to the aluminum fluorometer frame, so that the end of the tube was located at the same depth as the instrument pressure windows (0.4 m). These were attached via silicon tubing to a digital peristaltic pump with a 120 mL/min flow rate. Samples were analyzed for Total Petroleum Hydrocarbon (TPH) using a method developed by DFO in-house (Cole et al., 2007; King et al., 2015) for Gas Chromatograph (GC) - Flame Ionization Detector (FID) analysis. An eight point calibration was generated using standards prepared from the appropriate crude oil stock that was used to generate the TPH samples (e.g. ANS, IFO 120 and SLC). Peak quantification was performed using relative response factors. Samples were analyzed for benzene, toluene, ethylbenzene and xylene (BTEX) using EPA Method 8240 (purge and trap), modified by running a GC - Mass Spectrometer (MS) in selected ion monitoring mode to include ethylbenzene. BTEX standards were prepared in 40 mL purge and trap vials; and samples and standards were analyzed using this method, along with sample blanks and duplicate samples.

ED_001324_00000745-00009

TPH and BTEX results are not shown here in detail but can be found in the EPA 600/F-16/250 Report (2016).

RESULTS & DISCUSSION

A total of 72 experiments were conducted in replicate, where water ranged in temperature from 4.9 - 20.3 °C, with 11 °C serving as the cut off between warm and cold water tests. Previous experiments within the BIO flume tank facility have assessed dispersion effectiveness as a function of energy dissipation rate and particle size distribution (Li et al. 2009a) and demonstrated that DE is strongly dependent on wave conditions, dispersant type, and oil type (Lee et al. 2009) and highly correlated with *in-situ* droplet size distribution (Li et al. 2008; Li et al. 2009a). Here, DE was evaluated via response monitoring tools (fluorescence and particle size analyzers) during high-pressure subsurface injection experiments.

Dispersant-to-Oil Ratio (DOR) Effects- Addition of either Corexit 9500 or Finasol OSR 52 chemical dispersants to Alaskan North Slope (ANS), IFO 120 and South Louisiana Crude (SLC) oils resulted in a decrease in the Volume Mean Diameter (VMD) and shifted the Droplet Size Distribution (DSD) to smaller droplets for warm water treatments (Figure 2). For ANS, dispersions created without chemical dispersants or Dispersant-to-oil ratio (DOR) = 1:100 yielded VMD larger than 70 μm and exhibited unimodal DSD. Dispersions created with DOR = 1:20 yielded VMD between < 70 μm size range with a bimodal distribution. SLC oil was more dispersible compared to ANS for treatments with and without chemical dispersant. Bimodal distribution was observed during DOR = 1:20 and some DOR = 1:100 experiments indicating that the jet release of this particular oil into warm water produced smaller droplets than the ANS. During the DWH spill, droplets ≤ 70μm were considered small enough to remain in suspension

ED_001324_00000745-00010

and were monitored as a proxy for evaluating oil dispersion efficiency. This suggests that produced SLC droplets from a DOR = 1:20 or 1:100 dispersant injection, and ANS droplets at DOR = 1:20 would likely remain dispersed in the presence of mixing energy given the larger proportion of small droplet sizes observed. In general, Corexit 9500 produced slightly smaller droplets compared to Finasol OSR 52 for warm water treatments. The addition of Corexit 9500 or Finasol OSR 52 to IFO 120 during warm temperature experiments resulted in a shift in DSD and a decrease in VMD; however bimodal distribution was not achieved and even DOR = 1:20 did not yield VMD less than 70 μm in most cases. This suggests that dispersant addition to this oil at warm temperatures would not yield droplet sizes that would likely remain in suspension.

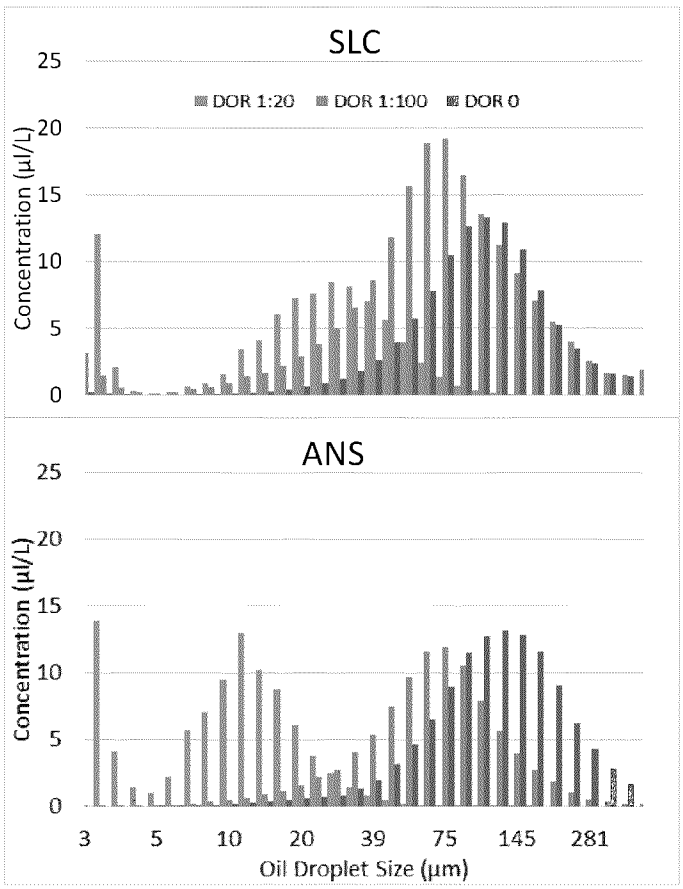

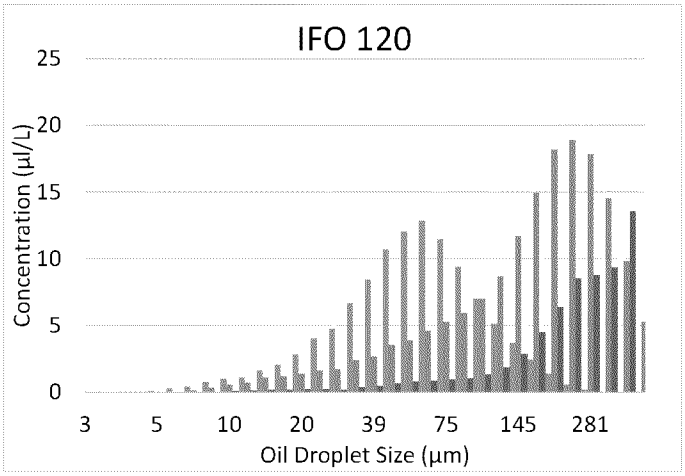

Figure 2. LISST DSD for SLC, ANS and IFO 120 with Corexit 9500 at three DOR treatments in warm water. Histograms represent averages obtained at the 2 minute time stamp during each experiment.

Water Temperature Effects - For ANS, dispersion with < 70 µm droplet VMD was observed for the DOR = 1:20 treatments at both cold and warm water temperatures (Figure 3). Water temperature did not appear to influence the DSD or VMD for this lighter crude oil. However, a temperature effect was observed on the Total Particle Concentration (TPC), where lower temperatures were coincident with fewer particles dispersed within the plume for a given volume of oil injected. This may be due to enhanced density differences between the oil and water at colder temperatures, thus quicker rise time of the produced droplets. For the addition of Corexit 9500 or Finasol OSR 52 to IFO 120 at cold water temperatures, smaller droplet sizes were not observed, where DOR = 1:20 remained above 200 µm. This suggests that dispersant addition to this oil at cold temperatures would not yield droplet sizes that would likely remain in suspension.

ANS IFO 120

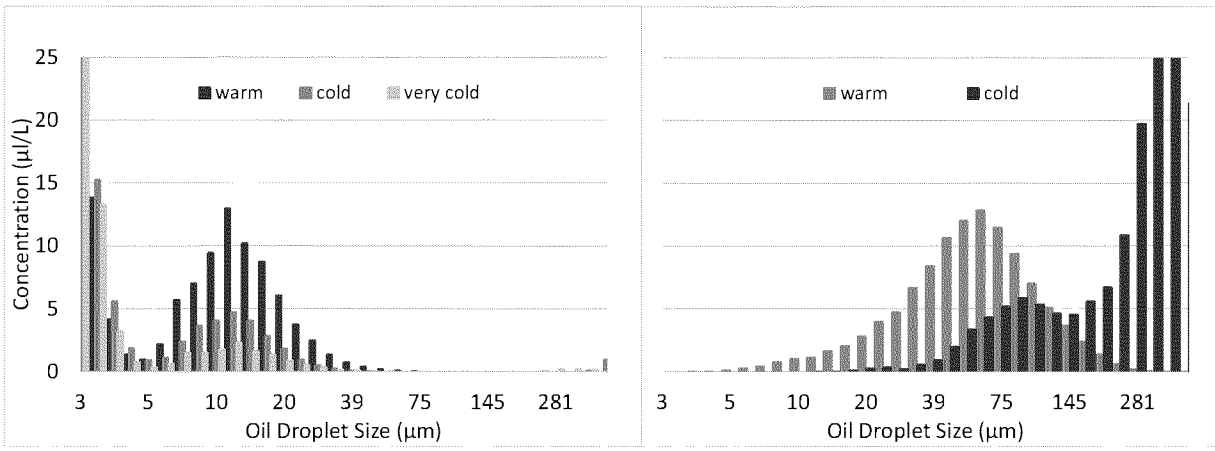

Figure 3. LISST DSD for ANS and IFO 120 with Corexit 9500 at DOR = 1:20 and varying water temperature.

For experiments conducted at water temperatures < 5 °C, the LISST particle size analyzer yielded unexpected DSD where even a unimodal distribution was not measured. Chemistry and *in situ* fluorescence data indicate that the oil was in fact dispersed adequately. This suggests potential operational problems < 5 °C, even though it is within the operating temperature (manufacturer manual). Additional testing of cold water temperature limits is recommended.

Upstream and Downstream Particle Fractionation - Histograms representing the particle concentration for a given size class from the upstream and downstream LISSTs suggest dilution and fractionation of particles within the plume. The downstream LISST positioned further from the jet release serves as an indication of plume evolution through the tank. For all oil and DOR treatments, dilution in particles (decrease in TPC) within the plume expectedly occurred. Also evident is a shift to smaller particles for all DOR treatments as the plume moves through the tank, where size fractionation was dependent on DOR treatment (Figure 4). Physical dispersion (DOR 0) treatments for lighter oils were found to have the largest shift in

DSD and VMD between the upstream and downstream LISSTs suggesting the largest effect of particle fractionation in the plume. Where the decrease in TPC suggests plume dilution in the tank, the DSD shift to smaller particles suggests that within each experiment larger droplets were removed from the plume within 6 minutes of the oil release, most likely rising to the surface of the tank. The effect was least observed in the DOR 1:20 treatments where dilution occurred but the presence of smaller droplets (with lower rise times) at the point of release most likely didn't allow for fractionation. The effects of fractionation were observed in warm and cold treatments.

Time series particle size data allows for evaluating plume dynamics over the duration of the experiments. Figure 5 depicts time series contour plots of the plume, where colored contours represent the particle concentration (normalized to max value for comparison purposes) for given droplet sizes through time. These plots allow for ascertaining how the DSD shifts over the duration of the release as the plume moves in the horizontal direction in the tank. For ANS, data suggest that the leading edge of the plume, as detected by the upstream LISST, exhibited a wide range in DSD during the first few minutes after release. As the plume advances down the tank, the DSD becomes narrower with a shift in the VMD for the DOR = 1:100 and 0 treatments. DSD remained similar for the DOR = 1:20 treatment. Warm and cold water treatments exhibit similar trends.

ED_001324_00000745-00014

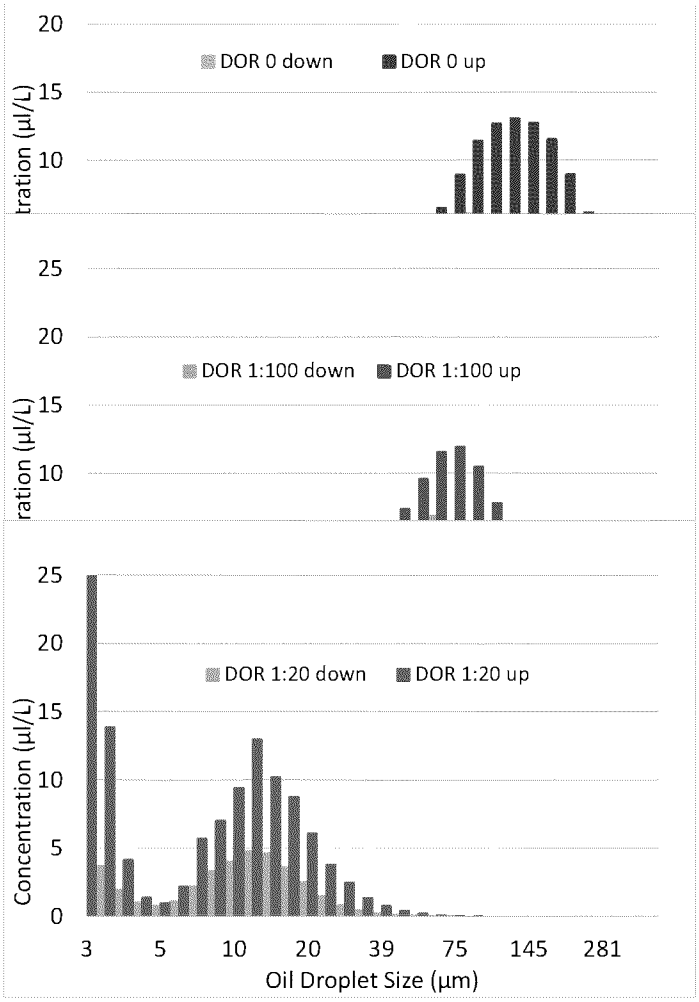

Figure 4. Upstream and downstream LISST Droplet Size Distribution and particle concentration for ANS with Corexit 9500 during warm water treatments.

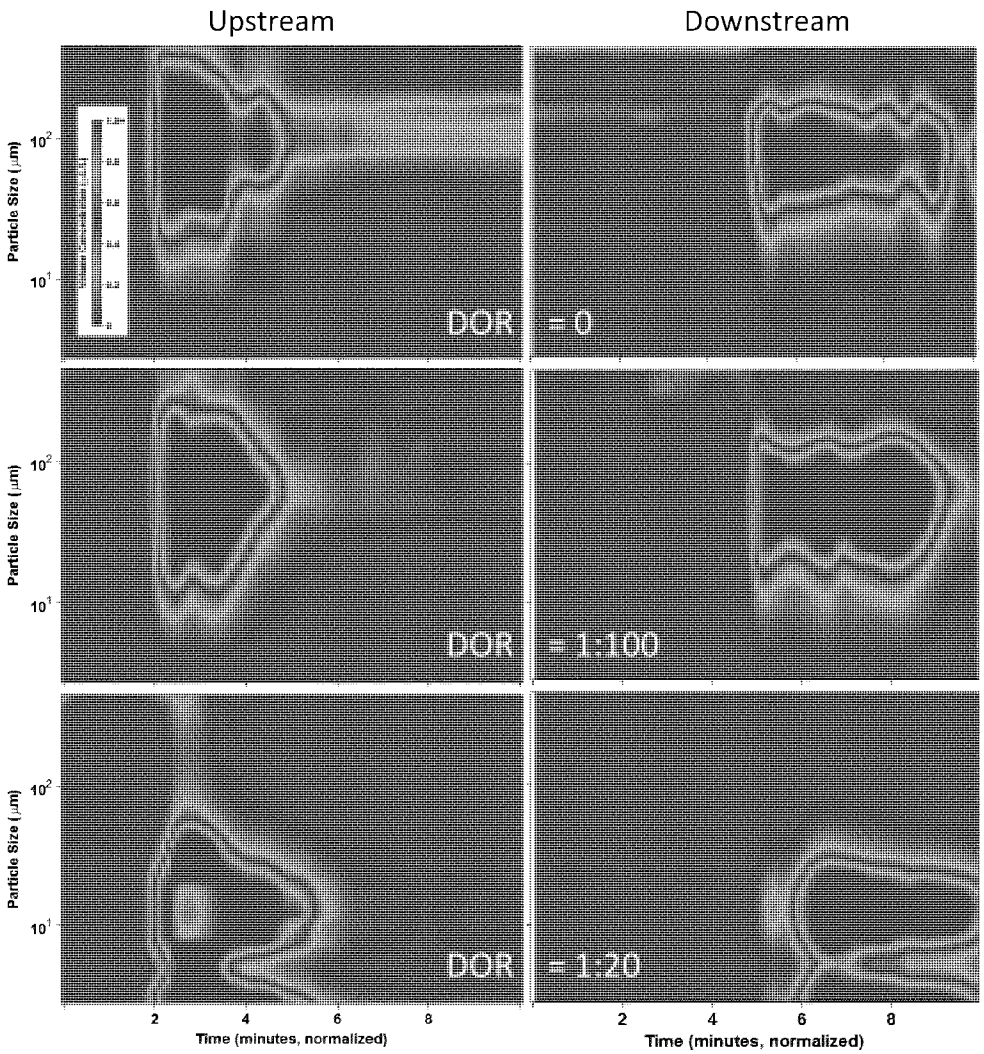

Figure 5. Time series contours of droplet size distribution and particle concentration from the upstream (left panels) and downstream (right panels) LISSTs for ANS with Corexit 9500 during warm water treatments.

<u>Plume Fluorescence Intensity</u> – In addition to the plume transport of particles (oil droplets), dissolved hydrocarbons were also measured via discrete samples and by proxy using fluorescence intensity. The reliability of *in situ* fluorescence measurements as a proxy for oil concentration within physically and chemically dispersed oil has been demonstrated previously

within the tank (Conmy et al., 2014). Here, *in situ* fluorescence serves as a good proxy for oil concentration during the subsurface injection experiments. However, heterogeneity of the produced plumes and the short time scale of experiments (~10 min) led to difficulties in correlations between the plume particle size analyses and chemistry results. This is in part due to discrete samples representing 15 second averages as opposed to instantaneous measures given by fluorometers and particle size analyzers. Thus, although general trends were similar, exact matchups between *in situ* data streams and discrete samples proved to be challenging (Figure 6). Given the experimental design, fluorescence was found to be better suited for correlation with total particle concentration (Figure 7). Depicted are the in situ fluorescence and TPC data during a warm water experiment of ANS with (left) and without (right) Corexit 9500. When exposed to dispersant, fluorescence estimates of dissolved hydrocarbons was higher compared to oil alone treatments, and signal persisted for longer periods of time. Whereas a sharper decay in the fluorescence intensity and the TPH values were observed for the physically dispersed oil.

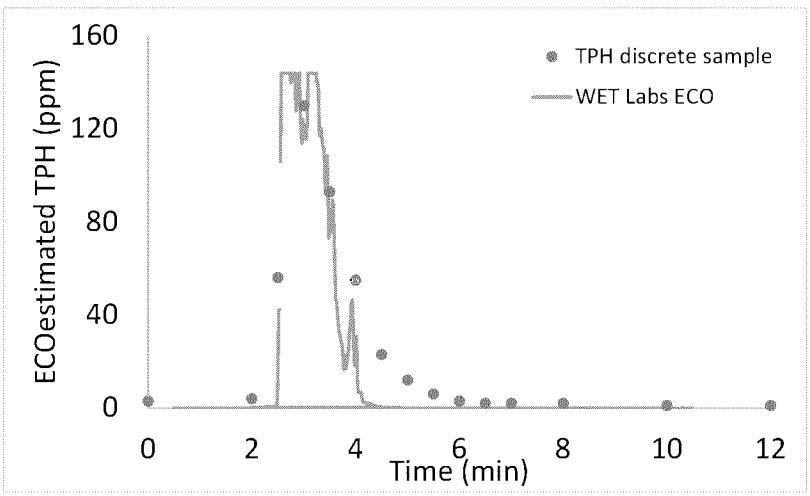

Figure 6. Fluorescence intensity and TPH samples for a warm water treatment using SLC

at DOR = 1:20.

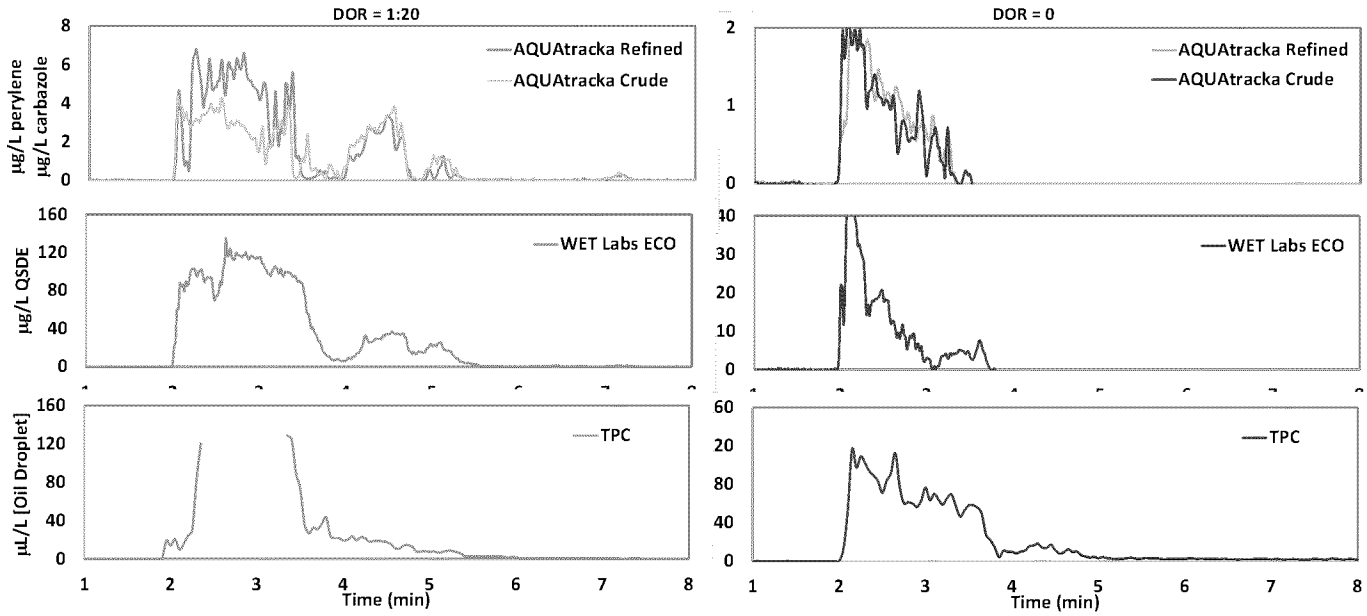

Figure 7. Fluorescence intensity and TPC as a function of time for ANS warm water treatment.

CONCLUSIONS

In situ oil droplet size distribution, particle concentration and fluorescence data from this study are essential for better understanding dispersion effectiveness and for refining droplet formation and trajectory models, such as modified Weber Number technique (Johansen et al., 2013) and the VDROP-J model (Zhou et al., 2014). Thus, findings from this study have implications for predicting the behavior of oil and plume formation, decision-making pertaining to SSDI as a countermeasure, and assessing the transport and fate of slicks and subsurface plumes in support of emergency response operations during any future deep water spills.

ED_001324_00000745-00018

REFERENCES

Conmy, R. N., et al. (2014) Submersible Optical Sensors Exposed to Chemically Dispersed Crude Oil: Wave Tank Simulations for Improved Oil Spill Monitoring. Environ. Sci. Technol. 48(3): 1803-1810.

Cole, M.G., T. King, K. Lee (2007) Analytical technique for extracting hydrocarbons from water using sample container as extraction vessel in combination with a roller apparatus. Anal. Chem., 77: 2210-17.

CRRC Report (2010) Coastal Response Research Center Deepwater Horizon Dispersant USE Meeting Report, May 26-27, 2010, 108 pp.

EPA 600/F-16/250 Federal Report (2016) Dispersant Effectiveness, In-Situ Droplet Size Distribution and Numerical Modeling to Assess Subsurface Dispersant Injection as a Deepwater Blowout Oil Spill Response Option *and* Evaluation of Oil Fluorescence Characteristics to Improve Forensic Response Tools; IAA No. E12PG00037 for DOI BSEE, 144 pp.

Joint Analysis Group Report (2010) Review of Data to Examine Subsurface Oil in the Vicinity of DWH MC-252, May 19-June 19, 2010; 29 pp.

Johansen, O., et al. (2013) Droplet breakup in subsea oil releases - Part 2: Predictions of droplet size distributions with and without injection of chemical dispersants. Mar. Poll. Bull. 73(1): 327-335.

Lee, K., Li, Z., Boufadel, M.C., Venosa, A.D. and Scott Miles, M. (2009) Wave tank studies on

ED_001324_00000745-00019

dispersant effectiveness as a function of energy dissipation rate and particle size distribution. Final report submitted to NOAA/CRRC/UNH, 67 pp.

Li, Z., Lee, K., King, T., Boufadel, M.C. and Venosa, A.D., (2008) Oil droplet size distribution as a function of energy dissipation rate in an experimental wave tank 2008 International Oil Spill Conference. American Petroleum Institute, Washington D.C., Savannah, GA, pp. 621-626.

Li, Z., Lee, K., King, T., Boufadel, M.C. and Venosa, A.D., (2009a) Evaluating crude oil chemical dispersion efficacy in a flow-through wave tank under regular non-breaking wave and breaking wave conditions. Mar. Poll. Bull., 58: 735-744.

Li, Z., Lee, K., King, T., Boufadel, M.C. and Venosa, A.D., (2009b) Evaluating Chemical Dispersant Efficacy in an Experimental Wave Tank: 2, Significant Factors Determining *In Situ* Oil Droplet Size Distribution. Environ. Engin. Sci., 26(9): 1407-1418.

Li, Z., Lee, K., King, T., Boufadel, M.C. and Venosa, A.D., (2010) Effects of temperature and wave conditions on chemical dispersion efficacy of heavy fuel oil in an experimental flow-through wave tank. Mar. Poll. Bull., 60(9): 1550-9.

NRC Report (2005) National Research Council Oil Spill Dispersants: Efficacy and Effects, Washington, DC, 400 pp.

Wickley-Olsen, E., Boufadel, M.C., King, T., Li, Z., Lee, K., Venosa, A.D. (2007) Regular and breaking waves in wave tank for dispersion effectiveness testing. In: Proceedings of the 30th Arctic and Marine Oil spill Program (AMOP) Technical Seminar, Edmonton, AB, Canada. Environment Canada, Ottawa, Ontario, Canada, pp. 161–187.

Zhao, L., et al. (2014). Evolution of droplets in subsea oil and gas blowouts: Development and validation of the numerical model VDROP-J. Mar. Poll. Bull., 83(1): 58-69.

ED_001324_00000745-00020

Oil plume simulations: Tracking oil droplet size distribution and fluorescence within high-pressure release jets

R.N. Conmy[1], B. Robinson [2], T. King [2], M. Boufadel[3], S. Ryan[2], C. McIntyre[2], M. I. Abercrombie[4], K. Lee [2,5]

[1]U.S. Environmental Protection Agency, Office of Research and Development, 26 MLK Drive West, Cincinnati, OH 45255, USA

[2] Bedford Institute of Oceanography, Fisheries and Oceans Canada, 1 Challenger Dr, Dartmouth, NS, B2Y 4A2, Canada

[3] New Jersey Institute of Technology, Department of Civil and Environmental Engineering, University Heights, Newark, NJ 07102, USA

[4]University of South Florida, College of Marine Science, 140 7th Ave South, St. Petersburg, FL 33701, USA

[5] Commonwealth Scientific and Industrial Research Organisation, Oceans and Atmosphere Flagship, PO Box 1130, Bentley WA 6102, Australia

ABSTRACT

Optical measurements have been used during oil spill response for more than three decades to determine oil presence in slicks and plumes. Oil surveillance approaches range from simple (human eyeball) to the sophisticated (sensors on AUVs, aircraft, satellites). *In situ* fluorometers and particle size analyzers were deployed during the Deepwater Horizon (DWH) Gulf of Mexico oil spill to track shallow and deep subsea plumes. Uncertainties regarding instrument specifications and capabilities during DWH necessitated performance testing of sensors exposed to simulated, dispersed oil plumes. Seventy two wave tank experiments were conducted at the Bedford Institute of Oceanography. Simulated were oil releases with varying parameters such as oil release rate, oil temperature (reservoir temp ~ 80 $_{o}$C), water temperature (<8 $_{o}$C and >15 $_{o}$C), oil type, dispersant type (Corexit 9500 and Finasol OSR52) and dispersant to oil ratio (DOR). Plumes of Alaskan North Slope Crude, South Louisiana Crude and IFO-120

ED_001324_00000746-00001

oils were tracked using *in situ* fluorescence, droplet size distribution (DSD), total petroleum hydrocarbons (TPH) and benzene-toluene-ethylbenzene-xylene (BTEX). Results offer valuable information on the behavior and dispersibility of oils over a range of viscosity, DOR and environmental conditions. Findings have implications for fate and transport models, where DSD, chemistry and fluorescence are all impacted by release variables. This research was supported by the Bureau of Safety and Environmental Enforcement.

INTRODUCTION

The 2010 *Deepwater Horizon* (DWH) oil spill highlighted the pressing need for a better understanding of the interaction of chemical dispersants and crude oil at ocean depth. Early in the blowout release, partial emulsification of oil and heterogeneous slicks were observed as it rose to the surface from 1500-m depth (JAG report, 2010). As a countermeasure, Sub-Sea Dispersant Injection (SSDI) was used, where dispersants were injected directly at the release point as a possible means to increase dispersion efficiency and to potentially reduce the amount of dispersant needed if applied at the air-sea interface (CRRC Report, 2010). Potential advantages of this application during a continuous oil release included the fact that the fresh (unweathered) oil was considered well suited for dispersion, operators were able to inject the dispersant directly into the oil stream thereby maximizing dispersant/oil contact, sufficient control of DOR (Dispersant-to-Oil Ratio) could be maintained, injection may minimize the need for surface application because of reduced oil surfacing, and optimized subsurface application would likely promote formation of smaller and stable oil droplets, enhancing biodegradation (Lee et al., 2009). The Unified Area Command (UAC) coordinated a large-scale environmental monitoring program to track and characterize dispersed subsurface oil plumes based on field data and transport modeling outputs. Oil Droplet Size Distribution (DSD) and fluorescence intensity

ED_001324_00000746-00002

from submersible sensors were used as an indication of Dispersion Effectiveness (DE) onboard vessels, where concentrations were monitored to evaluate oil dispersion (presence of small droplets ≤ 70 μm) based on previous studies for surface dispersant applications (Li et al., 2009a). Monitoring provided sound evidence of the presence of oil-bearing small particles both in surface waters and in the subsurface plume (JAG Report, 2010). SSDI correlated with a higher proportion of low molecular weight compounds in subsea waters compared to surface, suggesting that SSDI may have promoted the formation of small oil droplets in the deep sea and thus would have the potential for enhancing the weathering and dissolution of oil in the water column.

Uncertainties still exist, however, regarding the effectiveness of this application. For example, assumptions of the optimal DOR are based on empirical data mostly obtained from bench-scale experiments designed for testing at standard temperatures and pressures (STP), whereas conditions at a wellhead on the ocean floor or anywhere along a riser could be significantly different. Hence, DOR for direct injection needs to be better understood. Although theoretical analyses and experiments suggest that oil jet breakup is insensitive to the absolute value of hydrostatic pressure for incompressible liquid-liquid systems (Masutani and Adams 2000), the effects of several ambient environmental factors on SSDI, including high release pressure, high oil temperature, low water temperature, and the presence of methane and suspended sediments in the oil plume and/or surrounding water column remain to be clarified. Improved understanding on the influence of these factors and the interaction of oil and chemical dispersant under a range of turbulent regimes at depth is required for informed decision-making for future SSDI use.

ED_001324_00000746-00003

For evaluating DE, standard laboratory tests are inherently limited in simulating operational performance under realistic environmental conditions in part due to space constraints that are critical for transport and dilution efficiency (NRC, 2005). Meso-scale tanks capable of generating waves and flume flows to simulate ocean conditions help to address this issue. One such tank facility at the Bedford Institute of Oceanography (BIO; Dartmouth, Nova Scotia) has been used previously to assess chemical dispersant effectiveness for various oil types as a function of energy dissipation rate and particle size distribution (Li et al. 2009b) and demonstrated that the effectiveness of a dispersant is strongly dependent on wave conditions, dispersant type, and oil type (Wickley-Olsen et al. 2007; Li et al. 2008; Lee et al. 2009). A strong correlation has been established between dispersion effectiveness and *in situ* DSD within the hydrodynamic regime, particularly energy dissipation rate, under a variety of wave conditions (Li et al. 2008; Li et al. 2009b), where flume mode can simulate the effects of underwater currents on dispersion and dilution of oil (Li et al. 2009a; Li et al. 2010). Experiments have also shown the reliability of fluorescence intensity as a proxy for oil concentration within oil dispersions (Conmy et al., 2014).

Presented here are results from a series of high pressure jet releases of oil within the BIO flume tank to assess the operational performance of SSDI. DSD and fluorescence intensity were used as a proxy for dispersion efficiency for treatments with (chemically-enhanced dispersion) and without (physical dispersion) chemical dispersants. The objective of this work was to evaluate the effects of water temperature and dispersant-to-oil ratio on DE of three oils at high reservoir temperatures. Findings help (1) to determine the applicability of existing *in situ* monitoring technologies for SSDI and (2) inform efforts to integrate DSD into deepwater blowout plume formation models that enable prediction of the dispersed oil droplets under high-

ED_001324_00000746-00004

flow subsurface release velocities. DWH spill monitoring program DSD and fluorescence data played a significant role in supporting emergency response operations, fate and transport modeling, and impact assessment. Findings from this study have implications for efforts in support of future deep-water spill preparedness.

METHODS

Flume Tank Description - Oil dispersion experiments were conducted using Alaska North Slope crude oil (ANS), South Louisiana Crude (SLC) and Intermediate Fuel Oil 120 (IFO 120) with Corexit 9500 and Finasol OSR 52 chemical dispersants in the 32m long flow-through carbon steel flume tank (31,000 L) at BIO. Seawater was pulled from the Bedford Basin (50cm below surface) via two smaller centrifugal pumps (110 gpm), and filtered through high-flow polypropylene bag filters (5 and 25 μm) to a fiberglass holding tank (25,000 L) that supplies seawater for the system to ensure that a constant flow rate is maintained. Two high-flow centrifugal pumps (600 gpm) provided flow to generate horizontal water currents in the tank, where flow gauges on influent and effluent pipes were monitored and valve adjustments made to obtain a balanced flow rate throughout experiments. Water current velocities were measured in the tank using an ADV (Nortek Vectrino) to maintain consistent horizontal water current velocities (3.5 cm/s) at all measured depths. At the completion of experiments, oil absorbent pads removed oil from the water surface. Effluent wastewater was filtered over layers of polypropylene PomPom Oil-Mops to remove insoluble oil from the water prior to discharging, where effluent samples were collected and PomPom's were changed if oil concentrations exceed the minimum guidelines (10 ppm) for wastewater discharge in Canada.

Subsurface Oil Injection System - A custom subsurface oil injection system was used to generate dispersed oil plumes in the tank (Figure 1), consisting of a 2 L stainless steel pressure

vessel and a series of valves and pressure gauges, fastened to the outer wall of the tank. Inside the tank, a fitting connects the outer assembly to a nozzle (2.4 mm), which extends mid-width perpendicular to the tank wall (9 m downstream from the influent pipe) and is angled at the tip to direct the discharge plume downstream and use horizontal length of the tank to capture the plume movement. For each experiment, oil or oil/dispersant premix is added to the pressure vessel in order to reduce the influence of any additional confounding factor of mixing effectiveness. Copper coil within the pressure vessel connects to a water bath to permit oil heating to 80°C, and then pressurized (40 psi for ANS and SLC; 60 psi for IFO 120) with compressed Nitrogen. A ball valve connected to the vessel controls the oil release through the subsurface nozzle into the tank. Release time and total volume (determined by mass) of oil injected are recorded. After each experiment, the subsurface injector system was cleaned by flushing with toluene, acetone and fresh water.

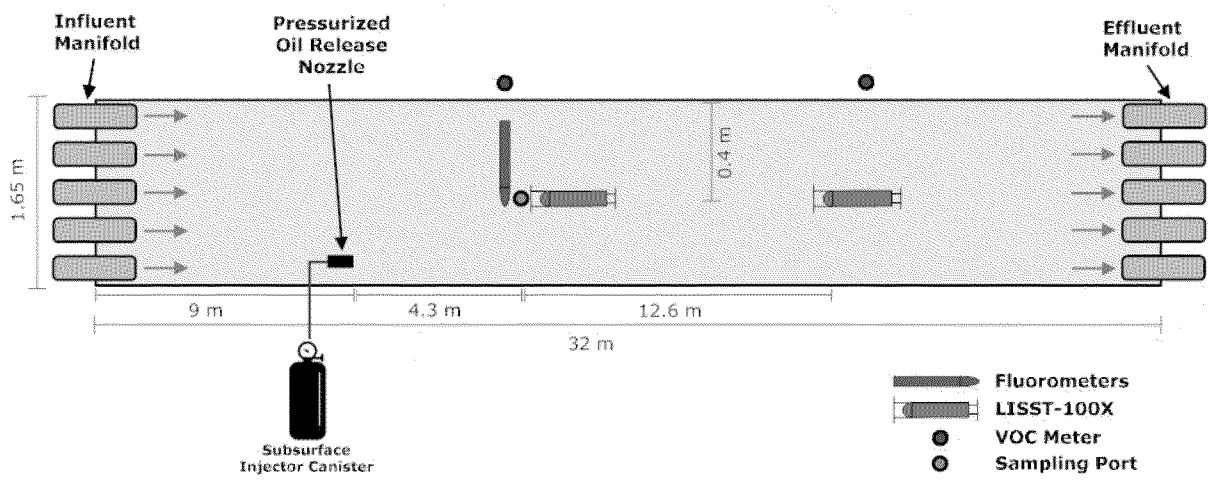

Figure 1. Schematic diagram showing the location of the subsurface injector and *in situ* instrumentation submerged within the tank.

ED_001324_00000746-00006

Submersible Sensor Deployment - Sensors were mounted on an aluminum frame located 4.3 m from the oil release point with their pressure windows and at a depth of 0.4 m. The instruments were attached to a crosspiece support bar, so that they were all located the same distance downstream from the oil release point with the pressure window pointed directly towards the bottom of the tank. Data acquisition systems were used to control and collect data with real-time displays from the *in situ* fluorometers. A total of six *in situ* hydrocarbon fluorometers were evaluated during this study; Chelsea Technologies Group UV Aquatrackas - Refined and Crude models, Turner Designs Group Cyclops - Fine and Crude models, Sea Bird – Wet Labs Inc ECO-FLU, and GmBH Trios. Sampling rates and units of signal intensity varied for each instrument with one reading every 5 seconds for GmBH (μg/L PAH), every 3 seconds for Cyclops (auto-gain feature; mV), and every 1 second for the ECO and Aquatrackas (μg/L QSDE, μg/L perylene and μg/L carbazole, respectively. Oil droplet size was measured *in situ* using two LISST-100X (Laser *in-situ* Scattering and Transmissometry) particle size analyzers (Sequoia Scientific, Inc), measuring particle size from 2.5 – 500 μm. The first LISST (upstream LISST) was located immediately after the fluorometer package support frame at a distance of 5.1 m from the oil release point and the second LISST (downstream LISST) was located at 16.9 m from the oil release point and both at a depth of 0.4 m (Figure 1). Placement was informed by the numerical modeling efforts conducted previously in the tank to maximize oil droplet detection without saturating the instrument. Real-time data was provided by LISST-SOP data acquisition software (ver. 5) with a sample acquisition rate of one measurement every 3 seconds. Underwater video of oil droplets and the transport of the plume were captured using a GoPro Hero4 digital camera, as well as a Sony RX100 III digital camera with underwater housing.

Submersible Sensor Data Processing - LISST data files were processed using a statistically-based quality control script written using the R statistical package. This script identifies and removes "Over Range" samples (defined as 0 μL/L) and outliers. Outliers are defined as any reading that is greater than the moving mean (5 data points before and after the targeted time point) of the dataset multiplied by four times the standard deviation (over the same interval as the moving mean). Due to the potential for one or more extreme outliers to skew both the moving mean and standard deviation calculations for points around them, this outlier detection routine is run iteratively, excluding previously flagged points, until no more outliers are detected. The script then calculates the Total Particle Concentration (TPC), Volume Mean Diameter (VMD), and Particle Size Concentration (PSC). It then detects the plume curve (if present) and time-normalizes the data based on that location. Data are presented as Droplet Size Distribution (DSD). Plots presented include data 2 minutes before and 8 minutes after the start of the plume curve. Data from the Downstream LISST were normalized so that the plume began at t = 5 min in order to visually convey that the plume was detected in the tank roughly 3 min after detection by the LISST further upstream near point of injection release. Similar to the LISST data, a script was used to detect outliers in the fluorometry data. Curve detection was performed and the data was time-normalized to include 2 minutes of data before, and 8 minutes of data after the start of the plume curve. The baseline of the plume curve was calculated using data points observed in the first minute preceding the start of the curve and this baseline was subtracted from the data. Finally, factory calibration factors were applied to the data.

Experimental Design -. Seawater temperature and salinity in the tank were recorded using a handheld probe (YSI Incorporated, Yellow Springs, OH). Prior to experiments, the tank was operated in recirculation mode (10 minutes) to allow current flow to stabilize. Five minutes

ED_001324_00000746-00008

prior to oil injection, data-logging on all instruments was started and background seawater samples were collected. After oil injection, the real-time readout of the fluorometer signal was monitored for the first spike in signal intensity (usually after 2 minutes), and bottle chemistry sample collection began. The experiments ran for 12 minutes and the tank was cleaned using Big Orange Degreaser, to prevent any potential contamination between experiments. Instrument windows were cleaned using disposable alcohol wipes. Water samples were returned to the lab and stored at 4°C.

Discrete Chemistry Samples - Water samples for chemical analysis were collected at various time points throughout the experiments. Three ¼" stainless steel tubes were attached to the aluminum fluorometer frame, so that the end of the tube was located at the same depth as the instrument pressure windows (0.4 m). These were attached via silicon tubing to a digital peristaltic pump with a 120 mL/min flow rate. Samples were analyzed for Total Petroleum Hydrocarbon (TPH) using a method developed by DFO in-house (Cole et al., 2007; King et al., 2015) for Gas Chromatograph (GC) - Flame Ionization Detector (FID) analysis. An eight point calibration was generated using standards prepared from the appropriate crude oil stock that was used to generate the TPH samples (e.g. ANS, IFO 120 and SLC). Peak quantification was performed using relative response factors. Samples were analyzed for benzene, toluene, ethylbenzene and xylene (BTEX) using EPA Method 8240 (purge and trap), modified by running a GC - Mass Spectrometer (MS) in selected ion monitoring mode to include ethylbenzene. BTEX standards were prepared in 40 mL purge and trap vials; and samples and standards were analyzed using this method, along with sample blanks and duplicate samples. TPH and BTEX results are not shown here in detail but can be found in the EPA 600/F-16/250 Report (2016).

RESULTS & DISCUSSION

ED_001324_00000746-00009

A total of 72 experiments were conducted in replicate, where water ranged in temperature from 4.9 - 20.3 $_{o}$C, with 11 $_{o}$C serving as the cut off between warm and cold water tests. Previous experiments within the BIO flume tank facility have assessed dispersion effectiveness as a function of energy dissipation rate and particle size distribution (Li et al. 2009a) and demonstrated that DE is strongly dependent on wave conditions, dispersant type, and oil type (Lee et al. 2009) and highly correlated with *in-situ* droplet size distribution (Li et al. 2008; Li et al. 2009a). Here, DE was evaluated via response monitoring tools (fluorescence and particle size analyzers) during high-pressure subsurface injection experiments.

Dispersant-to-Oil Ratio (DOR) Effects- Addition of either Corexit 9500 or Finasol OSR 52 chemical dispersants to Alaskan North Slope (ANS), IFO 120 and South Louisiana Crude (SLC) oils resulted in a decrease in the Volume Mean Diameter (VMD) and shifted the Droplet Size Distribution (DSD) to smaller droplets for warm water treatments (Figure 2). For ANS, dispersions created without chemical dispersants or Dispersant-to-oil ratio (DOR) = 1:100 yielded VMD > 70 μm and exhibited unimodal DSD. Dispersions created with DOR = 1:20 yielded VMD < 70 μm size range with a bimodal DSD. SLC oil was more dispersible compared to ANS for treatments with and without chemical dispersant. Bimodal distribution was observed during DOR = 1:20 and some DOR = 1:100 experiments indicating that the jet release of this particular oil into warm water produced smaller droplets than the ANS. During the DWH spill, droplets ≤ 70μm were considered small enough to remain in suspension and were monitored as a proxy for evaluating oil dispersion efficiency. This suggests that produced SLC droplets from a DOR = 1:20 or 1:100 dispersant injection, and ANS droplets at DOR = 1:20 would likely remain dispersed in the presence of mixing energy given the larger proportion of small droplet sizes observed. In general, Corexit 9500 produced slightly smaller

droplets compared to Finasol OSR 52 for warm water treatments. The addition of Corexit 9500 or Finasol OSR 52 to IFO 120 during warm temperature experiments resulted in a shift in DSD and a decrease in VMD; however bimodal distribution was not achieved and even DOR = 1:20 did not yield VMD less than 70 µm in most cases. This suggests that dispersant addition to this oil at warm temperatures would not yield droplet sizes that would likely remain in suspension.

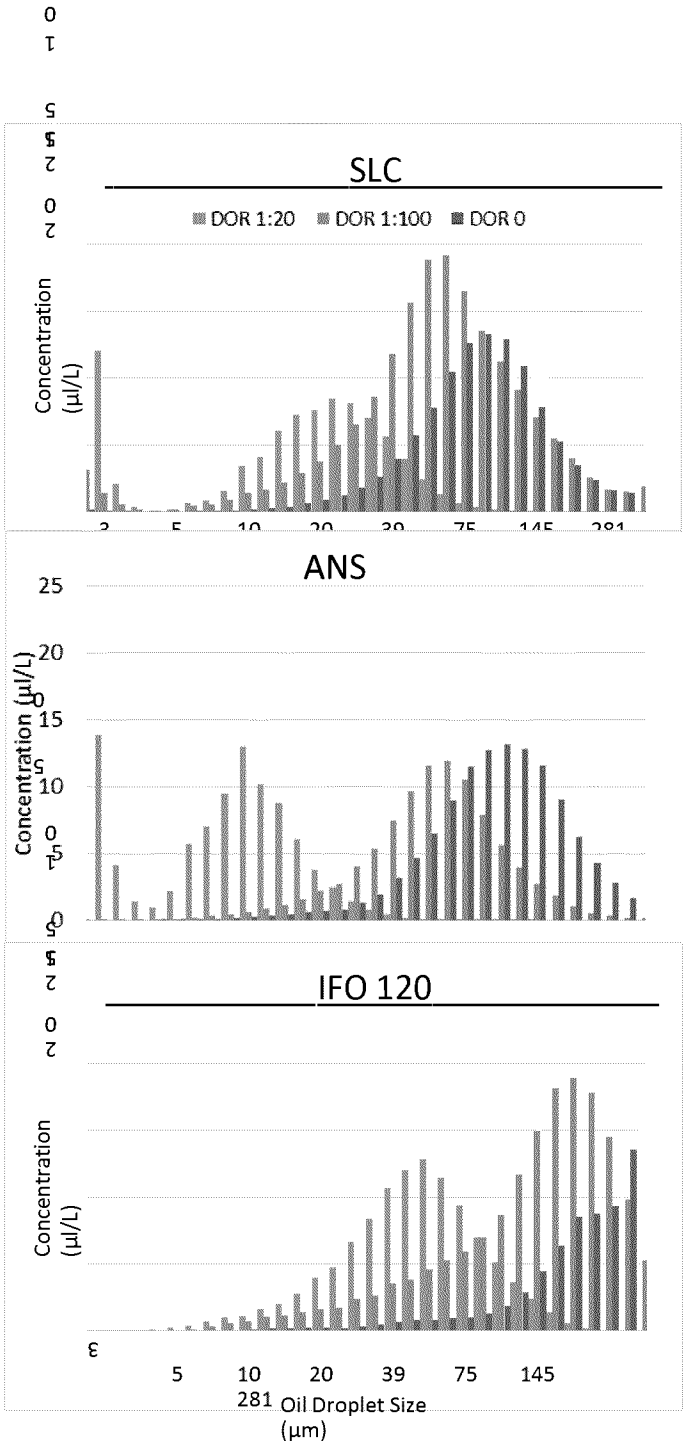

Figure 2. LISST DSD for SLC, ANS and IFO 120 with Corexit 9500 at three DOR treatments in warm water. Histograms represent averages obtained at the 2 minute time stamp during each experiment.

Water Temperature Effects - For ANS, dispersion with < 70 μm droplet VMD was observed for the DOR = 1:20 treatments at both cold and warm water temperatures (Figure 3). Water temperature did not appear to influence the DSD or VMD for this lighter crude oil. However, a temperature effect was observed on the Total Particle Concentration (TPC), where lower temperatures coincided with fewer particles dispersed within the plume for a given volume of oil injected. This may be due to enhanced density differences between the oil and water at colder temperatures, thus quicker rise time of the produced droplets. For the addition of Corexit 9500 or Finasol OSR 52 to IFO 120 at cold water temperatures, smaller droplet sizes were not observed, where DOR = 1:20 remained above 200 μm. This suggests that dispersant addition to this oil at cold temperatures would not yield droplet sizes that would likely remain in suspension.

ED_001324_00000746-00012

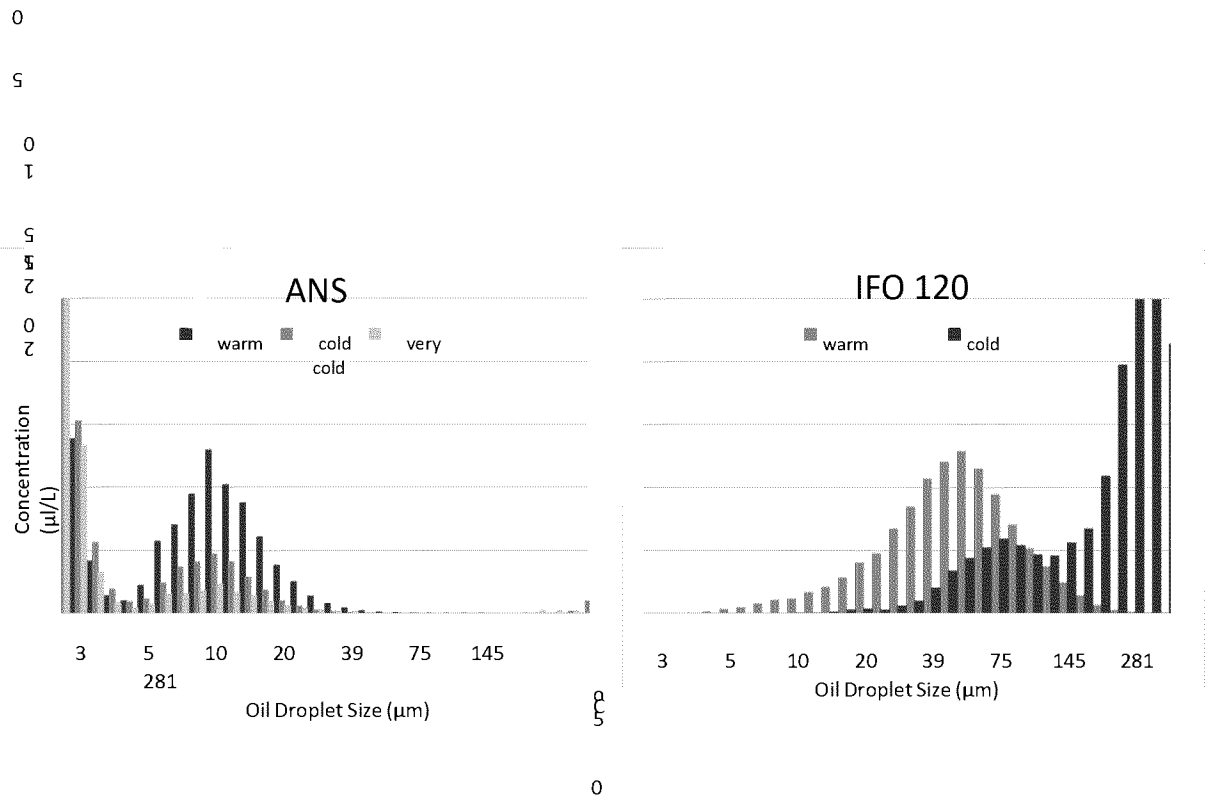

Figure 3. LISST DSD for ANS and IFO 120 with Corexit 9500 at DOR = 1:20 and varying water temperature.

For experiments conducted at water temperatures < 5 $_{o}$C, the LISST particle size analyzer yielded unexpected DSD where even a unimodal distribution was not measured. Chemistry and *in situ* fluorescence data indicate that the oil was in fact dispersed adequately. This suggests potential operational problems of the LISST at < 5 $_{o}$C, even though it is within the operating temperature (manufacturer manual). Additional testing of cold water temperature limits is recommended.

Upstream and Downstream Particle Fractionation - Histograms representing the particle concentration for a given size class from the upstream and downstream LISSTs suggest dilution and fractionation of particles within the plume. The downstream LISST positioned further from the jet release serves as an indication of plume evolution through the tank. For all oil and DOR treatments, dilution in particles (decrease in TPC) within the plume expectedly occurred. Also evident is a shift to smaller particles for all DOR treatments as the plume

moves through the tank, where size fractionation was dependent on DOR treatment (Figure 4). Physical dispersion (DOR 0) treatments for lighter oils were found to have the largest shift in DSD and VMD between the upstream and downstream LISSTs suggesting the largest effect of particle fractionation in the plume. Where the decrease in TPC suggests plume dilution in the tank, the DSD shift to smaller particles suggests that within each experiment larger droplets were removed from the plume within 6 minutes of the oil release, most likely rising to the surface of the tank. The effect was least observed in the DOR 1:20 treatments where dilution occurred but the presence of smaller droplets (with lower rise times) at the point of release most likely didn't allow for fractionation. The effects of fractionation were observed in warm and cold treatments.

Time series particle size data allows for evaluating plume dynamics over the duration of the experiments. Figure 5 depicts time series contour plots of the plume, where colored contours represent the particle concentration (normalized to max value for comparison purposes) for given droplet sizes through time. These plots allow for ascertaining how the DSD shifts over the duration of the release as the plume moves in the horizontal direction in the tank. For ANS, data suggest that the leading edge of the plume, as detected by the upstream LISST, exhibited a wide range in DSD during the first few minutes after release. As the plume advances down the tank, the DSD becomes narrower with a shift in the VMD for the DOR = 1:100 and 0 treatments. DSD remained similar for the DOR = 1:20 treatment. Warm and cold water treatments exhibit similar trends.

ED_001324_00000746-00014

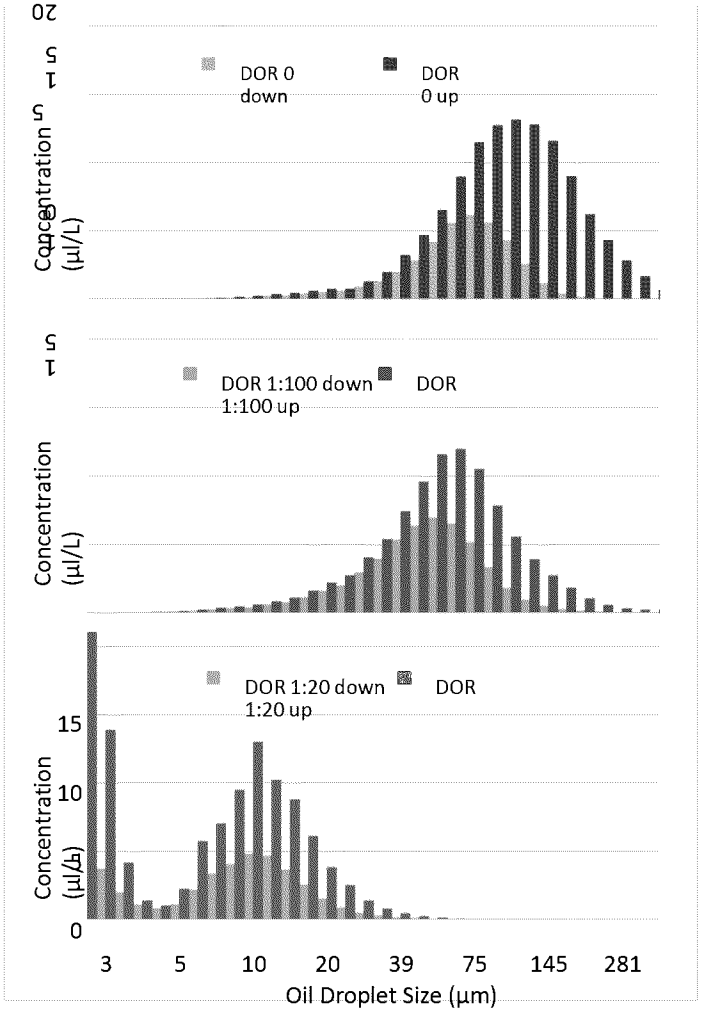

Figure 4. Upstream and downstream LISST Droplet Size Distribution and particle concentration for ANS with Corexit 9500 during warm water treatments.

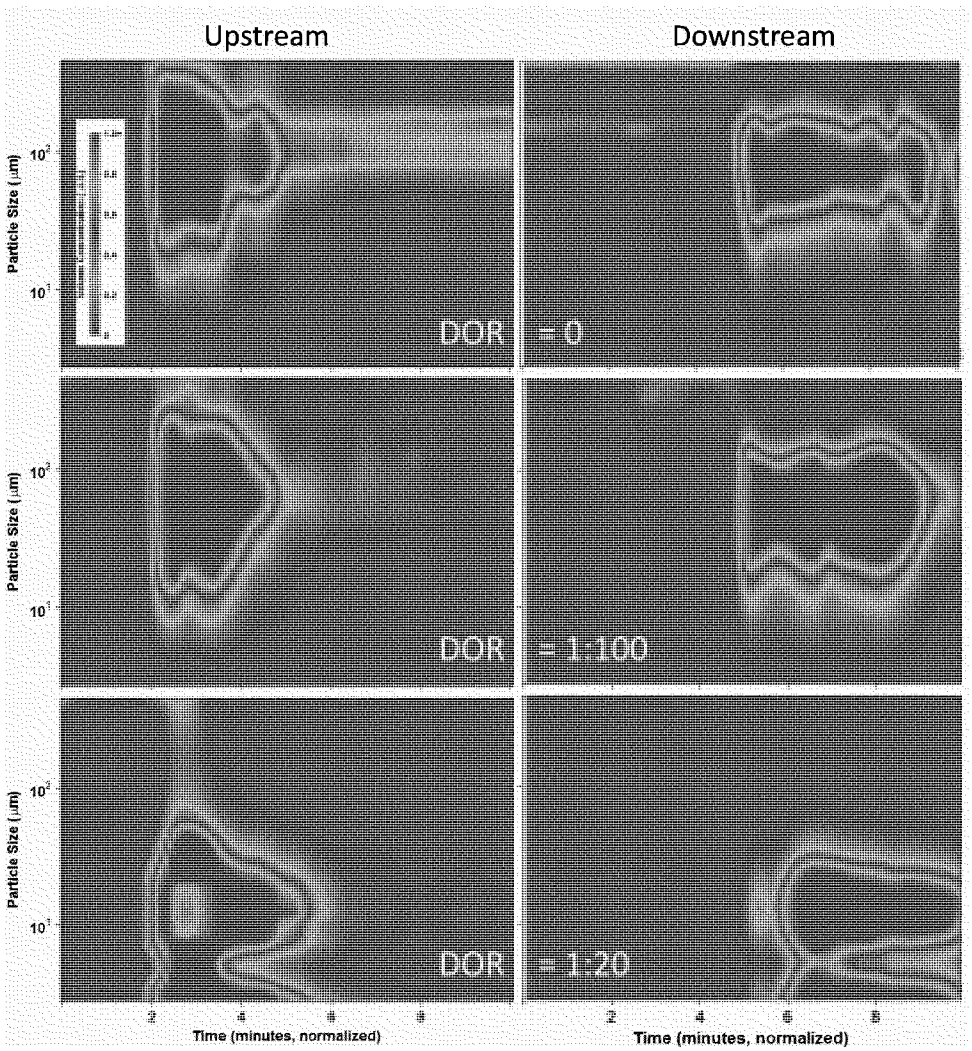

Figure 5. Time series contours of droplet size distribution and particle concentration from the upstream (left panels) and downstream (right panels) LISSTs for ANS with Corexit 9500 during warm water treatments.

Plume Fluorescence Intensity – In addition to the plume transport of particles (oil droplets), dissolved hydrocarbons were also measured via discrete samples and by proxy using fluorescence intensity. The reliability of *in situ* fluorescence measurements as a proxy for oil concentration within physically and chemically dispersed oil has been demonstrated previously within the tank (Conmy et al., 2014). Here, *in situ* fluorescence serves as a good proxy for oil

concentration during the subsurface injection experiments. However, heterogeneity of the produced plumes and the short time scale of experiments (~10 min) led to difficulties in correlations between the plume particle size analyses and chemistry results. This is in part due to discrete samples representing 15 second averages as opposed to instantaneous measures given by fluorometers and particle size analyzers. Thus, although general trends were similar, exact matchups between *in situ* data streams and discrete samples proved to be challenging (Figure 6). Given the experimental design, fluorescence was found to be better suited for correlation with total particle concentration (Figure 7). Depicted are the in situ fluorescence and TPC data during a warm water experiment of ANS with (left) and without (right) Corexit 9500. When exposed to dispersant, fluorescence estimates of dissolved hydrocarbons was higher compared to oil alone treatments, and signal persisted for longer periods of time. Whereas a sharper decay in the fluorescence intensity and the TPH values were observed for the physically dispersed oil.

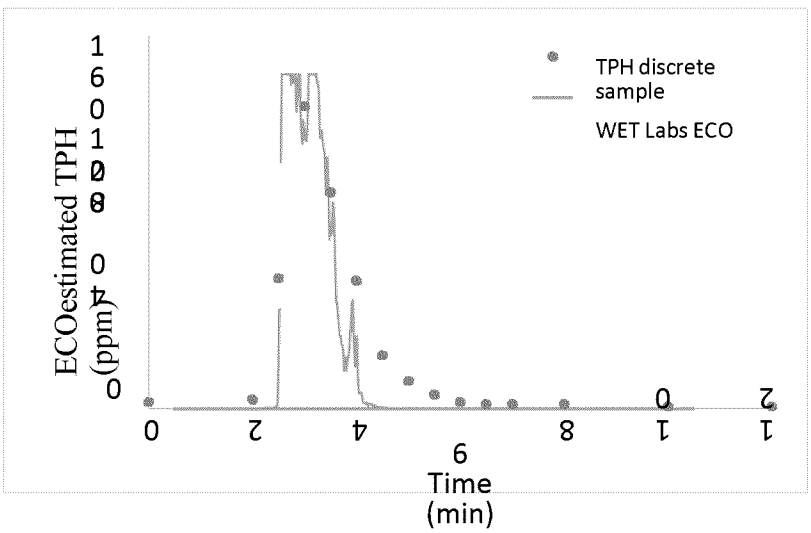

Figure 6. Fluorescence intensity and TPH samples for a warm water treatment using SLC at DOR = 1:20.

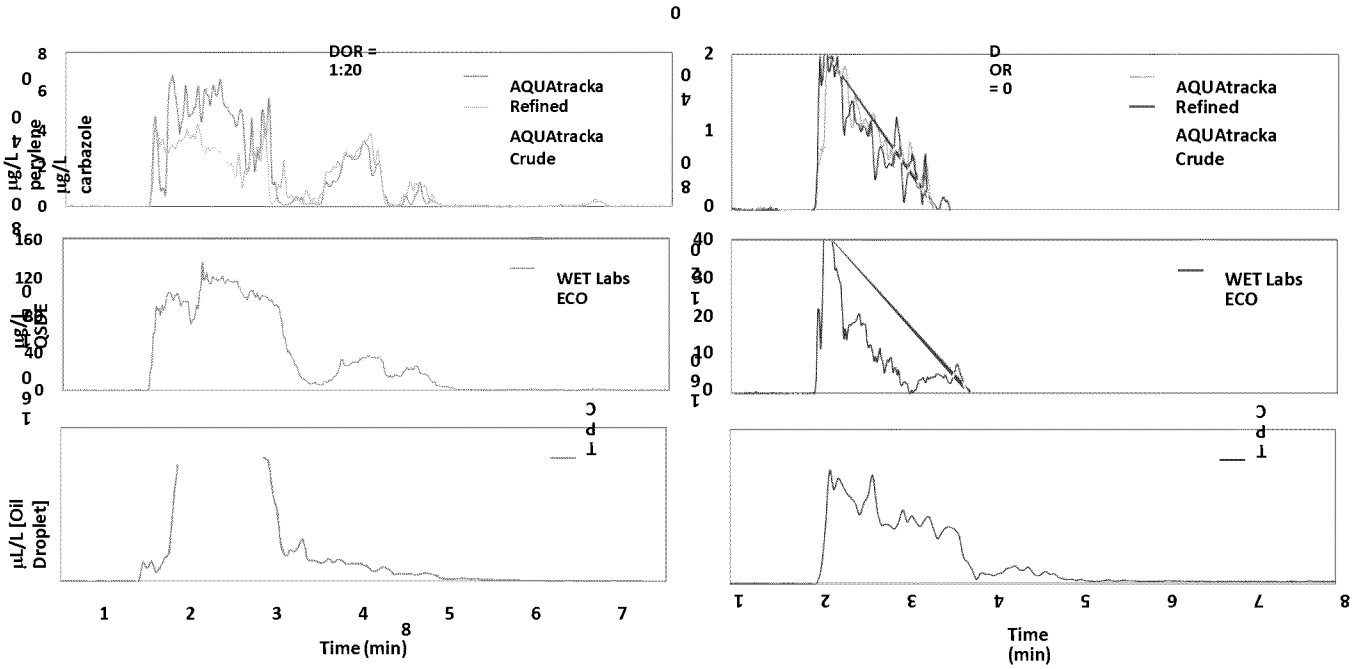

Figure 7. Fluorescence intensity and TPC as a function of time for ANS warm water treatment.

CONCLUSIONS

In situ oil droplet size distribution, particle concentration and fluorescence data from this study are essential for better understanding dispersion effectiveness and for refining droplet formation and trajectory models, such as modified Weber Number technique (Johansen et al., 2013) and the VDROP-J model (Zhou et al., 2014). Thus, findings from this study have implications for predicting the behavior of oil and plume formation, decision-making pertaining to SSDI as a countermeasure, and assessing the transport and fate of slicks and subsurface plumes in support of emergency response operations during any future deepwater spills.

ED_001324_00000746-00018

REFERENCES

Conmy, R. N., et al. (2014) Submersible Optical Sensors Exposed to Chemically Dispersed Crude Oil: Wave Tank Simulations for Improved Oil Spill Monitoring. Environ. Sci. Technol. 48(3): 1803-1810.

Cole, M.G., T. King, K. Lee (2007) Analytical technique for extracting hydrocarbons from water using sample container as extraction vessel in combination with a roller apparatus. Anal. Chem., 77: 2210-17.

CRRC Report (2010) Coastal Response Research Center Deepwater Horizon Dispersant USE Meeting Report, May 26-27, 2010, 108 pp.

EPA 600/F-16/250 Federal Report (2016) Dispersant Effectiveness, In-Situ Droplet Size Distribution and Numerical Modeling to Assess Subsurface Dispersant Injection as a Deepwater Blowout Oil Spill Response Option *and* Evaluation of Oil Fluorescence Characteristics to Improve Forensic Response Tools; IAA No. E12PG00037 for DOI BSEE, 144 pp.

Joint Analysis Group Report (2010) Review of Data to Examine Subsurface Oil in the Vicinity of DWH MC-252, May 19-June 19, 2010; 29 pp.

Johansen, O., et al. (2013) Droplet breakup in subsea oil releases - Part 2: Predictions of droplet size distributions with and without injection of chemical dispersants. Mar. Poll. Bull. 73(1): 327-335.

Lee, K., Li, Z., Boufadel, M.C., Venosa, A.D. and Scott Miles, M. (2009) Wave tank studies on dispersant effectiveness as a function of energy dissipation rate and particle size distribution. Final report submitted to NOAA/CRRC/UNH, 67 pp.

Li, Z., Lee, K., King, T., Boufadel, M.C. and Venosa, A.D., (2008) Oil droplet size distribution

ED_001324_00000746-00019

as a function of energy dissipation rate in an experimental wave tank 2008 International Oil

Spill Conference. American Petroleum Institute, Washington D.C., Savannah, GA, pp. 621-626.

Li, Z., Lee, K., King, T., Boufadel, M.C. and Venosa, A.D., (2009a) Evaluating crude oil chemical dispersion efficacy in a flow-through wave tank under regular non-breaking wave and breaking wave conditions. Mar. Poll. Bull., 58: 735-744.

Li, Z., Lee, K., King, T., Boufadel, M.C. and Venosa, A.D., (2009b) Evaluating Chemical Dispersant Efficacy in an Experimental Wave Tank: 2, Significant Factors Determining *In Situ* Oil Droplet Size Distribution. Environ. Engin. Sci., 26(9): 1407-1418.

Li, Z., Lee, K., King, T., Boufadel, M.C. and Venosa, A.D., (2010) Effects of temperature and wave conditions on chemical dispersion efficacy of heavy fuel oil in an experimental flow-through wave tank. Mar. Poll. Bull., 60(9): 1550-9.

NRC Report (2005) National Research Council Oil Spill Dispersants: Efficacy and Effects, Washington, DC, 400 pp.

Wickley-Olsen, E., Boufadel, M.C., King, T., Li, Z., Lee, K., Venosa, A.D. (2007) Regular and breaking waves in wave tank for dispersion effectiveness testing. In: Proceedings of the 30th Arctic and Marine Oil spill Program (AMOP) Technical Seminar, Edmonton, AB, Canada. Environment Canada, Ottawa, Ontario, Canada, pp. 161–187.

Zhao, L., et al. (2014). Evolution of droplets in subsea oil and gas blowouts: Development and validation of the numerical model VDROP-J. Mar. Poll. Bull., 83(1): 58-69.

ED_001324_00000746-00021